

Научном већу Института за физику

Предмет: Молба за покретање поступка за стицање звања виши научни сарадник

С обзиром да испуњавам критеријуме прописане од стране Министарства за просвету, науку и технолошки развој за стицање научног звања виши научни сарадник, као и критеријуме прописане Правилником о стицању научних звања, молим Научно веће Института за физику да покрене поступак за мој избор у наведено звање.

У прилогу достављам:

1. Мишљење руководиоца пројекта
2. Кратку биографију
3. Преглед научне активности
4. Елементе за квалитативну оцену научног доприноса
5. Елементе за квантитативну оцену научног доприноса
6. Списак објављених радова и њихове копије
7. Списак цитата
8. Докторску диплому и уверење о њеној нострификацији
9. Докторску тезу

Са поштовањем,

др Димитрије Степаненко

Naučnom veću Instituta za fiziku u Beogradu

Beograd, 9. maj 2013. g.

Predmet: Mišljenje rukovodioca projekta o izboru dr Dimitrija Stepanenka u zvanje viši naučni saradnik

Kao rukovodilac projekta osnovnih istraživanja Ministarstva prosvete, nauke i tehnološkog razvoja ON171032 pod nazivom „Fizika nanostrukturnih oksidnih materijala i jako korelisanih sistema“, saglasna sam sa pokretanjem postupka za izbor dr Dimitrija Stepanenka u zvanje viši naučni saradnik.

Za sastav Komisije za izbor predlažem:

- (1) dr Antun Balaž, viši naučni saradnik, IPB,
- (2) dr Zorana Dohčević-Mitrović, naučni savetnik, IPB,
- (3) prof. dr Zoran Radović, redovni profesor, FF.

Rukovodilac projekta

dr Zorana Dohčević-Mitrović

Biografija

Dimitrije Stepanenko

Dimitrije Stepanenko je rođen 13. 7. 1974. u Vranju, gde je završio osnovnu školu i Gimnaziju. Tokom školovanja u osnovnoj i srednjoj školi učestvovao je na takmičenjima iz fizike i osvojio brojne nagrade. Osvojio je pohvalu na međunarodnom takmičenju “First step to Nobel prize in physics” koji je organizovala Akademija nauka Poljske. Osvojio je prvu nagradu na državnom takmičenju iz fizike i bio je izabran u tim za međunarodnu fizičku olimpijadu 1993. na koju nacionalni tim nije otišao.

Studirao je na Fizičkom fakultetu Univerziteta u Beogradu, gde je 1998. godine diplomirao na smeru Teorijska i eksperimentalna fizika, sa prosečnom ocenom tokom studija 9.68. Tokom studija radio je u Istraživačkoj stanici Petnica.

Po diplomiranju odlazi na postdiplomske studije na Univerzitet u Bostonu (Boston University) gde je proveo dve godine kao stipendista univerziteta (Presidential University Graduate Fellowship). Od 2001. nastavlja postdiplomske studije na Državnom Univerzitetu Floride (Florida State University). Doktorat iz teorijske fizike kondenzovanog stanja odbranio je 2005. godine. Doktorat je nostrifikovan na Univerzitetu u Beogradu, rešenjem br. 06-613-7554/4-11, 30. januara 2012. Tokom postdiplomskih studija dobio je Dirak-Helmanovu nagradu za teorijsku fiziku 2004. godine. Tema naučnog rada tokom doktorskih studija bila je kontrola spinova u kvantnim tačkama. Razvio je principe korišćenja spin-orbitne interakcije za kontrolu spinova koristeći električna polja kao klasične kontrolne veličine. Tokom studija radio je kao asistent u nastavi i izvođenju računskih i eksperimentalnih vežbi na dodiplomskim studijama. Radio je i kao asistent na postdiplomskom kursu kvantne mehanike. Saradivao je na istraživanju u Nacionalnoj laboratoriji za jaka magnetna polja (National High Magnetic Field Laboratory). Boravio je u istraživačkim grupama u IBM istraživačkom centru (IBM T. J. Watson Research Center) i na Univerzitetu Ohaja (Ohio University).

Posle doktorata radi na Univerzitetu u Bazelu (Universität Basel), Švajcarska, u grupama Guida Burkarda i Daniela Losa. Držao je odabrana predavanja i računске vežbe na naprednim kursevima fizike kondenzovanog stanja i fizike mnogočestičnih sistema i učestvovao je u nastavi na uvodnim kursevima fizike i primenjene matematike. Pored nastavka istraživanja kontrole spinova u kvantnim tačkama, radi na procesiranju kvantne informacije u molekularnim magnetima, optičkim

metodama kontrole nuklearnih spinova u poluprovodničkim nanostrukturama i kvantnom transportu šupljina. Učestvovao je u istraživanjima na projektima Švajcarske nacionalne fondacije (SNF), Evropske komisije na Marie Curie projektu MagMaNet i FP7 projektima MolSpinQIP i ELFOS, kao i u istraživanjima u oblasti kvantne informacije pod pokroviteljstvom agencija DOE i IARPA Sjedinjenih Američkih država. Pored istraživanja, na projektima MagMaNet, MolSPinQIP i ELFOS radio je i kao organizator lokalne grupe konzorcijuma na Univerzitetu u Bazelu. Boravio je na Institutu za nanonauke Univerziteta Modena i Regio Emilia u Modeni kao gostujući istraživač.

Pregled naučne aktivnosti

Dimitrije Stepanenko

Moć svakog računskog sistema, po tezi Čurča i Tjuringa (Church-Turing thesis), jednak je moći Tjuringove mašine. Ova pretpostavka omogućuje zasnivanje teorije računske kompleksnosti i predstavlja granicu razvoja računara. Za sve do sada poznate fizičke sisteme, osim za kvantne računare, pokazano je da zadovoljavaju ovu granicu. Zato su na trenutnom stepenu razvoja nauke kvantni računari jedina nada za prevazilaženje ograničenja u performansama računara nametnutih Čurč-Tjuringovom tezom. Među sistemima koji mogu poslužiti kao osnova za izgradnju kvantnih računara, spinovi su specifični po tome što su sve njihove osobine inherentno kvantne i opisane konačnim brojem stepeni slobode. Istraživanja kandidata bave se kontrolom spinova u nanostrukturama za potrebe obrade kvantne informacije.

Problem kontrole je važan u spinskim sistemima pošto, u limitu slabih i sporo promenljivih polja, spinovi direktno interaguju isključivo sa magnetnim poljima dok su potpuno neosetljivi na električna polja. Zato je svaka električna kontrola indirektna i koristi spin-orbitnu interakciju ili mnogočestične efekte koji proizilaze iz fermionskih korelacija među elektronskim spinovima. Sa druge strane, na prostornim i vremenskim skalama karakterističnim za nanosisteme, brzo promenljiva, jaka i lokalna električna polja je lakše proizvesti nego odgovarajuća magnetna polja. Vremenska skala za kvantnu kontrolu mora biti dovoljno kratka, kako dekoherencija ne bi izbrisala kvantne osobine računara. U principu, duža vremena dekoherencije su povezana sa manjim sistemima, pa svaka ostvariva arhitektura kvantnog računara mora pronaći ravnotežu između zahteva za laku kontrolu, koji daje prednost većim sistemima i zahteva za kvantnu koherentnost, koji daje prednost manjim. Kandidatovi radovi razmatraju kontrolu elektronskih spinova u kvantnim tačkama sa karakterističnim dimenzijama reda veličine deset do sto nanometra i molekularnim magnetima sa karakteristiknim dimenzijama od desetog dela nanometra do nekoliko nanometra.

Kandidat je razvio proceduru za kontrolu spinova u kvantnim tačkama koja koristi vremenski zavisnu spin-orbitnu interakciju. Pokazao je da je stepen kontrole ostvariv ovim sredstvima u principu dovoljan za izgradnju univerzalnog kvantnog računara baziranog na spinovima u kvantnim tačkama. U ovom predlogu, jedino korišćeno magnetno poje je vremenski nezavisno i konstantno. Sva vremenska zavisnost potrebna za kontrolu dolazi od naponskih impulsa dovedenih na elektrode koje definišu kvantne tačke.

Postojanje procedure za kontrolu spinova pomoću spin-orbitne interakcije, kao i činjenica da su najnaprednija eksperimentalna istraživanja kvantne kontrole urađena u heterostrukturama III-V poluprovodnika sa cink-blend strukturom koji pokazuju jaku spin-orbitnu interakciju postavlja problem eksperimentalnog određivanja forme i jačine ove interakcije. U kvantnim računarima koji ne koriste spin-orbitnu interakciju kao kontrolni mehanizam, njeno prisustvo modifikuje kvantna logička kola i zahteva korekcije u njihovoj primeni. Kandidat je predložio eksperimente kojima se jačina i forma interakcije mogu odrediti u realističnoj postavci koja uključuje i efekte spinova jezgara u materijalima koji čine heterostrukturu.

Kvantni računari su mogući zahvaljujući toleranciji na greške u primeni kvantnih logičkih kola. Ispravljanje grešaka se postiže kvantnim kodovima za ispravljanje grešaka koji omogućuju tačnu primenu kvantnih logičkih kola i u slučaju kada svaka kvantna operacija nosi mogućnost greške. Da bi kodovi za ispravljanje grešaka funkcionisali, verovatnoća greške u elementarnim operacijama mora biti ispod neke granične vrednosti, koja se kreće između 10^{-4} za standardne Šorove kodove i oko 10^{-1} za topološke kvantne kodove. U svakom slučaju, neophodno je smanjiti početnu verovatnoću greške pre primene procedure za njihovo ispravljanje. Pored grešaka koje proističu iz nepreciznosti u primeni kontrolnih procedura, kvantna logička kola uvek pokazuju i greške koje su posledica dekoherencije. U kvantnim tačkama, najznačajniji izvor dekoherencije je interakcija sa nuklearnim spinovima. Kandidat je razvio proceduru koja koristi slaba kvantna merenja u kvantnoj optici sa kvantnim tačkama za ublažavanje uticaja nuklearnih spinova na koherenciju elektronskih spinova. Ovaj metod se zasniva na merenju fotoemisije iz kvantnih tačaka u režimu elektromagnetski izazvane transparencije (EIT) i prilagođavanju parametara eksperimenta pretpostavljenom stanju nuklearnih spinova. Efekat merenja je priprema nuklearnih spinova u stanje koje slabo utiče na koherenciju elektronskih spinova. Na kraju procedure, vreme koherencije elektronskih spinova je veće za dva reda veličine od svoje početne vrednosti.

Kvantne osobine spinova, pored skladištenja tehnološki značajnih kvantnih informacija, određuju i transport na nanometarskim skalama. Najizrazitiji kvantni efekat u transportu su Aharonov-Bomove oscilacije provodnosti nanoprstenova u funkciji magnetnog polja. Kandidat je proučavao transport kroz poluprovodničke nanoprstenove i spinski zavisne kvantne efekte kod šupljina u III-V poluprovodnicima. Za razliku od elektrona, šupljine imaju spin $3/2$, koji dozvoljava anizotropnu interakciju spinova. Pokazao je da uticaj kvantnih diskretnih stepeni slobode na transport čini mezoskopski transport šupljina značajno različitim od sličnog transporta elektrona. Kao posledica netrivialne i anizotropne strukture spinskih stanja, transportne osobine šupljina ne mogu biti

određene samo jednim parametrom kao u slučaju elektrona, gde su sve transportne osobine funkcije transparentnosti barijere. Zbog nekompatibilnosti spinski-nezavisnog rasejanja i anizotropne spin-orbitne interakcije, spin šupljina se ne održava u rasejanju na barijeri, čak i kada je sama barijera spinski nezavisna.

Iako kvantne tačke omogućuju bogat izbor mehanizama za kontrolu spinova, one imaju i svojih mana. Jedna od njih je da su kvantne tačke proizvedene u kompleksnom laboratorijskom postupku, tako da nisu identične. Prirodna sredina u kojoj spinovi borave u identičnim okolinama i predstavljaju identične kubite su molekularni magneti. Kandidat je proučavao kontrolu spinova u molekularnim magnetima pomoću električnih polja. Predložio je mehanizam kojim spinovi u molekularnim magnetima bez simetrije u odnosu na inverziju interaguju sa električnim poljima. Pored teorijskog opisa interakcije, kandidat je predložio eksperimente bazirane na elektronskoj spinskoj rezonanci (ESR) u spoljnim električnim poljima koji mogu izdvojiti molekule u kojima je električna kontrola spina moguća.

Kratka analiza najznačajnijih radova

Vremenski zavisna spin-orbitna interakcija u implementaciji kvantnih logičkih kola:

- Anisotropic spin exchange in pulsed quantum gates; N. E. Bonesteel, D. Stepanenko, and D. P. DiVincenzo, *Physical Review Letters* **87**, 207901 (2001)
- Spin-orbit coupling and time-reversal symmetry in pulsed quantum gates; D. Stepanenko, G. Burkard, D. P. DiVincenzo, and Daniel Loss, *Physical Review B* **68**, 115306 (2003)
- Universal quantum computation through control of spin-orbit coupling; D. Stepanenko, N. E. Bonesteel, *Physical Review Letters* **93**, 140501 (2004)

Značaj spin-orbitne interakcije u kvantnim logičkim kolima na kvantnim tačkama određen je, sa jedne strane, jačinom interakcije koja je oko 10 puta slabija od dominantne izotropne izmenske interakcije, i , sa druge strane, zahtevom da verovatnoća greške u primeni kola ne prelazi oko 10^{-4} . Naivna primena kvantnog logičkog kola zasnovanog na izmenskoj interakciji koja potpuno zanemaruje postojanje spin-orbitne interakcije dovodi do greške sa verovatnoćom oko 10^{-2} . Zato je neophodno uzeti u obzir spin-orbitnu interakciju pri dizajnu kvantnih logičkih kola sa kvantnim tačkama.

U ovim radovima, problem spin-orbitne interakcije je detaljno proučen. Radovi su ukazali da je ona značajna zato što u njenom prisustvu hamiltonijani spinova na kvantnim tačkama, uzeti u različitim trenucima, ne komutiraju. Pokazano je kako se komutatori vremenski zavisnog hamiltonijana u različitim trenucima mogu iskoristiti da smanje grešku u primeni kola. Primenom razvijene procedure, greška koja je inicijalno efekat prvog reda, postaje efekat drugog reda u količniku jačine spin-orbitne i izotropne izmenske interakcije. Pokazano je da ovakvo smanjenje greške može nastati kod svih kontrolnih impulsa sa simetričnom vremenskom zavisnošću.

Dalja kontrola vremenske zavisnosti kontrolnih impulsa opisana je kvantnim logičkim kolima koja nije moguće izvesti samo pomoću izotropne spinske interakcije. Razvijen je jednostavan geometrijski opis skupa kvantnih logičkih kola koja se mogu primeniti kontrolom oblika impulsa. Uvedeni su parametri koji kvantitativno određuju dostupna kola, i pokazano je da ovaj skup zavisi od asimetrije impulsa i jačine spin-orbitne interakcije. Pokazano je da je ovaj skup dovoljan za konstrukciju univerzalnog skupa kvantnih logičkih kola, te da je zato primena kontrolnih impulsa različitih oblika dovoljna za funkcionisanje kvantnog računara. Podskup ovoh skupa, koji obuhvata kola generisana vremenski simetričnim impulsima je takođe dovoljan za primenu univerzalnog skupa kvantnih logičkih kola. Pošto je uloga kontrolnog parametra prenešena na oblik naponskog impulsa, ovakva konstrukcija eliminiše potrebu za kontrolom magnetnih polja.

Višespinski kubiti u kvantnim tačkama:

- Quantum gates between capacitively coupled double quantum dot two-spin qubits; Dimitrije Stepanenko, Guido Burkard, *Physical Review B* **75**, 085324 (2007)
- Singlet-triplet splitting in double quantum dots due to spin-orbit and hyperfine interactions; Dimitrije Stepanenko, Mark Rudner, Bertrand I. Halperin, and Daniel Loss, *Physical Review B* **85**, 075416 (2012)
- Exchange-based CNOT gates for singlet-triplet qubits with spin-orbit interaction; Jelena Klinovaja, Dimitrije Stepanenko, Bertrand I. Halperin, and Daniel Loss, *Physical Review B* **86**, 085423 (2012)

Najmanji sistem koji može pokazati sve elemente neophodne za kvantnu obradu informacija na kvantnim tačkama je dupla kvantna tačka. U ovom sistemu moguće je definisati kodirane kubite, u kojima je osnovna jedinica kvantne informacije sadržana u stanju dva elektronska spina na paru susednih kvantnih tačkaka. Zahtevi za kontrolu ovakvih kodiranih kubita različiti su od analognih

zahteva za kubite kodirane u jednom spinu.

Kandidat je razmatrao karakteristike duplih kvantnih tačaka bitne za kreiranje spletenih stanja dvospinskih kubita. Kreiranje spletenih stanja je neophodan korak u kvantnoj obradi informacija. Najmanji sistem kvantnih tačaka koji omogućava kreiranje spletenih stanja među duplim kvantnim tačkama sadrži četiri kvantne tačke. Dok je izmenska interakcija unutar duple kvantne tačke posledica preklapanja orbitala vezanih elektrona, među duplim kvantnim tačkama dominira dugodometna Kulonova interakcija vezanih elektrona. Pokazano je da u ovakvoj konfiguraciji impulsi koji implementiraju jednokubitne operacije na susednim duplim kvantnim tačkama proizvode i komponentu kvantnih logičkih operacija koja se može opisati jedino kao dvokubitno kolo. Otkriveno je da je dvokubitna komponenta određena jednim parametrom, koji je izračunat kao funkcija geometrije sistema. Novootkriveni parametar iskorišćen je za konstrukciju dvokubitnih kvantnih logičkih kola u paru duplih kvantnih tačaka.

Drugi način kreiranja spletenih stanja povezan je sa narušavanjem potpune rotacione simetrije u spinskom prostoru. Kandidat je razmotrio situaciju u kojoj, pored spin-orbitne interakcije, i spinovi jezgara u poluprovodničkoj nanostrukтури doprinose narušenju ove simetrije. Pod ovim realističnim uslovima, interpretacija eksperimenata u kojima se spin-orbitna interakcija meri pomoću cepanja degenerisanog energetskog nivoa koji se sastoji od singleta totalnog spina 0 i jednog od tripletnih nivoa sa totalnim spinom 1 nije jednoznačna. Kandidat je analizirao postavku ovakvih eksperimenata i pronašao teoretski opis pomoću koga se iz niza sistematskih eksperimenata ovog tipa mogu razlučiti spin-orbitna i nuklearna komponenta cepanja. Tako se, pored jačine spin-orbitne interakcije, određuje i jačina interakcije nuklearnih spinova sa kubitima kodiranim u parove jednoelektronskih kvantnih tačaka.

Kvantna optika i priprema nuklearnih spinova:

- Enhancement of electron spin coherence by optical preparation of nuclear spins; Dimitrije Stepanenko, Guido Burkard, Geza Giedke, and Atac Imamoglu, *Physical Review Letters* **96**, 136401 (2006)
- Optical preparation of nuclear spins coupled to a localized electron spin; Dimitrije Stepanenko and Guido Burkard, *Proceedings of the 4th International Symposium on Mesoscopic Superconductivity and Spintronics*, page 371, (2008)

Dekoherencija je proces u kome kvantne osobine fizičkog sistema, opisane netrivialnim statističkim operatorom, usled interakcije sa okolinom gube kvantna svojstva, tako da postaje moguće opisati ih klasičnim raspedelama verovatnoće. Fizički sistem se može koristiti kao kvantni računar sa niskom verovatnoćom greske samo unutar vremenskog intervala koji je ograničen vremenom dekoherencije. Kako kvantni kodovi za korekciju greške zahtevaju nisku početnu verovatnoću greške, neophodno je eliminisati ili ublažiti dekoherenciju nosača kvantne informacije. Kod elektronskih spinova u kvantnim tačkama jedan od najznačajnijih izvora dekoherencije je interakcija sa spinovima jezgara poluprovodničkih materijala u kojima su elektroni koji nose spinske kubite. Karakteristično vreme dekoherencije kubita zavisi od stanja spinova jezgara. Na primer, potpuna polarizacija spinova jezgara bi u potpunosti eliminisala ovakvu dekoherenciju. Nažalost, vreme dekoherencije dobija konačnu i brzo opadajuću vrednost kada polarizacija jezgrenih spinova opadne ispod maksimalne vrednosti. Eksperimentalno dostupne vrednosti polarizacije od oko 0.6-0.8 nažalost ne izazivaju značajno povećanje vremena koherencije.

Autor je razvio teoretski opis elektromagnetski izazvane transparentije (EIT) naelektrisanih ekscitona i elektrona u kvantnim tačkama fabrikovanim u materijalima koji sadrže jezgra sa spinom. Jezgra, putem Overhauserovog polja, pomeraju energije elektronskih i ekscitonskih nivoa koji učestvuju u fenomenu elektromagnetski izazvane transparentije. Overhauserovo polje je kvantni operator koji u opštem slučaju nema oštru vrednost u sistemu jezgrenih spinova. Autor je pokazao da merenje fotoemisije iz kvantne tačke u režimu EIT predstavlja slabo kvantno merenje Overhauserovog polja. Razvijen je algoritam kojim se informacija dobijena merenjem vremena u kojima nastaje fotoemisija pretače u informaciju o stanju Overhauserovog polja jezgara. Podešavanjem parametara elektromagnetnih polja koja izazivaju transparentiju u zavisnosti od izmerenih vremena fotoemisije, spinovi jezgara se mogu dovesti u stanje sa uskom raspodelom Overhauserovog polja. Zatim je pokazano da jezgra u ovakvom stanju ne utiču značajno na dekoherenciju elektrona.

Detaljni teoretski opis ovakvog pripremnog merenja dat je relativno jednostavnom stohastičkom jednačinom. U idealnom slučaju u kome su sve snage i talasne dužine pobuđujućih elektromagnetnih polja dostupne, svi detektori idealno efikasni, i sve elektromagnetna zračenja idealno monohromatska, pokazano je da primena opisanog postupka u potpunosti eliminiše dekoherenciju usled interakcije sa jezgrima. Kandidat je pokazao kako odstupanja od idealnog slučaja daju konačna vremena dekoherencije. Zaključeno je da u realističnim okolnostima ovakav način pripreme ansambla jezgrenih spinova pokazuje bolje rezultate od pokušaja polarizacije

jezgara.

Kvantni transport i diskretni stepeni slobode:

- Interference of heavy holes in an Aharonov-Bohm ring; Dimitrije Stepanenko, Minchul Lee, Guido Burkard, Daniel Loss, *Physical Review B* 79, 235301 (2009)
- Current-conserving Aharonov-Bohm interferometry with arbitrary spin interactions, Minchul Lee and Dimitrije Stepanenko; *Physical Review B* 85, 075316 (2012)

Transport kroz nanoskopske prstenove pokazuje oscilatornu zavisnost od fluksa magnetnog polja kroz prsten. Ove Aharonov-Bomove oscilacije su posledica kvantne interferencije elektrona koji prolaze kroz dve grane prstena. Aharonov-Bomove oscilacije u metalima ne pokazuju jake spinske efekte. Nasuprot tome, spin-orbitna interakcija u poluprovodničkim prstenovima modifikuje oscilacije zahvaljujući Aharonov-Kašerovom efektu, električnom analogonu Aharonov-Bomovog efekta. Kandidat je proučavao transport kroz poluprovodničke prstenove nanometarskih dimenzija u kojima niskoenergetska stanja poseduju netrivialnu spinsku teksturu.

Za razliku od elektrona sa dominantnom linearnom spin-orbitnom interakcijom, kod šupljina spin-orbitna interakcija je proporcionalna trećem stepenu komponenti kvaziimpulsa. Pokazano je da su u ovom slučaju niskoenergetska stanja opisana spinskom teksturom sa nekolinearnim osama kvantizacije spinova. Nasuprot analognim stanjima u sistemima sa linearnom spin-orbitnom interakcijom ove teksture su energetski zavisne. Zato je oblik Aharonov-Bomovih oscilacija šupljina različit od jednostavnih periodičnih oscilacija elektrona. Detaljno je proučen oblik oscilacija za dva karakteristična oblika spin-orbitne interakcije: Rašbin oblik izazvan asimetrijom vezivanja šupljina u dvodimenzionalni gas i Dreselhausov oblik izazvan asimetrijom kristalne strukture nosećih poluprovodnika. Pokazano je kako se na osnovu oblika oscilacija može odrediti dominantan oblik interakcije.

Pored razvoja praktičnog načina za razlikovanje Dreselhausovog od Rašbinog oblika spin-orbitne interakcije, kandidatove studije transporta šupljina kroz poluprovodničke prstenove ukazuju na ključnu ulogu spinskih tekstura u transportu. Prostorno-zavisno stanje spinskih ili uopšteno bilo kojih diskretnih unutrašnjih stepeni slobode izaziva interferencione efekte u transportu. Zato, za razliku od slučaja stanja sa energetski nezavisnom teksturom, transportne osobine prstena nisu date samo verovatnoćom transmisije. Pokazano je da opis provodnosti kroz prsten mora sadržati

dodatne parametre. Na osnovu razvijene teorije spinski zavisnog transporta kroz stanja sa teksturom, pokazano je da ovakvi sistemi mogu fonctionisati kao spinski filteri. I pored spinski nezavisnog rasejanja, spin nije održan u transportu.

Magnetizam u molekulima i kvantni računari sa molekularnim magnetima:

- Spin-electric coupling in molecular magnets; Mircea Trif, Filippo Troiani, Dimitrije Stepanenko, Daniel Loss, Physical Review Letters **101**, 217201 (2008)
- Spin-electric effect in molecular antiferromagnets; Mircea Trif, Filippo Troiani, Dimitrije Stepanenko, and Daniel Loss, Physical Review B **82**, 045429 (2010)
- Hyperfine-induced decoherence in triangular spin-cluster qubits; Filippo Troiani, Dimitrije Stepanenko, and Daniel Loss, Physical review B **86**, 161409 (2012)

U molekularnim magnetima, niskoenergetska stanja čine multipleti sa dobro definisanim spinskim uređenjem. Ova stanja nastaju kao posledica jake izmenske interakcije koja kod molekularnih feromagneta snižava energiju stanja sa najvećim totalnim spinom, a kod molekularnih antiferomagneta snižava energiju stanja sa najmanjim totalnim spinom. Unutar ovih multipleta, stanja su dalje opisana anizotropnim spinskim hamiltonianom, koji određuje osnovno stanje sa najvećom ili najmanjom projekcijom spina na osu kvantizacije. Niskoenergetska stanja razdvojena su barijerom kroz koju mogu tunelovati. Kvantno tunelovanje magnetizacije pokazuje da je niskoenergetska dinamika u molekularnim magnetima kvantna i koherentna tokom dugih vremenskih intervala.

U ovim radovima, kandidat je pokazao da se kvantnim stanjem pojedinih molekularnih magneta može manipulirati pomoću spoljnih električnih polja. Razvijen je opis mehanizma kojim spinovi u molekularnim antiferomagnetima interaguju sa električnim poljem. Interakcija je zasnovana na nedostatku simetrije molekula u odnosu na inverziju i postojanju električnih dipolnih momenta hemijskih veza među magnetnim centrima. Identifikovan je niskoenergetski skup stanja koji je opisan projekcijom ukupnog spina i kiralnošću spinske strukture. Pokazano je da se kiralnost ponaša kao pseudospin $1/2$, te da električna polja u ravni molekula interaguju sa kiralnošću ne utičući na totalni spin. U isto vreme, električna polja normalna na ravan molekula ne pokazuju nikakav uticaj na stanje molekula.

Rezultati ovih radova upućuju na mogućnost električne manipulacije spinskim stanjima. Jačina

interakcije zavisi od detaljne strukture molekula, koju nije moguće pouzdano predvideti numeričkim metodama. Zato je predložen niz eksperimenata kojim bi se identifikovali molekuli u kojima postoji jaka spin-električna interakcija. Pokazano je da su najizgledniji kandidati za električnu manipulaciju spinovima trougaoni molekuli kod kojih je antiferomagnetna izmenska interakcija između magnetnih centara indukovana nemagnetnim mostovima u ravni molekula. Predložena je manipulacija pomoću električnih polja u blizini vrhova skenirajućih tunelnih mikroskopa, ili pomoću električne komponente kvantizovanog polja unutar rezonantnih linijskih supljina. U oba slučaja, karakteristično vreme manipulacije je dovoljno kratko u odnosu na vreme koherencije spinskih stanja da omogući kvantnu kontrolu spinova.

Elementi za kvalitativnu analizu Dimitrije Stepanenko

1.

Pokazatelji uspeha u naučnom radu

1.1

Nagrade i priznanja:

- Presidential University Graduate Fellowship, Boston University. Stipendija za postdiplomske studije na Univerzitetu u Bostonu. Jedna do dve ovakve nagrade se dodeljuju studentima prirodnih nauka na ovom univerzitetu.
- Dirac-Hellman award for theoretical physics. Jedna nagrada godišnje se dodeljuje studentima postdiplomskih studija ili naučnim saradnicima na Državnom Univerzitetu Floride.

1.2

Uvodna predavanja na konferencijama i druga predavanja po pozivu

Transportne osobine nanostruktura u kojima su nosioci naelektrisanja i spina šupljine pobudile su interesovanje istraživača u oblasti spintronike i kvantnih mezoskopskih fenomena. Optička priprema nuklearnih spinova u poluprovodnicima je zanimljiva kako grupama koje se bave kvantnom optikom, tako i istraživačima koji eksperimentalno ispituju mogućnost izgradnje kvantnih računara. Električna kontrola spinova u molekulima je pobudila interesovanje kako istraživača kvantnog magnetizma, tako i hemičara koji pokušavaju da sintetišu molekule sa traženim svojstvima. Članovi kandidatove grupe su zato održali uvodna predavanja na konferencijama iz oblasti spintronike, kvantne informacije, fizike nanosistema, kondenzovanog stanja i neorganske hemije. Kandidat je autor sledećih uvodnih predavanja i predavanja po pozivu:

- Quantum transport of heavy holes through an Aharonov-Bohm ring: Spin and charge properties of low-dimensional systems, Advanced ICTP Workshop, Sibiu, Romania, June 29. – July 4. 2009.
- Spin-electric coupling for quantum computation and quantum optics: International Conference on Quantum Optics and Quantum Information, Kiev, Ukraine, May 28 -- June 1, 2010.
- Interaction of molecular spins with electric fields: European Conference on Molecular

Magnetism, Paris, France, November 22 -- 25, 2011.

- Molecular spins and electric fields: NORDFORSK Nanospintronics Workshop, Borgholm, Sweden, June 12 – 14, 2012.
- Optical preparation of nuclear spins coupled to a localized electron spin: International Symposium on mesoscopic superconductivity and spintronics, NTT Basic Research Laboratories, Japan, February 27 – March 2, 2006. Predavanje po pozivu na kome je kandidat koautor

Seminari na grupama sa kojima je kandidat saradivao:

- North Florida condensed matter meeting, Gainesville Florida, 2004.
- North Florida condensed matter meeting, Tallahassee Florida 2005.
- Colloquium of the quantum computing group, IBM T. J. Watson Research Center, Yorktown Heights, New York, USA, October 2004.
- Condensed matter seminar, Ohio University, Athens, Ohio, USA,
- S3 Group Seminar, Istituto Nazionale per la Fisica della Materia, Modena, Italy, 2010.
- 4 th NORDFORSK meeting, Norrköping, Sweden, 2010.
- QSIT Seminar, Joint Colloquium of ETH Zurich and University of Basel, Basel Switzerland, 2012.
- National Center of Competence in Research, Quantum Science and Technology (NCCR QSIT), Arosa meeting, Arosa Switzerland, 2009.

Kandidat je boravio kao gostujući istraživač u sledećim institucijama:

- Physics Department, Ohio University, Athens, Ohio, USA
- IBM T.J. Watson Research Center, Yorktown Heights, New York, USA
- Istituto Nazionale per la Fisica della Materia, Modena, Italy

1.4

Članstva u uređivačkim odborima časopisa, uređivanje monografija, recenzije naučnih radova i projekata

Kandidat radi kao recenzent za sledeće časopise:

- Physical Review Letters,

- Physical Review B,
- Physica Status Solidi,
- Europhysics Journal,
- New Journal of Physics,
- Journal of Physics B,
- Applied Physics Letters

2

Razvoj uslova za naučni rad, obrazovanje i formiranje naučnih kadrova

2.1

Doprinos razvoju nauke u zemlji

Kandidat saradjuje sa istraživačima na Institutu za Fiziku u Zemunu koji se bave magnetnim osobinama nanočestica. Nanonauke spadaju u jedan od prioriternih pravaca u strategiji razvoja nauke u Srbiji. Kandidatova istraživanja upotrebe kvantnih osobina magnetnog uređenja u obradi kvantnih informacija, kao i uticaja električnih polja na magnetizam molekula predstavljaju otvaranje novih oblasti istraživanja i otvaranje oblasti kvantnog magnetizma u Srbiji. Kandidat je održao seminare o magnetizmu u molekulima i o kvantnim računarima baziranim na kvantnim tačkama u Srbiji, tokom zime 2010.

- Seminar Instituta za fiziku
- Kolokvijum Fizičkog fakulteta

2.2

Mentorstvo pri izradi magistarskih i doktorskih radova, rukovođenje specijalističkim radovima

Kandidat je radio sa studentima postdiplomskih studija i učestvovao u istraživanjima koja su bila deo doktorske teze Mirče Trifa (Mircea Trif) na Univerzitetu u Bazelu. Istraživanja molekularnog magnetizma su rađena pod zajedničkim rukovodstvom Daniela Losa i kandidata.

2.3

Pedagoški rad

Tokom studija u Srbiji, kandidat je radio u Istraživačkoj stanici Petnica na programima fizike za srednjoškolce. Učestvovao je u nastavi na Univerzitetu u Bostonu (Boston University), Državnom Univerzitetu Floride (Florida State University) i Univerzitetu u Bazelu (Universität Basel).

Kao saradnik u nastavi, vodio je računске vežbe i ocenjivao studente na sledećim kursevima:

Boston University:

- Electricity and magnetism
- Classical mechanics
- Quantum physics

Florida State University:

- Quantum mechanics, postdiplomski kurs
- Experimental particle physics, 1/2 semestra laboratorijskih vežbi

Na Univerzitetu u Bazelu, pored računskih vežbi, kandidat je držao predavanja iz odabranih poglavlja na sledećim kursevima:

- Solid state physics
- Mathematical methods of physics
- Advanced condensed matter physics
- Electromagnetism
- Statistical physics
- Many-body theory
- Introduction to nanoscale science

2.4

Međunarodna saradnja

Istraživanja mezoskopskih kvantnih fenomena su zastupljena na mnogim institucijama, tako da je kandidat saradivao sa mnogobrojnim istraživačima. Najznačajnija saradnja ostvarena je sa sledećim grupama:

- Nacionalni institut za fiziku materijala (Istituto Nazionale per la Fisica della Materia) i

Univerzitet Modene i Regije Emilia (Universita degli Studi di Modena e Regio Emilia). U ovim institucijama deluje grupa istraživača koja se bavi molekularnim magnetizmom koristeći eksperimentalne, numeričke i teorijske metode. Kandidat je radio na efektima električnog polja u molekularnim magnetima i dekoherenciji molekularnih spinova.

- Kyung Hee University, Yongin, Korea. Kandidat je saradivao na istraživanju provodnosti šupljina u nanostrukturama. U okviru ove saradnje, ispitan je uticaj diskretnih stepeni slobode na električni i spinski transport, kao i efekti koherentne interferencije provodnih puteva u nanoprstenovima.
- Harvard University, Boston, Massachusetts, USA. Kandidat je radio na razvoju kvantnih logičkih kola sa spinovima u kvantnim tačkama, u saradnji sa grupom Bertranda Halperina. U planu je da ovi rezultati budu primenjeni na eksperimente u kojima bi se ostvarila kontrola spinova pomoću spin-orbitne interakcije i izmenske interakcije elektronskih i nuklearnih spinova.
- T. J. Watson Research Center, Yorktown Heights, New York, USA. Kandidat je saradivao sa Dejvidom Divinćenom (David DiVincenzo) na problemu kontrole spinova u kvantnim tačkama pomoću vremenski zavisne anizotropne interakcije.

3.

Organizacija naučnog rada

3.1

Rukovođenje projektima, potprojektima i zadacima

Na Univerzitetu u Bazelu, kandidat je od 2007. do danas, pored lokalnih projekata pod pokroviteljstvom Švajcarske nacionalne fondacije (SNF), radio i na projektima koji su finansirale i nadzirale spoljne agencije. Pošto odsek za teorijsku fiziku kondenzovanog stanja učestvuje istovremeno u velikom broju projekata, kandidat je preuzeo organizacione, upravljačke i popularizacione poslove na projektima koji su se ticali njegovih istraživanja. Kandidat je pisao delove predloga projekata koji se odnose na ulogu Univerziteta u Bazelu u konzorcijumima, formulisao planove istraživanja, planirao budžet, pisao izveštaje, predstavljao grupu na sastancima konzorcijuma i na sastancima na kojima su sponzori istraživanja ocenjivali postignute rezultate i planove za dalji rad. Kandidat je obavljao ovakve poslove na projektima MagMaNet, MolSpinQIP i ELFOS iz okvirnog programa FP7 Evropske komisije. U manjoj meri učestvovao je u upravljanju projektima koje je finansirala švajcarska nacionalna fondacija (SNF) i Office of the Director of National Intelligence Sjedinjenih Američkih Država kroz program IARPA (Intelligence

Advance Research Projects Activity). U ovim projektima kandidat je izveštavao o radu grupe u Bazelu.

4

Kvalitet naučnih rezultata

4.1

Uticajnost kandidatovih naučnih radova

Istraživanja kandidata bave se kvantnim efektima u mezoskopskim sistemima. Ova oblast je tesno povezana sa osobinama nanostrukturiranih materijala, kvantnom kontrolom i kvantnom optikom.

Kandidat je razmatrao do tada standardno zanemarivana odstupanja spinova od modela jake izotropne izmenske interakcije. Otvorio je problem spin-orbitne interakcije u kvantnim logičkim kolima i razvio metode koji, sa jedne strane, smanjuju njen uticaj na ponasanje spinova i, sa druge strane, omogućuju korišćenje ove interakcije kao dodatnog mehanizma za kvantnu kontrolu. Razvoj ovih metoda je još uvek predmet širokog interesovanja, i kandidat nastavlja ovu liniju istraživanja.

Interakcije spinova u kvantnim računarima sa brojnim stohastičkim sistemima u okolini postepeno uništavaju koherenciju spinova, čineći ih nepogodnim za prenos i obradu kvantne informacije. Kandidat je predložio proceduru kojom se kvantno-optički efekat elektromagnetno indukovane transparentije koristi za poboljšanje koherencije elektronskih spinova u kvantnim tačkama. Dinamika uspostavljanja i narušavanja transparentnosti opisana je kao slabo kvantno merenje. Razvijena procedura je korišćena u kasnijim studijama uticaja nuklearnih spinova na elektronske spinove. Ilustracija iz jednog od kandidatovih radova izabrana je za rubriku kaleidoskop časopisa Physical Review B, (sh)to predstavlja ekvivalent naslovne strane časopisa. Ilustracija se može videti na adresi: <<http://prb.aps.org/kaleidoscope/prb/85/7/075416>>.

Na nanometarskoj skali, kvantni efekti utiču na transport naelektrisanja i spina. Najbolje proučeni kvantni efekat u transportu su Aharonov-Bomove oscilacije u provodnosti prstenova. Ovaj efekat je prvo otkriven u metalnim strukturama. U poluprovodničkim strukturama vidljivi su i efekti električnog polja koji su opisani analognim Aharonov-Kašerovim efektom. Kandidat je razvio teoriju provodnosti nanometarskih prstenova u kojima su nosioci naelektrisanja šupljine. Zbog veće vrednosti spina i kubne forme spin-orbitne interakcije, transport šupljina jako zavisi od diskretnih

stepeni slobode. Kandidat je pokazao da provodnost može poslužiti za određivanje forme spin-orbitne interakcije u poluprovodnicima, kao i da provodnost nanostrukture sa šupljinama zahteva opis koji ne može zavisiti od samo jednog parametra kao u slučaju struktura sa elektronima.

Kvantna kontrola zahteva da sistem ostane koherentan tokom dugog vremena dok interaguje sa poljima koje je moguće kontrolisati u eksperimentalnim uslovima. Ovi zahtevi su u principu protivrečni. Kvantne tačke su relativno pogodne za manipulaciju, ali nisu identične, te zahtevaju prilagođavanje kontrole procedure svakoj tački ponaosob. Kandidat je razmatrao kontrolu u molekularnim magnetima kao alternativnim nosiocima kvantne informacije. Kod ovih molekula problem kontrole spinova je teži zato što spinovi ne interaguju direktno sa električnim poljima. Kandidat je predložio mehanizam spin-električne interakcije u molekulima, zasnovan na nedostatku simetrije molekula u odnosu na inverziju. Pokazano je da spinski stepeni slobode u trougaonim molekulima interaguju sa električnim poljima preko kiralnosti spinske teksture u osnovnom stanju. Razmatran je uticaj spin-električnog efekta na osobine molekula merljive u eksperimentu, razvijen je mikroskopski model interakcije na osnovu efektivnog Habardovog modela i predložen način za identifikovanje molekula pogodnih za manipulaciju. Studija dekoherencije kiralnih stepeni slobode pokazala je da su oni mnogo otporniji na dekoherenciju od ukupnog spina molekula. Ovi rezultati poslužili su kao osnova za dva trenutno aktivna FP7 projekta koje se bave kvantnom kontrolom spinova u molekulima.

4.2

Pozitivna citiranost kandidatovih radova

Ukupan broj citata na kandidatove radove je 311, sa 299 citata ne računajući autocitate. Citati daju kandidatov h-faktor 8. Kandidat je dobio više rezultata koji su otvorili nove oblasti u proučavanju kvantne kontrole. U radovima koji se bave vremenski zavisnom kontrolom spina, dekoherencijom izazvanom nuklearnim spinovima i električnom kontrolom spinova u molekulima, kandidatovi rezultati su standardne reference.

4.3

Ugled i uticajnost publikacija u kojima su kandidatovi radovi objavljeni

Kandidat je objavljivao u časopisu Physical Review Letters (četiri rada), najuglednijoj publikaciji koja se bavi isključivo fizikom i ravnopravno objavljuje eksperimentalne, numeričke i teorijske rezultate iz svih oblasti fizike. Najveći broj kandidatovih radova objavljen je u časopisu Physical

Review B, koji je najuglednija publikacija posvećena fizici kondenzovanog stanja. Po jedan rad je objavljen u časopisu *Inorganica Chimica Acta*, koji je posvećen hemiji i u zborniku radova sa međunarodne konferencije “4th International Symposium on Mesoscopic Superconductivity and Spintronics”. Časopisi *Physical Review Letters* i *Physical Review B* su vrhunski međunarodni časopisi kategorije M21, dok je *Inorganica Chimica Acta* međunarodni časopis kategorije M23.

4.4

Efektivni broj radova i broj radova normiran na osnovu broja koautora, ukupan broj kandidatovih radova, udeo samostalnih i koautorskih radova u njemu, kandidatov doprinos u radovima

Svi kandidatovi radovi koriste teorijske i numeričke metode i imaju ukupno između dva i pet autora. Ukupan broj radova je četrnaest. Tokom postdiplomskih studija kandidat je objavljivao radove u kolaboraciji sa svojim mentorom i saradnicima van svoje institucije. Pored nastavka istraživanja započetih na doktorskim studijama, radovi objavljeni posle doktorata obuhvataju nove oblasti kojima je kandidat proširio svoja interesovanja. Objavljivani su u kolaboraciji sa studentima Univerziteta u Bazelu, spoljnim saradnicima i vođom grupe za teoriju kondenzovanog stanja na Univerzitetu u Bazelu.

4.5

Stepen samostalnosti u naučnoistraživačkom radu i uloga u realizaciji radova u naučnim centrima u zemlji i inostranstvu

Kandidat je razvijao računске i numeričke metode potrebne za rešavanje problema i razvijao ideje u diskusijama sa koautorima. Za radove koji se bave provodnošću prstenova i spin-električnom interakcijom osnovna ideja za istraživanje potiče od kandidata, dok su za ostale radove ideje rezultat diskusija sa koautorima, tako da su zajedničke sa značajnim doprinosom kandidata. Svi teorijski rezultati imaju značajan doprinos kandidata, dok je numerički deo posla podeljen među koautorima. Oko jedne trećine numeričkih izračunavanja su rezultati kandidata, dok je ostatak samostalni doprinos ostalih koautora. Na radovima koji se bave spin-električnim efektom, pored doprinosa u formulisanju problema, doprinosa teorijskom razmatranju i numeričkim izračunavanjima, kandidat je još i organizovao podelu rada među koautorima.

Elementi za kvantitativnu ocenu naučnog doprinosa

Pošto se kandidat Dimitrije Stepanenko nakon povratka iz inostranstva bira direktno u zvanje viši naučni saradnik, prikazani su minimalni uslovi za izbor u zvanja naučnog saradnik, višeg naučnog saradnika kao i zbirni uslovi za oba zvanja. Nakon toga su prikazani kvantitativni rezultati kandidata u dosadašnjem radu i upoređeni sa zbirnim uslovima za izbor u zvanje viši naučni saradnik.

Zvanje	Minimalni broj bodova	
Naučni saradnik	Ukupno	16
	M10+M20+M31+M32+M33+M41+M42	10
	M11+M12+M21+M22+M23+M24	5
Viši naučni saradnik	Ukupno	48
	M10+M20+M31+M32+M33+M41+M42	40
	M11+M12+M21+M22+M23+M24	28
Zbirno za oba zvanja	Ukupno	64
	M10+M20+M31+M32+M33+M41+M42	50
	M10+M20+M31+M32+M33+M41+M42+M51	50
	M11+M12+M21+M22+M23+M24	33
	M11+M12+M21+M22+M23+M24+M31+M32+M41+M42	33

Rezultati kandidata

Kategorija	M bodova po radu	Broj radova	Ukupno M bodova
M21	8	11	88
M23	3	1	3
M32	1.5	3	4.5
M33	1	1	1
M34	0.5	14	7
M71	6	1	6
Ukupno			109.5

Poređenje minimalnih uslova sa ostvarenim rezultatima kandidata

Zbirno za oba zvanja	Uslov	Ostvareni rezultat
Ukupno	64	109.5
M10+M20+M31+M32+M33+M41+M42	50	96.5
M10+M20+M31+M32+M33+M41+M42+M51	50	96.5
M11+M12+M21+M22+M23+M24	33	91
M11+M12+M21+M22+M23+M24+M31+M32+M41+M42	33	95.5

Ne računajući autocitate, kandidatovi radovi su citirani **299** puta prema bazi ISI Web of knowledge (ukupno 311 puta). Kandidatov h-faktor je **8**.

Spisak radova Dimitrije Stepanenko

Radovi u vrhunskim međunarodnim časopisima (M21)

1. Hyperfine-induced decoherence in triangular spin-cluster qubits; Filippo Troiani, Dimitrije Stepanenko, and Daniel Loss, *Physical Review B* **86**, 161409 (2012)
2. Exchange-based CNOT gates for singlet-triplet qubits with spin-orbit interaction; Jelena Klinovaja, Dimitrije Stepanenko, Bertrand I. Halperin, and Daniel Loss, *Physical Review B* **86**, 085423 (2012)
3. Current-conserving Aharonov-Bohm interferometry with arbitrary spin interactions, Minchul Lee and Dimitrije Stepanenko; *Physical Review B* **85**, 075316 (2012)
4. Singlet-triplet splitting in double quantum dots due to spin-orbit and hyperfine interactions; Dimitrije Stepanenko, Mark Rudner, Bertrand I. Halperin, and Daniel Loss, *Physical Review B* **85**, 075416 (2012)
5. Spin-electric effects in molecular antiferromagnets; Mircea Trif, Filippo Troiani, Dimitrije Stepanenko, and Daniel Loss, *Physical Review B* **82**, 045429 (2010)
6. Interference of heavy holes in an Aharonov-Bohm ring, Dimitrije Stepanenko; Minchul Lee, Guido Burkard, and Daniel Loss, *Physical Review B* **79**, 235301 (2009)
7. Spin-electric coupling in molecular magnets; Mircea Trif, Filippo Troiani, Dimitrije Stepanenko, and Daniel Loss, *Physical Review Letters* **101**, 217201 (2008)
8. Quantum gates between capacitively coupled double quantum dot two-spin qubits; Dimitrije Stepanenko and Guido Burkard, *Physical Review B* **75**, 085324 (2007)
9. Enhancement of electron spin coherence by optical preparation of nuclear spins; Dimitrije Stepanenko, Guido Burkard, Geza Giedke, and Atac Imamoglu, *Physical Review Letters* **96**, 136401 (2006)

10. Universal quantum computation through control of spin-orbit coupling; D. Stepanenko and N. E. Bonesteel, *Physical Review Letters* **93**, 140501 (2004)
11. Spin-orbit coupling and time-reversal symmetry in pulsed quantum gates; D. Stepanenko, N. E. Bonesteel, D. P. DiVincenzo, G. Burkard, and Daniel Loss, *Physical Review B* **68**, 115306 (2003)

Publikacija koja ne ulazi u kvantitativne kriterijume zbog datuma objavljivanja

- 12*. Anisotropic spin exchange in pulsed quantum gates; N. E. Bonesteel, D. Stepanenko, and D. P. DiVincenzo, *Physical Review Letters* **87**, 207901 (2001)

Rad u međunarodnom časopisu (M23)

1. Quantum computing with molecular magnets; Dimitrije Stepanenko, Mircea Trif, and Daniel Loss, *Inorganica Chimica Acta* **361**, 3740 (2008)

Predavanja po pozivu sa međunarodnih skupova, štampana u izvodima (M32)

1. Molecular spins and electric fields: NORDFORSK Nanospintronics Workshop, Borgholm, Sweden, June 12 – 14, 2012.
2. Interaction of molecular spins with electric fields: European Conference on Molecular Magnetism, Paris, France, November 22 -- 25, 2011.
3. Spin-electric coupling for quantum computation and quantum optics: International Conference on Quantum Optics and Quantum Information, Kiev, Ukraine, May 28 -- June 1, 2010.

Saopštenje sa međunarodnog skupa, štampano u celini (M33)

1. Optical preparation of nuclear spins coupled to a localized electron spin; Dimitrije Stepanenko and Guido Burkard, *Proceedings of the 4th Symposium on Mesoscopic Superconductivity and Spintronics*, Atsugi, Japan, in *Controllable Quantum States*:

Saopštenja sa međunarodnih skupova, štampana u izvodu (M34)

1. Singlet-triplet splitting in double quantum dots due to spin-orbit and hyperfine interactions; Dimitrije Stepanenko, Mark Rudner, Bertrand I. Halperin, and Daniel Loss, March Meeting of the American Physical Society, Boston, Massachusetts, USA, March 2012.
2. Quantum control of molecular antiferromagnets: an approach based on electric fields; Mircea Trif, Dimitrije Stepanenko, Filippo Troiani, and Daniel Loss, March Meeting of the American Physical Society, Portland, Oregon, USA, March 2010.
3. Interference of heavy holes in an Aharonov-Bohm ring; Dimitrije Stepanenko, Minchul Lee, Guido Burkard, and Daniel Loss, Spring Meeting of the Deutsche Physikallische Gessellschaft, Regensburg, Germany, 2010.
4. Electric quantum control of spins in molecular magnets; Mircea Trif, Dimitrije Stepanenko, Filippo Troiani, And Daniel Loss, Spring Meeting of the Deutsche Physikallische Gessellschaft, Regensburg, Germany, 2010.
5. Quantum transport of heavy holes through an Aharonov-Bohm ring: Spin and charge properties of low-dimensional systems; Advanced ICTP Workshop, Sibiu, Romania, June 29. – July 4. 2009.
6. Spin-Electric Coupling in Molecular Magnets; Mircea Trif, Filippo Troiani, Dimitrije Stepanenko, Daniel Loss, March Meeting of the American Physical Society, Pittsburgh, Pennsylvania, USA, March 2009.
7. Interference of heavy holes in an Aharonov-Bohm ring; QSIT Arosa Meeting, Arosa, Switzerland, January 2009.
8. Quantum gates between capacitively coupled double quantum dot two-spin qubits; Guido Burkard, Dimitrije Stepanenko, March Meeting of the American Physical Society, Denver, Colorado, USA, March 2007.

9. Enhancement of electron spin coherence by optical preparation of nuclear spins; Dimitrije Stepanenko, Guido Burkard, Geza Giedke, and Atac Imamoglu, March Meeting of the American Physical Society, Denver, Colorado, USA, March 2007.
10. Quantum gates between capacitively coupled double quantum dot two-spin qubits; Dimitrije Stepanenko and Guido Burkard, 71. Annual Meeting of the Deutsche Physikalische Gesellschaft and DPG - spring meeting of the Division Condensed Matter, Regensburg, Germany, March 2007.
11. Enhancement of Electron Spin Coherence by Optical Preparation of Nuclear Spins; D. Stepanenko, G. Burkard, G. Giedke, A. Imamoglu, International Conference on Nanoscience and Technology, Basel, Switzerland, August 2006.
12. Anisotropic Spin Exchange in Coupled Quantum Dots; Kerwin Foster, Layla Hormozi, Dimitrije Stepanenko, and Nicholas Bonesteel, March Meeting of the American Physical Society, Los Angeles, California, USA, March 2005.
13. Control of Anisotropic Spin Exchange in Quantum Dots; Dimitrije Stepanenko, Layla Hormozi, Nicholas Bonesteel, March Meeting of the American Physical Society, Los Angeles, California, USA, March 2005.
14. Spin-orbit coupling and time-symmetric pulsing of quantum gates; D. Stepanenko, N. E. Bonesteel, G. Burkard, D. P. DiVincenzo, and Daniel Loss, March Meeting of the American Physical Society, Austin, Texas, USA, March 2003.

Publikacija koja ne ulazi u kvantitativne kriterijume zbog datuma objavljivanja

- 15*. Anisotropic spin exchange in pulsed quantum gates; D. Stepanenko, N. E. Bonesteel, and D. P. DiVincenzo, March Meeting of the American Physical Society, Indianapolis, Indiana, USA, March 2002.

Odbranjena doktorska disertacija (M71)

1. Symmetry and control in spin-based quantum computing, Florida State University and National High Magnetic Field Laboratory, Tallahassee, Florida, USA, 2005. Nostrifikacija

na Univerzitetu u Beogradu, rešenje broj 06-613-7554/4-11, novembra 2011.

Kandidatovi radovi su citirani 299 puta, ne računajući autocitate (ukupno 311 puta) u časopisima indeksiranim u ISI Web of Science . Kandidatov h-faktor je 8.

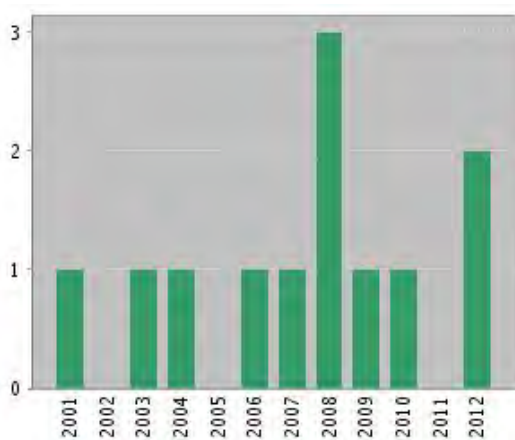
Web of Science[®] now with books

<< Back to previous page

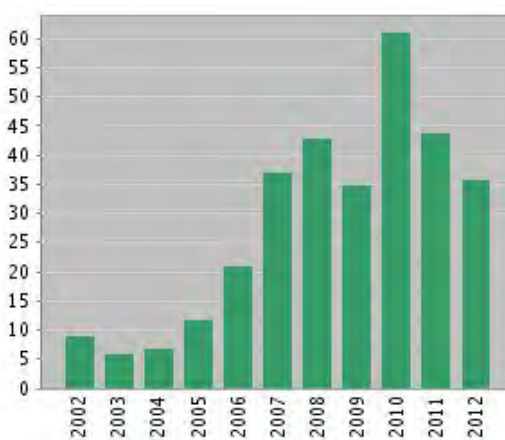
Citation Report From Marked List.

This report reflects citations to source items indexed within Web of Science. Perform a Cited Reference Search to include citations to items not indexed within Web of Science.

Published Items in Each Year



Citations in Each Year



Results found: 12
 Sum of the Times Cited [?]: 311
 Sum of Times Cited without self-citations [?]: 299
 Citing Articles [?]: 268
 Citing Articles without self-citations [?]: 260
 Average Citations per Item [?]: 25.92
 h-index [?]: 8

Results: 12

Page 1 of 2 Go

Sort by:

Publication Date -- newest to oldest

Use the checkboxes to remove individual items from this Citation Report

or restrict to items published between

1898 and 2012 Go

2008	2009	2010	2011	2012	Total	Average Citations per Year
43	35	61	44	36	311	28.27

- 1. Title: **Current-conserving Aharonov-Bohm interferometry with arbitrary spin interactions**
 Author(s): Lee, Minchul; Stepanenko, Dimitrije
 Source: PHYSICAL REVIEW B Volume: 85 Issue: 7 Article Number: 075316 DOI: 10.1103/PhysRevB.85.075316 Published: FEB 21 2012
- 2. Title: **Singlet-triplet splitting in double quantum dots due to spin-orbit and hyperfine interactions**
 Author(s): Stepanenko, Dimitrije; Rudner, Mark; Halperin, Bertrand I.; et al.
 Source: PHYSICAL REVIEW B Volume: 85 Issue: 7 Article Number: 075416 DOI: 10.1103/PhysRevB.85.075416 Published: FEB 16 2012
- 3. Title: **Spin electric effects in molecular antiferromagnets**
 Author(s): Trif, Mircea; Troiani, Filippo; Stepanenko, Dimitrije; et al.
 Source: PHYSICAL REVIEW B Volume: 82 Issue: 4 Article Number: 045429 DOI: 10.1103/PhysRevB.82.045429 Published: JUL 28 2010
- 4. Title: **Interference of heavy holes in an Aharonov-Bohm ring**

2008	2009	2010	2011	2012	Total	Average Citations per Year
0	0	0	0	0	0	0.00
0	0	0	0	2	2	2.00
0	0	1	7	4	12	4.00

<input checked="" type="checkbox"/>	Author(s): Stepanenko, Dimitrije; Lee, Minchul; Burkard, Guido; et al. Source: PHYSICAL REVIEW B Volume: 79 Issue: 23 Article Number: 235301 DOI: 10.1103/PhysRevB.79.235301 Published: JUN 2009	0	0	3	1	2	6	1.50
<input checked="" type="checkbox"/>	5. Title: Spin-Electric Coupling in Molecular Magnets Author(s): Trif, Mircea; Troiani, Filippo; Stepanenko, Dimitrije; et al. Source: PHYSICAL REVIEW LETTERS Volume: 101 Issue: 21 Article Number: 217201 DOI: 10.1103/PhysRevLett.101.217201 Published: NOV 21 2008	0	6	14	16	7	43	8.60
<input checked="" type="checkbox"/>	6. Title: Quantum computing with molecular magnets Author(s): Stepanenko, Dimitrije; Trif, Mircea; Loss, Daniel Source: INORGANICA CHIMICA ACTA Volume: 361 Issue: 14-15 Pages: 3740-3745 DOI: 10.1016/j.ica.2008.02.066 Published: OCT 1 2008	1	3	4	3	1	12	2.40
<input checked="" type="checkbox"/>	7. Title: OPTICAL PREPARATION OF NUCLEAR SPINS COUPLED TO A LOCALIZED ELECTRON SPIN Author(s): Stepanenko, Dimitrije; Burkard, Guido Book Editor(s): Takayanagi, H; Nitta, J; Nakano, H Conference: 4th International Symposium on Mesoscopic Superconductivity and Spintronics Location: NTT, Atsugi, JAPAN Date: FEB 27-MAR 02, 2006 Sponsor(s): Japan Sci & Technol Acgy; NTT Basic Res Labs Source: CONTROLLABLE QUANTUM STATES: MESOSCOPIC SUPERCONDUCTIVITY AND SPINTRONICS Pages: 371-376 DOI: 10.1142/9789812814623_0059 Published: 2008	0	0	0	0	0	0	0.00
<input checked="" type="checkbox"/>	8. Title: Quantum gates between capacitively coupled double quantum dot two-spin qubits Author(s): Stepanenko, Dimitrije; Burkard, Guido Source: PHYSICAL REVIEW B Volume: 75 Issue: 8 Article Number: 085324 DOI: 10.1103/PhysRevB.75.085324 Published: FEB 2007	6	5	2	3	2	21	3.50
<input checked="" type="checkbox"/>	9. Title: Enhancement of electron spin coherence by optical preparation of nuclear spins Author(s): Stepanenko, D; Burkard, G; Giedke, G; et al. Source: PHYSICAL REVIEW LETTERS Volume: 96 Issue: 13 Article Number: 136401 DOI: 10.1103/PhysRevLett.96.136401 Published: APR 7 2006	22	8	13	7	7	82	11.71
<input checked="" type="checkbox"/>	10. Title: Universal quantum computation through control of spin-orbit coupling Author(s): Stepanenko, D; Bonesteel, NE Source: PHYSICAL REVIEW LETTERS Volume: 93 Issue: 14 Article Number: 140501 DOI: 10.1103/PhysRevLett.93.140501 Published: OCT 1 2004	5	6	10	5	4	44	4.89

Results: 12

Page 1 of 2

Sort by:

Publication Date -- newest to oldest

Output Records

Step 1:

- Selected Records on page
- All records on page
- Records to

Step 2:

12 records matched your query of the 53,006,495 in the data limits you selected.

View in: [简体中文](#) | [English](#) | [日本語](#)

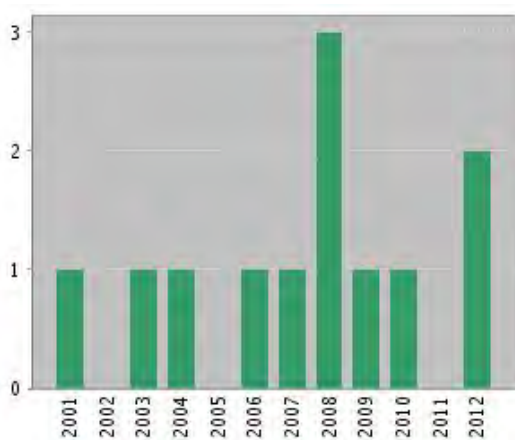
Web of Science[®] now with books

<< Back to previous page

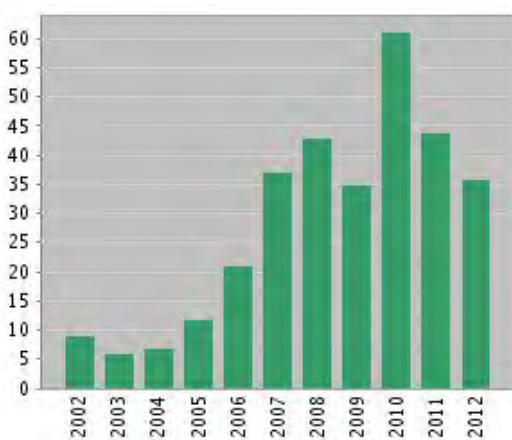
Citation Report From Marked List.

This report reflects citations to source items indexed within Web of Science. Perform a Cited Reference Search to include citations to items not indexed within Web of Science.

Published Items in Each Year



Citations in Each Year



Results found: 12
 Sum of the Times Cited [?]: 311
 Sum of Times Cited without self-citations [?]: 299
 Citing Articles [?]: 268
 Citing Articles without self-citations [?]: 260
 Average Citations per Item [?]: 25.92
 h-index [?]: 8

Results: 12 Page 2 of 2 Go Sort by: Publication Date -- newest to oldest

Use the checkboxes to remove individual items from this Citation Report or restrict to items published between

1898 and 2012 Go

	2008	2009	2010	2011	2012	Total	Average Citations per Year
	43	35	61	44	36	311	28.27

11. Title: **Spin-orbit coupling and time-reversal symmetry in quantum gates**
 Author(s): Stepanenko, D; Bonesteel, NE; DiVincenzo, DP; et al.
 Source: PHYSICAL REVIEW B Volume: 68 Issue: 11 Article Number: 115306 DOI: 10.1103/PhysRevB.68.115306 Published: SEP 15 2003

5	4	7	0	5	38	3.80
---	---	---	---	---	----	------

12. Title: **Anisotropic spin exchange in pulsed quantum gates**
 Author(s): Bonesteel, NE; Stepanenko, D; DiVincenzo, DP
 Source: PHYSICAL REVIEW LETTERS Volume: 87 Issue: 20 Article Number: 207901 DOI: 10.1103/PhysRevLett.87.207901 Published: NOV 12 2001

4	3	7	2	2	51	4.25
---	---	---	---	---	----	------

Results: 12 Page 2 of 2 Go Sort by: Publication Date -- newest to oldest

Output Records

Step 1:

- Selected Records on page
- All records on page

Step 2:

Save as text file Save

Records to

12 records matched your query of the 53,006,495 in the data limits you selected.

View in: | [简体中文](#) | [English](#) | [日本語](#)

© 2012 [Thomson Reuters](#) | [Terms of Use](#) | [Privacy Policy](#) | *Please give us your [feedback](#) on using Web of Knowledge.*

Web of Science[®] now with books

[<< Return to All Databases](#)

[<< Back to previous page](#)

Citing Articles

Title: **Anisotropic spin exchange in pulsed quantum gates**
 Author(s): **Bonesteel, NE ; Stepanenko, D ; DiVincenzo, DP**
 Source: **PHYSICAL REVIEW LETTERS** Volume: **87** Issue: **20** Article Number: **207901** DOI: **10.1103/PhysRevLett.87.207901** Published: **NOV 12 2001**

This article has been cited by articles indexed in the databases listed below. [\[more information\]](#)

51 in All Databases

51 in Web of Science

0 in BIOSIS Citation Index

0 in Chinese Science Citation Database

Results: **51**

Page of 2 [Go](#)

Sort by:

[Publication Date -- newest to oldest](#)

Hide Refine

Refine Results

Search within results for

[Search](#)

Web of Science Categories

[Refine](#)

- PHYSICS CONDENSED MATTER (23)
- PHYSICS ATOMIC MOLECULAR CHEMICAL (15)
- OPTICS (14)
- PHYSICS MULTIDISCIPLINARY (11)
- PHYSICS MATHEMATICAL (5)
- [more options / values...](#)

Document Types

[Refine](#)

- ARTICLE (49)
- PROCEEDINGS PAPER (4)
- REVIEW (1)
- [more options / values...](#)

Research Areas

- Authors**
- Group Authors**
- Editors**
- Source Titles**
- Book Series Titles**
- Conference Titles**
- Publication Years**
- Organizations-Enhanced**
- Funding Agencies**
- Languages**
- Countries/Territories**

(12) |
 |
 Save to: [ENDNOTE[®] WEB](#) |
 [Analyze Results](#) |
 [Create Citation Report](#)

[ENDNOTE[®]](#) |
 [ResearcherID](#) |
 [more options](#)

1. Title: **Exchange-based CNOT gates for singlet-triplet qubits with spin-orbit interaction**
 Author(s): **Klinovaja, Jelena; Stepanenko, Dimitrije; Halperin, Bertrand I.; et al.**
 Source: **PHYSICAL REVIEW B** Volume: **86** Issue: **8** Article Number: **085423** DOI: **10.1103/PhysRevB.86.085423** Published: **AUG 13 2012**
 Times Cited: **0** (from Web of Science)
[View abstract](#)
2. Title: **Effect of the Dzyaloshinskii-Moriya interaction on heat conductivity in one-dimensional quantum Ising chains**
 Author(s): **Li, W.; Zhang, Z.; Tong, P.**
 Source: **EUROPEAN PHYSICAL JOURNAL B** Volume: **85** Issue: **2**
 Article Number: **73** DOI: **10.1140/epjlb/e2012-20798-6** Published: **FEB 2012**
 Times Cited: **0** (from Web of Science)
[View abstract](#)
3. Title: **TWO-IMPURITY KONDO MODEL: SPIN-ORBIT INTERACTIONS AND ENTANGLEMENT**
 Author(s): **Johannesson, Henrik; Mross, David F.; Eriksson, Erik**
 Conference: **International Conference on Frustrated Spin Systems, Cold Atoms and Nanomaterials** Location: **Hanoi, VIETNAM** Date: **JUL 14-16, 2010**
 Source: **MODERN PHYSICS LETTERS B** Volume: **25** Issue: **12-13**
 Special Issue: **SI** Pages: **1083-1091** DOI: **10.1142/S0217984911026796**
 Published: **MAY 30 2011**
 Times Cited: **0** (from Web of Science)
[View abstract](#)
4. Title: **Singlet-triplet avoided crossings and effective g factor versus spatial orientation of spin-orbit-coupled quantum dots**

For advanced refine options, use

 Analyze Results

Author(s): Nowak, M. P.; Szafran, B.
Source: PHYSICAL REVIEW B Volume: **83** Issue: **3** Article Number:
035315 DOI: [10.1103/PhysRevB.83.035315](https://doi.org/10.1103/PhysRevB.83.035315) Published: **JAN 19 2011**
Times Cited: **2** (from Web of Science)

 [ View abstract]

5. Title: **Time-dependent configuration-interaction simulations of spin swap in spin-orbit-coupled double quantum dots**
Author(s): Nowak, M. P.; Szafran, B.
Source: PHYSICAL REVIEW B Volume: **82** Issue: **16** Article Number:
165316 DOI: [10.1103/PhysRevB.82.165316](https://doi.org/10.1103/PhysRevB.82.165316) Published: **OCT 12 2010**
Times Cited: **6** (from Web of Science)

 [ View abstract]

6. Title: **Spin-orbit coupling and anisotropic exchange in two-electron double quantum dots**
Author(s): Baruffa, Fabio; Stano, Peter; Fabian, Jaroslav
Source: PHYSICAL REVIEW B Volume: **82** Issue: **4** Article Number:
045311 DOI: [10.1103/PhysRevB.82.045311](https://doi.org/10.1103/PhysRevB.82.045311) Published: **JUL 21 2010**
Times Cited: **4** (from Web of Science)

 [ View abstract]

7. Title: **Optimal control landscape for the generation of unitary transformations with constrained dynamics**
Author(s): Hsieh, Michael; Wu, Rebing; Rabitz, Herschel; et al.
Source: PHYSICAL REVIEW A Volume: **81** Issue: **6** Article Number:
062352 DOI: [10.1103/PhysRevA.81.062352](https://doi.org/10.1103/PhysRevA.81.062352) Published: **JUN 30 2010**
Times Cited: **2** (from Web of Science)

 [ View abstract]

8. Title: **Coupling of bonding and antibonding electron orbitals in double quantum dots by spin-orbit interaction**
Author(s): Nowak, M. P.; Szafran, B.
Source: PHYSICAL REVIEW B Volume: **81** Issue: **23** Article Number:
235311 DOI: [10.1103/PhysRevB.81.235311](https://doi.org/10.1103/PhysRevB.81.235311) Published: **JUN 9 2010**
Times Cited: **3** (from Web of Science)

 [ View abstract]

9. Title: **Berezinskii-Kosterlitz-Thouless transition uncovered by the fidelity susceptibility in the XXZ model**
Author(s): Wang, Bo; Feng, Mang; Chen, Ze-Qian
Source: PHYSICAL REVIEW A Volume: **81** Issue: **6** Article Number:
064301 DOI: [10.1103/PhysRevA.81.064301](https://doi.org/10.1103/PhysRevA.81.064301) Published: **JUN 2 2010**
Times Cited: **7** (from Web of Science)

 [ View abstract]

10. Title: **Concatenated cranking representation of the Schrodinger equation and resolution to pulsed quantum operations with spin exchange**
Author(s): Ding, Zhi-Gang; Cen, Li-Xiang; Wang, ShunJin
Source: PHYSICAL REVIEW A Volume: **81** Issue: **3** Article Number:
032337 DOI: [10.1103/PhysRevA.81.032337](https://doi.org/10.1103/PhysRevA.81.032337) Published: **MAR 2010**
Times Cited: **2** (from Web of Science)

 [ View abstract]

11. Title: **Quantum computing with electron spins in quantum dots**
Author(s): Zak, Robert Andrzej; Roethlisberger, Beat; Chesi, Stefano; et al.
Source: RIVISTA DEL NUOVO CIMENTO Volume: **33** Issue: **7** Pages:
345-399 DOI: [10.1393/ncr/i2010-10056-y](https://doi.org/10.1393/ncr/i2010-10056-y) Published: **2010**
Times Cited: **7** (from Web of Science)

 [ View abstract]

12. Title: **Bloch sphere-like construction of SU(3) Hamiltonians using unitary integration**
 Author(s): Vinjanampathy, Sai; Rau, A. R. P.
 Source: JOURNAL OF PHYSICS A-MATHEMATICAL AND THEORETICAL Volume: **42** Issue: **42** Article Number: **425303** DOI: **10.1088/1751-8113/42/42/425303** Published: **OCT 23 2009**
 Times Cited: **2** (from Web of Science)
-  [ [View abstract](#)]
13. Title: **Selective suppression of Dresselhaus or Rashba spin-orbit coupling effects by the Zeeman interaction in quantum dots**
 Author(s): Szafran, B.; Nowak, M. P.; Bednarek, S.; et al.
 Source: PHYSICAL REVIEW B Volume: **79** Issue: **23** Article Number: **235303** DOI: **10.1103/PhysRevB.79.235303** Published: **JUN 2009**
 Times Cited: **3** (from Web of Science)
-  [ [View abstract](#)]
14. Title: **Influence of magnetic field on swap operation in Heisenberg XYZ model**
 Author(s): Liu, Jia; Zhang, Guo-Feng; Chen, Zi-Yu
 Source: PHYSICA B-CONDENSED MATTER Volume: **404** Issue: **8-11** Pages: **1116-1118** DOI: **10.1016/j.physb.2008.11.092** Published: **MAY 1 2009**
 Times Cited: **0** (from Web of Science)
-  [ [View abstract](#)]
15. Title: **Numerical study of a quantum dot structure for entanglement generation**
 Author(s): Giavaras, George
 Source: SEMICONDUCTOR SCIENCE AND TECHNOLOGY Volume: **23** Issue: **8** Article Number: **085010** DOI: **10.1088/0268-1242/23/10/085010** Published: **AUG 2008**
 Times Cited: **2** (from Web of Science)
-  [ [View abstract](#)]
16. Title: **Effect of spin-orbit interaction on entanglement of two-qubit Heisenberg XYZ systems in an inhomogeneous magnetic field**
 Author(s): Kheirandish, Fardin; Akhtarshenas, S. Javad; Mohammadi, Hamidreza
 Source: PHYSICAL REVIEW A Volume: **77** Issue: **4** Article Number: **042309** DOI: **10.1103/PhysRevA.77.042309** Published: **APR 2008**
 Times Cited: **33** (from Web of Science)
-  [ [View abstract](#)]
17. Title: **Theory of spin qubits in nanostructures**
 Author(s): Trauzettel, Bjoern; Borhani, Massoud; Trif, Mircea; et al.
 Source: JOURNAL OF THE PHYSICAL SOCIETY OF JAPAN Volume: **77** Issue: **3** Article Number: **031012** DOI: **10.1143/JPSJ.77.031012** Published: **MAR 2008**
 Times Cited: **3** (from Web of Science)
-   [ [View abstract](#)]
18. Title: **Effect of the Dzyaloshinski-Moriya term in the quantum (SWAP)(alpha) gate produced with exchange coupling**
 Author(s): Guerrero, Roberto J.; Rojas, F.
 Source: PHYSICAL REVIEW A Volume: **77** Issue: **1** Article Number: **012331** DOI: **10.1103/PhysRevA.77.012331** Published: **JAN 2008**
 Times Cited: **3** (from Web of Science)
-  [ [View abstract](#)]
19. Title: **Mutual information and swap operation in the two-qubit Heisenberg model with Dzyaloshinskii-Moriya anisotropic antisymmetric interaction**

Author(s): Zhang, Guo-Feng
 Source: JOURNAL OF PHYSICS-CONDENSED MATTER Volume: **19**
 Issue: **45** Article Number: **456205** DOI: **10.1088/0953-8984/19/45/456205** Published: **NOV 14 2007**
 Times Cited: **11** (from Web of Science)



[[View abstract](#)]

20. Title: **Interplay between the Dzyaloshinskii-Moriya anisotropic antisymmetric interaction and the SWAP operation in a two-qubit Heisenberg model**
 Author(s): Zhang, Guo-Feng; Zhou, Yue
 Source: PHYSICS LETTERS A Volume: **370** Issue: **2** Pages: **136-138**
 DOI: **10.1016/j.physleta.2007.05.051** Published: **OCT 15 2007**
 Times Cited: **0** (from Web of Science)



[[View abstract](#)]

21. Title: **Quantum computation in semiconductor quantum dots of electron-spin asymmetric anisotropic exchange**
 Author(s): Hao, Xiang; Zhu, Shiqun
 Source: PHYSICAL REVIEW A Volume: **76** Issue: **4** Article Number: **044306** DOI: **10.1103/PhysRevA.76.044306** Published: **OCT 2007**
 Times Cited: **7** (from Web of Science)



[[View abstract](#)]

22. Title: **Control and error prevention in condensed matter quantum computing devices**
 Author(s): Byrd, M. S.; Wu, L. -A.
 Conference: **30th International Workshop on Condensed Matter Theories (CMT30)** Location: **Max-Planck Inst Phys Komplexer Syst, Dresden, GERMANY** Date: **JUN 05-10, 2006**
 Source: INTERNATIONAL JOURNAL OF MODERN PHYSICS B Volume: **21** Issue: **13-14** Pages: **2505-2516** DOI: **10.1142/S0217979207043841**
 Published: **MAY 30 2007**
 Times Cited: **0** (from Web of Science)



[[View abstract](#)]

23. Title: **Quantum gates between capacitively coupled double quantum dot two-spin qubits**
 Author(s): Stepanenko, Dimitrije; Burkard, Guido
 Source: PHYSICAL REVIEW B Volume: **75** Issue: **8** Article Number: **085324** DOI: **10.1103/PhysRevB.75.085324** Published: **FEB 2007**
 Times Cited: **21** (from Web of Science)



[[View abstract](#)]

24. Title: **Spin-spin coupling in electrostatically coupled quantum dots**
 Author(s): Trif, Mircea; Golovach, Vitaly N.; Loss, Daniel
 Source: PHYSICAL REVIEW B Volume: **75** Issue: **8** Article Number: **085307** DOI: **10.1103/PhysRevB.75.085307** Published: **FEB 2007**
 Times Cited: **24** (from Web of Science)



[[View abstract](#)]

25. Title: **Detection and measurement of the Dzyaloshinskii-Moriya interaction in double quantum dot systems**
 Author(s): Chutia, Sucismita; Friesen, Mark; Joynt, Robert
 Source: PHYSICAL REVIEW B Volume: **73** Issue: **24** Article Number: **241304** DOI: **10.1103/PhysRevB.73.241304** Published: **JUN 2006**
 Times Cited: **16** (from Web of Science)



[[View abstract](#)]

26. Title: **Scheme for direct measurement of a general two-qubit Hamiltonian**
 Author(s): Devitt, SJ; Cole, JH; Hollenberg, LCL
 Source: PHYSICAL REVIEW A Volume: **73** Issue: **5** Article Number:

052317 DOI: [10.1103/PhysRevA.73.052317](https://doi.org/10.1103/PhysRevA.73.052317) Published: **MAY 2006**
Times Cited: **18** (from Web of Science)

 [ [View abstract](#)]

27. Title: [Quantum malware](#)
Author(s): Wu, Lian-Ao; Lidar, Daniel
Source: QUANTUM INFORMATION PROCESSING Volume: **5** Issue: **2**
Pages: **69-81** DOI: [10.1007/s11128-006-0014-5](https://doi.org/10.1007/s11128-006-0014-5) Published: **APR 2006**
Times Cited: **0** (from Web of Science)

 [ [View abstract](#)]

28. Title: [Design and control of spin gates in two quantum-dot arrays](#)
Author(s): Usaj, G; Balseiro, CA
Source: APPLIED PHYSICS LETTERS Volume: **88** Issue: **10** Article
Number: **103103** DOI: [10.1063/1.2181275](https://doi.org/10.1063/1.2181275) Published: **MAR 6 2006**
Times Cited: **2** (from Web of Science)

 [ [View abstract](#)]

29. Title: [Spin-based quantum dot quantum computing](#)
Author(s): Hu, X
Book Editor(s): Fabian, J; Fabian, J; Hohenester, U
Conference: **42th Schladming Winter School on Quantum Coherence in Matter - From Quarks to Solids** Location: **Schladming, AUSTRIA** Date: **FEB 28-MAR 06, 2004**
Sponsor(s): **Univ Graz, Div Theoret Phys**
Source: QUANTUM COHERENCE: FROM QUARKS TO SOLIDS Book
Series: **Lecture Notes in Physics** Volume: **689** Pages: **83-114**
Published: **2006**
Times Cited: **4** (from Web of Science)

 [ [View abstract](#)]

30. Title: [Recipes for spin-based quantum computing](#)
Author(s): Cerletti, V; Coish, WA; Gywat, O; et al.
Source: NANOTECHNOLOGY Volume: **16** Issue: **4** Pages: **R27-R49**
DOI: [10.1088/0957-4484/16/4/R01](https://doi.org/10.1088/0957-4484/16/4/R01) Published: **APR 2005**
Times Cited: **125** (from Web of Science)

 [ [View abstract](#)]

31. Title: [Spin manipulation of free two-dimensional electrons in Si/SiGe quantum wells](#)
Author(s): Tyryshkin, AM; Lyon, SA; Jantsch, W; et al.
Source: PHYSICAL REVIEW LETTERS Volume: **94** Issue: **12** Article
Number: **126802** DOI: [10.1103/PhysRevLett.94.126802](https://doi.org/10.1103/PhysRevLett.94.126802) Published: **APR 1 2005**
Times Cited: **57** (from Web of Science)








 [ [View abstract](#)]

32. Title: [Exchange gate in solid-state spin-quantum computation: The applicability of the Heisenberg model](#)
Author(s): Scarola, VW; Das Sarma, S
Source: PHYSICAL REVIEW A Volume: **71** Issue: **3** Article Number:
032340 DOI: [10.1103/PhysRevA.71.032340](https://doi.org/10.1103/PhysRevA.71.032340) Part: **Part a** Published:
MAR 2005
Times Cited: **25** (from Web of Science)

 [ [View abstract](#)]

33. Title: [Thermal entanglement of spins in an inhomogeneous magnetic field](#)
Author(s): Asoudeh, M; Karimipour, V
Source: PHYSICAL REVIEW A Volume: **71** Issue: **2** Article Number:
022308 DOI: [10.1103/PhysRevA.71.022308](https://doi.org/10.1103/PhysRevA.71.022308) Published: **FEB 2005**
Times Cited: **79** (from Web of Science)

 [ [View abstract](#)]

34. Title: **Universal quantum computation through control of spin-orbit coupling**
 Author(s): Stepanenko, D; Bonesteel, NE
 Source: PHYSICAL REVIEW LETTERS Volume: **93** Issue: **14** Article Number: **140501** DOI: **10.1103/PhysRevLett.93.140501** Published: **OCT 1 2004**
 Times Cited: **44** (from Web of Science)
-  [[View abstract](#)]
35. Title: **Quantum-cellular-automata pseudorandom maps**
 Author(s): Weinstein, YS; Hellberg, CS
 Source: PHYSICAL REVIEW A Volume: **69** Issue: **6** Article Number: **062301** DOI: **10.1103/PhysRevA.69.062301** Published: **JUN 2004**
 Times Cited: **7** (from Web of Science)
-  [[View abstract](#)]
36. Title: **Generation of entangled ancilla states for use in linear optics quantum computing**
 Author(s): Franson, JD; Donegan, MM; Jacobs, BC
 Source: PHYSICAL REVIEW A Volume: **69** Issue: **5** Article Number: **052328** DOI: **10.1103/PhysRevA.69.052328** Published: **MAY 2004**
 Times Cited: **7** (from Web of Science)
-  [[View abstract](#)]
37. Title: **Symmetry of anisotropic exchange interactions in semiconductor nanostructures**
 Author(s): Kavokin, KV
 Source: PHYSICAL REVIEW B Volume: **69** Issue: **7** Article Number: **075302** DOI: **10.1103/PhysRevB.69.075302** Published: **FEB 2004**
 Times Cited: **33** (from Web of Science)
-  [[View abstract](#)]
38. Title: **Anisotropic transport in a two-dimensional electron gas in the presence of spin-orbit coupling**
 Author(s): Schliemann, J; Loss, D
 Source: PHYSICAL REVIEW B Volume: **68** Issue: **16** Article Number: **165311** DOI: **10.1103/PhysRevB.68.165311** Published: **OCT 15 2003**
 Times Cited: **97** (from Web of Science)
-  [[View abstract](#)]
39. Title: **Spin-orbit coupling and time-reversal symmetry in quantum gates**
 Author(s): Stepanenko, D; Bonesteel, NE; DiVincenzo, DP; et al.
 Source: PHYSICAL REVIEW B Volume: **68** Issue: **11** Article Number: **115306** DOI: **10.1103/PhysRevB.68.115306** Published: **SEP 15 2003**
 Times Cited: **38** (from Web of Science)
-  [[View abstract](#)]
40. Title: **Dressed qubits**
 Author(s): Wu, LA; Lidar, DA
 Source: PHYSICAL REVIEW LETTERS Volume: **91** Issue: **9** Article Number: **097904** DOI: **10.1103/PhysRevLett.91.097904** Published: **AUG 29 2003**
 Times Cited: **18** (from Web of Science)
-  [[View abstract](#)]
41. Title: **Overview of spin-based quantum dot quantum computation**
 Author(s): Hu, XD; Das Sarma, S
 Conference: **2nd International Conference on Semiconductor Quantum Dots** Location: **UNIV TOKYO, KOMABA CAMPUS, TOKYO, JAPAN** Date: **SEP 30-OCT 03, 2002**
 Source: PHYSICA STATUS SOLIDI B-BASIC SOLID STATE

PHYSICS Volume: **238** Issue: **2** Pages: **360-365** DOI:
10.1002/pssb.200303094 Published: **JUL 2003**
 Times Cited: **12** (from Web of Science)



[[View abstract](#)]

42. Title: **Hydrogenic spin quantum computing in silicon: A digital approach**
 Author(s): Skinner, AJ; Davenport, ME; Kane, BE
 Source: PHYSICAL REVIEW LETTERS Volume: **90** Issue: **8** Article
 Number: **087901** DOI: **10.1103/PhysRevLett.90.087901** Published: **FEB
 28 2003**
 Times Cited: **100** (from Web of Science)



[[View abstract](#)]

43. Title: **Universal quantum logic from Zeeman and anisotropic exchange interactions**
 Author(s): Wu, LA; Lidar, DA
 Source: PHYSICAL REVIEW A Volume: **66** Issue: **6** Article Number:
062314 DOI: **10.1103/PhysRevA.66.062314** Published: **DEC 2002**
 Times Cited: **31** (from Web of Science)



[[View abstract](#)]

44. Title: **Magnetic anisotropy in the molecular complex V-15**
 Author(s): Konstantinidis, NP; Coffey, D
 Source: PHYSICAL REVIEW B Volume: **66** Issue: **17** Article Number:
174426 DOI: **10.1103/PhysRevB.66.174426** Published: **NOV 1 2002**
 Times Cited: **32** (from Web of Science)



[[View abstract](#)]

45. Title: **Effects of J-gate potential and uniform electric field on a coupled donor pair in Si for quantum computing**
 Author(s): Fang, AB; Chang, YC; Tucker, JR
 Source: PHYSICAL REVIEW B Volume: **66** Issue: **15** Article Number:
155331 DOI: **10.1103/PhysRevB.66.155331** Published: **OCT 15 2002**
 Times Cited: **18** (from Web of Science)



[[View abstract](#)]

46. Title: **Double-occupation errors induced by orbital dephasing in exchange-interaction quantum gates**
 Author(s): Barrett, SD; Barnes, CHW
 Source: PHYSICAL REVIEW B Volume: **66** Issue: **12** Article Number:
125318 DOI: **10.1103/PhysRevB.66.125318** Published: **SEP 15 2002**
 Times Cited: **9** (from Web of Science)



[[View abstract](#)]

47. Title: **Qubits as parafermions**
 Author(s): Wu, LA; Lidar, DA
 Source: JOURNAL OF MATHEMATICAL PHYSICS Volume: **43** Issue: **9**
 Pages: **4506-4525** DOI: **10.1063/1.1499208** Published: **SEP 2002**
 Times Cited: **20** (from Web of Science)



[[View abstract](#)]

48. Title: **Encoded universality for generalized anisotropic exchange Hamiltonians**
 Author(s): Vala, J; Whaley, KB
 Source: PHYSICAL REVIEW A Volume: **66** Issue: **2** Article Number:
022304 DOI: **10.1103/PhysRevA.66.022304** Published: **AUG 2002**
 Times Cited: **11** (from Web of Science)



[[View abstract](#)]

- 49. Title: **Comprehensive encoding and decoupling solution to problems of decoherence and design in solid-state quantum computing**
 Author(s): Byrd, MS; Lidar, DA
 Source: PHYSICAL REVIEW LETTERS Volume: **89** Issue: **4** Article Number: **047901** DOI: **10.1103/PhysRevLett.89.047901** Published: **JUL 22 2002**
 Times Cited: **55** (from Web of Science)



- 50. Title: **Power of anisotropic exchange interactions: Universality and efficient codes for quantum computing**
 Author(s): Wu, LA; Lidar, DA
 Source: PHYSICAL REVIEW A Volume: **65** Issue: **4** Article Number: **042318** DOI: **10.1103/PhysRevB.65.042318** Part: **Part a** Published: **APR 2002**
 Times Cited: **22** (from Web of Science)



Results: **51** Show 50 per page Page 1 of 2 Go Sort by: Publication Date -- newest to oldest

Output Records

Step 1:

- Selected Records on page
- All records on page
- Records to

Step 2:

- Authors, Title, Source
 - plus Abstract
- Full Record
 - plus Cited References

Step 3: [\[How do I export to bibliographic management software?\]](#)

Save to: ENDNOTE WEB ENDNOTE
ResearcherID
Save to other Reference Software Save
 (12)

51 records matched your query of the 53,033,624 in the data limits you selected.

View in: [简体中文](#) | [English](#) | [日本語](#)

Web of Science[®] now with books

<< Return to All Databases

<< Back to previous page

Citing Articles

Title: Anisotropic spin exchange in pulsed quantum gates
Author(s): Bonesteel, NE ; Stepanenko, D ; DiVincenzo, DP
Source: PHYSICAL REVIEW LETTERS Volume: 87 Issue: 20 Article Number: 207901 DOI: 10.1103/PhysRevLett.87.207901 Published: NOV 12 2001

This article has been cited by articles indexed in the databases listed below. [more information]

51 in All Databases

51 in Web of Science

0 in BIOSIS Citation Index

0 in Chinese Science Citation Database

Results: 51

Page 2 of 2 Go

Sort by:

Publication Date -- newest to oldest

Hide Refine

Refine Results

Search within results for

Search input field

Search

Web of Science Categories

Refine

- PHYSICS CONDENSED MATTER (23)
- PHYSICS ATOMIC MOLECULAR CHEMICAL (15)
- OPTICS (14)
- PHYSICS MULTIDISCIPLINARY (11)
- PHYSICS MATHEMATICAL (5)

Document Types

Refine

- ARTICLE (49)
- PROCEEDINGS PAPER (4)
- REVIEW (1)

- Research Areas
- Authors
- Group Authors
- Editors
- Source Titles
- Book Series Titles
- Conference Titles
- Publication Years
- Organizations-Enhanced
- Funding Agencies
- Languages
- Countries/Territories

Save to: ENDNOTE[®] WEB | Analyze Results | Create Citation Report

- 51. Title: Cancellation of spin-orbit effects in quantum gates based on the exchange coupling in quantum dots
Author(s): Burkard, G; Loss, D
Source: PHYSICAL REVIEW LETTERS Volume: 88 Issue: 4 Article Number: 047903 DOI: 10.1103/PhysRevLett.88.047903 Published: JAN 28 2002
Times Cited: 66 (from Web of Science)

View abstract

For advanced refine options, use

[Analyze Results](#)

Results: 51 [Show 50 per page](#)

Page 2 of 2 [Go](#)

Sort by: [Publication Date -- newest to oldest](#)

Output Records

Step 1:

- Selected Records on page
- All records on page
- Records to

Step 2:

- Authors, Title, Source
 - plus Abstract
- Full Record
 - plus Cited References

Step 3: [\[How do I export to bibliographic management software?\]](#)

Save to: [ENDNOTE® WEB](#) [ENDNOTE®](#)
[ResearcherID](#)
[Save to other Reference Software](#) [Save](#)
 (12)

51 records matched your query of the 53,033,624 in the data limits you selected.

View in: | [简体中文](#) | [English](#) | [日本語](#)

Web of Science[®] now with books

[<< Return to All Databases](#)

[<< Back to previous page](#)

Citing Articles

Title: **Spin-orbit coupling and time-reversal symmetry in quantum gates**
 Author(s): **Stepanenko, D ; Bonesteel, NE ; DiVincenzo, DP ; et al.**
 Source: **PHYSICAL REVIEW B** Volume: **68** Issue: **11** Article Number: **115306** DOI:
10.1103/PhysRevB.68.115306 Published: **SEP 15 2003**

This article has been cited by articles indexed in the databases listed below. [\[more information\]](#)

38 in All Databases

38 in Web of Science

0 in BIOSIS Citation Index

0 in Chinese Science Citation Database

Results: **38**

Page of 1

Sort by:

Hide Refine

Refine Results

Search within results for

Web of Science Categories

- PHYSICS CONDENSED MATTER (17)
- PHYSICS MULTIDISCIPLINARY (11)
- PHYSICS ATOMIC MOLECULAR CHEMICAL (6)
- OPTICS (5)
- MATERIALS SCIENCE MULTIDISCIPLINARY (3)
- [more options / values...](#)

Document Types

- ARTICLE (33)
- PROCEEDINGS PAPER (5)
- REVIEW (3)
- [more options / values...](#)

Research Areas

Authors

Group Authors

Editors

Source Titles

Book Series Titles

Conference Titles

Publication Years

Organizations-Enhanced

Funding Agencies

Languages

Countries/Territories

(12) |
 |
 |
 Save to: |
 |

1. Title: **Exchange-based CNOT gates for singlet-triplet qubits with spin-orbit interaction**
 Author(s): Klinovaja, Jelena; Stepanenko, Dimitrije; Halperin, Bertrand I.; et al.
 Source: PHYSICAL REVIEW B Volume: **86** Issue: **8** Article Number: **085423** DOI: **10.1103/PhysRevB.86.085423** Published: **AUG 13 2012**
 Times Cited: **0** (from Web of Science)

[View abstract](#)

2. Title: **Electron Mediated Mn-Mn Interaction in Quantum Dots**
 Author(s): Bak, Z.
 Conference: **European Conference on Physics of Magnetism (PM)**
 Location: **Poznan, POLAND** Date: **JUN 27-JUL 01, 2011**
 Source: ACTA PHYSICA POLONICA A Volume: **121** Issue: **5-6** Pages: **1219-1221** Published: **MAY-JUN 2012**
 Times Cited: **0** (from Web of Science)

[View abstract](#)

3. Title: **Spin manipulation and relaxation in spin-orbit qubits**
 Author(s): Borhani, Massoud; Hu, Xuedong
 Source: PHYSICAL REVIEW B Volume: **85** Issue: **12** Article Number: **125132** DOI: **10.1103/PhysRevB.85.125132** Published: **MAR 28 2012**
 Times Cited: **1** (from Web of Science)

[View abstract](#)

4. Title: **Singlet-triplet splitting in double quantum dots due to spin-orbit and hyperfine interactions**
 Author(s): Stepanenko, Dimitrije; Rudner, Mark; Halperin, Bertrand I.; et al.
 Source: PHYSICAL REVIEW B Volume: **85** Issue: **7** Article Number: **075416** DOI: **10.1103/PhysRevB.85.075416** Published: **FEB 16 2012**
 Times Cited: **2** (from Web of Science)

For advanced refine options, use

[Analyze Results](#)[View abstract](#)

5. Title: **Generation of entanglement between qubits in a one-dimensional harmonic oscillator**
 Author(s): Owen, E. T.; Dean, M. C.; Barnes, C. H. W.
 Source: PHYSICAL REVIEW A Volume: **85** Issue: **2** Article Number: **022319** DOI: **10.1103/PhysRevA.85.022319** Published: **FEB 14 2012**
 Times Cited: **0** (from Web of Science)

[View abstract](#)

6. Title: **Electric Field Control of Magnetic Coupling in a Double Quantum Dot System and Related Parasitic Electric Dipole Effect**
 Author(s): Bak, Z.
 Conference: **14th Czech and Slovak Conference on Magnetism** Location: **Kosice, SLOVAKIA** Date: **JUN 06-09, 2010**
 Sponsor(s): **Safarik Univ, Fac Sci; Inst Phys, Slovak Acad Sci; Slovak Phys Soc**
 Source: ACTA PHYSICA POLONICA A Volume: **118** Issue: **5** Pages: **957-958** Published: **NOV 2010**
 Times Cited: **1** (from Web of Science)

[View abstract](#)

7. Title: **Optimal control landscape for the generation of unitary transformations with constrained dynamics**
 Author(s): Hsieh, Michael; Wu, Rebing; Rabitz, Herschel; et al.
 Source: PHYSICAL REVIEW A Volume: **81** Issue: **6** Article Number: **062352** DOI: **10.1103/PhysRevA.81.062352** Published: **JUN 30 2010**
 Times Cited: **2** (from Web of Science)

[View abstract](#)

8. Title: **Proposal of a full Bell state analyzer for spin qubits in a double quantum dot**
 Author(s): Yokoshi, Nobuhiko; Imamura, Hiroshi; Kosaka, Hideo
 Source: PHYSICAL REVIEW B Volume: **81** Issue: **16** Article Number: **161305** DOI: **10.1103/PhysRevB.81.161305** Published: **APR 15 2010**
 Times Cited: **4** (from Web of Science)

[View abstract](#)

9. Title: **Theory of Anisotropic Exchange in Laterally Coupled Quantum Dots**
 Author(s): Baruffa, Fabio; Stano, Peter; Fabian, Jaroslav
 Source: PHYSICAL REVIEW LETTERS Volume: **104** Issue: **12** Article Number: **126401** DOI: **10.1103/PhysRevLett.104.126401** Published: **MAR 26 2010**
 Times Cited: **12** (from Web of Science)

[View abstract](#)

10. Title: **Concatenated cranking representation of the Schrodinger equation and resolution to pulsed quantum operations with spin exchange**
 Author(s): Ding, Zhi-Gang; Cen, Li-Xiang; Wang, ShunJin
 Source: PHYSICAL REVIEW A Volume: **81** Issue: **3** Article Number: **032337** DOI: **10.1103/PhysRevA.81.032337** Published: **MAR 2010**
 Times Cited: **2** (from Web of Science)

[View abstract](#)

11. Title: **Exchange coupling in silicon quantum dots: Theoretical considerations for quantum computation**
 Author(s): Li, Qiuzi; Cywinski, Lukasz; Culcer, Dimitrie; et al.
 Source: PHYSICAL REVIEW B Volume: **81** Issue: **8** Article Number: **085313** DOI: **10.1103/PhysRevB.81.085313** Published: **FEB 2010**
 Times Cited: **23** (from Web of Science)

[View abstract](#)

12. Title: **Electronic properties of quantum dot systems realized in semiconductor nanowires**
 Author(s): Salfi, J.; Roddaro, S.; Ercolani, D.; et al.
 Source: SEMICONDUCTOR SCIENCE AND TECHNOLOGY Volume: **25**
 Issue: **2** Special Issue: **SI** Article Number: **024007** DOI: **10.1088/0268-1242/25/2/024007** Published: **FEB 2010**
 Times Cited: **4** (from Web of Science)



[[View abstract](#)]

13. Title: **Adiabatic pumping in a double quantum dot structure with strong spin-orbit interaction**
 Author(s): Romeo, F.; Citro, R.
 Source: PHYSICAL REVIEW B Volume: **80** Issue: **16** Article Number: **165311** DOI: **10.1103/PhysRevB.80.165311** Published: **OCT 2009**
 Times Cited: **7** (from Web of Science)



[[View abstract](#)]

14. Title: **Electrical Measurement of a Two-Electron Spin State in a Double Quantum Dot**
 Author(s): Yokoshi, Nobuhiko; Imamura, Hiroshi; Kosaka, Hideo
 Source: PHYSICAL REVIEW LETTERS Volume: **103** Issue: **4** Article Number: **046806** DOI: **10.1103/PhysRevLett.103.046806** Published: **JUL 24 2009**
 Times Cited: **5** (from Web of Science)



[[View abstract](#)]

15. Title: **Aharonov-Casher Effect in Exchange Interactions in a Wigner Crystal**
 Author(s): Tserkovnyak, Yaroslav; Kindermann, Markus
 Source: PHYSICAL REVIEW LETTERS Volume: **102** Issue: **12** Article Number: **126801** DOI: **10.1103/PhysRevLett.102.126801** Published: **MAR 27 2009**
 Times Cited: **3** (from Web of Science)



[[View abstract](#)]

16. Title: **Dynamics of coupled spins in quantum dots with strong spin-orbit interaction**
 Author(s): Pfund, A.; Shorubalko, I.; Ensslin, K.; et al.
 Source: PHYSICAL REVIEW B Volume: **79** Issue: **12** Article Number: **121306** DOI: **10.1103/PhysRevB.79.121306** Published: **MAR 2009**
 Times Cited: **10** (from Web of Science)



[[View abstract](#)]

17. Title: **Crossover from the ballistic to the resonant tunneling transport for an ideal one-dimensional quantum ring with spin-orbit interaction**
 Author(s): Bellucci, S.; Onorato, P.
 Source: PHYSICAL REVIEW B Volume: **78** Issue: **23** Article Number: **235312** DOI: **10.1103/PhysRevB.78.235312** Published: **DEC 2008**
 Times Cited: **12** (from Web of Science)



[[View abstract](#)]

18. Title: **Spin-orbit coupling and the singlet-triplet transition in lateral double quantum dots**
 Author(s): Meza-Montes, L.; Destefani, Carlos F.; Ulloa, Sergio E.
 Source: PHYSICAL REVIEW B Volume: **78** Issue: **20** Article Number: **205307** DOI: **10.1103/PhysRevB.78.205307** Published: **NOV 2008**
 Times Cited: **13** (from Web of Science)



[[View abstract](#)]

19. Title: **Quantum computing with molecular magnets**
 Author(s): Stepanenko, Dimitrije; Trif, Mircea; Loss, Daniel

Source: INORGANICA CHIMICA ACTA Volume: **361** Issue: **14-15** Pages: **3740-3745** DOI: **10.1016/j.ica.2008.02.066** Published: **OCT 1 2008**
Times Cited: **12** (from Web of Science)



[[View abstract](#)]

20. Title: **Spin-orbit-mediated anisotropic spin interaction in interacting electron systems**
Author(s): Gangadharaiah, Suhas; Sun, Jianmin; Starykh, Oleg A.
Source: PHYSICAL REVIEW LETTERS Volume: **100** Issue: **15** Article Number: **156402** DOI: **10.1103/PhysRevLett.100.156402** Published: **APR 18 2008**
Times Cited: **46** (from Web of Science)



[[View abstract](#)]

21. Title: **Theory of spin qubits in nanostructures**
Author(s): Trauzettel, Bjoern; Borhani, Massoud; Trif, Mircea; et al.
Source: JOURNAL OF THE PHYSICAL SOCIETY OF JAPAN Volume: **77** Issue: **3** Article Number: **031012** DOI: **10.1143/JPSJ.77.031012**
Published: **MAR 2008**
Times Cited: **3** (from Web of Science)



[[View abstract](#)]

22. Title: **Quantum computation in semiconductor quantum dots of electron-spin asymmetric anisotropic exchange**
Author(s): Hao, Xiang; Zhu, Shiqun
Source: PHYSICAL REVIEW A Volume: **76** Issue: **4** Article Number: **044306** DOI: **10.1103/PhysRevA.76.044306** Published: **OCT 2007**
Times Cited: **7** (from Web of Science)



[[View abstract](#)]

23. Title: **Spin-spin coupling in electrostatically coupled quantum dots**
Author(s): Trif, Mircea; Golovach, Vitaly N.; Loss, Daniel
Source: PHYSICAL REVIEW B Volume: **75** Issue: **8** Article Number: **085307** DOI: **10.1103/PhysRevB.75.085307** Published: **FEB 2007**
Times Cited: **24** (from Web of Science)



[[View abstract](#)]

24. Title: **Tunable few-electron quantum dots in InAs nanowires**
Author(s): Shorubalko, I.; Pfund, A.; Leturcq, R.; et al.
Conference: **International Conference on Nanoscience and Technology**
Location: **Basel, SWITZERLAND** Date: **JUL 30-AUG 04, 2006**
Source: NANOTECHNOLOGY Volume: **18** Issue: **4** Article Number: **044014** DOI: **10.1088/0957-4484/18/4/044014** Published: **JAN 31 2007**
Times Cited: **11** (from Web of Science)



[[View abstract](#)]

25. Title: **Spin-orbit mediated control of spin qubits**
Author(s): Flindt, Christian; Sorensen, Anders S.; Flensberg, Karsten
Source: PHYSICAL REVIEW LETTERS Volume: **97** Issue: **24** Article Number: **240501** DOI: **10.1103/PhysRevLett.97.240501** Published: **DEC 15 2006**
Times Cited: **43** (from Web of Science)



[[View abstract](#)]

26. Title: **Scheme for direct measurement of a general two-qubit Hamiltonian**
Author(s): Devitt, SJ; Cole, JH; Hollenberg, LCL
Source: PHYSICAL REVIEW A Volume: **73** Issue: **5** Article Number: **052317** DOI: **10.1103/PhysRevA.73.052317** Published: **MAY 2006**
Times Cited: **18** (from Web of Science)



[[View abstract](#)]

27. Title: [Design and control of spin gates in two quantum-dot arrays](#)
Author(s): Usaj, G; Balseiro, CA
Source: APPLIED PHYSICS LETTERS Volume: **88** Issue: **10** Article Number: **103103** DOI: **10.1063/1.2181275** Published: **MAR 6 2006**
Times Cited: **2** (from Web of Science)



[[View abstract](#)]

28. Title: [Spin-based quantum dot quantum computing](#)
Author(s): Hu, X
Book Editor(s): Fabian, J; Fabian, J; Hohenester, U
Conference: **42th Schladming Winter School on Quantum Coherence in Matter - From Quarks to Solids** Location: **Schladming, AUSTRIA** Date: **FEB 28-MAR 06, 2004**
Sponsor(s): **Univ Graz, Div Theoret Phys**
Source: QUANTUM COHERENCE: FROM QUARKS TO SOLIDS Book Series: **Lecture Notes in Physics** Volume: **689** Pages: **83-114**
Published: **2006**
Times Cited: **4** (from Web of Science)



[[View abstract](#)]

29. Title: [Asymmetric exchange between electron spins in coupled semiconductor quantum dots](#)
Author(s): Badescu, SC; Lyanda-Geller, YB; Reinecke, TL
Source: PHYSICAL REVIEW B Volume: **72** Issue: **16** Article Number: **161304** DOI: **10.1103/PhysRevB.72.161304** Published: **OCT 2005**
Times Cited: **13** (from Web of Science)



[[View abstract](#)]

30. Title: [Spin-orbit effects in single-electron states in coupled quantum dots](#)
Author(s): Stano, P; Fabian, J
Source: PHYSICAL REVIEW B Volume: **72** Issue: **15** Article Number: **155410** DOI: **10.1103/PhysRevB.72.155410** Published: **OCT 2005**
Times Cited: **29** (from Web of Science)



[[View abstract](#)]

31. Title: [Holonomic quantum computation in decoherence-free subspaces](#)
Author(s): Wu, LA; Zanardi, P; Lidar, DA
Source: PHYSICAL REVIEW LETTERS Volume: **95** Issue: **13** Article Number: **130501** DOI: **10.1103/PhysRevLett.95.130501** Published: **SEP 23 2005**
Times Cited: **33** (from Web of Science)



[[View abstract](#)]

32. Title: [Spin-orbit coupling and anisotropy of spin splitting in quantum dots](#)
Author(s): Konemann, J; Haug, RJ; Maude, DK; et al.
Source: PHYSICAL REVIEW LETTERS Volume: **94** Issue: **22** Article Number: **226404** DOI: **10.1103/PhysRevLett.94.226404** Published: **JUN 10 2005**
Times Cited: **43** (from Web of Science)



[[View abstract](#)]

33. Title: [Recipes for spin-based quantum computing](#)
Author(s): Cerletti, V; Coish, WA; Gywat, O; et al.
Source: NANOTECHNOLOGY Volume: **16** Issue: **4** Pages: **R27-R49**
DOI: **10.1088/0957-4484/16/4/R01** Published: **APR 2005**
Times Cited: **125** (from Web of Science)



[[View abstract](#)]

34. Title: [Double occupancy errors in quantum computing operations: Corrections to adiabaticity](#)
Author(s): Requist, R; Schliemann, J; Abanov, AG; et al.

Source: PHYSICAL REVIEW B Volume: 71 Issue: 11 Article Number: 115315 DOI: 10.1103/PhysRevB.71.115315 Published: MAR 2005 Times Cited: 6 (from Web of Science)

 [ View abstract]

- 35. Title: **Universal quantum computation through control of spin-orbit coupling**
 Author(s): Stepanenko, D; Bonesteel, NE
 Source: PHYSICAL REVIEW LETTERS Volume: 93 Issue: 14 Article Number: 140501 DOI: 10.1103/PhysRevLett.93.140501 Published: OCT 1 2004
 Times Cited: 44 (from Web of Science)

 [ View abstract]

- 36. Title: **Symmetry of anisotropic exchange interactions in semiconductor nanostructures**
 Author(s): Kavokin, KV
 Source: PHYSICAL REVIEW B Volume: 69 Issue: 7 Article Number: 075302 DOI: 10.1103/PhysRevB.69.075302 Published: FEB 2004
 Times Cited: 33 (from Web of Science)

 [ View abstract]

- 37. Title: **Relaxation of candidate electron spin qubits**
 Author(s): Lyon, SA
 Book Editor(s): Smulko, JM; Blanter, Y; Dykman, M; et al.
 Conference: **Conference on Noise and Information in Nanoelectronics, Sensors and Standards II** Location: **Maspalomas, SPAIN** Date: **MAY 26-28, 2004**
 Sponsor(s): **SPIE**
 Source: NOISE AND INFORMATION IN NANO-ELECTRONICS, SENSORS, AND STANDARDS II Book Series: **PROCEEDINGS OF THE SOCIETY OF PHOTO-OPTICAL INSTRUMENTATION ENGINEERS (SPIE)** Volume: 5472 Pages: 97-106 DOI: 10.1117/12.550634 Published: 2004
 Times Cited: 1 (from Web of Science)

 [ View abstract]

- 38. Title: **Anisotropic transport in a two-dimensional electron gas in the presence of spin-orbit coupling**
 Author(s): Schliemann, J; Loss, D
 Source: PHYSICAL REVIEW B Volume: 68 Issue: 16 Article Number: 165311 DOI: 10.1103/PhysRevB.68.165311 Published: OCT 15 2003
 Times Cited: 97 (from Web of Science)

 [ View abstract]

Results: 38  Page 1 of 1  Sort by: 

Output Records








Step 1:

- Selected Records on page
- All records on page
- Records to

Step 2:

- Authors, Title, Source plus Abstract
- Full Record plus Cited References

Step 3: [\[How do I export to bibliographic management software?\]](#)

  Save to:  

 Save to other Reference Software   (12)

38 records matched your query of the 53,033,624 in the data limits you selected.

View in: | [简体中文](#) | [English](#) | [日本語](#)

Web of Science[®] now with books

[<< Return to All Databases](#)

[<< Back to previous page](#)

Citing Articles

Title: **Universal quantum computation through control of spin-orbit coupling**
 Author(s): **Stepanenko, D ; Bonesteel, NE**
 Source: **PHYSICAL REVIEW LETTERS** Volume: **93** Issue: **14** Article Number: **140501** DOI: **10.1103/PhysRevLett.93.140501** Published: **OCT 1 2004**

This article has been cited by articles indexed in the databases listed below. [\[more information\]](#)

44 in All Databases

44 in Web of Science

0 in BIOSIS Citation Index

0 in Chinese Science Citation Database

Results: **44**

Page of 1

Sort by:

Hide Refine

Refine Results

Search within results for

Web of Science Categories

- PHYSICS CONDENSED MATTER (24)
 - PHYSICS MULTIDISCIPLINARY (10)
 - PHYSICS APPLIED (7)
 - MATERIALS SCIENCE MULTIDISCIPLINARY (5)
 - NANOSCIENCE NANOTECHNOLOGY (5)
- [more options / values...](#)

Document Types

- ARTICLE (43)
 - PROCEEDINGS PAPER (1)
 - REVIEW (1)
- [more options / values...](#)






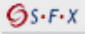





- Research Areas
- Authors
- Group Authors
- Editors
- Source Titles
- Book Series Titles
- Conference Titles
- Publication Years
- Organizations-Enhanced
- Funding Agencies
- Languages
- Countries/Territories








(12) |
 |
 |
 |
 |
 |

1. Title: **Resonant harmonic generation and collective spin rotations in electrically driven quantum dots**
 Author(s): Nowak, M. P.; Szafran, B.; Peeters, F. M.
 Source: PHYSICAL REVIEW B Volume: **86** Issue: **12** Article Number: **125428** DOI: **10.1103/PhysRevB.86.125428** Published: **SEP 18 2012**
 Times Cited: **0** (from Web of Science)
 []
2. Title: **Spin manipulation and relaxation in spin-orbit qubits**
 Author(s): Borhani, Massoud; Hu, Xuedong
 Source: PHYSICAL REVIEW B Volume: **85** Issue: **12** Article Number: **125132** DOI: **10.1103/PhysRevB.85.125132** Published: **MAR 28 2012**
 Times Cited: **1** (from Web of Science)
 []
3. Title: **Singlet-triplet splitting in double quantum dots due to spin-orbit and hyperfine interactions**
 Author(s): Stepanenko, Dimitrije; Rudner, Mark; Halperin, Bertrand I.; et al.
 Source: PHYSICAL REVIEW B Volume: **85** Issue: **7** Article Number: **075416** DOI: **10.1103/PhysRevB.85.075416** Published: **FEB 16 2012**
 Times Cited: **2** (from Web of Science)
 []
4. Title: **Configuration interaction calculations of the controlled phase gate in double quantum dot qubits**
 Author(s): Nielsen, Erik; Muller, Richard P.; Carroll, Malcolm S.
 Source: PHYSICAL REVIEW B Volume: **85** Issue: **3** Article Number: **035319** DOI: **10.1103/PhysRevB.85.035319** Published: **JAN 25 2012**
 Times Cited: **0** (from Web of Science)
 []

For advanced refine options, use

Analyze Results

5. Title: **Single Electron's Dynamical Behavior in a Two Dimensional Anisotropic Quantum Dot with Account of Rashba Effect**
Author(s): Sisakhti, Masoumeh; Golshan, Mohammad Mehdi; Sanaee, Maryam
Source: JOURNAL OF COMPUTATIONAL AND THEORETICAL NANOSCIENCE Volume: **8** Issue: **10** Pages: **2166-2171** DOI: **10.1166/jctn.2011.1939** Published: **OCT 2011**
Times Cited: **0** (from Web of Science)
-  [ View abstract]
6. Title: **Entanglement of electronic subbands and coherent superposition of spin states in a Rashba nanoloop**
Author(s): Safaiee, R.; Golshan, M. M.
Source: EUROPEAN PHYSICAL JOURNAL B Volume: **83** Issue: **4** Pages: **457-463** DOI: **10.1140/epjb/e2011-20142-x** Published: **OCT 2011**
Times Cited: **0** (from Web of Science)
-  [ View abstract]
7. Title: **Spintronic properties of graphene films grown on Ni(111) substrate**
Author(s): Gong, S. J.; Li, Z. Y.; Yang, Z. Q.; et al.
Source: JOURNAL OF APPLIED PHYSICS Volume: **110** Issue: **4** Article Number: **043704** DOI: **10.1063/1.3622618** Published: **AUG 15 2011**
Times Cited: **3** (from Web of Science)
-  [ View abstract]
8. Title: **Acoustically Induced Spin-Orbit Interactions Revealed by Two-Dimensional Imaging of Spin Transport in GaAs**
Author(s): Sanada, H.; Sogawa, T.; Gotoh, H.; et al.
Source: PHYSICAL REVIEW LETTERS Volume: **106** Issue: **21** Article Number: **216602** DOI: **10.1103/PhysRevLett.106.216602** Published: **MAY 26 2011**
Times Cited: **4** (from Web of Science)
-  [ View abstract]
9. Title: **Controllable Anisotropic Exchange Coupling between Spin Qubits in Quantum Dots**
Author(s): Shim, Yun-Pil; Oh, Sangchul; Hu, Xuedong; et al.
Source: PHYSICAL REVIEW LETTERS Volume: **106** Issue: **18** Article Number: **180503** DOI: **10.1103/PhysRevLett.106.180503** Published: **MAY 6 2011**
Times Cited: **2** (from Web of Science)
-  [ View abstract]
10. Title: **Manipulation of two spin qubits in a double quantum dot using an electric field**
Author(s): Shitade, Atsuo; Ezawa, Motohiko; Nagaosa, Naoto
Source: PHYSICAL REVIEW B Volume: **82** Issue: **19** Article Number: **195305** DOI: **10.1103/PhysRevB.82.195305** Published: **NOV 4 2010**
Times Cited: **2** (from Web of Science)
-  [ View abstract]
11. Title: **Suppression of Kondo-assisted cotunneling in a spin-1 quantum dot with spin-orbit interaction**
Author(s): Lucignano, Procolo; Fabrizio, Michele; Tagliacozzo, Arturo
Source: PHYSICAL REVIEW B Volume: **82** Issue: **16** Article Number: **161306** DOI: **10.1103/PhysRevB.82.161306** Published: **OCT 18 2010**
Times Cited: **3** (from Web of Science)
-  [ View abstract]

12. Title: **Time-dependent configuration-interaction simulations of spin swap in spin-orbit-coupled double quantum dots**
Author(s): Nowak, M. P.; Szafran, B.
Source: PHYSICAL REVIEW B Volume: **82** Issue: **16** Article Number: **165316** DOI: **10.1103/PhysRevB.82.165316** Published: **OCT 12 2010**
Times Cited: **6** (from Web of Science)
-  [[View abstract](#)]
13. Title: **Exchange cotunneling through quantum dots with spin-orbit coupling**
Author(s): Paaske, J.; Andersen, A.; Flensberg, K.
Source: PHYSICAL REVIEW B Volume: **82** Issue: **8** Article Number: **081309** DOI: **10.1103/PhysRevB.82.081309** Published: **AUG 31 2010**
Times Cited: **10** (from Web of Science)
-  [[View abstract](#)]
14. Title: **Spin-orbit coupling and anisotropic exchange in two-electron double quantum dots**
Author(s): Baruffa, Fabio; Stano, Peter; Fabian, Jaroslav
Source: PHYSICAL REVIEW B Volume: **82** Issue: **4** Article Number: **045311** DOI: **10.1103/PhysRevB.82.045311** Published: **JUL 21 2010**
Times Cited: **4** (from Web of Science)
-  [[View abstract](#)]
15. Title: **Coupling of bonding and antibonding electron orbitals in double quantum dots by spin-orbit interaction**
Author(s): Nowak, M. P.; Szafran, B.
Source: PHYSICAL REVIEW B Volume: **81** Issue: **23** Article Number: **235311** DOI: **10.1103/PhysRevB.81.235311** Published: **JUN 9 2010**
Times Cited: **3** (from Web of Science)
-  [[View abstract](#)]
16. Title: **Theory of Anisotropic Exchange in Laterally Coupled Quantum Dots**
Author(s): Baruffa, Fabio; Stano, Peter; Fabian, Jaroslav
Source: PHYSICAL REVIEW LETTERS Volume: **104** Issue: **12** Article Number: **126401** DOI: **10.1103/PhysRevLett.104.126401** Published: **MAR 26 2010**
Times Cited: **12** (from Web of Science)
-  [[View abstract](#)]
17. Title: **Quantum kinetic equation for spin relaxation and spin Hall effect in GaAs**
Author(s): Lee, H. C.; Mou, C. -Y.
Source: EUROPEAN PHYSICAL JOURNAL B Volume: **73** Issue: **2** Pages: **229-242** DOI: **10.1140/epjb/e2009-00437-3** Published: **JAN 2010**
Times Cited: **1** (from Web of Science)
-  [[View abstract](#)]
18. Title: **Biexciton in magnetic fields**
Author(s): Varga, Kalman
Source: FEW-BODY SYSTEMS Volume: **47** Issue: **1-2** Pages: **65-71** DOI: **10.1007/s00601-009-0062-3** Published: **JAN 2010**
Times Cited: **1** (from Web of Science)
-  [[View abstract](#)]
19. Title: **Quantum computing with electron spins in quantum dots**
Author(s): Zak, Robert Andrzej; Roethlisberger, Beat; Chesi, Stefano; et al.
Source: RIVISTA DEL NUOVO CIMENTO Volume: **33** Issue: **7** Pages: **345-399** DOI: **10.1393/ncr/i2010-10056-y** Published: **2010**
Times Cited: **7** (from Web of Science)

[View abstract](#)

20. Title: **Temporal behavior of entanglement between electronic spin and subband states in a Rashba nanoloop**
 Author(s): Safaiee, R.; Golshan, M. M.; Foroozani, N.
 Source: JOURNAL OF STATISTICAL MECHANICS-THEORY AND EXPERIMENT Article Number: **P11014** DOI: **10.1088/1742-5468/2009/11/P11014** Published: **NOV 2009**
 Times Cited: **4** (from Web of Science)

[View abstract](#)

21. Title: **Spin Precession in a Quasi-1D Rashba Quantum Loop**
 Author(s): Golshan, M. M.; Safaiee, R.; Foroozani, N.
 Source: JOURNAL OF COMPUTATIONAL AND THEORETICAL NANOSCIENCE Volume: **6** Issue: **10** Pages: **2235-2241** DOI: **10.1166/jctn.2009.1279** Published: **OCT 2009**
 Times Cited: **2** (from Web of Science)

[View abstract](#)

22. Title: **Two-impurity Kondo model with spin-orbit interactions**
 Author(s): Moss, David F.; Johannesson, Henrik
 Source: PHYSICAL REVIEW B Volume: **80** Issue: **15** Article Number: **155302** DOI: **10.1103/PhysRevB.80.155302** Published: **OCT 2009**
 Times Cited: **6** (from Web of Science)

[View abstract](#)

23. Title: **Dynamical Wobblations of Electronic Spin States in a Rashba Isotropic 2D Quantum Dot**
 Author(s): Safaiee, R.; Golshan, M. M.
 Source: JOURNAL OF COMPUTATIONAL AND THEORETICAL NANOSCIENCE Volume: **6** Issue: **5** Pages: **1045-1053** DOI: **10.1166/jctn.2009.1142** Published: **MAY 2009**
 Times Cited: **3** (from Web of Science)

[View abstract](#)

24. Title: **The Electronic Spin-Subbands States Entanglement in a Rashba 2D Isotropic Quantum Dot**
 Author(s): Safaiee, R.; Foroozani, N.; Golshan, M. M.
 Source: JOURNAL OF COMPUTATIONAL AND THEORETICAL NANOSCIENCE Volume: **6** Issue: **3** Pages: **686-691** DOI: **10.1166/jctn.2009.1095** Published: **MAR 2009**
 Times Cited: **2** (from Web of Science)

[View abstract](#)

25. Title: **Effects of quantum dot characteristics on electronic spin-subband state entanglement**
 Author(s): Safaiee, R.; Foroozani, N.; Golshan, M. M.
 Source: JOURNAL OF STATISTICAL MECHANICS-THEORY AND EXPERIMENT Article Number: **P02038** DOI: **10.1088/1742-5468/2009/02/P02038** Published: **FEB 2009**
 Times Cited: **2** (from Web of Science)

[View abstract](#)

26. Title: **Spin Rotations Induced by an Electron Running in Closed Trajectories in Gated Semiconductor Nanodevices**
 Author(s): Bednarek, S.; Szafran, B.
 Source: PHYSICAL REVIEW LETTERS Volume: **101** Issue: **21** Article Number: **216805** DOI: **10.1103/PhysRevLett.101.216805** Published: **NOV 21 2008**
 Times Cited: **13** (from Web of Science)

[View abstract](#)

27. Title: **Quantum computing with molecular magnets**

- Author(s): Stepanenko, Dimitrije; Trif, Mircea; Loss, Daniel
Source: INORGANICA CHIMICA ACTA Volume: **361** Issue: **14-15** Pages: **3740-3745** DOI: **10.1016/j.ica.2008.02.066** Published: **OCT 1 2008**
Times Cited: **12** (from Web of Science)

 [ [View abstract](#)]

28. Title: **Theory of spin qubits in nanostructures**
Author(s): Trauzettel, Bjoern; Borhani, Massoud; Trif, Mircea; et al.
Source: JOURNAL OF THE PHYSICAL SOCIETY OF JAPAN Volume: **77**
Issue: **3** Article Number: **031012** DOI: **10.1143/JPSJ.77.031012**
Published: **MAR 2008**
Times Cited: **3** (from Web of Science)

 [Full Text](#) [ [View abstract](#)]

29. Title: **Nuclear-induced time evolution of entanglement of two-electron spins in anisotropically coupled quantum dot**
Author(s): Sadiek, Gehad; Huang, Zhen; Aldossary, Omar; et al.
Source: MOLECULAR PHYSICS Volume: **106** Issue: **14** Pages: **1777-1786** DOI: **10.1080/00268970802290313** Published: **2008**
Times Cited: **2** (from Web of Science)

 [ [View abstract](#)]

30. Title: **Effect of the Dzyaloshinski-Moriya term in the quantum (SWAP)(alpha) gate produced with exchange coupling**
Author(s): Guerrero, Roberto J.; Rojas, F.
Source: PHYSICAL REVIEW A Volume: **77** Issue: **1** Article Number: **012331** DOI: **10.1103/PhysRevA.77.012331** Published: **JAN 2008**
Times Cited: **3** (from Web of Science)

 [ [View abstract](#)]

31. Title: **Ideal switching effect in periodic spin-orbit coupling structures**
Author(s): Gong, S. J.; Yang, Z. Q.
Source: JOURNAL OF PHYSICS-CONDENSED MATTER Volume: **19**
Issue: **44** Article Number: **446209** DOI: **10.1088/0953-8984/19/44/446209** Published: **NOV 7 2007**
Times Cited: **4** (from Web of Science)

 [ [View abstract](#)]

32. Title: **Quantum computation in semiconductor quantum dots of electron-spin asymmetric anisotropic exchange**
Author(s): Hao, Xiang; Zhu, Shiqun
Source: PHYSICAL REVIEW A Volume: **76** Issue: **4** Article Number: **044306** DOI: **10.1103/PhysRevA.76.044306** Published: **OCT 2007**
Times Cited: **7** (from Web of Science)

 [ [View abstract](#)]

33. Title: **Flying spin-qubit gates implemented through Dresselhaus and Rashba spin-orbit couplings**
Author(s): Gong, S. J.; Yang, Z. Q.
Source: PHYSICS LETTERS A Volume: **367** Issue: **4-5** Pages: **369-372**
DOI: **10.1016/j.physleta.2007.03.022** Published: **JUL 30 2007**
Times Cited: **2** (from Web of Science)

 [ [View abstract](#)]

34. Title: **Exchange-controlled single-electron-spin rotations in quantum dots**
Author(s): Coish, W. A.; Loss, Daniel
Source: PHYSICAL REVIEW B Volume: **75** Issue: **16** Article Number: **161302** DOI: **10.1103/PhysRevB.75.161302** Published: **APR 2007**
Times Cited: **19** (from Web of Science)

 [ [View abstract](#)]

35. Title: **Universal quantum computing with correlated spin-charge states**
Author(s): Kyriakidis, Jordan; Burkard, Guido
Source: PHYSICAL REVIEW B Volume: **75** Issue: **11** Article Number: **115324** DOI: **10.1103/PhysRevB.75.115324** Published: **MAR 2007**
Times Cited: **6** (from Web of Science)
-  [ [View abstract](#)]
36. Title: **Spin-spin coupling in electrostatically coupled quantum dots**
Author(s): Trif, Mircea; Golovach, Vitaly N.; Loss, Daniel
Source: PHYSICAL REVIEW B Volume: **75** Issue: **8** Article Number: **085307** DOI: **10.1103/PhysRevB.75.085307** Published: **FEB 2007**
Times Cited: **24** (from Web of Science)
-  [ [View abstract](#)]
37. Title: **Tunable few-electron quantum dots in InAs nanowires**
Author(s): Shorubalko, I.; Pfund, A.; Leturcq, R.; et al.
Conference: **International Conference on Nanoscience and Technology**
Location: **Basel, SWITZERLAND** Date: **JUL 30-AUG 04, 2006**
Source: NANOTECHNOLOGY Volume: **18** Issue: **4** Article Number: **044014** DOI: **10.1088/0957-4484/18/4/044014** Published: **JAN 31 2007**
Times Cited: **11** (from Web of Science)
-  [ [View abstract](#)]
38. Title: **Spin-orbit mediated control of spin qubits**
Author(s): Flindt, Christian; Sorensen, Anders S.; Flensberg, Karsten
Source: PHYSICAL REVIEW LETTERS Volume: **97** Issue: **24** Article Number: **240501** DOI: **10.1103/PhysRevLett.97.240501** Published: **DEC 15 2006**
Times Cited: **43** (from Web of Science)
-  [ [View abstract](#)]
39. Title: **RKKY interaction between quantum dot spins tuned by the quantum dot level**
Author(s): Yang, Mou; Li, Shu-Shen
Source: PHYSICAL REVIEW B Volume: **74** Issue: **7** Article Number: **073402** DOI: **10.1103/PhysRevB.74.073402** Published: **AUG 2006**
Times Cited: **3** (from Web of Science)
-  [ [View abstract](#)]
40. Title: **Electric-field inversion asymmetry: Rashba and Stark effects for holes in resonant tunneling devices**
Author(s): de Carvalho, H. B.; Brasil, M. J. S. P.; Lopez-Richard, V.; et al.
Source: PHYSICAL REVIEW B Volume: **74** Issue: **4** Article Number: **041305** DOI: **10.1103/PhysRevB.74.041305** Published: **JUL 2006**
Times Cited: **7** (from Web of Science)
-  [ [View abstract](#)]
41. Title: **Detection and measurement of the Dzyaloshinskii-Moriya interaction in double quantum dot systems**
Author(s): Chutia, Sucismita; Friesen, Mark; Joynt, Robert
Source: PHYSICAL REVIEW B Volume: **73** Issue: **24** Article Number: **241304** DOI: **10.1103/PhysRevB.73.241304** Published: **JUN 2006**
Times Cited: **16** (from Web of Science)
-  [ [View abstract](#)]
42. Title: **Design and control of spin gates in two quantum-dot arrays**
Author(s): Usaj, G; Balseiro, CA
Source: APPLIED PHYSICS LETTERS Volume: **88** Issue: **10** Article Number: **103103** DOI: **10.1063/1.2181275** Published: **MAR 6 2006**
Times Cited: **2** (from Web of Science)



- 43. Title: **Hologmic quantum computation in decoherence-free subspaces**
 Author(s): Wu, LA; Zanardi, P; Lidar, DA
 Source: PHYSICAL REVIEW LETTERS Volume: **95** Issue: **13** Article Number: **130501** DOI: **10.1103/PhysRevLett.95.130501** Published: **SEP 23 2005**
 Times Cited: **33** (from Web of Science)



- 44. Title: **Universal leakage elimination**
 Author(s): Byrd, MS; Lidar, DA; Wu, LA; et al.
 Source: PHYSICAL REVIEW A Volume: **71** Issue: **5** Article Number: **052301** DOI: **10.1103/PhysRevA.71.052301** Published: **MAY 2005**
 Times Cited: **23** (from Web of Science)



Results: **44** Show 50 per page Page of 1 Go Sort by: Publication Date – newest to oldest

Output Records

Step 1:

- Selected Records on page
- All records on page
- Records to

Step 2:

- Authors, Title, Source plus Abstract
- Full Record plus Cited References

Step 3: [\[How do I export to bibliographic management software?\]](#)

Save to: ENDNOTE® WEB ENDNOTE®
ResearcherID
Save to other Reference Software Save
 (12)

44 records matched your query of the 53,033,624 in the data limits you selected.

View in: [简体中文](#) | [English](#) | [日本語](#)

Web of Science[®] now with books

[<< Return to All Databases](#)

[<< Back to previous page](#)

Citing Articles Title: **Enhancement of electron spin coherence by optical preparation of nuclear spins**
 Author(s): **Stepanenko, D ; Burkard, G ; Giedke, G ; et al.**
 Source: **PHYSICAL REVIEW LETTERS** Volume: **96** Issue: **13** Article Number: **136401** DOI: **10.1103/PhysRevLett.96.136401** Published: **APR 7 2006**

This article has been cited by articles indexed in the databases listed below. [\[more information\]](#)

83 in *All Databases*

82 in *Web of Science*

0 in *BIOSIS Citation Index*

1 in *Chinese Science Citation Database*

Results: **82**

Page of 2

Sort by:

Hide Refine

Refine Results

Search within results for

Web of Science Categories

- PHYSICS CONDENSED MATTER (40)
 - PHYSICS MULTIDISCIPLINARY (26)
 - MULTIDISCIPLINARY SCIENCES (6)
 - OPTICS (6)
 - NANOSCIENCE NANOTECHNOLOGY (5)
- [more options / values...](#)

Document Types

- ARTICLE (72)
 - REVIEW (7)
 - PROCEEDINGS PAPER (5)
 - BOOK CHAPTER (3)
 - EDITORIAL MATERIAL (1)
- [more options / values...](#)

Research Areas

- Authors**
- Group Authors**
- Editors**
- Source Titles**
- Book Series Titles**
- Conference Titles**
- Publication Years**
- Organizations-Enhanced**
- Funding Agencies**
- Languages**

(12) |
 |
 |
 |
 |
 |

- 1. Title: **Manipulation of qubits in nonorthogonal collective storage modes**
 Author(s): Refsgaard, Jonas; Molmer, Klaus
 Source: PHYSICAL REVIEW A Volume: **86** Issue: **2** Article Number: **022302** DOI: **10.1103/PhysRevA.86.022302** Published: **AUG 1 2012**
 Times Cited: **0** (from Web of Science)
 []
- 2. Title: **Spin decoherence in graphene quantum dots due to hyperfine interaction**
 Author(s): Fuchs, Moritz; Rychkov, Valentin; Trauzettel, Bjoern
 Source: PHYSICAL REVIEW B Volume: **86** Issue: **8** Article Number: **085301** DOI: **10.1103/PhysRevB.86.085301** Published: **AUG 1 2012**
 Times Cited: **0** (from Web of Science)
 []
- 3. Title: **Effect of strain on hyperfine-induced hole-spin decoherence in quantum dots**
 Author(s): Maier, Franziska; Loss, Daniel
 Source: PHYSICAL REVIEW B Volume: **85** Issue: **19** Article Number: **195323** DOI: **10.1103/PhysRevB.85.195323** Published: **MAY 24 2012**
 Times Cited: **0** (from Web of Science)
 []
- 4. Title: **Persistent Narrowing of Nuclear-Spin Fluctuations in InAs Quantum Dots Using Laser Excitation**
 Author(s): Sun, Bo; Chow, Colin Ming Earn; Steel, Duncan G.; et al.
 Source: PHYSICAL REVIEW LETTERS Volume: **108** Issue: **18** Article Number: **187401** DOI: **10.1103/PhysRevLett.108.187401** Published: **MAY 1 2012**
 Times Cited: **0** (from Web of Science)

► Countries/Territories

For advanced refine options, use

[Analyze Results](#)



[[View abstract](#)]

5. Title: **Entanglement Dynamics of Electron Spins in Quantum Dots Under a Nonuniform Magnetic Field**
 Author(s): Zhou, Feng-Xue; Qi, Yi-Hong; Niu, Yue-Ping; et al.
 Source: JOURNAL OF THE KOREAN PHYSICAL SOCIETY Volume: **60**
 Issue: **8** Pages: **1238-1244** DOI: **10.3938/jkps.60.1238** Published: **APR 2012**
 Times Cited: **0** (from Web of Science)



[[View abstract](#)]

6. Title: **Dipolar broadening of nuclear spin resonance under dynamical pumping**
 Author(s): Tsypliyatsev, O.; Whittaker, D. M.
 Source: PHYSICAL REVIEW B Volume: **85** Issue: **12** Article Number: **125123** DOI: **10.1103/PhysRevB.85.125123** Published: **MAR 22 2012**
 Times Cited: **0** (from Web of Science)



[[View abstract](#)]

7. Title: **Persistent optical nuclear spin narrowing in a singly charged InAs quantum dot**
 Author(s): Sun, Bo; Yao, Wang; Xu, Xiaodong; et al.
 Source: JOURNAL OF THE OPTICAL SOCIETY OF AMERICA B-OPTICAL PHYSICS Volume: **29** Issue: **2** Pages: **A119-A126** Published: **FEB 2012**
 Times Cited: **0** (from Web of Science)



[[View abstract](#)]

8. Title: **Role of hyperfine interaction for cavity-mediated coupling between spin qubits**
 Author(s): Hildmann, Julia; Burkard, Guido
 Source: PHYSICAL REVIEW B Volume: **84** Issue: **20** Article Number: **205127** DOI: **10.1103/PhysRevB.84.205127** Published: **NOV 17 2011**
 Times Cited: **0** (from Web of Science)



[[View abstract](#)]

9. Title: **Generating Entanglement and Squeezed States of Nuclear Spins in Quantum Dots**
 Author(s): Rudner, M. S.; Vandersypen, L. M. K.; Vuletic, V.; et al.
 Source: PHYSICAL REVIEW LETTERS Volume: **107** Issue: **20** Article Number: **206806** DOI: **10.1103/PhysRevLett.107.206806** Published: **NOV 8 2011**
 Times Cited: **5** (from Web of Science)



[[View abstract](#)]

10. Title: **Generation of non-equilibrium thermal quantum discord and entanglement in a three-spin XX chain by multi-spin interaction and an external magnetic field**
 Author(s): Zhang, Xiu-xing; Li, Fu-li
 Source: PHYSICS LETTERS A Volume: **375** Issue: **46** Pages: **4130-4137**
 DOI: **10.1016/j.physleta.2011.10.004** Published: **NOV 7 2011**
 Times Cited: **3** (from Web of Science)










[[View abstract](#)]

11. Title: **Controlling transfer of quantum correlations among bi-partitions of a composite quantum system by combining different noisy environments**
 Author(s): Xiu-Xing, Zhang; Fu-Li, Li
 Source: CHINESE PHYSICS B Volume: **20** Issue: **11** Article Number: **110302** DOI: **10.1088/1674-1056/20/11/110302** Published: **NOV 2011**
 Times Cited: **0** (from Web of Science)



[[View abstract](#)]

12. Title: **Laser cooling and real-time measurement of the nuclear spin environment of a solid-state qubit**
Author(s): Togan, E.; Chu, Y.; Imamoglu, A.; et al.
Source: NATURE Volume: **478** Issue: **7370** Pages: **497-501** DOI: **10.1038/nature10528** Published: **OCT 27 2011**
Times Cited: **6** (from Web of Science)
-  [[View abstract](#)]
13. Title: **Controlling the nuclear polarization in quantum dots using optical pulse shape with a modest bandwidth**
Author(s): Carter, S. G.; Economou, Sophia E.; Shabaev, A.; et al.
Source: PHYSICAL REVIEW B Volume: **83** Issue: **11** Article Number: **115325** DOI: **10.1103/PhysRevB.83.115325** Published: **MAR 23 2011**
Times Cited: **3** (from Web of Science)
-  [[View abstract](#)]
14. Title: **Spectrum of an Electron Spin Coupled to an Unpolarized Bath of Nuclear Spins**
Author(s): Tsypliyatsev, Oleksandr; Loss, Daniel
Source: PHYSICAL REVIEW LETTERS Volume: **106** Issue: **10** Article Number: **106803** DOI: **10.1103/PhysRevLett.106.106803** Published: **MAR 8 2011**
Times Cited: **4** (from Web of Science)
-  [[View abstract](#)]
15. Title: **Hybridization and Spin Decoherence in Heavy-Hole Quantum Dots**
Author(s): Fischer, Jan; Loss, Daniel
Source: PHYSICAL REVIEW LETTERS Volume: **105** Issue: **26** Article Number: **266603** DOI: **10.1103/PhysRevLett.105.266603** Published: **DEC 22 2010**
Times Cited: **13** (from Web of Science)
-  [[View abstract](#)]
16. Title: **Nuclear Spin Cooling Using Overhauser-Field Selective Coherent Population Trapping**
Author(s): Issler, M.; Kessler, E. M.; Giedke, G.; et al.
Source: PHYSICAL REVIEW LETTERS Volume: **105** Issue: **26** Article Number: **267202** DOI: **10.1103/PhysRevLett.105.267202** Published: **DEC 21 2010**
Times Cited: **8** (from Web of Science)
-  [[View abstract](#)]
17. Title: **Feedback control of nuclear hyperfine fields in a double quantum dot**
Author(s): Yao, Wang; Luo, Yu
Source: EPL Volume: **92** Issue: **1** Article Number: **17008** DOI: **10.1209/0295-5075/92/17008** Published: **OCT 2010**
Times Cited: **0** (from Web of Science)
-  [[View abstract](#)]
18. Title: **Harnessing the GaAs quantum dot nuclear spin bath for quantum control**
Author(s): Ribeiro, Hugo; Petta, J. R.; Burkard, Guido
Source: PHYSICAL REVIEW B Volume: **82** Issue: **11** Article Number: **115445** DOI: **10.1103/PhysRevB.82.115445** Published: **SEP 24 2010**
Times Cited: **11** (from Web of Science)
-  [[View abstract](#)]
19. Title: **Spin dynamics in semiconductors**
Author(s): Wu, M. W.; Jiang, J. H.; Weng, M. Q.
Source: PHYSICS REPORTS-REVIEW SECTION OF PHYSICS LETTERS Volume: **493** Issue: **2-4** Pages: **61-236** DOI:

10.1016/j.physrep.2010.04.002 Published: **AUG 2010**
Times Cited: **94** (from Web of Science)



[View abstract]

20. Title: **Protection of center-spin coherence by a dynamically polarized nuclear spin core**
Author(s): Zhang, Wenxian; Hu, Jian-Liang; Zhuang, Jun; et al.
Source: PHYSICAL REVIEW B Volume: **82** Issue: **4** Article Number: **045314** DOI: **10.1103/PhysRevB.82.045314** Published: **JUL 23 2010**
Times Cited: **0** (from Web of Science)



[View abstract]

21. Title: **Dynamical cooling of nuclear spins in double quantum dots**
Author(s): Rudner, M. S.; Levitov, L. S.
Source: NANOTECHNOLOGY Volume: **21** Issue: **27** Article Number: **274016** DOI: **10.1088/0957-4484/21/27/274016** Published: **JUL 9 2010**
Times Cited: **2** (from Web of Science)



[View abstract]

22. Title: **Free-induction decay and envelope modulations in a narrowed nuclear spin bath**
Author(s): Coish, W. A.; Fischer, Jan; Loss, Daniel
Source: PHYSICAL REVIEW B Volume: **81** Issue: **16** Article Number: **165315** DOI: **10.1103/PhysRevB.81.165315** Published: **APR 15 2010**
Times Cited: **15** (from Web of Science)



[View abstract]

23. Title: **Non-equilibrium entanglement dynamics of a two-qubit Heisenberg XY system in the presence of an inhomogeneous magnetic field and spin-orbit interaction**
Author(s): Kheirandish, F.; Akhtarshenas, S. J.; Mohammadi, H.
Source: EUROPEAN PHYSICAL JOURNAL D Volume: **57** Issue: **1** Pages: **129-140** DOI: **10.1140/epjd/e2010-00003-2** Published: **MAR 2010**
Times Cited: **5** (from Web of Science)



[View abstract]

24. Title: **Quantum computing by optical control of electron spins**
Author(s): Liu, Ren-Bao; Yao, Wang; Sham, L. J.
Source: ADVANCES IN PHYSICS Volume: **59** Issue: **5** Pages: **703-802**
Article Number: **PII 925641728** DOI: **10.1080/00018732.2010.505452**
Published: **2010**
Times Cited: **14** (from Web of Science)



[View abstract]

25. Title: **Carrier spin dynamics in self-assembled quantum dots**
Author(s): Clarke, Edmund; Harbord, Edmund; Murray, Ray
Book Editor(s): Slavcheva, G; Roussignol, P
Source: OPTICAL GENERATION AND CONTROL OF QUANTUM COHERENCE IN SEMICONDUCTOR NANOSTRUCTURES Book Series: **Nanoscience and Technology** Pages: **39-61** DOI: **10.1007/978-3-642-12491-4_4** Published: **2010**
Times Cited: **0** (from Web of Science)



[View abstract]

26. Title: **Magnetic order in nuclear spin two-dimensional lattices due to electron-electron interactions**
Author(s): Simon, Pascal; Braunecker, Bernd; Loss, Daniel
Conference: **International Conference on Frontiers of Quantum and Mesoscopic Thermodynamics (FQMT '08)** Location: **Prague, CZECH REPUBLIC** Date: **JUL 28-AUG 02, 2008**
Source: PHYSICA E-LOW-DIMENSIONAL SYSTEMS & NANOSTRUCTURES Volume: **42** Issue: **3** Pages: **634-638** DOI: **10.1016/j.physe.2009.06.058** Published: **JAN 2010**

Times Cited: 0 (from Web of Science)

[View abstract](#)

27. Title: **Quantum computing with electron spins in quantum dots**
 Author(s): Zak, Robert Andrzej; Roethlisberger, Beat; Chesi, Stefano; et al.
 Source: RIVISTA DEL NUOVO CIMENTO Volume: **33** Issue: **7** Pages: **345-399** DOI: **10.1393/ncr/i2010-10056-y** Published: **2010**
 Times Cited: **7** (from Web of Science)

[View abstract](#)

28. Title: **Measurement of the Knight field and local nuclear dipole-dipole field in an InGaAs/GaAs quantum dot ensemble**
 Author(s): Auer, T.; Oulton, R.; Bauschulte, A.; et al.
 Source: PHYSICAL REVIEW B Volume: **80** Issue: **20** Article Number: **205303** DOI: **10.1103/PhysRevB.80.205303** Published: **NOV 2009**
 Times Cited: **3** (from Web of Science)

[View abstract](#)

29. Title: **Locking electron spins into magnetic resonance by electron-nuclear feedback**
 Author(s): Vink, Ivo T.; Nowack, Katja C.; Koppens, Frank H. L.; et al.
 Source: NATURE PHYSICS Volume: **5** Issue: **10** Pages: **764-768** DOI: **10.1038/NPHYS1366** Published: **OCT 2009**
 Times Cited: **45** (from Web of Science)

[View abstract](#)

30. Title: **Nuclear spins in nanostructures**
 Author(s): Coish, W. A.; Baugh, J.
 Source: PHYSICA STATUS SOLIDI B-BASIC SOLID STATE PHYSICS Volume: **246** Issue: **10** Pages: **2203-2215** DOI: **10.1002/pssb.200945229** Published: **OCT 2009**
 Times Cited: **35** (from Web of Science)

[View abstract](#)

31. Title: **Optically controlled locking of the nuclear field via coherent dark-state spectroscopy**
 Author(s): Xu, Xiaodong; Yao, Wang; Sun, Bo; et al.
 Source: NATURE Volume: **459** Issue: **7250** Pages: **1105-1109** DOI: **10.1038/nature08120** Published: **JUN 25 2009**
 Times Cited: **69** (from Web of Science)

[View abstract](#)

32. Title: **Pure quantum dephasing of a solid-state electron spin qubit in a large nuclear spin bath coupled by long-range hyperfine-mediated interactions**
 Author(s): Cywinski, Lukasz; Witzel, Wayne M.; Das Sarma, S.
 Source: PHYSICAL REVIEW B Volume: **79** Issue: **24** Article Number: **245314** DOI: **10.1103/PhysRevB.79.245314** Published: **JUN 2009**
 Times Cited: **38** (from Web of Science)

[View abstract](#)

33. Title: **Nuclear State Preparation via Landau-Zener-Stuckelberg Transitions in Double Quantum Dots**
 Author(s): Ribeiro, Hugo; Burkard, Guido
 Source: PHYSICAL REVIEW LETTERS Volume: **102** Issue: **21** Article Number: **216802** DOI: **10.1103/PhysRevLett.102.216802** Published: **MAY 29 2009**
 Times Cited: **24** (from Web of Science)

[View abstract](#)

34. Title: **Directing Nuclear Spin Flips in InAs Quantum Dots Using Detuned Optical Pulse Trains**

Author(s): Carter, S. G.; Shabaev, A.; Economou, Sophia E.; et al.
Source: PHYSICAL REVIEW LETTERS Volume: **102** Issue: **16** Article
Number: **167403** DOI: **10.1103/PhysRevLett.102.167403** Published:
APR 24 2009
Times Cited: **20** (from Web of Science)



[[View abstract](#)]

35. Title: **Effect of nuclear polarization on spin dynamics in a double quantum dot**
Author(s): Sarkka, J.; Harju, A.
Source: PHYSICAL REVIEW B Volume: **79** Issue: **8** Article Number:
085313 DOI: **10.1103/PhysRevB.79.085313** Published: **FEB 2009**
Times Cited: **2** (from Web of Science)



[[View abstract](#)]

36. Title: **Nuclear spin dynamics and Zeno effect in quantum dots and defect centers**
Author(s): Klauser, D.; Coish, W. A.; Loss, Daniel
Source: PHYSICAL REVIEW B Volume: **78** Issue: **20** Article Number:
205301 DOI: **10.1103/PhysRevB.78.205301** Published: **NOV 2008**
Times Cited: **17** (from Web of Science)



[[View abstract](#)]

37. Title: **Spin decoherence of a heavy hole coupled to nuclear spins in a quantum dot**
Author(s): Fischer, Jan; Coish, W. A.; Bulaev, D. V.; et al.
Source: PHYSICAL REVIEW B Volume: **78** Issue: **15** Article Number:
155329 DOI: **10.1103/PhysRevB.78.155329** Published: **OCT 2008**
Times Cited: **55** (from Web of Science)



[[View abstract](#)]

38. Title: **Entanglement generation via a completely mixed nuclear spin bath**
Author(s): Christ, H.; Cirac, J. I.; Giedke, G.
Source: PHYSICAL REVIEW B Volume: **78** Issue: **12** Article Number:
125314 DOI: **10.1103/PhysRevB.78.125314** Published: **SEP 2008**
Times Cited: **8** (from Web of Science)



[[View abstract](#)]

39. Title: **Suppressing spin qubit dephasing by nuclear state preparation**
Author(s): Reilly, D. J.; Taylor, J. M.; Petta, J. R.; et al.
Source: SCIENCE Volume: **321** Issue: **5890** Pages: **817-821** DOI:
10.1126/science.1159221 Published: **AUG 8 2008**
Times Cited: **113** (from Web of Science)



[[View abstract](#)]

40. Title: **Numerical study of a quantum dot structure for entanglement generation**
Author(s): Giavaras, George
Source: SEMICONDUCTOR SCIENCE AND TECHNOLOGY Volume: **23**
Issue: **8** Article Number: **085010** DOI: **10.1088/0268-1242/23/10/085010** Published: **AUG 2008**
Times Cited: **2** (from Web of Science)



[[View abstract](#)]

41. Title: **Quenching spin decoherence in diamond through spin bath polarization**
Author(s): Takahashi, Susumu; Hanson, Ronald; van Tol, Johan; et al.
Source: PHYSICAL REVIEW LETTERS Volume: **101** Issue: **4** Article
Number: **047601** DOI: **10.1103/PhysRevLett.101.047601** Published: **JUL 25 2008**
Times Cited: **42** (from Web of Science)



42. Title: **Coherent manipulation of single spins in semiconductors**
 Author(s): Hanson, Ronald; Awschalom, David D.
 Source: NATURE Volume: **453** Issue: **7198** Pages: **1043-1049** DOI: **10.1038/nature07129** Published: **JUN 19 2008**
 Times Cited: **108** (from Web of Science)



43. Title: **Spin dynamics in a double quantum dot: Exact diagonalization study**
 Author(s): Sarkka, J.; Harju, A.
 Source: PHYSICAL REVIEW B Volume: **77** Issue: **24** Article Number: **245315** DOI: **10.1103/PhysRevB.77.245315** Published: **JUN 2008**
 Times Cited: **5** (from Web of Science)



44. Title: **Quantum dynamics in electron-nuclei coupled spin system in quantum dots: Bunching, revival, and quantum correlation in electron-spin measurements**
 Author(s): Cakir, Ozguer; Takagahara, Toshihide
 Source: PHYSICAL REVIEW B Volume: **77** Issue: **11** Article Number: **115304** DOI: **10.1103/PhysRevB.77.115304** Published: **MAR 2008**
 Times Cited: **5** (from Web of Science)



45. Title: **Exponential decay in a spin bath**
 Author(s): Coish, W. A.; Fischer, Jan; Loss, Daniel
 Source: PHYSICAL REVIEW B Volume: **77** Issue: **12** Article Number: **125329** DOI: **10.1103/PhysRevB.77.125329** Published: **MAR 2008**
 Times Cited: **34** (from Web of Science)



46. Title: **Long-time electron spin storage via dynamical suppression of hyperfine-induced decoherence in a quantum dot**
 Author(s): Zhang, Wenxian; Konstantinidis, N. P.; Dobrovitski, V. V.; et al.
 Source: PHYSICAL REVIEW B Volume: **77** Issue: **12** Article Number: **125336** DOI: **10.1103/PhysRevB.77.125336** Published: **MAR 2008**
 Times Cited: **34** (from Web of Science)



47. Title: **Dynamic nuclear polarization with single electron spins**
 Author(s): Petta, J. R.; Taylor, J. M.; Johnson, A. C.; et al.
 Source: PHYSICAL REVIEW LETTERS Volume: **100** Issue: **6** Article Number: **067601** DOI: **10.1103/PhysRevLett.100.067601** Published: **FEB 15 2008**
 Times Cited: **56** (from Web of Science)



48. Title: **Electrical control of spin relaxation in a quantum dot**
 Author(s): Amasha, S.; MacLean, K.; Radu, Iuliana P.; et al.
 Source: PHYSICAL REVIEW LETTERS Volume: **100** Issue: **4** Article Number: **046803** DOI: **10.1103/PhysRevLett.100.046803** Published: **FEB 1 2008**
 Times Cited: **85** (from Web of Science)



49. Title: **Control of electron spin decoherence in mesoscopic nuclear spin baths**
 Author(s): Liu, Ren-Bao; Yao, Wang; Sham, L. J.
 Source: INTERNATIONAL JOURNAL OF MODERN PHYSICS B Volume: **22** Issue: **1-2** Pages: **27-32** DOI: **10.1142/S0217979208046013** Published: **JAN 20 2008**
 Times Cited: **1** (from Web of Science)

 [ [View abstract](#)]

- 50. Title: [Decoherence in solid-state qubits](#)
 Author(s): Chirolli, Luca; Burkard, Guido
 Source: ADVANCES IN PHYSICS Volume: 57 Issue: 3 Pages: 225-285
 DOI: 10.1080/00018730802218067 Published: 2008
 Times Cited: 15 (from Web of Science)

 [ [View abstract](#)]

Results: 82  Page 1 of 2   Sort by: 

Output Records





Step 1:

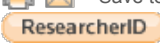
- Selected Records on page
- All records on page
- Records to

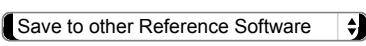

Step 2:



- Authors, Title, Source
 - plus Abstract
- Full Record
 - plus Cited References

Step 3: [\[How do I export to bibliographic management software?\]](#)

  Save to:  



  (12)

82 records matched your query of the 53,033,624 in the data limits you selected.

View in: | [简体中文](#) | [English](#) | [日本語](#)

Web of Science[®] now with books

[<< Return to All Databases](#)

[<< Back to previous page](#)

Citing Articles Title: **Enhancement of electron spin coherence by optical preparation of nuclear spins**
 Author(s): **Stepanenko, D ; Burkard, G ; Giedke, G ; et al.**
 Source: **PHYSICAL REVIEW LETTERS** Volume: **96** Issue: **13** Article Number: **136401** DOI: **10.1103/PhysRevLett.96.136401** Published: **APR 7 2006**

This article has been cited by articles indexed in the databases listed below. [\[more information\]](#)

83 in *All Databases*

82 in *Web of Science*

0 in *BIOSIS Citation Index*

1 in *Chinese Science Citation Database*

Results: **82**

Page of 2

Sort by:

Hide Refine

Refine Results

Search within results for

Web of Science Categories

- PHYSICS CONDENSED MATTER (40)
 - PHYSICS MULTIDISCIPLINARY (26)
 - MULTIDISCIPLINARY SCIENCES (6)
 - OPTICS (6)
 - NANOSCIENCE NANOTECHNOLOGY (5)
- [more options / values...](#)

Document Types

- ARTICLE (72)
 - REVIEW (7)
 - PROCEEDINGS PAPER (5)
 - BOOK CHAPTER (3)
 - EDITORIAL MATERIAL (1)
- [more options / values...](#)

- Research Areas
- Authors
- Group Authors
- Editors
- Source Titles
- Book Series Titles
- Conference Titles
- Publication Years
- Organizations-Enhanced
- Funding Agencies
- Languages

(12) |
 |
 |
 |
 |
 |

- 51. Title: **Magnetic ordering of nuclear spins in an interacting two-dimensional electron gas**
 Author(s): Simon, Pascal; Braunecker, Bernd; Loss, Daniel
 Source: PHYSICAL REVIEW B Volume: **77** Issue: **4** Article Number: **045108** DOI: **10.1103/PhysRevB.77.045108** Published: **JAN 2008**
 Times Cited: **19** (from Web of Science)
 []
- 52. Title: **Spin dynamics in InAs nanowire quantum dots coupled to a transmission line**
 Author(s): Trif, Mircea; Golovach, Vitaly N.; Loss, Daniel
 Source: PHYSICAL REVIEW B Volume: **77** Issue: **4** Article Number: **045434** DOI: **10.1103/PhysRevB.77.045434** Published: **JAN 2008**
 Times Cited: **33** (from Web of Science)
 []
- 53. Title: **Magnetic Ordering of Nuclear Spins in an Interacting 2D Electron Gas as a Consequence of Non-Analyticities in the 2D Fermi Liquid**
 Author(s): Simon, Pascal; Braunecker, Bernd; Loss, Daniel
 Source: PROGRESS OF THEORETICAL PHYSICS SUPPLEMENT Issue: **176** Pages: **302-321** Published: **2008**
 Times Cited: **0** (from Web of Science)
 []
- 54. Title: **Quantum State Transfer from a Photon to an Electron Spin in Quantum Dots and Quantum Dynamics of Electron-Nuclei Coupled System**
 Author(s): Takagahara, T.; Cakir, Oezguer
 Book Author(s): Henneberger, F; Benson, O
 Source: SEMICONDUCTOR QUANTUM BITS Pages: **179-198** DOI:

► Countries/Territories

For advanced refine options, use

[Analyze Results](#)

10.1142/9789814241199_0008 Published: 2008
Times Cited: 0 (from Web of Science)



55. Title: **Electron and Hole Spin Dynamics and Decoherence in Quantum Dots**
Author(s): Klauser, D.; Bulaev, D. V.; Coish, W. A.; et al.
Book Author(s): Henneberger, F; Benson, O
Source: SEMICONDUCTOR QUANTUM BITS Pages: 229-247 DOI: 10.1142/9789814241199_0010 Published: 2008
Times Cited: 2 (from Web of Science)



56. Title: **Magnetic Order in Kondo-Lattice Systems due to Electron-Electron Interactions**
Author(s): Braunecker, Bernd; Simon, Pascal; Loss, Daniel
Book Editor(s): Goan, HS; Chen, YN
Conference: 2nd International Workshop on Solid-State Quantum Computing/Mini-School on Quantum Information Science Location: Taipei, TAIWAN Date: JUN 23-27, 2008
Sponsor(s): Natl Sci Council; Natl Ctr Theoret Sci S; Natl Ctr Theoret Sci N; Acad Sinica, Res Ctr Appl Sci; Natl Cheng Kung Univ; Ctr Theoret Sci; Natl Taiwan Univ, Dept Phys; Natl Taiwan Univ, Coll Sci
Source: SOLID-STATE QUANTUM COMPUTING, PROCEEDINGS Book Series: AIP Conference Proceedings Volume: 1074 Pages: 62-67
Published: 2008
Times Cited: 0 (from Web of Science)



[[View abstract](#)]

57. Title: **OPTICAL PREPARATION OF NUCLEAR SPINS COUPLED TO A LOCALIZED ELECTRON SPIN**
 Author(s): Stepanenko, Dimitrije; Burkard, Guido
Book Editor(s): Takayanagi, H; Nitta, J; Nakano, H
Conference: 4th International Symposium on Mesoscopic Superconductivity and Spintronics Location: NTT, Atsugi, JAPAN Date: FEB 27-MAR 02, 2006
Sponsor(s): Japan Sci & Technol Acgy; NTT Basic Res Labs
Source: CONTROLLABLE QUANTUM STATES: MESOSCOPIC SUPERCONDUCTIVITY AND SPRINTRONICS Pages: 371-376 DOI: 10.1142/9789812814623_0059 Published: 2008
Times Cited: 0 (from Web of Science)



[[View abstract](#)]

58. Title: **Electrically driven reverse overhauser pumping of nuclear spins in quantum dots**
Author(s): Rudner, M. S.; Levitov, L. S.
Source: PHYSICAL REVIEW LETTERS Volume: 99 Issue: 24 Article Number: 246602 DOI: 10.1103/PhysRevLett.99.246602 Published: DEC 14 2007
Times Cited: 22 (from Web of Science)


















[[View abstract](#)]

59. Title: **Quantum dynamics of electron-nuclei coupled system in quantum dots**
Author(s): Cakir, Oezguer; Takagahara, Toshihide
Conference: 2nd International Symposium on Nanometer-Scale Quantum Physics Location: Tokyo Inst Technol, Tokyo, JAPAN Date: JAN 24-26, 2007
Sponsor(s): Minist Educ, Culture, Sports, Sci & Technol; Tokyo Tech Res Ctr; Physical Soc Japan; Japan Soc Appl Phys
Source: PHYSICA E-LOW-DIMENSIONAL SYSTEMS & NANOSTRUCTURES Volume: 40 Issue: 2 Pages: 379-382 DOI: 10.1016/j.physe.2007.06.026 Published: DEC 2007
Times Cited: 1 (from Web of Science)



[[View abstract](#)]

60. Title: **Observation of extremely slow hole spin relaxation in self-assembled quantum dots**
 Author(s): Heiss, D.; Schaeck, S.; Huebl, H.; et al.
 Source: PHYSICAL REVIEW B Volume: **76** Issue: **24** Article Number: **241306** DOI: **10.1103/PhysRevB.76.241306** Published: **DEC 2007**
 Times Cited: **77** (from Web of Science)
-  [ [View abstract](#)]
61. Title: **Exactly solvable spin dynamics of an electron coupled to a large number of nuclei; the electron-nuclear spin echo in a quantum dot**
 Author(s): Kozlov, G. G.
 Source: JOURNAL OF EXPERIMENTAL AND THEORETICAL PHYSICS Volume: **105** Issue: **4** Pages: **803-815** DOI: **10.1134/S1063776107100159** Published: **OCT 2007**
 Times Cited: **8** (from Web of Science)
-  [ [View abstract](#)]
62. Title: **Spins in few-electron quantum dots**
 Author(s): Hanson, R.; Kouwenhoven, L. P.; Petta, J. R.; et al.
 Source: REVIEWS OF MODERN PHYSICS Volume: **79** Issue: **4** Pages: **1217-1265** DOI: **10.1103/RevModPhys.79.1217** Published: **OCT-DEC 2007**
 Times Cited: **596** (from Web of Science)
-  [ [View abstract](#)]
63. Title: **Control of electron spin decoherence caused by electron-nuclear spin dynamics in a quantum dot**
 Author(s): Liu, Ren-Bao; Yao, Wang; Sham, L. J.
 Source: NEW JOURNAL OF PHYSICS Volume: **9** Article Number: **226** DOI: **10.1088/1367-2630/9/7/226** Published: **JUL 11 2007**
 Times Cited: **47** (from Web of Science)
-   [ [View abstract](#)]
64. Title: **Dynamical control of electron spin coherence in a quantum dot: A theoretical study**
 Author(s): Zhang, Wenxian; Dobrovitski, V. V.; Santos, Lea F.; et al.
 Source: PHYSICAL REVIEW B Volume: **75** Issue: **20** Article Number: **201302** DOI: **10.1103/PhysRevB.75.201302** Published: **MAY 2007**
 Times Cited: **31** (from Web of Science)
-  [ [View abstract](#)]
65. Title: **Quantum description of nuclear spin cooling in a quantum dot**
 Author(s): Christ, H.; Cirac, J. I.; Giedke, G.
 Source: PHYSICAL REVIEW B Volume: **75** Issue: **15** Article Number: **155324** DOI: **10.1103/PhysRevB.75.155324** Published: **APR 2007**
 Times Cited: **27** (from Web of Science)
-  [ [View abstract](#)]
66. Title: **Dynamical nuclear spin polarization and the Zamboni effect in gated double quantum dots**
 Author(s): Ramon, Guy; Hu, Xuedong
 Source: PHYSICAL REVIEW B Volume: **75** Issue: **16** Article Number: **161301** DOI: **10.1103/PhysRevB.75.161301** Published: **APR 2007**
 Times Cited: **24** (from Web of Science)
-  [ [View abstract](#)]
67. Title: **Electric dipole spin resonance for heavy holes in quantum dots**
 Author(s): Bulaev, Denis V.; Loss, Daniel
 Source: PHYSICAL REVIEW LETTERS Volume: **98** Issue: **9** Article Number: **097202** DOI: **10.1103/PhysRevLett.98.097202** Published: **MAR 2 2007**

Times Cited: **27** (from Web of Science)

68. Title: **Nonequilibrium thermal entanglement**
 Author(s): Quiroga, Luis; Rodriguez, Ferney J.; Ramirez, Maria E.; et al.
 Source: PHYSICAL REVIEW A Volume: **75** Issue: **3** Article Number: **032308** DOI: **10.1103/PhysRevA.75.032308** Published: **MAR 2007**
 Times Cited: **20** (from Web of Science)



69. Title: **Single-electron spin decoherence by nuclear spin bath: Linked-cluster expansion approach**
 Author(s): Saikin, S. K.; Yao, Wang; Sham, L. J.
 Source: PHYSICAL REVIEW B Volume: **75** Issue: **12** Article Number: **125314** DOI: **10.1103/PhysRevB.75.125314** Published: **MAR 2007**
 Times Cited: **37** (from Web of Science)



70. Title: **Modelling decoherence in quantum spin systems**
 Author(s): Zhang, Wenxian; Konstantinidis, N.; Al-Hassanieh, K. A.; et al.
 Source: JOURNAL OF PHYSICS-CONDENSED MATTER Volume: **19** Issue: **8** Article Number: **083202** DOI: **10.1088/0953-8984/19/8/083202**
 Published: **FEB 28 2007**
 Times Cited: **38** (from Web of Science)



71. Title: **Restoring coherence lost to a slow interacting mesoscopic spin bath**
 Author(s): Yao, Wang; Liu, Ren-Bao; Sham, L. J.
 Source: PHYSICAL REVIEW LETTERS Volume: **98** Issue: **7** Article Number: **077602** DOI: **10.1103/PhysRevLett.98.077602** Published: **FEB 16 2007**
 Times Cited: **93** (from Web of Science)



72. Title: **Universal set of quantum gates for double-dot spin qubits with fixed interdot coupling**
 Author(s): Hanson, Ronald; Burkard, Guido
 Source: PHYSICAL REVIEW LETTERS Volume: **98** Issue: **5** Article Number: **050502** DOI: **10.1103/PhysRevLett.98.050502** Published: **FEB 2 2007**
 Times Cited: **51** (from Web of Science)



73. Title: **Quantum gates between capacitively coupled double quantum dot two-spin qubits**
 Author(s): Stepanenko, Dimitrije; Burkard, Guido
 Source: PHYSICAL REVIEW B Volume: **75** Issue: **8** Article Number: **085324** DOI: **10.1103/PhysRevB.75.085324** Published: **FEB 2007**
 Times Cited: **21** (from Web of Science)



74. Title: **Suppression of electron spin decoherence in a quantum dot**
 Author(s): Zhang, Wenxian; Dobrovitski, V. V.; Santos, Lea F.; et al.
 Conference: **37th Winter Colloquium on the Physics of Quantum Electronics** Location: **Snowbird, UT** Date: **JAN 02-06, 2007**
 Source: JOURNAL OF MODERN OPTICS Volume: **54** Issue: **16-17** Pages: **2629-2640** DOI: **10.1080/09500340701534857** Published: **2007**
 Times Cited: **5** (from Web of Science)



75. Title: **Theoretical aspects of quantum state transfer, correlation measurement and electron-nuclei coupled dynamics in quantum dots**
 Author(s): Takagahara, Toshihide; Cakir, Oezguer
 Source: JOURNAL OF NANOPHOTONICS Volume: **1** Article Number: **011593** DOI: **10.1117/1.2828099** Published: **2007**
 Times Cited: **2** (from Web of Science)



[[View abstract](#)]

76. Title: **Coherent population trapping in a single-hole-charged quantum dot**
 Author(s): Imamoglu, A.
 Source: PHYSICA STATUS SOLIDI B-BASIC SOLID STATE PHYSICS Volume: **243** Issue: **14** Pages: **3725-3729** DOI: **10.1002/pssb.200642282** Published: **NOV 2006**
 Times Cited: **3** (from Web of Science)



[[View abstract](#)]

77. Title: **Electron spin and nuclear spin manipulation in semiconductor nanosystems**
 Author(s): Hirayama, Yoshiro; Yusa, Go; Sasaki, Satoshi
 Source: PHYSICA STATUS SOLIDI B-BASIC SOLID STATE PHYSICS Volume: **243** Issue: **14** Pages: **3764-3772** DOI: **10.1002/pssb.200642259** Published: **NOV 2006**
 Times Cited: **0** (from Web of Science)



[[View abstract](#)]

78. Title: **Hyperfine interaction induced decoherence of electron spins in quantum dots**
 Author(s): Zhang, Wenxian; Dobrovitski, V. V.; Al-Hassanieh, K. A.; et al.
 Source: PHYSICAL REVIEW B Volume: **74** Issue: **20** Article Number: **205313** DOI: **10.1103/PhysRevB.74.205313** Published: **NOV 2006**
 Times Cited: **37** (from Web of Science)



[[View abstract](#)]

79. Title: **Quantum physics - A spin solo**
 Author(s): Burkard, Guido
 Source: NATURE Volume: **442** Issue: **7104** Pages: **749-750** DOI: **10.1038/442749a** Published: **AUG 17 2006**
 Times Cited: **0** (from Web of Science)



80. Title: **Driven coherent oscillations of a single electron spin in a quantum dot**
 Author(s): Koppens, F. H. L.; Buizert, C.; Tielrooij, K. J.; et al.
 Source: NATURE Volume: **442** Issue: **7104** Pages: **766-771** DOI: **10.1038/nature05065** Published: **AUG 17 2006**
 Times Cited: **554** (from Web of Science)



[[View abstract](#)]

81. Title: **Nuclear spin state narrowing via gate-controlled Rabi oscillations in a double quantum dot**
 Author(s): Klauser, D; Coish, WA; Loss, D
 Source: PHYSICAL REVIEW B Volume: **73** Issue: **20** Article Number: **205302** DOI: **10.1103/PhysRevB.73.205302** Published: **MAY 2006**
 Times Cited: **98** (from Web of Science)



[[View abstract](#)]

82. Title: **Knight-field-enabled nuclear spin polarization in single quantum dots**
 Author(s): Lai, CW; Maletinsky, P; Badolato, A; et al.
 Source: PHYSICAL REVIEW LETTERS Volume: **96** Issue: **16** Article Number: **167403** DOI: **10.1103/PhysRevLett.96.167403** Published: **APR 28 2006**

Times Cited: 107 (from Web of Science)

 [[View abstract](#)]

Results: 82 [Show 50 per page](#) Page 2 of 2 [Go](#) Sort by: [Publication Date -- newest to oldest](#)

Output Records




Step 1:

- Selected Records on page
- All records on page
- Records to

Step 2:

- Authors, Title, Source
 - plus Abstract
- Full Record
 - plus Cited References

Step 3: [\[How do I export to bibliographic management software?\]](#)



 Save to: [ENDNOTE WEB](#) [ENDNOTE](#)
[ResearcherID](#)
[Save to other Reference Software](#) [Save](#)
 (12)

82 records matched your query of the 53,033,624 in the data limits you selected.

View in: [简体中文](#) | [English](#) | [日本語](#)

Web of Science[®] now with books

[<< Return to All Databases](#)

[<< Back to previous page](#)

Citing Articles Title: **Quantum gates between capacitively coupled double quantum dot two-spin qubits**

Author(s): **Stepanenko, Dimitrije ; Burkard, Guido**
 Source: **PHYSICAL REVIEW B** Volume: **75** Issue: **8** Article Number: **085324** DOI: **10.1103/PhysRevB.75.085324** Published: **FEB 2007**

This article has been cited by articles indexed in the databases listed below. [\[more information\]](#)

21 in All Databases

21 in Web of Science

0 in BIOSIS Citation Index

1 in Chinese Science Citation Database

Results: **21**

Page of 1

Sort by:

Hide Refine

Refine Results

Search within results for

Web of Science Categories

- PHYSICS CONDENSED MATTER (9)
 - PHYSICS APPLIED (5)
 - NANOSCIENCE NANOTECHNOLOGY (4)
 - OPTICS (4)
 - PHYSICS ATOMIC MOLECULAR CHEMICAL (4)
- [more options / values...](#)

Document Types

- ARTICLE (21)
- Research Areas
- Authors
- Group Authors
- Editors
- Source Titles
- Book Series Titles
- Conference Titles
- Publication Years
- Organizations-Enhanced
- Funding Agencies
- Languages
- Countries/Territories

For advanced refine options, use

(12) |
 |
 |
 Save to: |
 |

1. Title: **Universal quantum computing with spin and valley states**
 Author(s): Rohling, Niklas; Burkard, Guido
 Source: NEW JOURNAL OF PHYSICS Volume: **14** Article Number: **083008** DOI: **10.1088/1367-2630/14/8/083008** Published: **AUG 10 2012**
 Times Cited: **0** (from Web of Science)

[View abstract]

2. Title: **Configuration interaction calculations of the controlled phase gate in double quantum dot qubits**
 Author(s): Nielsen, Erik; Muller, Richard P.; Carroll, Malcolm S.
 Source: PHYSICAL REVIEW B Volume: **85** Issue: **3** Article Number: **035319** DOI: **10.1103/PhysRevB.85.035319** Published: **JAN 25 2012**
 Times Cited: **0** (from Web of Science)





[View abstract]

3. Title: **Electrically controlled quantum gates for two-spin qubits in two double quantum dots**
 Author(s): Ramon, Guy
 Source: PHYSICAL REVIEW B Volume: **84** Issue: **15** Article Number: **155329** DOI: **10.1103/PhysRevB.84.155329** Published: **OCT 31 2011**
 Times Cited: **1** (from Web of Science)

[View abstract]

4. Title: **Low-noise conditional operation of singlet-triplet coupled quantum dot qubits**
 Author(s): Yang, Shuo; Das Sarma, S.
 Source: PHYSICAL REVIEW B Volume: **84** Issue: **12** Article Number: **121306** DOI: **10.1103/PhysRevB.84.121306** Published: **SEP 23 2011**
 Times Cited: **0** (from Web of Science)

[View abstract]

5. Title: **Low-Density Quantum Dot Molecules by Selective Etching Using in Droplet as a Mask**
Author(s): Lee, Jihoon; Wang, Zhiming M.; Hirono, Yusuke; et al.
Source: IEEE TRANSACTIONS ON NANOTECHNOLOGY Volume: **10**
Issue: **3** Pages: **600-605** DOI: **10.1109/TNANO.2010.2056695**
Published: **MAY 2011**
Times Cited: **0** (from Web of Science)
-  [ [View abstract](#)]
6. Title: **Harnessing the GaAs quantum dot nuclear spin bath for quantum control**
Author(s): Ribeiro, Hugo; Petta, J. R.; Burkard, Guido
Source: PHYSICAL REVIEW B Volume: **82** Issue: **11** Article Number: **115445** DOI: **10.1103/PhysRevB.82.115445** Published: **SEP 24 2010**
Times Cited: **11** (from Web of Science)
-  [ [View abstract](#)]
7. Title: **Various Quantum- and Nano-Structures by III-V Droplet Epitaxy on GaAs Substrates**
Author(s): Lee, J. H.; Wang, Zh. M.; Kim, E. S.; et al.
Source: NANOSCALE RESEARCH LETTERS Volume: **5** Issue: **2** Pages: **308-314** DOI: **10.1007/s11671-009-9481-9** Published: **FEB 2010**
Times Cited: **8** (from Web of Science)
-   [ [View abstract](#)]
8. Title: **Implementation of Quantum Fourier Transform and Its Applications via Quantum-Dot Spins and Microcavity**
Author(s): Dong Ping; Zheng Xiao-Hu; Zhang Gang; et al.
Source: COMMUNICATIONS IN THEORETICAL PHYSICS Volume: **52**
Issue: **3** Pages: **425-430** Published: **SEP 2009**
Times Cited: **0** (from Web of Science)
-  [ [View abstract](#)]
9. Title: **On the complex behavior of strain relaxation in (In,Ga)As/GaAs(001) quantum dot molecules**
Author(s): Hanke, M.; Dubsloff, M.; Schmidbauer, M.; et al.
Source: APPLIED PHYSICS LETTERS Volume: **95** Issue: **2** Article Number: **023103** DOI: **10.1063/1.3176409** Published: **JUL 13 2009**
Times Cited: **0** (from Web of Science)
-  [ [View abstract](#)]
10. Title: **The Control on Size and Density of InAs QDs by Droplet Epitaxy (April 2009)**
Author(s): Lee, Jihoon H.; Wang, Zhiming M.; Salamo, Gregory J.
Source: IEEE TRANSACTIONS ON NANOTECHNOLOGY Volume: **8**
Issue: **4** Pages: **431-436** DOI: **10.1109/TNANO.2009.2021654**
Published: **JUL 2009**
Times Cited: **9** (from Web of Science)
-  [ [View abstract](#)]
11. Title: **Parity-measurement-based entanglement concentration**
Author(s): Cao, Zhuo-Liang; Dong, Ping
Source: PHYSICA B-CONDENSED MATTER Volume: **404** Issue: **14-15**
Pages: **1917-1919** DOI: **10.1016/j.physb.2009.03.011** Published: **JUL 1 2009**
Times Cited: **2** (from Web of Science)
-  [ [View abstract](#)]
12. Title: **Tunable resonant tunneling through a system of capacitively coupled double quantum dots**
Author(s): Yuan, R. Y.; Wang, R. Z.; Yan, H.

Source: PHYSICA E-LOW-DIMENSIONAL SYSTEMS & NANOSTRUCTURES Volume: **41** Issue: **4** Pages: **558-563** DOI: **10.1016/j.physe.2008.10.012** Published: **FEB 2009**
Times Cited: **0** (from Web of Science)



[View abstract]

13. Title: **Discrete quantum Fourier transform in coupled semiconductor double quantum dot molecules**
Author(s): Dong, Ping; Yang, Ming; Cao, Zhuo-Liang
Source: PHYSICS LETTERS A Volume: **373** Issue: **1** Pages: **30-32**
DOI: **10.1016/j.physleta.2008.11.005** Published: **DEC 22 2008**
Times Cited: **2** (from Web of Science)



[View abstract]

14. Title: **Dispersive coupling between the superconducting transmission line resonator and the double quantum dots**
Author(s): Guo, Guo-Ping; Zhang, Hui; Hu, Yong; et al.
Source: PHYSICAL REVIEW A Volume: **78** Issue: **2** Article Number: **020302** DOI: **10.1103/PhysRevA.78.020302** Part: **Part a** Published: **AUG 2008**
Times Cited: **9** (from Web of Science)



[View abstract]

15. Title: **Dynamical polarization processes in double quantum dots coupled in series**
Author(s): Michalek, G.; Bulka, B. R.
Source: JOURNAL OF PHYSICS-CONDENSED MATTER Volume: **20** Issue: **27** Article Number: **275244** DOI: **10.1088/0953-8984/20/27/275244** Published: **JUL 9 2008**
Times Cited: **0** (from Web of Science)



[View abstract]

16. Title: **Evolution of InGaAs quantum dot molecules**
Author(s): Lee, J. H.; Sablon, K.; Wang, Zh. M.; et al.
Source: JOURNAL OF APPLIED PHYSICS Volume: **103** Issue: **5** Article Number: **054301** DOI: **10.1063/1.2890149** Published: **MAR 1 2008**
Times Cited: **13** (from Web of Science)



[View abstract]

17. Title: **Eliminating interactions between non-neighboring qubits in the preparation of cluster states in quantum molecules**
Author(s): Guo, Guo-Ping; Hao, Xiao-Jie; Tu, Tao; et al.
Source: EUROPEAN PHYSICAL JOURNAL B Volume: **61** Issue: **2** Pages: **141-146** DOI: **10.1140/epjb/e2008-00053-9** Published: **JAN 2008**
Times Cited: **3** (from Web of Science)



[View abstract]

18. Title: **Controlled-NOT gate for multiparticle qubits and topological quantum computation based on parity measurements**
Author(s): Zilberberg, Oded; Braunecker, Bernd; Loss, Daniel
Source: PHYSICAL REVIEW A Volume: **77** Issue: **1** Article Number: **012327** DOI: **10.1103/PhysRevA.77.012327** Published: **JAN 2008**
Times Cited: **11** (from Web of Science)



[View abstract]

19. Title: **General quantum phase estimation and calibration of a timepiece in a quantum dot system**
Author(s): Dong, Ping; Cao, Zhuo-Liang
Source: JOURNAL OF PHYSICS-CONDENSED MATTER Volume: **19** Issue: **37** Article Number: **376216** DOI: **10.1088/0953-8984/19/37/376216** Published: **SEP 19 2007**
Times Cited: **2** (from Web of Science)



- 20. Title: **Quantum computation and Bell-state measurements with double-dot molecules**
 Author(s): Zhang, Hui; Guo, Guo-Ping; Tu, Tao; et al.
 Source: PHYSICAL REVIEW A Volume: **76** Issue: **1** Article Number: **012335** DOI: **10.1103/PhysRevA.76.012335** Published: **JUL 2007**
 Times Cited: **10** (from Web of Science)



- 21. Title: **One-step preparation of cluster states in quantum-dot molecules**
 Author(s): Guo, Guo-Ping; Zhang, Hui; Tu, Tao; et al.
 Source: PHYSICAL REVIEW A Volume: **75** Issue: **5** Article Number: **050301** DOI: **10.1103/PhysRevA.75.050301** Published: **MAY 2007**
 Times Cited: **29** (from Web of Science)



Results: **21** Page of 1 Sort by:

Output Records

Step 1:

- Selected Records on page
- All records on page
- Records to

Step 2:

- Authors, Title, Source
 - plus Abstract
- Full Record
 - plus Cited References

Step 3: [\[How do I export to bibliographic management software?\]](#)

Save to:

 (12)

21 records matched your query of the 53,033,624 in the data limits you selected.

View in: [简体中文](#) | [English](#) | [日本語](#)

Web of Science[®] now with books

[<< Return to All Databases](#)

[<< Back to previous page](#)

Citing Articles

Title: **Spin-Electric Coupling in Molecular Magnets**
 Author(s): **Trif, Mircea ; Troiani, Filippo ; Stepanenko, Dimitrije ; et al.**
 Source: **PHYSICAL REVIEW LETTERS** Volume: **101** Issue: **21** Article Number: **217201** DOI: **10.1103/PhysRevLett.101.217201** Published: **NOV 21 2008**

This article has been cited by articles indexed in the databases listed below. [\[more information\]](#)

43 in All Databases

43 in Web of Science

1 in BIOSIS Citation Index

0 in Chinese Science Citation Database

Results: **43**

Page of 1

Sort by:

Hide Refine

Refine Results

Search within results for

Web of Science Categories

- PHYSICS CONDENSED MATTER (24)
- PHYSICS MULTIDISCIPLINARY (8)
- PHYSICS ATOMIC MOLECULAR CHEMICAL (5)
- CHEMISTRY MULTIDISCIPLINARY (3)
- CHEMISTRY PHYSICAL (3)
- [more options / values...](#)

Document Types

- ARTICLE (39)
- PROCEEDINGS PAPER (3)
- REVIEW (2)
- BOOK CHAPTER (1)
- [more options / values...](#)

Research Areas

Authors

Group Authors

Editors

Source Titles

Book Series Titles

Conference Titles

Publication Years

Organizations-Enhanced

Funding Agencies

Languages

(12) |
 |
 |
 Save to: |
 |

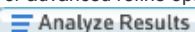
|
 |
 [more options](#)

1. Title: **Entanglement in a three spin system controlled by electric and magnetic fields**
 Author(s): Luczak, Jakub; Bulka, Bogdan R.
 Source: JOURNAL OF PHYSICS-CONDENSED MATTER Volume: **24** Issue: **37** Article Number: **375303** DOI: **10.1088/0953-8984/24/37/375303** Published: **SEP 19 2012**
 Times Cited: **0** (from Web of Science)
 [View abstract](#)
2. Title: **Electric Field Control of the Spin State in Mixed-Valence Magnetic Molecules**
 Author(s): Bosch-Serrano, Cristian; Clemente-Juan, Juan M.; Coronado, Eugenio; et al.
 Source: CHEMPHYSICHEM Volume: **13** Issue: **11** Pages: **2662-2665** DOI: **10.1002/cphc.201200383** Published: **AUG 6 2012**
 Times Cited: **0** (from Web of Science)

3. Title: **Molecular analog of multiferroics: Electric and magnetic field effects in many-electron mixed-valence dimers**
 Author(s): Bosch-Serrano, Cristian; Clemente-Juan, Juan M.; Coronado, Eugenio; et al.
 Source: PHYSICAL REVIEW B Volume: **86** Issue: **2** Article Number: **024432** DOI: **10.1103/PhysRevB.86.024432** Published: **JUL 25 2012**
 Times Cited: **0** (from Web of Science)
 [View abstract](#)
4. Title: **A Combined Experimental and Computational Study of the Magnetic Superexchange within a Triangular (mu 3-O)-Pyrazolato-Fell3 Complex**
 Author(s): Sameera, W. M. C.; Pintero, Dalice M.; Herchel, Radovan; et al.

► **Countries/Territories**

For advanced refine options, use

 **Analyze Results**

Source: EUROPEAN JOURNAL OF INORGANIC CHEMISTRY Issue: **21**
Pages: **3500-3506** DOI: **10.1002/ejic.201200206** Published: **JUL 2012**
Times Cited: **0** (from Web of Science)

 [ [View abstract](#)]

5. Title: **Inelastic low-temperature transport through a quantum dot with a Mn ion**
Author(s): Niu, Peng-Bin; Yao, Hui; Li, Zhi-Jian; et al.
Source: JOURNAL OF MAGNETISM AND MAGNETIC MATERIALS Volume: **324** Issue: **14** Pages: **2324-2329** DOI: **10.1016/j.jmmm.2012.02.124** Published: **JUL 2012**
Times Cited: **0** (from Web of Science)

 [ [View abstract](#)]

6. Title: **Magnetic of trinuclear nickel complexes-building blocks of single-molecule agpropemrtiesnets**
Author(s): Klimov, A. V.; Berdinskii, V. L.
Source: RUSSIAN JOURNAL OF INORGANIC CHEMISTRY Volume: **57** Issue: **3** Pages: **411-415** DOI: **10.1134/S0036023612030126** Published: **MAR 2012**
Times Cited: **0** (from Web of Science)

 [ [View abstract](#)]

7. Title: **First-principles studies of spin-orbit and Dzyaloshinskii-Moriya interactions in the {Cu-3} single-molecule magnet**
Author(s): Nossa, J. F.; Islam, M. F.; Canali, C. M.; et al.
Source: PHYSICAL REVIEW B Volume: **85** Issue: **8** Article Number: **085427** DOI: **10.1103/PhysRevB.85.085427** Published: **FEB 22 2012**
Times Cited: **0** (from Web of Science)

 [ [View abstract](#)]

8. Title: **Localized states on triangular traps and low-temperature properties of the antiferromagnetic Heisenberg and repulsive Hubbard models**
Author(s): Maksymenko, M.; Derzhko, O.; Richter, J.
Source: EUROPEAN PHYSICAL JOURNAL B Volume: **84** Issue: **3** Pages: **397-408** DOI: **10.1140/epjb/e2011-20706-8** Published: **DEC 2011**
Times Cited: **2** (from Web of Science)

 [ [View abstract](#)]

9. Title: **Molecular Nanomagnets as Quantum Simulators**
Author(s): Santini, P.; Carretta, S.; Troiani, F.; et al.
Source: PHYSICAL REVIEW LETTERS Volume: **107** Issue: **23** Article Number: **230502** DOI: **10.1103/PhysRevLett.107.230502** Published: **NOV 30 2011**
Times Cited: **2** (from Web of Science)

 [ [View abstract](#)]

10. Title: **Electric polarization, toroidal moment, spin canting, and chirality induced by Dzialoshinsky-Moriya interactions in a V-3 cluster analog of multiferroics**
Author(s): Belinsky, Moisey I.
Source: PHYSICAL REVIEW B Volume: **84** Issue: **6** Article Number: **064425** DOI: **10.1103/PhysRevB.84.064425** Published: **AUG 24 2011**
Times Cited: **0** (from Web of Science)

 [ [View abstract](#)]

11. Title: **Canonical perturbation theory for inhomogeneous systems of interacting fermions**
Author(s): Kostyrko, Tomasz; Bulka, Bogdan R.
Source: PHYSICAL REVIEW B Volume: **84** Issue: **3** Article Number: **035123** DOI: **10.1103/PhysRevB.84.035123** Published: **JUL 26 2011**
Times Cited: **2** (from Web of Science)

[\[+...View abstract \]](#)

12. Title: **Measuring the state of a single-molecule magnet with a microstrip resonator**
 Author(s): Fan, Thomas; Tsifrinovich, Vladimir I.
 Source: PHYSICAL REVIEW B Volume: **84** Issue: **2** Article Number: **024410** DOI: **10.1103/PhysRevB.84.024410** Published: **JUL 7 2011**
 Times Cited: **1** (from Web of Science)

[\[+...View abstract \]](#)

13. Title: **Encapsulation of single-molecule magnets in carbon nanotubes**
 Author(s): Gimenez-Lopez, Maria del Carmen; Moro, Fabrizio; La Torre, Alessandro; et al.
 Source: NATURE COMMUNICATIONS Volume: **2** Article Number: **407**
 DOI: **10.1038/ncomms1415** Published: **JUL 2011**
 Times Cited: **3** (from Web of Science)

[\[+...View abstract \]](#)

14. Title: **Quantum nanojunctions as spintronic logic operators: Gate response in a two input ballistic interferometer**
 Author(s): Bellucci, S.; Onorato, P.
 Source: JOURNAL OF APPLIED PHYSICS Volume: **109** Issue: **12**
 Article Number: **123715** DOI: **10.1063/1.3598127** Published: **JUN 15 2011**
 Times Cited: **0** (from Web of Science)

[\[+...View abstract \]](#)

15. Title: **Low-Temperature Properties of the Quantum Heisenberg Antiferromagnet on Some One-Dimensional Lattices Containing Equilateral Triangles**
 Author(s): Maksymenko, M.; Derzhko, O.; Richter, J.
 Source: ACTA PHYSICA POLONICA A Volume: **119** Issue: **6** Pages: **860-862** Published: **JUN 2011**
 Times Cited: **2** (from Web of Science)

[\[+...View abstract \]](#)

16. Title: **Macroscopic quantum dynamics of toroidal moment in Ising-type rare-earth clusters**
 Author(s): Plokhov, D. I.; Zvezdin, A. K.; Popov, A. I.
 Source: PHYSICAL REVIEW B Volume: **83** Issue: **18** Article Number: **184415** DOI: **10.1103/PhysRevB.83.184415** Published: **MAY 18 2011**
 Times Cited: **2** (from Web of Science)

[\[+...View abstract \]](#)

17. Title: **Quantum memory coupled to cavity modes**
 Author(s): Pedrocchi, Fabio L.; Chesi, Stefano; Loss, Daniel
 Source: PHYSICAL REVIEW B Volume: **83** Issue: **11** Article Number: **115415** DOI: **10.1103/PhysRevB.83.115415** Published: **MAR 10 2011**
 Times Cited: **2** (from Web of Science)

[\[+...View abstract \]](#)

18. Title: **Measurement of a Quantum State of a Single Molecule Magnet with Magnetic Resonance Force Microscopy**
 Author(s): Fan, Thomas; Tsifrinovich, Vladimir I.
 Source: JOURNAL OF COMPUTATIONAL AND THEORETICAL NANOSCIENCE Volume: **8** Issue: **3** Pages: **503-508** DOI: **10.1166/jctn.2011.1715** Published: **MAR 2011**
 Times Cited: **0** (from Web of Science)

[\[+...View abstract \]](#)

19. Title: [Entanglement in finite spin rings with noncollinear Ising interaction](#)
 Author(s): Troiani, F.
 Source: PHYSICAL REVIEW A Volume: **83** Issue: **2** Article Number: **022324** DOI: [10.1103/PhysRevA.83.022324](#) Published: **FEB 24 2011**
 Times Cited: **0** (from Web of Science)
-  [[View abstract](#)]
20. Title: [Linear and nonlinear Stark effect in a triangular molecule](#)
 Author(s): Bulka, Bogdan R.; Kostyrko, Tomasz; Luczak, Jakub
 Source: PHYSICAL REVIEW B Volume: **83** Issue: **3** Article Number: **035301** DOI: [10.1103/PhysRevB.83.035301](#) Published: **JAN 10 2011**
 Times Cited: **4** (from Web of Science)
-  [[View abstract](#)]
21. Title: [Molecular spins for quantum information technologies](#)
 Author(s): Troiani, Filippo; Affronte, Marco
 Source: CHEMICAL SOCIETY REVIEWS Volume: **40** Issue: **6** Pages: **3119-3129** DOI: [10.1039/c0cs00158a](#) Published: **2011**
 Times Cited: **7** (from Web of Science)
-  [[View abstract](#)]
22. Title: [Magnetism on a Mesoscopic Scale: Molecular Nanomagnets Bridging Quantum and Classical Physics](#)
 Author(s): Konstantinidis, Nikolaos P.; Sundt, Alexander; Nehr Korn, Joscha; et al.
 Book Editor(s): Spalek, J
 Conference: **Joint European Magnetic Symposia (JEMS)** Location: **Jagiellonian Univ, Krakow, POLAND** Date: **AUG 23-28, 2010**
 Sponsor(s): **Jagiellonian Univ, Inst Phys**
 Source: JOINT EUROPEAN MAGNETIC SYMPOSIA (JEMS) Book Series: **Journal of Physics Conference Series** Volume: **303** Article Number: **012003** DOI: [10.1088/1742-6596/303/1/012003](#) Published: **2011**
 Times Cited: **1** (from Web of Science)
-   [[View abstract](#)]
23. Title: [Oxo-centered carboxylate-bridged trinuclear complexes deposited on Au\(111\) by a mass-selective electrospray](#)
 Author(s): Corradini, Valdis; Cervetti, Christian; Ghirri, Alberto; et al.
 Source: NEW JOURNAL OF CHEMISTRY Volume: **35** Issue: **8** Pages: **1683-1689** DOI: [10.1039/c1nj20080a](#) Published: **2011**
 Times Cited: **2** (from Web of Science)
-  [[View abstract](#)]
24. Title: [Decoherence of intermolecular entanglement in exchange-coupled nanomagnets](#)
 Author(s): Szallas, A.; Troiani, F.
 Source: PHYSICAL REVIEW B Volume: **82** Issue: **22** Article Number: **224409** DOI: [10.1103/PhysRevB.82.224409](#) Published: **DEC 8 2010**
 Times Cited: **4** (from Web of Science)
-  [[View abstract](#)]
25. Title: [Quantum circuits based on coded qubits encoded in chirality of electron spin complexes in triple quantum dots](#)
 Author(s): Hsieh, Chang-Yu; Hawrylak, Pawel
 Source: PHYSICAL REVIEW B Volume: **82** Issue: **20** Article Number: **205311** DOI: [10.1103/PhysRevB.82.205311](#) Published: **NOV 9 2010**
 Times Cited: **4** (from Web of Science)
-  [[View abstract](#)]
26. Title: [First-principles study of spin-electric coupling in a {Cu-3} single molecular magnet](#)

Author(s): Islam, M. Fhokrul; Nossa, Javier F.; Canali, Carlo M.; et al.
 Source: PHYSICAL REVIEW B Volume: **82** Issue: **15** Article Number:
155446 DOI: [10.1103/PhysRevB.82.155446](https://doi.org/10.1103/PhysRevB.82.155446) Published: **OCT 26 2010**
 Times Cited: **6** (from Web of Science)



[[View abstract](#)]

27. Title: [Spin Quantum Bit with Ferromagnetic Contacts for Circuit QED](#)

Author(s): Cottet, Audrey; Kontos, Takis
 Source: PHYSICAL REVIEW LETTERS Volume: **105** Issue: **16** Article
 Number: **160502** DOI: [10.1103/PhysRevLett.105.160502](https://doi.org/10.1103/PhysRevLett.105.160502) Published:
OCT 15 2010
 Times Cited: **12** (from Web of Science)



[[View abstract](#)]

28. Title: [Probing local magnetization in molecular heterometallic Cr₂Cu trimer](#)

Author(s): Lorusso, G.; Corradini, V.; Candini, A.; et al.
 Source: PHYSICAL REVIEW B Volume: **82** Issue: **14** Article Number:
144420 DOI: [10.1103/PhysRevB.82.144420](https://doi.org/10.1103/PhysRevB.82.144420) Published: **OCT 11 2010**
 Times Cited: **4** (from Web of Science)



[[View abstract](#)]

29. Title: [Self-correcting quantum memory in a thermal environment](#)

Author(s): Chesi, Stefano; Roethlisberger, Beat; Loss, Daniel
 Source: PHYSICAL REVIEW A Volume: **82** Issue: **2** Article Number:
022305 DOI: [10.1103/PhysRevA.82.022305](https://doi.org/10.1103/PhysRevA.82.022305) Published: **AUG 6 2010**
 Times Cited: **9** (from Web of Science)



[[View abstract](#)]

30. Title: [Spin electric effects in molecular antiferromagnets](#)

Author(s): Trif, Mircea; Troiani, Filippo; Stepanenko, Dimitrije; et al.
 Source: PHYSICAL REVIEW B Volume: **82** Issue: **4** Article Number:
045429 DOI: [10.1103/PhysRevB.82.045429](https://doi.org/10.1103/PhysRevB.82.045429) Published: **JUL 28 2010**
 Times Cited: **12** (from Web of Science)



[[View abstract](#)]

31. Title: [Magnetic strong coupling in a spin-photon system and transition to classical regime](#)

Author(s): Chiorescu, I.; Groll, N.; Bertaina, S.; et al.
 Source: PHYSICAL REVIEW B Volume: **82** Issue: **2** Article Number:
024413 DOI: [10.1103/PhysRevB.82.024413](https://doi.org/10.1103/PhysRevB.82.024413) Published: **JUL 14 2010**
 Times Cited: **14** (from Web of Science)



[[View abstract](#)]

32. Title: [Family of Exactly Solvable Models with an Ultimate Quantum Paramagnetic Ground State](#)

Author(s): Schmidt, Kai Phillip; Laad, Mukul
 Source: PHYSICAL REVIEW LETTERS Volume: **104** Issue: **23** Article
 Number: **237201** DOI: [10.1103/PhysRevLett.104.237201](https://doi.org/10.1103/PhysRevLett.104.237201) Published: **JUN 7 2010**
 Times Cited: **1** (from Web of Science)



[[View abstract](#)]

33. Title: [Chirality of Triangular Antiferromagnetic Clusters as a Qubit](#)

Author(s): Georgeot, B.; Mila, F.
 Source: PHYSICAL REVIEW LETTERS Volume: **104** Issue: **20** Article
 Number: **200502** DOI: [10.1103/PhysRevLett.104.200502](https://doi.org/10.1103/PhysRevLett.104.200502) Published:
MAY 21 2010
 Times Cited: **8** (from Web of Science)



[[View abstract](#)]

34. Title: **Spin chirality and nontrivial charge dynamics in frustrated Mott insulators: spontaneous currents and charge redistribution**
 Author(s): Khomskii, D. I.
 Conference: **International Conference on Magnetism** Location: **Karlsruhe, GERMANY** Date: **JUL 26-31, 2009**
 Source: JOURNAL OF PHYSICS-CONDENSED MATTER Volume: **22**
 Issue: **16** Article Number: **164209** DOI: **10.1088/0953-8984/22/16/164209** Published: **APR 28 2010**
 Times Cited: **7** (from Web of Science)



[[View abstract](#)]

35. Title: **Single-Molecule Nanomagnets**
 Author(s): Friedman, Jonathan R.; Sarachik, Myriam P.
 Book Editor(s): Langer, JS
 Source: ANNUAL REVIEW OF CONDENSED MATTER PHYSICS, VOL 1 Book Series: **Annual Review of Condensed Matter Physics** Volume: **1**
 Pages: **109-128** DOI: **10.1146/annurev-conmatphys-070909-104053**
 Published: **2010**
 Times Cited: **9** (from Web of Science)



[[View abstract](#)]

36. Title: **EPR and inelastic neutron scattering in spin-frustrated V(3) and Cu(3) nanomagnets with Dzialoshinsky-Moriya exchange**
 Author(s): Belinsky, Moisey I.
 Book Editor(s): Goll, G; Lohneysen, HV; Loidl, A; et al.
 Conference: **International Conference on Magnetism (ICM 2009)**
 Location: **Karlsruhe, GERMANY** Date: **JUL 26-31, 2009**
 Sponsor(s): **Univ Karlsruhe; Forschungszentrum Karlsruhe; Int Union Pure & Appl Phys; City Karlsruhe; German Natl Sci Fdn; European Commission COST MPNS**
 Source: INTERNATIONAL CONFERENCE ON MAGNETISM (ICM 2009) Book Series: **Journal of Physics Conference Series** Volume: **200**
 Article Number: **072011** DOI: **10.1088/1742-6596/200/7/072011**
 Published: **2010**
 Times Cited: **1** (from Web of Science)



[Full Text](#)

[[View abstract](#)]

37. Title: **Quantum computing with electron spins in quantum dots**
 Author(s): Zak, Robert Andrzej; Roethlisberger, Beat; Chesi, Stefano; et al.
 Source: RIVISTA DEL NUOVO CIMENTO Volume: **33** Issue: **7** Pages: **345-399** DOI: **10.1393/ncr/i2010-10056-y** Published: **2010**
 Times Cited: **7** (from Web of Science)



[[View abstract](#)]

38. Title: **Toroidal moment in the molecular magnet V-15**
 Author(s): Zvezdin, A. K.; Kostyuchenko, V. V.; Popov, A. I.; et al.
 Source: PHYSICAL REVIEW B Volume: **80** Issue: **17** Article Number: **172404** DOI: **10.1103/PhysRevB.80.172404** Published: **NOV 2009**
 Times Cited: **4** (from Web of Science)



[[View abstract](#)]

39. Title: **Anapole moment and spin-electric interactions in rare-earth nanoclusters**
 Author(s): Popov, A. I.; Plokhov, D. I.; Zvezdin, A. K.
 Source: EPL Volume: **87** Issue: **6** Article Number: **67004** DOI: **10.1209/0295-5075/87/67004** Published: **SEP 2009**
 Times Cited: **6** (from Web of Science)



[[View abstract](#)]

40. Title: **Spin-frustrated V-3 and Cu-3 nanomagnets with Dzialoshinsky-Moriya exchange. 1. Inelastic neutron scattering and EPR in scalene, isosceles and equilateral trimers**
 Author(s): Belinsky, Moisey I.
 Source: CHEMICAL PHYSICS Volume: **361** Issue: **3** Pages: **137-151**
 DOI: **10.1016/j.chemphys.2009.05.012** Published: **JUL 15 2009**

Times Cited: 3 (from Web of Science)



- 41. Title: **Spin-frustrated V-3 and Cu-3 nanomagnets with Dzialoshinsky-Moriya exchange. 2. Spin structure, spin chirality and tunneling gaps**
 Author(s): Belinsky, Moisey I.
 Source: CHEMICAL PHYSICS Volume: 361 Issue: 3 Pages: 152-167
 DOI: 10.1016/j.chemphys.2009.05.013 Published: JUL 15 2009
 Times Cited: 2 (from Web of Science)



- 42. Title: **Tailoring effective exchange interactions via domain walls in coupled Heisenberg rings**
 Author(s): Srinivasa, Vanita; Levy, Jeremy
 Source: PHYSICAL REVIEW B Volume: 80 Issue: 2 Article Number: 024414
 DOI: 10.1103/PhysRevB.80.024414 Published: JUL 2009
 Times Cited: 3 (from Web of Science)



- 43. Title: **Exactly solvable Ising-Heisenberg chain with triangular XXZ-Heisenberg plaquettes**
 Author(s): Antonosyan, Diana; Bellucci, Stefano; Ohanyan, Vadim
 Source: PHYSICAL REVIEW B Volume: 79 Issue: 1 Article Number: 014432
 DOI: 10.1103/PhysRevB.79.014432 Published: JAN 2009
 Times Cited: 17 (from Web of Science)



Results: 43 Show 50 per page Page 1 of 1 Go Sort by: Publication Date -- newest to oldest

Output Records

Step 1: Selected Records on page All records on page Records to

Step 2: Authors, Title, Source plus Abstract Full Record plus Cited References

Step 3: [\[How do I export to bibliographic management software?\]](#)
 Save to: ENDNOTE® WEB ENDNOTE® ResearcherID
 Save to other Reference Software Save
 + (12)

43 records matched your query of the 53,033,624 in the data limits you selected.

View in: [简体中文](#) | [English](#) | [日本語](#)

All Databases

Select a Database

Web of Science

Additional Resources

[Search](#) | [Author Finder](#) | [Cited Reference Search](#) | [Advanced Search](#) | [Search History](#)
Web of Science[®] now with books[<< Return to All Databases](#)[<< Back to previous page](#)

Citing Articles

Title: **Quantum computing with molecular magnets**Author(s): **Stepanenko, Dimitrije ; Trif, Mircea ; Loss, Daniel**Source: **INORGANICA CHIMICA ACTA** Volume: **361** Issue: **14-15** Pages: **3740-3745** DOI:**10.1016/j.ica.2008.02.066** Published: **OCT 1 2008**This article has been cited by articles indexed in the databases listed below. [\[more information\]](#)

12 in All Databases

 12 in Web of Science

0 in BIOSIS Citation Index

0 in Chinese Science Citation Database

Results: 12

 Page 1 of 1 [Go](#)

Sort by:

Refine Results

Search within results for

[Search](#)Web of Science Categories [Refine](#) CHEMISTRY INORGANIC NUCLEAR (6) CHEMISTRY PHYSICAL (3) PHYSICS CONDENSED MATTER (3) CHEMISTRY MULTIDISCIPLINARY (2) CHEMISTRY ORGANIC (1)[more options / values...](#)Document Types [Refine](#) ARTICLE (6) REVIEW (4) PROCEEDINGS PAPER (3)[more options / values...](#)

Research Areas

Authors

Group Authors

Editors

Source Titles

Book Series Titles

Conference Titles

Publication Years

Organizations-Enhanced

Funding Agencies

Languages

Countries/Territories



(12)



Save to:

[ENDNOTE® WEB](#)[Analyze Results](#)[Create Citation Report](#)[ENDNOTE®](#)[ResearcherID](#)[more options](#)

Title: **Cyanido-Bridged Fe(III)-Mn(III) Heterobimetallic Materials Built From Mn(III) Schiff Base Complexes and Di- or Tri-Cyanido Fe(III) Precursors**

Author(s): Senapati, Tapas; Pichon, Celine; Ababei, Rodica; et al.

Source: INORGANIC CHEMISTRY Volume: 51 Issue: 6 Pages: 3796-

3812 DOI: 10.1021/ic2027708 Published: MAR 19 2012

Times Cited: 0 (from Web of Science)

[View abstract](#)

Title: **Single molecule magnets and the Lipkin-Meshkov-Glick model**

Author(s): Campos, J. A.; Hirsch, J. G.

Source: REVISTA MEXICANA DE FISICA Volume: 57 Issue: 3

Supplement: S Pages: 56-61 Published: JUL 2011

Times Cited: 0 (from Web of Science)

[View abstract](#)

Title: **Beyond the spin model: exchange coupling in molecular magnets with unquenched orbital angular momenta**

Author(s): Palii, Andrei; Tsukerblat, Boris; Klokishner, Sophia; et al.

Source: CHEMICAL SOCIETY REVIEWS Volume: 40 Issue: 6 Pages:

3130-3156 DOI: 10.1039/c0cs00175a Published: 2011

Times Cited: 14 (from Web of Science)

[View abstract](#)

Title: **Direct and two-phonon Orbach-Aminov type spin-lattice relaxation in molecular magnet V(15)**

Author(s): Tarantul, Alex; Tsukerblat, Boris

Book Group Author(s): IOP

Conference: International Conference on Resonances in Condensed







Matter Location: Fed Univ, Kazan, RUSSIA Date: JUN 21-25, 2011

For advanced refine options, use

[Analyze Results](#)

Source: INTERNATIONAL CONFERENCE ON RESONANCES IN CONDENSED MATTER: ALTSHULER100 Book Series: **Journal of Physics Conference Series** Volume: **324** Article Number: **012007** DOI: **10.1088/1742-6596/324/1/012007** Published: **2011** Times Cited: **0** (from Web of Science)

 [Full Text](#) [[View abstract](#)]

5. Title: **Magnetic relaxation in V-15 cluster: Direct spin-phonon transitions**
 Author(s): Tarantul, Alex; Tsukerblat, Boris
 Source: INORGANICA CHIMICA ACTA Volume: **363** Issue: **15** Pages: **4361-4367** DOI: **10.1016/j.ica.2010.07.080** Published: **DEC 10 2010** Times Cited: **2** (from Web of Science)
-  [[View abstract](#)]
6. Title: **Magneto-optical interactions in single-molecule magnets: Low-temperature photon-induced demagnetization**
 Author(s): Donnio, B.; Riviere, E.; Terazzi, E.; et al.
 Source: SOLID STATE SCIENCES Volume: **12** Issue: **8** Pages: **1307-1313** DOI: **10.1016/j.solidstatesciences.2010.06.003** Published: **AUG 2010** Times Cited: **0** (from Web of Science)
-  [[View abstract](#)]
7. Title: **Microspectroscopic Analysis of the X-Ray-induced Photoreduction in Fe- and Mn-containing SMMs**
 Author(s): Schmidt, Norman; Scheurer, Andreas; Sperner, Stefan; et al.
 Source: ZEITSCHRIFT FUR NATURFORSCHUNG SECTION B-A JOURNAL OF CHEMICAL SCIENCES Volume: **65** Issue: **3** Pages: **390-398** Published: **MAR 2010** Times Cited: **4** (from Web of Science)
-  [[View abstract](#)]
8. Title: **Magnetic exchange between metal ions with unquenched orbital angular momenta: basic concepts and relevance to molecular magnetism**
 Author(s): Palii, Andrei; Tsukerblat, Boris; Modesto Clemente-Juan, Juan; et al.
 Source: INTERNATIONAL REVIEWS IN PHYSICAL CHEMISTRY Volume: **29** Issue: **1** Pages: **135-230** Article Number: **PII 918980501** DOI: **10.1080/01442350903435256** Published: **2010** Times Cited: **19** (from Web of Science)
-  [[View abstract](#)]
9. Title: **Structural variety and magnetic properties of polynuclear assemblies based on 2-aminoglucose and tritopic triaminoguanidine ligands**
 Author(s): Plass, Winfried
 Source: COORDINATION CHEMISTRY REVIEWS Volume: **253** Issue: **19-20** Pages: **2286-2295** DOI: **10.1016/j.ccr.2008.12.002** Published: **OCT 2009** Times Cited: **13** (from Web of Science)
-  [[View abstract](#)]
10. Title: **Jahn-Teller Effect in Molecular Magnetism: An Overview**
 Author(s): Tsukerblat, Boris; Klokishner, Sophia; Palii, Andrew
 Book Editor(s): Koppel, H; Yarkony, DR; Barentzen, H
 Conference: **19th International Jahn-Teller Symposium** Location: **Univ Campus, Heidelberg, GERMANY** Date: **AUG 25-29, 2008**
 Source: JAHN-TELLER EFFECT: FUNDAMENTALS AND IMPLICATIONS FOR PHYSICS AND CHEMISTRY Book Series: **Springer Series in Chemical Physics** Volume: **97** Pages: **555-619** Published: **2009** Times Cited: **3** (from Web of Science)
-  [[View abstract](#)]

11. Title: **Bimetallic cyanido-bridged magnetic materials derived from manganese(III) Schiff-base complexes and pentacyanonitrosylferrate(II) precursor**
 Author(s): Ababei, Rodica; Li, Yang-Guang; Roubeau, Olivier; et al.
 Conference: **3rd International Symposium on Molecular Materials**
 Location: **Toulouse, FRANCE** Date: **JUL, 2008**
 Source: NEW JOURNAL OF CHEMISTRY Volume: **33** Issue: **6** Pages: **1237-1248** DOI: **10.1039/b903399h** Published: **2009**
 Times Cited: **13** (from Web of Science)



[[View abstract](#)]

12. Title: **Molecular magnetism: A philosophical perspective from a biased point of view**
 Author(s): Dei, Andrea
 Source: INORGANICA CHIMICA ACTA Volume: **361** Issue: **12-13** Pages: **3344-3355** DOI: **10.1016/j.ica.2008.02.032** Published: **SEP 1 2008**
 Times Cited: **0** (from Web of Science)



[[View abstract](#)]

Results: **12** [Show 50 per page](#) Page of 1 Sort by: [Publication Date -- newest to oldest](#)

Output Records

Step 1:

- Selected Records on page
 All records on page
 Records to

Step 2:

- Authors, Title, Source
 plus Abstract
 Full Record
 plus Cited References

Step 3: [\[How do I export to bibliographic management software?\]](#)

Save to: [ENDNOTE® WEB](#) [ENDNOTE®](#)
[ResearcherID](#)
 [Save](#)
 (12)

12 records matched your query of the 53,033,624 in the data limits you selected.

View in: | [简体中文](#) | [English](#) | [日本語](#)

Web of Science[®] now with books

[<< Return to All Databases](#)

[<< Back to previous page](#)

Citing Articles

Title: **Interference of heavy holes in an Aharonov-Bohm ring**
 Author(s): **Stepanenko, Dimitrije ; Lee, Minchul ; Burkard, Guido ; et al.**
 Source: **PHYSICAL REVIEW B** Volume: **79** Issue: **23** Article Number: **235301** DOI: **10.1103/PhysRevB.79.235301** Published: **JUN 2009**

This article has been cited by articles indexed in the databases listed below. [\[more information\]](#)

- 6 in All Databases
- 6 in Web of Science
- 0 in BIOSIS Citation Index
- 0 in Chinese Science Citation Database

Results: 6 Page 1 of 1 Sort by:

Hide Refine

Refine Results

Search within results for

Web of Science Categories

- PHYSICS CONDENSED MATTER (3)
- PHYSICS MULTIDISCIPLINARY (2)
- PHYSICS APPLIED (1)
- [more options / values...](#)

Document Types

- ARTICLE (6)
- Research Areas
- Authors
- Group Authors
- Editors
- Source Titles
- Book Series Titles
- Conference Titles
- Publication Years
- Organizations-Enhanced
- Funding Agencies
- Languages
- Countries/Territories

For advanced refine options, use

(12) |
 |
 |
 Save to: |
 |

- 1. Title: **In-plane mapping of buried InGaAs quantum rings and hybridization effects on the electronic structure**
 Author(s): Teodoro, M. D.; Malachias, A.; Lopes-Oliveira, V.; et al.
 Source: JOURNAL OF APPLIED PHYSICS Volume: 112 Issue: 1 Article Number: 014319 DOI: 10.1063/1.4733964 Published: JUL 1 2012
 Times Cited: 0 (from Web of Science)
- 2. Title: **Current-conserving Aharonov-Bohm interferometry with arbitrary spin interactions**
 Author(s): Lee, Minchul; Stepanenko, Dimitrije
 Source: PHYSICAL REVIEW B Volume: 85 Issue: 7 Article Number: 075316 DOI: 10.1103/PhysRevB.85.075316 Published: FEB 21 2012
 Times Cited: 0 (from Web of Science)
- 3. Title: **Generalized eigenvalue problem criteria for multiband-coupled systems: hole mixing phenomenon study**
 Author(s): Mendoza-Alvarez, A.; Flores-Godoy, J. J.; Fernandez-Anaya, G.; et al.
 Source: PHYSICA SCRIPTA Volume: 84 Issue: 5 Article Number: 055702 DOI: 10.1088/0031-8949/84/05/055702 Published: NOV 2011
 Times Cited: 0 (from Web of Science)
- 4. Title: **Anomalous spin-related quantum phase in mesoscopic hole rings**
 Author(s): Jaaskelainen, M.; Zulicke, U.
 Source: PHYSICAL REVIEW B Volume: 81 Issue: 15 Article Number: 155326 DOI: 10.1103/PhysRevB.81.155326 Published: APR 15 2010
 Times Cited: 2 (from Web of Science)

 [ View abstract]

- 5. Title: **Discovery of a Novel Linear-in-k Spin Splitting for Holes in the 2D GaAs/AIAs System**
 Author(s): Luo, Jun-Wei; Chantis, Athanasios N.; van Schilfgaarde, Mark; et al.
 Source: PHYSICAL REVIEW LETTERS Volume: **104** Issue: **6** Article Number: **066405** DOI: **10.1103/PhysRevLett.104.066405** Published: **FEB 12 2010**
 Times Cited: **4** (from Web of Science)

 [ View abstract]

- 6. Title: **Tunable spin currents in a biased Rashba ring**
 Author(s): Moldoveanu, V.; Tanatar, B.
 Source: PHYSICAL REVIEW B Volume: **81** Issue: **3** Article Number: **035326** DOI: **10.1103/PhysRevB.81.035326** Published: **JAN 2010**
 Times Cited: **9** (from Web of Science)

 [ View abstract]

Results: **6**  Show 50 per page  Page of 1   Sort by:  Publication Date -- newest to oldest 

Output Records





Step 1:


- Selected Records on page
- All records on page
- Records to

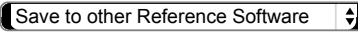

Step 2:



- Authors, Title, Source
 - plus Abstract
- Full Record
 - plus Cited References

Step 3: [\[How do I export to bibliographic management software?\]](#)

  Save to:  



  (12)

6 records matched your query of the 53,006,495 in the data limits you selected.

View in: | [简体中文](#) | [English](#) | [日本語](#)

Web of Science[®] now with books

[<< Return to All Databases](#)

[<< Back to previous page](#)

Citing Articles

Title: **Spin electric effects in molecular antiferromagnets**
 Author(s): **Trif, Mircea ; Troiani, Filippo ; Stepanenko, Dimitrije ; et al.**
 Source: **PHYSICAL REVIEW B** Volume: **82** Issue: **4** Article Number: **045429** DOI: **10.1103/PhysRevB.82.045429** Published: **JUL 28 2010**

This article has been cited by articles indexed in the databases listed below. [\[more information\]](#)

12 in All Databases

12 in Web of Science

0 in BIOSIS Citation Index

0 in Chinese Science Citation Database

Results: **12**

Page of 1

Sort by:

Hide Refine

Refine Results

Search within results for

Web of Science Categories

- PHYSICS CONDENSED MATTER (9)
 - MATERIALS SCIENCE MULTIDISCIPLINARY (2)
 - CHEMISTRY INORGANIC NUCLEAR (1)
 - CHEMISTRY PHYSICAL (1)
 - NANOSCIENCE NANOTECHNOLOGY (1)
- [more options / values...](#)

Document Types

- ARTICLE (12)
- Research Areas
- Authors
- Group Authors
- Editors
- Source Titles
- Book Series Titles
- Conference Titles
- Publication Years
- Organizations-Enhanced
- Funding Agencies
- Languages
- Countries/Territories

For advanced refine options, use

(12) |
 |
 |
 Save to: |
 |

1. Title: **Entanglement in a three spin system controlled by electric and magnetic fields**
 Author(s): Luczak, Jakub; Bulka, Bogdan R.
 Source: JOURNAL OF PHYSICS-CONDENSED MATTER Volume: **24** Issue: **37** Article Number: **375303** DOI: **10.1088/0953-8984/24/37/375303** Published: **SEP 19 2012**
 Times Cited: **0** (from Web of Science)
 []
2. Title: **First-principles studies of spin-orbit and Dzyaloshinskii-Moriya interactions in the {Cu-3} single-molecule magnet**
 Author(s): Nossa, J. F.; Islam, M. F.; Canali, C. M.; et al.
 Source: PHYSICAL REVIEW B Volume: **85** Issue: **8** Article Number: **085427** DOI: **10.1103/PhysRevB.85.085427** Published: **FEB 22 2012**
 Times Cited: **0** (from Web of Science)
 []
3. Title: **Density-functional-based prediction of a spin-ordered open-shell singlet in an unpassivated graphene nanofilm**
 Author(s): Pederson, Mark R.
 Source: PHYSICA STATUS SOLIDI B-BASIC SOLID STATE PHYSICS Volume: **249** Issue: **2** Pages: **283-291** DOI: **10.1002/pssb.201100796** Published: **FEB 2012**
 Times Cited: **0** (from Web of Science)
 []
4. Title: **Factorizing magnetic fields triggered by the Dzyaloshinskii-Moriya interaction: Application to magnetic trimers**
 Author(s): Florez, J. M.; Vargas, P.
 Source: JOURNAL OF MAGNETISM AND MAGNETIC MATERIALS Volume: **324** Issue: **1** Pages: **83-89** DOI:

10.1016/j.jmmm.2011.07.052 Published: JAN 2012
Times Cited: 1 (from Web of Science)

 [ View abstract]

5. Title: **Quantum magnetoelectric effect in the molecular crystal Dy₃**
Author(s): Plokhov, D. I.; Popov, A. I.; Zvezdin, A. K.
Source: PHYSICAL REVIEW B Volume: **84** Issue: **22** Article Number: **224436** DOI: **10.1103/PhysRevB.84.224436** Published: **DEC 28 2011**
Times Cited: **1** (from Web of Science)

 [ View abstract]

6. Title: **Electric polarization, toroidal moment, spin canting, and chirality induced by Dzialoshinsky-Moriya interactions in a V-3 cluster analog of multiferroics**
Author(s): Belinsky, Moisey I.
Source: PHYSICAL REVIEW B Volume: **84** Issue: **6** Article Number: **064425** DOI: **10.1103/PhysRevB.84.064425** Published: **AUG 24 2011**
Times Cited: **0** (from Web of Science)

 [ View abstract]

7. Title: **Electric Polarization Induced by Neel Order without Magnetic Superlattice: Experimental Study of Cu₃Mo₂O₉ and Numerical Study of a Small Spin Cluster**
Author(s): Kuroe, Haruhiko; Hosaka, Tomohiro; Hachiuma, Suguru; et al.
Source: JOURNAL OF THE PHYSICAL SOCIETY OF JAPAN Volume: **80** Issue: **8** Article Number: **083705** DOI: **10.1143/JPSJ.80.083705**
Published: **AUG 2011**
Times Cited: **2** (from Web of Science)

  [ View abstract]

8. Title: **Canonical perturbation theory for inhomogeneous systems of interacting fermions**
Author(s): Kostyrko, Tomasz; Bulka, Bogdan R.
Source: PHYSICAL REVIEW B Volume: **84** Issue: **3** Article Number: **035123** DOI: **10.1103/PhysRevB.84.035123** Published: **JUL 26 2011**
Times Cited: **2** (from Web of Science)

 [ View abstract]

9. Title: **Quantum memory coupled to cavity modes**
Author(s): Pedrocchi, Fabio L.; Chesì, Stefano; Loss, Daniel
Source: PHYSICAL REVIEW B Volume: **83** Issue: **11** Article Number: **115415** DOI: **10.1103/PhysRevB.83.115415** Published: **MAR 10 2011**
Times Cited: **2** (from Web of Science)

 [ View abstract]

10. Title: **Tuning the Energy Level Alignment at the SnPc/Ag(111) Interface Using an STM Tip**
Author(s): Toader, Marius; Hietschold, Michael
Source: JOURNAL OF PHYSICAL CHEMISTRY C Volume: **115** Issue: **7** Pages: **3099-3105** DOI: **10.1021/jp111478v** Published: **FEB 24 2011**
Times Cited: **7** (from Web of Science)

 [ View abstract]

11. Title: **Magnetic relaxation in basic iron(III) carboxylate [Fe₃O(O₂CPh)₆(H₂O)₃]ClO₄ center dot py**
Author(s): Georgopoulou, Anastasia N.; Sanakis, Yiannis; Boudalis, Athanassios K.
Source: DALTON TRANSACTIONS Volume: **40** Issue: **24** Pages: **6371-6374** DOI: **10.1039/c1dt10323g** Published: **2011**
Times Cited: **4** (from Web of Science)

 [ View abstract]

- 12. Title: **First-principles study of spin-electric coupling in a {Cu-3} single molecular magnet**
 Author(s): Islam, M. Fhokrul; Nossa, Javier F.; Canali, Carlo M.; et al.
 Source: PHYSICAL REVIEW B Volume: **82** Issue: **15** Article Number: **155446** DOI: **10.1103/PhysRevB.82.155446** Published: **OCT 26 2010**
 Times Cited: **6** (from Web of Science)



[[View abstract](#)]

Results: **12** [Show 50 per page](#) Page of 1 [Go](#) Sort by: [Publication Date -- newest to oldest](#)

Output Records

Step 1:

- Selected Records on page
- All records on page
- Records to

Step 2:

- Authors, Title, Source
 - plus Abstract
- Full Record
 - plus Cited References

Step 3: [\[How do I export to bibliographic management software?\]](#)

Save to: [ENDNOTE® WEB](#) [ENDNOTE®](#)
[ResearcherID](#)
[Save to other Reference Software](#) [Save](#)
 (12)

12 records matched your query of the 53,006,495 in the data limits you selected.

View in: | [简体中文](#) | [English](#) | [日本語](#)

Web of Science[®] now with books

<< Return to All Databases

Citing Articles Title: Singlet-triplet splitting in double quantum dots due to spin-orbit and hyperfine interactions
Author(s): Stepanenko, Dimitrije ; Rudner, Mark ; Halperin, Bertrand I. ; et al.
Source: PHYSICAL REVIEW B Volume: 85 Issue: 7 Article Number: 075416 DOI: 10.1103/PhysRevB.85.075416 Published: FEB 16 2012

This article has been cited by articles indexed in the databases listed below. [more information]

- 2 in All Databases
2 in Web of Science
0 in BIOSIS Citation Index
0 in Chinese Science Citation Database

Results: 2 Page 1 of 1 Go Sort by: Publication Date -- newest to oldest

Hide Refine

Refine Results

Search within results for

Search

- Web of Science Categories
Document Types
Research Areas
Authors
Group Authors
Editors
Source Titles
Book Series Titles
Conference Titles
Publication Years
Organizations-Enhanced
Funding Agencies
Languages
Countries/Territories

For advanced refine options, use

Analyze Results

+ (12) Save to: ENDNOTE WEB Analyze Results Create Citation Report
ENDNOTE ResearcherID more options

- 1. Title: Exchange-based CNOT gates for singlet-triplet qubits with spin-orbit interaction
Author(s): Klinovaja, Jelena; Stepanenko, Dimitrije; Halperin, Bertrand I.; et al.
Source: PHYSICAL REVIEW B Volume: 86 Issue: 8 Article Number: 085423
DOI: 10.1103/PhysRevB.86.085423 Published: AUG 13 2012
Times Cited: 0 (from Web of Science)
View abstract
2. Title: Spectroscopy of Spin-Orbit Quantum Bits in Indium Antimonide Nanowires
Author(s): Nadj-Perge, S.; Pribiag, V. S.; van den Berg, J. W. G.; et al.
Source: PHYSICAL REVIEW LETTERS Volume: 108 Issue: 16 Article Number: 166801 DOI: 10.1103/PhysRevLett.108.166801 Published: APR 19 2012
Times Cited: 7 (from Web of Science)
View abstract

Results: 2 Show 50 per page Page 1 of 1 Go Sort by: Publication Date -- newest to oldest

Output Records

Step 1: Selected Records on page Step 2: Authors, Title, Source Step 3: [How do I export to bibliographic management software?] Save to: ENDNOTE WEB ENDNOTE

- All records on page
- Records to
- plus Abstract
- Full Record
- plus Cited References

ResearcherID

Save to other Reference Software

Save

+ (12)

2 records matched your query of the 53,006,495 in the data limits you selected.

View in: | [简体中文](#) | [English](#) | [日本語](#)

© 2012 [Thomson Reuters](#) | [Terms of Use](#) | [Privacy Policy](#) | *Please give us your [feedback](#) on using Web of Knowledge.*

From: Sergei Kilin <kilin@dragon.bas-net.by>
To: Dimitrije.Stepanenko@unibas.ch
Subject: ICQOQI'2010
Date: Wed, 7 Apr 2010 22:53:19 +0300 (EEST) (04/07/2010 09:53:19 PM)

Dear Dr. Stepanenko,

I am sending you with a great pleasure an official invitation to the XIII International Conference on Quantum Optics and Quantum Information 2010. It will be very nice if you join the meeting and deliver an invited talk. I really hope that you can attend the Conference.

With my best regards,

Sergei Kilin

XIII International Conference on Quantum Optics and Quantum Information
(ICQOQI'2010)
May 28-June 1, 2010, Kyiv, Ukraine

Dear Dr. Stepanenko,

Organizing Committee of the XIII International Conference on Quantum Optics and Quantum Information invites you to take part in the activities of the meeting and deliver an invited talk.

XIII International Conference on Quantum Optics and Quantum Information organized by National Academy of Sciences of Ukraine, National Academy of Sciences of Belarus, Institute of Physics of NAS of Ukraine, M. M. Bogolyubov Institute for Theoretical Physics of NAS of Ukraine, B.I.Stepanov Institute of Physics of NAS of Belarus, Ukrainian Physical Society and Belarussian Physical Society will be held on May 28-June 1, 2010 in the city of Kyiv on the base of Presidium of NAS of Ukraine.

General idea of the conference is to bring together scientists and engineers from different fields (optics, atomic and molecular physics, solid state physics, computer science) which actively contribute to the field of Quantum Optics and Quantum information.

The traditional style for this Conference is the oral presentations followed by rather informal discussions during poster sessions. This International Conference will be the next one of a series of very successful meetings that were held in Minsk during the last 20 years in 1986, 1988, 1990, 1992, 1994, 1996, 1998, 2000, 2002, 2004, 2006, 2008.

If you have joint projects with quantum optics and quantum information scientists in the FSU or plan to start such an activity, it is a good chance to choose this event for your local meeting with colleagues.

The main topics include

- * TRADITIONAL QUANTUM OPTICS PROBLEMS, QUANTUM IMAGING
- * MATERIALS AND DEVICES FOR QUANTUM OPTICS AND QUANTUM INFORMATION:
 - nanophotonics
 - spintronics
 - strong optical nonlinearities
 - laser sources for quantum cryptography, including single photon sources and ultrashort lasers
 - single photon detectors
 - single quantum objects (molecules, atoms, solid state impurities, quantum dots, electrons, electron and nuclear spins): detection, control and manipulation
- * ENTANGLEMENT
 - characterization, creation and detection
 - entanglement in many bodies systems
 - metrology using entanglement
- * BUILDING HARDWARE FOR SCALABLE QUANTUM COMPUTERS
 - trapped ions
 - atomic systems (optical lattices)
 - solid state systems
 - photon based quantum information processing
- * QUANTUM MEMORY AND QUANTUM REPEATERS
- * INTERFACES BETWEEN PHOTONS AND ATOMIC QUBITS
- * QUANTUM ALGORITHMS
- * QUANTUM SIMULATIONS
- * FIBER-BASED AND FREE-SPACE QKD SYSTEMS

Conference language: English.

FOR REGISTRATION,
please send the following information to the Organizers by E-mail:
icqo2008@basnet.by or by fax: 375 172 84 08 79 by March, 15, 2010:

Family name:
First name:
Affiliation:
Mailing address:
Postal code:
City/Town:
Country:

Fax (with country code):

E-mail:

Title of the report:

Please also prepare the Abstract of the report (0.5 page) as a plain text or write it in TeX and send by E-mail by April, 20, 2010.

Usually we publish the reports as full length papers in Optics and Spectroscopy Journal after the meeting. So, it would be very nice if you keep this in mind and start preparing the manuscript in advance. Manuscripts should be prepared in LaTeX format.

ICQOQI'2010 SCHEDULE

The opening session (May 28, 10.00) and the following Plenary Session of the conference will be held in the conference hall of the Presidium of National Academy of Sciences of Ukraine. All the other sessions (May 29 - June 1) will be held in the Conference center of the Hotel Rus, located in the center of Kyiv. Welcome party will be held on May 28 on a riverboat traveling on the Dnepr River with beautiful panoramic views of the city. Conference dinner will take place on May 30 at the restaurant of Hotel Rus.

ACCOMMODATION

The participants are proposed to be accommodated in Hotel Rus, which offers the special rates for the conference participants. To book the room in Hotel Rus the accommodation form, available at the page <http://reserv.hotelrus.kiev.ua/cc.php> should be filled and sent to the hotel by fax or email given in the form. There are additional services proposed by the hotel: airport transfer and buffet lunches during the conference break between the morning and afternoon sessions. If you are interested in these services, please fill the corresponding boxes of the form. For safety of the transfer of your credit card information the proper fields should be filled in by hand. The accommodation form should be sent before 25th April 2010.

REGISTRATION FEE

Regular registration fee: 260 EURO (if paid by May, 15) or 300 EURO (if paid after May, 15).

Accompanying persons fee: 185 EURO (if paid by May, 15) or 225 EURO (if paid after May, 15).

Students' fee: 160 EURO (if paid by May, 15) or 200 EURO (if paid after May, 15).

Members' of Ukrainian, Belorussian and Russian Physical Societies fee: 110 EURO (if paid by May, 15) or 150 EURO (if paid after May, 15).

The regular conference registration fee covers: the admission to the conference sessions, the conference materials, the conference welcome party, and the conference coffee-breaks. The conference Registration fee should be paid by all

participants including invited and plenary speakers.

Accompanying person's registration fee covers the same points, as the regular one, except conference materials, and provides a full access to all the conference activities.

Optional fee include the conference dinner (40 EURO). The full conference fee is calculated as a sum of Registration fee and Optional fees.

The payment can be done by bank transfer or by credit cards (the details will be sent additionally).

REGISTRATION FEE PAYMENT

The payment can be done by bank transfer (preferable, see the details below) or on the conference site. If you need pro-forma invoice for registration fee payment, please request the Organizers by email icqoqi2010@basnet.by.

REQUISITES FOR BANK TRANSFER:

In the case of bank transfer the conference fee should be sent to the official partner of the conference, Advanced Laboratory Technologies Europe Ltd. Please note, that the deadline for bank transfer is May 17, 2010.

ADVANCED LABORATORY TECHNOLOGIES EUROPE LTD.

324-326 Regent Street, Suite 404
London W1B 3HH, UK

Beneficiary Bank: Nordea Bank Danmark A/S
Strandgave 3
Copenhagen DK-0900
Denmark

SWIFT: NDEADKKK
Sort Code: 2040

Account number 5036306396
IBAN: DK4620005036306396 EUR

Bank charges must be paid by the participant. Please make sure that bank transaction fees do not reduce the amount of payment. Please indicate your full name on the bank transfer. If payment is made for more than one person or by a company, please indicate all names.

For any questions concerning fee payment please contact Mr. Dmitry Melinevsky (dem@alt.ua), the representative of Advanced Laboratory Technologies Europe Ltd.

HISTORY OF ICQOQI

The information on traditions and activities of this series of seminars can be also found in special issues of Optics and Spectroscopy v.82 (1997) p.813, v.87 (1999) p.533, v.91(2001) No.3,4

v.94(2003) No.5 (http://www.maik.ru/contents/optics/optics5_3v94cont.htm),
v.99(2005) No.2(http://www.maik.ru/contents/optics/optics2_5v99cont.htm),
v.99(2005) No.3(http://www.maik.ru/contents/optics/optics3_5v99cont.htm),
v.103 (2007) No.1 (http://www.maik.ru/contents/optics/optics1_7v103cont.htm),
v.103 (2007) No.2 (http://www.maik.ru/contents/optics/optics2_7v103cont.htm),
v.103 (2007) No.3 (http://www.maik.ru/contents/optics/optics3_7v103cont.htm).

Conference Co chairs

Sergei Kilin
Leonid Yatsenko

Mailing address:
B.I.Stepanov Institute of Physics
National Academy of Sciences of Belarus
Nezavisimosti Avenue 68,
220072, Minsk
BELARUS

Contact Phone: 375 17 284 28 45
Fax: 375 172 84 08 79
e-mail: icqoqi2010@basnet.by
For updates visit <http://master.basnet.by>

Second Circular

ECMM2011

The third European Conference on Molecular Magnetism Paris, November 22-25, 2011

<http://www.ecmm-paris2011.u-psud.fr/>

Organized at "Les Cordeliers", 15, rue de l'école de médecine, 75006, Paris
(http://www.upmc.fr/fr/culture/patrimoine/sites_historiques/les_cordeliers.html) by

Université Paris Sud 11
Université Pierre et Marie Curie
Centre National de la Recherche Scientifique
Université Versailles-Saint Quentin
European Institute of Molecular Magnetism

INVITED SPEAKERS

(<http://www.ecmm-paris2011.u-psud.fr/spip.php?rubrique7>)

●Andreas Heinrich

IBM Research Center, Almaden
United States of America

http://domino.research.ibm.com/comm/research_people.nsf/pages/heinrich.index.html

●Mikhail Katsnelson

Institute for Molecules and Materials, Radboud University of Nijmegen
The Netherlands

<http://www.theorphys.science.ru.nl/people/katsnelson/>

●Stephen Mann FRS

Centre for Organized Matter Chemistry, University of Bristol
United Kingdom

<http://www.chm.bris.ac.uk/inorg/mann/webpage.htm>

●Jose Antonio Real

Department of Chemistry, Valencia University
Spain

<http://www.uv.es/smolmat/index.html>

●Dimitrije Stepanenko

Department of Physics, University of Basel
Switzerland

<http://quantumtheory.physik.unibas.ch/stepanenko/>

INVITED SPEAKERS (Olivier Kahn session)

Organized under the auspices of the French Academy of Science

●Bruno Chaudret, member of the French Academy of Science

Laboratoire de Chimie de Coordination du CNRS and Laboratoire de Physique et de Chimie des Nano-Objets, Toulouse, France

http://www.academie-sciences.fr/membres/C/Chaudret_Bruno.htm

●Jean-Jacques Girerd

Université Paris Sud 11, Institut de Chimie Moléculaire et des Matériaux d'Orsay, Orsay, France

<http://www.icmo.u-psud.fr/Labos/LCI/cv/jjg.php>

●Laureate of the Olivier Kahn Award



INSTITUT DE FRANCE
Académie des sciences



UPMC
SORBONNE UNIVERSITÉS

REGISTRATION

(<http://www.ecmm-paris2011.u-psud.fr/spip.php?rubrique10>)

Deadline for registration: 30 July 2011

PhD students

- Conference fee: 210€
- Conference fee and conference dinner attendance: 270€

Post-doctoral researcher

- Conference fee: 250€
- Conference fee and conference dinner attendance: 310€

Scientist

- Conference fee: 470€
- Conference fee and conference dinner attendance: 530€

Conference fee includes: Attendance at the sessions, lunches, refreshments throughout the meeting, conference bag including book of abstracts, free on-site wifi access
Please note that accommodation is not included in registration fee

ABSTRACT SUBMISSION

(<http://www.ecmm-paris2011.u-psud.fr/spip.php?rubrique11>)

Deadlines for abstract submission:

- **Oral communication 1 May 2011**
- **Poster communication 15 June 2011**

Abstract submission is strictly restricted to one per attendee. Submitting more than one abstract will cause systematic rejection. Please also note that there will be a limited number of presented posters.

ACCOMMODATION

<http://www.ecmm-paris2011.u-psud.fr/spip.php?rubrique13>)

Accommodation is not included in the registration fee. Delegates can book hotel rooms around the conference site, which is in the centre of Paris. A list of hotels will soon be provided on the website

VENUE

(<http://www.ecmm-paris2011.u-psud.fr/spip.php?rubrique12>)

The conference site in the centre of Paris at the following address: Les Cordeliers, 15, rue de l'école de médecine, 75006, Paris.

The closet stations are:

Metro Odéon, Line 4 or 10

RER B : Saint-Michel or Luxembourg

RER C : Saint-Michel



INSTITUT DE FRANCE
Académie des sciences



UPMC
SORBONNE UNIVERSITÉS

CONFERENCE PROGRAMM SCHEME

(<http://www.ecmm-paris2011.u-psud.fr/spip.php?rubrique8>)

Tuesday <i>november 22</i>	Wednesday <i>november 23</i>	Thursday <i>november 24</i>	Friday <i>november 25</i>
	9H00-9H40 PLENARY 2		9H00-9H40 PLENARY 4
	9H40-10H COMM8	O. KAHN SESSION	9H40-10H COMM20
	10H-10H20 COMM9		10H-10H20 COMM21
	10H20-10H40 COMM10		10H20-10H40 COMM22
	10H40-11H10 COFFEE BREAK	10H40-11H10 COFFEE BREAK	10H40-11H10 COFFEE BREAK
	11H10-11H30 COMM11		11H10-11H30 COMM23
	11H30-11H50 COMM12	O. KAHN SESSION	11H30-11H50 COMM24
	11H50-12H10 COMM13		11H50-12H10 COMM25
	12H10-12H30 COMM14		12H10-12H30 COMM26
12H30-14H REGISTRATION	12H30-14H30		12H30-14H30
14H-14H40 PLENARY 1	BUFFET & POSTER SESSION	13H00-15H00	BUFFET & POSTER SESSION
14H40-15H00 COMM1	14H30-15H10 PLENARY 3	BUFFET & POSTER SESSION	14H30-15H10 PLENARY 5
15H00-15H20 COMM2	15H10-15h30 COMM15	15H00-19H30 FREE TIME	15H10-15h30 COMM27
15H20-15H40 COMM3	15h30-15h50 COMM16		15h30-15h50 COMM28
15H40-16H00 COMM4	15H50-16H20 COFFEE BREAK		15H50-16H20 COFFEE BREAK
16H00-16H30 COFFEE BREAK	16H20-16H40 COMM17		16H20-16H40 COMM29
16H30-16H50 COMMS5	16H40-17H00 COMM18		16H40-17H00 COMM30
16H50-17H10 COMM6	17H00-17H20 COMM19		17H00-17H30 CLOSING ceremony
17H10-17H30 COMM7			
17H30-19H POSTER SESSION & COCKTAIL		19H30: CONFERENCE DINNER	



31/03/2012

Invitation to participate in the 5th Workshop of the NordForsk network: *Nanospintronics: theory and simulations.*

Dear Dr. Stepanenko,

The NordForsk network on nanospintronics that I coordinate will organize its 5th annual meeting at Borgholm on the island of Öland, off the coast of Kalmar, in the period June 12-14, 2012.

Highlights of the workshop are: (i) studies of individual magnetic impurities in semiconductors, which could lead to the realization of a novel class of versatile spin transistors consisting of one magnetic atom; (ii) new theoretical approaches studying the time evolutions of individual atomic spins (iii) and the recent detection of a special type of “quasi-particles” known as Majorana fermions, in semiconductor nanowires attached to superconducting leads.

More information on the workshop and on the network can be found at:

<http://lnu.se/research-groups/condensed-matter-physics/nanospintronics-network-/workshops/fifth-nordforsk-nanospintronics-workshop?l=en>

It is my pleasure to invite you to give a talk at the workshop. I would be grateful if you could let me know by May 16 whether or not you accept this invitation, and the title and abstract of your presentation. The network will reimburse living expenses and provide a contribution toward travel expenses.

Best wishes,

Carlo Maria Canali

Prof. Carlo Maria Canali

Linnaeus University, School of Computer Science, Physics, and Mathematics
Norra vägen 49, 391 82 Kalmar, Sweden

Phone +46(0)480-446995 Fax +46(0)480-446192 E-mail Carlo.Canali@lnu.se

Web <http://lnu.se/employee/carlo.canali?l=en>



[Previous abstract](#) | [Graphical version](#) | [Text version](#) | [Next abstract](#)

Session S23 - Quantum Computing I.

FOCUS session, Thursday morning, March 21

203, Indiana Convention Center

[S23.008] [Anisotropic Spin Exchange in Pulsed Quantum Gates](#)

Dimitrije Stepanenko, N.E. Bonesteel (NHMFL and Dept. of Physics, Florida State University), David DiVincenzo (IBM Research Division, T. J. Watson Research Center)

The exchange interaction between spins is a promising physical resource for carrying out two qubit quantum gates in quantum computers. For the idealized case of vanishing spin-orbit coupling, this interaction has the isotropic form $J \mathbf{S}_1 \cdot \mathbf{S}_2$, and the resulting quantum gates can be used for universal quantum computation with appropriate qubit coding. However, for any realistic implementation, there will be small anisotropic corrections to this purely isotropic form. When carrying out a quantum gate by pulsing this interaction, these corrections will not, in general, commute with themselves at different times. This makes the problem of determining the resulting quantum gate nontrivial. To address this, we derive an effective Hamiltonian which produces the same quantum gate as a given pulse, but which does commute with itself at different times. Through a symmetry analysis of this effective Hamiltonian we show that time-symmetric pulsing of the coupling automatically eliminates several undesirable terms. Further, we show that well-chosen pulse shapes produce an effectively isotropic exchange gate which can be used for universal quantum computation.

[Part S of program listing](#)



[Previous abstract](#) | [Graphical version](#) | [Text version](#) | [Next abstract](#)

Session X19 - Quantum Information Science: Semiconductors I.

ORAL session, Thursday afternoon, March 06

Room 11AB, Austin Convention Center

[X19.010] Spin-Orbit Coupling and Time-Symmetric Pulsing of Quantum Gates

D. Stepanenko, N.E. Bonesteel (Dept. of Physics and NHMFL, Florida State University), G. Burkard, D.P. DiVincenzo (IBM Research Division, T. J. Watson Research Center), D. Loss (Dept. of Physics and Astronomy, University of Basel)

We study the effect of spin-orbit coupling on quantum gates produced by pulsing the exchange interaction in double quantum dots. Spin-orbit coupling enters as a small spin rotation when electrons tunnel between dots. For an adiabatic pulse the gate is described by a unitary operator U acting on the four-dimensional Hilbert space of two qubits. Taking the spin-orbit precession axis to be parallel to \hat{z} , symmetry requires that $U = \exp[-i\lambda(S_1 \cdot S_2 + \beta(S_1^x S_2^y - S_1^y S_2^x) + \gamma(S_1^x S_2^x + S_1^y S_2^y) + \alpha(S_1^z - S_2^z)/2)]$. If $\lambda = \pi/2$ and $\alpha = 0$ the gate $U_g = U e^{i\pi S_2^z} U$ is independent of β and γ and, together with single spin rotations, can be used to form a controlled-not gate. This simple construction is spoiled if $\alpha \neq 0$. We give a nonperturbative proof that $\alpha = 0$ for time-symmetric pulsing. The effect of time asymmetry is studied by numerically integrating the Schrödinger equation using parameters appropriate for GaAs. We find $\alpha = C s r$ where s and r are dimensionless measures of spin-orbit coupling and pulse time asymmetry, respectively, and C is a number of order 1.

[Part X of program listing](#)

Abstract Submitted
for the MAR05 Meeting of
The American Physical Society

Control of Anisotropic Spin Exchange in Quantum Dots DIMITRIJE STEPANENKO, LAYLA HORMOZI, NICHOLAS BONESTEEL, Dept. of Physics, NHMFL and MARTECH, Florida State University, KERWIN FOSTER, Dillard University — To first order in spin-orbit coupling, the exchange interaction between spins in coupled quantum dots has the form $J(\mathbf{S}_1 \cdot \mathbf{S}_2 + \vec{\beta} \cdot (\mathbf{S}_1 \times \mathbf{S}_2))$. Recently we have shown that the ability to control the Dzyaloshinski-Moriya vector $\vec{\beta}$ is a potentially useful resource for quantum computation.¹ Here we study microscopically the degree of this control for coupled quantum dots in III-V semiconductors. At the level of the Hund-Mulliken (HM) approximation, in which one orbital is kept per dot, spin-orbit coupling enters as a small spin precession during interdot tunneling. $\vec{\beta}$ is proportional to this precession angle, and its dependence on dot parameters (e.g., interdot distance and dot size) can be strongly enhanced by ferromagnetic direct exchange. We determine the range of effective $\vec{\beta}$ values in quantum gates produced by pulsing the exchange interaction through numerical integration of the Schrödinger equation. Anisotropy in any particular gate is determined by the pulse duration, which is limited by decoherence for slow pulses and adiabaticity for fast pulses. The effects of going beyond the HM approximation, keeping more than one orbital per dot, are also discussed.

¹D.Stepanenko, N.E.Bonesteel, PRL **93**, 140501 (2004).

Dimitrije Stepanenko
Dept. of Physics, NHMFL and MARTECH, Florida State University

Date submitted: 01 Dec 2004

Electronic form version 1.4

Abstract Submitted
for the MAR05 Meeting of
The American Physical Society

Anisotropic Spin Exchange in Coupled Quantum Dots KERWIN FOSTER, Dillard University, LAYLA HORMOZI, DIMITRIJE STEPANENKO, NICHOLAS BONESTEEL, Dept. of Physics and NHMFL, Florida State University — We study the effect of spin-orbit coupling on the exchange interaction between spins in coupled quantum dots in III-V semiconductors. Our motivation is recent work showing that spin-orbit induced anisotropic corrections to the isotropic Heisenberg exchange are potentially useful for quantum computation.¹ We show that ferromagnetic direct exchange *enhances* the anisotropy of the interaction by reducing the size of the isotropic term — an important effect if these terms are going to be used for quantum computation. If only one orbital is kept per dot (Hund-Mulliken approximation) the effect of ferromagnetic direct exchange is overestimated for large dots.² This can be seen, for example, by noting that the calculated isotropic exchange coupling becomes *negative* in zero magnetic field for some interdot distances, in violation of the Lieb-Mattis theorem. To reliably estimate the enhancement of the anisotropy, we therefore work within an approximation in which more than one orbital is kept per dot, and show that this new approximation is applicable to a wider range of dot parameters. Apart from the improved reliability of the approximation, adding more orbitals gives new insight into the symmetry of the resulting interaction.

¹D. Stepanenko and N.E. Bonesteel, PRL **93**, 140501 (2004).

²G. Burkard, D. Loss, and D.P. DiVincenzo, PRB **59**, 2070 (1999).

Dimitrije Stepanenko
Dept. of Physics and NHMFL, Florida State University

Date submitted: 01 Dec 2004

Electronic form version 1.4

Abstract Submitted
for the MAR07 Meeting of
The American Physical Society

Enhancement of electron spin coherence by optical preparation of nuclear spins DIMITRIJE STEPANENKO, GUIDO BURKARD, University of Basel, GEZA GIEDKE, Max Planck Institute for Quantum Optics, Garching, ATAC IMAMOGLU, ETH Zurich — We study a large ensemble of nuclear spins interacting with a single electron spin in a quantum dot under optical excitation and photon detection. When a pair of applied laser fields satisfy two-photon resonance between the two ground electronic spin states, detection of light scattering from the intermediate exciton state acts as a weak quantum measurement of the effective magnetic (Overhauser) field due to the nuclear spins. If the spin were driven into a coherent population trapping state where no light scattering takes place, then the nuclear state would be projected into an eigenstate of the Overhauser field operator and electron decoherence due to nuclear spins would be suppressed: we show that this limit can be approached by adapting the laser frequencies when a photon is detected. We use a Lindblad equation to describe the time evolution of the driven system under photon emission and detection. Numerically, we find an increase of the electron coherence time from 5 ns to 500 ns after a preparation time of 10 microseconds.

Dimitrije Stepanenko
University of Basel

Date submitted: 17 Nov 2006

Electronic form version 1.4

Abstract Submitted
for the MAR07 Meeting of
The American Physical Society

Quantum gates between capacitively coupled double quantum dot two-spin qubits GUIDO BURKARD, DIMITRIJE STEPANENKO, University of Basel — We study the two-qubit controlled-not gate operating on qubits encoded in the spin state of a pair of electrons in a double quantum dot. We assume that the electrons can tunnel between the two quantum dots encoding a single qubit, while tunneling between the quantum dots that belong to different qubits is forbidden. Therefore, the two qubits interact exclusively through the direct Coulomb repulsion of the electrons. We find that entangling two-qubit gates can be performed by the electrical biasing of quantum dots and/or tuning of the tunneling matrix elements between the quantum dots within the qubits. The entangling interaction can be controlled by tuning the bias through the resonance between the singly-occupied and doubly-occupied singlet ground states of a double quantum dot.

Guido Burkard
University of Basel

Date submitted: 09 Nov 2006

Electronic form version 1.4

HL 11.1 Mon 14:45 H15

Quantum gates between capacitively coupled double quantum dot two-spin qubits — •Dimitrije Stepanenko and Guido Burkard — Department of Physics and Astronomy, University of Basel, Klingelbergstrasse 82, CH-4056 Basel, Switzerland

We study the two-qubit controlled-not gate operating on qubits encoded in the spin state of a pair of electrons in a double quantum dot. We assume that the electrons can tunnel between the two quantum dots encoding a single qubit, while tunneling between the quantum dots that belong to different qubits is forbidden. Therefore, the two qubits interact exclusively through the direct Coulomb repulsion of the electrons. We find that entangling two-qubit gates can be performed by the electrical biasing of quantum dots and/or tuning of the tunneling matrix elements between the quantum dots within the qubits. The entangling interaction can be controlled by tuning the bias through the resonance between the singly-occupied and doubly-occupied singlet ground states of a double quantum dot.

**Program of the
QSIT Arosa Meeting
January 21 – 23, 2009 in Arosa**

Wednesday, January 21, 2008

14h00	Arrival	
16h00 – 18h00	Poster Session	
19h00	Dinner	
	Chair: Klaus Ensslin	
20h30 – 20h45	Welcome	Klaus Ensslin
20h45 – 21h15	Coherent pumping of a Mott insulator: Fermi golden rule versus Rabi oscillations	Fabian Hassler
21h15 – 22h00	Generation and Tomography of Two-Qubit entangled states in superconducting circuits	Peter J. Leek <i>and</i> Stefen Filipp
22h00	Welcome Apéro	

Thursday, January 22, 2008

7h30	Breakfast	
	Chair: Cyril Stark	
8h30 – 9h00	A new approach to quantifying information	Roger Colbeck
9h00 – 9h30	Solid State Quantum Memories for Quantum Repeaters	Hugues de Riedmatten
9h30 – 10h00	Spin-orbit interaction as a tool for spin manipulation in semiconductors	Matthias Studer
10h00	Coffee Break	
	Chair: Susanne Dröscher	
10h30 – 11h15	Dragging of quantum dot resonances <i>and</i> Optical signatures of the Kondo effect in a quantum dot	Alex Högele
11h15 – 12h00	Rydberg Stark deceleration and trapping of molecules <i>and</i> Deceleration and magnetic trapping of hydrogen atoms	Hakan Tureci Stephen Hogan Alex Wiederkehr
12h00	Skiing	
17h00 – 18h30	Poster Session	
19h00	Dinner	
	Chair: Gabriel Puebla	
20h30 – 21h15	Dynamical Coupling between a Bose-Einstein Condensate and a Cavity Optical Lattice <i>and</i> A Mott insulator of fermionic atoms in an optical lattice	Christine Guerlin
21h15 – 22h00	Phonon driven current in a double quantum dot <i>and</i> Photon driven current in a double quantum dot	Niels Strohmaier Urszula Gasser-Szerrer
22h00	Award Ceremony of the ski race	Bruno Küng

Friday, January 23, 2008

7h30	Breakfast	
	Chair: Christian May	
8h30 – 9h00	Symmetry implies independence	Dejan Dukaric
9h00 – 9h30	Interference of heavy holes in an Aharonov-Bohm ring	Dimitrije Stepanenko
9h30 – 10h00	Introduction to device-independent security	Esther Hänggi
10h00	Coffee Break	
	Chair: Kristian Baumann	
10h30 – 11h15	Single Molecule Quantum Optics	Martin Pototschnig <i>and</i> Robert Lettow
11h15 – 11h45	Fermionized photons in an array of driven dissipative cavities	Iacopo Carusotto
11h45 – 12h00	Poster Quiz: Solutions and awards	Tilman Esslinger
12h00	End of the Meeting	

Verhandlungen Φ

der Deutschen Physikalischen Gesellschaft e.V.

Regensburg 2010 – individual program

[Parts](#) | [Days](#) | [Selection](#) | [Search](#) | [Help](#)

MA: Fachverband Magnetismus

MA 2: Bio- and Molecular Magnetism

MA 2.2, Monday, 11:00–11:15, H10

selection status for this contribution:

Electric quantum control of spins in molecular magnets — •MIRCEA TRIF¹,
DIMITRIJE STEPANENKO¹, FILIPPO TROIANI², and DANIEL LOSS¹ — ¹Department of Physics,
University of Basel, Klingelbergstrasse 82, CH-4056 Basel, Switzerland

— ²CNR-INFM National Research Center S3 c/o Dipartimento di Fisica via G.
Campi 213/A, 41100, Modena, Italy

Single molecule magnets show clear signatures of coherent behavior. The control of the spins can allow for the quantum information processing and study of quantum dynamics. Electric fields are good for quantum control at the nanoscale. There are many SMMs and it is hard to predict which ones are suitable for control. Here, we provide two tools for the search for suitable SMMs. We analyze the form and mechanisms that lead to spin-electric coupling in the molecules with the shape of regular polygons. We find that the SEC in triangles is governed by the modification of the exchange interaction, while in pentagon the spin-electric coupling proceeds via spin-orbit interaction. The symmetry analysis leaves the coupling constant undetermined, and we apply a Hubbard model to single-molecule magnet to find a connection between the spin-electric coupling and the properties of the chemical bonds in a molecule. We study the experimental signatures of spin-electric coupling in the standard experiments, NMR, ESR, and thermodynamics.

Verhandlungen Φ

der Deutschen Physikalischen Gesellschaft e.V.

Regensburg 2010 – individual program

[Parts](#) | [Days](#) | [Selection](#) | [Search](#) | [Help](#)

HL: Fachverband Halbleiterphysik

HL 26: Spin-controlled Transport II

HL 26.7, Tuesday, 15:45–16:00, H14

selection status for this contribution:

Interference of heavy holes in an Aharonov-Bohm ring — •DIMITRIJE STEPANENKO¹, MINCHUL LEE², GUIDO BURKARD³, and DANIEL LOSS¹ — ¹University of Basel, Basel, Switzerland — ²Kyung Hee University, Yongin, Korea — ³University of Konstanz, Konstanz, Germany

We study the coherent transport of heavy holes through a one-dimensional ring in the presence of spin-orbit coupling. Spin-orbit interaction of holes, cubic in the in-plane components of momentum, gives rise to an angular momentum dependent spin texture of the eigenstates and influences transport. We analyze the dependence of the resulting differential conductance of the ring on hole polarization of the leads and the signature of the textures in the Aharonov-Bohm oscillations when the ring is in a perpendicular magnetic field. We find that the polarization-resolved conductance reveals whether the dominant spin-orbit coupling is of Dresselhaus or Rashba type, and that the cubic spin-orbit coupling can be distinguished from the conventional linear coupling by observing the four-peak structure in the Aharonov-Bohm oscillations.

Abstract Submitted
for the MAR09 Meeting of
The American Physical Society

Spin-Electric Coupling in Molecular Magnets MIRCEA TRIF, Department of Physics, University of Basel, Klingelbergstrasse 82, CH-4056 Basel, Switzerland, FILIPPO TROIANI, DIMITRIJE STEPANENKO, DANIEL LOSS, BASEL/MODENA COLLABORATION — We study the triangular antiferromagnet Cu_3 in external electric fields, using symmetry group arguments and a Hubbard model approach. We identify a spin-electric coupling caused by an interplay between spin exchange, spin-orbit interaction, and the chirality of the underlying spin texture of the molecular magnet. This coupling allows for the electric control of the spin (qubit) states, e.g. by using an STM tip or a microwave cavity. We propose an experimental test for identifying molecular magnets exhibiting spin-electric effects.

Mircea Trif
Department of Physics, University of Basel,
Klingelbergstrasse 82, CH-4056 Basel, Switzerland

Date submitted: 18 Dec 2008

Electronic form version 1.4

Abstract Submitted
for the MAR10 Meeting of
The American Physical Society

Quantum control of molecular antiferromagnets: an approach based on electric fields MIRCEA TRIF, DIMITRIJE STEPANENKO, University of Basel, FILIPPO TROIANI, CNR-INFN National Research Center, Modena, DANIEL LOSS, University of Basel — Single molecule magnets show clear signatures of coherent behavior, and have a wide variety of effective low-energy spin Hamiltonian suitable for encoding qubits and spin-based quantum information processing. At the nanoscale, the preferred mechanism for control of quantum systems involves application of electric fields, which can be locally applied, and rapidly switched. In this work, we provide the tools for the search for single molecule magnets suitable for electric control. We analyze the mechanisms that leads to spin-electric coupling in the molecules with the shape of regular polygons. We find that the spin-electric coupling in triangular molecules is governed by the modification of the exchange interaction, while in pentagonal molecules the spin-electric coupling proceeds via spin-orbit interaction. We apply a Hubbard model to single-molecule magnet to find a connection between the spin-electric coupling and the properties of the chemical bonds in a molecule. We study the experimental signatures of spin-electric coupling in nuclear magnetic resonance, electron spin resonance, magnetization, electric polarization, and specific heat of the molecules.

Mircea Trif
University of Basel

Date submitted: 23 Nov 2009

Electronic form version 1.4

Abstract Submitted
for the MAR12 Meeting of
The American Physical Society

Sorting Category: 08.1.1 (T)

Singlet-triplet splitting in double dots due to spin orbit and hyperfine interactions DIMITRIJE STEPANENKO, University of Basel, MARK RUDNER, BERTRAND I. HALPERIN, Harvard University, DANIEL LOSS, University of Basel — We analyze the low-energy spectrum of a detuned double quantum dot in the presence of magnetic fields, spin orbit interaction, and nuclear spins, and focus on the regime of spin blockade. Starting from a realistic model for two interacting electrons in a double dot, we derive perturbatively an effective two-level Hamiltonian in the vicinity of an avoided crossing between singlet and triplet levels, which are coupled by the spin-orbit and hyperfine interactions. We evaluate the level splitting at the anticrossing in various parameter regimes, and show that it depends on two controllable parameters: the angle between the external magnetic field and the internal spin orbit field, and on the detuning, as well as on the difference between nuclear fields in the two dots. We identify a parameter regime where spin orbit and hyperfine terms can become of equal strength and propose a protocol for tuning their relative sizes.

Prefer Oral Session
 Prefer Poster Session

Dimitrije Stepanenko
Dimitrije.Stepanenko@unibas.ch
University of Basel

Date submitted: 19 Jan 2012

Electronic form version 1.4

Anisotropic Spin Exchange in Pulsed Quantum Gates

N. E. Bonesteel and D. Stepanenko

Department of Physics and National High Magnetic Field Laboratory, Florida State University, Tallahassee, Florida 32310

D. P. DiVincenzo

IBM Research Division, T. J. Watson Research Center, Yorktown Heights, New York 10598

(Received 2 July 2001; published 30 October 2001)

We show how to eliminate the first-order effects of the spin-orbit interaction in the performance of a two-qubit quantum gate. Our procedure involves tailoring the time dependence of the coupling between neighboring spins. We derive an effective Hamiltonian which permits a systematic analysis of this tailoring. Time-symmetric pulsing of the coupling automatically eliminates several undesirable terms in this Hamiltonian. Well chosen pulse shapes can produce an effectively isotropic exchange gate, which can be used in universal quantum computation with appropriate coding.

DOI: 10.1103/PhysRevLett.87.207901

PACS numbers: 03.67.Lx, 71.70.Ej, 85.35.Be

The exchange interaction between spins is a promising physical resource for constructing two-qubit quantum gates in quantum computers [1–5]. In the idealized case of vanishing spin-orbit coupling, this interaction is isotropic, and any Hamiltonian describing time-dependent exchange between two spin-1/2 qubits, $H_0(t) = J(t)\mathbf{S}_1 \cdot \mathbf{S}_2$, commutes with itself at different times. Thus, the resulting quantum gate depends on $J(t)$ only through its time integral—a convenient simplification, particularly because, when carrying out quantum gates, the exchange interaction should be pulsed adiabatically on time scales longer than $\hbar/\Delta E$, where ΔE is a typical level spacing associated with the internal degrees of freedom of the qubits [3]. In addition, isotropic exchange alone has been shown to be sufficient for universal quantum computation, provided the logical qubits of the computer are properly encoded [6,7].

Given the potential advantages of isotropic exchange for quantum gates, it is important to understand the effect of the inevitable anisotropic corrections due to spin-orbit coupling. When these corrections are included, the Hamiltonian describing time-dependent exchange is

$$H(t) = J(t)[\mathbf{S}_1 \cdot \mathbf{S}_2 + \mathcal{A}(t)], \quad (1)$$

where

$$\mathcal{A}(t) = \boldsymbol{\beta}(t) \cdot (\mathbf{S}_1 \times \mathbf{S}_2) + \mathbf{S}_1 \cdot \boldsymbol{\Gamma}(t) \cdot \mathbf{S}_2. \quad (2)$$

Here $\boldsymbol{\beta}(t)$ is the Dzyaloshinski-Moriya vector, which is first order in spin-orbit coupling, and $\boldsymbol{\Gamma}(t)$ is a symmetric tensor which is second order in spin-orbit coupling [8]. Although these corrections may be small, they will, in general, not be zero unless forbidden by symmetry. For example, Kavokin has recently estimated that $\boldsymbol{\beta}(t)$ could be on the order of 0.01 for coupled quantum dots in GaAs [9].

In this Letter, we construct the quantum gates produced by pulsing $H(t)$. This is nontrivial because $H(t)$ typically does not commute with itself at different times. We represent the resulting gates using an effective Hamiltonian $\overline{H}(t)$, which we derive perturbatively in powers of the

spin-orbit coupling. $\overline{H}(t)$ is simple to work with because it *does* commute with itself at different times. As an application of this effective Hamiltonian, we use it to tailor pulse forms that effectively eliminate any first-order anisotropic corrections.

The quantum gate obtained by pulsing a particular $H(t)$ is found by solving the time-dependent Schrödinger equation $i\frac{d}{dt}|\Psi(t)\rangle = H(t)|\Psi(t)\rangle$, where $|\Psi(t)\rangle$ is the state vector describing the two spin-1/2 qubits (here, and in what follows, $\hbar = 1$). In general this problem cannot be solved analytically. However, since we expect spin-orbit coupling to be small, it is natural to attempt a perturbative solution in powers of $\boldsymbol{\beta}(t)$ and $\boldsymbol{\Gamma}(t)$. To do this, it is first necessary to solve the unperturbed [$\mathcal{A}(t) = 0$] problem exactly. This corresponds to pulsing the isotropic exchange interaction, for which the unitary time evolution operator at time t is

$$\begin{aligned} U_0(t) &= T \exp\left(-i \int_{-\infty}^t J(t')\mathbf{S}_1 \cdot \mathbf{S}_2 dt'\right) \\ &= \exp[-ix(t)\mathbf{S}_1 \cdot \mathbf{S}_2], \end{aligned} \quad (3)$$

where

$$x(t) = \int_{-\infty}^t J(t') dt'. \quad (4)$$

Here T is the usual Dyson time ordering, and the second equality in (3) follows from the fact that isotropic exchange commutes with itself at different times. The unperturbed quantum gate produced by a full pulse is then $U_0(t \rightarrow \infty) = \exp(-i\lambda\mathbf{S}_1 \cdot \mathbf{S}_2)$, where $\lambda = \int_{-\infty}^{\infty} J(t) dt$ is the pulse strength. This is a well studied class of quantum gates [1]. For $\lambda = \pi$ the result is a simple swap, and for $\lambda = \pi/2$ it is a “square root of swap” which, in conjunction with single-qubit rotations, can be used to construct a controlled-not gate [1].

We now consider the effect of the anisotropic corrections $\mathcal{A}(t)$. Given the evolution operator for the unperturbed system, it is possible to recast the problem

in the interaction picture by introducing the state vector $|\Psi_I(t)\rangle \equiv U_0^\dagger(t)|\Psi(t)\rangle$ which satisfies the Schrödinger equation $i\frac{d}{dt}|\Psi_I(t)\rangle = J(t)\mathcal{A}_I(t)|\Psi_I(t)\rangle$, where $\mathcal{A}_I(t) = U_0^\dagger(t)\mathcal{A}(t)U_0(t)$. A formal expression for the unitary operator describing a full pulse in this picture is then

$$U_I = T \exp\left(-i \int_{-\infty}^{\infty} J(t)\mathcal{A}_I(t) dt\right). \quad (5)$$

Expanding the exponential in (5) generates the standard time-dependent perturbation theory expansion for U_I in powers of $\mathcal{A}_I(t)$. Returning to the Schrödinger picture, the unitary operator describing the full quantum gate is $U = \exp(-i\lambda\mathbf{S}_1 \cdot \mathbf{S}_2)U_I$.

Rather than simply carrying out the perturbation expansion for U_I , it is useful to parametrize the resulting quantum gate in terms of an effective Hamiltonian of the form

$$\overline{H}(t) = J(t)(\mathbf{S}_1 \cdot \mathbf{S}_2 + \overline{\mathcal{A}}), \quad (6)$$

where the time dependence of $J(t)$ is the same as in $H(t)$, and $\overline{\mathcal{A}}$ is independent of time. Unlike $H(t)$, the effective Hamiltonian $\overline{H}(t)$ commutes with itself at different times. Thus, after a full pulse, $\overline{H}(t)$ yields the quantum gate $\overline{U} = \exp[-i\lambda(\mathbf{S}_1 \cdot \mathbf{S}_2 + \overline{\mathcal{A}})]$. Our goal is then to find the operator $\overline{\mathcal{A}}$ for which \overline{U} is equal to the quantum gate produced by a full pulse of $H(t)$.

Because $H(t)$ is traceless at all times t , the corresponding unitary time evolution operator has determinant 1, i.e., $U \in \text{SU}[4]$. Requiring that our effective Hamiltonian produces the same quantum gate then implies that $\overline{\mathcal{A}}$ must also be a traceless Hermitian operator. The most general such operator acting on the Hilbert space of two qubits can be written

$$\begin{aligned} \overline{\mathcal{A}} = & \overline{\boldsymbol{\beta}} \cdot (\mathbf{S}_1 \times \mathbf{S}_2) + \mathbf{S}_1 \cdot \overline{\boldsymbol{\Gamma}} \cdot \mathbf{S}_2 \\ & + \frac{\overline{\boldsymbol{\alpha}}}{2} \cdot (\mathbf{S}_1 - \mathbf{S}_2) + \frac{\overline{\boldsymbol{\mu}}}{2} \cdot (\mathbf{S}_1 + \mathbf{S}_2), \end{aligned} \quad (7)$$

where $\overline{\boldsymbol{\Gamma}}$ is a symmetric tensor. This can be seen by noting that $\overline{\mathcal{A}}$ is indeed traceless and Hermitian, and has 15 independent real valued parameters, the number of degrees of freedom for a 4×4 traceless Hermitian matrix.

Before proceeding it is instructive to classify the terms in $\overline{\mathcal{A}}$ according to their symmetry properties under inversion ($\mathbf{S}_1 \leftrightarrow \mathbf{S}_2$) and time reversal ($\mathbf{S}_i \rightarrow -\mathbf{S}_i$). Under inversion $\overline{\boldsymbol{\beta}}$ and $\overline{\boldsymbol{\alpha}}$ change sign, while $\overline{\boldsymbol{\Gamma}}$ and $\overline{\boldsymbol{\mu}}$ do not. Since $\boldsymbol{\beta}(t)$ also changes sign under inversion this implies that $\overline{\boldsymbol{\beta}}$ and $\overline{\boldsymbol{\alpha}}$ are first order in spin-orbit coupling, while $\overline{\boldsymbol{\Gamma}}$ and $\overline{\boldsymbol{\mu}}$ are second order. Under time reversal $\overline{\boldsymbol{\alpha}}$ and $\overline{\boldsymbol{\mu}}$ change sign, while $\overline{\boldsymbol{\beta}}$ and $\overline{\boldsymbol{\Gamma}}$ are unaffected. We therefore expect that for time-reversal symmetric pulses, i.e., pulses for which $H(t_0 - t) = H(t)$ (where t_0 is the center of the pulse), $\overline{\boldsymbol{\alpha}}$ and $\overline{\boldsymbol{\mu}}$ will vanish.

To determine $\overline{\mathcal{A}}$ for a given pulse, we note that the requirement that $U = \overline{U}$ implies

$$\begin{aligned} T \exp\left(-i \int_{-\infty}^{\infty} J(t)\mathcal{A}_I(t) dt\right) \\ = T \exp\left(-i \int_{-\infty}^{\infty} J(t)\overline{\mathcal{A}}_I(t) dt\right), \end{aligned} \quad (8)$$

where $\overline{\mathcal{A}}_I(t) = U_0^\dagger(t)\overline{\mathcal{A}}U_0(t)$. Expanding both sides of (8) to a given order in spin-orbit coupling and equating matrix elements yields a set of 15 independent equations. These equations can then be solved for the parameters in $\overline{\mathcal{A}}$ in terms of $J(t)$, $\boldsymbol{\beta}(t)$, and $\boldsymbol{\Gamma}(t)$.

We have carried out this calculation to obtain the following expressions valid to second order in spin-orbit coupling [i.e., second order in $\boldsymbol{\beta}(t)$ and first order in $\boldsymbol{\Gamma}(t)$]:

$$\overline{\boldsymbol{\alpha}} = \frac{1}{2 \sin(\lambda/2)} \int_{-\infty}^{\infty} \boldsymbol{\beta}(t) \sin\left(x(t) - \frac{\lambda}{2}\right) J(t) dt, \quad (9)$$

$$\overline{\boldsymbol{\beta}} = \frac{1}{2 \sin(\lambda/2)} \int_{-\infty}^{\infty} \boldsymbol{\beta}(t) \cos\left(x(t) - \frac{\lambda}{2}\right) J(t) dt, \quad (10)$$

$$\overline{\boldsymbol{\mu}} = \frac{1}{4\lambda} \int_{-\infty}^{\infty} J(t_1) dt_1 \int_{-\infty}^{t_1} J(t_2) dt_2 \{[\boldsymbol{\beta}(t_1) \times \boldsymbol{\beta}(t_2)] \cos[x(t_1) - x(t_2)] + 2(\overline{\boldsymbol{\alpha}} \times \overline{\boldsymbol{\beta}}) \sin[x(t_1) - x(t_2)]\}, \quad (11)$$

and

$$\overline{\boldsymbol{\Gamma}}_{ab} = \frac{1}{\lambda} \int_{-\infty}^{\infty} \boldsymbol{\Gamma}_{ab}(t) J(t) dt + \frac{1}{4\lambda} \int_{-\infty}^{\infty} J(t_1) dt_1 \int_{-\infty}^{t_1} J(t_2) dt_2 I_{ab}(t_1, t_2) \sin[x(t_1) - x(t_2)], \quad (12)$$

where

$$I_{ab}(t_1, t_2) = 2[\boldsymbol{\beta}(t_1) \cdot \boldsymbol{\beta}(t_2) - \overline{\boldsymbol{\beta}}^2 - \overline{\boldsymbol{\alpha}}^2] \delta_{ab} - [\beta_a(t_1)\beta_b(t_2) + \beta_a(t_2)\beta_b(t_1) - 2\overline{\beta}_a\overline{\beta}_b - 2\overline{\alpha}_a\overline{\alpha}_b]. \quad (13)$$

The criterion for the validity of these expressions is that $|\lambda\boldsymbol{\beta}|, |\lambda\overline{\boldsymbol{\alpha}}| \ll 1$, where the factor of λ is included because it is the product $\lambda\overline{\mathcal{A}}$ that enters the unitary operator U . It is then apparent that, for any finite $\boldsymbol{\beta}(t)$ and $\boldsymbol{\Gamma}(t)$, our expansion breaks down when $\lambda \rightarrow 2\pi n$ for $n = \pm 1, \pm 2, \dots$, because $\sin(\lambda/2) \rightarrow 0$ at these points.

However, for $\lambda \rightarrow 0$, while $\overline{\boldsymbol{\alpha}}$ and $\overline{\boldsymbol{\beta}}$ may diverge, $\lambda\overline{\boldsymbol{\alpha}}$ and $\lambda\overline{\boldsymbol{\beta}}$ will always remain finite, and so, provided $\boldsymbol{\beta}(t)$ and $\boldsymbol{\Gamma}(t)$ are small, our expansion remains valid in this limit [10].

As expected from symmetry considerations, we find that $\overline{\boldsymbol{\beta}}$ and $\overline{\boldsymbol{\alpha}}$ are first order in spin-orbit coupling, while $\overline{\boldsymbol{\Gamma}}$

and $\overline{\boldsymbol{\mu}}$ are second order. It is also readily verified that for a time-reversal symmetric pulse the integrals (9) and (11) for $\overline{\boldsymbol{\alpha}}$ and $\overline{\boldsymbol{\mu}}$ vanish. Thus, these non-time-reversal symmetric terms are generated only by pulses that are themselves not time-reversal symmetric.

Given the possibility of using the exchange interaction alone to perform universal quantum computation [6,7], which depends crucially on the interaction being as close to isotropic as possible, a natural question arises: Is it possible to ameliorate the effect of spin-orbit induced anisotropy on exchange-based quantum gates? We show below that the answer is yes—by carefully shaping pulses, it is possible to effectively eliminate the first-order anisotropy terms leaving only a residual second-order anisotropy.

There are two first-order terms in $\overline{H}(t)$, $\overline{\boldsymbol{\alpha}}$ and $\overline{\boldsymbol{\beta}}$. We have already seen how to eliminate $\overline{\boldsymbol{\alpha}}$. By choosing a time-reversal symmetric pulse both $\overline{\boldsymbol{\alpha}}$ and $\overline{\boldsymbol{\mu}}$ will vanish from $\overline{H}(t)$. Although $\overline{\boldsymbol{\beta}}$ cannot similarly be eliminated, for appropriate pulse forms it can be effectively eliminated by performing a local rotation in spin space.

Let $\mathbf{S}'_2 = \mathbf{R} \cdot \mathbf{S}_2$ where \mathbf{R} is a rotation matrix constructed to eliminate $\overline{\boldsymbol{\beta}}$ from $\overline{H}(t)$ so that

$$\overline{H}(t) = J(t)(\mathbf{S}_1 \cdot \mathbf{S}'_2 + \mathbf{S}_1 \cdot \overline{\boldsymbol{\Pi}}' \cdot \mathbf{S}'_2), \quad (14)$$

where $\overline{\boldsymbol{\Pi}}'$ is a symmetric tensor. The precise form of this rotation depends on both $\overline{\boldsymbol{\beta}}$ and $\overline{\boldsymbol{\Pi}}$ and cannot be expressed simply. However, up to second order in $\overline{\boldsymbol{\beta}}$, it is given by

$$\mathbf{R}_{ab} = \delta_{ab} + \sum_c \epsilon_{abc} \overline{\beta}_c - (\overline{\beta}^2 \delta_{ab} - \overline{\beta}_a \overline{\beta}_b)/2 + O(\overline{\beta}^3), \quad (15)$$

and this is sufficient for our purpose of eliminating first-order anisotropy. Using (15) one finds the residual anisotropy in (14) is, up to second order in $\overline{\boldsymbol{\beta}}$,

$$\overline{\boldsymbol{\Pi}}'_{ab} = \overline{\boldsymbol{\Pi}}_{ab} + (\overline{\beta}^2 \delta_{ab} - \overline{\beta}_a \overline{\beta}_b)/2 + O(\overline{\beta}^4). \quad (16)$$

Thus, in this rotated coordinate system the first-order anisotropy vanishes and all corrections to the isotropic exchange interaction are second order in spin-orbit coupling.

The ability to eliminate $\overline{\boldsymbol{\beta}}$ from $\overline{H}(t)$ by simply rotating one qubit with respect to the other indicates a procedure for eliminating the first-order effects of spin-orbit coupling in any quantum computer that uses tunable exchange for quantum gates. Suppose that symmetric pulses are used, so that $\overline{\boldsymbol{\alpha}} = 0$, and pulse forms are chosen so that $\overline{\boldsymbol{\beta}}$ is the same for all pulse strengths λ . Then, if the qubits in the computer form a linear array, or any arrangement for which there are no closed loops of qubits connected by two-qubit gates, it will be possible to define a *local spin-space coordinate system* in which the effective interaction between any two neighboring qubits has the form (14). While this procedure does not completely eliminate the anisotropy, it does reduce it from an effect that is first order in spin-orbit coupling to one that is second order.

To demonstrate how (10) can be used to tailor pulse shapes that lead to the same $\overline{\boldsymbol{\beta}}$ for all pulse strengths λ , consider the family of pulses,

$$J(t; \lambda) = J_0(\lambda) \text{sech}^2[2t/\tau(\lambda)], \quad (17)$$

where $J_0(\lambda)$ and $\tau(\lambda)$ are, respectively, the pulse height and width, and the pulse strength is $\lambda = \int_{-\infty}^{\infty} J(t; \lambda) dt = J_0(\lambda)\tau(\lambda)$. To evaluate (10) it is also necessary to know the time dependence of $\boldsymbol{\beta}(t)$. Determining the precise form of this dependence will require a detailed microscopic study of the specific realization of the exchange interaction being considered. Here we take, as the simplest possible illustrative model, a linear dependence on $J(t; \lambda)$,

$$\boldsymbol{\beta}(t) = \boldsymbol{\beta}_1 J(t; \lambda), \quad (18)$$

for which the integral (10) can be performed analytically, with the result

$$\overline{\boldsymbol{\beta}} = \boldsymbol{\beta}_1 \frac{4J_0(\lambda)}{\lambda^2} [2 - \lambda \cot(\lambda/2)]. \quad (19)$$

Also, because these pulses are time-reversal symmetric, (9) gives $\overline{\boldsymbol{\alpha}} = 0$.

Equation (19) can be used to exploit the freedom to choose $J_0(\lambda)$ and $\tau(\lambda)$, while keeping $J_0(\lambda)\tau(\lambda) = \lambda$, to shape pulses that keep $\overline{\boldsymbol{\beta}}$ fixed for different pulse strengths. For example, if the pulse parameters for $\lambda = \pi$ (swap) are fixed to be $J_0(\pi)$ and $\tau(\pi)$, then, for general λ , one should take

$$J_0(\lambda) = J_0(\pi) \frac{2\lambda^2}{\pi^2} \frac{1}{2 - \lambda \cot(\lambda/2)}, \quad (20)$$

and

$$\tau(\lambda) = \tau(\pi) \frac{\pi}{2\lambda} [2 - \lambda \cot(\lambda/2)]. \quad (21)$$

These pulse forms are shown in Fig. 1 for various values of pulse strength λ . Note that, as λ increases, the pulse height *decreases*. This is because $\overline{\boldsymbol{\beta}}$ becomes increasingly sensitive to $\boldsymbol{\beta}(t)$ with increasing λ until, in the limit $\lambda \rightarrow 2\pi$, the pulse height must go to zero if $\overline{\boldsymbol{\beta}}$ is to be kept constant. Although our perturbation expansion for $\overline{\mathcal{A}}$ breaks down as $\lambda \rightarrow 2\pi$, for this example the pulse heights are chosen so that the parameters in $\overline{\mathcal{A}}$ remain small, and we are always within the perturbative regime. The pulse forms defined by (20) and (21) are therefore valid, even in this singular limit. Of course, in practice, pulses near $\lambda = 2\pi$ will be problematic because of the diverging pulse length.

Once the first-order corrections to $\overline{H}(t)$ are eliminated, the residual second-order anisotropy can be found by first evaluating (12) and then performing the local rotation to eliminate $\overline{\boldsymbol{\beta}}$. As a specific example, consider the special case for which the form of the pulsed Hamiltonian is

$$H(t) = J(t)\mathbf{S}_1 \cdot \mathbf{R}(t) \cdot \mathbf{S}_2, \quad (22)$$

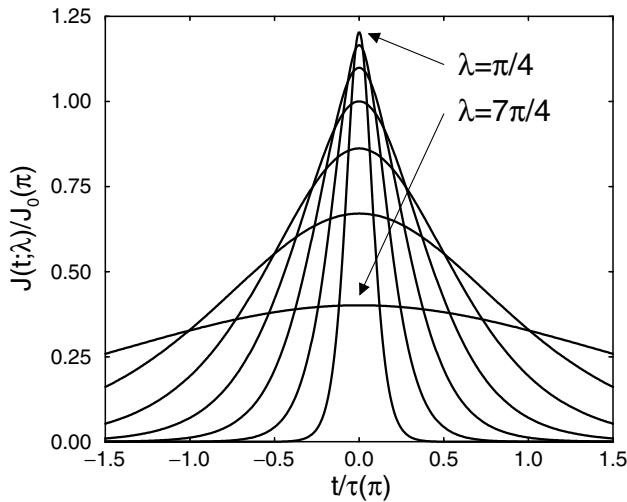


FIG. 1. Pulse forms tailored to produce the same $\bar{\beta}$ for different pulse strengths λ for the example described in the text. Of the pulses shown, the narrowest with the highest peak is for $\lambda = \pi/4$. λ then increases in increments of $\pi/4$ as the peak height decreases until, for the widest pulse with the lowest peak, $\lambda = 7\pi/4$. As $\lambda \rightarrow 2\pi$ the pulse height goes to zero.

where $\mathbf{R}(t)$ is a time-dependent rotation matrix. Such rotated exchange is, in fact, precisely the form of anisotropy found microscopically when spin-orbit corrections are included in the usual Hubbard model treatment of superexchange [11,12]. It has also been suggested that this form is appropriate for localized electrons in semiconductors [9]. In the present context, (22) is of interest because, if the rotation matrix $\mathbf{R}(t)$ were independent of time, our local rotation scheme would eliminate anisotropy to *all* orders, rather than just to first order in spin-orbit coupling. It is therefore natural to ask to what degree the fact that $\mathbf{R}(t)$ depends on time spoils this hidden symmetry.

For the particular form of anisotropic exchange in (22), the symmetric anisotropy term is, to second order in $\beta(t)$,

$$\mathbb{I}_{ab}(t) = -[\beta(t)^2 \delta_{ab} - \beta_a(t)\beta_b(t)]/2 + O[\beta(t)^4]. \quad (23)$$

For this $\mathbb{I}(t)$, if we continue to take the pulse form (17) and $\beta(t)$ from (18) then the expression (12) can be evaluated *analytically*. After performing the local rotation to eliminate $\bar{\beta}$ we find, using (16), that the residual anisotropy in $\bar{H}(t)$ is

$$\begin{aligned} \bar{\mathbb{I}}'_{ab} = & \frac{8J_0(\lambda)^2}{3\lambda^4} [\lambda^2 + 6\lambda \cot(\lambda/2) - 12] \\ & \times (\beta_1^2 \delta_{ab} - \beta_{1a}\beta_{1b}) + O(\beta_1^4). \quad (24) \end{aligned}$$

Thus even for the rotated exchange (22), if the rotation depends on time we are still left with residual second-order anisotropy after a pulse.

In summary, we have studied the effects of anisotropic corrections due to spin-orbit coupling on quantum gates produced by pulsing the exchange interaction between two spin-1/2 qubits. These quantum gates are parametrized by an effective Hamiltonian that commutes with itself at different times and produces the same quantum gate as a given pulse. Expressions for the various parameters in this effective Hamiltonian are obtained perturbatively in powers of spin-orbit coupling and used to shape pulses that effectively eliminate first-order spin-orbit corrections to quantum gates. The ability to reduce spin-orbit effects from first order to second order should be useful for any quantum computing scheme which relies on isotropic exchange.

N.E.B. and D.S. acknowledge support from the U.S. Department of Energy through Grant No. DE-FG02-97ER45639 and the National Science Foundation through Grant No. DMR-0103034. D.P.D. is grateful for support from the National Security Agency and the Advanced Research and Development Activity through Army Research Office Contracts No. DAAG55-98-C-0041 and No. DAAD19-01-C-0056.

-
- [1] D. Loss and D.P. DiVincenzo, Phys. Rev. A **57**, 120 (1998).
 - [2] B. E. Kane, Nature (London) **393**, 133 (1998).
 - [3] G. Burkard, D. Loss, and D.P. DiVincenzo, Phys. Rev. B **59**, 2070 (1999).
 - [4] X. Hu and S. Das Sarma, Phys. Rev. A **61**, 062301 (2000).
 - [5] R. Vrijen *et al.*, Phys. Rev. A **62**, 012306 (2000).
 - [6] D. Bacon *et al.*, Phys. Rev. Lett. **85**, 1758 (2000).
 - [7] D.P. DiVincenzo *et al.*, Nature (London) **408**, 339 (2000).
 - [8] I. Dzyaloshinski, J. Phys. Chem. Solids **4**, 241 (1958); T. Moriya, Phys. Rev. **120**, 91 (1960).
 - [9] K. V. Kavokin, Phys. Rev. B **64**, 075305 (2001).
 - [10] $\bar{\alpha}$ and $\bar{\beta}$ will diverge as $\lambda \rightarrow 0$ only if $J(t)$ changes sign. If $J(t)$ is always positive (or always negative), our expressions for the parameters in $\bar{\mathcal{A}}$ can be simplified by changing integration variables from t to $x = x(t)$ and using the fact that $dx = J(t)dt$. It is then easily seen that $\bar{\alpha}$ and $\bar{\beta}$ remain finite as $\lambda \rightarrow 0$ for these pulses.
 - [11] L. Shekhtman, O. Entin-Wohlman, and A. Aharony, Phys. Rev. Lett. **69**, 836 (1992).
 - [12] N.E. Bonesteel, Phys. Rev. B **47**, 11 302 (1993).

Spin-orbit coupling and time-reversal symmetry in quantum gates

D. Stepanenko and N. E. Bonesteel

Department of Physics and National High Magnetic Field Laboratory, Florida State University, Tallahassee, Florida 32310, USA

D. P. DiVincenzo and G. Burkard

IBM Research Division, T.J. Watson Research Center, Yorktown Heights, New York 10598, USA

Daniel Loss

Department of Physics and Astronomy, University of Basel, Klingelbergstrasse 82, CH-4056 Basel, Switzerland

(Received 7 April 2003; published 12 September 2003)

We study the effect of spin-orbit coupling on quantum gates produced by pulsing the exchange interaction between two single-electron quantum dots. Spin-orbit coupling enters as a small spin precession when electrons tunnel between dots. For adiabatic pulses the resulting gate is described by a unitary operator acting on the four-dimensional Hilbert space of two qubits. If the precession axis is fixed, time-symmetric pulsing constrains the set of possible gates to those which, when combined with single qubit rotations, can be used in a simple controlled-NOT construction. Deviations from time-symmetric pulsing spoil this construction. The effect of time asymmetry is studied by numerically integrating the Schrödinger equation using parameters appropriate for GaAs quantum dots. Deviations of the implemented gate from the desired form are shown to be proportional to dimensionless measures of both spin-orbit coupling and time asymmetry of the pulse.

DOI: 10.1103/PhysRevB.68.115306

PACS number(s): 03.67.Lx, 73.21.La

I. INTRODUCTION

A promising proposal for building a solid-state quantum computer is based on the notion of using electron spins trapped in quantum dots as qubits.¹ In such a device, two-qubit quantum gates would be carried out by turning on and off the exchange interaction between spins on neighboring dots through suitable pulsing of gate voltages.

When performing such a quantum gate, if nonadiabatic errors²⁻⁴ can be safely ignored,⁵ both the initial and final states of the two dots will be in the four-dimensional Hilbert space of two qubits. In the absence of spin-orbit coupling, and neglecting the dipolar interaction between spins, the unitary transformation resulting from such a pulsed exchange gate will necessarily have the form

$$U = \exp - i\lambda \mathbf{S}_A \cdot \mathbf{S}_B, \quad (1)$$

where λ is a dimensionless measure of the pulse strength. This simple isotropic form is a consequence of symmetry—if spin and space decouple exactly, as they do in the nonrelativistic limit, then the system is perfectly isotropic in spin space. Up to an irrelevant overall phase, gates (1) are the most general unitary operators with this symmetry acting on a two-qubit Hilbert space.

These isotropic exchange gates are useful for quantum computation. In conjunction with single qubit rotations, they can be used in a simple construction of a controlled-NOT gate.¹ It has also been shown that, even without single qubit rotations, isotropic exchange gates can be used for universal quantum computing with proper encoding of logical qubits.^{6,7}

When the effects of spin-orbit coupling are included, well-isolated single-electron dots will have a twofold Kram-

ers degeneracy and so can still be used as qubits. However, when carrying out a quantum gate the total spin will no longer be a good quantum number. As a result there will inevitably be corrections to the isotropic exchange gates (1). Motivated by this fact, a number of authors have considered *anisotropic* gates of the form

$$U = \exp - i\lambda [\mathbf{S}_A \cdot \mathbf{S}_B + \boldsymbol{\beta} \cdot (\mathbf{S}_A \times \mathbf{S}_B) + \gamma (\mathbf{S}_A \cdot \mathbf{S}_B - (\hat{\boldsymbol{\beta}} \cdot \mathbf{S}_A)(\hat{\boldsymbol{\beta}} \cdot \mathbf{S}_B))], \quad (2)$$

and shown that they have several useful properties. For example, in Ref. 8 it was shown that the controlled-NOT construction of Ref. 1 is robust against anisotropic corrections of the form appearing in Eq. (2). It has also been shown that, when combined with a controllable Zeeman splitting, gates (2) form a universal set.⁹

The anisotropic terms which appear in Eq. (2) are not the most general corrections to Eq. (1) which can occur when carrying out an exchange gate in the presence of spin-orbit coupling. It is therefore important to ask under what conditions these corrections can be restricted to have this desired form. The key observation motivating the present work is that, up to an irrelevant overall phase, gates (2) are the most general two-qubit quantum gates which are both axially symmetric, i.e., symmetric under rotations about an axis parallel to the vector $\boldsymbol{\beta}$ in spin space, and symmetric under time reversal ($\mathbf{S}_\mu \rightarrow -\mathbf{S}_\mu, \mu = A, B$). It follows that if these symmetries can be maintained throughout the gate operation, and provided nonadiabatic errors can be neglected, the resulting quantum gate is *guaranteed* to have form (2). Of course, symmetry alone cannot determine the values of λ , $\boldsymbol{\beta}$, and γ . However, in practice we envision these parameters will be

determined through experimental calibration rather than microscopic calculation. Therefore we emphasize symmetry as a useful guiding principle.

In this paper we study the effect of spin-orbit coupling on exchange-based quantum gates. For concreteness we consider a system of two single-electron quantum dots in GaAs. The contribution of spin-orbit coupling to the exchange interaction between localized spins in GaAs has been studied by Kavokin¹⁰ within the Heitler-London approximation, and by Gor'kov and Krotkov¹¹ who derived the exact asymptotic exchange interaction between hydrogenlike bound states at large separation.

Here we follow Ref. 2 and work within the Hund-Mulliken approximation, keeping one orbital per dot, and allowing double occupancy. In this approximation, the effect of spin-orbit coupling is to induce a small spin precession whenever an electron tunnels from one dot to another. The Hamiltonian governing the two-dot system is therefore axially symmetric in spin space with the symmetry axis being the precession axis of the spin. If the direction of the precession axis does not change while the gate is being pulsed, then the resulting quantum gate will also be axially symmetric.

An additional useful symmetry principle, first suggested in Ref. 12, is that any time-dependent Hamiltonian $H_p(t)$ which is time-reversal symmetric at all times t , and which is then pulsed in a time-symmetric way [$H_p(t) = H_p(-t)$], will lead to a gate which can be described in terms of an effective time-independent Hamiltonian H which is also time-reversal symmetric. Here we give a proof of this result.

Taken together these two results imply that, within the Hund-Mulliken approximation, if the spin-orbit precession axis is fixed and nonadiabatic errors can be ignored, the unitary transformation produced by pulsing the exchange interaction between two quantum dots will necessarily have the desired form (2), provided the gate is pulsed in a time-symmetric way.

This paper is organized as follows. In Sec. II we derive the Hund-Mulliken Hamiltonian for a double quantum dot system in the presence of spin-orbit coupling. In Sec. III we develop an effective spin Hamiltonian description which can be applied to pulsing our double dot system, and we review the robust controlled-NOT construction of Ref. 8. The implications of time-symmetric pulsing are then studied in Sec. IV, and in Sec. V we present numerical results showing the effect of small time asymmetry of the pulse. Finally, in Sec. VI we summarize the results of the paper.

II. HUND-MULLIKEN HAMILTONIAN

We consider a system of two laterally confined quantum dots with one electron in each dot. For concreteness we assume the dots are formed in a two-dimensional electron gas (2DEG) realized in a GaAs heterostructure.

The system is modeled by the Hamiltonian

$$H = T + C + H_{SO}. \quad (3)$$

Here $T + C$ is the Hamiltonian studied in Ref. 2, where $T = \sum_i h_i$ with

$$h_i = \frac{1}{2m} \left(\mathbf{p}_i - \frac{e}{c} \mathbf{A}(\mathbf{r}_i) \right)^2 + V(\mathbf{r}_i), \quad (4)$$

and $C = e^2/\epsilon|\mathbf{r}_1 - \mathbf{r}_2|$ is the Coulomb repulsion between electrons. We take the 2DEG the dots are formed in to lie in the xy plane, and for GaAs we take $m = 0.067m_e$ and $\epsilon = 13.1$. For completeness we include a vector potential $\mathbf{A} = (-y, x, 0)B/2$ which couples the orbital motion of the electrons to a uniform magnetic field $\mathbf{B} = B\hat{\mathbf{z}}$. We will see in Sec. III that this orbital coupling does not affect any of our arguments based on time-reversal symmetry, while a nonzero Zeeman coupling does.

As in Ref. 2 lateral confinement of the dots is modeled by the double-well potential,

$$V(x, y) = \frac{m\omega_0^2}{2} \left(\frac{1}{4a^2} (x^2 - a^2)^2 + y^2 \right). \quad (5)$$

This potential describes two quantum dots sitting at the points $(x, y) = (\pm a, 0)$. In the limit of large separation the dots decouple into two harmonic wells with frequency ω_0 .

Spin-orbit coupling enters the Hamiltonian through the term

$$H_{SO} = \sum_{i=1,2} \boldsymbol{\Omega}(\mathbf{k}_i) \cdot \mathbf{S}_i, \quad (6)$$

where $\hbar\mathbf{k} = \mathbf{p} - e/c\mathbf{A}$. Time-reversal symmetry requires that $\boldsymbol{\Omega}(\mathbf{k})$ is an odd function of \mathbf{k} , $\boldsymbol{\Omega}(\mathbf{k}) = -\boldsymbol{\Omega}(-\mathbf{k})$. Thus $\boldsymbol{\Omega}$ is nonzero only in the absence of inversion symmetry.

For definiteness, we take the 2DEG in which the dots are formed to lie in the plane perpendicular to the [001] structural direction, which then points along the z axis. However, we allow the x axis, which is parallel to the displacement vector of the two dots, to have any orientation with respect to the [100] and [010] structural axes. To describe the dependence of $\boldsymbol{\Omega}$ on \mathbf{k} it is then convenient to introduce unit vectors $\hat{\mathbf{e}}_{[110]}$ and $\hat{\mathbf{e}}_{[\bar{1}10]}$ which point in the [110] and $[\bar{1}10]$ structural directions, respectively, and define $k_{[110]} = \mathbf{k} \cdot \hat{\mathbf{e}}_{[110]}$ and $k_{[\bar{1}10]} = \mathbf{k} \cdot \hat{\mathbf{e}}_{[\bar{1}10]}$. We then have, following Kavokin,¹⁰

$$\boldsymbol{\Omega}(\mathbf{k}) \approx (f_D - f_R)k_{[110]}\hat{\mathbf{e}}_{[\bar{1}10]} + (f_D + f_R)k_{[\bar{1}10]}\hat{\mathbf{e}}_{[110]}. \quad (7)$$

Here f_D is the Dresselhaus contribution^{13,14} due to the bulk inversion asymmetry of the zinc-blende crystal structure of GaAs, and f_R is the Rashba contribution¹⁵ due to the inversion asymmetry of the quantum well used to form the 2DEG. These quantities depend on details of the 2DEG confining potential and so will vary from system to system.

It was pointed out in Ref. 16 that H_{SO} has a special symmetry when $f_D = \pm f_R$. This can be seen directly from Eq. (7). When $f_D = f_R$ ($f_D = -f_R$) the direction of $\boldsymbol{\Omega}$ is independent of \mathbf{k} and is fixed to be parallel to $\hat{\mathbf{e}}_{[110]}$ ($\hat{\mathbf{e}}_{[\bar{1}10]}$). The full Hamiltonian (3) is then invariant under rotations in spin space about this axis. We will see below that this special case has a number of attractive features.

In the limit of decoupled dots, and ignoring spin-orbit coupling, the single-electron ground states will be the Fock-Darwin ground states centered at $(x, y) = (\pm a, 0)$,

$$\phi_{\pm a}(x, y) = \sqrt{\frac{m\omega}{\pi\hbar}} e^{-m\omega[(x\mp a)^2 + y^2]/2\hbar} e^{\pm iay/2l_B^2}. \quad (8)$$

Here $\omega = \sqrt{\omega_0^2 + \omega_L^2}$ is the frequency of the magnetically squeezed oscillator where $\omega_L = eB/2mc$ is the Larmor frequency and $l_B = \sqrt{\hbar c/eB}$ is the magnetic length. In zero magnetic field, the size of these wave functions is set by the effective ‘‘Bohr radius’’ $a_B = \sqrt{\hbar/m\omega_0}$.

The Fock-Darwin states can be orthogonalized to obtain the Wannier states

$$\Phi_A = \frac{1}{\sqrt{1-2Sg+g^2}} (\phi_a - g\phi_{-a}), \quad (9)$$

$$\Phi_B = \frac{1}{\sqrt{1-2Sg+g^2}} (\phi_{-a} - g\phi_a), \quad (10)$$

where $S = \langle \phi_{-a} | \phi_a \rangle$ and $g = (1 - \sqrt{1 - S^2})/S$. We can then introduce second quantized operators $c_{A\alpha}^\dagger$ ($c_{A\alpha}$) and $c_{B\alpha}^\dagger$ ($c_{B\alpha}$) which create (annihilate) electrons in the states Φ_A and Φ_B with spin $\alpha = \uparrow, \downarrow$.

In the Hund-Mulliken approximation we keep one orbital per dot and allow for double occupancy. This amounts to restricting the full Hilbert space of the problem to the six-dimensional Hilbert space spanned by the states

$$|S_1\rangle = \frac{1}{\sqrt{2}} (c_{A\uparrow}^\dagger c_{B\downarrow}^\dagger - c_{A\downarrow}^\dagger c_{B\uparrow}^\dagger) |0\rangle, \quad (11)$$

$$|S_2\rangle = \frac{1}{\sqrt{2}} (c_{A\uparrow}^\dagger c_{A\downarrow}^\dagger + c_{B\downarrow}^\dagger c_{B\uparrow}^\dagger) |0\rangle, \quad (12)$$

$$|S_3\rangle = \frac{1}{\sqrt{2}} (c_{A\uparrow}^\dagger c_{A\downarrow}^\dagger - c_{B\downarrow}^\dagger c_{B\uparrow}^\dagger) |0\rangle, \quad (13)$$

$$|T_-\rangle = c_{A\downarrow}^\dagger c_{B\downarrow}^\dagger |0\rangle, \quad (14)$$

$$|T_0\rangle = \frac{1}{\sqrt{2}} (c_{A\uparrow}^\dagger c_{B\downarrow}^\dagger + c_{A\downarrow}^\dagger c_{B\uparrow}^\dagger) |0\rangle, \quad (15)$$

$$|T_+\rangle = c_{A\uparrow}^\dagger c_{B\uparrow}^\dagger |0\rangle. \quad (16)$$

In terms of second quantized operators, the Hund-Mulliken Hamiltonian acting in this space, up to an irrelevant overall additive constant, can be written

$$H_{HM} = \sum_{\alpha, \beta = \uparrow, \downarrow} -[c_{A\alpha}^\dagger (t_H \delta_{\alpha\beta} + i\mathbf{P} \cdot \boldsymbol{\sigma}_{\alpha\beta}) c_{B\beta} + \text{H.c.}] + V(\mathbf{S}_A \cdot \mathbf{S}_B + 3/4) + U_H(n_{A\uparrow} n_{A\downarrow} + n_{B\uparrow} n_{B\downarrow}). \quad (17)$$

Here

$$\mathbf{S}_\mu = \frac{1}{2} \sum_{\alpha, \beta = \uparrow, \downarrow} c_{\mu\alpha}^\dagger \boldsymbol{\sigma}_{\alpha\beta} c_{\mu\beta} \quad (18)$$

is the spin operator on site $\mu = A, B$,

$$V = \langle S_1 | C | S_1 \rangle - \langle T_0 | C | T_0 \rangle \quad (19)$$

is the ferromagnetic direct exchange,

$$U_H = \langle S_2 | C | S_2 \rangle - \langle S_1 | C | S_1 \rangle \quad (20)$$

is the Coulomb energy cost of doubly occupying a dot, and

$$t_H = \langle \Phi_A | h | \Phi_B \rangle \quad (21)$$

is the interdot tunneling amplitude.

The only contribution from spin-orbit coupling is the matrix element

$$i\mathbf{P} = \langle \Phi_A | \boldsymbol{\Omega}(\mathbf{k}) | \Phi_B \rangle = \langle \Phi_A | \frac{1}{\hbar} \left(p_x - \frac{e}{c} A_x \right) | \Phi_B \rangle \boldsymbol{\eta}, \quad (22)$$

where

$$\boldsymbol{\eta} = (f_D - f_R) \cos \theta \hat{\mathbf{e}}_{[\bar{1}10]} + (f_D + f_R) \sin \theta \hat{\mathbf{e}}_{[110]}. \quad (23)$$

Here θ is the angle the x axis makes with the $[110]$ structural direction. This term introduces a small spin precession about an axis parallel to \mathbf{P} through an angle $\phi = 2 \arctan(P/t_H)$ when an electron tunnels between dots.

It is convenient to express the spin-orbit matrix element as $\mathbf{P} = s \mathbf{1}_{SO}$ where

$$s = \frac{\sqrt{(f_D - f_R)^2 \cos^2 \theta + (f_D + f_R)^2 \sin^2 \theta}}{a_B \hbar \omega_0} \quad (24)$$

is a dimensionless measure of the strength of spin-orbit coupling. As stated above, f_D and f_R depend on details of the potential confining the electron to the 2DEG. Thus θ , f_D , and f_R are all parameters that, in principle, can be engineered to control the value of s . For example, if $\theta = 0$ then $s = |f_D - f_R| / (a_B \hbar \omega_0)$. Thus, for this orientation of the dots, if it is possible to design a system in which $f_D = f_R$, s can be made to vanish. Even if such perfect cancellation cannot be achieved, minimizing the difference $f_D - f_R$ will reduce s .

In what follows we leave s as a free parameter. We estimate that for GaAs quantum dots $s < 0.1$ for typical parameters.¹⁰ The remaining contribution to the matrix element \mathbf{P} is then

$$\mathbf{1}_{SO} = \frac{\hbar \omega_0}{2} \frac{1 - g^2}{1 - 2Sg + g^2} \frac{d}{b} e^{-d^2 b(2 - 1/b^2)} \hat{\boldsymbol{\eta}}, \quad (25)$$

where $d = a/a_B$ is a dimensionless measure of the distance between dots, $b = \sqrt{1 + \omega_L^2/\omega_0^2}$, and $\hat{\boldsymbol{\eta}} = \boldsymbol{\eta}/\eta$. The geometry of our model system is shown schematically in Fig. 1.

In what follows we envision pulsing quantum gates by varying the distance d between dots as a function of time. In doing this, we will assume that throughout the pulse the values of f_D and f_R do not change. If this is the case s will be constant and all of the time dependence of \mathbf{P} will be due to

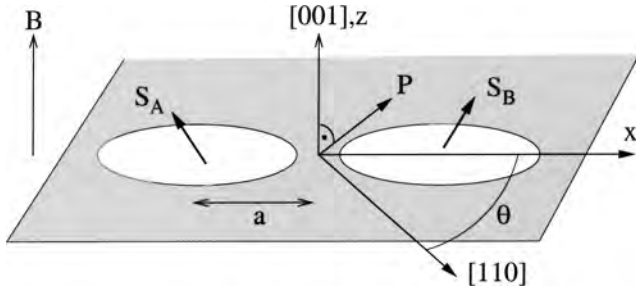


FIG. 1. Sketch of the GaAs double quantum dot system considered in this paper. There is one electron per dot, and the dot separation is $2a$. The dots are taken to lie in the plane perpendicular to both the $[001]$ axis and an applied magnetic field B . The displacement of the dots makes an angle θ with the $[110]$ axis. Due to spin-orbit coupling electron spins precess about an axis parallel to \mathbf{P} when tunneling between dots.

\mathbf{l}_{SO} . In addition, the direction of the vector \mathbf{P} will not change as a function of time. The Hamiltonian H_{HM} will therefore be invariant under rotations in spin space about a single fixed axis parallel to \mathbf{P} throughout the pulse. We will refer to such a pulse as having axial symmetry.

It is important to note that this axial symmetry is approximate. In general f_D and f_R will depend on time as the gate is pulsed, though in principle the system can be engineered to minimize this effect. Also, for general f_D and f_R the appearance of only one vector in spin space is a consequence of restricting the Hilbert space to one orbital per dot. If more orbitals are included then more spin-orbit matrix elements will appear in the Hamiltonian, corresponding typically to different spin-precession axes, thus breaking the axial symmetry. However, as shown above, if $f_D = \pm f_R$ then the full Hamiltonian (3) is axially symmetric—thus for this special case all spin-precession axes will be parallel and axial symmetry will not just be an artifact of the Hund-Mulliken approximation. In Sec. V we discuss the effect deviations from axial symmetry will have on our results.

Given an axially symmetric pulse, it is convenient to take the z axis in spin space to be parallel to \mathbf{P} . For this choice, the states $|T_+\rangle$ and $|T_-\rangle$ decouple, each having energy V .

Another useful symmetry of H_{HM} is invariance under $c_{A\alpha} \rightarrow c_{B,-\alpha}$ and $c_{B\alpha} \rightarrow c_{A,-\alpha}$. This transformation changes the sign of the states $|S_1\rangle$, $|S_2\rangle$, and $|T_0\rangle$, while leaving $|S_3\rangle$ invariant. It follows that the state $|S_3\rangle$ also decouples with energy U_H . The matrix representation of H_{HM} in the remaining nontrivial $|T_0\rangle$, $|S_1\rangle$, $|S_2\rangle$ basis is then

$$H_{HM} = \begin{pmatrix} V & 0 & -2iP \\ 0 & 0 & -2t_H \\ 2iP & -2t_H & U_H \end{pmatrix}. \quad (26)$$

III. EFFECTIVE SPIN HAMILTONIAN

We now consider pulsing the Hamiltonian H_{HM} by varying the distance between the dots, the barrier height, or some combination of the two, in such a way that the two electron spins interact for a finite period of time, but are well sepa-

rated at the beginning and end of the pulse. We assume the initial state of the system is in the four-dimensional Hilbert space describing two qubits, i.e., the space spanned by the singly occupied states $|S_1\rangle$, $|T_0\rangle$, $|T_-\rangle$, and $|T_+\rangle$. As the pulse is carried out, the eigenstates of H_{HM} at any given instant in time can be grouped into four low-energy states separated by a gap of order U_H from two high-energy states. If the pulse is sufficiently adiabatic on a time scale set by $\sim \hbar/U_H$, the amplitude for nonadiabatic transitions which would leave the system in the excited state $|S_2\rangle$ at the end of the pulse can be made negligibly small.⁵ If this condition holds, the final state of the system can also be assumed to be in the four-dimensional Hilbert space of two qubits. We will see that this condition is easily achieved in Sec. V.

One way to theoretically study the effect of such a pulse would be to first reduce H_{HM} to an effective anisotropic spin Hamiltonian acting on the four-dimensional low-energy Hilbert space and then consider pulsing this effective model.¹² The problem with this approach is that any such effective spin Hamiltonian will only be valid if the pulse is adiabatic, not only on the time scale \hbar/U_H , but also on the much longer time scale set by the inverse of the small energy splittings within the low-energy space due to the spin-orbit induced anisotropic terms. However, it is precisely the nonadiabatic transitions induced by these terms which give rise to the quantum gate corrections we would like to compute.

Although we may not be able to define an instantaneous effective spin Hamiltonian during the pulse, we can define one which describes the net effect of a full pulse. This definition amounts to parametrizing the quantum gate produced by the pulse as

$$U = e^{-i\tau H}, \quad (27)$$

where U acts on the four-dimensional Hilbert space of the initial and final spin states. H is then an effective spin Hamiltonian, i.e., it can be expressed entirely in terms of the spin operators \mathbf{S}_A and \mathbf{S}_B , and τ is a measure of the pulse duration. Note the definition of τ is arbitrary because it is the product τH which determines U . Here, and in the remainder of this paper, we work in units in which $\hbar = 1$.

If we assume exact axial symmetry throughout the pulse, the effective spin Hamiltonian must be invariant under rotations about the z axis in spin space and must also leave the states $|T_+\rangle$ and $|T_-\rangle$ degenerate. The most general such spin Hamiltonian, up to an irrelevant additive term proportional to the identity operator, is

$$\begin{aligned} \tau H(\lambda; \alpha, \beta, \gamma) = & \lambda \left(\mathbf{S}_A \cdot \mathbf{S}_B + \frac{\alpha}{2} (S_{Az} - S_{Bz}) \right. \\ & + \beta (S_{Ax} S_{By} - S_{Ay} S_{Bx}) \\ & \left. + \gamma (S_{Ax} S_{Bx} + S_{Ay} S_{By}) \right), \end{aligned} \quad (28)$$

and we denote the corresponding quantum gate as

$$U(\lambda; \alpha, \beta, \gamma) = e^{-i\tau H(\lambda; \alpha, \beta, \gamma)}. \quad (29)$$

When $\alpha = 0$, this is precisely gate (2) for $\boldsymbol{\beta} \parallel \hat{\mathbf{z}}$.

The controlled-NOT construction originally proposed in Ref. 1 is based on the sequence of gates

$$U_g = U(\pi/2; 0, 0, 0) e^{i\pi S_{Az}} U(\pi/2; 0, 0, 0), \quad (30)$$

where $U(\pi/2; 0, 0, 0) = \exp[-i[(\pi/2)\mathbf{S}_A \cdot \mathbf{S}_B]]$ is a square root of swap gate. The controlled-NOT gate is then

$$U_{CNOT} = e^{i(\pi/2)S_{Az}} e^{i(\pi/2)S_{Bz}} U_g. \quad (31)$$

Remarkably, it was shown in Ref. 8 that if $\lambda = \pi/2$ and $\alpha = 0$ this construction is robust against the β and γ corrections, i.e., the gate

$$U_g = U(\pi/2; 0, \beta, \gamma) e^{i\pi S_{Az}} U(\pi/2; 0, \beta, \gamma) \quad (32)$$

is independent of β and γ .

For completeness, we briefly review the arguments of Ref. 8. Due to axial symmetry, the action of the gate $U(\lambda; \alpha, \beta, \gamma)$ on the states $|T_+\rangle$ and $|T_-\rangle$ is trivial and independent of α, β , and γ ,

$$U(\lambda; \alpha, \beta, \gamma) |T_\pm\rangle = e^{-i\lambda/4} |T_\pm\rangle. \quad (33)$$

We can then introduce a pseudospin description of the remaining space, where $|S_1\rangle$ is pseudospin down and $|T_0\rangle$ is pseudospin up. The action of the gate $U(\lambda; \alpha, \beta, \gamma)$ on this pseudospin space is a simple rotation,

$$U(\lambda; \alpha, \beta, \gamma) \Rightarrow e^{i\lambda/4} e^{-i\mathbf{b} \cdot \boldsymbol{\tau}/2}, \quad (34)$$

where $\mathbf{b} = \lambda(\alpha, \beta, \gamma + 1)$ and the components of $\boldsymbol{\tau} = (\tau_x, \tau_y, \tau_z)$ are pseudospin Pauli matrices. At the same time, the action of the single qubit rotation entering U_g is

$$e^{i\pi S_{Az}} \Rightarrow i\tau_x. \quad (35)$$

Thus to show that the controlled-NOT construction is independent of β and γ if $\alpha = 0$ we need only show that the product

$$e^{-i\mathbf{b} \cdot \boldsymbol{\tau}/2} \tau_x e^{-i\mathbf{b} \cdot \boldsymbol{\tau}/2} \quad (36)$$

is independent of β and γ if $\alpha = 0$. This condition has a simple geometric interpretation. It is the requirement that a rotation about an axis parallel to \mathbf{b} , followed by a 180° rotation about the x axis, and then a repeat of the initial rotation must be equivalent to a simple 180° rotation about the x axis. This will trivially be the case if the vector $\mathbf{b} = \lambda(\alpha, \beta, \gamma + 1)$ lies in the yz plane. Thus, if $\alpha = 0$, this condition is satisfied and the Controlled-NOT construction is exact. Conversely, if $\alpha \neq 0$ the construction is spoiled.

IV. TIME-REVERSAL SYMMETRY

In this section we prove the following general result. Any time-dependent Hamiltonian $H_P(t)$ which is time-reversal symmetric for all t , and for which the time dependence is itself symmetric, i.e., $H_P(t_0 - t) = H_P(t_0 + t)$ for all t , will generate a unitary evolution operator $U = \exp[-i\tau H]$ where H is a time-independent effective Hamiltonian which is also time-reversal symmetric. We then show that this theorem implies that the parameter α , which spoils the controlled-NOT

construction described in Sec. III, is equal to zero for time-symmetric pulsing.

The time-reversal operation for any quantum system can be represented by an antiunitary operator Θ .¹⁷ An orthonormal basis $\{|M_i\rangle\}$ for the Hilbert space of this system is then said to be a time-symmetric basis if

$$\Theta|M_i\rangle = |M_i\rangle \quad (37)$$

for all i .

For any Hamiltonian H acting on a state $|M_i\rangle$ in this basis we can write

$$H|M_i\rangle = \sum_j \langle M_j|H|M_i\rangle |M_j\rangle. \quad (38)$$

Under time reversal H is transformed into $\Theta H \Theta^{-1}$. Using the invariance of the $\{|M_i\rangle\}$ basis and the antiunitarity of Θ we can then also write

$$\Theta H \Theta^{-1} |M_i\rangle = \Theta H |M_i\rangle \quad (39)$$

$$= \Theta \sum_j \langle M_j|H|M_i\rangle |M_j\rangle \quad (40)$$

$$= \sum_j \langle M_j|H|M_i\rangle^* |M_j\rangle. \quad (41)$$

Comparing Eqs. (38) and (41) leads to the conclusion that if H is time-reversal symmetric, i.e., $H = \Theta H \Theta^{-1}$, then the Hamiltonian matrix is purely real in the $\{|M_i\rangle\}$ basis, while if H is antisymmetric under Θ , i.e., $H = -\Theta H \Theta^{-1}$, then the Hamiltonian matrix is purely imaginary.

Since H is real in the $\{|M_i\rangle\}$ basis if and only if H is time-reversal symmetric it follows that the unitary operator $U = \exp[-i\tau H]$ is self-transpose, i.e., $U = U^T$, if and only if H is time-reversal symmetric.

Now consider a time-dependent pulse described by the Hamiltonian $H_P(t)$. We assume that $H_P(t)$ is time-reversal symmetric at all times, i.e., $H_P(t) = \Theta H_P(t) \Theta^{-1}$ for all t . The corresponding unitary evolution operator U which evolves the system from time t_I to t_F can be written as

$$U = \lim_{N \rightarrow \infty} U(t_N) U(t_{N-1}) \cdots U(t_2) U(t_1), \quad (42)$$

where

$$U(t_i) = e^{-i\Delta t H_P(t_i)} \quad (43)$$

with $\Delta t = (t_F - t_I)/N$ and $t_1 \equiv t_I$ and $t_N \equiv t_F$.

Since $H_P(t_i)$ is time-reversal symmetric, the above arguments imply $U^T(t_i) = U(t_i)$ when $U(t_i)$ is expressed in the time-symmetric basis $\{|M_i\rangle\}$. Thus, in this basis, we have

$$U^T = \lim_{N \rightarrow \infty} [U(t_N) U(t_{N-1}) \cdots U(t_2) U(t_1)]^T \quad (44)$$

$$= \lim_{N \rightarrow \infty} U^T(t_1) U^T(t_2) \cdots U^T(t_{N-1}) U^T(t_N) \quad (45)$$

$$= \lim_{N \rightarrow \infty} U(t_1) U(t_2) \cdots U(t_{N-1}) U(t_N). \quad (46)$$

For a time-symmetric pulse $H_P(t_i) = H_P(t_{N+1-i})$ and so $U(t_i) = U(t_{N+1-i})$. This allows us to reverse the order of the operators in Eq. (46) which then implies

$$U^T = U. \quad (47)$$

Thus if we write U in terms of an effective Hamiltonian,

$$U = e^{-i\tau H}, \quad (48)$$

the matrix elements of H must be real in the time-symmetric basis. H must therefore be time-reversal symmetric, i.e., $H = \Theta H \Theta^{-1}$.

To apply this theorem to the present problem we take the time-reversal operator for our two-electron system to be

$$\Theta = e^{i\pi S_{Ay}} e^{i\pi S_{By}} K. \quad (49)$$

Here the antiunitary operator K is defined so that when acting on a given state it takes the complex conjugate of the amplitudes of that state when expressed in the Hund-Mulliken basis defined in Sec. II. Note that this basis is constructed using the Fock-Darwin states, and if a magnetic field is present these states will be necessarily complex valued when expressed in the position basis. As defined here, the antiunitary operator K only takes the complex conjugates of the amplitudes in the Hund-Mulliken basis, *it does not take the complex conjugate of the Fock-Darwin states themselves*. Thus, if a magnetic field is present, Θ should be viewed as an *effective* time-reversal symmetry operator. This is a technical point which does not affect any of our conclusions (provided the Zeeman coupling can be ignored—see below). The key property that we will need in what follows is that spin changes sign under time reversal, and it is readily verified that for our definition of Θ ,

$$\Theta \mathbf{S}_\mu \Theta^{-1} = -\mathbf{S}_\mu \quad (50)$$

for $\mu = A, B$ even in the presence of a magnetic field.

Under Θ , the Hund-Mulliken basis states transform as follows,

$$\Theta |S_i\rangle = |S_i\rangle \quad \text{for } i = 1, 2, 3, \quad (51)$$

$$\Theta |T_0\rangle = -|T_0\rangle, \quad (52)$$

$$\Theta |T_+\rangle = |T_-\rangle, \quad (53)$$

$$\Theta |T_-\rangle = |T_+\rangle. \quad (54)$$

The states $|S_i\rangle$ therefore form a time-symmetric basis for the singlet states. A time-symmetric basis for the triplet states is given by

$$|\tilde{T}_0\rangle = i|T_0\rangle, \quad (55)$$

$$|\tilde{T}_a\rangle = \frac{1}{\sqrt{2}}(|T_+\rangle + |T_-\rangle), \quad (56)$$

$$|\tilde{T}_b\rangle = \frac{i}{\sqrt{2}}(|T_-\rangle - |T_+\rangle), \quad (57)$$

all of which are eigenstates of Θ with eigenvalue $+1$.

The matrix representation of H_{HM} in the time-reversal invariant $|\tilde{T}_0\rangle, |S_1\rangle, |S_2\rangle$ basis is

$$H_{HM} = \begin{pmatrix} V & 0 & -2P \\ 0 & 0 & -2t_H \\ -2P & -2t_H & U_H \end{pmatrix}, \quad (58)$$

which is real, reflecting the effective time-reversal symmetry of H_{HM} . Note that this would not be the case if H_{HM} included the Zeeman coupling of electron spins to an external magnetic field. While for typical field strengths the Zeeman coupling is small,² for some parameters it can be comparable to the spin-orbit corrections considered here. If this is the case our conclusions following from effective time-reversal symmetry will no longer be valid. Of course in zero magnetic field exact time-reversal symmetry is guaranteed.

We now consider pulsing a time dependent $H_{HM}(t)$ adiabatically so that, according to the arguments of Sec. III, the resulting gate can be parametrized by an effective spin Hamiltonian H . Since at all times t the Hund-Mulliken Hamiltonian is time-reversal symmetric, if the pulse itself is time symmetric, i.e., $H_{HM}(t) = H_{HM}(-t)$ where we take the center of the pulse to be at $t=0$, then the above theorem implies that the effective spin Hamiltonian H will also be time-reversal symmetric. Thus $H = \Theta H \Theta^{-1}$, and since $\Theta \mathbf{S}_\mu \Theta^{-1} = -\mathbf{S}_\mu$ this implies H must be quadratic in the spin operators, and so $\alpha = 0$. The resulting gate will therefore have the desired form (2).

For completeness we also consider here the case of time-antisymmetric pulsing. If $H_P(t) = -H_P(-t)$ then

$$U(t) = e^{-i\Delta t H_P(t)} = e^{i\Delta t H_P(-t)} = U(-t)^{-1}, \quad (59)$$

and the resulting quantum gate is

$$U = \lim_{N \rightarrow \infty} U(t_1) U(t_2) \cdots U(t_{N/2}) U(t_{N/2})^{-1} \cdots U(t_2)^{-1} U(t_1)^{-1} = 1. \quad (60)$$

The net effect of any time-antisymmetric pulse is thus simply the identity transformation.

V. MODEL CALCULATIONS

We have seen from symmetry arguments that time-symmetric pulsing of an axially symmetric Hamiltonian, such as H_{HM} when f_D and f_R are constant, which is itself time-reversal symmetric at all times, will automatically produce a gate of form (2), provided the pulse is adiabatic so that the initial and final states of the system are in the four-dimensional Hilbert space of two qubits. It is natural to then ask what the effect of the inevitable deviations from time-symmetric pulsing will be on the resulting gate. To investigate this we have performed some simple numerical simulations of coupled quantum dots.

In our calculations, we imagine pulsing the dots by varying the dimensionless distance d between them according to

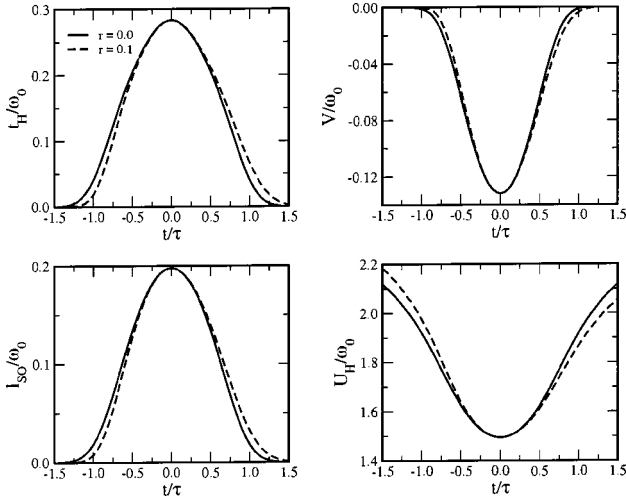


FIG. 2. Time dependence of matrix elements appearing in the Hund-Mulliken description of a double quantum dot when the displacement of the dots is varied according to Eq. (61) with $d_0=1$. Results are for GaAs parameters in zero magnetic field with $\hbar\omega_0=3$ meV and are plotted vs the dimensionless quantity t/τ for two values of the time-asymmetry parameter, $r=0$ (solid line) and $r=0.1$ (dashed line).

$$d(t) = d_0 + \left(\frac{t}{\tau + rt} \right)^2. \quad (61)$$

Here d_0 is the distance at the point of closest approach, τ is a measure of the pulse duration, and r is a dimensionless measure of the time asymmetry of the pulse. This form describes the generic behavior of any pulse for times near the pulse maximum ($t=0$). Note that for large $|t|$, and for $r \neq 0$, the distance $d(t)$ will saturate, and has a singularity for negative t . We have taken r to be small enough so that the dots decouple long before this leads to any difficulty.

For our calculations, we work in zero magnetic field and take $\hbar\omega_0=3$ meV and $d_0=1$, corresponding to $a \approx 20$ nm at closest approach. The resulting time dependences of the parameters in H_{HM} are shown in Fig. 2. Note that the spin-orbit matrix element plotted in this figure is l_{SO} , while the spin-orbit matrix element appearing in H_{HM} is $\mathbf{P} = sl_{SO}\hat{\mathbf{z}}$, where s is the dimensionless measure of spin-orbit coupling introduced in Sec. II.

For a given pulse $H_{HM}(t)$ we integrate the time-dependent Schrödinger equation to obtain the evolution operator U for the full pulse. If the pulse is adiabatic then the matrix elements of U which couple the singly occupied states $|S_1\rangle$ and $|T_0\rangle$ to the doubly occupied state $|S_2\rangle$ can be made negligibly small.⁵ The quantum gate is then obtained by simply truncating U to the 4×4 matrix acting on the two-qubit Hilbert space. By taking the log of this matrix we obtain $\tau H = i \ln U$ and thus the parameters $\lambda, \alpha, \beta, \gamma$. Note that when calculating $\ln U$, there are branch cuts associated with each eigenvalue of U , and as a consequence τH is not uniquely determined. We resolve this ambiguity by requiring that as the pulse height is reduced to zero and U goes continuously to the identity that $\tau H \rightarrow 0$ without crossing any branch cuts.

TABLE I. Symmetry properties of the pulse parameters r and s , and gate parameters λ , α , β , and γ under parity P and time reversal T .

	r	s	λ	α	β	γ
P	+	-	+	-	-	+
T	-	+	+	-	+	+

We fix the pulse width τ by requiring that if we turn off spin-orbit coupling ($s=0$) we obtain a $\lambda = \pi/2$ pulse, i.e., a square root of swap. For the parameters used here we find this corresponds to taking $\tau = 23.9/\omega_0 \approx 5$ ps. We have checked that these pulses are well into the adiabatic regime. The magnitudes of the matrix elements coupling singly occupied states to the doubly occupied state $|S_2\rangle$ are on the order of $|\langle S_1|U|S_2\rangle| \sim 10^{-6}$ and $|\langle T_0|U|S_2\rangle| \sim s10^{-6}$.

Once τ is fixed, there are two parameters characterizing each pulse, s and r , and four parameters characterizing the resulting gate, λ , α , β , and γ . The transformation properties of these parameters under parity (P) and time reversal (T) are summarized in Table I. These properties follow from the fact that (i) under time reversal $\mathbf{S}_\mu \rightarrow -\mathbf{S}_\mu$ and $r \rightarrow -r$, while $\mathbf{P} = sl_{SO}\hat{\mathbf{z}}$ is invariant, and (ii) under parity $\mathbf{S}_A \leftrightarrow \mathbf{S}_B$ and $\mathbf{P} \rightarrow -\mathbf{P}$, while r is invariant. Note that, as defined in Sec. II, the parameter s is positive. Here we allow s to change sign when the direction of the vector \mathbf{P} is reversed, thus under parity $s \rightarrow -s$.

These symmetry properties imply that if s and r are small, the parameters of the effective Hamiltonian will be given approximately by

$$\alpha \approx C_\alpha r s, \quad (62)$$

$$\beta \approx C_\beta s, \quad (63)$$

$$\gamma \approx C_\gamma s^2, \quad (64)$$

$$\lambda \approx \lambda_0 + C_\lambda s^2, \quad (65)$$

where the coefficients should be of order 1. For the pulses we consider here $\lambda_0 = \pi/2$.

The results of our calculations are shown in Fig. 3. Each point corresponds to a separate numerical run. The plots for λ , β , and γ show their dependence on s when $r=0$. The dependence of the parameter α on pulse asymmetry is shown by plotting α/s versus r . For the s values we have studied, up to $|s|=0.1$, the numerical results for α/s are essentially independent of s for a given r . These results are clearly consistent with the above symmetry analysis.

Now consider carrying out a controlled-NOT gate using the scheme reviewed in Sec. III. For this construction to work it is necessary that $\lambda = \pi/2$. In our calculations we have fixed τ so that $\lambda = \pi/2$ for $s=r=0$. Thus, when spin-orbit coupling is included

$$\lambda \approx \pi/2 + C_\lambda s^2. \quad (66)$$

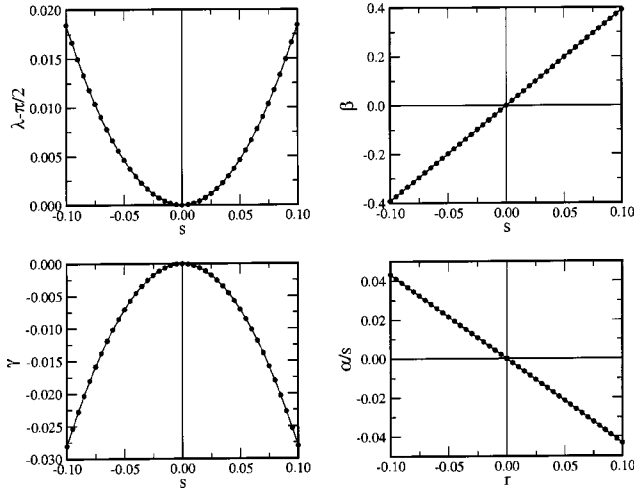


FIG. 3. Parameters appearing in the effective spin Hamiltonian derived from pulses depicted in Fig. 2. The parameters α , β , and γ are shown as functions of s for the case $r=0$ (time-symmetric pulses). For α the quantity α/s is plotted vs r . We have verified that the ratio α/s is essentially independent of s for all values we have considered ($|s| \leq 0.1$).

In order to keep $\lambda = \pi/2$ it will therefore be necessary to adjust the pulse width τ slightly to correct for spin-orbit effects.

The central result of this paper is summarized by the equation

$$\alpha \approx C_{\alpha} r s. \quad (67)$$

As shown in Sec. III, any nonzero α will lead to corrections to the Controlled-NOT construction. For time-symmetric pulses $r=0$ and these corrections will vanish. Equation (67) can then be used to estimate the errors due to any time asymmetry of the pulse, and to put design restrictions on the allowed tolerance for such asymmetry.

It is important to note that while the results presented here are for a specific model, all of the key arguments are based on symmetry and so are quite general. Given any time-reversal invariant two-qubit system with axial symmetry, if pulsed adiabatically in a time-symmetric way the resulting gate will have form (2).

While nearly perfect time-symmetric pulsing can presumably be achieved with sufficiently accurate pulse control, we expect that exact, or nearly exact, axial symmetry will be more difficult to realize. The results of this paper give some useful design guidelines for achieving this goal. For example, we have shown that within the Hund-Mulliken approximation axial symmetry is maintained provided the ratio f_D/f_R is kept constant throughout the pulse. As pointed out in Sec. III, however, even if quantum dots can be engineered so that this is the case, corrections beyond the Hund-Mulliken approximation will still, in general, lead to deviations from exact axial symmetry. Only when the special condition $f_D = \pm f_R$ is satisfied will the full Hamiltonian describing the system be axially symmetric. Achieving this

special condition is therefore the ideal case to strive for experimentally in order to guarantee axially symmetric quantum gates.

Even if perfect axial symmetry cannot be achieved, time-symmetric pulsing will still restrict the resulting gate to be invariant under time reversal. Thus, up to an irrelevant overall phase, this gate will necessarily have the form

$$U = \exp -i\lambda (\mathbf{S}_A \cdot \mathbf{S}_B + \boldsymbol{\beta} \cdot (\mathbf{S}_A \times \mathbf{S}_B) + \mathbf{S}_A \cdot \boldsymbol{\Gamma} \cdot \mathbf{S}_B). \quad (68)$$

Here $\boldsymbol{\Gamma}$ is a symmetric tensor which will, in general, deviate from the axial form of the γ term in Eq. (2) leading to corrections to the controlled-NOT construction. However, because $\boldsymbol{\Gamma}$ is even under parity it will still be second order in spin-orbit coupling,¹² and thus the deviations from Eq. (2) will also be second order. We conclude that even in the absence of exact axial symmetry, the corrections to the Controlled-NOT construction will be second order in spin-orbit coupling, rather than first order.

VI. CONCLUSIONS

In this paper we have studied spin-orbit corrections to exchange-based quantum gates, emphasizing symmetry arguments. In particular, we have shown that adiabatic time-symmetric pulsing of any Hamiltonian which (i) describes two well-defined spin-1/2 qubits at the beginning and end of the pulse, (ii) is time-reversal symmetric at all times during the pulse, and (iii) is axially symmetric in spin space with a fixed symmetry axis, will automatically produce a gate of form (2). Together with single qubit rotations, for $\lambda = \pi/2$ this gate can then be used in a simple Controlled-NOT construction. This result is quite general.

As a specific example we have studied a GaAs double quantum dot system within the Hund-Mulliken approximation. In this approximation spin-orbit coupling enters as a small spin precession when an electron tunnels between dots. If the direction of this precession axis is constant throughout the pulse the resulting gate will be axially symmetric and have form Eq. (29). The deviation of this gate from the desired gate (2) is then characterized by a single dimensionless parameter α which spoils the Controlled-NOT construction. Using symmetry arguments, as well as numerical calculations, we have shown that $\alpha \approx C_{\alpha} s r$ where s and r are, respectively, dimensionless measures of spin-orbit coupling and time asymmetry of the pulse. Thus time-symmetric pulsing ($r=0$) ensures the anisotropic corrections will have the desired form.

In any system without spatial inversion symmetry, spin-orbit coupling will inevitably lead to anisotropic corrections to the exchange interaction between spins. According to current estimates,¹⁸ fault-tolerant quantum computation will require realizing quantum gates with an accuracy of one part in 10^4 . Thus, even if spin-orbit coupling is weak, the design of any future quantum computer which uses the exchange interaction will have to take these anisotropic corrections into account. We believe the symmetry based analysis presented in this paper provides a useful framework for studying these effects.

ACKNOWLEDGMENTS

D.S. and N.E.B. acknowledge support from the National Science Foundation through NIRT Grant No. DMR-0103034. D.P.D.V. is supported in part by the National Security Agency and the Advanced Research and Development

Activity through Army Research Office Contract No. DAAD19-01-C-0056. He thanks the Institute for Quantum Information at Cal Tech (supported by the National Science Foundation under Grant No. EIA-0086038) for its hospitality during the initial stages of this work. D.L. thanks Swiss NSF, NCCR Nanoscience, DARPA, and ARO.

-
- ¹D. Loss and D.P. DiVincenzo, Phys. Rev. A **57**, 120 (1998).
²G. Burkard, D. Loss, and D.P. DiVincenzo, Phys. Rev. B **59**, 2070 (1999).
³G. Burkard, D. Loss, D.P. DiVincenzo, and J.A. Smolin, Phys. Rev. B **60**, 11404 (1999).
⁴X. Hu and S. Das Sarma, Phys. Rev. A **61**, 062301 (2000).
⁵J. Schliemann, D. Loss, and A.H. MacDonald, Phys. Rev. B **63**, 085311 (2001).
⁶D. Bacon, J. Kempe, D.A. Lidar, and K.B. Whaley, Phys. Rev. Lett. **85**, 1758 (2000).
⁷D.P. DiVincenzo, D. Bacon, J. Kempe, G. Burkard, and K.B. Whaley, Nature (London) **408**, 339 (2000).
⁸G. Burkard and D. Loss, Phys. Rev. Lett. **88**, 047903 (2002).
⁹L.-A. Wu and D. Lidar, Phys. Rev. A **66**, 062314 (2002).
¹⁰K.V. Kavokin, Phys. Rev. B **64**, 075305 (2001); cond-mat/0212347.
¹¹L.P. Gor'kov and P.L. Krotkov, Phys. Rev. B **67**, 033203 (2003).
¹²N.E. Bonesteel, D. Stepanenko, and D.P. DiVincenzo, Phys. Rev. Lett. **87**, 207901 (2001).
¹³G. Dresselhaus, Phys. Rev. **100**, 580 (1955).
¹⁴M.I. Dyakonov and V.Yu. Kachorovskii, Fiz. Techn. Poluprov. **20**, 178 (1986) [Sov. Phys. Semicond. **20**, 110 (1986)].
¹⁵E.L. Rashba, Fiz. Tverd. Tela (Leningrad) **2**, 1224 (1960) [Sov. Phys. Solid State **2**, 1109 (1960)]; Y.A. Bychkov and E.I. Rashba, J. Phys. C **17**, 6039 (1984).
¹⁶J. Schliemann, J.C. Egues, and D. Loss, Phys. Rev. Lett. **90**, 146801 (2003).
¹⁷For an excellent discussion of time-reversal symmetry see, K. Gottfried, *Quantum Mechanics* (Addison-Wesley, Reading, MA, 1989), pp. 314–322.
¹⁸D. Aharonov and M. Ben-Or, quant-ph/9906129 (unpublished).

Universal Quantum Computation through Control of Spin-Orbit Coupling

D. Stepanenko and N. E. Bonesteel

National High Magnetic Field Laboratory and Department of Physics, Florida State University, Tallahassee, Florida 32310, USA
(Received 12 March 2004; published 29 September 2004)

We propose a method for quantum computation which uses control of spin-orbit coupling in a linear array of single electron quantum dots. Quantum gates are carried out by pulsing the exchange interaction between neighboring electron spins, including the anisotropic corrections due to spin-orbit coupling. Control over these corrections, even if limited, is sufficient for universal quantum computation over qubits encoded into pairs of electron spins. The number of voltage pulses required to carry out either single-qubit rotations or controlled-NOT gates scales as the inverse of a dimensionless measure of the degree of control of spin-orbit coupling.

DOI: 10.1103/PhysRevLett.93.140501

PACS numbers: 03.67.Lx, 71.70.Ej, 73.21.La

Several quantum computation schemes are based on using the spin-1/2 degrees of freedom of electrons or certain nuclei as qubits [1–3]. For example, in the proposal of Loss and DiVincenzo [1], qubits are taken to be spins of single electrons trapped in quantum dots. Here we present a method for using spin-orbit coupling in such a system to perform universal quantum computation.

In many spin-based quantum computation schemes two-qubit gates are carried out by switching on and off the exchange interaction between neighboring spins [4,5]. For perfectly isotropic exchange, these two-qubit gates conserve total spin and so have too much symmetry to form a universal set; i.e., they cannot be used to carry out arbitrary unitary transformations on single-spin qubits. A universal set can be realized if single-spin rotations are possible [1], but it is generally believed these will be harder to achieve than two-qubit gates. An attractive alternative is to use an encoding scheme for which isotropic exchange alone is universal [6]. This requires encoding logical qubits into three or more spins [7,8].

Spin-orbit coupling leads to anisotropic corrections to the exchange interaction [9] which, under certain conditions elaborated on below, retains a residual rotational symmetry about a fixed axis. For many purposes these corrections are innocuous. The resulting exchange gates still form a universal set when combined with single-spin rotations [10,11]. And, through a combination of pulse shaping and locally defined spin quantization axes, they can be made effectively isotropic, although in general only to second order in spin-orbit coupling, so that exchange-only encoding can be used [12,13].

The partial reduction in symmetry, from isotropic to axial, can also simplify the requirements for universal quantum computation. In [14] it was shown that the XY interaction is universal for qubits encoded into only two spins, provided there is a third ancillary spin for each qubit. And in [15] it was shown that any axially symmetric anisotropic corrections, when combined with single-spin rotations about an axis perpendicular to the symmetry axis of the exchange, can be used to construct a universal set of gates for unencoded qubits.

In this Letter we propose a new method for quantum computation based on the ability to *control* the spin-orbit induced anisotropic corrections to the exchange interaction in a linear array of GaAs quantum dots. Our proposal requires encoding logical qubits into pairs of neighboring spins, similar to the encoding used in [16–18]. However, unlike these proposals, which require an inhomogeneous Zeeman field in addition to exchange, our proposal employs only the spin-orbit corrected exchange interaction.

Spin-orbit coupling is a relativistic effect which occurs because an electron moving in an electric field experiences a magnetic field which couples to its spin. In solids, the \mathbf{k} -dependent spin splitting due to spin-orbit coupling is described by the Hamiltonian $H_{SO} = \Omega(\mathbf{k}) \cdot \mathbf{S}$, where \mathbf{k} and \mathbf{S} are, respectively, crystal momentum and spin. Time-reversal symmetry implies $\Omega(\mathbf{k}) = -\Omega(-\mathbf{k})$; thus $\Omega \neq 0$ only in the absence of inversion symmetry. For a (001) two-dimensional electron gas (2DEG) in GaAs there are two sources of inversion asymmetry contributing to Ω . Taking k_x and k_y to be along the [100] and [010] crystal axes, respectively, the Dresselhaus contribution, $\Omega_D = f_D(-k_x, k_y, 0)$, is due to the bulk inversion asymmetry of the zinc blende structure of GaAs, with coupling f_D inversely proportional to the square of the width of the 2DEG [19], and the Rashba contribution, $\Omega_R = f_R(k_y, -k_x, 0)$, is due to the structural inversion asymmetry of the quantum well forming the 2DEG [20].

In the Hund-Mulliken description of two quantum dots, one Wannier orbital is kept per dot. Let t denote the tunneling amplitude between these orbitals in the absence of spin-orbit coupling. The effect of H_{SO} is to induce a small spin precession during this tunneling. If the dots lie in the (001) plane and are aligned in the [110] direction, the precession axis is fixed to be along the $[1\bar{1}0]$ direction [21]. The precession angle, η , then satisfies

$$\tan \frac{\eta}{2} = s \frac{a_0 \omega_0}{\sqrt{2} t} \langle \Psi_1 | (k_x + k_y) | \Psi_2 \rangle, \quad (1)$$

where Ψ_i is the Wannier state associated with dot i , and

$$s = \frac{f_D - f_R}{a_0 \omega_0} \quad (2)$$

is a dimensionless measure of the strength of spin-orbit coupling. Here a_0 and ω_0 are, respectively, the linear size and level spacing of a single isolated dot.

If the spin precession axis is fixed during gate operation, and the z axis in spin space is chosen to be parallel to this axis, exchange gates in the presence of spin-orbit coupling will have the form [11]

$$U_{12}(\lambda; \alpha, \beta, \gamma) = e^{-i\lambda H}, \quad (3)$$

where

$$H = \mathbf{S}_1 \cdot \mathbf{S}_2 + \frac{\alpha}{2}(S_1^z - S_2^z) + \beta(S_1^x S_2^y - S_1^y S_2^x) + \gamma(S_1^x S_2^z + S_1^y S_2^z) - \frac{1}{4}. \quad (4)$$

Here λ is the integrated strength of the dominant isotropic part of the interaction, and the parameters α , β , and γ characterize deviations from perfect isotropy. The constant $-1/4$ in H corresponds to a particular choice for the overall phase of U which will be convenient in what follows. For small s , $\alpha = C_\alpha s$, $\beta = C_\beta s$, and $\gamma = C_\gamma s^2$ [11]. C_β and C_γ are both of order 1 and depend on the shape and duration of the voltage pulse, though they cannot in general be set to 0. For a generic pulse, C_α is also of order 1 but, because α is odd under time reversal, it can be set to 0 by time-symmetric pulsing [12].

We envision two methods for controlling these anisotropic corrections. One is to control the width and shape of the potential confining the electrons to the 2DEG, thus controlling f_D and f_R , and hence s . For $f_D = f_R$ [22], s can even be set to zero. The other is to control the coefficients C_α , C_β , and C_γ by pulse shaping, as described above (see also [12]). Using these methods, it should be possible to achieve a *continuous range* of gates of the form (3), corresponding to small values of the parameter s . To ensure approximate axial symmetry, we assume a linear array of (001) quantum dots aligned along the [110] direction, as shown in Fig. 1. Note that corrections beyond Hund-Mulliken (i.e., involving more than one orbital per dot) will lead to deviations from perfect axial symmetry and will be a source of error. Here we assume these corrections are small enough to be ignored.

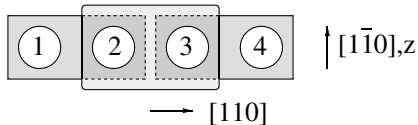


FIG. 1. Four quantum dots forming two neighboring logical qubits, 12 and 34. The dots lie in the (001) plane and are aligned along the [110] direction. The spin-orbit induced spin precession axis is parallel to the $[1\bar{1}0]$ direction. Exchange gates between spins within a logical qubit are used for single-qubit rotations. Two-qubit gates are carried out using exchange gates acting on spins 2 and 3.

Because of axial symmetry, the total S_z quantum number of this array will be conserved. It follows that the gates (3) cannot form a universal set if single spins are chosen to represent qubits. We therefore adopt the two-spin encoding scheme of [16–18]. To describe this encoding, we associate a pseudospin space with every nearest-neighbor pair of spins i and $i + 1$ spanned by the states

$$|S\rangle_{i,i+1} = \frac{1}{\sqrt{2}}(|\uparrow_i \downarrow_{i+1}\rangle - |\downarrow_i \uparrow_{i+1}\rangle), \quad (5)$$

$$|T_0\rangle_{i,i+1} = \frac{1}{\sqrt{2}}(|\uparrow_i \downarrow_{i+1}\rangle + |\downarrow_i \uparrow_{i+1}\rangle), \quad (6)$$

where $|S\rangle_{i,i+1}$ is pseudospin up and $|T_0\rangle_{i,i+1}$ is pseudospin down. The Hilbert space orthogonal to this pseudospin space is then spanned by the states $|T_+\rangle_{i,i+1} = |\uparrow_i \uparrow_{i+1}\rangle$ and $|T_-\rangle_{i,i+1} = |\downarrow_i \downarrow_{i+1}\rangle$. Given our phase convention, the gates (3) leave this space invariant,

$$U_{i,i+1}(\lambda, \boldsymbol{\phi}) |T_\pm\rangle_{i,i+1} = |T_\pm\rangle_{i,i+1}, \quad (7)$$

and so are entirely determined by their action on the pseudospin space,

$$U_{i,i+1}(\lambda, \boldsymbol{\phi}) = e^{i\lambda/2} e^{-i\boldsymbol{\phi} \cdot \boldsymbol{\sigma}^{(i,i+1)}/2}. \quad (8)$$

Here $\boldsymbol{\phi} = \lambda(\alpha, \beta, \gamma + 1)$ and the components of $\boldsymbol{\sigma} = (\sigma_x, \sigma_y, \sigma_z)$ are Pauli matrices, with the superscript $(i, i + 1)$ indicating that they act on the pseudospin space associated with spins i and $i + 1$. These gates then correspond to pseudospin rotations through the angle

$$\phi = \lambda(1 + 2\gamma + \alpha^2 + \beta^2 + \gamma^2)^{1/2} = \lambda + O(s^2), \quad (9)$$

about an axis parallel to $\boldsymbol{\phi}$.

In what follows we assume time-symmetric pulsing, so that $\alpha = 0$ for all gates. The available pseudospin rotation axes will then lie in the yz plane. Allowing nonzero α through time-asymmetric pulsing does not appreciably simplify any of our constructions. Given the ability to control the remaining anisotropic terms β and γ , either through direct control of s , or through pulse shaping, there will be a continuous range of available rotation axes. For a given rotation angle, ϕ , these axes will sweep out a wedge shape in the yz plane as shown in Fig. 2. The degree of control of spin-orbit coupling is then characterized by the angular size of this wedge, which we denote θ_m . We expect that θ_m will depend weakly on ϕ and will be on the order of the largest possible value of $|s|$. Note that the wedge of allowed rotation axes need not include the z axis, corresponding to $s = 0$, although as noted above it may be possible to achieve this through cancellation of the Dresselhaus and Rashba contributions.

For logical qubits encoded into the pseudospin spaces of dots i and $i + 1$, with i odd, and computational basis states $|0_L\rangle_{i,i+1} = |S\rangle_{i,i+1}$, and $|1_L\rangle_{i,i+1} = |T_0\rangle_{i,i+1}$ (see Fig. 1), we now show how pseudospin rotations can be used to perform single-qubit rotations and controlled-NOT (CNOT) gates, thus providing a universal set of quantum gates [23].

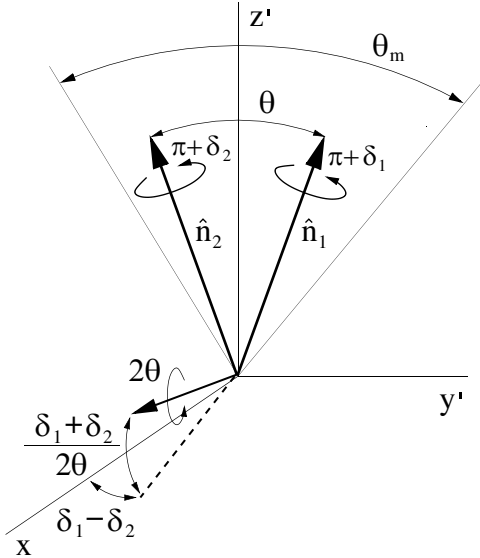


FIG. 2. Rotation axes in the pseudospin space of two neighboring spins. The wedge lying in the plane perpendicular to x and sweeping out the angle θ_m contains rotation axes which can be achieved using time-symmetric pulses and control of spin-orbit coupling. Successive π rotations about $\hat{\mathbf{n}}_1$ and $\hat{\mathbf{n}}_2$, with $\hat{\mathbf{n}}_1 \cdot \hat{\mathbf{n}}_2 = \cos\theta$, result in a 2θ rotation about the x axis. The effect of errors in the rotation angles, δ_1 and δ_2 , on the net rotation axis is also shown. Here $\hat{z}' \parallel (\hat{\mathbf{n}}_1 + \hat{\mathbf{n}}_2)$ and $\hat{y}' = \hat{z}' \times \hat{x}$.

Consider an arbitrary rotation about the x axis. This operation can be performed by a sequence of π rotations about available axes lying in the wedge. Figure 2 shows two such axes, \mathbf{n}_1 and \mathbf{n}_2 , making an angle $\theta \leq \theta_m$. A π rotation about \mathbf{n}_1 followed by a π rotation about \mathbf{n}_2 then results in a 2θ rotation about the x axis. The sense of this rotation can be reversed by reversing the order of the π rotations. Since a continuous range of axes within the wedge is available, a rotation about the x axis through an arbitrary angle Θ can be carried out by an even number, $2[\Theta/(2\theta_m)] + 2$, of π rotations, where $[x]$ denotes the greatest integer function of x . The standard Euler construction can then be used to generate arbitrary single-qubit rotations, with the number of pulses required growing as $1/\theta_m$ as θ_m goes to zero.

As θ_m is reduced, this construction also becomes increasingly sensitive to errors. To see this, let the rotation angles about $\mathbf{n}_{1(2)}$ be $\pi + \delta_{1(2)}$, where $\delta_{1(2)}$ are errors. If we take the z' axis to be parallel to $\mathbf{n}_1 + \mathbf{n}_2$ and the y' axis parallel to $\hat{z}' \times \hat{x}$ then the composition of these two rotations will yield an overall $2\theta + O(\delta^2/\theta)$ rotation about an axis deviating from the \hat{x} axis by an angle $\delta_1 - \delta_2$ in the y' direction and $(\delta_1 + \delta_2)/2\theta$ in z' direction (see Fig. 2). Thus, the larger θ_m is, the more robust this construction is against errors.

Now consider the two logical qubits shown in Fig. 1. A two-qubit gate between the 12 qubit and the 34 qubit can be carried out by a sequence of pulses acting on spins 2 and 3. Because the pseudospin space of spins 2 and 3 does not correspond to a logical qubit, rotations in this space

will, in general, mix in noncomputational states resulting in leakage errors. To avoid such errors, the net unitary transformation must be diagonal in the $\{\uparrow_1\downarrow_2\uparrow_3\downarrow_4, \uparrow_1\downarrow_2\downarrow_3\uparrow_4, \downarrow_1\uparrow_2\uparrow_3\downarrow_4, \downarrow_1\uparrow_2\downarrow_3\uparrow_4\}$ basis of the four spins. The most general unitary operator of the form (8) for which this is the case consists of a rotation about the x axis in pseudospin space. It follows that the net gate must be of the form

$$U_{23}(\Lambda, \Phi) = \prod_k U_{23}(\lambda_k; \phi_k) = e^{i(\Lambda/2)} e^{-i(\Phi/2)\sigma_x^{(2,3)}}, \quad (10)$$

where $\Lambda = \sum_k \lambda_k$ is the net phase and Φ is the rotation angle about the x axis produced by the sequence of rotations $\{\phi_k\}$. Note that both Λ and Φ are defined modulo 4π .

The gate (10) can be expressed in terms of operators acting on the logical qubits as follows:

$$U_{23}(\Lambda, \Phi) = e^{i(\Lambda/4)} e^{i(\Lambda/4)\sigma_x^{(1,2)}\sigma_x^{(3,4)}} e^{i(\Phi/4)\sigma_x^{(1,2)}} e^{i(\Phi/4)\sigma_x^{(3,4)}}. \quad (11)$$

By casting this gate in its canonical form [24], it can be shown to be equivalent to a CNOT gate, up to single-qubit rotations, if and only if

$$\Lambda = \sum_k \lambda_k = (2n + 1)\pi. \quad (12)$$

Below we outline two procedures for simultaneously satisfying (10) and (12).

For the first procedure, let $R_x(\pi)$ be a π rotation about the x axis. Using the single-qubit rotation scheme described above, this rotation can be performed through a sequence of $2n = 2[\pi/(2\theta_m)] + 2$ rotations about available axes. If $A(\phi)$ is then a ϕ rotation about a particular available axis lying in the yz plane, the sequence of rotations $A(\phi)R_x(\pi)A(\phi)$ will have the form (10) with $\Phi = (2n + 1)\pi$ regardless of the value of ϕ . According to (9) the contribution of $R_x(\pi)$ to the total phase Λ will then be $2n\pi + \mu$, where $\mu \sim O(s^2/\theta_m) \sim O(s)$. To satisfy (12) we therefore require $\phi = \pi/2 + O(s)$, where the $O(s)$ adjustment must be chosen so that $\lambda = \pi/2 - \mu/2$ for $A(\phi)$ and thus $\Lambda = (2n + 1)\pi$. This procedure is similar to those proposed in the two-spin encoding schemes of [15–18]. The main difference is that in these constructions the R_x rotation is generated by an inhomogeneous Zeeman field, whereas in ours it is generated entirely by a sequence of exchange gates corresponding to π rotations in the wedge of available axes. Again, as θ_m goes to zero, the number of required pulses scales as $1/\theta_m$ and the construction becomes increasingly sensitive to errors.

The second procedure requires more pulses in the limit of small θ_m but is simpler and less susceptible to error. The idea is to perform a sequence of 2π pseudospin rotations about any available axis or axes and use the spin-orbit induced mismatch between ϕ and λ to accrue the extra π phase required to satisfy (12). The resulting gate will then have the form (10) with $\Phi = 2n\pi$, where n

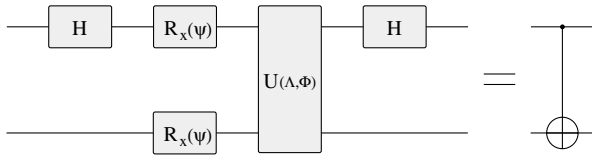


FIG. 3. Proposed CNOT construction. Each line corresponds to a logical qubit. $U(\Lambda, \Phi)$ is defined in (10) with $\Lambda = (2n + 1)\pi$. The value of Φ depends on the procedure used to carry out the CNOT. $H = (\sigma_x + \sigma_z)/\sqrt{2}$ is a Hadamard gate and $R_x(\psi)$ is a single-qubit rotation about the x axis through an angle ψ equal modulo 2π to $(\Phi + \Lambda)/2$.

is the number of 2π rotations. According to (9), for the i th rotation the corresponding phase factor will be $\lambda_i = 2\pi + \nu_i$, where $\nu_i \sim O(s^2)$. For a sequence to satisfy the constraint (12) the sum of all phases, and hence $\sum_i \nu_i$, must be an *odd* multiple of π . Given control of spin-orbit coupling, there will be a continuous range of achievable ν values for each 2π rotation, with $\nu_1 < \nu < \nu_2$, where $\nu_1, \nu_2 \sim O(s^2)$. If this range includes 0, then (12) can always be satisfied with $\lceil \pi/\nu_{\max} \rceil + 1$ rotations, where $\nu_{\max} = \max(|\nu_1|, |\nu_2|)$. If this range does not include 0 it will still always be possible to satisfy (12) with, at most, $\lceil \nu_{\max}/(\nu_2 - \nu_1) \rceil + 2 + \lceil \pi/\nu_{\max} \rceil$ rotations.

Regardless of which procedure is used, single-qubit gates acting on logical qubits 12 and 34 are required to complete the CNOT construction. One procedure for doing this is shown in Fig. 3.

Initialization can be performed by switching on the interaction between pairs of spins forming logical qubits and cooling. If s is set to 0 for this initialization, logical qubits will equilibrate to $|0_L\rangle$. If s cannot be set to 0, they will equilibrate to a state which can be rotated to $|0_L\rangle$. Readout can be performed using a modified version of the scheme proposed by Kane [2]. By switching on tunneling between dots forming a logical qubit, and raising the voltage of one dot so that it becomes doubly occupied if and only if the final state is a singlet, the qubit measurement can be converted to a charge measurement which can be performed using a single electron transistor. If the spin-orbit induced spin precession cannot be turned off during this process, it will not correspond to a measurement in the $\{|0_L\rangle, |1_L\rangle\}$ basis, but rather a measurement along a pseudospin axis nearly parallel to z . Again this does not cause any fundamental problems.

To carry out fault tolerant quantum computation, it must be possible to perform 10^5 gates within the spin decoherence time, τ_s [25]. In GaAs quantum dots, with pulse times of 1 ps [4] and $\tau_s \sim 10 \mu s$ [26], we estimate θ_m must be greater than 0.1 to do this. Given estimates of the size of anisotropic exchange in GaAs [9], we believe this is feasible.

To summarize, we propose a method for quantum computation based on controlling the spin-orbit induced

anisotropic corrections to the exchange interaction, with the degree of control characterized by the parameter θ_m . For two-spin encoding of logical qubits, single-qubit rotations and CNOT gates can be carried out with the number of pulses for each scaling as $1/\theta_m$ for small θ_m . For this scheme to be useful it is clearly desirable to design a system for which θ_m is as large as possible.

This work is supported by the National Science Foundation through NIRT Grant No. DMR-0103034.

- [1] D. Loss and D.P. DiVincenzo, Phys. Rev. A **57**, 120 (1998).
- [2] B. E. Kane, Nature (London) **393**, 133 (1998).
- [3] R. Vrijen *et al.*, Phys. Rev. A **62**, 012306 (2000).
- [4] G. Burkard, D. Loss, and D. P. DiVincenzo, Phys. Rev. B **59**, 2070 (1999).
- [5] X. Hu and S. Das Sarma, Phys. Rev. A **61**, 062301 (2000).
- [6] D. Bacon *et al.*, Phys. Rev. Lett. **85**, 1758 (2000).
- [7] D. P. DiVincenzo *et al.*, Nature (London) **408**, 339 (2000).
- [8] C. S. Hellberg, quant-ph/0304150.
- [9] K.V. Kavokin, Phys. Rev. B **64**, 075305 (2001); **69**, 075302 (2004).
- [10] G. Burkard and D. Loss, Phys. Rev. Lett. **88**, 047903 (2002).
- [11] D. Stepanenko *et al.*, Phys. Rev. B **68**, 115306 (2003).
- [12] N. E. Bonesteel, D. Stepanenko, and D. P. DiVincenzo, Phys. Rev. Lett. **87**, 207901 (2001).
- [13] L.-A. Wu and D. A. Lidar, Phys. Rev. Lett. **91**, 097904 (2003).
- [14] J. Kempe and K. B. Whaley, Phys. Rev. A **65**, 052330 (2002).
- [15] L.-A. Wu and D. A. Lidar, Phys. Rev. A **66**, 062314 (2002).
- [16] J. Levy, Phys. Rev. Lett. **89**, 147902 (2002).
- [17] S. C. Benjamin, Phys. Rev. A **64**, 054303 (2001).
- [18] D. A. Lidar and L.-A. Wu, Phys. Rev. Lett. **88**, 017905 (2002).
- [19] G. Dresselhaus, Phys. Rev. **100**, 580 (1955); M. I. Dyakonov and V. Yu. Kachorovskii, Sov. Phys. Semicond. **20**, 110 (1986).
- [20] E. I. Rashba, Fiz. Tverd. Tela (Leningrad) **2**, 1224 (1960) [Sov. Phys. Solid State **2**, 1109 (1960)]; Y. A. Bychkov and E. I. Rashba, J. Phys. C **17**, 6039 (1984).
- [21] We assume symmetry of the in-plane fields with respect to reflection through the $(1\bar{1}0)$ plane.
- [22] John Schliemann, J.C. Egues, and Daniel Loss, Phys. Rev. Lett. **90**, 146801 (2003).
- [23] M. A. Nielsen and I. L. Chuang, *Quantum Computation and Quantum Information* (Cambridge University Press, Cambridge, U.K., 2000).
- [24] B. Kraus and J. I. Cirac, Phys. Rev. A **63**, 062309 (2001); K. Hammerer, G. Vidal, and J. I. Cirac, Phys. Rev. A **66**, 062321 (2002).
- [25] J. Preskill, Proc. R. Soc. London A **454**, 385 (1998).
- [26] R. de Sousa and S. Das Sarma, Phys. Rev. B **67**, 033301 (2003).

Enhancement of Electron Spin Coherence by Optical Preparation of Nuclear Spins

Dimitrije Stepanenko and Guido Burkard

Department of Physics and Astronomy, University of Basel, Klingelbergstrasse 82, CH-4056 Basel, Switzerland

Geza Giedke and Atac Imamoglu

Institute of Quantum Electronics, ETH Zürich, CH-8093 Zürich, Switzerland

(Received 15 December 2005; published 3 April 2006)

We study a large ensemble of nuclear spins interacting with a single electron spin in a quantum dot under optical excitation and photon detection. At the two-photon resonance between the two electron-spin states, the detection of light scattering from the intermediate exciton state acts as a weak quantum measurement of the effective magnetic (Overhauser) field due to the nuclear spins. In a coherent population trapping state without light scattering, the nuclear state is projected into an eigenstate of the Overhauser field operator, and electron decoherence due to nuclear spins is suppressed: We show that this limit can be approached by adapting the driving frequencies when a photon is detected. We use a Lindblad equation to describe the driven system under photon emission and detection. Numerically, we find an increase of the electron coherence time from 5 to 500 ns after a preparation time of 10 μ s.

DOI: 10.1103/PhysRevLett.96.136401

PACS numbers: 71.70.Jp, 03.67.Pp, 78.67.Hc

Introduction.—Single electron spins localized in small artificial structures, such as semiconductor quantum dots (QDs), have become available and to a large extent controllable [1–4]. Of particular interest is the phase coherence of electron spins as single quantum objects, both from a fundamental physics point of view and because of their potential use as quantum bits (qubits) for quantum information processing [5,6].

A number of physical mechanisms that lead to the gradual reduction of the quantum phase coherence (decoherence) of the electron spin have been analyzed [7]. It has been established experimentally [2–4] and theoretically [8–13] that, in a GaAs QD, the predominant decoherence mechanism is the hyperfine coupling to the nuclear spins in the host material. For an unpolarized ensemble of N nuclei and an effective hyperfine interaction energy A , the dephasing time in a weak magnetic field is $T_2^* \sim 1/\sigma \sim \sqrt{N}/A$, where σ is the width of the distribution of nuclear field values h_z parallel to the field. In a typical GaAs QD with $A \sim 90 \mu\text{eV}$ or $A/g\mu_B = 3.5 \text{ T}$ [14], the number of Ga and As nuclei (spin $I = 3/2$) is $N \sim 5 \times 10^5$ and $T_2^* \sim 5 \text{ ns}$; this value is supported by the experimental evidence [4,15]. The T_2^* decay originates from nuclear ensemble averaging and can be prolonged by narrowing the nuclear spin distribution [12]. Another strategy is to polarize the nuclear spins [8], but this requires a polarization close to 100% which is currently not available [12]. Two schemes have been proposed to achieve a narrowing of the nuclear spin distribution, based on electron transport [16] and gate-controlled electronic Rabi oscillations [17].

Here we analyze an optical scheme for nuclear spin preparation that makes use of spin-flip two-photon (Raman) resonance in a driven three-level system (TLS), in analogy to electromagnetically induced transparency (EIT) in atoms [18,19]. The lowest electronic states in a

QD formed in a III-V semiconductor (e.g., GaAs) that are optically active under σ_+ circularly polarized excitation are the Zeeman-split ground state of a single localized conduction-band (E_C) electron and the negatively charged exciton (trion) $|X\rangle$, i.e., two electrons (spin up and down) plus one valence band heavy hole (hh) with angular momentum $J_{z'} = +3/2$ (Fig. 1). The $J = 3/2$ sector in the valence band is split into light hole and hh states along the axis z' of strong QD confinement. Here we assume excitation from the hh ($J_{z'} = \pm 3/2$) subband only. The axis z in

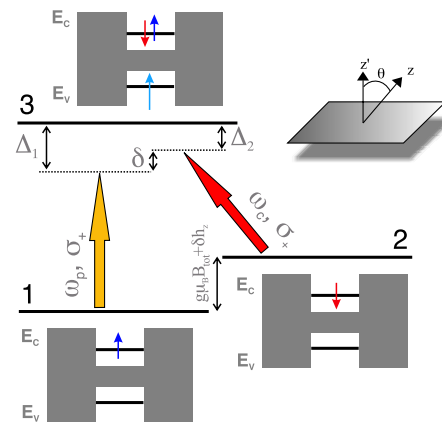


FIG. 1 (color online). Three-level system. State 1 (2) is a spin-up (-down) conduction-band (E_C) electron, with splitting $g\mu_B B_{\text{tot}} + \delta h_z$, where δh_z is the z component of the nuclear (Overhauser) field fluctuations. State 3 is a trion with $J_{z'} = 3/2$. Two laser fields with frequencies ω_p and ω_c are applied near the 13 and 23 resonances with detunings $\Delta_{1,2}$. For a σ_+ circularly polarized excitation (along z'), both transitions are allowed for $\theta \neq 0$ and transitions to the $J_{z'} = -3/2$ states are forbidden. Inset: Structural axis z' , leading to a splitting in E_V and spin quantization axis $z \parallel \mathbf{B}_{\text{tot}}$ in E_C where $\cos \theta = z \cdot z' < 1$.

E_C is parallel to the total magnetic field \mathbf{B}_{tot} , and we assume that the axes z and z' enclose an angle $\theta > 0$. The spin-up and -down states in E_C are then $|\uparrow\rangle \equiv |\uparrow\rangle_z = \cos(\theta)|\uparrow\rangle_{z'} + \sin(\theta)|\downarrow\rangle_{z'}$ and $|\downarrow\rangle \equiv |\downarrow\rangle_z = \cos(\theta)|\downarrow\rangle_{z'} - \sin(\theta)|\uparrow\rangle_{z'}$. Two circularly polarized (σ_+) continuous-wave lasers at the frequencies $\omega_p = \omega_X - \omega_l - \Delta_1$ and $\omega_c = \omega_X - \omega_l - \Delta_2$ stimulate the transitions between $|\uparrow\rangle$ and $|X\rangle$ and between $|\downarrow\rangle$ and $|X\rangle$, while the trion with $J_{z'} = -3/2$ is not excited.

The narrowing of the nuclear field distribution ν is based on light scattering in a TLS, where two long-lived (spin) states are coupled resonantly to an excited state that decays by spontaneous emission. When the two lasers satisfy exact two-photon resonance $\delta = \Delta_1 - \Delta_2 = 0$, one of the eigenstates of the system is a superposition of the two spin states with a vanishing excited state $|X\rangle$ component. The TLS at $\delta = 0$ is driven to this dark state with a vanishing light scattering rate [19]. The population of $|X\rangle$ and, thus, the photon scattering rate is nonzero for $\delta \neq 0$. In the presence of the nuclear spins, this resonance moves to $\delta = \delta h_z$, where δh_z is the deviation of the nuclear field (along z) from its mean $\langle h_z \rangle$. The absence of photon emission during a waiting time t constitutes a weak measurement of the quantum operator δh_z . In the limit $t \rightarrow \infty$, it becomes a strong measurement, projecting the nuclear state onto $|\delta h_z = 0\rangle$ (width $\sigma = 0$), thus eliminating electron decoherence due to the fluctuating field δh_z .

Model.—The Hamiltonian for the TLS coupled to nuclei is $H = H_0 + H_{\text{int}} + H_{\text{hf}}$, where $H_0 = -(\hbar\omega_z/2)\Sigma_z + \hbar\omega_X P_X$, with $\Sigma_i = \sigma_i \otimes \mathbb{0}$, the block-diagonal 3×3 matrix with the Pauli matrix σ_i in the upper left corner and 0 elsewhere, and $P_X = |X\rangle\langle X| = (001)^T(001)$. The spin splitting is given as $\hbar\omega_z = g\mu_B B_{\text{tot}} = |g\mu_B \mathbf{B} + \langle \mathbf{h} \rangle|$, the sum of the external magnetic and the mean nuclear fields. The nuclear (Overhauser) field operator is $\mathbf{h} = \sum_{i=1}^N A_i \mathbf{I}_i$, where $A_i = a_i v_0 |\Psi(\mathbf{r}_i)|^2$, and $\Psi(\mathbf{r}_i)$ denotes the electron wave function at the position \mathbf{r}_i of the i th atomic nucleus, v_0 is the volume of the unit cell, and a_i is the hyperfine coupling strength for the nuclear species at site i . The classical laser fields in the rotating wave approximation (RWA) are described by [19] $H_{\text{int}} = \Omega_p e^{i\omega_p t} |X\rangle \langle \uparrow| + \Omega_c e^{i\omega_c t} |X\rangle \langle \downarrow| + \text{H.c.}$ The coupling of the electron spin to the quantum fluctuations of \mathbf{h} is described by $H_{\text{hf}} = -\frac{1}{2} \delta \mathbf{h} \cdot \Sigma$, where $\delta \mathbf{h} = \mathbf{h} - \langle \mathbf{h} \rangle$. In the rotating frame $\tilde{\Psi}(t) = U(t)\Psi(t)$, with $U(t) = e^{-i\omega_p t} P_\uparrow + e^{-i\omega_c t} P_\downarrow + P_X$, where $P_\uparrow = |\uparrow\rangle\langle \uparrow|$ and $P_\downarrow = |\downarrow\rangle\langle \downarrow|$, we find $\tilde{H}(t) = U(t) \times [H(t) + \hbar\omega_p P_\uparrow + \hbar\omega_c P_\downarrow] U(t)^\dagger$ and, up to a constant (we drop the tilde and use H for the Hamiltonian henceforth),

$$H(t) = -\frac{\hbar}{2} \begin{pmatrix} \delta & 0 & \Omega_p \\ 0 & -\delta & \Omega_c \\ \Omega_p & \Omega_c & -\Delta \end{pmatrix} - \frac{\hbar}{2} \delta h_z \Sigma_z + H_\perp, \quad (1)$$

where $\Delta = \Delta_1 + \Delta_2$. The hyperfine flip-flop terms $H_\perp = \hbar(\delta h_+ \Sigma_- e^{i(\omega_p - \omega_c)t} + \delta h_- \Sigma_+ e^{-i(\omega_p - \omega_c)t})/4$ are oscillating rapidly at the frequency $\omega_p - \omega_c = g\mu_B B_{\text{tot}}/\hbar - \delta$

and can be neglected in the RWA [20], leading to a block-diagonal Hamiltonian $H = \text{diag}(H_1, H_2, \dots, H_K)$, with

$$H_k = -\frac{\hbar}{2} \begin{pmatrix} \delta h_z^k + \delta & 0 & \Omega_p \\ 0 & -\delta h_z^k - \delta & \Omega_c \\ \Omega_p & \Omega_c & -\Delta \end{pmatrix}, \quad (2)$$

where δh_z^k for $k = 1, 2, \dots, K$ are the eigenvalues of the operator δh_z and $K = (2I + 1)^N$ is the dimension of the nuclear spin Hilbert space. The state of the TLS combined with the nuclear spins is described by the density matrix ρ , which we divide up into 3-by-3 blocks $\rho_{kk'}$ and which evolves according to the generalized master equation [19]

$$\dot{\rho} = \mathcal{L}\rho \equiv \frac{1}{i\hbar} [H, \rho] + \mathcal{W}\rho, \quad (3)$$

with the Hamiltonian equation (1) and the dissipative term $\mathcal{W}\rho = \sum_{\alpha=\uparrow, \downarrow} \Gamma_{X\alpha} (2\sigma_{\alpha X} \rho \sigma_{X\alpha} - \sigma_{XX} \rho - \rho \sigma_{XX})/2 + \sum_{\beta=\downarrow, X} \gamma_\beta (2\sigma_{\beta\beta} \rho \sigma_{\beta\beta} - \sigma_{\beta\beta} \rho - \rho \sigma_{\beta\beta})/2$, where $\sigma_{ij} = \sigma_{ij} \otimes \mathbb{1} = |i\rangle\langle j|$. The rate $\Gamma_{X\alpha}$ describes the radiative decay of $|X\rangle$ into $\alpha = |\uparrow\rangle, |\downarrow\rangle$, while γ_β is the pure dephasing rate of state $\beta = |\downarrow\rangle, |X\rangle$ with respect to $|\uparrow\rangle$. Since H is block-diagonal, Eq. (3) leads to the closed form

$$\dot{\rho}_{kk'} = \frac{1}{i\hbar} (H_k \rho_{kk'} - \rho_{kk'} H_{k'}) + \mathcal{W}\rho_{kk'}. \quad (4)$$

The diagonal blocks obey the familiar Lindblad equation,

$$\dot{\rho}_{kk} = \mathcal{L}_k \rho_{kk}, \quad \mathcal{L}_k = -i[H_k, \rho] + \mathcal{W}\rho. \quad (5)$$

Stationary state.—We start with the factorized state $\rho_0 = \chi_0 \otimes \nu_0$, with arbitrary initial density matrices χ_0 and $\nu_0 = \sum_{kk'} \nu_{kk'} |\delta h_z^k\rangle \langle \delta h_z^{k'}|$ of the TLS and the nuclear ensemble, where $|\delta h_z^k\rangle$ are eigenstates of δh_z . We assume a Gaussian $\nu_{kk} = (2\pi)^{-1/2} \sigma^{-1} \exp[-(\delta h_z^k)^2/2\sigma^2]$, with the width $\sigma = \sigma_0 = A/\sqrt{N}$, plotted as a solid line in Fig. 2(a). For our numerics, we choose $A = 90 \mu\text{eV}$, $N \approx 5 \times 10^5$, corresponding to $\sigma_0 \approx 0.13 \mu\text{eV} \approx 0.2\hbar\Gamma$, with $\Gamma = 1$ ns, and a sample of $n \ll K$ states ($n \sim 4000$) [21]. Because of the hyperfine coupling, the TLS and the nuclei are entangled in the stationary state $\bar{\rho} = \sum_{kk'} \bar{\rho}_{kk'} \otimes |\delta h_z^k\rangle \langle \delta h_z^{k'}|$ with $\dot{\bar{\rho}} = \mathcal{L}\bar{\rho} = 0$. We derived an analytical expression for the 3-by-3 diagonal blocks $\bar{\rho}_{kk}$ of $\bar{\rho}$ as a function of all parameters, including δh_k .

Evolution of the observed system.—In order to enhance the electron-spin coherence, we aim at *narrowing* the nuclear spin distribution ν_{kk} . For a Gaussian distribution, this amounts to decreasing the width σ , thus increasing the electron coherence time $t_0 \approx 1/2\sigma$. Ideally, we would perform a projective measurement P on the nuclear spins, $P\bar{\rho}_{kk}P \propto \delta(\delta h_z^k - \delta)$. A successive approximation of P is achieved by monitoring the photon emission from the QD. The longer the period t during which no photon is emitted, the higher is the probability for δh_z to be at the two-photon resonance, $\delta h_z = \delta$.

To describe the state of the system conditional on a measurement record, we use the *conditional density matrix*

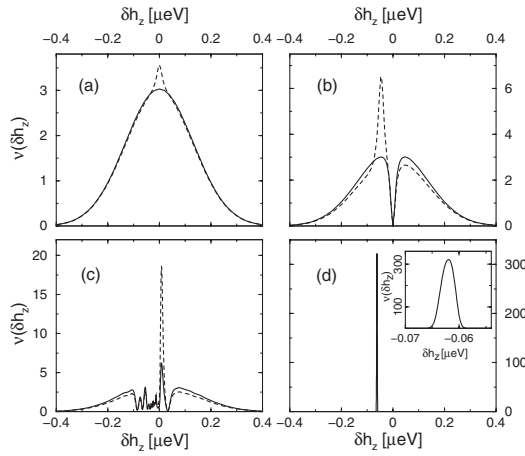


FIG. 2. Conditional evolution of the nuclear spin distribution $\nu(\delta h_z^k) = \nu_{kk}$. (a) During the first period t_1 without photon emission, the initial Gaussian distribution (solid line) develops a peak at the two-photon resonance (dashed line). (b) Change of $\nu(\delta h_z)$ after emission at t_1 (solid line), until before emission time t_2 of the second photon (dashed line). The two-photon resonance δ is shifted to the position of the left maximum (adaptive technique). The depleted region around $\delta h_z^k = 0$ develops at t_1 . (c) Analogous situation between t_{11} and t_{12} . (d) $\nu(\delta h_z)$ is obtained after a total time of $10 \mu\text{s}$. Inset: Magnification of peak in (d). The width of $\nu(\delta h_z)$ is reduced by a factor of ≈ 100 compared to the initial width in (a). The parameters are $\Omega_c = \Omega_p = 0.2 \text{ ns}^{-1}$, $\Delta = 0$, $\Gamma_{X\uparrow} = \Gamma_{X\downarrow} = 1 \text{ ns}^{-1}$, and $\gamma_I = \gamma_X = 0.001 \text{ ns}^{-1}$.

ρ^c . In the absence of photon emission, ρ^c obeys Eq. (5) with \mathcal{L}_k replaced by $\mathcal{L}_k - \mathcal{S}$, where the collapse operator \mathcal{S} describes spontaneous emission of the state $|X\rangle$ into $|\uparrow\rangle$ and $|\downarrow\rangle$ with rates $\Gamma_{X\uparrow}$ and $\Gamma_{X\downarrow}$ [22],

$$\dot{\rho}_{kk}^c = (\mathcal{L}_k - \mathcal{S})\rho_{kk}^c, \quad \mathcal{S}\rho = \sum_{\alpha=\uparrow,\downarrow} \Gamma_{X\alpha} \sigma_{\alpha X} \rho \sigma_{X\alpha}. \quad (6)$$

We have numerically calculated ρ^c in the absence of emitted photons for a duration t . We plot the updated distribution ν_{kk} from $\nu = \text{Tr}_\Lambda \rho^c$ as a dashed line in Fig. 2(a). We find that the *a posteriori* ν_{kk} is concentrated around the two-photon resonance. As the off-diagonal elements (coherences) of ν are constrained by positivity, $|\nu_{kk'}| \leq \sqrt{\nu_{kk}\nu_{k'k'}}$, they are also reduced by the narrowing of ν_{kk} . This process is eventually stopped by a photon emission.

Photon emission.—The stationary emission rate is [22]

$$\Gamma_{\text{em}} = \text{Tr} \mathcal{S} \bar{\rho}(t) = \Gamma \sum_k (\rho_{kk})_{XX} \nu_{kk}, \quad (7)$$

where $\Gamma = \Gamma_{X\uparrow} + \Gamma_{X\downarrow}$. The average photon number during time t is $\langle N_{\text{ph}} \rangle = t \Gamma_{\text{em}}$, and the *a priori* probability for $N_{\text{ph}} = 0$ is, according to Poissonian statistics, $P_{\text{dark}}(t) = \exp(-\Gamma_{\text{em}} t)$. The waiting time distribution for photon emissions is $p_{\text{wait}}(t) = \Gamma_{\text{em}}^{-1} \exp(-\Gamma_{\text{em}} t)$ with mean $\langle t \rangle = \Gamma_{\text{em}}^{-1}$. The narrowing of ν_{kk} , Eqs. (6) and (7), leads to a decreasing Γ_{em} and an increasing $\langle t \rangle$.

With Eq. (7), we find the update rule for ν upon photon emission, $\nu' = \text{Tr}_\Lambda \mathcal{S} \rho^c / \text{Tr} \mathcal{S} \rho^c$, or

$$\nu'_{kk} = \frac{\nu_{kk} (\rho_{kk})_{XX}}{\sum_j \nu_{jj} (\rho_{jj})_{XX}}, \quad (8)$$

where ν_{kk} and $(\rho_{kk})_{XX} = \langle X | \rho_{kk} | X \rangle$ are taken before the emission. The population in the Overhauser field δh_z corresponding to the two-photon resonance $\delta h_z = \delta$ is depleted by the photon emission [Fig. 2(b), solid line].

Adaptive technique.—The stationary, isolated TLS at the two-photon resonance is in a dark state. However, the coupling to the nuclei introduces a nonzero probability for occupation of $|X\rangle$ and for photon emission. Since the detection of a photon provides information about δh_z , the photon emission does not necessarily signify a failed attempt to narrow the nuclear field distribution but can be used as an input for the next weak measurement with adjusted frequencies of the driving lasers, $\omega'_p = \omega_p + \epsilon/2$ and $\omega'_c = \omega_c - \epsilon/2$, so that the new two-photon resonance condition is $\delta h_z = \delta'$, where $\delta' = \delta + \epsilon$ while $\Delta' = \Delta$. We choose ϵ such that the new resonance with the Overhauser field lies in one of the two maxima δh_z^{max} formed after the photon emission; see Fig. 2(b). This situation is described by Eq. (2) with the substitution $\delta \rightarrow \delta + \delta h_z^{\text{max}}$. The adaptive technique also works by changing only one of the laser frequencies. Right after the photon emission, the TLS is in one of the single electron states $|\uparrow\rangle$ or $|\downarrow\rangle$. Within a time $1/\Gamma$, much faster than any nuclear time scale, the system will reach the new stationary state. The photon emission from the QD can again be monitored, leading to an enhanced nuclear population at the new resonance [Fig. 2(b), dashed line], thus further narrowing the nuclear distribution. Repeating this procedure leads to a nuclear width that is limited only by the width of the EIT resonance [Figs. 2(c) and 2(d)].

Electron-spin decoherence.—The electron-spin coherence is quantified using the expectation value of the raising operator $S_+(t)$ in a state $|x_+\rangle$ that is prepared perpendicular to the total field \mathbf{B}_{tot} and is freely precessing about the fluctuating nuclear field δh_z , $\langle S_+(t) \rangle \equiv \langle x_+ | S_+(t) | x_+ \rangle$. We obtain $\langle S_+(t) \rangle = (\hbar/2) \sum_k \nu_{kk} \exp(it \delta h_z^k)$, which we plot in Fig. 3 at various stages in an adaptive optical measurement scheme. As the off-diagonal elements $\nu_{kk'}$ for $k \neq k'$ do not enter $\langle S_+(t) \rangle$ and Eq. (4) decouples, these results are valid for any ν_0 consistent with the chosen Overhauser field probability distribution. We make a Gaussian fit $\langle S_+(t) \rangle \propto \exp(-t^2/t_0^2)$ for short times t and plot the coherence time t_0 as a function of the total waiting time in Fig. 4. This is the main result of our theoretical analysis: The repeated observation of the QD photon emission and adaptation of the laser frequencies ω_c and ω_p after each photon emission leads to a pronounced enhancement of the electron coherence time, for the realistic parameters chosen, from $t_0 = 5 \text{ ns}$ to $\approx 500 \text{ ns}$ within a total observation time of $10 \mu\text{s}$.

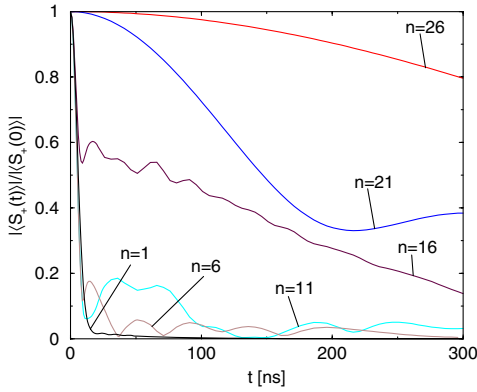


FIG. 3 (color online). Electron coherence function $|\langle S_+(t) \rangle|/|\langle S_+(0) \rangle|$ vs electronic precession time t calculated from $\nu(\delta h_z)$ in Fig. 2 after emission of the n th photon ($n = 1, 6, \dots, 26$). The initial decay is approximately Gaussian.

Imperfect detectors.—We cannot expect to have perfect photon detectors at our disposal; therefore, we discuss here the case of a detector with efficiency $e < 1$. For an imperfect detector, Eq. (6) becomes $\dot{\rho}_{kk}^c = (\mathcal{L}_k - e\mathcal{S})\rho_{kk}^c$, reflecting that photons are detected with probability e . We have numerically analyzed the case of $e = 10\%$ (other parameters as above) and find $t_0 \approx 460$ ns after a somewhat longer preparation time $t = 50 \mu\text{s}$. This is still much shorter than the time after which the nuclear spin decays, around 0.01 s due to higher-order hyperfine flip-flop terms [17], but possibly longer due to Knight-shift gradient effects. Nuclear flip-flop processes occur on a time scale of $\approx 100 \mu\text{s}$ [14] but are ineffective in changing h_z in a magnetic field that enforces nuclear spin conservation and, thus, preserve h_z for short-range flip-flops while long-range flip-flops are suppressed by the Knight-shift gradient. This picture is supported by the observed slow (≥ 1 s) decay of polarized nuclear spins in contact with donors in GaAs [23]. While a quantitative theory for the relevant time scale of nuclear spin decay due to nuclear-

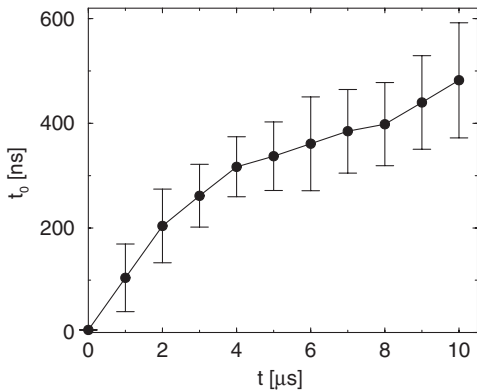


FIG. 4. Characteristic time t_0 of the initial Gaussian decay of $|\langle S_+(t) \rangle|/|\langle S_+(0) \rangle|$ in Fig. 3 as a function of the optical preparation time t , averaged over 50 numerical runs (error bars indicate the standard deviation).

dipole interactions is missing, the arguments given above suggest that our picture of a slow decay is reasonable.

Conclusions.—We find that it is possible to efficiently enhance the quantum phase coherence of an electron spin in a QD surrounded by a large ensemble of nuclear spins by a continuous weak measurement of the Overhauser field using optical excitation at a two-photon resonance of the TLS formed by $|\uparrow\rangle$, $|\downarrow\rangle$, and $|X\rangle$. An intriguing question is whether the electron-spin coherence can be enhanced by a quantum Zeno type effect to the point where it is ultimately determined by spin-orbit interaction: Since the reservoir correlation time of dominant electron-spin decoherence due to flip-flop terms of the hyperfine interaction is $\sim 1 \mu\text{s}$, this would most likely require high efficiency detection of the scattered photons.

We thank W.A. Coish, D. Klauser, D. Loss, M.D. Lukin, and J.M. Taylor for discussions. We acknowledge funding from the Swiss National Science Foundation (SNF) and through NCCR Nanoscience.

- [1] J.M. Elzerman *et al.*, Phys. Rev. B **67**, 161308 (2003).
- [2] A.C. Johnson *et al.*, Nature (London) **435**, 925 (2005).
- [3] F.H.L. Koppens *et al.*, Science **309**, 1346 (2005).
- [4] J.R. Petta *et al.*, Science **309**, 2180 (2005).
- [5] D. Loss and D.P. DiVincenzo, Phys. Rev. A **57**, 120 (1998).
- [6] A. Imamoglu *et al.*, Phys. Rev. Lett. **83**, 4204 (1999).
- [7] V. Cerletti *et al.*, Nanotechnology **16**, R27 (2005).
- [8] G. Burkard, D. Loss, and D.P. DiVincenzo, Phys. Rev. B **59**, 2070 (1999).
- [9] A. Khaetskii, D. Loss, and L. Glazman, Phys. Rev. Lett. **88**, 186802 (2002).
- [10] I.A. Merkulov, A.L. Efros, and M. Rosen, Phys. Rev. B **65**, 205309 (2002).
- [11] A. Khaetskii, D. Loss, and L. Glazman, Phys. Rev. B **67**, 195329 (2003).
- [12] W.A. Coish and D. Loss, Phys. Rev. B **70**, 195340 (2004).
- [13] W.A. Coish and D. Loss, Phys. Rev. B **72**, 125337 (2005).
- [14] D. Paget *et al.*, Phys. Rev. B **15**, 5780 (1977).
- [15] The decay of a spin echo envelope, being a measure for $T_2 \geq T_2^*$, can be much slower [4].
- [16] G. Giedke *et al.*, quant-ph/0508144.
- [17] D. Klauser, W.A. Coish, and D. Loss, cond-mat/0510177 [Phys. Rev. B (to be published)].
- [18] S.E. Harris, Phys. Today **50**, No. 7, 36 (1997).
- [19] M. Fleischhauer, A. Imamoglu, and J.P. Marangos, Rev. Mod. Phys. **77**, 633 (2005).
- [20] The neglected flip-flop terms contribute to electron-spin decoherence due to higher-order terms.
- [21] Smaller sample sizes ($n \sim 100$) also give reliable results due to the block-diagonal H . Denser sampling is used to resolve the sharp final distribution.
- [22] H.J. Carmichael, *An Open Systems Approach to Quantum Optics* (Springer, Berlin, 1993).
- [23] D. Paget, Phys. Rev. B **25**, 4444 (1982).

Quantum gates between capacitively coupled double quantum dot two-spin qubits

Dimitrije Stepanenko and Guido Burkard

Department of Physics and Astronomy, University of Basel, Klingelbergstrasse 82, CH-4056 Basel, Switzerland

(Received 13 October 2006; revised manuscript received 8 January 2007; published 27 February 2007)

We study the two-qubit controlled-NOT gate operating on qubits encoded in the spin state of a pair of electrons in a double quantum dot. We assume that the electrons can tunnel between the two quantum dots encoding a single qubit, while tunneling between the quantum dots that belong to different qubits is forbidden. Therefore, the two qubits interact exclusively through the direct Coulomb repulsion of the electrons. We find that entangling two-qubit gates can be performed by the electrical biasing of quantum dots and/or tuning of the tunneling matrix elements between the quantum dots within the qubits. The entangling interaction can be controlled by tuning the bias through the resonance between the singly occupied and doubly occupied singlet ground states of a double quantum dot.

DOI: [10.1103/PhysRevB.75.085324](https://doi.org/10.1103/PhysRevB.75.085324)

PACS number(s): 73.21.La, 03.67.Lx, 85.35.Be

I. INTRODUCTION

The spin 1/2 of a single electron trapped in a quantum dot (QD) is a promising candidate for a carrier of quantum information in a quantum computer.¹ To perform a quantum computation, we need to have all the unitary operations from some universal set of quantum gates at our disposal.² One such universal set consists of all the single-qubit quantum gates and a two-qubit controlled-NOT (CNOT) quantum gate. Quantum computation over the single-spin qubits with the logical states corresponding to the spin orientations $|\uparrow\rangle$ and $|\downarrow\rangle$ can, in principle, be achieved using an external magnetic field or with g -factor engineering for the single-qubit operations and with the time-dependent isotropic exchange interaction $H_{ex}(t)=J(t)\mathbf{S}_1\cdot\mathbf{S}_2$ for manipulating a pair of qubits encoded into spins \mathbf{S}_1 and \mathbf{S}_2 .¹

Control of electron spins in quantum dots is in the focus of many intense experimental investigations. Manipulation of pairs of electron spins using the tunable isotropic exchange interaction has already been demonstrated in several experiments.³⁻⁵ Such control was used in a study of the QD spin decoherence due to the hyperfine coupling to the surrounding nuclear spins, where the splitting between the singlet states with the total spin $S^{tot}=0$, where $\mathbf{S}^{tot}=\mathbf{S}_1+\mathbf{S}_2$, and the triplet states with $S^{tot}=1$ was used to turn the singlet-triplet mixing caused by the hyperfine interaction on and off. An important result of these studies is that the coherence time of an electron spin in a quantum dot is very long if the decoherence due to the interaction with the nuclear spins can be suppressed. The spin coherence times can be improved by the manipulation of nuclear spins,⁶⁻⁸ in principle, allowing for elaborate sequences of operations to be performed. Single-spin control is based on the local manipulation of the magnetic field or g factor¹ or on electron-spin-resonance methods^{9,10} and has only recently been demonstrated experimentally.¹¹

The difficulty of single-spin control has inspired a number of proposals for quantum computation based on the encoding of qubits into more than one spin. These encoding schemes reduce the requirement on the control over electron spins, but have the drawback of introducing so-called leakage errors, in which the state of encoded qubit “leaks” out of the set of computational states. Standard error-correction proce-

dures can be modified to prevent this kind of error.¹² A universal set of quantum gates operating on qubits encoded into states of three quantum dot spins with equal total spin quantum numbers can be implemented through control of the isotropic exchange coupling H_{ex} alone.¹³⁻¹⁵ Control over interactions that are symmetric only with respect to rotations about a fixed axis in spin space allows for the construction of a universal set of quantum gates that operate over qubits encoded into a pair of spins. One such encoding is into the orthogonal states $|\uparrow\downarrow\rangle$ and $|\downarrow\uparrow\rangle$ of two spins 1/2. A universal set of quantum gates over such qubits can, in principle, be performed by the control over H_{ex} , with the anisotropy provided by an external static homogeneous magnetic field and a site-dependent g factor.^{16,17}

We consider a variant of the two-spin encoding where the logical zero $|0_L\rangle$ and the logical one $|1_L\rangle$ quantum states are the singlet and the triplet with zero projection of the total spin to the symmetry axis z ($S_z^{tot}=0$); e.g., for lateral QDs, the z axis is the normal to the plane of the heterostructure,

$$|0_L\rangle = \frac{1}{\sqrt{2}}(|\uparrow\downarrow\rangle - |\downarrow\uparrow\rangle), \quad (1)$$

$$|1_L\rangle = \frac{1}{\sqrt{2}}(|\uparrow\downarrow\rangle + |\downarrow\uparrow\rangle).$$

These qubits can be manipulated by an axially symmetric interaction to produce a universal set of quantum gates. The interaction with an inhomogeneous Zeeman field and the isotropic exchange,^{16,17} the interaction with an inhomogeneous Zeeman field and an anisotropic spin-orbit coupling,¹⁸ and the spin-orbit coupling alone¹⁹ were all proposed as a way of producing a universal set of quantum gates operating on singlet-triplet two-spin qubit [Eq. (1)]. Recently, it was suggested that an architecture based on singlet-triplet qubits individually addressed using the isotropic exchange interaction and inhomogeneous magnetic field and coupled through Coulomb interactions of the electrons is scalable and, in principle, realizable.²⁰

In this paper, we study a particular realization of entangling two-qubit gates between singlet-triplet qubits [Eq. (1)], where each qubit is represented by a pair of tunnel-coupled single-electron quantum dots, as proposed in Ref. 20. In this

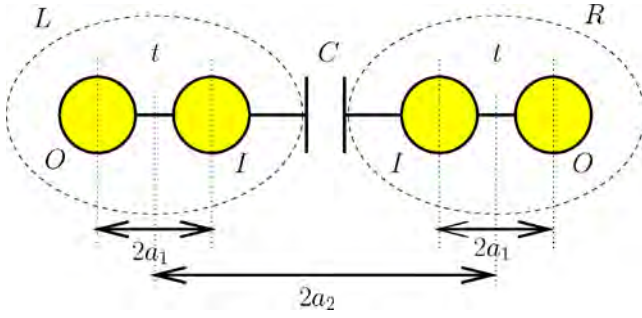


FIG. 1. (Color online) Double-double quantum dot (DDQD) setup. The four single-electron quantum dots are aligned along a fixed direction. The spins of the electrons on two quantum dots, inner (I) and outer (O), separated by a distance $2a_1$ encode a qubit. Two such double quantum dot (DQD) qubits, left (L) and right (R), at the distance $2a_2$ are separated by an impenetrable barrier. The tunneling matrix element t within the DQDs carrying the qubits and the bias ϵ of the inner dots with respect to the outer are equal on both DQDs and can be electrically tuned. The Coulomb interaction between the DQD is represented by the capacitor C .

realization, the double quantum dots are separated by a barrier, which is impenetrable for the electrons, so that the qubits are coupled exclusively through the Coulomb repulsion of electrons, while the exchange terms between electrons on different double quantum dots vanish. The setup of this double-double quantum dot (DDQD) is illustrated in Fig. 1.

The Coulomb interaction is spin independent, leading to an isotropic interaction $J\mathbf{S}_1 \cdot \mathbf{S}_2$ between tunnel-coupled spins \mathbf{S}_1 and \mathbf{S}_2 . The anisotropic correction to this interaction is dominated by the spin-orbit coupling induced term $J\boldsymbol{\beta} \cdot (\mathbf{S}_1 \times \mathbf{S}_2) + O(|\boldsymbol{\beta}|^2)$. The relative strength of the anisotropic interaction in quantum dot systems is estimated to be $|\boldsymbol{\beta}| \sim 0.1 - 0.01$.^{21,22} The influence of the anisotropic corrections can be reduced in specific implementations of the quantum gates.^{23,24} Coupling of singlet and triplet states in a DQD induced by the anisotropy would introduce errors in a quantum gate operation at the rate of approximately $|\boldsymbol{\beta}|^2$ for a generic implementation of the entangling gates and at the rate $|\boldsymbol{\beta}|^4$ if the methods of Ref. 24 are applied. In our study of a two-qubit gate operation, we will only consider the case of isotropic interaction and neglect the weak anisotropy. In this case, transitions between spin-singlet and spin-triplet states on a DQD are forbidden. Due to this spin symmetry, the four-electron Hamiltonian is block diagonal,

$$H = \text{diag}(H_{SS}, H_{ST}, H_{TS}, H_{TT}). \quad (2)$$

The nonzero blocks H_{ab} , where $a, b = S, T$, act on the states in which electron pairs on each DQD are either in the singlet (S) or in a triplet (T) state of the total spin $S^{\text{tot}} = 0$ or $S^{\text{tot}} = 1$.

Our main results are the effective low-energy spin interaction and a scheme to perform a two-qubit CNOT gate in an electrically controlled DDQD system. The effective low-energy spin interaction in this setup has the form

$$H = J(\mathbf{S}_{LI} \cdot \mathbf{S}_{LO} + \mathbf{S}_{RI} \cdot \mathbf{S}_{RO}) + E_e |SS\rangle\langle SS|. \quad (3)$$

Two pairs of spins, \mathbf{S}_{LI} and \mathbf{S}_{LO} on the left (L) qubit and \mathbf{S}_{RI} and \mathbf{S}_{RO} on the right (R) qubit (see Fig. 1), interact via the

isotropic exchange interaction of strength J and the entangling interaction of strength E_e that shifts the energy of the singlet-singlet state. We show how the entangling two-qubit quantum gates for universal quantum computation can be performed through the electrical control of E_e .

The triplet states with $S_z^{\text{tot}} = 0, \pm 1$ are degenerate in the absence of a magnetic field. A uniform magnetic field \mathbf{B} , pointing along the z axis normal to the plane of QDs, causes a Zeeman splitting $g\mu_B \mathbf{B} \cdot \mathbf{S}$ between the $S_z^{\text{tot}} = 0$ states and the states with $S_z^{\text{tot}} = 1, S_z^{\text{tot}} = \pm 1$. Our results apply to both the isotropic ($\mathbf{B} = 0$) and the anisotropic but axially symmetric ($\mathbf{B} \neq 0$) case if we take the $S_z^{\text{tot}} = 0$ state to represent the qubit $|1_L\rangle$ state.

A two-qubit quantum gate can, in principle, be performed by adiabatically varying the tunneling amplitude t and the bias ϵ within the DQD. A generic voltage pulse will modify the electrostatic potential in the quantum dots. We use the tunneling amplitude and the bias to describe this potential. In a more general approach, the new potential would be calculated as a solution to the electrostatic problem with external voltages specifying the boundary conditions. However, the wave functions of electrons are well localized at the positions of the quantum dots, and the parameters t and ϵ capture the possible variation of the electron Hamiltonian. In a naive picture, the tunneling and bias are controlled by separate electrodes. Another important issue is independent control over the two parameters. In principle, a change in the gate potentials will modify both parameters. The control will, however, be approximately independent as long as the quantum dots are well separated. In practice, it is much simpler to change the bias ϵ while t remains fixed.²⁷ The control parameters ϵ and t have to vary slowly on the time scale set by the energy splitting between the states of a given spin configuration. During the gate application, the orbital components of the S and T states are different due to the Pauli principle that forbids the electrons in a spin triplet to share their orbital state (see Fig. 2). As opposed to t and ϵ that are determined by gate voltages and can be changed more or less at will, the Coulomb interaction is set by the geometry of the system and therefore fixed. We show how the control of the parameters t and ϵ , or even ϵ alone, can nevertheless be used to implement entangling two-qubit gates on encoded singlet-triplet qubits through its influence on the Coulomb terms.

When an adiabatic gate is applied, the lowest-energy state in each block H_{ab} , of energy E_{ab} , where $a, b = S, T$ [see Eq. (2)], acquires a phase $\phi_{ab} = \int_{t_i}^{t_f} E_{ab}(t') dt' / \hbar$. The energy E_{ab} becomes time dependent through the time dependence of the parameters t and ϵ in the interval $t_i < t' < t_f$. The resulting interaction is described by an effective four-dimensional two-qubit Hamiltonian acting in the space spanned by the lowest-energy states $|SS\rangle$, $|ST\rangle$, $|TS\rangle$, and $|TT\rangle$ in the corresponding blocks H_{ab} , and has the form of Eq. (3).

In the regime of strong bias, $|\epsilon - U| \gg t$, where U is the on-site Coulomb repulsion, we investigate the DDQD system using perturbation theory. For the case of arbitrary bias ϵ , we numerically diagonalize the Hamiltonian [Eq. (2)]. We show that the two-qubit quantum gate can be operated by tuning the bias ϵ so that the amplitude of the doubly occupied state in the lowest-energy spin singlet becomes appreciable. In

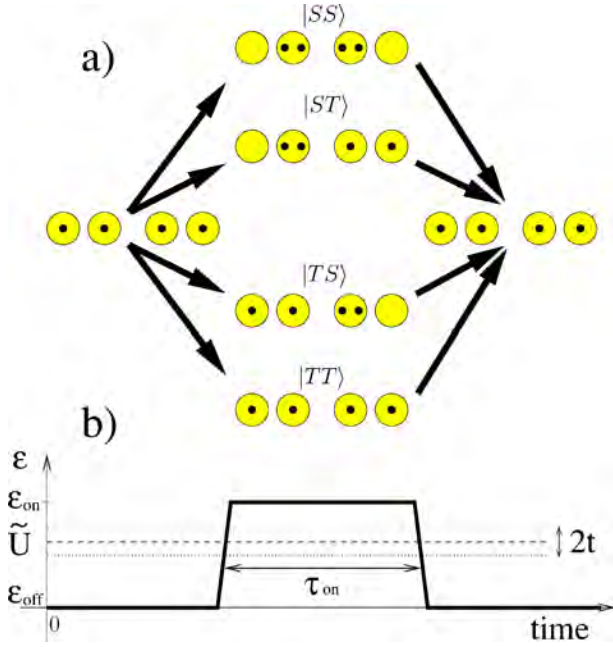


FIG. 2. (Color online) Two-qubit quantum gate. (a) When the inner quantum dots of the two double quantum dots system are strongly biased ($\epsilon > \tilde{U} + t$), the ground state is the doubly occupied inner dot. Due to the Pauli principle, only the spin singlets (S) can tunnel into the doubly occupied states on their QDs. As the bias ϵ is reduced, the states again become degenerate. (b) A quantum gate is performed by sending a bias pulse $\epsilon(t')$. Each qubit state $|ab\rangle$ acquires a phase $\phi_{ab} = \int_{-\infty}^{\infty} E_{ab}(t') dt' / \hbar$, where $E_{ab}(t')$ is the ground-state energy of the Hamiltonian at time t' reduced to the appropriate spin subspace, resulting in a two-qubit quantum gate.

this “on” state with a large double occupancy amplitude, entanglement is generated between the two-spin qubits. The entanglement generation is suppressed in the “off” regime with weak bias and tunneling. Therefore, the generation of entanglement between the two two-spin qubits encoded into DDQD can be efficiently controlled using the bias ϵ alone. Together with the single-qubit operation, this control is sufficient for universal quantum computing.

This paper is organized as follows. In Sec. II, we introduce our model of the DDQD system, followed by the discussion of the control through voltage pulses. In Sec. III, we focus on the case of the strongly biased ($|\epsilon - U| \gg t$) DDQD system and calculate the interaction between the qubits. The constraint of the strong bias is lifted in Sec. IV, where we numerically find the interaction between the qubits, valid at an arbitrary bias ϵ . In Sec. V, we outline the construction of a CNOT gate based on the resources for the control over a pair of qubits deduced from the results of Secs. III and IV. Our results are summarized in Sec. VI. The technical details of the calculation are collected in the Appendix.

II. MODEL

For the purpose of finding the effective low-energy spin Hamiltonian, the excited orbital states of single quantum dots can be neglected, leading to the Hund-Mulliken (HM) ap-

proximation with one orbital per dot.^{9,25} In the HM approximation, the state space of the two-electron system in a double quantum dot (DQD) encoding the left ($q=L$) or the right ($q=R$) qubit is spanned by three singlet basis states, $|\bar{S}\rangle$, $|D_I\rangle$, and $|D_O\rangle$, and one triplet basis state, $|T_0\rangle$,

$$|\bar{S}\rangle = \frac{1}{\sqrt{2}}(c_{qI\uparrow}^\dagger c_{qO\downarrow}^\dagger - c_{qI\downarrow}^\dagger c_{qO\uparrow}^\dagger)|0\rangle, \quad (4)$$

$$|D_I\rangle = c_{qI\uparrow}^\dagger c_{qI\downarrow}^\dagger|0\rangle, \quad (5)$$

$$|D_O\rangle = c_{qO\uparrow}^\dagger c_{qO\downarrow}^\dagger|0\rangle, \quad (6)$$

$$|T_0\rangle = \frac{1}{\sqrt{2}}(c_{qI\uparrow}^\dagger c_{qO\downarrow}^\dagger + c_{qI\downarrow}^\dagger c_{qO\uparrow}^\dagger)|0\rangle, \quad (7)$$

where c_k is the annihilation operator for an electron in the state $k=(q_k, p_k, s_k)$ on the qubit $q_k=L, R$, with position $p_k=I, O$, where I stands for inner and O for outer quantum dot within a qubit, and spin $s_k=\uparrow, \downarrow$. The vacuum $|0\rangle$ is the state of empty QDs.

In the standard notation, the singlet states of a DQD are denoted by $|(n, m)S\rangle$, where n is the number of electrons on the left QD and m is the number of electrons on the right QD. Our singly occupied singlet is then expressed as $|\bar{S}\rangle \equiv |(1, 1)S\rangle$. The doubly occupied singlet states on the left, $q=L$, DQD are $|D_I\rangle \equiv |(0, 2)S\rangle$ and $|D_O\rangle \equiv |(2, 0)S\rangle$. On the right, $q=R$, DQD the definitions are reversed, $|D_I\rangle \equiv |(2, 0)S\rangle$ and $|D_O\rangle \equiv |(0, 2)S\rangle$.

The orbital states annihilated by c_k approximate the ground states of the single-particle Hamiltonian,

$$H_1 = \sum_i \frac{1}{2m} \left[\mathbf{p}_i - \frac{e}{c} \mathbf{A}(\mathbf{r}_i) \right]^2 + V(\mathbf{r}_i), \quad (8)$$

describing an electron in the magnetic field $\mathbf{B}=\nabla \times \mathbf{A}$ and confined to the system of quantum dots by the electrostatic potential V . The quantum dots form in the minima of this potential, which is locally harmonic with the frequency ω_0 . The ground states of H_1 localized in these wells are the translated Fock-Darwin states.⁹

The HM Hamiltonian is of the generic form

$$H = t \sum_{k,l} (\delta_{q_k q_l} \delta_{s_k s_l} c_{q_k l s_k}^\dagger c_{q_l s_l} + \text{H.c.}) - \epsilon \sum_{k, p_k=I} c_k^\dagger c_k + \frac{1}{2} \sum_{klmn} \langle kl | V_C | mn \rangle c_k^\dagger c_l^\dagger c_n c_m. \quad (9)$$

The intra-DQD tunneling term $\propto t$ preserves the electron spin. The bias ϵ of the inner ($p_k=I$) QDs with respect to the outer ($p_k=O$) QDs is taken to be symmetric; i.e., the energy of both inner dots is lowered by the same amount. The two-body Coulomb interaction is denoted by V_C . Near the center of the quantum dot, the electrostatic potential is approximately harmonic and we assume that the wave functions of the electrons annihilated by the operators c_k are well approximated by the orthogonalized Fock-Darwin ground states.

The impenetrable barrier that separates the DQDs imposes the conservation of the number of $L(R)$ electrons, $\hat{n}_{L(R)} = \sum_{p=L,O; s=\uparrow, \downarrow} \hat{n}_{L(R)ps}$, where $\hat{n}_{qps} = c_{qps}^\dagger c_{qps}$. The $\hat{n}_{L(R)}$ conserving terms, proportional to the interaction matrix elements $\langle kl|V_C|mn\rangle$ in Eq. (9), where the indices k, l, m, n denote the single QD ground states, can be divided into intra-DQD terms where $q_k = q_l = q_m = q_n$ and inter-DQD terms that satisfy $q_k \neq q_l$ and $q_m \neq q_n$. All the other terms, e.g., the ones that annihilate two electrons on the left (L) DQD and create two on the right (R) DQD, violate the conservation of the electron numbers and therefore vanish.

A. Interaction within a double quantum dot

The terms for the interaction within a DQD in Eq. (9) were discussed in Ref. 9. They renormalize the one-body tunneling matrix element $t \rightarrow t_H = t + \langle \bar{S}|V_C|D_{I(O)}\rangle / \sqrt{2}$, introduce the on-site repulsion $U = \langle D_{I(O)}|V_C|D_{I(O)}\rangle$ of two electrons on the same QD, and cause transitions between the two doubly occupied DQD states with the matrix element $X = \langle D_{I(O)}|V_C|D_{O(I)}\rangle$. Also, the Coulomb interaction on a DQD contributes $V_+ = \langle \bar{S}|V_C|\bar{S}\rangle$ to the electrostatic energy of the symmetric and $V_- = \langle T_0|V_C|T_0\rangle$ to the antisymmetric singly occupied orbitals of two electrons in a DQD,⁹ giving rise to a direct exchange interaction between spins. As a result, the electrons on a DQD are described by an extended Hubbard model with the isotropic exchange interaction,⁹

$$J = V_- - V_+ - \frac{U_H}{2} + \frac{1}{2} \sqrt{U_H^2 + 16t_H^2}, \quad (10)$$

where $U_H = U - V_+ + X$ is the effective on-site repulsion.

B. Interaction between the double quantum dots

The Coulomb interaction between the DQDs produces three new classes of direct terms in the Hamiltonian, while the exchange terms between the DQD vanish due to the impenetrable barrier.

In the first class are the terms proportional to the number operators $\hat{n}_{qps}\hat{n}_{\bar{q}p's'}$, describing the electrostatic repulsion of the electrons in states qps and $\bar{q}p's'$, where $\bar{L}=R$ and $\bar{R}=L$. For a pair of identical DQDs, there are three such terms: the interaction of a pair of electrons on the inner QDs, $U_N = \langle qIs, \bar{q}Is'|V_C|qIs, \bar{q}Is'\rangle$, the interaction of an electron on the inner QD of one DQD and an electron in the outer QD of the other DQD, $U_M = \langle qIs, \bar{q}Os|V_C|qIs, \bar{q}Os\rangle$, and the interaction of electrons on the outer QDs, $U_F = \langle qOs, \bar{q}Os|V_C|qOs, \bar{q}Os\rangle$ [Fig. 3(a)].

In the second class are the terms proportional to $\hat{n}_{qps}c_{\bar{q}p's'}^\dagger c_{\bar{q}p's'}$, where $\bar{I}=O$ and $\bar{O}=I$. These terms describe the spin-independent correction to the tunneling matrix element in the \bar{q} qubit due to the interaction with an electron in the state qps . The two parameters that determine the tunneling corrections are $T_{p'} = \langle qps, \bar{q}p's'|V_C|q\bar{p}s, \bar{q}p's'\rangle$, and are due to the interaction with an electron in the $p'=I, O$ orbital in the other DQD [Fig. 3(b)].

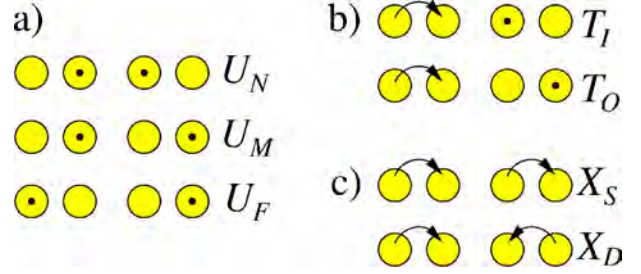


FIG. 3. (Color online) Effects of the direct Coulomb interaction between double quantum dots (DQDs). All the exchange terms between the DQDs vanish due to the impenetrable barrier. (a) The Coulomb repulsion between the electrons on different double quantum dots contributes to the energy of the system. In the case of identical DQDs separated by an impenetrable barrier, there are three such contributions, coming from the electrons in orbitals that are near (U_N), at a medium distance (U_M), or far apart (U_F). (b) The tunneling matrix elements within a DQD are renormalized by T_I or T_O due to the interaction with an electron on the inner or the outer dot of the other DQD. (c) The interaction enables the correlated hopping processes in which electrons simultaneously tunnel in both DQDs. In one such process, the electrons tunnel to the same side (either left or right) with the matrix element X_S . In the other correlated hopping process, electrons simultaneously tunnel into the inner or outer quantum dots of their double quantum dots with the matrix element X_D .

The terms in the third class are proportional to $c_{qps}^\dagger c_{\bar{q}p's'}^\dagger c_{\bar{q}p's'} c_{qps}$ and describe the processes in which electrons in both DQD tunnel simultaneously [Fig. 3(c)]. The two independent matrix elements for these processes are $X_S = \langle qps, \bar{q}p's'|V_C|q\bar{p}s, \bar{q}p's'\rangle$, describing the tunneling from the inner to the outer orbital in one DQD and from the outer to the inner in the other, and $X_D = \langle qps, \bar{q}p's'|V_C|q\bar{p}s, \bar{q}p's'\rangle$, describing the simultaneous tunneling into inner or outer orbitals in both DQDs. For the system in zero magnetic field, these two matrix elements are equal, $X_S = X_D$.

C. Control of the interaction

In order to describe the influence of the intra-DQD tunneling t and the bias ϵ on the spectrum of the DDQD, we have to model the dependence of the Hamiltonian on these external parameters. In an experiment, both t and ϵ are controlled by applying voltages to the electrodes that define the quantum dots. The exact form of the voltage-dependent DDQD binding potential was studied using the Schrödinger-Poisson equation,²⁶ but here we do not attempt to calculate the dependence of the Hamiltonian [Eq. (2)] on ϵ and t from first principles.

Instead, we adopt a quartic double-well model for the potential of a DQD centered at $(\pm a_2, 0)$ of the form⁹

$$V(x, y) = \frac{m\omega_0^2}{2} \left\{ \frac{1}{4a_1^2} [(x \mp a_2)^2 - a_1^2]^2 + y^2 \right\}, \quad (11)$$

where m is the electron effective mass, $2a_1$ is the distance between the approximately harmonic wells in a DQD, and $2a_2$ is the distance between the DQD double-well minima. In

the limit of well separated dots, $a_{1,2} \gg a_B$, where a_B is the QD Bohr radius given by $a_B^2 = \hbar/m\omega_0$, and near the local minima of the quartic potential well at $(\pm a_2 \pm a_1, 0)$, the potential is approximately harmonic with the frequency ω_0 . The Fock-Darwin ground-state wave functions in this harmonic potential centered at $(x_c, 0)$ and in the magnetic field B normal to the plane of the dots, described in the symmetric gauge by the vector potential $\mathbf{A} = B(-y, x, 0)/2$, are

$$\phi_{x_c}(x, y) = \sqrt{\frac{m\omega}{\pi\hbar}} e^{-m\omega[(x-x_c)^2 + y^2]/2\hbar + im\omega_L x_c y/\hbar}, \quad (12)$$

where $\omega_L = eB/2mc$ is the electron Larmor frequency and $\omega = \sqrt{\omega_0^2 + \omega_L^2}$ is the resulting confinement frequency with both electrostatic and magnetic contributions. We will use the magnetic compression factor $b = \omega/\omega_0$ to measure the strength of the magnetic field, consistent with the notation in Ref. 9.

The translated single-electron Fock-Darwin states $\phi_{\pm a_2 \pm a_1}(x, y)$ define the state space of the variational HM approximation for a DDQD. The tunneling matrix element between the Fock-Darwin ground states in the local minima of the potential [Eq. (11)] is our control parameter t ,⁹

$$t \equiv \langle \phi_{\pm a_2 + a_1} | H_1 | \phi_{\pm a_2 - a_1} \rangle = \frac{3}{8} \frac{S}{1 + S^2} \left(\frac{a_1^2}{a_B^2} + \frac{1}{b} \right), \quad (13)$$

where $S = \langle \phi_{\pm a_2 + a_1} | \phi_{\pm a_2 - a_1} \rangle = \exp[-d_1^2(2b - 1/b)]$ is the overlap between the Fock-Darwin ground states in a DQD and $d_1 = a_1/a_B$ is the distance between the QDs within the DQD in the units of the QD Bohr radius.

As t is changed by external voltages, we assume that the overlap S between the oscillator states remains consistent with the relation in Eq. (13), which is valid for the double-well potential V . All the Coulomb matrix elements can be expressed in terms of S so that after solving Eq. (13) for the overlap, they become functions of t (see the Appendix). The bias ϵ is modeled as an energy shift of the orbitals, so that the inner $p_k = l$ orbitals have their energy reduced by ϵ .

The two-qubit gates are applied by time-dependent tuning of the tunneling matrix element t and/or the bias ϵ in the DQDs using voltage pulses. In a typical experiment, the control of the QD energies through ϵ is much easier to achieve than the control over tunneling matrix element t .²⁷ The reason behind this is that the energy bias is linear in applied voltage, while the tunneling is typically exponential.

The structure of the energy levels is particularly simple in the limit of zero tunneling $t=0$. In this limit, the eigenstates are the Hund-Mulliken basis states [Eqs. (4)–(7)]. Their energies are determined by the bias ϵ , the external magnetic field B , and the direct Coulomb interaction that is set by the device geometry. A drastic change in the structure of the DDQD spectrum as a function of bias ϵ appears at the crossings of the lowest-energy singlet states within a DQD. Each of the singlet states $|\bar{S}\rangle$, $|D_I\rangle$, and $|D_O\rangle$ is lowest in energy for some values of the bias ϵ (Fig. 4). A crossing occurs when either the positive bias overcomes the effective on-site repulsion \tilde{U} , making the state with both electrons in an inner dot $|D_I\rangle$ the lowest in energy, or the negative bias makes $|D_O\rangle$ the

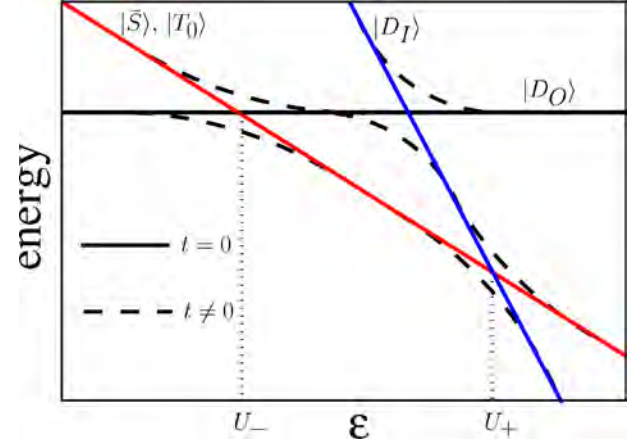


FIG. 4. (Color online) Illustration of the double quantum dot energy levels as a function of the bias ϵ . The energy of the singlet state with doubly occupied outer quantum dot, $|D_O\rangle$, is independent of the bias. The energies of the singly occupied singlet, $|\bar{S}\rangle$, and the singly occupied triplet, $|T_0\rangle$, state are lowered with the increasing bias as they have a contribution of -2ϵ from the biased inner quantum dots. The energy of the singlet with doubly occupied inner quantum dots, $|D_I\rangle$, is lowered with the increasing bias faster than the energy of $|\bar{S}\rangle$ and $|T_0\rangle$ state due to the bias contribution of -4ϵ . When the tunneling t is zero, the lowest-energy levels cross at the bias U_{\pm} , leading to a drastic change of the effective spin interaction. For nonzero tunneling, the levels anticross, but the effective spin interaction still changes significantly when we tune the system from one side of the anticrossing to the other.

lowest in energy (see Fig. 5). We use the effective on-site repulsion \tilde{U} to emphasize the fact that it includes not only the repulsion of two electrons in the same dot, denoted by U , but also the energy of the interaction with the electrons on the other DQD. We will also use two special values of the effective on-site repulsion, U_{\pm} . Due to the dependence of the effective on-site repulsion on the state of the other DQD, the lowest-energy singlet-singlet DDQD state can consist of dif-

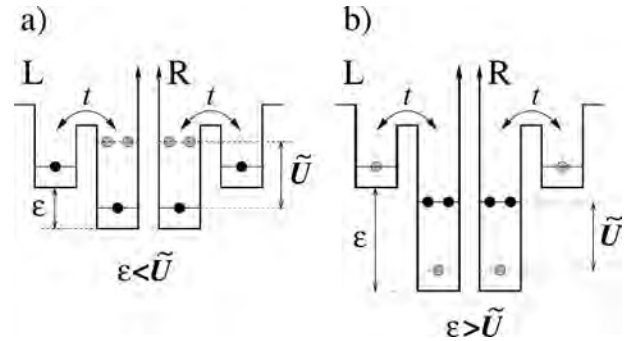


FIG. 5. Bias dependence of the double-double quantum dot (DDQD) ground state. (a) When the bias ϵ of the inner quantum dots with respect to the outer ones is weaker than the effective on-site Coulomb repulsion \tilde{U} , the charge configurations of the lowest-energy singlet and triplet states consists of singly occupied orbitals. (b) When $\epsilon > \tilde{U}$, the lowest-energy singlet has a doubly occupied inner quantum dot, while the orbital state of the lowest-energy triplet remains unchanged.

ferent singlets on the two dots, as in $|\bar{S}, D_I\rangle$ and $|D_I, \bar{S}\rangle$. In the strong-bias regions, the lowest-energy singlets are doubly occupied states. For $\epsilon - U_+ \gg t$, the lowest-energy singlet is $|D_I D_I\rangle$, and for $U_- - \epsilon \gg t$, the lowest-energy singlet is $|D_O D_O\rangle$. The second doubly occupied singlet state is separated by an energy gap $\approx 2|\epsilon|$ from the lowest-energy state.

III. STRONG BIAS

To develop an intuitive picture of the operation of an entangling two-qubit gate and the mechanisms for its control, we consider the simple case of strong bias. We show how the switching between the strong-bias regime ($\epsilon - U_+ \gg t$) and the weak-bias regime, in which the dominant interaction is the on-site repulsion, provides us with control over the entangling interaction E_e . The boundary of the strong-bias regime considered here is set by $U_+ = (3U_N - 2U_M - U_F - 2V_- + 2U)/2$. A similar strong-bias regime with the lowest-energy singlet $|D_O, D_O\rangle$ exists for $U_- - \epsilon \gg t$, where $U_- = (3U_F - 2U_M - U_N - 2V_- + 2U)/2$, but we do not consider it here in detail. In both of these regimes, a wide energy gap $\approx 2|\epsilon|$ to the second doubly occupied state allows us to neglect that state. This approximation reduces the dimensions of the Hamiltonian blocks H_{ab} [Eq. (2)] and allows for a perturbative solution.

Since the only available DQD states in the strong-bias regime are the triplet, $|T_0\rangle$, and two singlets, $|\bar{S}\rangle$ and $|D_I\rangle$, the H_{TT} block of Eq. (2) is one dimensional, H_{ST} and H_{TS} are two dimensional, and H_{SS} is four dimensional. For the present discussion of the strong-bias regime, we choose the zero of the energy scale at $4\hbar\omega - 2\epsilon + U + 2V_+ + U_N + 2U_M + U_F$, setting the expectation value of the energy of four singly occupied QDs with the DQDs in the electron singlet states to zero, $\langle \bar{S}, \bar{S} | H | \bar{S}, \bar{S} \rangle = 0$. Using the expressions for the Hamiltonian matrix elements given in the Appendix, we find the matrices of the H_{ab} blocks ($a, b = S, T$). The energy of the $|TT\rangle$ state is then

$$E_{TT} = 2(V_- - V_+). \quad (14)$$

The two-dimensional blocks H_{TS} and H_{ST} are related by the symmetry under exchange of the double quantum dots $L \leftrightarrow R$ and in the bases $\{|\bar{S}, T_0\rangle, |D_I, T_0\rangle\}$ and $\{|T_0, \bar{S}\rangle, |T_0, D_I\rangle\}$, and have the identical matrix form

$$H_{TS} = H_{ST} = V_- - V_+ + \begin{pmatrix} 0 & \sqrt{2}t_S \\ \sqrt{2}t_S & V_D - \epsilon \end{pmatrix}, \quad (15)$$

where $t_S = -t_H + T_S$ is the renormalized hopping matrix element and $V_D = U - V_+ + U_N - U_F$ is the electrostatic energy cost of doubly occupying the $p_k = I$ state in the presence of the triplet DQD. With our choice of the zero of the energy scale, the ground-state energies of H_{ST} and H_{TS} are

$$E_{ST} = E_{TS} = V_- - V_+ + \frac{1}{2}(V_D - \epsilon) - \frac{1}{2}\sqrt{(V_D - \epsilon)^2 + 8t_S^2}. \quad (16)$$

From the energies E_{ST} and E_{TS} , we extract the isotropic exchange part of the low-energy four-spin Hamiltonian [Eq. (3)] as

$$J = E_{TT} - E_{ST} = E_{TT} - E_{TS}. \quad (17)$$

The resulting exchange interaction strength is

$$J = V_- - V_+ - \frac{1}{2}(V_D - \epsilon) + \frac{1}{2}\sqrt{(V_D - \epsilon)^2 + 8t_S^2}. \quad (18)$$

Comparing this result with the case of an unbiased isolated double quantum dot [Eq. (10)], we see that the effect of the strong bias ϵ and the presence of another DQD behind the impenetrable barrier is the change of the effective on-site repulsion to the value $V_D - \epsilon$ and a reduction of the effective tunneling matrix element because of the large gap to the excited doubly occupied state. As a consequence of this gap, the isotropic exchange in the limit of noninteracting DQDs and weak tunneling is $J = V_- - V_+ + 2t_H^2/(U - V_+ - \epsilon)$, with the hopping contribution reduced to half of the result expected from the standard Hubbard model in the unbiased case, $4t_H^2/U_H$.⁹

The four-dimensional block H_{SS} in the basis $\{|\bar{S}, \bar{S}\rangle, (|\bar{S}, D_I\rangle + |D_I, \bar{S}\rangle)/\sqrt{2}, |D_I, D_I\rangle, (|\bar{S}, D_I\rangle - |D_I, \bar{S}\rangle)/\sqrt{2}\}$ is

$$H_{SS} = \begin{pmatrix} 0 & 2t_S & 2X_D & 0 \\ 2t_S & V_D - \epsilon + 2X_S & 2t_I & 0 \\ 2X_D & 2t_I & E_{DD} & 0 \\ 0 & 0 & 0 & V_D - \epsilon - 2X_S \end{pmatrix}, \quad (19)$$

where t_I is the tunneling matrix element renormalized by the spectator DQD in the doubly occupied state, and

$$E_{DD} = 2U + 3U_N - 2U_M - U_F - 2V_+ - 2\epsilon \quad (20)$$

accounts for the repulsion energy of four electrons in the $p_k = I$ orbitals and the bias ϵ (see the Appendix). Due to the symmetry with respect to exchange of the DQDs, $L \leftrightarrow R$, the antisymmetric state $(|\bar{S}, D_I\rangle - |D_I, \bar{S}\rangle)/\sqrt{2}$ decouples from the other, symmetric, states.

In the limit of large and positive bias, $|\epsilon - V_D| \gg t_{SI}, X_{SI/D}$, all the tunneling and correlated hopping terms in the Hamiltonian H_{SS} can be taken to be small. The unperturbed Hamiltonian is then diagonal and the ground-state energy is E_{DD} . This situation is relevant because all the small terms are proportional to the overlap S of the localized states in the quantum dots, which is small for weakly tunnel-coupled QDs, and we can reach this regime by applying external voltage to make $|\epsilon - V_D|$ large enough.

Operating the system in the strong-bias regime causes a qualitative change to the effective low-energy Hamiltonian by turning on the entanglement generating term E_e in Eq. (3),

$$E_e = E_{TT} - 2E_{ST} + E_{SS}. \quad (21)$$

For a weak bias and in the absence of tunneling, the entanglement generating E_e term is zero, as can be checked from the energies of the states $|\bar{S}, \bar{S}\rangle$, $|T_0, \bar{S}\rangle$, and $|T_0, T_0\rangle$,

given in the Appendix. This is not true in the case of a strong bias, where the entangling interaction of the strength $E_e = U_N - 2U_M + U_F \neq 0$ is present even if the tunneling terms are zero. In the strong-bias regime, the conditions for $E_e = 0$ are $t_I = t_S$, $X_S = X_D$, and $E_{DD} = 2(V_D - \epsilon)$. While the first two conditions are satisfied when there is no tunneling, the third is independent of the tunneling. It is only satisfied in the limit of long distance between DQDs, $a_2 \gg a_1$ (see Fig. 1). The tunneling causes a second-order correction to E_{SS} ,

$$E_{SS} = E_{DD} + \frac{4t_I^2}{E_{DD} - (V_D - \epsilon)} + \frac{4X_D^2}{E_{DD}}, \quad (22)$$

and the corresponding correction to E_e .²⁸ Since the basic control mechanism relies on turning the entangling interaction on and off in the $E_e \neq 0$ and $E_e = 0$ regimes, the control is robust against small imperfections. For example, if the quantum dots are not identical or the distances between the QDs within two DQDs are different, the value of E_e would change, but it could still be turned on and off using external voltages.

We have calculated the matrix elements of the Coulomb interaction using the basis of single-electron Wannier states obtained by orthogonalizing the Fock-Darwin ground states centered at the quantum dot positions, following Ref. 9. The resulting matrix elements can all be expressed in terms of the distances between the quantum dots and the tunneling matrix element t between QD in DQD. These results are summarized in the Appendix. Together with Eqs. (3), (18), and (22), they provide a model of the low-energy Hamiltonian of a pair of qubits realized on a DDQD in the strong-bias regime. This model can describe a two-qubit quantum gate realized by adiabatically switching the value of the control parameter ϵ so that the qubit goes from the weak-bias regime to the strong-bias regime and back.

In an array of DQDs, where each encodes a qubit, a quantum gate can be applied by bringing the pairs of neighboring qubits that we would like to entangle into the $E_e \neq 0$ regime, while keeping $E_e = 0$ for all the other pairs. Each QD can play the role of either an inner or an outer QD, depending on the neighbor with which the entanglement is created. The Hamiltonian [Eq. (3)] and the gates generated by it are invariant under the interchange of the inner and outer QDs within a qubit.

In summary, the interaction of the DQDs causes a change in the parameters of the extended Hubbard model coupling strength [Eq. (10)] so that the energies and hopping matrix elements on one DQD depend on the state of the other. Also, the processes in which the hopping of electrons on the two DQDs is correlated and mediated by the direct Coulomb interaction become possible (see Fig. 3). The coupling between the DQDs causes an effective spin interaction that deviates from the form of exchange-coupled qubits, adding the entangling term E_e to Eq. (3). This deviation creates the entanglement between the two qubits. The generation of entanglement can be efficiently controlled by changing the bias ϵ .

IV. GENERAL BIAS

The study of a DDQD system in the strong-bias regime presented in Sec. III allows for a simple perturbative solution

and offers an insight into the mechanism of entanglement generation. However, it lacks sufficient predictive power for a general analysis of a realistic two-qubit quantum gate: When switching on and off the entangling interaction, a continuous voltage pulse is applied, and the system undergoes a smooth transition from the strong-bias regime to the unbiased (or merely biased) regime and vice versa. During this transition, the system has to pass through an intermediate weak-bias regime where the perturbative expansion [Eq. (22)] breaks down.

In this section, we calculate the full HM Hamiltonian of the four quantum dots, including both $|D_I\rangle$ and $|D_O\rangle$ states. This calculation allows us to predict the quantum gate generated by an arbitrarily shaped adiabatic pulse of the control parameters t and ϵ . The main difference in the system's description is that now we take into account both doubly occupied states $|D_I\rangle$ and $|D_O\rangle$ in each DQD. Therefore, we are working in the entire Hilbert space of the HM approximation, and the strong-bias requirement is not important. Now, H_{TT} is one dimensional, H_{ST} and H_{TS} are three dimensional, and H_{SS} is nine dimensional.

Following the discussion of Sec. III, the effective low-energy spin Hamiltonian H [Eq. (3)] is determined by the energies E_{ab} , where $a, b = S, T$, of the lowest-energy states of a given spin configuration. Due to the $L \leftrightarrow R$ symmetry, H is the sum of the isotropic exchange terms and the entangling term. We proceed by calculating the matrix elements of the Hamiltonian as a function of the tunneling matrix element t and the bias ϵ . The results of this calculation are given in the Appendix. Numerical diagonalization of the resulting Hamiltonian gives the energies E_{ab} for each of the blocks H_{ab} , where $a, b = S, T$. Finally, we extract the effective low-energy Hamiltonian parameters J and E_e using Eqs. (17) and (21).

The dependence of the isotropic exchange coupling on the bias $J(\epsilon)$ is illustrated in Fig. 6. In the zero-tunneling limit, we can identify three regions of qualitatively different behaviors of $J(\epsilon)$. For strong and negative bias, $\epsilon < U_-$, corresponding to the $|D_O D_O\rangle$ lowest-energy singlet state, the isotropic exchange coupling is decreasing linearly with the bias. In the intermediate region, $U_- < \epsilon < U_+$, the exchange coupling is absent. For strong and positive bias, $U_+ < \epsilon$, the exchange coupling grows linearly with ϵ . The asymmetric placement of the $J=0$ plateau is a consequence of the different repulsion energies of the electrons in the inner and outer QDs. As the tunneling is turned on, the isotropic exchange couplings become larger due to the mixing of the doubly occupied states in the plateau region. For a zero magnetic field, the coupling J is positive. In a finite field, there is a region with negative J , consistent with the analysis of Ref. 9 and the experimental findings of Ref. 29.

A plot of the entanglement generating interaction E_e is given in Fig. 7. The zero-tunneling value of E_e shows a structure determined by the Coulomb energies of the basis states [Eqs. (4)–(7)]. In a wide plateau of small bias, the entangling interaction vanishes because all of the lowest-energy states of definite spin are products of $|\bar{S}\rangle$ and $|T_0\rangle$. Since the direct exchange interaction $V_- - V_+$ is zero in the absence of tunneling, those two states are equal in energy. When the bias overcomes the on-site repulsion, the lowest-

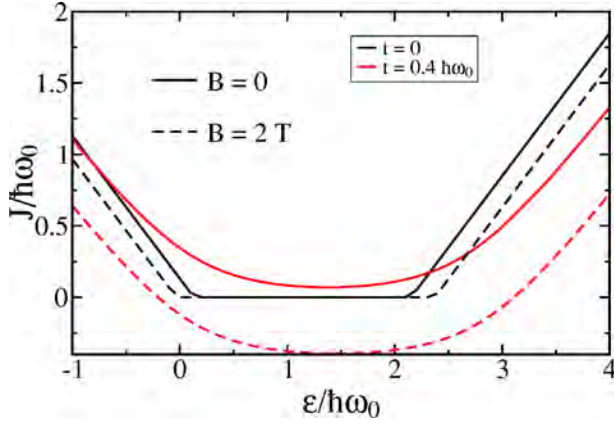


FIG. 6. (Color online) Isotropic exchange coupling J as a function of the bias ϵ . In the regions of strong positive and negative bias, the exchange coupling is approximately linear $J \propto |\epsilon|$. In the intermediate region, the exchange is zero in the zero-tunneling limit and becomes nonzero as the tunneling is turned on. The coupling J is always positive in the absence of a magnetic field. The external magnetic field drives J to negative values in a relatively wide range of values of the tunneling matrix element and bias. The confinement energy of the quantum dots is chosen to be $\hbar\omega_0 = 3$ meV, which corresponds to a quantum dot Bohr radius $a_B = 20$ nm in GaAs. The distances between the dots are chosen to be $2a_1 = 1.6a_B$ and $2a_2 = 3a_B$.

energy states of H_{SS} , H_{ST} , and H_{TS} change. The degenerate lowest-energy states of H_{SS} are either $|\bar{S}D_I\rangle$ and $|D_I\bar{S}\rangle$, in the region of large bias on the right of the plateau, or $|\bar{S}D_O\rangle$ and $|D_O\bar{S}\rangle$, in the region of smaller bias to the left of the plateau. Simultaneously, the analogous states with $|\bar{S}\rangle$ replaced by $|T\rangle$ become the lowest-energy states in H_{ST} and H_{TS} . In these two regions, E_e is a linear function of ϵ , $E_e = U_N - U_F$

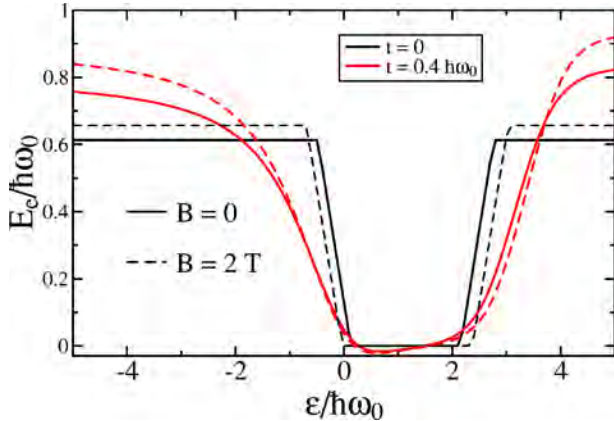


FIG. 7. (Color online) Entangling interaction E_e as a function of bias. The plots correspond to different values of the tunneling matrix elements t within the double quantum dots in the absence of a magnetic field and in an external magnetic field of $B = 2$ T. The $t = 0$ plot indicates the regions of different lowest-energy singlets and the positions of crossings. The strength of the entangling interaction E_e can be changed significantly by tuning the bias ϵ at a fixed tunneling matrix element t . Parameters used in this plot are the same as in Fig. 6.

$-U - \epsilon$ on the left and $E_e = -U_N + U_F - U + \epsilon$ on the right of the plateau. When the absolute value of the bias is even higher, the lowest-energy state in H_{SS} is $|D_I D_I\rangle$ for a very strong and positive bias and $|D_O D_O\rangle$ for a very strong and negative bias. These regions are characterized by an ϵ -independent $E_e = U_N - 2U_M + U_F$ for large $|\epsilon|$. The values U_{\pm} for the bias ϵ at which the changes in zero-tunneling lowest-energy states occur depend on the geometry of the device, described by the distances $2a_1$ and $2a_2$ (Fig. 1) and the quantization energy $\hbar\omega_0$, and correspond to the changes in behavior of the exchange coupling strength J .

The zero-tunneling case shows a desirable feature in that E_e , the quantity that determines the entanglement between the qubits, can be switched on and off by tuning ϵ . However, the regions of different E_e cannot be reached by adiabatic pulses in the $t \rightarrow 0$ limit. Turning on the tunneling t between the QDs will introduce transitions between previously disconnected regions, and the adiabatic gates become possible. The simple $t = 0$ picture of the entanglement generated by a difference in Coulomb energies is perturbed by the transitions. It is no longer possible to turn off E_e throughout the plateau region by a change in ϵ alone. In the plateau region, E_e is generically nonzero, but small. Therefore, in order to turn off the entangling interaction when t is kept constant, it is desirable to keep t small and to tune ϵ to a value where $E_e = 0$.

V. QUANTUM GATE OPERATION

For a quantum gate applied by the time-dependent Hamiltonian [Eq. (2)], with the parameters t and ϵ changing adiabatically on the time scale set by the energy gap between the states within the blocks H_{ab} , the applied gate is determined by the splittings between the lowest-lying states in each of the subspaces of the definite spin. If the energies of the lowest-energy states in singlet-singlet, singlet-triplet, triplet-singlet, and triplet-triplet subspaces are $E_{SS}(t)$, $E_{ST}(t) = E_{TS}(t)$, and $E_{TT}(t)$, respectively, the gate applied by an adiabatic pulse starting at the time t_i and finishing at t_f will be $\mathcal{U} = \text{diag}(\phi_{SS}, \phi_{ST}, \phi_{TS}, \phi_{TT})$, with the phases

$$\phi_{ab} = \exp - \frac{i}{\hbar} \int_{t_i}^{t_f} E_{ab}(t) dt. \quad (23)$$

With the ability to turn the entangling interaction on and off and perform single-qubit gates, it is possible to perform a CNOT gate on a pair of qubits encoded into spin states of DQD. We consider a quantum gate implemented by first adiabatically turning on the entangling interaction for a period τ_{on} , and then again adiabatically switching to the Hamiltonian with the entangling interaction off for the time interval τ_{off} . The lowest-energy states in each of the SS , ST , TS , and TT subspaces will acquire a phase dependent on the control parameters ϵ and t and the pulse durations. In the on state, the Hamiltonian that describes the ground states in all

the spin subspaces is, up to a constant, $H_{\text{on}} = \text{diag}(E_e, J_{\text{on}}, J_{\text{on}}, 2J_{\text{on}})$, where E_e is the strength of the entangling interaction in the *on* regime and J_{on} is the corresponding exchange coupling. After the DDQD was in the on state for the time τ_{on} , the applied gate is

$$\mathcal{U}_{\text{on}} = \exp - i \frac{\tau_{\text{on}}}{\hbar} H_{\text{on}}. \quad (24)$$

Similarly, during the subsequent period of duration τ_{off} when the entangling interaction is set to zero, the applied gate is

$$\mathcal{U}_{\text{off}} = \exp - i \frac{\tau_{\text{off}}}{\hbar} H_{\text{off}}, \quad (25)$$

where $H_{\text{off}} = \text{diag}(0, J_{\text{off}}, J_{\text{off}}, 2J_{\text{off}})$ in analogy with the on regime. The resulting gate is

$$\mathcal{U} = \mathcal{U}_{\text{off}} \mathcal{U}_{\text{on}} = \exp - i \begin{pmatrix} \phi & 0 & 0 & 0 \\ 0 & \lambda & 0 & 0 \\ 0 & 0 & \lambda & 0 \\ 0 & 0 & 0 & 2\lambda \end{pmatrix}, \quad (26)$$

where $\hbar\lambda = J_{\text{on}}\tau_{\text{on}} + J_{\text{off}}\tau_{\text{off}}$ is the integrated strength of the exchange coupling in DQD and $\hbar\phi = E_e\tau_{\text{on}}$ is the integrated strength of the entangling interaction.

The CPHASE gate, which is equivalent to CNOT up to single-qubit rotations, is obtained when the gate parameters satisfy $\phi = m\pi$ and $\lambda = n\pi$, for an odd integer m and an arbitrary integer n . In order to complete a CNOT, we follow a pulse of on-state Hamiltonian of the duration $\tau_{\text{on}} = m\pi\hbar/E_e$ by a pulse of the off-state Hamiltonian with the duration $\tau_{\text{off}} = \hbar(n\pi - J_{\text{on}}\tau_{\text{on}}/\hbar)/J_{\text{off}}$. The resulting gate is $\text{diag}(-1, -1, -1, 1) = -\text{CPHASE}$, for odd n and $\text{diag}(-1, 1, 1, 1)$, which is equal to CPHASE with the X gate applied to both qubits before and after \mathcal{U} . For any integer n ,

$$\text{CPHASE} \sim (\xi \otimes \xi) \mathcal{U} (\xi \otimes \xi), \quad (27)$$

where $\xi = \exp[i\pi[1 + (-1)^n]\sigma_x/4]$. In order to complete the CNOT, we apply the one-qubit Haddamard gates $H = (X + Z)/\sqrt{2}$ to the target qubit both before and after the entangling gate \mathcal{U} . The entire construction can be represented as

$$\text{CNOT} = (\mathbf{1} \otimes H) (\xi \otimes \xi) \mathcal{U} (\xi \otimes \xi) (\mathbf{1} \otimes H). \quad (28)$$

Note that the CNOT construction necessarily involves the single-qubit rotations about pseudospin axes different from z . Such operations can be performed using the asymmetric bias within a DQD that encodes the qubit in an inhomogeneous external magnetic field.²⁷ The entangling part of a CNOT gate can be performed by pulsing the bias ϵ only and keeping the tunneling t constant. Therefore, control over the bias ϵ and the availability of an inhomogeneous magnetic field are sufficient for the universal quantum computing with two-spin qubits.

VI. CONCLUSION

We have analyzed two-qubit gates in a pair of qubits, each encoded into singlet and triplet states of a DQD and coupled

by Coulomb repulsion. A two-qubit CNOT gate, which together with the single-qubit rotations forms a universal set of quantum gates, can be performed by tuning the bias of the inner dots with respect to the outer ones. We identify the entangling interaction strength E_e as a quantity that has to be controlled in order to implement a CNOT with the aid of single-qubit rotations.

The dependence of E_e on the externally controllable bias ϵ and the tunneling matrix element t shows that it can, in principle, be turned on and off by changing ϵ alone, if sufficiently low values of t are available.

The largest change in E_e comes from a tuning of the system through the resonance between the singly occupied state and the doubly occupied state on a DQD. At the side of the resonance with a singly occupied ground state, and far from the resonance, the entangling interaction E_e is caused by inter-DQD correlation and is small. On the other side of the resonance, with a doubly occupied DQD ground state, the entangling interaction is caused by the direct Coulomb repulsion and it is much stronger. Two-qubit gates necessary for a universal set of gates can be performed by switching between the strong and weak entanglement generation regimes using voltage pulses.

ACKNOWLEDGMENTS

We thank M. Trif and D. Klauser for discussions. We acknowledge funding from the Swiss National Science Foundation (SNF) and through NCCR Nanoscience.

APPENDIX: HUND-MULLIKEN 16×16 HAMILTONIAN

The full Hund-Mulliken Hamiltonian is block diagonal due to the symmetry of the interactions with respect to arbitrary rotations in spin space. In reality, this symmetry is broken by the weak spin-orbit coupling interaction that we have neglected. The blocks are the one-dimensional H_{TT} , the two three-dimensional H_{TS} and H_{ST} , and the nine-dimensional H_{SS} , where T stands for a triplet and S for a singlet state on a DQD. In this appendix, we present the matrices of these blocks as functions of the system geometry and the control parameters.

There is only one TT state and its energy is

$$H_{TT} = E_{TT} = 2V_- + U_N + 2U_M + U_F - 2\epsilon. \quad (A1)$$

The three-dimensional blocks H_{TS} and H_{ST} are related by the symmetry operation of exchanging the DQD, and if we choose the basis $\{|T_0, \bar{S}\rangle, |T_0, D_I\rangle, |T_0, D_O\rangle\}$ for the TS and $\{|\bar{S}, T_0\rangle, |D_I, T_0\rangle, |D_O, T_0\rangle\}$ for the ST subspace, they can both be represented by the matrix

$$H_{TS} = H_{ST} = \begin{pmatrix} C_{TS} & \sqrt{2}t_S & \sqrt{2}t_S \\ \sqrt{2}t_S & C_{TI} & X \\ \sqrt{2}t_S & X & C_{TO} \end{pmatrix}. \quad (A2)$$

The nine-dimensional block of singlet states, in the direct product basis composed out of the two-electron states [Eq. (4)–(6)], is

$$H_{SS} = \begin{pmatrix} C_{SS} & \sqrt{2}t_S & \sqrt{2}t_S & \sqrt{2}t_S & 2X_D & 2X_S & \sqrt{2}t_S & 2X_S & 2X_D \\ \sqrt{2}t_S & C_{SI} & X & 2X_S & \sqrt{2}t_I & 0 & 2X_D & \sqrt{2}t_I & 0 \\ \sqrt{2}t_S & X & C_{SO} & 2X_D & 0 & \sqrt{2}t_O & 2X_S & 0 & \sqrt{2}t_O \\ \sqrt{2}t_S & 2X_S & 2X_D & C_{IS} & \sqrt{2}t_I & \sqrt{2}t_I & X & 0 & 0 \\ 2X_D & \sqrt{2}t_I & 0 & \sqrt{2}t_I & C_{II} & X & 0 & X & 0 \\ 2X_S & 0 & \sqrt{2}t_O & \sqrt{2}t_I & X & C_{IO} & 0 & 0 & X \\ \sqrt{2}t_S & 2X_D & 2X_S & X & 0 & 0 & C_{OS} & \sqrt{2}t_O & \sqrt{2}t_O \\ 2X_S & \sqrt{2}t_I & 0 & 0 & X & 0 & \sqrt{2}t_O & C_{OI} & X \\ 2X_D & 0 & \sqrt{2}t_O & 0 & 0 & X & \sqrt{2}t_O & X & C_{OO} \end{pmatrix}. \quad (\text{A3})$$

We do not antisymmetrize with respect to the permutations of electrons that belong to different quantum dots and have nonoverlapping orbital wave functions. The matrix elements of the Hamiltonian that describe the Coulomb interaction within a DQD (intra-DQD terms), U , t , X , V_+ , and V_- , were analyzed in Ref. 9. The inter-DQD elements depend on the following matrix elements of the Coulomb interaction between the product states of the $|qps\rangle$ electrons localized in the qubit q and the quantum dot p and having a spin s :

$$X_S = \langle LIs, RIs' | V_C | LOs, ROs' \rangle, \quad (\text{A4})$$

$$X_D = \langle LIs, ROs' | V_C | LOs, RIs' \rangle, \quad (\text{A5})$$

$$T_O = \langle LOs, ROs' | V_C | LIs, ROs' \rangle, \quad (\text{A6})$$

$$T_I = \langle LIs, RIs' | V_C | LIs, ROs' \rangle. \quad (\text{A7})$$

In zero magnetic field, we find that $X_S = X_D$.

The off-diagonal elements are determined by

$$t_S = T_O + T_I - t_H, \quad (\text{A8})$$

$$t_I = 2T_I - t_H, \quad (\text{A9})$$

$$t_O = 2T_O - t_H, \quad (\text{A10})$$

and the diagonal elements are given by

$$C_{TT} = 2V_- + U_N + 2U_M + U_F - 2\epsilon, \quad (\text{A11})$$

$$C_{TS} = V_+ + V_- + U_N + 2U_M + U_F - 2\epsilon, \quad (\text{A12})$$

$$C_{TI} = V_- + U + 2U_N + 2U_M - 3\epsilon, \quad (\text{A13})$$

$$C_{TO} = V_- + U + 2U_M + 2U_F - \epsilon, \quad (\text{A14})$$

$$C_{SS} = U_N + 2U_M + U_F + 2V_+ - 2\epsilon, \quad (\text{A15})$$

$$C_{SI} = 2U_M + 2U_F + U + V_+ - 3\epsilon, \quad (\text{A16})$$

$$C_{SO} = 2U_M + 2U_F + U + V_+ - \epsilon, \quad (\text{A17})$$

$$C_{II} = 4U_N + 2U - 4\epsilon, \quad (\text{A18})$$

$$C_{IO} = 4U_M + 2U - 2\epsilon, \quad (\text{A19})$$

$$C_{OO} = 4U_F + 2U, \quad (\text{A20})$$

where the symmetry with respect to exchange of the DQDs leads to $C_{AB} = C_{BA}$, where $A, B \in \{T, S, I, O\}$.

To represent the matrix elements in terms of the system parameters, the single QD quantization energy $\hbar\omega_0$, tunneling matrix element within an isolated DQD t , the bias ϵ , and the interdot distances a_1 and a_2 , we have to adopt a model for the binding potential of a DQD and the orbitals of Hund-Mulliken approximation. We assume that the QD orbitals are Wannier functions obtained by orthogonalization of the Fock-Darwin ground states centered at the positions of the QDs within a DQD, $(a_2 \pm a_1, 0)$ and $(-a_2 \pm a_1, 0)$. The Wannier orbitals are of the generic form

$$|W_{q,I}\rangle = N(|\phi_{q,I}\rangle - g|\phi_{q,O}\rangle), \quad (\text{A21})$$

$$|W_{q,O}\rangle = N(-g|\phi_{q,I}\rangle + |\phi_{q,O}\rangle), \quad (\text{A22})$$

where $|\phi_{q,I(O)}\rangle$ is the Fock-Darwin ground state on the dot belonging to the qubit $q=L, R$ and the inner (I) or outer (O) QD [Eq. (12)]. The Wannier orbitals are determined by the overlap of these wave functions, $S = \langle \phi_{q,I} | \phi_{q,O} \rangle = \exp[-d_1^2(2b-1/b)]$, through the mixing $g = (1 - \sqrt{1-S^2})/S$ and normalization constant $N = 1/\sqrt{1-2gS+g^2}$.

The Coulomb interaction matrix elements for the DQD centered at $\pm a_2 = \pm d_2 a_B$ and QDs within a DQD displaced by $\pm a_1 = \pm d_1 a_B$ from the center of the DQD are then expressed as

$$U_N = cN^4 \left\{ f(d_2 - d_1, 0) + 2g^2(1 + S^2)f(d_2, 0) + g^4 f(d_1 + d_2, 0) + 2S^2 g^2 f(d_2, d_1) - 4gS \left[f\left(d_2 - \frac{d_1}{2}, \frac{d_1}{2}\right) + g^2 f\left(d_2 + \frac{d_1}{2}, \frac{d_1}{2}\right) \right] \right\}, \quad (\text{A23})$$

$$\begin{aligned}
 U_F = cN^4 & \left\{ f(d_2 + d_1, 0) + 2g^2(1 + S^2)f(d_2, 0) \right. \\
 & + g^4f(d_2 - d_1, 0) + 2S^2g^2f(d_2, d_1) \\
 & \left. - 4gS \left[f\left(d_2 + \frac{d_1}{2}, \frac{d_1}{2}\right) + g^2f\left(d_2 - \frac{d_1}{2}, \frac{d_1}{2}\right) \right] \right\}, \quad (\text{A24})
 \end{aligned}$$

$$\begin{aligned}
 U_M = cN^4 & \left\{ (1 + g^4)f(d_2, 0) + g^2\{f(d_1 + d_2, 0) \right. \\
 & + f(d_1 - d_2, 0) + 2S^2[f(d_2, 0) + f(d_2, d_1)]\} \\
 & \left. - 2gS(1 + g^2) \left[f\left(d_2 + \frac{d_1}{2}, \frac{d_1}{2}\right) + f\left(d_2 - \frac{d_1}{2}, \frac{d_1}{2}\right) \right] \right\}, \quad (\text{A25})
 \end{aligned}$$

$$\begin{aligned}
 T_O = cN^4 & \left\{ S \left[(1 + 3g^2)f\left(d_2 + \frac{d_1}{2}, \frac{d_1}{2}\right) \right. \right. \\
 & + (g^4 + 3g^2)f\left(d_2 - \frac{d_1}{2}, \frac{d_1}{2}\right) \\
 & \left. - (g + g^3)[(1 + S^2)f(d_2, 0) + S^2f(d_2, d_1)] \right. \\
 & \left. - gf(d_2 + d_1, 0) - g^3f(d_2 - d_1, 0) \right\}, \quad (\text{A26})
 \end{aligned}$$

$$\begin{aligned}
 T_I = cN^4 & \left\{ S \left[(1 + 3g^2)f\left(d_2 - \frac{d_1}{2}, \frac{d_1}{2}\right) \right. \right. \\
 & + (g^4 + 3g^2)f\left(d_2 + \frac{d_1}{2}, \frac{d_1}{2}\right) \\
 & \left. - (g + g^3)[(1 + S^2)f(d_2, 0) + S^2f(d_2, d_1)] \right. \\
 & \left. - gf(d_2 - d_1, 0) - g^3f(d_2 + d_1, 0) \right\}, \quad (\text{A27})
 \end{aligned}$$

$$\begin{aligned}
 X_S = cN^4 & \left\{ (S^2 + 2g^2 + g^4S^2)f(d_2, 0) \right. \\
 & + g^2[f(d_1 + d_2, 0) + f(d_1 - d_2, 0) + 2S^2f(d_2, d_1)] \\
 & \left. - 2S(g + g^3) \left[f\left(d_2 + \frac{d_1}{2}, \frac{d_1}{2}\right) + f\left(d_2 - \frac{d_1}{2}, \frac{d_1}{2}\right) \right] \right\}, \quad (\text{A28})
 \end{aligned}$$

$$\begin{aligned}
 X_D = cN^4 & \left\{ S^2(1 + g^4)f(d_2, d_1) + g^2[f(d_1 + d_2, 0) + f(d_2 - d_1, 0) \right. \\
 & + 2(1 + S^2)f(d_2, 0)] - 2S(g + g^3) \\
 & \left. \times \left[f\left(d_2 + \frac{d_1}{2}, \frac{d_1}{2}\right) + f\left(d_2 - \frac{d_1}{2}, \frac{d_1}{2}\right) \right] \right\}, \quad (\text{A29})
 \end{aligned}$$

in terms of the overlaps of the harmonic oscillator wave functions S , the mixing factor g , and the function

$$f(d, l) = \sqrt{b} \exp[-\alpha(d, l)] I_0(\alpha(d, l)), \quad (\text{A30})$$

where $\alpha(d, l) = bd^2 - (b - 1/b)l^2$. We use the contraction factor $b = \omega/\omega_0$ to measure the magnetic field strength. The overall strength of the Coulomb interaction is set by $c = \sqrt{\pi/2}e^2/\kappa\hbar\omega_0a_B$, where e is the electron charge, κ is the dielectric constant, and $\hbar\omega_0$ is the single isolated QD quantization energy.⁹

To model the dependence of the matrix elements on the externally controllable tunneling matrix element t , we use the connection between the tunneling and the overlap $S = S(t)$ that holds for the quartic double well, Eq. (13) and assume that it holds throughout the gate operation.

¹D. Loss and D. P. DiVincenzo, Phys. Rev. A **57**, 120 (1998).

²M. Nielsen and I. Chuang, *Quantum Computation and Quantum Information* (Cambridge University Press, Cambridge, 2000).

³J. R. Petta, A. C. Johnson, J. M. Taylor, E. A. Laird, A. Yacoby, M. D. Lukin, C. M. Marcus, M. P. Hanson, and A. C. Gossard, Science **309**, 2180 (2005).

⁴A. C. Johnson, J. R. Petta, J. M. Taylor, A. Yacobi, M. D. Lukin, C. M. Marcus, M. P. Hanson, and A. C. Gossard, Nature (London) **435**, 925 (2005).

⁵F. H. L. Koppens, J. A. Folk, J. M. Elzerman, R. Hanson, L. H. Willems van Beveren, I. T. Vink, H. P. Tranitz, W. Wegscheider, L. P. Kouwenhoven, and L. M. K. Vandersypen, Science **309**, 1346 (2005).

⁶W. A. Coish and D. Loss, Phys. Rev. B **72**, 125337 (2005).

⁷D. Stepanenko, G. Burkard, G. Giedke, and A. Imamoglu, Phys. Rev. Lett. **96**, 136401 (2006).

⁸D. Klauser, W. A. Coish, and D. Loss, Phys. Rev. B **73**, 205302 (2006).

⁹G. Burkard, D. Loss, and D. P. DiVincenzo, Phys. Rev. B **59**, 2070 (1999).

¹⁰H.-A. Engel and D. Loss, Phys. Rev. Lett. **86**, 4648 (2001).

¹¹F. H. L. Koppens, C. Buizert, K. J. Tielrooij, I. T. Vink, K. C. Nowack, T. Meunier, L. P. Kouwenhoven, and L. M. K. Vandersypen, Nature (London) **442**, 766 (2006).

¹²P. Aliferis and B. M. Terhal, Quantum Inf. Comput. **7**, 139 (2007).

¹³D. Bacon, J. Kempe, D. A. Lidar, and K. B. Whaley, Phys. Rev. Lett. **85**, 1758 (2000).

¹⁴J. Kempe, D. Bacon, D. A. Lidar, and K. B. Whaley, Phys. Rev. A **63**, 042307 (2001).

¹⁵D. P. DiVincenzo, D. Bacon, J. Kempe, G. Burkard, and K. B. Whaley, Nature (London) **408**, 339 (2000).

¹⁶J. Levy, Phys. Rev. Lett. **89**, 147902 (2002).

¹⁷S. C. Benjamin, Phys. Rev. A **64**, 054303 (2001).

¹⁸L.-A. Wu and D. A. Lidar, Phys. Rev. A **66**, 062314 (2002).

¹⁹D. Stepanenko and N. E. Bonesteel, Phys. Rev. Lett. **93**, 140501 (2004).

²⁰J. M. Taylor, H.-A. Engel, W. Dür, A. Yacoby, C. M. Marcus, P. Zoller, and M. D. Lukin, Nat. Phys. **1**, 177 (2005).

²¹K. V. Kavokin, Phys. Rev. B **64**, 075305 (2001).

- ²²K. V. Kavokin, Phys. Rev. B **69**, 075302 (2004).
- ²³G. Burkard and D. Loss, Phys. Rev. Lett. **88**, 047903 (2002).
- ²⁴N. E. Bonesteel, D. Stepanenko, and D. P. DiVincenzo, Phys. Rev. Lett. **87**, 207901 (2001).
- ²⁵X. Hu and S. Das Sarma, Phys. Rev. A **61**, 062301 (2000).
- ²⁶A. Weichselbaum and S. E. Ulloa, Phys. Rev. B **74**, 085318 (2006).
- ²⁷R. Hanson and G. Burkard, Phys. Rev. Lett. **98**, 050502 (2007).
- ²⁸We have done a similar calculation of the second-order correction to the E_e in the weak-bias regime, valid in the region where $U_- - \epsilon \gg t \gg \epsilon - U_+$. The resulting correction to the $E_e=0$ zeroth-order result contains terms of the order X_D^2 and X_S^2 . It is caused by the correlated hopping processes, and its size is $\propto t^4$.
- ²⁹D. M. Zumbühl, C. M. Marcus, M. P. Hanson, and A. C. Gossard, Phys. Rev. Lett. **93**, 256801 (2004).

Spin-Electric Coupling in Molecular Magnets

Mircea Trif,¹ Filippo Troiani,² Dimitrije Stepanenko,¹ and Daniel Loss¹

¹*Department of Physics, University of Basel, Klingenbergstrasse 82, CH-4056 Basel, Switzerland*

²*CNR-INFM National Research Center S3 c/o Dipartimento di Fisica via G. Campi 213/A, 41100, Modena, Italy*

(Received 8 May 2008; published 20 November 2008)

We study the triangular antiferromagnet Cu_3 in external electric fields, using symmetry group arguments and a Hubbard model approach. We identify a spin-electric coupling caused by an interplay between spin exchange, spin-orbit interaction, and the chirality of the underlying spin texture of the molecular magnet. This coupling allows for the electric control of the spin (qubit) states, e.g., by using an STM tip or a microwave cavity. We propose an experimental test for identifying molecular magnets exhibiting spin-electric effects.

DOI: 10.1103/PhysRevLett.101.217201

PACS numbers: 75.50.Xx, 03.67.Lx

Single-molecule magnets (SMMs) [1] have emerged as a fertile testing ground for investigating quantum effects at the nanoscale, such as tunneling of magnetization [2,3], or coherent charge transport [4–6], or the decoherence and the transition from quantum to classical behavior [7]. SMMs with antiferromagnetic coupling between spins are especially promising for the encoding and manipulation of quantum information [8–11], for they act as effective two-level systems, while providing additional auxiliary states that can be exploited for performing quantum gates. Intra- and intermolecular couplings of SMMs can be engineered by molecular and supramolecular chemistry [12], enabling a bottom-up design of molecule-based devices [13].

While the properties of SMMs can be chemically modified, the fast control required for quantum information processing remains a challenge. The standard spin-control technique is electron spin resonance (ESR) driven by ac magnetic fields $B_{ac}(t)$ [7]. For manipulation on the time scale of 1 ns, B_{ac} should be of the order of 10^{-2} T, which, however, is difficult to achieve. The spatial resolution of 1 nm, required for addressing a single molecule, is also prohibitively small. At these spatial and temporal scales, the electric control is preferable, because strong electric fields can be applied to small regions by using, for example, STM tips [14,15], see Fig. 1(a). Also, the quantized electric field inside a microwave cavity can be used [16–19] to control single qubits and to induce coupling between them even if they are far apart. Electric control of spins has been studied in multiferroic materials [20] and semiconductor spintronics [21], focusing on the control of a large number of spins and producing macroscopic magnetization and spin currents. Here, we are interested in control over a single molecular spin system.

We identify and study an efficient spin-electric coupling mechanism in SMMs which is based on an interplay of spin exchange, spin-orbit interaction (SOI), and lack of inversion symmetry. Spin-electric effects induced solely by SOI have been proposed [22] and experimentally demonstrated [23] in quantum dots. However, these SOI effects scale

with the system size L as L^3 [22], making them irrelevant for the much smaller SMMs. Thus, additional ingredients—such as broken symmetries—must be present in SMMs for an efficient coupling between spin and applied electric field.

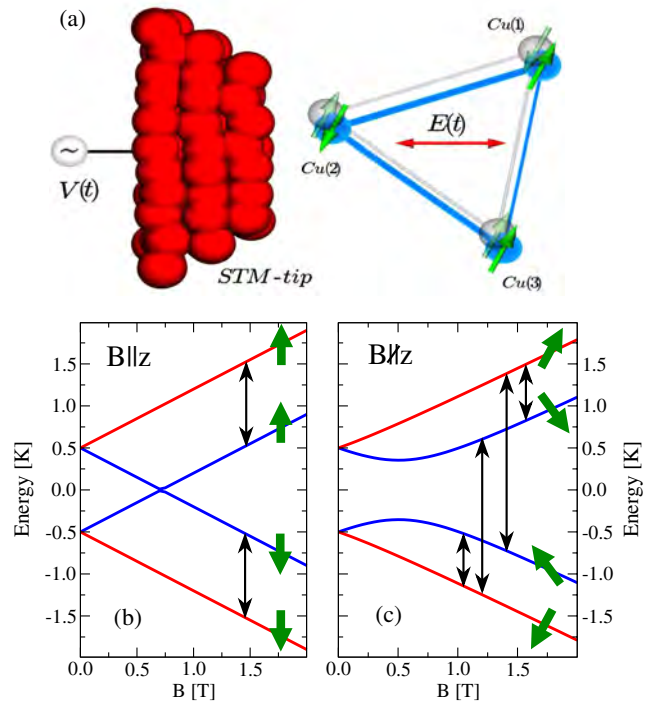


FIG. 1 (color online). (a) Cu_3 -triangle exposed to an electric field $\mathbf{E}(t)$ created by, e.g., an STM-tip. For $\mathbf{E} = 0$, the exchange couplings, represented by the thickness of Cu-Cu bonds, are equal (light triangle). A finite \mathbf{E} affects the (super-) exchange coupling in a directional way (dark triangle). (b),(c) Low-energy $S = 1/2$ states of Cu_3 in a magnetic field \mathbf{B} , with the zero-field SOI splitting $\Delta_{\text{SO}} = 1$ K. Light (red) and dark (blue) lines represent the states with $\chi = +1(-1)$. If $\mathbf{B} \parallel z$ (b), the transitions induced by \mathbf{E} (thin arrows) conserve S_z ; for $\mathbf{B} \not\parallel z$ (c), these transitions result in a change of spin orientation (thick arrows).

In the following, we demonstrate the possibility of such spin-electric effects in SMMs by focusing on a specific example, namely, an equilateral spin triangle, Cu_3 [24]. In this SMM, the low-energy states exhibit a chiral spin texture and, due to the absence of inversion symmetry, electric fields couple states of opposite chirality. Moreover, SOI couples the chirality to the total spin, and thus an effective spin-electric interaction eventually emerges.

Spin-electric coupling.—At low energies, the Cu_3 can be described in terms of an effective spin Hamiltonian. There, the states are labeled by the quantum numbers of three spins-1/2 \mathbf{s}_i (one for each Cu^{2+} ion), and the orbital states are quenched. The (super-) exchange and SOI are then expressed as Heisenberg and Dzyaloshinski-Moriya interaction of spins, [24],

$$H_0 = \sum_{i=1}^3 J_{ii+1} \mathbf{s}_i \cdot \mathbf{s}_{i+1} + \sum_{i=1}^3 \mathbf{D}_{ii+1} \cdot \mathbf{s}_i \times \mathbf{s}_{i+1}. \quad (1)$$

The D_{3h} symmetry of the triangle implies several relations between the coupling constants [25]. We neglect the intrinsic deformation of Cu_3 triangle that makes one of the sides slightly shorter. Since $J_{pq} \sim 5$ K and $|\mathbf{D}_{pq}| \sim 0.5$ K, the Heisenberg terms determine the gross structure of the energy spectrum, and the Dzyaloshinski-Moriya terms the fine one. In particular, since $J_{pq} > 0$, the ground state multiplet has total spin $S = 1/2$, and the gap to the first excited $S = 3/2$ quadruplet is $\Delta_H \equiv 3J/2$. The $S = 1/2$ subspace is spanned by the symmetry-adapted states $|\chi, M\rangle$, i.e.,

$$|\pm 1, +1/2\rangle \equiv (|\uparrow\uparrow\uparrow\rangle + \epsilon_{\pm} |\uparrow\uparrow\downarrow\rangle + \epsilon_{\mp} |\uparrow\downarrow\uparrow\rangle) / \sqrt{3}, \quad (2)$$

$$|\pm 1, -1/2\rangle \equiv (|\uparrow\downarrow\downarrow\rangle + \epsilon_{\pm} |\downarrow\uparrow\downarrow\rangle + \epsilon_{\mp} |\downarrow\downarrow\uparrow\rangle) / \sqrt{3}, \quad (3)$$

with $\epsilon_{\pm} = e^{\pm i2\pi/3}$, that are simultaneous eigenstates of the chirality operator C_z and of S_z (total spin), for the respective eigenvalues χ and M . Here, we have introduced the chirality \mathbf{C} with components

$$C_x = (-2/3)(\mathbf{s}_1 \cdot \mathbf{s}_2 - 2\mathbf{s}_2 \cdot \mathbf{s}_3 + \mathbf{s}_3 \cdot \mathbf{s}_1), \quad (4)$$

$$C_y = (2/\sqrt{3})(\mathbf{s}_1 \cdot \mathbf{s}_2 - \mathbf{s}_3 \cdot \mathbf{s}_1), \quad (5)$$

$$C_z = (4/\sqrt{3})\mathbf{s}_1 \cdot (\mathbf{s}_2 \times \mathbf{s}_3). \quad (6)$$

They satisfy $[C_k, C_l] = i2\epsilon_{klm} C_m$ and $[C_k, S_l] = 0$, and act as Pauli matrices in the $|\chi = \pm 1\rangle$ bases.

Next, we study the effect of an electric field \mathbf{E} on the Cu_3 -spins using general symmetry group arguments. The low-energy $|E'_{\pm}, S = 1/2\rangle$ ($|A'_2, S = 3/2\rangle$) spin-orbital states form two E' (four A'_2) irreducible representations (IRs) of D_{3h} , with the $S = 1/2$ states lower in energy [24,25]. The states $|E'_{\pm}, S_z\rangle$ transform in the same way as the chiral states $|\chi = \pm 1, S_z\rangle$, Eqs. (2) and (3), with orbitals localized on the Cu ions corresponding to the triangle

vertices. An electric field \mathbf{E} couples to Cu_3 via $e\mathbf{E} \cdot \mathbf{R}$, where e is the electron charge, and $\mathbf{R} = \sum_{j=1}^3 \mathbf{r}_j$. The Z component of \mathbf{R} transforms as A'_2 IR, while the components $X_{\pm} = \pm X + iY$ in the Cu_3 plane transform as the two-dimensional IR E' . From the Wigner-Eckart theorem, it follows that the only nonzero matrix elements of \mathbf{R} are $e\langle E'_{+}, S_z | X_{-} | E'_{-}, S_z \rangle = e\langle E'_{-}, S_z | X_{+} | E'_{+}, S_z \rangle = 2id$, with d real denoting the electric dipole coupling. The resulting coupling between the \mathbf{E} -field and chirality in the spin-Hamiltonian model takes the compact form $\delta H_E = d\mathbf{E}' \cdot \mathbf{C}_{\parallel}$, where $\mathbf{E}' = \mathcal{R}_z(\phi)\mathbf{E}$ is rotated by $\phi = 7\pi/6 - 2\theta$ about z , and $\mathbf{C}_{\parallel} = (C_x, C_y, 0)$.

To emphasize that the spin-electric effect derived above is based on exchange, we reinterpret our results in terms of spin interactions. In an equilateral triangle, and in the absence of electric field, the spin Hamiltonian is given by Eq. (1) with equal exchange couplings $J_{i,i+1} \equiv J$. Using then Eqs. (4) and (5), we find

$$\delta H_E = \frac{4dE}{3} \sum_{i=1}^3 \sin[2(1-i)\pi/3 + \theta] \mathbf{s}_i \cdot \mathbf{s}_{i+1}, \quad (7)$$

where θ is the angle between an in-plane \mathbf{E} -field and the vector \mathbf{r}_{12} pointing from site 1 to 2. This form of δH_E shows that the \mathbf{E} -field lowers the symmetry by introducing direction-dependent corrections to the exchange couplings $J_{i,i+1}$. E.g., if $\theta = \pi/2$, $\delta J_{23} = \delta J_{31} \neq \delta J_{12}$. Intrinsic deformation of the molecule can be described as an internal electric field \mathbf{E}_{mol} , giving Eq. (7) with $\mathbf{E} \rightarrow \mathbf{E} + \mathbf{E}_{\text{mol}}$. The lack of inversion symmetry is crucial for the linear spin-electric coupling, since the electric field \mathbf{E} is odd under inversion, and the spin is even.

Next, we turn to the SOI. The most general form of SOI allowed by the D_{3h} symmetry reads, $H_{\text{SO}} = \sum_{i=1}^3 [\lambda_{\text{SO}}^{\parallel} T_{A'_2} s_z^i + \lambda_{\text{SO}}^{\perp} (T_{E'_+} s_-^i + T_{E'_-} s_+^i)]$, where $\lambda_{\text{SO}}^{\perp}$ ($\lambda_{\text{SO}}^{\parallel}$) is the effective SOI coupling constant for the A'_2 - (E'_{\pm} -) irreducible representation, and $T_{A'_2}$ ($T_{E'_{\pm}}$) is the corresponding irreducible tensor operator in the orbital space [25]. Using again symmetry group arguments, we find that the SOI Hamiltonian acting in the $S = 1/2$ subspace reads $\delta H_{\text{SO}} = \Delta_{\text{SO}} C_z S_z$, where $\Delta_{\text{SO}} = \lambda_{\text{SO}}^{\parallel}$. The states are therefore split into two Kramers doublets $|E'_{\pm}, S_z = \pm 1/2\rangle$ and $|E'_{\pm}, S_z = \mp 1/2\rangle$. Using Eq. (6), δH_{SO} can be reduced to the Dzyaloshinski-Moriya interaction, given in Eq. (1). The coupling to a magnetic field \mathbf{B} is given by $\mathbf{B} \cdot \bar{\mathbf{g}} \cdot \mathbf{S}$, with the Bohr magneton absorbed in the $\bar{\mathbf{g}}$ -tensor. Because of the D_{3h} -symmetry, $\bar{\mathbf{g}}$ is diagonal with components $g_{xx} = g_{yy} = g_{\perp}$ in the Cu_3 -plane and $g_{zz} = g_{\parallel}$ normal to it.

Combining δH_E and δH_{SO} , we finally obtain the effective low-energy Hamiltonian in the presence of SOI and electric and magnetic fields,

$$H_{\text{eff}}^{\text{spin}} = \Delta_{\text{SO}} C_z S_z + g_{\perp} \mathbf{B}_{\perp} \cdot \mathbf{S} + g_{\parallel} B_z S_z + d\mathbf{E}' \cdot \mathbf{C}_{\parallel}. \quad (8)$$

From this we see that an in-plane \mathbf{E} -field causes rotations

of the chirality pseudospin. To illustrate the role of \mathbf{B} , we focus on the case $\mathbf{E} \parallel \mathbf{r}_{31}$, giving $\delta H_E = -dEC_x$. For $\mathbf{B} \parallel z$, the eigenstates coincide with those of S_z , and thus \mathbf{E} will not induce transitions between $|\pm, 1/2\rangle$ and $|\pm, -1/2\rangle$, but will do so in subspaces of given M ; see Fig. 1. For $\mathbf{B} \nparallel z$, instead, the system eigenstates for $\mathbf{E} = 0$ are no longer eigenstates of S_z , and thus the electric-field induced transitions result in spin flips; see Fig. 1(c).

The form of spin Hamiltonian, Eq. (8), is set by symmetry alone, but a microscopic evaluation of electric dipole coupling d requires an *ab initio* approach which is beyond the scope of this work. However d can be directly accessed in experiments, e.g., by standard ESR measurements in static electric fields; see Fig. 2. We can estimate d , $|\mathbf{E}|$ and the spin-manipulation (Rabi) time resulting from Eq. (8) as follows. For d between $d_{\min} = 10^{-4}eR_{12}$ and $d_{\max} = eR_{12}$ and for $E \approx 10^2$ kV/cm, obtainable near an STM tip, see Fig. 1(a), the Rabi time is $\tau_{\text{Rabi}} \approx 0.1\text{--}10^3$ ps. The condition $dE \ll \Delta_H$ for the validity of $H_{\text{eff}}^{\text{spin}}$ in Eq. (8) provides another lower bound on the spin-manipulation time, namely $\tau_{\text{Rabi}}^{\min} \approx 10$ ps. The spin control is not affected by the time-independent \mathbf{E}_{mol} .

Hubbard approach.—In order to gain further insight into the interplay between the exchange interaction and the electric field \mathbf{E} , we introduce an N_s -site Hubbard model of the triangular spin chain, with Cu ions represented by the sites on the vertices and the bridging atoms by sites on the sides, see Fig. 3(a). The corresponding Hamiltonian reads, $H_H = \sum_{i,\sigma} [(U_i/2)n_{i,\sigma}n_{i,-\sigma} + \epsilon_i n_{i,\sigma} + (t_{ii+1}c_{i,\sigma}^\dagger c_{i+1,\sigma} + \text{H.c.})]$, where U_i is the repulsion on site i , t_{ii+1} the hopping matrix element, $\sigma = \uparrow, \downarrow$, and $\sum_{i,\sigma} n_i^\sigma = N_e$. The coupling of the system to \mathbf{E} is

$$H_E = e\mathbf{E} \cdot \sum_{i,\sigma} [n_{i,\sigma}\mathbf{r}_i + (\tilde{\mathbf{r}}_{ii+1}c_{i,\sigma}^\dagger c_{i+1,\sigma} + \text{H.c.})]. \quad (9)$$

In the single-site terms, the expectation value of the electron position \mathbf{r} in the Wannier state $|\phi_i\rangle$ is identified with the ion position $\mathbf{r}_i = \langle \phi_i | \mathbf{r} | \phi_i \rangle$. The two-site terms describe the electric-field assisted hopping of electrons between neighboring sites, with $\tilde{\mathbf{r}}_{ii+1} = \langle \phi_i | \mathbf{r} | \phi_{i+1} \rangle = (\alpha_{ii+1}^\parallel + \alpha_{ii+1}^\perp \mathbf{e}_z \times) \mathbf{r}_{ii+1}$, and $\mathbf{r}_{ii+1} = \mathbf{r}_{i+1} - \mathbf{r}_i$. We now focus on the two main mechanisms giving antiferromagnetic coupling, namely, direct exchange and superexchange (models A and B, Fig. 2(a)) for $|t_{ij}| \ll U_i$. In both cases, the low-energy subspace (\mathcal{S}_0) is defined by the states ($|\alpha^0\rangle$) where the magnetic ions at the triangle vertices are singly occupied. For $E = 0$, the projection of these states onto \mathcal{S}_0 ($|\Psi_{1-8}^0\rangle$) coincides with the $S = 1/2$ and $S = 3/2$ eigenstates of the Heisenberg Hamiltonian. The degeneracy in the $S = 1/2$ multiplet is lifted by \mathbf{E} .

In Fig. 3(b), we show the overlap between the projected ground state $|\Psi_1^0\rangle$ and the $|S = 1/2, S_{12} = 0, 1\rangle$ states for a given S_z as function of the direction of \mathbf{E} (angle θ). The results coincide with the ones from Eq. (7), for both models A and B. In addition, we find that the splitting ($\Delta_{21} \equiv E_2 - E_1$) between the two lowest energies varies by less than 5% with θ , in agreement with H_E^{spin} that predicts no θ -dependence at all.

In Fig. 3(c) we isolate the contribution to Δ_{21} arising from the single- and two-site terms. All these contributions scale linearly with $|\mathbf{E}|$ for every θ . The dependence of Δ_{21} on t , however, is model dependent. In particular, in model A, the contributions to Δ_{21} arising from the single- and two-site terms scale as $(t/U)^3$ and (t/U) , respectively, and

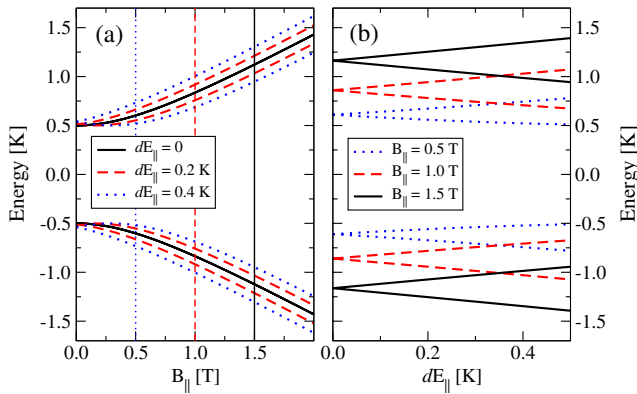


FIG. 2 (color online). Low-energy spectrum of the undeformed Cu_3 molecule. (a) Energy levels of the Cu_3 molecule in an in-plane magnetic field B_{\parallel} (black solid line), split as a static in-plane electric field E_{\parallel} is turned on (dashed red line and dotted blue line). (b) The electric dipole coupling d is given by the slope of energy levels as a function of E_{\parallel} in a constant magnetic field [vertical lines in (a)]. Intrinsic deformation gives $\mathbf{E} \rightarrow \mathbf{E} + \mathbf{E}_{\text{mol}}$, allowing to measure \mathbf{E}_{mol} as the field \mathbf{E} at which the levels cross.

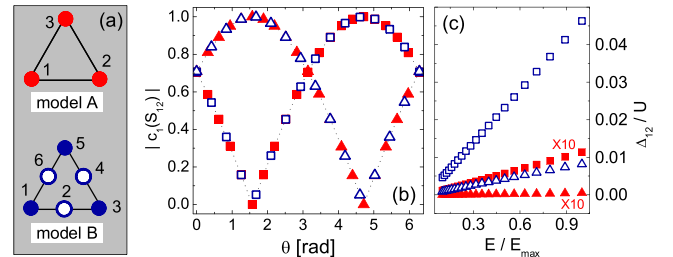


FIG. 3 (color online). (a) Hubbard models A and B of the spin triangle. Model A: $N_e = N_s = 3$, $t_i = t$, $U_i = U$, and $\epsilon_i = \alpha_{ii+1}^\parallel = 0$. Model B: $N_e = 9$, $N_s = 6$, $\alpha_{ii+1}^\parallel = 0$, $\alpha_{ii+1}^\perp = \alpha$, $t_i = t$, $\epsilon_{3k-2} - \epsilon_{3k-1} = \epsilon$, $U_{3k-2} - U_{3k-1} = U$ ($k, k' = 1, 2, 3$). (b) Overlap between the projected ground state of $H_H + H_E$ ($|\Psi_1^0\rangle$), and the eigenstates of $\mathbf{s}_1 \cdot \mathbf{s}_2$ with $S_{12} = 0$ (squares) and $S_{12} = 1$ (triangles), as function of the angle θ between the triangle side 1-2 and an in-plane \mathbf{E} . The filled (empty) symbols correspond to the A (B) model, whereas the dotted lines give the components of the δH_E ground state. In both models, $t/U = 0.1$, $eRE/U = 2.5 \times 10^{-2}$, and $\alpha = 0.1$. (c) Dependence of Δ_{21} on the amplitude E , for $\mathbf{E} \parallel y$ and $eRE_{\text{max}}/U = 2.5 \times 10^{-2}$. Filled (empty) symbols refer to the A (B) model, and squares (triangles) to $\alpha = 0.1$ ($\alpha = 0$) two-site contributions.

$d = 4t|e\tilde{r}_{12}^y|/U$. Analogous power-law dependences are found in model *B*, where the single-site (two-site) contribution scales as $(t/U)^4$ ($(t/U)^3$), and two-site terms dominate in both models. Additional mechanisms, such as the relative displacements of the ions, can contribute to the coupling between spin and electric field.

Spin coupling to cavity electric fields.—Exchange coupling of SMMs has been demonstrated in dimers [26]. The use of this short-range and (so far) untunable interaction requires additional resources for quantum information processing [27]. Efficient spin-electric interaction, on the other hand, provides a route to long-range and switchable coupling between SMM qubits. In particular, microwave cavities are suitable for reaching the strong-coupling regime for various qubit systems [16–19]. Here, we propose to use such cavities to control single SMMs and, moreover, to couple the spin qubits of distant SMMs placed inside the same cavity.

The interaction of a single SMM with the cavity field reads, $\delta H_E = d\mathbf{E}'_0 \cdot \mathbf{C}_{\parallel}(b^\dagger + b)$, where \mathbf{E}'_0 is the rotated electric field of amplitude $|\mathbf{E}'_0| \propto \sqrt{\hbar\omega/\mathcal{V}}$ inside the cavity of volume \mathcal{V} [17], and b is the annihilation operator for the photon mode of frequency ω . The low-energy Hamiltonian of N SMMs interacting with the cavity mode is $H_{s\text{-ph}} = \sum_j (\Delta_{\text{SO}} C_z^{(j)} S_z^{(j)} + \mathbf{B} \cdot \hat{\mathbf{g}} \cdot \mathbf{S}^{(j)} + H_{\text{int}}^{(j)}) + \omega b^\dagger b$, where

$$H_{\text{int}}^{(j)} = dE_0(e^{i\varphi_j} C_-^{(j)} + e^{-i\varphi_j} C_+^{(j)})(b + b^\dagger), \quad (10)$$

with $C_\pm^{(j)} = C_x^{(j)} \pm iC_y^{(j)}$ and $\varphi_j = 7\pi/6 - 2\theta_j$. In the rotating wave approximation $H_{s\text{-ph}}$ reduces to the well-known Tavis-Cummings model [28] when the spins are in eigenstates of $S_z^{(j)}$, and $\mathbf{B} \parallel \hat{z}$. However, if $\mathbf{B} \not\parallel \hat{z}$ it is possible to couple both chiralities and total spins of distant molecules. Typically, the electric fields in cavities are weaker, $|\mathbf{E}'_0| \approx 1$ V/cm for $\hbar\omega \approx 0.1$ meV [19], than the ones near STM tips, thus giving $\tau_{\text{Rabi}} \approx 0.01\text{--}100$ μs . Obviously, decreasing the cavity volume \mathcal{V} would give shorter τ_{Rabi} . Coupling of distant SMMs can be controlled by tuning two given molecules in and out of resonance with the cavity mode, e.g., by applying additional local electric fields. For example, when $\mathbf{B} = 0$ the coupling constant between distant molecules is $J \approx d^2 E_0^2 / (\Delta_{\text{SO}} - \omega)$, with the typical chirality flipping time $0.05\text{--}500$ μs . Further effects such as the state transfer between stationary and flying qubits, or the SMM-photon entanglement, can be observed in a system described by $H_{s\text{-ph}}$.

In conclusion, we find an exchange-based mechanism that couples electric fields to spins in triangular molecular antiferromagnets. While our results are derived for Cu_3 , analogous symmetry arguments are expected to apply to

other molecular magnets that lack inversion symmetry, such as V_{15} [29], Co_3 [30], Dy_3 [31], Mn_{12} [2,3], etc.

We thank D. Klauser, M. Affronte and V. Bellini for useful discussions. We acknowledge financial support from the Swiss NSF, the NCCR Nanoscience Basel; the Italian MIUR under FIRB Contract No. RBIN01EY74; the EU under MagMaNet, QuEMolNa and MolSpinQIP.

-
- [1] D. Gatteschi, R. Sessoli, and J. Villain, *Molecular Nanomagnets* (Oxford Univ. Press, New York, 2007).
 - [2] J.R. Friedman *et al.*, Phys. Rev. Lett. **76**, 3830 (1996).
 - [3] L. Thomas *et al.*, Nature (London) **383**, 145 (1996).
 - [4] C. Romeike *et al.*, Phys. Rev. Lett. **96**, 196601 (2006).
 - [5] M.N. Leuenberger and E.R. Mucciolo, Phys. Rev. Lett. **97**, 126601 (2006).
 - [6] J. Lehmann and D. Loss, Phys. Rev. Lett. **98**, 117203 (2007).
 - [7] A. Ardavan *et al.*, Phys. Rev. Lett. **98**, 057201 (2007).
 - [8] M. Leuenberger and D. Loss, Nature (London) **410**, 789 (2001).
 - [9] F. Meier, J. Levy, and D. Loss, Phys. Rev. B **68**, 134417 (2003).
 - [10] F. Troiani *et al.*, Phys. Rev. Lett. **94**, 207208 (2005).
 - [11] J. Lehmann *et al.*, Nature Nanotech. **2**, 312 (2007).
 - [12] M. Affronte *et al.*, Angew. Chem., Int. Ed. **44**, 6496 (2005).
 - [13] L. Bogania and W. Wernsdorfer, Nature Mater. **7**, 179 (2008).
 - [14] C.F. Hirjibehedin, C.P. Lutz, and A.J. Heinrich, Science **312**, 1021 (2006).
 - [15] A.C. Bleszynski *et al.*, Phys. Rev. B **77**, 245327 (2008).
 - [16] A. Wallraff *et al.*, Nature (London) **431**, 162 (2004).
 - [17] G. Burkard and A. Imamoglu, Phys. Rev. B **74**, 041307 (2006).
 - [18] A. André *et al.*, Nature Phys. **2**, 636 (2006).
 - [19] M. Trif, V.N. Golovach, and D. Loss, Phys. Rev. B **77**, 045434 (2008).
 - [20] M. Fiebig, V.V. Eremanko, and I.E. Chupis, *Magneto-electric Interaction Phenomena in Crystals* (Kluwer Academic, Dordrecht, 2004).
 - [21] D.D. Awschalom, D. Loss, and N. Samarth, *Semiconductor Spintronics and Quantum Computation* (Springer-Verlag, Berlin Heidelberg, 2002).
 - [22] V.N. Golovach, M. Borhani, and D. Loss, Phys. Rev. B **74**, 165319 (2006).
 - [23] K.C. Nowack *et al.*, Science **318**, 1430 (2007).
 - [24] K.-Y. Choi *et al.*, Phys. Rev. Lett. **96**, 107202 (2006).
 - [25] B. Tsukerblat, *Group Theory in Chemistry and Spectroscopy* (Academic, New York, 1994).
 - [26] W. Wernsdorfer *et al.*, Nature (London) **416**, 406 (2002).
 - [27] F. Troiani *et al.*, Phys. Rev. Lett. **94**, 190501 (2005).
 - [28] M. Tavis and F.W. Cummings, Phys. Rev. **170**, 379 (1968).
 - [29] I. Chiorescu *et al.*, Phys. Rev. Lett. **84**, 3454 (2000).
 - [30] M.C. Juan *et al.*, Inorg. Chem. **44**, 3389 (2005).
 - [31] J. Luzon *et al.*, Phys. Rev. Lett. **100**, 247205 (2008).



Review

Quantum computing with molecular magnets

Dimitrije Stepanenko*, Mircea Trif, Daniel Loss

Department of Physics, University of Basel, Klingelbergstrasse 82, CH-4056 Basel, Switzerland

ARTICLE INFO

Article history:

Received 29 January 2008

Accepted 29 February 2008

Available online 7 March 2008

Dedicated to Dante Gatteschi

Keywords:

Single molecule magnets

Quantum computing

ABSTRACT

We discuss the potential of molecular magnets as the building blocks of a quantum computer. The simplification in the control procedure for the quantum gates in many-spin systems coming from the high symmetry is shown to lead to a relatively simple way to address the spin degrees of freedom in molecular magnets. The advantage of an anisotropic effective spin interaction in memory applications is demonstrated on the example of the Grover quantum search algorithm in a generic easy-axis molecular magnet. Electric control of the coupling between the spins is shown to enable two-qubit quantum gates in polyoxometalates.

© 2008 Elsevier B.V. All rights reserved.

Contents

1. Introduction	3740
2. Quantum computer, similarities and differences with the classical computer	3741
3. Qubits in many-spin systems	3742
4. Grover quantum search algorithm in molecular magnets	3742
5. Quantum computing with electrically gated molecular magnets	3743
6. Summary	3745
Acknowledgments	3745
References	3745

1. Introduction

Information processing using quantum mechanics, or more specifically quantum computing, is among the most prominent fields of science in the last 15 years. The motivation behind this effort comes both from the technological appeal of new and better computers and from the fundamental scientific questions about the nature of information and the physical limits on our ability to process it. Quantum mechanics enters this discussion with understanding that an abstract information is always embedded in some real world objects and therefore it is governed by the laws of nature which are quantum [1]. From the point of view of technology, the appeal of quantum computers comes from the fact that there are problems that are tractable on quantum computers which are believed to be intractable on classical ones. The most fa-

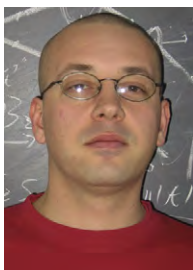
mous such problem is factoring of integers into their prime factors [2], suggesting that quantum computers may be intrinsically more powerful than classical ones.

Conceptually, a computer is any machine that can manipulate information following a predefined set of instructions. Quantitative description of the computational power of different computers is the main problem of complexity theory, a branch of computer science. A similar problem, asking whether mathematics can be done by following a predefined set of rules was stated by Hilbert [3]. The negative answer to this problem, provided by Turing [4], and independently by Church [5], has created the field of computer science and paved the way to the realization of modern computers.

The relevance of quantum computing outside computer science stems from the so-called Church–Turing thesis. This conjecture claims that the resources needed to solve any problem are essentially the same on any computer. If the Church–Turing thesis is true, all the fascinating development of computing machines is simply due to the improved technology, and not due to any

* Corresponding author.

E-mail address: Dimitrije.Stepanenko@unibas.ch (D. Stepanenko).



Dimitrije Stepanenko was born in Vranje, Serbia in 1974. He received a Ph.D. in condensed matter physics from the Florida State University and the National High Magnetic Field Laboratory in the US in 2005. Since then, he worked as a postdoctoral researcher at the University of Basel, with Guido Burkard and then with Daniel Loss. His research interests are in coherent control of electron and nuclear spins in mesoscopic structures and quantum computing with spins in quantum dots and molecular magnets.



Mircea Trif was born in Baia Mare, Romania in 1982. He studied Physics in Cluj Napoca, Romania where he graduated with a Master Degree in Theoretical Physics. Since 2005 he is pursuing a doctoral degree in Theoretical Physics under the supervision of Prof. Daniel Loss at University of Basel, Switzerland. His research interests cover effects of spin-orbit interaction on the electron and hole spins dynamics in semiconductor nanostructures and molecular magnets.



Daniel Loss was born in Wintherthur, Switzerland in 1958. He received a Ph.D. in Theoretical Physics at the University of Zurich in 1985. He stayed there as postdoctoral researcher for four more years before moving to the US in 1989. From 1989 to 1991 he worked as postdoctoral researcher in the group of Prof. Dr. A. J. Leggett, Urbana, and from 1991 to 1993 at IBM Research Center, NY (USA). In 1993, he moved to Vancouver (Canada) to become Assistant and then Associate Professor of Physics at Simon Fraser University. In 1996 he returned to Switzerland to become full Professor of Theoretical Physics at the University of Basel. He received several prestigious fellowships, is a

Fellow of the American Physical Society, and was awarded the Humboldt Research Prize in 2005. His research interests include many aspects of the theory of condensed matter systems with a particular focus on spin-dependent and phase-coherent phenomena in semiconducting nanostructures and molecular magnets.

fundamental difference in the basic organization of the computing machine. It is believed (but not proven) that a quantum computer does not obey the Church–Turing thesis.

Powerful computers that cannot be built are useless, and it is crucial to know whether the model of a quantum computer describes a machine that can be built, and how such a machine can be built. Based on our current knowledge of quantum mechanics it is possible to build a quantum computer. However, the realization of such a machine seems to be a hard task. There have been several proposals for implementing a quantum computer. The purpose of this article is to review the possibilities for quantum information processing in molecular magnets. We will look into requirements for a quantum computer, the DiVincenzo criteria [6], and describe the possibilities for satisfying them in molecular magnets.

2. Quantum computer, similarities and differences with the classical computer

Quantum computers are model devices that process information encoded in quantum states. The model of a quantum computer is built in analogy to a classical computer. It consists of a collection of quantum two-level systems that store the quantum information. In that sense a qubit is analogous to a bit in a classical digital computer. The quantum state of a single qubit, $|\psi\rangle = \alpha|0\rangle + \beta|1\rangle$, is an arbitrary normalized linear combination of the logical basis states $|0\rangle$ and $|1\rangle$. The state of N qubits is, in analogy to the spin state of N spin-1/2 particles,

$$|\Psi\rangle = \sum_{x=\{00\dots 0\}}^{x=\{11\dots 1\}} \alpha_x |x\rangle, \quad (1)$$

an arbitrary superposition of the 2^N basis states in which every qubit is in one of the computational basis states.

As in classical computers the computation is a transformation from an initial state at the beginning of the computation, $|00\dots 0\rangle$, to the final state that encodes the result. This transformation is carried out in a series of operations. For the quantum computer the operations are unitary operations on the state (1). Every quantum operation U can be decomposed into a series of operations U_i acting on a single, i th, qubit and U_{ij} acting on a pair of qubits, i and j [7]. This allows one to measure the complexity of a quantum computation by

counting the elementary operations needed to perform it. From the practical point of view, this reduction to the single- and two-qubit quantum gates is an immense simplification, because the direct n -qubit operation would require control of an n -qubit interaction. Therefore, the control over interaction of single qubits with external fields, leading to single qubit quantum gates, and over the interaction of pairs of qubits, leading to two-qubit quantum gates is sufficient for an arbitrary quantum computation.

During computation, the evolution of the state of a quantum computer is governed by quantum gates applied to the qubits. Any interaction with the qubit environment other than the controlled application of the quantum gates produces errors. Similar error generating processes are suppressed in classical digital computers, because small changes in signal levels within digital computer circuitry do not alter the information. It is not possible to make the quantum information digital without losing the advantage of a quantum computer over the classical one. Recovering from the errors using redundant coding, used for classical communication over noisy channels does have a direct quantum extension to the quantum error correcting codes [8]. Quantum error correction works only if the probability of error in a gate operation is below some threshold value ϵ_{th} . The value of ϵ_{th} depends on the actual form of the errors and the estimates are $\epsilon_{\text{th}} \sim 10^{-2} - 10^{-6}$. In a qubit with coherence time T_2 , this puts an upper limit on the switching time τ_{switch} of quantum gates

$$\frac{\tau_{\text{switch}}}{T_2} \leq \epsilon_{\text{th}}. \quad (2)$$

The low value of the threshold requires long coherence times of the qubits and short switching times of the gates.

At the end of the computation the result is read out by measuring the state of the qubits. Quantum computation produces answers that are encoded in well-defined computational states and the readout requires only the measurement of few qubits.

By looking at the requirements posed on the quantum computer we arrive at five DiVincenzo criteria: for a working quantum computer we must have

- a well-defined two-dimensional subspace that is well isolated and scalable, i.e. it must be easy to add an extra qubit to the computer,

- a procedure to prepare the qubits in an initial state, like $|00\dots 0\rangle$,
- an implementation of one- and two-qubit quantum gates,
- coherence times long enough compared to switching time to allow for the error correction to be efficient,
- the possibility to measure the qubits at the end of computation.

These criteria describe the minimal set of requirements for any quantum computing implementation. We would like to emphasize that all of the criteria from the list must be met in a single device at the same time and in the same experiment. A more detailed overview of the requirements a quantum system must satisfy in order to perform quantum computation can be found in [9].

3. Qubits in many-spin systems

A qubit can be encoded in any two-dimensional state space, regardless of the system that it describes. Quantum computation can also be done on systems with the larger dimension of the state space, like three-dimensional qutrits. Such encodings do not bring additional advantage in computational power over qubit encoding, and we will not discuss them.

Molecular magnets are systems of interacting magnetic atoms, and to a very good approximation can be described as a set of interacting spins [10]. Given the complexity of the underlying interactions between the magnetic ions, we can naively expect that the control over a molecular magnet would be much more difficult than the control over qubits with a natural two-dimensional state space, like the electron spin. It is only due to clear separation of energy scales and the high symmetry of the molecule that the low-energy behavior is comparatively simple and, at least in principle controllable. At the root of this simplification is the fact that the strongest interaction in the system, Coulomb repulsion, is spin-independent. The low-energy manifold of states is then well approximated as a multiplet of the fixed total spin. Within this manifold, the molecule is described by the spin Hamiltonian of a large spin. In order to use a single molecule as a qubit it is then necessary to isolate a two-level subsystem for encoding the quantum information.

When the exchange coupling in a molecule is antiferromagnetic, the ground state as a rule is a multiplet of the lowest total spin. This can lead to a true spin-1/2 ground state multiplet. In that case the symmetry of the molecule becomes crucial and the resulting low-energy behavior of the system is to a large extent determined by the symmetry alone.

The problem of encoding a qubit into a system of interacting spins, analogous to the spins in molecular magnets, was studied in antiferromagnetic spin clusters [11]. A coupled spin system a lowest-energy multiplet of the total spin $1/2$, $S^{\text{tot}} = 1/2$, retains the main advantage of the natural spin-1/2 encoding since the energy gap to the excited states prevents the qubit state from leaking out of the computational space. While the description of the state in terms of individual spins is not simple, its symmetry assures that the interaction with the external fields is easily controlled. The advantage of the cluster of spins over the single spin comes with the increased size of the qubit. Quantum control over larger qubits does not require engineering of the external fields on prohibitively short length scale. The overhead comes as a modest increase in control complexity and in coherence times.

As an example that illustrates the simplification of the control, we consider the case of two coupled large spins with anisotropic single-spin Hamiltonians

$$H = J s_1 \cdot s_2 + k_z (s_{1,z}^2 + s_{2,z}^2). \quad (3)$$

Two large spins s_1 and s_2 interact via exchange and show single-spin anisotropy. The low-energy eigenstates have a general form

$$|0(1)\rangle = \sum_{m_1=-s_1+1}^{s_1} \alpha_{m_1}^{0(1)} \left| m_1, \frac{1}{2} - m_1 \right\rangle. \quad (4)$$

Note that the symmetry under rotations about the anisotropy axis z has drastically simplified the states (4) which include only a multiplet of a constant S_z^{tot} , since $[H, S_z^{\text{tot}}] = 0$. The effective interaction, derived from the full system at low energy still has a simple form:

$$H_* = J_* s^I \cdot s^{II}. \quad (5)$$

We see that the effective interaction H_* is just the exchange in the space of cluster spins s^I and s^{II} , with a new coupling constant J_* . Therefore, the problem of control is shielded from the complexities of the actual interaction and amounts to the control of a single parameter $J_*(t)$, in analogy with exchange-coupled quantum dots [12].

For a generic spin system at low energy, the spin interaction is not of the isotropic form (5). The point-group symmetry of the molecule is smaller than the spherical symmetry and the spin-orbit coupling introduces anisotropy in the effective spin interaction. The effects of anisotropy on quantum gates can be suppressed using appropriately designed time-dependence of the control pulses [13], or used to produce quantum gates unavailable in the systems with isotropic interaction [14].

4. Grover quantum search algorithm in molecular magnets

The most striking advantage of quantum computers over classical ones is the exponential speedup with respect to the best known classical algorithm, as in the factoring problem. There are, however, other problems where quantum computers offer a different kind of advantage. One such problem is the so-called quantum search. In the standard version of the problem we are given a database that is not ordered in any way, and asked to retrieve a specific element from it. We can visualize this as searching through a phone book in order to find the name corresponding to a given telephone number. In the classical case, the best strategy is to successively retrieve and check one element after another. On average, the item will be found after $N/2$ queries of the database, where N is the number of entries. In the quantum version of the problem, we are allowed to use quantum queries and ask for the superpositions of the database entries. Using the Grover algorithm [15], the task of finding the item is accomplished using $O(\sqrt{N})$ queries. This speedup is not as spectacular as the speedup in the factoring problem. The advantage is seen in going from a higher to a lower order polynomial. However, it can be proved (and it is almost obvious) that there is no classical search algorithm that scales better than linear in the size of the database, while we do not know how efficient is the best classical algorithm for factoring.

A related search problem, also posed and solved by Grover [16], is the quantum version of the 'game of twenty questions'. In the classical game we are allowed to query the database about all the entries at once, and the only constraint is that the answer to every question must be either yes or no. For example, we can ask if there is an element we are looking for among the first $N/2$ database elements. Such questions can be answered only if the database is ordered. In the classical case, the search needs at least $\sim \log_2 N$ queries. A truly surprising result is that the quantum version of this search can be completed in a single quantum query. The price for this great reduction of the number of queries is in the queries complexity.

Quantum search algorithm requires an oracle, the computing element that can recognize the elements we are searching for,

and it requires that the oracle be quantum. That means that the oracle performs a unitary transformation:

$$O|x\rangle = (-1)^{f(x)}|x\rangle, \quad (6)$$

where $|x\rangle$ is a computational basis state (1) that addresses the database entry, and the function f is defined by $f(x) = 1$ if the element is the one we are searching for, and $f(x) = 0$ otherwise. In words, the computational basis states that encode solutions to the search problem are marked by the oracle which changes their sign. The search proceeds by applying the Grover iteration that after $\sim\sqrt{N}$ repeats produces a solution to the search problem. The essential part of the Grover iteration that cannot be applied in a classical settings is the application of the oracle to the state:

$$|\Psi_{\text{mix}}\rangle = \left(\frac{1}{\sqrt{2}}(|0\rangle + |1\rangle)\right)^{\otimes N}, \quad (7)$$

which represents the query of all of the registers at once. Note that the oracle still only needs to recognize the solution to the search problem. It does not know how many solutions are in the database, nor what their nature is. In contrast to factoring, the Grover search algorithm does not require entanglement for its operation [17].

In the most powerful application the Grover quantum search algorithm enables retrieval of a record from a database using a single quantum query. This astonishing speedup requires some knowledge about the solutions to the search problem that is not present in its standard statement, and comes at a price of the query being more complex. Therefore, a system that allows for a complex quantum query is valuable as a memory element. The molecular magnets are capable of supporting this kind of Grover query [18], thanks to the strong anisotropy present in the molecular magnets low-energy manifold. Molecular magnets can therefore serve as memory elements with large information density and potentially short access time.

Taking a look at the mixed state $|\Psi_{\text{mix}}\rangle$, we can immediately see where the complexity of a quantum query lies. It has to access all the records in a database at once. In a molecular magnet the different states correspond to the different energy levels of a large spin. A query would then proceed through accessing all the transitions between the different states in a controllable fashion. If the levels were equidistant, as in $H^{\text{eq}} = \hbar\omega^{\text{eq}}S_z$, all the transition frequencies between the neighboring levels would be equal, and it would be impossible to access each transition separately.

Molecular magnets have an advantage of a highly anisotropic spin Hamiltonian with nonequidistant energy levels. A typical spin Hamiltonian reads

$$H_{\text{spin}} = H_a + V, \quad (8)$$

where $H_a = -AS_z^2 - BS_z^4$, ($A \gg B > 0$) represents the spin anisotropy with the easy axis along z , and $V = g\mu_B H \cdot S$ is the Zeeman coupling between the external magnetic field B and the spin S . In addition to (8), the molecular magnet experiences tunneling between $|m\rangle$ -states, and the spin-phonon coupling. At low temperatures, and in the bias field regime $g\mu_B \delta H_z > E_{\text{mm}'}$, where $E_{\text{mm}'}$ are the tunnel splittings between $|m\rangle$ -states, the tunneling and spin-phonon interaction are suppressed. Spin evolution is then controlled by H_a and V .

Using two kinds of ac magnetic fields that give rise to the 'low' and 'high' Zeeman coupling term [18]

$$V_{\text{low}}(t) = g\mu_B H_0(t) \cos(\omega_0 t) S_z, \quad (9)$$

$$V_{\text{high}}(t) = \sum_{m=-m_0}^{s-1} \frac{g\mu_B H_m(t)}{2} (e^{i(\omega_m t + \phi_m)} S_+ + e^{-i(\omega_m t + \phi_m)} S_-), \quad (10)$$

where the 'low' field corresponds to the linear polarization of the field along the easy axis that causes the transitions that do not change the quantum number m , and the 'high' transitions correspond to left circular polarization σ^- and cause transitions with $\Delta m = -1$. Right circular polarization σ^+ would cause $\Delta m = +1$ transitions, and the choice of circular polarization allows selective addressing of the states in just one of the wells $S_z > 0$, or $S_z < 0$, when starting from the large spin with maximal projection on the z -axis.

Under the influence of the combined driving $V(t) = V_{\text{low}}(t) + V_{\text{high}}(t)$, and with rectangular pulse shape ($H_k(t) = H_k$, if $-T/2 < t < T/2$, $H_k(t) = 0$ otherwise), the molecular magnet transition amplitudes are given by the S -matrix, given in a perturbation series as

$$S = \sum_j S^{(j)}, \quad (11)$$

where the transitions involving n photons of different frequencies are

$$S_{m,s}^{(n)} = \sum_F \Omega_m \frac{2\pi}{i} \left(\frac{g\mu_B}{2\hbar}\right)^n \frac{\prod_{k=m}^{s-1} H_k e^{i\phi_k} H_0^{m-m_0} p_{m,s}(F)}{(-1)^{q_F} q_F! r_s(F)! \omega_0^{n-1}} \times \delta^{(T)} \left(\omega_{m,s} - \sum_{k=m}^{s-1} \omega_k - (m - m_0) \omega_0 \right). \quad (12)$$

Here, the n th order S -matrix is given in terms of the external control fields, parameterized in terms of H_k , H_0 , and ϕ_k , and the constants q_F , $r_s(F)$, and $p_{m,s}(F)$ that all depend on a particular tunneling path F . The Dirac delta function of the duration T assures energy conservation between the initial and final states.

Procedure for writing in a state into a molecular magnet consists of sending in a single ESR pulse that will bring a magnet from the initial state $|m\rangle = |-s\rangle$ to the final state:

$$|f\rangle = \sum_{m=-m_0}^s \sum_{j=0}^n S_{m,s}^{(j)} |m\rangle. \quad (13)$$

where the S -matrix has to be calculated up to n th order. Due to the resonance condition being different for different levels, it is possible to adjust the frequencies so that the amplitudes of all the states $|m\rangle$ in (13) are of comparable modulus. This would not be possible in a system with an equidistant spectrum where the population of higher levels has to proceed through higher order perturbation with all the perturbative terms coming into resonance at the same frequency. In an actual molecular magnet, like Mn_{12} , the frequencies would lie in a range between 20 and 300 GHz and the ratio between the largest and the smallest field strength at different frequencies would be ~ 30 .

To find the capacity of a single molecular magnet to store information, we can assume that each molecule can store two digits, one for each circular polarization of the write and read pulse. Each digit can be in one of $N = 2^{s-1}$ states, which for $s = 10$ (Mn_{12}) is 2.6×10^5 . The total time of a full write-read cycle is $\tau_c = 10^{-10}$ s. Therefore, molecular magnets can be used as a dense and efficient memory device.

5. Quantum computing with electrically gated molecular magnets

The control over quantum operations can be the most involved requirement for a quantum computer. There is no single best way to apply quantum gates valid for every qubit, and each qubit type requires a specific control mechanism. The molecular magnets stand out among other proposed qubits by combining the size that is much larger than the atomic systems and much smaller than

solid-state devices such as quantum dots. The magnetic properties of molecular magnets can be changed in a wide range during chemical synthesis. A wide variety of available molecules promises that there are many potentially interesting systems for quantum computing applications among them.

In solid-state settings, the qubits based on spin typically show longer coherence times than the charge-based qubits. The paradigmatic way of producing a solid-state qubit is to isolate an island of electrons in a piece of semiconductor and contact it by metallic electrodes. When the island is small enough, typically 10–100 nm, voltages on electrodes can control the number of electrons in the island, all the way to single electron regime and the empty island. In these regimes, the energy of the electron is quantized due to confinement in a small volume, and these structures are called quantum dots, or artificial atoms. This procedure of preparing an electronic system with a discrete set of energy levels by carving it out of a piece of semiconductor is a typical top-down approach. The drawback of such an approach is that each and every quantum dot has to be lithographically defined, and the scalability of such structures can be an issue. The top-down production gives quantum dots with different electrostatic confinement, and spins can feel such differences through spin–orbit coupling. The molecular magnets are designed from bottom up, using synthetic chemistry and starting from identical atoms. Quantum computers that consist of a coupled set of molecular magnets is guaranteed to have all of its qubits identical.

If the spin of a molecular magnet represents a qubit, the quantum computer can be realized as a set of qubits connected in a cluster [11]. The interaction of qubits is mediated by the intervening binding groups. This kind of control is exhausted once the mol-

ecules are assembled. Application of a quantum gate requires control over spins while the gates are applied, at very fast time scales. Such time scales favor electrical over magnetic control, because it is generically much easier to produce electric fields that vary on very short time scales than it is the case with magnetic fields. Strong electric fields can be applied to molecular magnets using a scanning tunneling microscope tip, or by coupling the molecule to a strip-line [19].

An experimental setup for applying the two-qubit gates on spins in a molecular magnet cannot be directly deduced from the solid-state counterpart. The reason for this is that the spin coupling in a molecular magnet is mostly determined by its chemistry, and reacts very weakly to the external fields that are under experimental control on the short time scales characteristic for the quantum gates. As an example of a two-qubit system, we can consider a polyoxometalate molecule $[\text{PMo}_{12}\text{O}_{40}(\text{VO})_2]^{q-}$ [20,21] that consists of a central mixed-valence core based on the $[\text{PMo}_{12}\text{O}_{40}]$ Keggin unit [22], capped by two vanadyl groups containing two localized spins. Quite generically, the low-energy spin Hamiltonian of such a structure has a relatively simple form [21]:

$$H = -J(n_c)S_L \cdot S_R - J_C(S_L + S_R) \cdot s_c + (\epsilon_0 - eV_g)n_c + Un_c(n_c - 1)/2. \quad (14)$$

Here, the first term describes the indirect exchange coupling of the left (S_L) and right (S_R) vanadyl group spins, with the coupling strength $J(n_c)$ which depends on the number of excess electrons on the central core n_c . The second term describes symmetric coupling of the spin on the central core s_c to the vanadyl group spins. The molecule is also electrostatically coupled to the control gate voltage V_g , and the orbital energy of an added electron is ϵ_0 , as described by the third term. The last term in (14) describes the Coulomb repulsion energy cost of changing the number of electrons on the core. For the application of the quantum gates, the crucial part of the Hamiltonian (14) is the dependence of the exchange coupling between the vanadyl spins on the charge of the core $J(n_c)$. The control over the central core charge allows for implementation of the exchange gates:

$$U(\lambda) = \exp(-i\lambda S_L \cdot S_R), \quad (15)$$

where the parameter λ completely determines the gate. If we choose to encode the qubits into spin states of the vanadyl groups,

$$|0\rangle = |S_z^{(\text{VO})} = 1/2\rangle, \quad |1\rangle = |S_z^{(\text{VO})} = -1/2\rangle, \quad (16)$$

then one particular exchange gate, $\sqrt{\text{SWAP}} = U(\pi/2)$ is sufficient for universal quantum computation, provided that it can be applied between any pair of neighboring qubits [12]. Assuming that the exchange coupling is negligible for the core in equilibrium $J(n_c = 0) = 0$, and writing the Hamiltonian (14) in the $n_c = 1$ sector as

$$H_1 = -(J_1 - J_C)S_L \cdot S_R - \frac{J_C}{2}S^2, \quad (17)$$

where $S = S_L + S_R + s_c$ is the total spin of the molecule, it can be shown that the $\sqrt{\text{SWAP}}$ gate is obtained for the gate time τ_{gate} and the exchange coupling in the $n_c = 1$ sector J_1 that satisfy the relations:

$$\tau_{\text{gate}} = \frac{4\pi}{3} \frac{\hbar}{|J_C|} m, \quad \frac{J_1}{J_C} = \text{sgn}J_C + \frac{3}{8} \frac{1 - 4n}{m}, \quad (18)$$

where $n(\neq 0)$ and m are arbitrary integers.

This control scheme assumes that the exchange coupling can be changed with the required precision. A quick look at (14) implies that we must also control the charge of the core with high precision and high temporal resolution. The process of electron tunneling from the control electrode to the core and back is however governed by quantum effects and the degree to which it can be

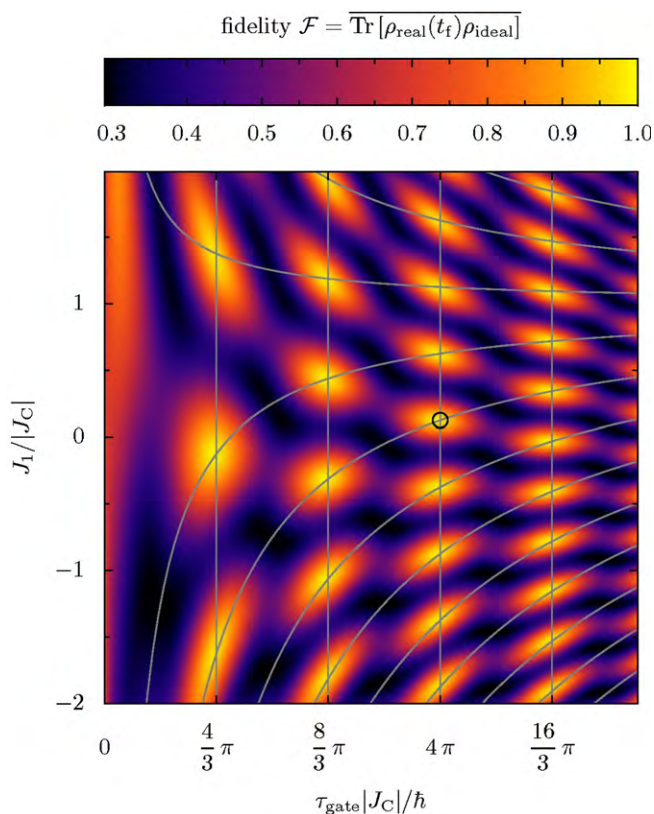


Fig. 1. Numerical evaluation of the average fidelity of $\sqrt{\text{SWAP}}$ quantum gate as a function of the gate time τ_{gate} and the ratio of indirect exchange coupling J_1 between the vanadyl groups and the coupling of vanadyl groups to the central core J_C . The solid lines track the gate parameters that lead to an ideal gate in the approximation of the direct control of n_c .

controlled by an external voltage can be found by solving for the quantum evolution of the system comprising the molecule and the electrodes under the influence of time-dependent voltage V_g (14) [21].

One figure of merit for a real quantum gate is the fidelity

$$\mathcal{F} = \overline{\text{Tr}[\rho_{\text{real}}(t_f)\rho_{\text{ideal}}]} \quad (19)$$

Here, $\rho_{\text{real}}(t_f)$ is the density matrix of the qubits at the end of the quantum gate operation at the time t_f , ρ_{ideal} is the density matrix of the involved qubits that were operated upon by an ideal gate, and the overbar means the average over the initial two-qubit states. Intuitively, the fidelity is an average overlap of the state produced by the real quantum gate with the desired state that an ideal gate would produce. Numerical analysis of the electrically gated quantum dots shows [21] that the fidelities as large as $\mathcal{F} = 0.99$ are possible for this implementation of the quantum $\sqrt{\text{SWAP}}$ gate (Fig. 1). An important lesson from this exercise is that the complex structure of the molecule does not necessarily give a complex interaction of the spins and that due to the constrained form of the effective interaction the control problem has some degree of robustness.

6. Summary

We have reviewed how the complexities of a generic molecular magnet, a structure of many interacting spins are tamed by symmetry, so that the low-energy properties of a collection of spins can be controlled by simple means. Molecular magnets offer an advantage in memory applications due to their highly anisotropic spectrum, and allow for an application of the Grover search algorithm. Finally we have described a proposal for quantum informa-

tion processing in polyoxometalates that uses electric control over spins to perform the two-qubit quantum gates.

Acknowledgments

Financial support by the EU RTN QuEMolNa, the EU NoE MAG-MANet, the NCCR Nanoscience, and the Swiss NSF is gratefully acknowledged.

References

- [1] D.P. DiVincenzo, D. Loss, *Superlattices Microstruct.* 23 (1998) 419.
- [2] P.W. Shor, in: *Proceedings of the 35th Annual Symposium on the Foundations of Computer Science*, IEEE Computer Society Press, Los Alamos, 1994, p. 124.
- [3] D. Hilbert, *Nachrichten von der Königl. Gesellschaft der Wiss., zu Göttingen*, 1900, p. 253.
- [4] A.M. Turing, *Proc. London Math. Soc.* 42 (1936) 200.
- [5] A. Church, *Am. J. Math.* 58 (1936) 345.
- [6] D.P. DiVincenzo, *Science* 270 (1995) 255.
- [7] D.P. DiVincenzo, *Phys. Rev. A* 51 (1995) 1015.
- [8] P.W. Shor, *Phys. Rev. A* 52 (1995) R2493.
- [9] V. Cerletti, W.A. Coish, O. Gywat, D. Loss, *Nanotechnology* 16 (2005) R27.
- [10] D. Gatteschi, R. Sessoli, J. Villain, *Molecular Nanomagnets*, Oxford University Press, Oxford, 2006.
- [11] F. Meier, J. Levy, D. Loss, *Phys. Rev. B* 68 (2003) 134417.
- [12] D. Loss, D.P. DiVincenzo, *Phys. Rev. A* 57 (1998) 120.
- [13] D. Stepanenko, N.E. Bonesteel, D.P. DiVincenzo, G. Burkard, D. Loss, *Phys. Rev. B* 68 (2003) 115306.
- [14] D. Stepanenko, N.E. Bonesteel, *Phys. Rev. Lett.* 93 (2004) 140501.
- [15] L.K. Grover, *Phys. Rev. Lett.* 79 (1997) 325.
- [16] L.K. Grover, *Phys. Rev. Lett.* 79 (1997) 4709.
- [17] S. Lloyd, *Phys. Rev. A* 61 (1999) R010301.
- [18] M. Leuenberger, D. Loss, *Nature* 410 (2001) 789.
- [19] M. Trif, V.N. Golovach, D. Loss, *Phys. Rev. B* 77 (2008) 045434.
- [20] Q. Chen, C.L. Hill, *Inorg. Chem.* 35 (1996) 2403.
- [21] J. Lehmann, A. Gaita-Ariño, E. Coronado, D. Loss, *Nat. Nanotechnol.* 2 (2007) 312.
- [22] J. Keggins, *Nature* 131 (1933) 908.

Interference of heavy holes in an Aharonov-Bohm ring

Dimitrije Stepanenko,¹ Minchul Lee,² Guido Burkard,³ and Daniel Loss¹

¹*Department of Physics, University of Basel, Klingelbergstrasse 82, CH-4056 Basel, Switzerland*

²*Centre de Physique Théorique, UMR6207, Case 907, Luminy, 13288 Marseille Cedex 9, France*

³*Department of Physics, University of Konstanz, D-78457 Konstanz, Germany*

(Received 16 January 2009; revised manuscript received 26 April 2009; published 1 June 2009)

We study the coherent transport of heavy holes through a one-dimensional ring in the presence of spin-orbit coupling. Spin-orbit interaction of holes, cubic in the in-plane components of momentum, gives rise to an angular momentum-dependent spin texture of the eigenstates and influences transport. We analyze the dependence of the resulting differential conductance of the ring on hole polarization of the leads and the signature of the textures in the Aharonov-Bohm oscillations when the ring is in a perpendicular magnetic field. We find that the polarization-resolved conductance reveals whether the dominant spin-orbit coupling is of Dresselhaus or Rashba type, and that the cubic spin-orbit coupling can be distinguished from the conventional linear coupling by observing the four-peak structure in the Aharonov-Bohm oscillations.

DOI: 10.1103/PhysRevB.79.235301

PACS number(s): 73.23.-b, 03.65.Vf, 71.70.Ej, 73.63.-b

I. INTRODUCTION

Conductance of mesoscopic rings threaded by the magnetic flux shows Aharonov-Bohm oscillations¹ due to the phase a quantum state acquires when it winds around the magnetic flux. An analogous effect in rings made of semiconductors with spin-orbit coupling occurs due to the spin precession as an electron orbits the ring, giving rise to the Aharonov-Casher phase.² Both the Aharonov-Bohm and the Aharonov-Casher effects are manifestations of quantum coherence in mesoscopic systems, and provide a way to study the quantum interference in mesoscopic conductors.³⁻⁶ They lead to universal conductance fluctuations⁷ and persistent spin and charge currents.⁸⁻¹⁰ From a more practical point of view, the conductance that depends on the magnetic flux in the case of Aharonov-Bohm effect, or on the strength of spin-orbit coupling in the case of Aharonov-Casher effect, paves the way for novel applications in mesoscopic electronic and spintronic devices. For example, the Aharonov-Casher phase can be modified by applying a backgate voltage to the device and changing the Rashba coupling constant.¹¹ This enables spintronic devices that require neither any ferromagnetic materials nor the control over magnetic field to operate.¹¹⁻¹⁴

Recently, a number of experimental^{15,16} and theoretical⁴ studies have investigated transport of heavy holes in rings. These studies are relevant because of the strong spin-orbit coupling of heavy holes confined to the ring,¹⁵ and long coherence length ($\sim 3 \mu\text{m}$ in carbon-doped GaAs), making the interference effects in transport observable. The material parameters of holes allow for spintronic applications.¹⁷ In coherent spin-orbit coupled systems, the transport shows an intriguing interplay of Aharonov-Bohm and Aharonov-Casher effects.¹⁸ Apart from showing strong spin-orbit coupling and long coherence lengths, the heavy holes interact through a novel form of the spin-orbit coupling that is cubic in the in-plane components of momentum. This form of spin-orbit coupling influences the interference effects in transport.

In this work, we study the conductance of a ring of heavy holes tunnel coupled to two external leads. This is in contrast

to previous studies which consider rings that are strongly coupled to the leads,⁴ or are in a diffusive regime and can be described using semiclassical trajectories,¹⁹ or described in a lattice model.²⁰ Studies of the conduction through quantum dots embedded in an Aharonov-Bohm ring have focused on the effects of interaction on the transport,²¹⁻²³ while we study the interference of many available paths. In these setups, the interference effects can be traced to the Aharonov-Bohm and Aharonov-Casher phases accumulated by a spin experiencing a time-dependent field while moving along a trajectory through the ring. In the adiabatic limit, this approach leads to geometric phases.²⁴ On the other hand, in our tunneling setup, the quantum effects in transport arise from the interference of tunneling paths through the eigenstates of the ring. The interference is then related to the magnetic field dependence of the eigenstates of a hole confined to the ring, and not to the phase accumulated by a spin following quasiclassical trajectory.

The states $|\Psi_{\text{hh}}\rangle$ of a heavy hole orbiting a ring can be described in terms of pseudospin textures. At a position ϕ along the ring, the heavy-hole state is

$$\langle\phi|\Psi_{\text{hh}}\rangle = \psi_+(\phi)|j_z = 3/2\rangle + \psi_-(\phi)|j_z = -3/2\rangle, \quad (1)$$

and it determines a unique direction \mathbf{n} in the pseudospin space for which $\langle\phi|\Psi_{\text{hh}}\rangle$ is an eigenstate of pseudospin projection to the axis \mathbf{n} , i.e., $|\Psi_{\text{hh}}\rangle \propto |\sigma_{\mathbf{n}} = 1\rangle$. We identify the $|j_z = \pm 3/2\rangle$ heavy-hole states with pseudospin 1/2 pointing in $\pm z$ direction, $|\sigma_z = \pm 1\rangle$. The pseudospin texture associates the direction \mathbf{n} with every point ϕ on the ring (Figs. 1 and 2) so that the states in Eq. (1) can be represented in terms of spin texture as

$$\langle\phi|\Psi_{\text{hh}}\rangle = e^{i\lambda(\phi)}|\sigma_{\mathbf{n}(\phi)} = 1\rangle, \quad (2)$$

with the texture defined by the position-dependent unit vector $\mathbf{n}(\phi)$ and the position-dependent overall phase $\lambda(\phi)$. The textures of heavy-hole eigenstates depend on the hole-orbital momentum κ so that the holes arrive at the connecting leads with different pseudospins, causing an interference pattern in the resulting conductance.

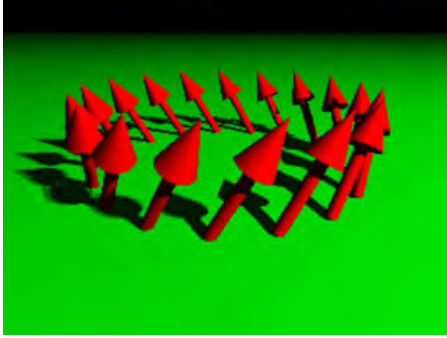


FIG. 1. (Color online) Hole pseudospin texture of the Dresselhaus-only eigenstate.

In the measurement of conductance as a function of flux through a semiconductor ring, the Aharonov-Casher effect manifests itself through an additional structure in the Aharonov-Bohm oscillations due to spin precession in the arms of the ring.¹⁵ In the approximation of spin-orbit coupling that is linear in momentum, the conductance oscillations reveal a splitting of Aharonov-Bohm peak in the Fourier transform of resistivity as a function of the external magnetic field.²⁵ However, the spin-orbit coupling of holes in *III-V* semiconductors is, in lowest order, cubic in the hole momentum.²⁶ In this case, the spin texture of the orbiting carrier depends on the momentum (see below) and profoundly influences the transport. Therefore, for the carriers with cubic spin-orbit coupling, the Aharonov-Casher phase can be controlled by changing the momentum of the carriers, without the need to modify the coupling constant. This point is especially important in the structures fabricated in symmetric quantum wells where the Rashba coupling is absent, and the Dresselhaus spin-orbit coupling is given by the crystalline structure. Even though the coupling constant is fixed, due to the cubic form of spin-orbit coupling, the Aharonov-Casher phase can still be indirectly controlled through the manipulation of the carrier momentum. In addition, the Dresselhaus and Rashba terms produce different patterns in conductance as a function of backgate voltage so that the conductance in phase-coherent rings reveals the dominant type of spin-orbit coupling.

The remainder of the paper is organized as follows: In Sec. II, we describe the confinement of heavy holes to a ring



FIG. 2. (Color online) Hole pseudospin texture of the Rashba-only eigenstate.

and derive the effective one-dimensional Hamiltonian. In Sec. III, we solve for the hole eigenstates and eigenenergies. In Sec. IV, we introduce the tunneling model of hole transport through the ring. In Sec. V, we present the resulting differential conductance of the ring. We conclude in Sec. VI.

II. HEAVY HOLES IN A ONE-DIMENSIONAL RING

Heavy holes confined to the two-dimensional hole gas (2DHG) are described with $H=H_0+H_{SO}+H_Z$, where $H_0=\mathbf{p}^2/2m_{hh}$ is the standard kinetic term, $H_Z=(1/2)\mu_B\mathbf{B}\cdot\mathbf{g}\cdot\boldsymbol{\sigma}$ is the Zeeman coupling to the magnetic field \mathbf{B} , μ_B being the Bohr magneton, \mathbf{g} the gyromagnetic tensor of the confined holes, and $\boldsymbol{\sigma}$ the vector of the pseudospin Pauli matrices. We consider a material with large splitting between heavy holes and light holes bands, and assume that only the heavy holes band is populated. The spin-orbit interaction of heavy holes is, in lowest order, cubic in the in-plane components of the momentum,²⁶

$$H_{SO}=(i\alpha p_-^3+\beta p_-p_+p_-)\sigma_++\text{H.c.}, \quad (3)$$

where α and β are, respectively, interaction strengths of Rashba and Dresselhaus spin-orbit coupling, and $O_{\pm}=O_x\pm iO_y$, ($O=p,\sigma$). The pseudospin represents the two heavy-hole states $|\sigma_z=\pm 1\rangle=|j=3/2,j_z=\pm 3/2\rangle$. This is in sharp contrast to the electrons in a two-dimensional electron gas (2DEG), where the spin-orbit is in the lowest-order linear in momentum. Effects of spin-orbit coupling in general depend on the confinement, both to the 2DHG and to the ring. We will treat the spin-orbit coupling strengths α and β as free parameters and absorb the influence of the electrostatic potential that confines the holes to two dimensions into their values. In particular, if the confinement to two dimensions is caused by a symmetric potential, the Rashba coupling vanishes, $\alpha=0$. We neglect the orbital effects of the magnetic fields so that \mathbf{p} is the kinetic momentum of the hole.

In order to illustrate the spin structure of ring eigenstates, we will first solve for the eigenvalues and wave functions of the heavy holes confined to the ring in the absence of magnetic field. Later, we take the magnetic field into account and find that it causes modification of the quantization condition and the Zeeman coupling.

The two-dimensional hole gas is confined to the ring by a radial potential $V(r)$ that has a deep minimum in the interval $a-w/2 < r < a+w/2$, where a is the radius of the ring and w is its width. States of the hole orbiting the ring in the limit of strong confinement are products of the ground-state radial wave function in the potential $V(r)$, and a function of the angular coordinate $\Psi(\phi)$. For strong radial confinement, the motion of the hole in the ring is described by an effective Hamiltonian that depends only on the angular coordinate along the ring and all the properties of the radial wave function enter the problem only through the parameters of the effective one-dimensional Hamiltonian. The description in terms of the effective one-dimensional Hamiltonian is valid when both the energy spacing of the 2DHG confinement and the energy spacing of the radial confinement are much larger than the energies associated with the motion along the ring.

We find an effective Hamiltonian for the ring by introducing the confinement potential $V(r)$ in the radial direction in

H_{SO} and reducing it to the subspace of the lowest radial mode, in analogy with Ref. 27. Typically these results were obtained by introducing a model potential and explicitly calculating the angular Hamiltonian for the lowest radial mode. The resulting one-dimensional effective Hamiltonian for the harmonic radial confinement was found for the case of linear²⁷ and cubic Rashba¹⁹ spin-orbit coupling. We note that generically the solution to the radial problem in an arbitrary potential can lead to divergences in the effective Hamiltonian. This can be avoided by working directly with the radial wave function in the form of a harmonic-oscillator ground state. In this work, we employ a different approach, and calculate the effective Hamiltonian for a general radial wave function. The resulting effective one-dimensional Hamiltonian is

$$\begin{aligned}
H = & -\frac{1}{2m_{\text{hh}}a^2}\partial_\phi^2 + [i\alpha e^{3i\phi}(F_0 + F_1\partial_\phi + F_2\partial_\phi^2 + F_3\partial_\phi^3) \\
& + \beta e^{i\phi}(G_0 + G_1\partial_\phi + G_2\partial_\phi^2 + G_3\partial_\phi^3)]\sigma_- \\
& + [-i\alpha e^{-3i\phi}(F_0 - F_1\partial_\phi + F_2\partial_\phi^2 - F_3\partial_\phi^3) \\
& + \beta e^{-i\phi}(G_0 - G_1\partial_\phi + G_2\partial_\phi^2 - G_3\partial_\phi^3)]\sigma_+. \quad (4)
\end{aligned}$$

where $G_0=i(R_0+R_1-R_2)$, $G_1=-(R_1+R_2)$, $G_2=i(R_2-2R_3)$, and $G_3=-R_3$; $F_0=i(R_0-3R_1+3R_2)$, $F_1=-3R_1+9R_2-8R_3$, $F_2=i(-3R_2+6R_3)$, and $F_3=R_3$. The parameters that depend on the radial confinement are $R_j=\langle r^{-j}\partial_r^{3-j} \rangle_{\text{radial}}$, where the expectation value is taken in the ground-state radial wave function. The parameters R_j and $j=0, \dots, 3$ satisfy consistency conditions that reduce the number of free parameters to two. We keep the explicit dependence of the independent expectation values in the radial state. The constraints are $R_2=R_3/2$ and $R_0=-3R_1/2$. The constraints can be proven using integration by parts in the radial part of the Schrödinger equation, under the assumption that the radial part of the wave function vanishes at the origin together with its derivatives up to order 3. We have checked that this conclusion holds in the limit of a series of potentials that converge to the hard wall. Also, note that the relation between R_0 and R_1 is satisfied for the radial wave functions of the harmonic confinement for which R_3 diverges.¹⁹ We can take the values R_0 and R_3 as the free parameters of the ring confinement. For a ring of radius a and width w , $R_3 \propto a^{-3}$ and $R_0 \propto a^{-1}w^{-2}$.

Before embarking on the solution of the one-dimensional problem, let us briefly discuss the resulting Hamiltonian. Depending on the radius and the width of the ring, different terms in the spin-orbit interaction become more or less important. Also, we see an enhancement of the spin-orbit effects in narrow and small rings. We see that the strength of the spin-orbit coupling terms depends on the width of the one-dimensional ring w through the parameter $1/(aw^2)$. This means that the spin-orbit coupling terms can be enhanced in a very narrow ring. In this limit, however, the spin-orbit coupling is effectively linear. Therefore, the effects of the cubic spin-orbit coupling presented here will be pronounced in the rings of intermediate widths, and the strength of radial confinement that is strong enough for the approximation of the single radial mode to hold.

III. SPECTRUM AND EIGENSTATES OF THE ORBITING HOLES

The effective Hamiltonian [Eq. (4)] describes a ring of heavy holes in the presence of both Dresselhaus and Rashba spin-orbit interaction, when $\alpha \neq 0$ and $\beta \neq 0$. Our goal is to understand the role of cubic spin-orbit coupling in transport, and contrast its effects to the standard linear spin-orbit coupling, experienced by the electrons in a similar configuration. We will therefore focus on the two limits that allow for a simple solution, namely, Dresselhaus-only interaction ($\alpha=0$), and Rashba-only interaction ($\beta=0$) that was previously studied in Ref. 19. While restricting the domain of validity of our results, these approximations emphasize the physical picture of the eigenstates in terms of holes orbiting the ring, and the associated texture of the hole pseudospin. Apart from allowing a simple solution and providing a simple picture of the eigenstates, these two limits are also, in principle, realizable in practice. In the semiconductor heterostructures that confine holes to the 2DHG, the strength of the Rashba term is governed by the asymmetry of the confining potential in the direction perpendicular to the 2DHG plane. For a highly asymmetric potential the Rashba term is dominant, but it vanishes when the holes are confined by a symmetric potential well.

A. Dresselhaus ($\alpha=0$) case

Eigenstates of the effective Hamiltonian [Eq. (4)] are specified by two quantum numbers, $\kappa=(2n+1)/2$, where n is an integer, and the texture quantum number $\tau=\uparrow, \downarrow$, which takes on two discrete values. The Dresselhaus interaction eigenstates Ψ^d are

$$\Psi_{\kappa\uparrow}^d = e^{i\kappa\phi} \begin{pmatrix} \cos \frac{\theta^d(\kappa)}{2} e^{-(i/2)(\phi+\pi/2)} \\ \sin \frac{\theta^d(\kappa)}{2} e^{(i/2)(\phi+\pi/2)} \end{pmatrix}, \quad (5)$$

$$\Psi_{\kappa\downarrow}^d = e^{i\kappa\phi} \begin{pmatrix} -\sin \frac{\theta^d(\kappa)}{2} e^{-(i/2)(\phi+\pi/2)} \\ \cos \frac{\theta^d(\kappa)}{2} e^{(i/2)(\phi+\pi/2)} \end{pmatrix}, \quad (6)$$

where the texture angle $\theta^d(\kappa)$ is

$$\theta^d(\kappa) = \tan^{-1} \left\{ \frac{2m_{\text{hh}}\beta}{R_3^{2/3}} \left[\frac{2}{3}R_0 + \left(\kappa^2 - \frac{5}{4} \right) R_3 \right] \right\}. \quad (7)$$

The states represent a hole that orbits the ring with angular-momentum κ and well-defined spin texture. At the point on the ring with the angle ϕ , the spin-state $\langle \phi = \phi_0 | \Psi_{\kappa\uparrow}^d \rangle$ corresponds to the spin that is tilted by the angle $\theta^d(\kappa)$ from the normal to the plane of the ring, and the azimuthal angle is $\Phi = \phi_0 + \pi/2$ so that the projection of the spin to the plane of the ring is always tangential to the ring (see Fig. 1). The spin state associated with the other texture, $\langle \phi = \phi_0 | \Psi_{\kappa\downarrow}^d \rangle$, corresponds to the spin with the tilt angle $\pi - \theta^d$, and the same azimuthal angle. The crucial difference with respect to the

eigenstates of the ring with linear spin-orbit coupling is that the texture of the state depends on the momentum quantum number κ even in the absence of magnetic fields. Therefore, the states of different momentum show different spin textures.

Energies depend on both momentum and the texture,

$$E_{\kappa,\uparrow(\downarrow)}^d = \frac{1}{2m_{\text{hh}}R_3^{2/3}} \left(\kappa^2 + \frac{1}{4} \pm \frac{\kappa}{\cos \theta^d(\kappa)} \right). \quad (8)$$

The pairs of eigenstates ($\Psi_{\kappa,\uparrow}, \Psi_{-\kappa,\downarrow}$) form Kramers doublets, $E_{\kappa,\uparrow}^d = E_{-\kappa,\downarrow}^d$.

B. Rashba ($\beta=0$) case

When the spin-orbit coupling is of the Rashba type, the momentum $\kappa=(2n+1)/2$ for integer n is still a good quantum number, and there are still two textures, $\tau=\uparrow$ and $\tau=\downarrow$ for every value of κ . The eigenstates Ψ^r are

$$\Psi_{\kappa,\uparrow}^r = e^{i\kappa\phi} \begin{pmatrix} \cos \frac{\theta^r(\kappa)}{2} e^{-3i/2\phi} \\ \sin \frac{\theta^r(\kappa)}{2} e^{3i/2\phi} \end{pmatrix}, \quad (9)$$

$$\Psi_{\kappa,\downarrow}^r = e^{i\kappa\phi} \begin{pmatrix} -\sin \frac{\theta^r(\kappa)}{2} e^{-3i/2\phi} \\ \cos \frac{\theta^r(\kappa)}{2} e^{3i/2\phi} \end{pmatrix}, \quad (10)$$

with the Rashba texture angle $\theta^r(\kappa)$

$$\theta^r(\kappa) = \tan^{-1} \left\{ \frac{2m_{\text{hh}}\alpha}{R_3^{2/3}} \left[\frac{2}{3}R_0 + \left(\frac{13}{12} - \frac{1}{3}\kappa^2 \right) R_3 \right] \right\}. \quad (11)$$

As for the Dresselhaus case, the eigenstates represent a hole with well-defined pseudospin texture that orbits the ring. The texture is however quite different. The pseudospin $\langle \phi = \phi_0 | \Psi_{\kappa,\uparrow}^r \rangle$ is tilted away from the normal to the ring plane by the angle $\theta^r(\kappa)$ that, in contrast to the Dresselhaus case, can vary in the full range $\theta^r \in [0, \pi]$, while the Dresselhaus spin-orbit coupling allows only for $\theta^d \in [0, \pi/2]$, except for $\kappa = 1/2$ and unrealistically large R_3 . The pseudospin projection to the plane of the ring, that was always tangential in the Dresselhaus case, now makes three full rotations on each orbit (see Fig. 2). The pseudospin of the opposite texture $\langle \phi = \phi_0 | \Psi_{\kappa,\downarrow}^r \rangle$ has the tilt angle $\theta = \pi - \theta^r(\kappa)$, and the same projection to the ring plane.

Energies in the Rashba case again depend on the momentum and texture

$$E_{\kappa,\uparrow(\downarrow)}^r = \frac{1}{2m_{\text{hh}}R_3^{2/3}} \left(\kappa^2 + \frac{9}{4} \pm \frac{\kappa}{\cos \theta^r(\kappa)} \right). \quad (12)$$

The time-reversal symmetry imposes Kramers degeneracy, and the states in the Kramers doublet ($\Psi_{\kappa,\uparrow}^r, \Psi_{-\kappa,\downarrow}^r$) have the same energy $E_{\kappa,\uparrow}^r = E_{-\kappa,\downarrow}^r$.

C. Magnetic field

Our preceding calculation of the eigenstates and eigenenergies did not take into account the interaction of holes with

the magnetic field \mathbf{B} . In this subsection, we will find the spectrum and the eigenstates of a heavy hole in the presence of a magnetic field normal to the ring. This calculation includes the change in the quantization condition for the orbital momentum κ and the Zeeman term H_Z , but neglects the modification of the lowest energy radial wave function due to the magnetic confinement. This approximation neglects the modification of the radial confinement, described by R_1 and R_3 in Eq. (4) due to magnetic field. This approximation is valid for weak magnetic fields $r_c \gg a$ that give the cyclotron radius r_c much larger than the ring-radius a , as well as for the magnetic fields of arbitrary strength confined to the interior of the ring.

The requirement that the wave function of an orbiting hole is single valued, $\langle \phi = 2\pi | \Psi_{\kappa\tau} \rangle = \langle \phi = 0 | \Psi_{\kappa\tau} \rangle$ gives the quantization-condition $\kappa = (2n+1)/2$, for integer n . In the absence of Zeeman coupling, the complete spectrum of the ring is periodic in the flux with the period Φ_0 . This perfect periodicity of the spectrum is broken by the Zeeman interaction.

For the magnetic field in z direction, normal to the plane of the ring, it is possible to account exactly for the effects of Zeeman term $H_Z = bS_z$, where $b = g_{zz}\mu_B B$ is the magnetic field in with absorbed Bohr magneton μ_B and the gyromagnetic tensor component g_{zz} . For 2DHG the g tensor is highly anisotropic, and to a good approximation the only nonzero component is g_{zz} . Therefore, this approximation is valid also for the magnetic fields with in-plane components, with the adjustment that $\mathbf{B} \rightarrow (\mathbf{B} \cdot \mathbf{e}_z)\mathbf{e}_z$, since only the z component impacts both the Aharonov-Bohm flux and the Zeeman term.

The Zeeman interaction couples the states of the same orbital momentum κ and opposite textures. The energies and eigenstates in the presence of Zeeman interaction are $(|\kappa,\uparrow\rangle, |\kappa,\downarrow\rangle) \rightarrow (|\kappa+\rangle, |\kappa-\rangle)$ and $(E_{\kappa,\uparrow}, E_{\kappa,\downarrow}) \rightarrow (E_{\kappa,+}, E_{\kappa,-})$, where

$$E_{\kappa,\pm} = \frac{1}{2}(E_{\kappa,\uparrow} + E_{\kappa,\downarrow}) \pm \sqrt{\frac{1}{4}\delta(\kappa)^2 + b^2 + b \cos \theta(\kappa)\delta(\kappa)}. \quad (13)$$

The eigenstates in the presence of Zeeman interaction keep the κ quantum numbers, but the states of opposite textures get mixed

$$\begin{pmatrix} |\kappa+\rangle \\ |\kappa-\rangle \end{pmatrix} = \begin{pmatrix} \cos \frac{\Theta(\kappa)}{2} & -\sin \frac{\Theta(\kappa)}{2} \\ -\sin \frac{\Theta(\kappa)}{2} & \cos \frac{\Theta(\kappa)}{2} \end{pmatrix} \begin{pmatrix} |\kappa,\uparrow\rangle \\ |\kappa,\downarrow\rangle \end{pmatrix}, \quad (14)$$

where the mixing angle $\Theta(\kappa)$ is

$$\Theta(\kappa) = \arccos \frac{\frac{1}{2}\delta(\kappa) + b \cos \theta(\kappa)}{\sqrt{\frac{1}{4}\delta(\kappa)^2 + b^2 + b \cos \theta(\kappa)\delta(\kappa)}}. \quad (15)$$

Here $\delta(\kappa) = E_{\kappa,\uparrow} - E_{\kappa,\downarrow}$ is the energy difference of the two states with momentum κ and opposite textures.

IV. TUNNELING MODEL OF CONDUCTION

We consider a system of heavy holes confined to a ring-shaped geometry and contacted by a pair of leads (Fig. 3).

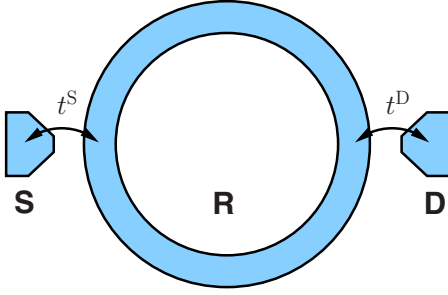


FIG. 3. (Color online) Geometry of the ring of heavy holes coupled to a pair of leads. The heavy holes in the ring (R) experience the spin-orbit coupling. Due to this coupling, the eigenstates of holes confined to the ring have a spin texture. The ring is coupled to the source (S) and drain (D) electrodes via tunneling of holes. The tunneling is assumed to conserve the hole spin.

The lead density of states is assumed to be wide and flat. In order to elucidate the pseudospin structure of the leads, we allow for an arbitrary pseudospin density-matrix $\rho^{S(D)}$ in the source(drain) lead.

The spin textures revealed in the eigenstates of heavy holes confined to a ring influence the transport properties when the ring is coupled to electrodes. For example, the hole of a given pseudospin entering the ring from the source electrode can propagate via different $\Psi_{\kappa\tau}$ eigenstates, and arrive at the drain electrode with different pseudospin orientations. The pseudospin states at the drain electrode will interfere, and the probability of transmission will depend on the pseudospin orientations. Since the pseudospin orientations at the drain electrode depend on the hole-momentum κ through the texture of the state $\Psi_{\kappa\tau}$ we may expect that the transmission of the ring, and therefore the resulting conductance will also depend on the momentum of the incoming hole. This momentum dependence is absent in the electronic systems where the texture is determined solely by the spin-orbit coupling constant.²⁸ Therefore, we expect new effects of spin interference in transport of carriers that are subject to the cubic spin-orbit coupling.

The interference of heavy holes will be observable if their coherence length λ_{coh} is longer than the ring circumference λ_{ring} . At the same time, the spin-orbit length λ_{SO} that a hole must transverse in the ring in order to experience an appreciable pseudospin rotation must be at least comparable to λ_{ring} . The resulting set of constraints $\lambda_{\text{coh}} \gg \lambda_{\text{ring}} \sim \lambda_{\text{SO}}$ can be achieved in the heavy-hole structures based on carbon-doped GaAs.^{15,25}

In order to find the transmission through the ring, we introduce a tunneling Hamiltonian model for the ring coupled to source and drain electrodes. The tunneling Hamiltonian description is valid when the overlap of the electrode states and the ring states is small, $|\phi_{k\sigma}(\mathbf{x})\Psi_{\kappa\tau}(\mathbf{x})| \ll 1$ for every point \mathbf{x} within the system, and every pair of states $(\kappa\tau, k\sigma)$.

The tunneling between either electrode and the ring occurs on the length-scale λ_{tun} that is much shorter than the spin-orbit length, $\lambda_{\text{tun}} \ll \lambda_{\text{SO}}$. Therefore, unless there are magnetic impurities in the boundary region between the ring and the leads, the tunneling will preserve the true hole spin, re-

sulting in the hole pseudospin conservation in tunneling, and the pseudospin independence of the tunneling amplitudes.

The tunneling Hamiltonian reads

$$H_T = H_S + H_D + H_R + H_T, \quad (16)$$

where the three noninteracting Hamiltonians

$$H_S = \sum_{k\sigma} \epsilon_{k\sigma}^S s_{k\sigma}^\dagger s_{k\sigma}, \quad (17)$$

$$H_D = \sum_{k\sigma} \epsilon_{k\sigma}^D d_{k\sigma}^\dagger d_{k\sigma}, \quad (18)$$

$$H_R = \sum_{\kappa\tau} \epsilon_{\kappa\tau} r_{\kappa\tau}^\dagger r_{\kappa\tau}, \quad (19)$$

describe decoupled source electrode, drain electrode, and the ring. The operators $s_{k\sigma}$ ($d_{k\sigma}$) annihilate a hole of momentum k and pseudospin $\sigma = \uparrow, \downarrow$ in the source(drain) electrode, while the operators $r_{\kappa\tau}$ and $\tau = \uparrow, \downarrow$ annihilate a hole in the ring state $\Psi_{\kappa\tau}$. The ring energies $\epsilon_{\kappa\tau}$ are given by Eqs. (8) and (12). The tunneling term H_T describes processes when a hole hops from an electrode to the ring and back,

$$H_{\text{tun}} = \sum_{k\sigma, \kappa\tau} (t_{k\sigma, \kappa\tau}^S s_{k\sigma}^\dagger r_{\kappa\tau} + t_{k\sigma, \kappa\tau}^D d_{k\sigma}^\dagger r_{\kappa\tau} + \text{H.c.}). \quad (20)$$

The tunneling matrix elements, $t_{k\sigma, \kappa\tau}^{S(D)}$ are determined by the details of the potential barrier between the electrodes and the ring. We are interested in the consequences of nontrivial spin textures in the transport of holes through a ring. The potential barrier is due to electric fields, and its influence on the spin and the hole pseudospin can come only from the spin-orbit coupling. Here we assume that the holes of arbitrary pseudospin see the same potential. This assumption is valid for a potential which is nonzero only in a tunneling region of the linear dimension much smaller than the spin-orbit length.

Under these assumptions, we can model the tunneling matrix elements as

$$t_{k\sigma, \kappa\tau}^{S(D)} = t_{k, \kappa}^{S(D)} \langle k\sigma | S(D) | \phi_{S(D)} \rangle \langle \phi_{S(D)} | \kappa\tau \rangle, \quad (21)$$

where the spin- and texture-independent matrix elements $t_{k, \kappa}^{S(D)}$ describe the tunneling in the absence of spin-orbit coupling, and the spin- and texture-dependent factor is proportional to the overlap of the spin and texture part of the wave function at the position $\phi_{S(D)}$ of the source (drain) junction.

The resulting tunneling Hamiltonian H_{tun} is a generalization of the Fano-Anderson model²⁹ to the many isolated levels in a continuum with different couplings to the continuum states in the leads. Since the tunneling term H_T in Eq. (20) is bilinear in the operators that describe the uncoupled system, it is in principle exactly solvable. However, the exact solution for the eigenstates is simple and transparent only in the case of a single level.^{18,30} The exact solution requires inversion of an $N \times N$ matrix, where N is the number of relevant ring states. Instead of solving for the eigenstates, we calculate the current through the ring using the Keldysh technique.³¹

The current through a region coupled to the leads via a tunneling Hamiltonian was considered by Meir and Win-

green in Ref. 32. Quite generally, the current is

$$I = \frac{e}{h} \int d\epsilon [f_S(\epsilon) - f_D(\epsilon)] \text{Tr}[\mathbf{G}^A \mathbf{\Gamma}^D \mathbf{G}^R \mathbf{\Gamma}^S(\epsilon)], \quad (22)$$

where $f_{S(D)}$ are Fermi distribution functions in the source and drain electrodes, $\mathbf{G}^{R(A)}$ are retarded (advanced) Green functions of the ring coupled to the leads, and $\mathbf{\Gamma}^{S(D)}$ are the escape rates of the ring states to the source (drain) electrode. The trace is taken over the ring states $\kappa\tau$. At zero-temperature $T=0$, the differential conductance $g(\epsilon)$ for the carriers of energy ϵ can be directly read off from Eq. (22) (for finite temperature T , see below) as $g(\epsilon) = \text{Tr}[\mathbf{G}^A \mathbf{\Gamma}^D \mathbf{G}^R \mathbf{\Gamma}^S(\epsilon)]$.

The Green functions in frequency space $\mathbf{G}^{R(A)}(\omega)$ are expressed in terms of the self-energy as

$$\mathbf{G}^{R(A)}(\omega) = \frac{1}{[\mathbf{g}^{R(A)}(\omega)]^{-1} - \Sigma^{R(A)}(\omega)}. \quad (23)$$

Here, $\mathbf{g}^{R(A)}$ is the retarded(advanced) Green function of the ring. In our noninteracting case, the self-energy $\Sigma^{R(A)}$ is given exactly as a sum of contributions coming from the excursion of the hole through the electrodes,

$$\Sigma_{\kappa_1\tau_1, \kappa_2\tau_2}^{R(A)}(\omega) = \sum_{k\sigma, L} (t_{k\sigma, \kappa_1\tau_1}^L)^* g_{k\sigma}^{LR(A)}(\omega) t_{k\sigma, \kappa_2\tau_2}^L, \quad (24)$$

where $g_{k\sigma}^{LR(A)}(\omega)$ are retarded (advanced) Green functions of decoupled leads, being diagonal in $k\sigma$.

The escape rates $\mathbf{\Gamma}^{S/D}$ describe the processes in which a hole escapes from the ring into a lead and gets replaced by another hole. They are defined as

$$\mathbf{\Gamma}_{\kappa_1\tau_1, \kappa_2\tau_2}^{S/D}(\omega) = 2\pi \sum_{k\sigma} t_{k\sigma, \kappa_1\tau_1}^{S/D} (t_{k\sigma, \kappa_2\tau_2}^{S/D})^* \delta(\omega - \epsilon_{k\sigma}^{S/D}). \quad (25)$$

The current through the ring is determined by Eqs. (22)–(25), once we incorporate the tunneling matrix elements Eq. (21). The current will depend on the pseudospin states in the leads. The effects of the texture in the ring eigenstates will be visible in the conductance if the states in the ring are polarized. We thus consider general pseudospin-density matrices in the source (drain) electrode

$$\rho^{S(D)} = \frac{1}{2}(1 + \mathbf{P}^{S(D)} \cdot \boldsymbol{\sigma}), \quad (26)$$

where the direction of $\mathbf{P}^{S(D)}$, defines the axis of partial polarization $|\mathbf{P}^{S(D)}| \leq 1$ in the source(drain) lead.

We proceed by calculating the current using Eq. (22), with the spin-dependent density of states in the escape rates [Eq. (25)], and assuming that the bands in the leads are wide and flat. Our calculation is numerical and includes a finite number (184) of states in the ring. This approach produces results that do not change in the range of low values of ω with the addition of new levels. Another reason for truncating the number of levels is the fact that the dispersion relations for heavy holes in the ring Eqs. (8) and (12) predict unphysical states that are bound to the ring by strong spin-orbit coupling.

V. DIFFERENTIAL CONDUCTANCE OF A HEAVY-HOLE RING

In this section, we discuss the influence of nontrivial pseudospin textures in the eigenstates of the heavy-hole ring to its conductance. In the tunneling picture, we can distinguish two basic sources of the varying conductance. One source is the discrete spectrum of the ring that in the limit of weak tunneling produces a series of peaks in the conductance when the chemical potential of the leads aligns with the discrete energy levels of the ring. As we increase the tunneling matrix elements the levels broaden due to the coupling to the leads, and eventually begin to overlap. Interference of the transitions from the source lead to the drain lead via ring eigenstates is the second source of variations in the conductance.

We illustrate the interplay of these two mechanisms that modify conductance by studying pseudospin-resolved current in the ring. Then, we study the polarization-resolved conductance and show the qualitative differences between Dresselhaus- and Rashba-coupled holes, which allow for the determination of the dominant type of coupling.

Magnetic flux threaded through the ring causes Aharonov-Bohm oscillations in the conductance that are further modified by the pseudospin textures. The standard technique for observing these oscillations is by looking for the peaks in the Fourier transform of the conductance as a function of magnetic field that correspond to the period of one flux quantum. We show that the structure of Aharonov-Bohm oscillations in direct space, i.e., before the Fourier transform, offers a signature of the cubic spin-orbit coupling in the form of easily recognizable four-peak structure in the oscillations. We trace the emergence of this split-peak structure to dependence of the energy spectrum of an orbiting hole on the flux through the ring, and show that the form of the periodic conductance is drastically different between the cubic and linear spin-orbit coupling.

The possibility of experimental observation of the pseudospin-resolved conductance is determined by the widths of the ring energy levels compared to their splitting. In our system, the levels broaden due to tunneling. In experiment, an additional thermal broadening will further smear the conductance peaks. We study the disappearance of pseudospin-split conductance with temperature, and suggest the regime favorable for resolving the pseudospin components.

In this section, the energy is measured in units of E_R , the energy of $\kappa=1$ orbital state in a ring without spin-orbit coupling, $E_R = \hbar^2 / 2m_{\text{hh}} R_3^{-2/3}$. For a typical ring of radius $R_3^{-2/3} \sim 0.5 \mu\text{m}$, $E_R \approx 1 \mu\text{eV}$.

A. Level broadening and interference

The dependence of conductivity on the tunnel coupling strength and carrier energy is illustrated in Fig. 4 which shows the conductance between unpolarized leads. In the limit of zero tunneling, $|t| \rightarrow 0$, the peaks in the conductance appear at the energies of an isolated ring. As the tunneling is increased, the levels become broader, due to the tunneling of holes between the ring and the lead. Our calculation includes

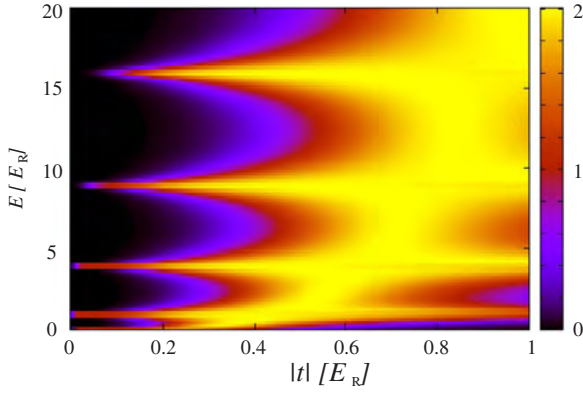


FIG. 4. (Color online) Tunneling dependence of differential conductance between unpolarized leads with Dresselhaus spin-orbit coupling ($\alpha=0, \beta=0.3$) in the leads. The differential conductance $g(\epsilon)$ in units of the conductance quantum $G_0=h/e$ is plotted as a function of the absolute value of the tunneling matrix element between the states of uncoupled leads of the ring, and the chemical potential of the leads. At small tunneling, the conductance shows peaks when the chemical potential of the ring aligns with the energy levels of the ring. As the tunneling grows, the peaks become wider and begin to overlap.

contributions of an arbitrary number of such “excursions.” The calculation is done at zero temperature (for the thermal broadening see below). With strong enough tunneling, the broadening of the ring levels leads to their overlap. The resulting conductance in the overlapping region is not a simple sum of the conductances of pseudospin components. Since the tunneling involves many ring levels in a coherent way, the resulting conductance shows a signature of interference. In Fig. 5, we show the interference term at a fixed tunneling strength. The conductance g^{+0} between the pseudospin-

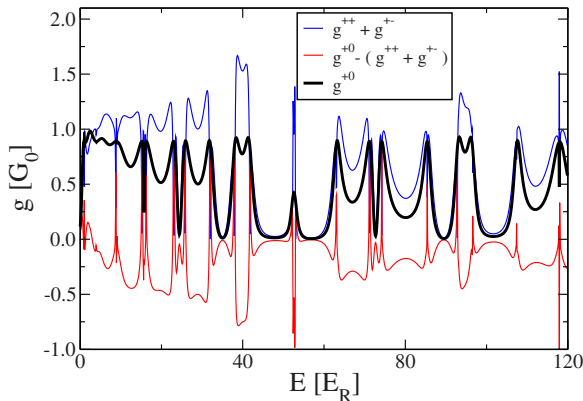


FIG. 5. (Color online) When the broadening of the ring levels is strong enough to produce the overlap of the energy levels, the tunneling processes through various states in the ring interfere. Pseudospin textures affect this tunneling. The conductance g^{+0} between the pseudospin-polarized source lead and the unpolarized drain lead (thick black line) is not equal to the sum of conductances $g^{++} + g^{+-}$ between the polarized source and drain leads with parallel polarizations g^{++} and the conductance between polarized source and drain lead with the antiparallel polarization g^{+-} [thin dark (blue) line]. The difference $g^{+0} - (g^{++} + g^{+-})$ is the contribution of the interference term [thin bright (red)] line.

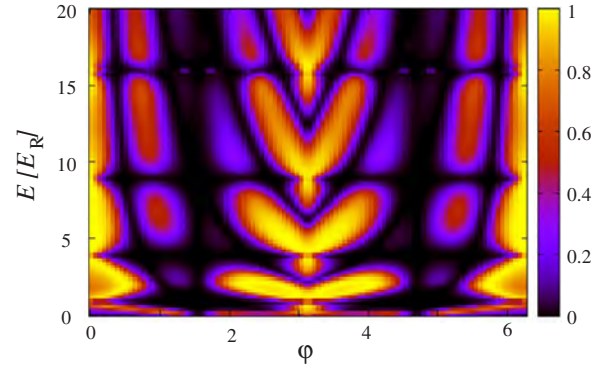


FIG. 6. (Color online) Conductance between the completely in-plane polarized source and drain leads for Dresselhaus ($\alpha=0, \beta=0.3$) spin-orbit coupled holes. The position of the source lead is $\phi_S=0$, while the position of the drain lead ϕ_D varies between 0 and 2π . For each drain position, the differential conductance is plotted as a function of the ring Fermi energy. The radial structure of the pseudospin textures is seen in the traces of conductance at a fixed energy.

polarized source lead and the unpolarized drain lead (thick black line) is not equal to the sum of conductances $g^{++} + g^{+-}$ between the polarized source and drain leads with parallel polarizations g^{++} and the conductance between polarized source and drain lead with the antiparallel polarization g^{+-} (thin dark blue line). The difference $g^{+0} - (g^{++} + g^{+-})$ is the contribution of the interference term (thin bright red) line.

B. In-plane spin textures

The conductance between the leads polarized in the direction normal to the plane of the ring does not show the full difference between the Dresselhaus- and Rashba-coupling induced textures. Namely, the most striking difference between the two textures is in the projection of the pseudospin to the plane of the ring, see Figs. 1 and 2, which is qualitatively different for the two forms of the cubic spin-orbit coupling. The in-plane component of the Dresselhaus-only eigenstate winds once around the z axis as the ring is transversed, and always stays tangential to the ring. The in-plane component of the Rashba state, on the other hand, winds three times as the ring is transversed.

The winding of in-plane polarization is the same for all the states in the ring and leaves a signature in the conductance. We calculate the conductance between the fully polarized leads with the polarization vector \mathbf{P} in the plane of the ring, and with the varying position of the drain lead along the ring, Figs. 6 and 7. We note that the conductance patterns in the Rashba case show more islands of conductivity at a fixed carrier energy as the position of the drain lead is encircling the ring. The reason for the additional islands is that the lead pseudospin aligns with the in-plane projection of the pseudospin of ring eigenstates at the position of the junction. Aligned pseudospins increase the conductivity and create the islands. The in-plane projection of the Dresselhaus eigenstate pseudospin texture aligns with lead polarization for one junc-

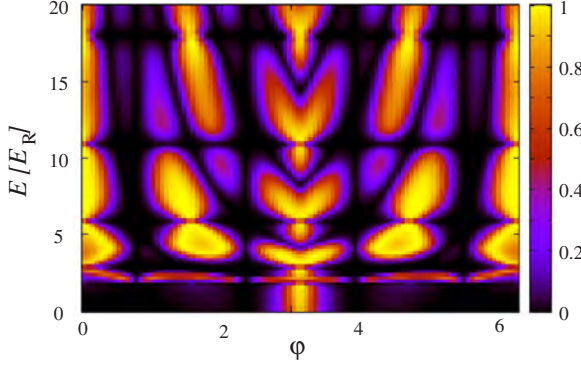


FIG. 7. (Color online) Conductance between the completely in-plane polarized source and drain leads for Rashba ($\alpha=0.3, \beta=0$) spin-orbit coupled holes. The position of the source lead is $\phi_S=0$, while the position of the drain lead ϕ_D varies between 0 and 2π . For each drain position, the differential conductance is plotted as a function of the ring Fermi energy. Compare with the case of Dresselhaus spin-orbit coupling.

tion position, while this alignment occurs for three positions in the case of Rashba coupling.

C. Modified Aharonov-Bohm oscillations

Conductance measurements between the polarized leads and with the control over the chemical potential of the ring are difficult to achieve. Typical experiments measure the conductance as a function of the magnetic field that threads a magnetic flux through the ring and introduces the Zeeman coupling. In our model of tunneling conductance the Aharonov-Bohm phase can be incorporated in the boundary conditions for the ring wave function, using the singular gauge. This leads to a quantization condition for $\kappa - \Phi/\Phi_0$, where Φ is the flux threaded through the ring, and Φ_0 is the flux quantum. The effect of the flux is thus the shift of all the κ quantum numbers. As a consequence, the energy levels and the pseudospin textures change. The new texture angles $\theta^{d/r}$ and the new energies $E_{\kappa, \tau}$ are still given by Eqs. (8), (7), (12), and (11), but with the shifted values of the orbital quantum number $\kappa \rightarrow \kappa + \Phi/\Phi_0$.

The gross features of the Aharonov-Bohm oscillations can be understood in terms of a simplified picture based on interference of levels that lie close in energy. The spectra of the ring in zero magnetic field, and in the presence of weak spin-orbit coupling consists of pairs of closely spaced Kramers doublets ($\Psi_{\kappa, \uparrow}, \Psi_{-\kappa, \downarrow}$) and ($\Psi_{\kappa+1, \downarrow}, \Psi_{-\kappa-1, \uparrow}$). The gap between these doublets scales as $\beta^2(\alpha^2)$ for weak Dresselhaus (Rashba) spin-orbit coupling, while all the other states are separated by larger gaps that originate from the kinetic-energy terms and persist in the absence of spin-orbit coupling. Therefore, we can approximately describe the conductance by transition amplitudes

$$T = \begin{pmatrix} T^{+,+} & T^{+,-} \\ T^{-,+} & T^{-,-} \end{pmatrix}, \quad (27)$$

where the matrix element $T^{s_1 s_2}$ stands for the amplitude for a hole of pseudospin $\pm 1/2$ for $s_1 = \pm$ in the source lead to

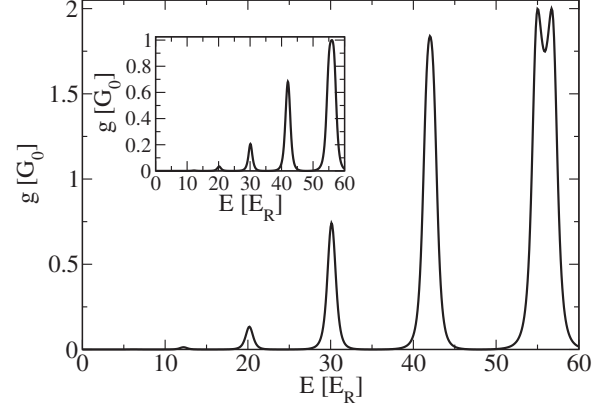


FIG. 8. Conductance of the ring threaded by a half of flux quantum. Leads are unpolarized. Note that the conductance is not zero due to tunneling through off-resonant states. The inset shows the conductance of the same ring with the same flux, but between polarized leads. The peak at $\epsilon_F \approx 55E_R$ shows that the split peak in the main plot is due to the conductance of the holes of different polarizations.

tunnel into the drain lead with the pseudospin $\pm 1/2$ for $s_2 = \pm$. Taking into account only the tunneling through the four closely spaced levels and in the absence of the flux through the ring, the transition amplitudes are

$$T_0 = 2 \sin(\kappa\pi) \cos\left(\frac{d_0}{2}\right) \begin{pmatrix} \cos\frac{s_0}{2} & i \sin\frac{s_0}{2} \\ i \sin\frac{s_0}{2} & \cos\frac{s_0}{2} \end{pmatrix}, \quad (28)$$

where $s_0 = \theta^{d/r}(\kappa) + \theta^{d/r}(\kappa+1)$ and $d_0 = \theta^{d/r}(\kappa) - \theta^{d/r}(\kappa+1)$ are the sum and the difference of the texture angles of the involved states. Similar considerations for the case of a ring threaded by the magnetic-flux $\Phi = \Phi_0/2$ equal to half the flux quantum gives

$$T_{1/2} = 2 \cos(\kappa\pi) \cos\left(\frac{d_{1/2}}{2}\right) \begin{pmatrix} \cos\frac{s_{1/2}}{2} & i \sin\frac{s_{1/2}}{2} \\ i \sin\frac{s_{1/2}}{2} & \cos\frac{s_{1/2}}{2} \end{pmatrix}, \quad (29)$$

where the relevant sums are now $s_{1/2} = \theta^{d/r}(\kappa+1/2) + \theta^{d/r}(\kappa+3/2)$ and $d_{1/2} = \theta^{d/r}(\kappa+1/2) - \theta^{d/r}(\kappa+3/2)$. The quantum number κ is a half of an odd integer and $T_{1/2} = 0$. Therefore, this simplified description correctly predicts the minima in conductance when half a flux quantum threads the ring. The conductance value is zero in this simple model, but it turns out to be nonzero when the additional levels are included in the more detailed model. When the additional levels in the ring are included, the conductance can be nonzero in the ring threaded by half of flux quantum; see Fig. 8. The currents transmitted through the ring carry hole polarization, as can be seen from the figures. The peak in the unpolarized conductance near the energy $\epsilon = 54E_R$ is split, while the polarized conductance shows a single peak of roughly half the height. The components of the split peak correspond to pseudospin components with high polarization up and down, described

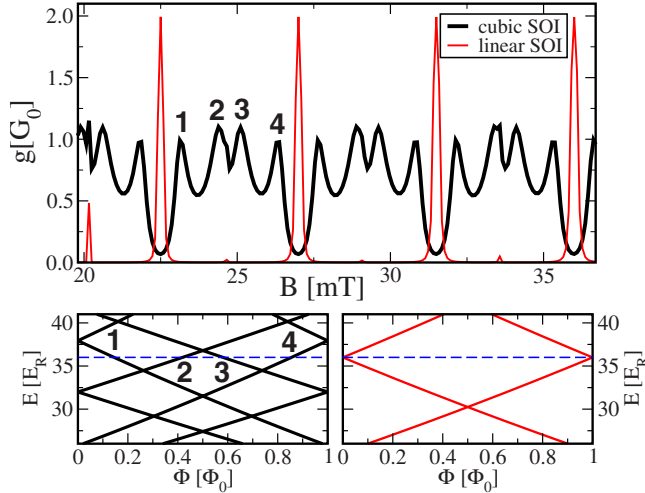


FIG. 9. (Color online) Aharonov-Bohm oscillations for different types of spin-orbit coupling. (a) The conductance of the ring as a function of the magnetic field shows oscillations with the period that corresponds to a flux quantum threading the ring for both linear [(red) light] and cubic [(black) dark] spin-orbit coupling, but with markedly different conductance within a period. (b) and (c) The four-peak structure [labels 1–4 in (a)] for the cubic spin-orbit interaction, and the single-peak structure for the linear spin-orbit coupling can be traced to the magnetic fields at which an energy level in the ring aligns with the leads [labels 1–4 in (b)]. Calculations for both plots are done for the lead chemical potential of $36E_R \approx 36 \mu\text{eV}$, close to an energy level of an isolated ring in the absence of spin-orbit coupling, Dresselhaus cubic spin-orbit coupling ($\beta=0.3$), and the linear spin-orbit coupling model is derived from the cubic one by setting $R_3=0$.

by pseudospin density matrices [Eq. (26)] with $\mathbf{P} \approx \mathbf{e}_z$ and $\mathbf{P} \approx -\mathbf{e}_z$. This splitting is a clear signature of pseudospin-dependent transport.

The standard setup for a study of conductance oscillations as a function of the magnetic field consists of measuring the conductance at a fixed lead chemical potential and sweeping the external magnetic field. The conductance then typically reveals the oscillations with the period $T_{AB} = S\Phi_0^{-1}$, with S being the ring surface area and Φ_0 the flux quantum. The spin-orbit coupling was found to modify these oscillations.¹⁵ In our model the conductance is modified due to the presence of four closely spaced energy levels that correspond to each peak in the conductance. At zero flux these four levels are the Kramers doublets ($\Psi_{\kappa,\uparrow}, \Psi_{-\kappa,\downarrow}$) and ($\Psi_{\kappa+1,\downarrow}, \Psi_{-(\kappa+1),\uparrow}$). The splitting between these pairs in the absence of magnetic field is of second order in spin-orbit coupling. As the magnetic flux is threaded through the ring the quartet of levels splits, with two of the levels with $\kappa > 0$ gaining energy, and the levels with $\kappa < 0$ losing it. In addition the Zeeman coupling splits these levels further. This behavior is in sharp contrast to the linear spin-orbit coupling case where there are at most two states of any given energy.

The four-peak structure within the maximum of conductance in Aharonov-Bohm oscillations represents a signature of the cubic spin-orbit coupling (see Fig. 9). The period of oscillations is equal for both types of coupling, but the shape of the peaks is drastically different. The four-peak structure

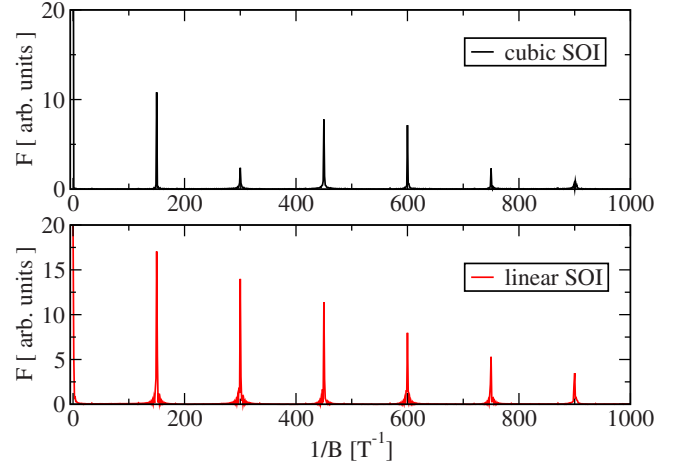


FIG. 10. (Color online) Fourier spectra of the ring conductance as function of the magnetic field. The upper panel [(black) dark] shows the conductance spectrum of the ring with cubic spin-orbit coupling, and the lower panel [(red) light] shows the conductance spectrum of the ring with linear spin-orbit coupling. The ring radius is set to $R_3^{-3/2} = 0.5 \mu\text{m}$, and the lead chemical potential is $36E_R$. The structure of base frequency and the higher harmonics is the consequence of the Aharonov-Bohm oscillations. The two cases can be distinguished by the relative size of the harmonics.

is most visible when the leads are tuned into the vicinity of a ring energy level. At these energies, in contrast, the linear spin-orbit coupling produces a single-peak structure.

Fourier spectra of conductance fluctuations were reported to show the signature of spin-orbit coupling in the diffusive regime, seen in the splitting of peaks in the Fourier spectrum.^{15,16} We have compared the Fourier spectra of our results in the case of linear and cubic form of spin-orbit coupling (Fig. 10). In our tunneling model, the Fourier spectra of the ring with linear spin-orbit coupling differs from the spectra of the ring with the cubic spin-orbit coupling in the relative size of the base and higher harmonic. The shape of the peaks in Fourier spectrum does not show significant differences. Therefore, the signature of the cubic spin-orbit coupling is clearly visible in the direct-space Aharonov-Bohm oscillations, and very hard to discern in the Fourier transform.

D. Thermal broadening

The split peaks in differential conductance as function of lead chemical potential will be visible if the distance between the peaks is larger than their width. As an illustration of the effects of temperature $T > 0$, we will investigate the broadening of pseudospin-resolved peak at half-flux quantum $\Phi = \Phi_0/2$ (Fig. 11). For the parameters we used, the splitting of the peaks is $\sim 3 \mu\text{eV} \approx 30 \text{ mK}$, and requires low temperatures to resolve. The broadening that impairs resolving of the split peaks has a temperature-independent contribution due to tunneling to the leads, and it is further increased due to the temperature. We study the thermal broadening of the conductivity using Eq. (22), and finding the conductance g at finite temperatures. We find that the conductance is in-

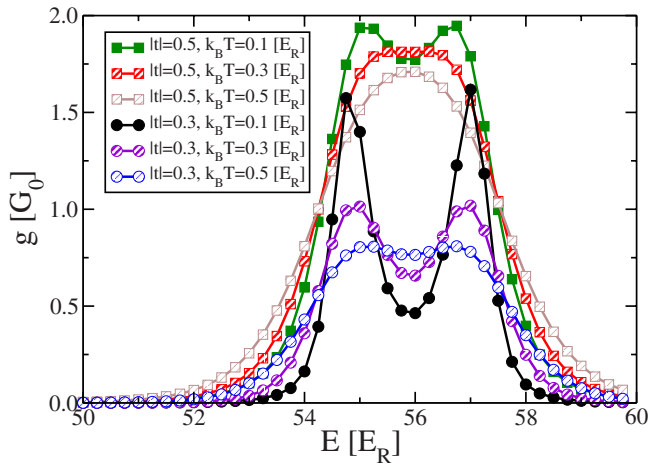


FIG. 11. (Color online) Thermal broadening of differential conductance g . Components of the split peak in the differential conductance (inset in Fig. 8) merge into a single peak as the temperature is raised. The squares represent the conductance of the ring with stronger tunneling between the leads and the ring, $|t|=0.5E_R$, while the circles represent the conductivity for weaker tunneling $|t|=0.3E_R$. Weaker tunnel coupling allows the splitting to be resolved at higher temperatures.

deed broadened at finite temperatures (Fig. 11). However, the visibility of the peaks and the resolution of peaks can be improved if the peaks are narrower or the splitting is larger. The peak splitting grows with the absolute value of the momentum, $|\kappa|$, and can be observed at higher temperatures if the momentum of the interfering states is larger. In summary, the favorable conditions for the observation of pseudospin-dependent conductance are weak tunneling and low temperatures. Both of these conditions aim at reducing the line width of the peaks. Another way to resolve the pseudospins is to perform an experiment with the higher chemical potential in the leads, and observe the splitting of the higher-energy peak. These peaks are further separated in energy, due to the cubic spin-orbit coupling.

VI. CONCLUSIONS

We have investigated the conductance of a mesoscopic ring of heavy holes tunnel coupled to leads. In the coherent

regime, the transport through the ring is dominated by the energy spectrum and the pseudospin texture of the orbiting hole eigenstates. Due to the cubic form of spin-orbit interaction, the pseudospin texture of the hole eigenstates is momentum dependent, as opposed, e.g., to the electrons with linear spin-orbit coupling.

The hole transport proceeds through tunneling between the source and the drain lead via various ring eigenstates, with the phase of each tunneling path modified due to the spin texture. The effects of interference between the tunneling paths are visible in the conductance when the tunnel broadening is sufficient to make the ring energy levels overlap. We have demonstrated that the dominant type of spin-orbit interaction can be deduced from the pseudospin-dependent conductance between the polarized leads.

Aharonov-Bohm oscillations appear in the tunneling approach as a consequence of the evolution the ring spectrum as the magnetic flux is threaded through the ring. Approximately periodic evolution of the peaks leads directly to the approximately periodic conductance oscillations. We have explained the four-peak shape of the Aharonov-Bohm oscillations in the direct space as a direct consequence of fourfold near degeneracy of the orbiting hole energy levels. This particular shape of Aharonov-Bohm oscillations is a signature of the cubic spin-orbit coupling, but it is not visible in the Fourier transform of the conductance.

The pseudospin splitting of the conductance peaks, caused by pseudospin textures of the ring eigenstates is clearly visible at zero temperature and low tunneling, but disappears when the combined thermal and tunnel broadening becomes comparable to the size of the splitting.

ACKNOWLEDGMENTS

We thank M. Trif, J. C. Egues, and C. Bruder for useful discussions. We acknowledge financial support from the Swiss SNF, the NCCR Nanoscience Basel, the EU under “MagMaNet” and “MolSpinQIP,” the Brain Korea 21 Project, the DFG within Grants No. SPP 1285 “Spintronics” and No. FOR 912.

¹Y. Aharonov and D. Bohm, Phys. Rev. **115**, 485 (1959).

²Y. Aharonov and A. Casher, Phys. Rev. Lett. **53**, 319 (1984).

³M. Lee and M. Y. Choi, J. Phys. A **37**, 973 (2004).

⁴M. F. Borunda, X. Liu, A. A. Kovalev, X.-J. Liu, T. Jungwirth, and J. Sinova, Phys. Rev. B **78**, 245315 (2008).

⁵T. Bergsten, T. Kobayashi, Y. Sekine, and J. Nitta, Phys. Rev. Lett. **97**, 196803 (2006).

⁶M. Pletyukhov and U. Zülicke, Phys. Rev. B **77**, 193304 (2008).

⁷C. P. Umbach, S. Washburn, R. B. Laibowitz, and R. A. Webb, Phys. Rev. B **30**, 4048 (1984).

⁸O. Entin-Wohlman, Y. Imry, and A. Aharony, Phys. Rev. Lett. **91**, 046802 (2003).

⁹D. Loss, P. Goldbart, and A. V. Balatsky, Phys. Rev. Lett. **65**,

1655 (1990).

¹⁰D. Loss and P. M. Goldbart, Phys. Rev. B **45**, 13544 (1992).

¹¹J. Nitta, F. E. Meijer, and H. Takayanagi, Appl. Phys. Lett. **75**, 695 (1999).

¹²R. Citro, F. Romeo, and M. Marinaro, Phys. Rev. B **74**, 115329 (2006).

¹³R. Citro and F. Romeo, Phys. Rev. B **75**, 073306 (2007).

¹⁴R. Citro and F. Romeo, Phys. Rev. B **77**, 193309 (2008).

¹⁵B. Grbic, R. Leturcq, T. Ihn, K. Ensslin, D. Reuter, and A. D. Wieck, Phys. Rev. Lett. **99**, 176803 (2007).

¹⁶B. Habib, E. Tutuc, and M. Shayegan, Appl. Phys. Lett. **90**, 152104 (2007).

¹⁷M. G. Pala, M. Governale, J. König, and U. Zülicke, EPL **65**,

- 850 (2004).
- ¹⁸H.-A. Engel and D. Loss, Phys. Rev. Lett. **93**, 136602 (2004).
- ¹⁹A. A. Kovalev, M. F. Borunda, T. Jungwirth, L. W. Molenkamp, and J. Sinova, Phys. Rev. B **76**, 125307 (2007).
- ²⁰S. Souma and B. K. Nikolić, Phys. Rev. B **70**, 195346 (2004).
- ²¹W. Hofstetter, J. König, and H. Schoeller, Phys. Rev. Lett. **87**, 156803 (2001).
- ²²J. König and Y. Gefen, Phys. Rev. B **65**, 045316 (2002).
- ²³P. Simon, O. Entin-Wohlman, and A. Aharony, Phys. Rev. B **72**, 245313 (2005).
- ²⁴D. Loss, H. Schoeller, and P. M. Goldbart, Phys. Rev. B **48**, 15218 (1993).
- ²⁵J.-B. Yau, E. P. De Poortere, and M. Shayegan, Phys. Rev. Lett. **88**, 146801 (2002).
- ²⁶D. V. Bulaev and D. Loss, Phys. Rev. Lett. **95**, 076805 (2005).
- ²⁷F. E. Meijer, A. F. Morpurgo, and T. M. Klapwijk, Phys. Rev. B **66**, 033107 (2002).
- ²⁸B. Molnár, F. M. Peeters, and P. Vasilopoulos, Phys. Rev. B **69**, 155335 (2004).
- ²⁹U. Fano, Phys. Rev. **124**, 1866 (1961).
- ³⁰D. Averin, J. Appl. Phys. **73**, 2593 (1993).
- ³¹H. Haug and A.-P. Jauho, *Quantum Kinetics in Transport and Optics of Semiconductors* (Springer, New York, 1996).
- ³²Y. Meir and N. S. Wingreen, Phys. Rev. Lett. **68**, 2512 (1992).

Spin electric effects in molecular antiferromagnetsMircea Trif,¹ Filippo Troiani,² Dimitrije Stepanenko,¹ and Daniel Loss¹¹*Department of Physics, University of Basel, Klingelbergstrasse 82, CH-4056 Basel, Switzerland*²*CNR-INFM National Research Center S3, Istituto Nanoscienze-CNR, via G. Campi 213/A, 41100 Modena, Italy*

(Received 24 January 2010; published 28 July 2010)

Molecular nanomagnets show clear signatures of coherent behavior and have a wide variety of effective low-energy spin Hamiltonians suitable for encoding qubits and implementing spin-based quantum information processing. At the nanoscale, the preferred mechanism for the control of a quantum systems is the application of electric fields, which are strong, can be locally applied, and rapidly switched. In this work, we provide the theoretical tools for identifying molecular nanomagnets suitable for electric control. By group-theoretical symmetry analysis we find that the spin-electric coupling in triangular molecules is governed by the modification of the exchange interaction and is possible even in the absence of spin-orbit coupling. In pentagonal molecules the spin-electric coupling can exist only in the presence of spin-orbit interaction. This kind of coupling is allowed for both $s=1/2$ and $s=3/2$ spins at the magnetic centers. Within the Hubbard model, we find a relation between the spin-electric coupling and the properties of the chemical bonds in a molecule, suggesting that the best candidates for strong spin-electric coupling are molecules with nearly degenerate bond orbitals. We also investigate the possible experimental signatures of spin-electric coupling in nuclear magnetic resonance and electron spin resonance spectroscopy, as well as in the thermodynamic measurements of magnetization, electric polarization, and specific heat of the molecules.

DOI: [10.1103/PhysRevB.82.045429](https://doi.org/10.1103/PhysRevB.82.045429)

PACS number(s): 75.50.Xx, 03.67.Lx

I. INTRODUCTION

The control of coherent quantum dynamics is a necessary prerequisite for quantum information processing. This kind of control is achieved through coupling of the internal quantum degrees of freedom of a suitable microscopic or mesoscopic system to an external classical or quantum field that can readily be manipulated on the characteristic spatial and temporal scales of the quantum system.

The molecular nanomagnets (MNs) (Refs. 1 and 2) represent a class of systems that show rich quantum behavior. At low energies, the MNs behave as a large spin or a system of only few interacting spins. The behavior of this spin system can be designed to some degree by altering the chemical structure of the molecules and ranges from a single large spin with high anisotropy barrier to small collections of ferromagnetically or antiferromagnetically coupled spins with various geometries and magnetic anisotropies. This versatility of available effective spin systems makes the MNs promising carriers of quantum information.³ While the interaction with magnetic fields provides a straightforward access to the spins in an MN, it is preferable to use electric fields for the quantum control of spins since the electric fields are easier to control on the required short spatial and temporal scales. In this work, we explore the mechanisms of spin-electric coupling and study the ways in which an MN with strong spin-electric coupling can be identified.

Quantum behavior of MNs is clearly manifested in the quantum tunneling of magnetization.^{4–11} A prototypical example of quantum tunneling of magnetization is the hysteresis loop of an MN with a large spin and high anisotropy barrier. The height of the barrier separating the degenerate states of different magnetization leads to long-lived spin configurations with nonzero magnetic moment in the absence of external fields. The transitions between magnetization states

in the MN driven through a hysteresis loop occur in tunneling events that involve coherent change in a many-spin state. These transitions have been observed as stepwise changes in magnetization in single-molecule ferromagnets.^{7,8,12–14} Similar tunneling between spin configurations are predicted in antiferromagnetic molecules,^{15,16} and the observed hysteresis was explained in terms of the photon bottleneck and Landau-Zener transitions.^{17–20} The transitions between spin states are coherent processes and show the signatures of interference between transition paths,^{21–23} as well as the effects of Berry phase in tunneling.^{21–27}

Spin systems within molecular nanomagnets offer a number of attractive features for studying the quantum coherence and for the applications in quantum information processing.³ A wide variety of spin states and couplings between them allows for encoding qubits. Chemical manipulation offers a way to modify the structure of low-energy spin states.²⁸ Coherence times of up to $\sim 3 \mu\text{s}$ (Ref. 29) which can persist up to relatively high temperatures on the order of a few kelvin are sensitive to the isotopic composition of the molecule. A universal set of quantum gates can be applied in a system of coupled antiferromagnetic ring molecules, without the need for local manipulation.³⁰ The presence of many magnetic centers with the coupled spins allows for the construction of spin cluster qubits that can be manipulated by relatively simple means.³¹ In polyoxometalates, the spin structure of the molecule is sensitive to the addition of charge, and controlled delivery and removal of charges via a scanning tunneling microscope (STM) tip can produce useful quantum gates.³² Chemical bonds between the molecules can be engineered to produce the permanent coupling between the molecular spins and allow for interaction between the qubits.^{33,34}

Sensitivity of molecular state to the addition of charge was demonstrated in the tunneling through single molecules³⁵ and used to control the spin state of a MN.³⁶

Transport studies of the MNs can provide a sensitive probe of their spin structure.^{27,37–40}

The most straightforward and traditional way of controlling magnetic molecules is by applying an external magnetic field. With carefully crafted electron spin resonance (ESR) pulses, it is possible to perform the Grover algorithm, or use the low-energy sector of the molecular nanomagnet as a dense classical memory.³ Unfortunately, the approaches based on magnetic fields face a significant drawback in the large-scale quantum control application. Typically, the quantum manipulation has to be performed on very short spatial and temporal scales, while the local application of rapidly varying magnetic field presents a challenging experimental problem. For that reason, the schemes for quantum computing tend to rely on modifying the spin dynamics that is caused by intramolecular interaction, rather than on the direct manipulation of spins.⁴¹

The electric fields offer an attractive alternative for spin manipulation in the molecular nanomagnets.⁴² One major advantage is that they can be applied to a very small volume via an STM tip^{43,44} and rapidly turned on and off by applying voltage pulses to the electrodes placed close to the molecules that are being manipulated. Switchable coupling between different nanomagnets is essential for qubit implementation. At present, this can be implemented only locally, and the interaction is practically untunable. The use of microwave cavities can offer a solution to this problem. By placing the nanomagnets inside a microwave cavity, one can obtain a fully controllable, long-range interaction between them.⁴² This coupling relies on the presence of a quantum electric field inside such a cavity, which mediates the interaction between distant nanomagnets. The interaction can be tuned by tuning each molecule in- or out-of-resonance with the cavity field using local electric or magnetic fields.⁴² The spins, however, do not couple directly to the electric fields, classical or quantum, and therefore any electric spin manipulation is indirect and involves the modification of molecular orbitals or the spin-orbit interaction (SOI). Alternatively, the flying spin qubits can be manipulated by tailoring the exchange interactions and moving the domain walls in spin chains.^{45,46}

The description of the molecular nanomagnets in terms of spins is an effective low-energy theory that does not carry information about the orbital states. However, it is still possible to predict the form of spin-electric coupling from symmetry considerations and single out the molecules in which such a coupling is possible. In particular, the molecules with the triangular arrangement of antiferromagnetically coupled spin-1/2 magnetic centers interact with external electric field through chirality of their spin structure.^{42,47} The same coupling of chirality to the external electric field was derived for the triangular Mott insulators.⁴⁸

While the symmetry of a molecule sets the form of spin-electric coupling, no symmetry analysis can predict the size of the corresponding coupling constant. The coupling strength will depend on the underlying mechanism that correlates the spin and orbital states, and on the detailed structure of low-energy molecular orbitals. To identify molecules that can be efficiently manipulated by electric fields, it is necessary to perform an extensive search among the molecules with the right symmetries and look for the ones that

also have a large coupling constant. Unfortunately, this search has to proceed by *ab initio* calculations of the coupling constants for a class of molecules of a given symmetry or by an indiscriminate experimental scanning of all of the available molecules.

We will consider the spin electric coupling in the language of effective model, namely, either the spin Hamiltonian or the Hubbard model. In reality the mechanism behind the spin-electric coupling involves either the modification of the electronic orbitals in an external field and the Coulomb repulsion of electrons or the much weaker direct spin-orbit coupling to the external fields. A derivation of spin-electric coupling from this realistic picture would require the knowledge of electronic orbitals from an *ab initio* calculation and the distribution of electric field within the molecule. Both of these problems require substantial computational power and cannot be performed routinely. Since the electric field acts primarily on the orbital degrees of freedom and the spin Hamiltonian carries no information about the orbital states, we provide a description in terms of a Hubbard model that still contains some information about the orbital states. We can then describe the properties of the molecule that allow for strong spin-electric coupling in the language of orbitals that offers some intuitive understanding of the underlying mechanisms of interaction.

The main body of the paper is divided into three largely independent sections that deal with the symmetry analysis, Hubbard model description, and experimental signatures of the spin-electric coupling. In Sec. II, we consider the general form of spin-electric coupling in the ring-shaped molecules. Based on the symmetry analysis, we identify the parameters of the spin Hamiltonian that can change in the electric field and cause spin-electric coupling. We find that the low-energy sector of the rings with odd number of spins (odd-spin rings) contains two Kramers doublets. Electric fields cause transitions between these states. The even-spin rings possess a nondegenerate $S=0$ ground state, making their low-energy sector unsuitable for electric manipulation. Among the odd-spin rings, we find that generically the triangular molecules show strongest coupling to electric fields. In triangles, the spin-electric coupling mechanism that is of the first order in electric field does not involve the spin-orbit coupling. Instead, the spin-electric coupling in the odd-spin rings with more than three spins requires it.

In Sec. III, we describe the molecules in terms of Hubbard model and find how the spin-electric coupling can be attributed to changes of Hubbard model parameters in the electric field. We show that the spin Hamiltonian description arises in the limit of spins well localized on the magnetic centers, and the symmetry-based results are confirmed in this limit. In addition, we consider a Hubbard model of a single superexchange bridge between magnetic centers. We find that the various symmetries of the bridge and the reduction in symmetry in external electric fields specifies the coupling between the spins on magnetic centers.

In Sec. IV, we identify the response of an MN with spin-electric coupling in the standard measurements of ESR, nuclear magnetic resonance (NMR), magnetization, polarization, linear magnetoelectric effect, and specific heat. Our conclusions are summarized in Sec. V.

II. SYMMETRY ANALYSIS OF ANTIFERROMAGNETIC SPIN RINGS

Spin chains whose ground state multiplet consists of two quasidegenerate $S=1/2$ doublets represent suitable candidates for the manipulation of the spin state by pulsed electric fields. Such a ground-state multiplet characterizes a number of frustrated spin rings, consisting of an odd number of half-integer spins. Rings containing an even number of antiferromagnetically coupled spins show no frustration, and in consequence the ground state is a nondegenerate $S=0$ state.

Symmetry analysis is one of the most powerful tools for investigating molecules. By identifying the point group symmetry associated with a given molecule, one can readily read the energy level structure of the system, as well as the allowed transitions induced by external perturbations. In even-spin molecular systems, the symmetry analysis is done by using the so called single-valued point groups.⁴⁹ In an odd-spin system instead, double valued point groups are usually used in order to describe the states, the splittings and the allowed transitions (magnetic or electric).⁴⁹ In the presence of spin-orbit interaction the splittings can be accounted for either by single group analysis (perturbatively) or by double group analysis (exact).

Using both the single group and double group analysis we pinpoint the transitions that arise in the absence or only in the presence of SOI. Therefore, the electric dipole transitions present in the single group are a consequence of the modified exchange interaction and can arise even in the absence of SOI, while the ones that show up only in the double group analysis are a consequence of the SOI (or modification of SOI in electric field).

We expect that the molecules that lack inversion symmetry are going to show stronger spin-electric coupling so that the odd-spin rings are the prime candidates for observing such effects. The importance of inversion stems from the fact that the electric field, being odd under inversion, can only cause transitions between the states of opposite parity in inversion symmetric molecules. Unless there is an accidental degeneracy, these transitions will be suppressed by an energy of the order of intramolecular exchange interaction. In the following we consider prototypical examples odd-spin ring systems and, in the Sec. II D, summarize the symmetry requirements for the existence of spin-electric coupling.

A. Triangle of $s=1/2$ spins

The low-energy properties of most molecular nanomagnets are well described in terms of spin degrees of freedom alone. Within the spin Hamiltonian approach, the coupling of external electric fields to the molecule can be accounted by suitably renormalizing the physical parameters. In the following, we use the symmetry of the molecules to calculate the changes of spin Hamiltonian parameters, to identify the system's eigenstates, and to deduce the allowed transitions. Quantitative estimates of the parameters entering the spin Hamiltonian require *ab initio* calculations⁵⁰ or comparison with experiments. The simplest example of a spin system which may couple to an external electric field in a nontrivial way is a triangle of $s=1/2$ spins, for example, the Cu₃

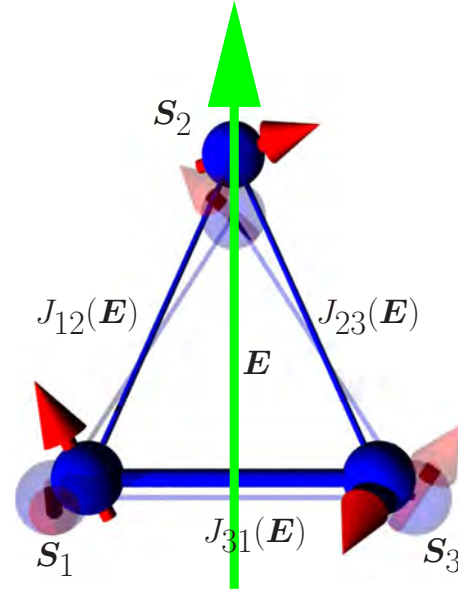


FIG. 1. (Color online) Schematics of the $s_i=1/2$ triangular molecule in electric field. The antiferromagnetic exchange couplings, represented by the bonds with thickness proportional to J_{ii+1} , are modified in electric field. In the absence of electric field, exchange couplings are equal $J_{ii+1}=J_{jj+1}$, here represented in gray (fade blue online). The black (blue online) triangle represents the exchange interaction strengths in electric field.

MN.^{51,52} The schematics of such a spin system in the presence of an electric field is shown in Fig. 1. Its spin Hamiltonian, in the absence of external fields, reads:

$$H_{\text{spin}} = \sum_{i=1}^N J_{ii+1} \mathbf{s}_i \cdot \mathbf{s}_{i+1} + \sum_{i=1}^N \mathbf{D}_{ii+1} \cdot (\mathbf{s}_i \times \mathbf{s}_{i+1}), \quad (1)$$

with $N=3$ and $\mathbf{s}_4 \equiv \mathbf{s}_1$. The first term in Eq. (1) represents the isotropic Heisenberg exchange Hamiltonian with the exchange couplings J_{ii+1} between the spins \mathbf{s}_i and \mathbf{s}_{i+1} , and the second term represents the Dzyalozhinsky-Moriya (DM) interaction due to the presence of SOI in the molecule, with the DM vectors \mathbf{D}_{ii+1} . The states of the spin triangle can be found by forming the direct product of the SU(2) representations of three spins $S=1/2$: $D_{\text{tot}} = D^{(1/2) \otimes 3} = 2D^{(1/2)} \oplus D^{(3/2)}$, meaning there are eight states in total. The point group symmetry of the molecule is D_{3h} ,⁵¹ which imposes the following restrictions on the spin Hamiltonian parameters: $J_{ii+1} \equiv J$ and $D_{ii+1}^{x,y} \equiv 0$, and $D_{ii+1}^z \equiv D_z$. The spin states in a form adapted to the rotational symmetry C_3 of the system are

$$|\psi_{M=1/2}^{(k)}\rangle = \frac{1}{\sqrt{3}} \sum_{j=0}^2 \epsilon_j^k C_3^j |\downarrow\uparrow\uparrow\rangle, \quad (2)$$

$$|\psi_{M=3/2}\rangle = |\uparrow\uparrow\uparrow\rangle, \quad (3)$$

where $\epsilon_j = \exp(2i\pi j/3)$ and $j=0,1,2$. The states with opposite spin projection $M'=-M$, i.e., with all spins flipped can be written in an identical way (not shown). These states are already the symmetry adapted basis functions of the point

group D_{3h} . Moreover, these are eigenstates of the chirality operator

$$C_z = \frac{1}{4\sqrt{3}} \mathbf{s}_1 \cdot (\mathbf{s}_2 \times \mathbf{s}_3), \quad (4)$$

with $C_z|\psi_M^{(1,2)}\rangle = \pm|\psi_M^{(1,2)}\rangle$, $C_z|\psi_M^{(0)}\rangle = 0$, and $C_z|\psi_{M=\pm 3/2}\rangle = 0$. The above states in Eq. (3) carry different total spin. There are two spin $S=1/2$ states, corresponding to $k=1, 2$, and a spin $S=3/2$ state corresponding to $k=0$. Obviously, the states $|\psi_{M=\pm 3/2}\rangle$ have $S=3/2$.

Note that the quantum numbers $j=0, 1, 2$, and chirality $C_z=0, \pm 1$ describe the same states. Since $\{e^{2i\pi C_z/3}\} \equiv \{e^{2i\pi j/3}\}$, we can use either of the two quantum numbers to classify the states. For an arbitrary $2n+1$ odd-spin chain with $n=1, 2, \dots$ the same arguments hold. We can either use the set $\{e^{2i\pi k/3}\}$ with $k=0, 1, \dots, 2n$, or $\{e^{2i\pi C_z/3}\}$ with $C_z=0 \pm 1, \dots, \pm n$ to quantify the states. The advantage of using one or another will show up in the next section when we treat the SOI.

1. Single valued group analysis of the $s=1/2$ spin triangle

In the single valued point group D_{3h} , the states $|\psi_{M=\pm 1/2}^{(k)}\rangle$ with $k=1, 2$ form the basis of the two dimensional irreducible representation E' , while the states $|\psi_{M=\pm 1/2}^{(0)}\rangle$, and the $|\psi_{M=\pm 3/2}\rangle$ transform as A'_2 . The allowed electric transitions in the system are determined by the transformation properties of the basis states.

The simplest and possibly the dominant dependence of the spin Hamiltonian on the applied electric field comes via the modification of the exchange interactions, like depicted in Fig. 1. This gives rise to the following term in the spin Hamiltonian:

$$\delta H_0(\mathbf{E}) = \sum_{i=1}^3 \delta J_{ii+1}(\mathbf{E}) \mathbf{s}_i \cdot \mathbf{s}_{i+1}, \quad (5)$$

where $\delta J_{ii+1}(\mathbf{E}) \approx \mathbf{d}_{ii+1} \cdot \mathbf{E}$, with \mathbf{d}_{ii+1} being vectors that describe the electric-dipole coupling of the bond $\mathbf{s}_i - \mathbf{s}_{i+1}$ to the electric field \mathbf{E} in leading order. There are three such vector parameters and thus nine scalar parameters in total. However, symmetry will allow to drastically reduce the number of free parameters by providing relations between them. The $S=3/2$ states of the unperturbed spin Hamiltonian form the multiplet ${}^4A'_2$, while the $S=1/2$ states form two multiplets ${}^2E'$.⁴⁹ The electric dipole Hamiltonian is $H_{e-d} = -e \sum_i \mathbf{E} \cdot \mathbf{r}_i \equiv -e \mathbf{E} \cdot \mathbf{R}$, with e standing for the electron charge, \mathbf{r}_i being the coordinates of the i th electron, and $\mathbf{R} = \sum_i \mathbf{r}_i$. The nonzero electric dipole matrix elements of H_{e-d} in the D_{3h} symmetric molecule are

$$\langle \psi_M^{(1,2)} | -eX | \psi_{M'}^{(2,1)} \rangle = i \langle \psi_M^{(1,2)} | -eY | \psi_{M'}^{(2,1)} \rangle \equiv d \delta_{MM'}, \quad (6)$$

proportional to the effective electric dipole parameter d . The value of d is not determined by symmetry and has to be found by some other means (*ab initio*, Hubbard modeling, experiments, etc.). All the other matrix elements are zero. The electric field acts only in the low-energy sector, which allows us to write the effective spin-electric coupling Hamiltonian acting in the lowest quadruplet as

$$H_{e-d}^{\text{eff}} = d \mathbf{E}' \cdot \mathbf{C}_{\parallel}, \quad (7)$$

where $\mathbf{E}' = \mathcal{R}_z(7\pi/6 - 2\theta) \mathbf{E}$, with $\mathcal{R}_z(\phi)$ describing the rotation with an angle ϕ about the z axis, and θ is the angle between in-plane component \mathbf{E}_{\parallel} of the electric field \mathbf{E} and the bond $\mathbf{s}_1 - \mathbf{s}_2$. For $\mathbf{C}_{\parallel} = (C_x, C_y, 0)$ we have

$$C_x = \sum_M (|\psi_M^{(1)}\rangle \langle \psi_M^{(2)}| + |\psi_M^{(2)}\rangle \langle \psi_M^{(1)}|), \quad (8)$$

$$C_y = i \sum_M (|\psi_M^{(1)}\rangle \langle \psi_M^{(2)}| - |\psi_M^{(2)}\rangle \langle \psi_M^{(1)}|). \quad (9)$$

The low-energy spectrum in the presence of electric field and the related states can be expressed in terms of the spin Hamiltonian Eq. (5) so that we find anisotropic variations of the exchange coupling constants,

$$\delta J_{ii+1}(\mathbf{E}) = \frac{4d}{3} |\mathbf{E}_{\parallel}| \cos\left(\frac{2\pi}{3}i + \theta\right), \quad (10)$$

which depend on the angle θ and the projection of the electric field \mathbf{E} on the plane of the triangle. In the $s_i = 1/2$ triangle the \mathbf{C} operators can be written as

$$C_x = -\frac{2}{3} (\mathbf{s}_1 \cdot \mathbf{s}_2 - 2\mathbf{s}_2 \cdot \mathbf{s}_3 + \mathbf{s}_3 \cdot \mathbf{s}_1), \quad (11)$$

$$C_y = \frac{2}{\sqrt{3}} (\mathbf{s}_1 \cdot \mathbf{s}_2 - \mathbf{s}_3 \cdot \mathbf{s}_1), \quad (12)$$

with $[C_i, C_j] = 2i\epsilon_{ijk} C_k$ (ϵ_{ijk} are the Levi-Civita symbols).^{42,48} From the above relations we can conclude that (i) only the electric field component perpendicular to the bond and lying in the plane of the molecule gives rise to spin-electric coupling; (ii) there is only one free parameter d describing the coupling of the spin system to electric fields and $\mathbf{d}_{ii+1} = 4d/3 [\sin(2i\pi/3), \cos(2i\pi/3), 0]$.

The SOI in a D_{3h} symmetric MN is constrained by the transformation properties of the localized orbitals. It reads

$$H_{\text{SO}} = \lambda_{\text{SO}}^{\parallel} T_{A_2} S_z + \lambda_{\text{SO}}^{\perp} (T_{E'_+} S_- + T_{E'_-} S_+), \quad (13)$$

with T_{Γ} being tensor operators transforming according to the irreducible representation Γ .⁴⁹ The nonzero matrix elements of this SOI Hamiltonian in the low-energy quadruplet read $\langle \psi_M^{(1,2)} | H_{\text{SO}} | \psi_{M'}^{(1,2)} \rangle = \pm M \lambda_{\text{SO}}^{\parallel} \delta_{MM'}$ so that the SOI takes the following effective form:

$$H_{\text{SO}} = \Delta_{\text{SO}} C_z S_z, \quad (14)$$

with $\Delta_{\text{SO}} = \lambda_{\text{SO}}^{\parallel}$ and $S_z = \sum_i^3 s_i^z$. An effective SOI Hamiltonian is obtained also from the DM SOI Hamiltonian in Eq. (1). The constraints $D_{ii+1}^{x,y} = 0$ and $D_{ii+1}^z \equiv D_z$ on the DM vectors due to D_{3h} symmetry of the molecule give rise to the same effective SOI in Eq. (14), with $D_z = \lambda_{\text{SO}}^{\parallel}$. Thus, as expected, the molecular SOI and the DM SOI give rise to the same effective SOI Hamiltonian acting in the low energy quadruplet. Like in the case of the electric dipole parameter d , finding $D_z(\lambda_{\text{SO}}^{\parallel})$ requires more than symmetry, like *ab initio* methods or experiments. The transverse SOI, with interaction strength $\lambda_{\text{SO}}^{\perp}$ does not act within the low-energy space, and its effect will

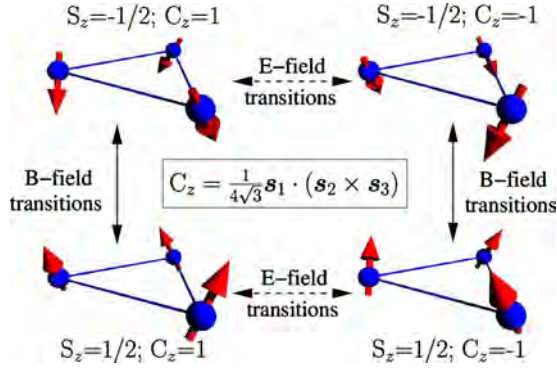


FIG. 2. (Color online) The spin transitions in the $s_f=1/2$ triangle induced by electric and magnetic fields. The electric field causes transitions between the states of opposite chiralities C_z and equal spin projections S_z (horizontal arrows), while the magnetic field instead causes transitions between the states of opposite spin projections S_z and equal chiralities C_z (vertical arrows).

appear only in higher orders of perturbation theory in λ_{SO}^\perp/J .

An external magnetic field couples to the spin via the Zeeman term $H_Z = \mathbf{B} \cdot \bar{g}\mathbf{S}$, with $\bar{g} = \text{diag}\{g_\parallel, g_\parallel, g_\perp\}$ being the g -factor tensor in D_{3h} . The full effective Hamiltonian describing the low-energy quadruplet in the presence of SOI, electric field, and magnetic field reads

$$H_{\text{eff}} = \Delta_{SO} C_z S_z + \mathbf{B} \cdot \bar{g}\mathbf{S} + d\mathbf{E}' \cdot \mathbf{C}_\parallel. \quad (15)$$

Note that $[\mathbf{C}, \mathbf{S}] = 0$, and chirality and spin act as independent spin $1/2$ degrees of freedom. Furthermore, in the absence of SOI the chirality \mathbf{C} and the spin \mathbf{S} evolve independently. However, the SOI couples the two and provides with means for electric control of both spin and chirality. Vice versa, magnetic fields can also couple to chirality due to SOI. Also, while magnetic fields (time-dependent) cause transitions between states of opposite spin projection M but with the same chirality C_z , the electric field does the opposite: it causes transitions between states of opposite chirality C_z , but carrying the same M . Full control of the lowest quadruplet is thus realized in the presence of both electric and magnetic fields, as can be seen in Fig. 2.

2. Double valued group states of the $s=1/2$ spin triangle

The double groups provide a formalism that takes into account the fact that the rotation of a half-integer spin by the angle 2π does not produce the identity transformation on its quantum state. The double group representations allow to nonperturbatively describe the magnetic and electric transitions in the presence of spin-orbit interaction (see Chapter 10 of Ref. 49). The lowest quadruplet consists of two Kramers doublets, transforming like \bar{E}' and \bar{E}'' , respectively. The $S=3/2$ states transform as \bar{E}' (for $M=\pm 1/2$) and \bar{E}'' ($M=\pm 3/2$). Thus, the $S=1/2$ states mix with the $S=3/2$ states, but only the ones transforming according to the same representations, i.e., there is no mixing between \bar{E}' and \bar{E}'' due to spin-orbit interaction. The magnetic dipole transitions take place between \bar{E}' and \bar{E}'' , and within \bar{E}' and \bar{E}'' , respectively, while electric dipole transitions take place only between \bar{E}'

and \bar{E}'' . The selection rules for the electric transitions are $\Delta M = \pm 2$, while for the magnetic transitions these are $\Delta M = 0, \pm 1$. We see that there are allowed electric dipole transitions also within the $S=3/2$ subspace.

We can now establish several selection rules for the SOI, electric field, and magnetic field induced transitions. Note that the above analysis was exact in SOI. However, it is instructive to treat electric field, magnetic fields, and SOI on the same footing. First, we find that the electric dipole transitions fulfill the selection rules $\Delta C_z = \pm 1$ and $\Delta S_z = 0$, meaning that electric field only couples states within the lowest quadruplet. The SOI transitions show a richer structure. We can separate the SOI interaction in two parts: the perpendicular SOI, quantified by D_z in the DM interaction Hamiltonian, and the in-plane SOI, quantified by $D_{x,y}$ in the DM interaction Hamiltonian, respectively. By doing so, we find that the D_z SOI terms obey the selection rules $\Delta C_z = 0$ and $\Delta S_z = 0$, while for the $D_{x,y}$ terms we get the selection rules $\Delta C_z = \pm 1$ and $\Delta S_z = \pm 1$. Due to the cyclic boundary conditions the relation $C_z = 1 + 1 \equiv C_z = -1$ holds. Moreover, for a $2n+1$ spin ring with $n=1, 2, \dots$, this relation is generalized to $C_z = n + 1 \equiv C_z = -n$. We see that in-plane SOI ($D_{x,y}$ terms) do not cause any splitting in the ground state and can lead to observable effects only in second order in perturbation theory in $D_{x,y}/J$. Also, note that if σ_h symmetry is present, $D_{x,y} \equiv 0$ and thus there are no in-plane SOI effects at all. Modification of these terms due to an in-plane external electric field \mathbf{E} , however, lead to different selection rules: changes in D_z terms lead to $\Delta C_z = \pm 1$ and $\Delta S_z = 0$, while modification of $D_{x,y}$ lead to $\Delta C_z = 0, \pm 2$ and $\Delta S_z = \pm 1$. The magnetic field transitions obey the selection rules $\Delta S_z = 0, \pm 1$ and $\Delta C_z = 0$. Thus, we can make clear distinction between pure electric field transitions, SOI-mediated electric transitions, and magnetic transitions. This distinction between the electric and magnetic field induced transitions could be used to extract the spin-electric coupling strength parameter d from spectroscopic measurements.

B. Spin $s=3/2$ triangle

The spin $s=3/2$ triangle has a more complex level structure than the $s=1/2$ triangle due to its higher spin. The spin Hamiltonian, however, is similar to the one in Eq. (1) for $s=1/2$, and the reduction in the representation of three spins $S=3/2$ is $D_{\text{tot}} = D^{(3/2) \otimes 3} = 2D^{(1/2)} \oplus 4D^{(3/2)} \oplus 3D^{(5/2)} \oplus 2D^{(7/2)} \oplus D^{(9/2)}$, a total of 64 spin states. The $s=3/2$ triangle states can be defined according to their transformation properties under threefold rotations C_3 in D_{3h} and are of the following form:

$$|\psi_M^{(k,i)}\rangle = P_k^3 |M, i\rangle, \quad (16)$$

$$P_k^3 = \frac{1}{\sqrt{3}} \sum_{j=0}^2 \epsilon_j^k C_3^j, \quad (17)$$

where $\epsilon_j^k = \exp(2i\pi jk/3)$, C_3^j are the threefold rotation of order j , and $j, k=0, 1, 2$. The states $|M, i\rangle \equiv |\sigma_1 \sigma_2 \sigma_3\rangle$ represent all possible states (i states in total) with a given spin projection M ($\equiv \sum_k \sigma_k$) that cannot be transformed into each other

TABLE I. Nonsymmetry adapted states of the $s=3/2$ spin triangle. We use $|\uparrow(\downarrow)\rangle=|\pm 3/2\rangle$ and $|\uparrow(\downarrow)\rangle=|\pm 1/2\rangle$.

M	i			
	1	2	3	4
1/2	$ \downarrow\uparrow\uparrow\rangle$	$ \uparrow\downarrow\downarrow\rangle$	$ \downarrow\uparrow\uparrow\rangle$	$ \downarrow\uparrow\uparrow\rangle$
3/2	$ \downarrow\uparrow\uparrow\rangle$	$ \downarrow\uparrow\uparrow\rangle$	$ \downarrow\uparrow\uparrow\rangle$	$ \uparrow\uparrow\uparrow\rangle$
5/2	$ \uparrow\uparrow\uparrow\rangle$	$ \downarrow\uparrow\uparrow\rangle$	0	0
7/2	$ \uparrow\uparrow\uparrow\rangle$	0	0	0
9/2	$ \uparrow\uparrow\uparrow\rangle$	0	0	0

by application of the rotation operator C_3^j . These states are showed in Table I.

The corresponding states with all spins flipped, namely, with $M'=-M$, can be written in a similar form (not shown). Having identified the symmetric states in terms of the spin states, we proceed to analyze the allowed transitions induced in the spin systems by magnetic and electric field, both within the single valued group and double valued group representations.

1. Single valued group states of the $s=3/2$ triangle

The above states are basis of the point group D_{3h} , but not eigenstates of the total spin operator \mathbf{S}^2 . The total spin eigenstates can be written as linear combinations of states with given M , S , and chirality (k): $|\psi_{S,M}^{(k)}\rangle = \sum_{l(M)} a_{k,l}^S |\psi_{M'}^{(k,l)}\rangle$, where $l(M)$ is the number of different states with a given M . The coefficients $a_{k,l}$ are to be identified so that these states satisfy $\mathbf{S}^2|\psi_{S,M}^{(k)}\rangle = S(S+1)|\psi_{S,M}^{(k)}\rangle$, with $S=1/2, 3/2, 5/2, 7/2, 9/2$. The states with $k=0$ are all transforming according to the A_2' representation, while the states with $k=1, 2$ are organized in doublets, being the bases of the two dimensional representation E' . The magnetic and electric transitions are similar to the ones in the $s=1/2$ triangle, in the absence of SOI. The electric field causes transitions only between states with the same M and S , but opposite chirality $C_z=(1/2\sqrt{3})\mathbf{s}_1\cdot(\mathbf{s}_2\times\mathbf{s}_3)$ (this is different from the triangle with $s_i=1/2$ spins in each of the vertices). As for the $s=1/2$ spin triangle, there are electric dipole transitions within the $S=1/2$ quadruplet, even in the absence of SOI. The ground state is fourfold degenerate consisting of two $S=1/2$ eigenstates,

$$|\psi_{M=1/2}^{(1)}\rangle = \frac{1}{\sqrt{10}}[|\psi_{M=1/2}^{(1,1)}\rangle + \sqrt{3}|\psi_{M=1/2}^{(1,2)}\rangle - (\epsilon_1 - \epsilon_2)(|\psi_{M=1/2}^{(1,3)}\rangle - |\psi_{M=1/2}^{(1,4)}\rangle)], \quad (18)$$

$$|\psi_{M=1/2}^{(2)}\rangle = \frac{1}{\sqrt{10}}[|\psi_{M=1/2}^{(2,1)}\rangle + \sqrt{3}|\psi_{M=1/2}^{(2,2)}\rangle + (\epsilon_1 - \epsilon_2)(|\psi_{M=1/2}^{(2,3)}\rangle - |\psi_{M=1/2}^{(2,4)}\rangle)]. \quad (19)$$

As in the case of the $s=1/2$ triangle, electric-field induced transitions take place between the states of opposite chirality C_z and same spin projection M . Besides, the lowest quadruplet states are still organized as spin and chirality eigenstates that are split in the presence of SOI.

In the original spin Hamiltonian in Eq. (1) the electric field causes modification of the spin Hamiltonian parameters. As for the spin $s=1/2$ triangle, the strongest effect comes from modification of the isotropic exchange interaction so that

$$\delta H_0(\mathbf{E}) = \sum_{i=1}^3 \delta J_{ii+1}(\mathbf{E}) \mathbf{s}_i \cdot \mathbf{s}_{i+1}, \quad (20)$$

with $\delta J_{ii+1}(\mathbf{E}) = dE \cos(2\pi i/3 + \theta)$, where θ is the angle between the projection of the external electric field \mathbf{E} to the molecule's plane and the $\mathbf{s}_1-\mathbf{s}_2$ bond, and $i=0, 1, 2$. The effect of the electric field on the lowest quadruplet is found to be similar to the spin $s=1/2$ case. While the SOI splits the two chiral states without mixing them (at least in lowest order), the electric field, on the other hand, mixes the chiral states. The effective Hamiltonian acting in the lowest quadruplet reads

$$H_{\text{eff}} = \Delta_{\text{SO}} C_z S_z + \mathbf{B} \cdot \bar{\mathbf{g}} \mathbf{S} + d' \mathbf{E} \cdot \mathbf{C}_{\parallel}. \quad (21)$$

Above, $d' = 3d/2$, $\mathbf{C}_{\parallel} = (C_x, C_y, 0)$, with $C_x = \sum_M |\psi_M^{(1)}\rangle \langle \psi_M^{(2)}| + |\psi_M^{(2)}\rangle \langle \psi_M^{(1)}|$ and $C_x = i \sum_M (|\psi_M^{(1)}\rangle \langle \psi_M^{(2)}| - |\psi_M^{(2)}\rangle \langle \psi_M^{(1)}|)$, and Δ_{SO} stands for the SO splitting. However, in this situation the in-plane chirality operators $C_{x,y}$ cannot be written in a simple form as a function of the individual spin operators, as opposed to the $s=1/2$ triangle.

2. Double valued group states of the $s=3/2$ triangle

The double group representation allows us to identify the couplings between different spin states induced by the SOI and to identify the allowed magnetic dipole transitions. Due to SOI, the electric field induced spin transitions will take place also outside the spin quadruplet. In the absence of extra degeneracies (induced, for example, by external magnetic fields), however, these transitions are strongly reduced due the gap of the order J . We can then focus, as for the $S=1/2$ triangle, only on the lowest quadruplet. These states are organized in two Kramer doublets \bar{E}' and \bar{E}'' transforming as $M = \pm 1/2$ and $M = \pm 3/2$.

As in the case of the $s=1/2$ triangle, the electric field induced transitions take place between \bar{E}' and \bar{E}'' , with the selection rules $\Delta M = \pm 2$. Magnetic transitions instead take place both within and between \bar{E}' and \bar{E}'' , satisfying the selection rules $\Delta M = 0, \pm 1$.

If we now treat the SOI, electric field, and magnetic fields on the same footing, we arrive at the same selection rules as for the $s=1/2$ triangle, namely, $\Delta C_z = \pm 1$ and $\Delta S_z = 0$ for electric transitions, $\Delta C_z = 0, \pm 1$ and $\Delta S_z = 0, \pm 1$ for SOI transitions, and $\Delta C_z = 0$ and $\Delta S_z = 0, \pm 1$ for magnetic transitions, respectively.

C. Spin $s=1/2$ pentagon

We now analyze the spin-electric coupling in a pentagonal molecule with a spin $s=1/2$ in each of the vertices, like depicted schematically in Fig. 3. As in the case of the spin triangle, an external electric field \mathbf{E} gives rise to modification of exchange couplings J_{ii+1} . However, the net spin-electric

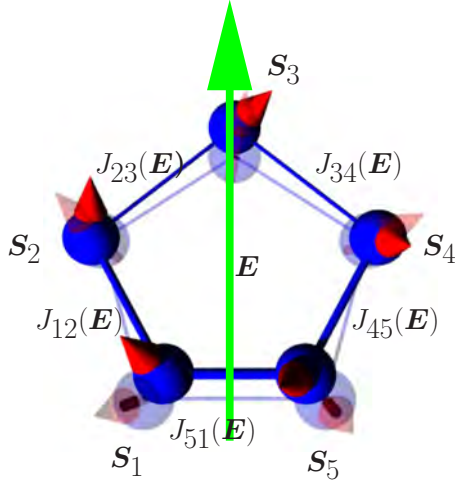


FIG. 3. (Color online) Schematics of a pentagonal spin ring molecule in electric field \mathbf{E} , light (green) arrow. The molecule in the absence of electric field is depicted in fade colors, while the full colors represent the molecules in electric field. Thickness of the bonds represents the strength of antiferromagnetic exchange interaction between the spins. An electric field modifies the strengths of spin exchange couplings J_{ii+1} .

coupling in the lowest spin sector can only be mediated by SOI, i.e., via the DM interaction.

To make the analysis simpler, we assume in the following that the pentagonal spin molecule possesses a D_5 point group symmetry, thus no horizontal reflection plane σ_h . However, no generality is lost since lower symmetry implies more allowed transitions in the spin system. If, for example, in the lower symmetric situation some transitions are forbidden, these transitions will be also forbidden in the higher symmetry case. The Hamiltonian is given in Eq. (1) with $N=5$. The states of the pentagon are found from the product of the individual spin representations $D_{tot}=D^{(1/2)\otimes 5}=5D^{(1/2)}\oplus 4D^{(3/2)}\oplus D^{(5/2)}$, meaning there are 32 spin states in total. As before, these states can be organized in a symmetry adapted basis in the following way:

$$|\psi_M^{(k,i)}\rangle = P_5^k |M, i\rangle, \quad (22)$$

$$P_5^k = \frac{1}{\sqrt{5}} \sum_{j=0}^4 \epsilon_j^k C_5^j, \quad (23)$$

where $\epsilon_j^k = \exp(2i\pi jk/5)$ with $k, j=0, \dots, 5$, C_5^j are the five-fold rotations of order j . The states $|M, i\rangle \equiv |\sigma_1 \sigma_2 \sigma_3 \sigma_4 \sigma_5\rangle$ represent all possible states (i states in total) with a given spin projection $M (\equiv \sum_k \sigma_k)$ that cannot be transformed into each other by application of the rotation operator C_5^j . These states are showed in Table II and the corresponding states with all spins flipped, i.e., $M \rightarrow -M$ states (not shown). In the absence of SOI there is no mixing of different k states, i.e. the chirality is a good quantum number. In this case the chirality is quantified by the operator $C_z = 1/(2\sqrt{5+2\sqrt{5}}) \sum_i \mathbf{s}_i \cdot (\mathbf{s}_{i+1} \times \mathbf{s}_{i+2})$ (the prefactor is chosen for convenience; see below). The ground-state quadruplet consists of two Kramers doublets with spin $S=1/2$. In the fol-

TABLE II. Spin $s=1/2$ pentagon nonsymmetry adapted states.

M	i	
	1	2
1/2	$ \uparrow\uparrow\downarrow\downarrow\rangle$	$ \uparrow\downarrow\downarrow\uparrow\rangle$
3/2	$ \downarrow\uparrow\uparrow\uparrow\rangle$	0
5/2	$ \uparrow\uparrow\uparrow\uparrow\rangle$	0

lowing we inspect the level structure of these four states in terms of the above symmetry adapted states.

1. Single valued group $s=1/2$ pentagon

We focus here only on the four lowest energy states, which are two pairs of $S=1/2$ states. The first (second) pair is given by linear combination of states with $k=1(k=-1)$ and spin projection $M=\pm 1/2$. We obtain

$$|\psi_{S=1/2, M=\pm 1/2}^{(k)}\rangle = \frac{1}{\sqrt{3}} \left[\frac{1}{2 \cos\left(\frac{2k\pi}{5}\right)} |\psi_{M=\pm 1/2}^{(k,1)}\rangle + 2\epsilon_2^k \cos\left(\frac{2\pi}{5}\right) |\psi_{M=\pm 1/2}^{(k,2)}\rangle \right], \quad (24)$$

so that $C_z |\psi_{M=\pm 1/2}^{(k)}\rangle = (-1)^k |\psi_{M=\pm 1/2}^{(k)}\rangle$. These states (for a given M projection) form the basis of the two-dimensional irreducible representation E_1 . We are now in positions to investigate the allowed electric dipole transitions within this lowest subspace. The in-plane electric dipole $\mathbf{d}=(d_x, d_y)$ forms a basis of the irreducible representation E_1 in D_5 .⁴⁹ By calculating the product $E_1 \otimes E_1 \otimes E_1 = 2E_1 \oplus 2E_2$, with E_2 being another two-dimensional irreducible representation of D_5 , we see that the totally symmetric representation A_1 of D_5 is absent. Therefore, there are *no* electric dipole transitions within the four-dimensional subspace in the absence of SOI.

As in the previous two cases, the coupling of the spin Hamiltonian to electric field comes via modification of the spin Hamiltonian parameters. If only the modification of the isotropic exchange Hamiltonian is taken into account, the spin-electric Hamiltonian takes the same form as in Eq. (7), with $\delta J_{ii+1}(\mathbf{E}) = dE \cos(2i\pi/5 + \theta)$, $i=1, \dots, 5$. The parameter d quantifies the electric dipole coupling of each of the bonds and θ is the angle between the electric field \mathbf{E} and the bond $\mathbf{s}_1 - \mathbf{s}_2$. Note that d is in principle non-zero in D_5 point group symmetry. However, the matrix elements of the spin-electric Hamiltonian within the lowest quadruplet are all zero, i.e., $\langle \psi_{S=1/2, M}^{(k)} | \delta H_{e-d}(\mathbf{E}) | \psi_{S=1/2, M'}^{(k')} \rangle \equiv 0$. This means that electric field has no effect on the lowest quadruplet, as found out also by purely symmetry arguments. Therefore, we may expect that the spin-electric coupling in pentagonal spin molecule is caused by SO effects.

2. Double valued group $s=1/2$ pentagon

The lowest four states in the double group D_5^2 are described by the two dimensional irreducible representations

$\bar{E}'_1(M = \pm 1/2)$ and $\bar{E}'_1(M = \pm 3/2)$. Since both the magnetic μ and electric \mathbf{d} dipoles transform as E_1 in D'_5 , both electric and magnetic transitions will take place between the same pair of states. The products of the irreducible representations that labels the states in the low-energy quadruplet read $\bar{E}'_1 \otimes \bar{E}'_2 = E_1 \oplus E_2$, $\bar{E}'_1 \otimes \bar{E}'_1 = A_1 \oplus A_2 \oplus E_1$ and $\bar{E}'_2 \otimes \bar{E}'_2 = A_1 \oplus A_2 \oplus E_2$. These equalities imply the same selection rules in the lowest subspace as for the spin triangle case: $\Delta M = \pm 2$ for electric dipole transitions, and $\Delta M = 0, \pm 1$ for the magnetic ones.

The main feature of the pentagonal spin ring is the absence of electric dipole transitions in the lowest quadruplet in the absence of SOI. This is to be contrasted with the spin triangle case, where spin-electric coupling exists in the ground state even in the absence of SOI. This feature finds its explanation in the interplay between the selection rules for electric field transitions and the ones for the SOI. In fact, these selection rules are by no means different from the triangular spin rings. Since the ground state is spanned by four states with chirality $C_z = -1, 1$ and spin $S_z = \pm 1/2$, we see that the condition $\Delta C_z = \pm 1$ for the electric field transitions implies no electric field coupling within the ground state. In the presence of SOI though, spin electric coupling is still possible, but it will be $(D_{x,y}/J)$ times smaller than in triangles. Spin-electric coupling can arise also via modification of the DM vectors $D_{x,y,z}$ in electric field. However, the selection rules for this transitions are, like for the triangle, $\Delta C_z = 0, \pm 2$ and $\Delta S_z = 0, \pm 1$. This means direct splitting in the ground state, and thus we expect that for pentagonal spin rings the electric dipole response will be much weaker.

D. Symmetry requirements for the existence of spin-electric coupling

There are two general features that allow for the manipulation of the MN state vector within the ground-state multiplet, through pulsed electric fields. (For simplicity, we refer to the case where such coupling is not mediated by spin-orbit interaction and appears in a triangular molecule.)

Firstly, in order for the spin-electric Hamiltonian to be linear in the electric field, permanent electric dipoles \mathbf{d}_{ij} must be present on the bridge(s) that mediate the coupling of spins i and j . These dipole moments must depend on the relative orientation of \mathbf{s}_i and \mathbf{s}_j , see Fig. 4. Besides, in order for the electric field to modify differently the super-exchange couplings J_{ij} between different pairs of spins, the dipoles \mathbf{d}_{ij} must point in different directions from one another. In the present case (10), the \mathbf{d}_{ij} are orthogonal to the vectors \mathbf{R}_{ij} , other in-plane components being forbidden by symmetry. If the dipoles associated with the spin pairs are all along the same direction, instead, the electric field can only induce equal renormalizations of all the exchange couplings ($\delta J_{ij} \equiv \delta J$). As a consequence, the spin-electric Hamiltonian δH_E would commute with H_0 and could not induce transitions between eigenstates of the unperturbed Hamiltonian. In a recent study of spin crossover effect,⁵³ the total molecular electric dipole moment was shown to cause influence the spin state of the molecule. In the mechanism considered here, we require only the existence of the bridge dipole mo-

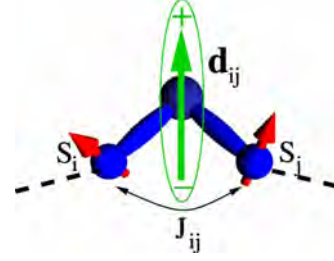


FIG. 4. (Color online) Dipole moment of an unperturbed bridge. In the first order, external electric fields couple to the electric dipole moments of the bridges that connect the spins at magnetic centers. The different orientations of the bridge dipole moments $\mathbf{d}_{ij} \neq \mathbf{d}_{kl}$ lead to inhomogeneous variations of the resulting exchange interactions between the spins $\delta J_{ij} \neq \delta J_{kl}$.

ment, while the total dipole moment of the molecule may be zero.

Secondly, given the existence of a spin-electric coupling, we require that this allows nontrivial manipulations of the MN quantum state within the low-energy multiplet. In particular, in the case of triangle, our proposal relies on the existence of a four-dimensional ground-state multiplet (with $S = 1/2$), whose states are identified by the spin projection $|S_z| = 1/2$ and by chirality C_z . This condition is fulfilled by rings consisting of an odd number of half integer and equivalent spins. Within these class of systems, triangles are particularly suited because the two eigenstates of chirality can be coupled in first order by the spin-electric Hamiltonian even in the absence of spin-orbit interaction.

Both the above criteria can be formulated in terms of inversion symmetry. As far as the first criterion is concerned, the superexchange bridges that magnetically couple \mathbf{s}_i and \mathbf{s}_j must lack an inversion center, though this condition is not sufficient in order for the bridge to possess a permanent electric dipole. Regarding the level structure and selection rules (second criterion), the presence of an odd number of equivalent spins in the ring implies the lack of an inversion center for the molecule as a whole.

III. HUBBARD MODEL OF A MOLECULAR NANOMAGNET

Spin Hamiltonian models of molecular nanomagnets are based on the assumption that the spins on magnetic centers are the only relevant degrees of freedom. This assumption of fully quenched and localized orbitals allows for the relatively simple predictions of spin structure in the low-energy states of the molecule. However, since the orbital dynamics plays a crucial role in the spin-electric coupling, spin Hamiltonian models are unable to predict the corresponding coupling constants. In this section, we relax the assumption of quenched and localized orbitals and treat the orbital degrees of freedom of electrons on magnetic ions within a Hubbard model. This provides an intuitive picture of spin-electric coupling in terms of the deformation of the molecular orbitals induced by the external field. Besides, in the limit of strong quenching of the orbitals, the Hubbard model reproduces a spin Hamiltonian, similar to the results found in the studies of

cuprates^{54–56} and multiferroics.^{57,58} In particular, we find the relation between modifications of the electronic hopping matrix elements induced by the field and that of the spin-electric coupling in the spin Hamiltonian, thus providing a guide for the estimate of the size of spin-electric coupling in a molecule.

The outline of the present section is the following. In Sec. III A, we introduce the Hubbard model of a spin chain with the shape of regular n -tagon and derive the resulting symmetry constraints for the hopping parameters. In Sec. III B we assume a direct electron hopping between magnetic sites and derive the spin Hamiltonian of a spin triangle from the Hubbard model in the limit of large on-site repulsions; we thus express the coupling to electric fields in terms of the Hubbard model parameters. In Sec. III C, we introduce a Hubbard model of a magnetic coupling in the case where this is mediated by a nonmagnetic bridge between the magnetic centers; also in this case, we find a connection between the modification of the bridge and spin-electric coupling.

A. Parameters of the Hubbard model of molecular nanomagnets

Magnetic properties of molecular nanomagnets are governed by the spin state of few electrons in the highest partially occupied atomic orbitals, split by the molecular field. The spin density is localized on the magnetic centers,⁵⁹ and thus the low-energy magnetic properties are correctly described by quantum models of interacting localized spins.^{60,61}

The response of molecular nanomagnets to electric fields, as a matter of principle, does not have to be governed by the electrons occupying the same orbitals that determine the molecule's spin. However, the quantum control of single molecule magnets by electric fields depends on the electrons that both react to electric fields and produce the magnetic response. Therefore, the models of molecular nanomagnets that consider only few orbitals can provide useful information about the electric control of spins.

Hubbard model provides a simplified description of orbital degrees of freedom by including only one or few localized orbitals on each magnetic center. Furthermore, the interaction between electrons is accounted for only by introducing the energies of the atomic configurations with different occupation numbers. The Hubbard model of the MN is given by

$$H_H = \left[\sum_{i,j} \sum_{\alpha,\beta} c_{i\alpha}^\dagger \left(t \delta_{\alpha\beta} + \frac{i \mathbf{P}_{ij}}{2} \cdot \boldsymbol{\sigma}_{\alpha\beta} \right) c_{j\beta} + \text{H.c.} \right] + \sum_j U_j (n_{j\uparrow}, n_{j\downarrow}), \quad (25)$$

where $c_{j\sigma}^\dagger (c_{j\sigma})$ creates (annihilates) an electron with spin $\sigma = \uparrow, \downarrow$ on the orbital localized on j th atom, and $n_{j\sigma} = c_{j\sigma}^\dagger c_{j\sigma}$ is the corresponding number operator. Model parameters U_j describe the energy of $n_{j\uparrow(\downarrow)}$ spin up(down) electrons on the site j . Hopping parameters t_{ij} and \mathbf{P}_{ij} describe the spin-independent and spin-dependent hopping between sites i and j .

We assume that the largest energy scale is the splitting between the energy of the highest occupied atomic orbital and lowest unoccupied one, induced by the molecular crystal field: this justifies the inclusion of one orbital only for each magnetic center. The on-site repulsion energy is the next largest energy scale in the problem, being U_j larger than the hopping coefficients. Among these, processes involving states of different spin, mediated by spin-orbit interaction, are described by the x and y components of \mathbf{P}_{ij} . The parameters $P_{ij,z}$, instead, describe the difference of the hopping matrix elements between spin-up and spin-down electrons. In the following, we shall consider both the case where electron hopping takes place directly between neighboring magnetic ions and that where the magnetic interaction is mediated by bridges of nonmagnetic atoms. Hubbard model with spin-dependent hopping was used to describe the spin-orbit coupling in cuprates⁶² and multiferroics.⁵⁷ The Hubbard Hamiltonian can be approximated by a spin Hamiltonian model in the limit $|t_{ij}|, |\mathbf{P}_{ij}| \ll U_j$. The symmetry constraints on the spin Hamiltonian parameters can be deduced from those on the Hubbard model parameters.⁵⁴ If the spin-independent hopping dominates ($|t| \gg |\mathbf{P}|$), the resulting spin Hamiltonian will contain the Heisenberg exchange terms and a small additional spin-anisotropic interaction. If $|t| \approx |\mathbf{P}|$, the size of spin-dependent interactions in the spin Hamiltonian will be comparable to the Heisenberg terms. Both these cases appear in the molecule nanomagnets.^{18,51,63,64}

Symmetry of the molecule imposes constraints to the Hubbard model, thus reducing the number of free parameters. The on-site repulsion parameters U_j are equal for all equivalent magnetic ions. In the molecules of the form of regular n -tagon, all of the spin-independent hopping parameters are equal due to the C_n symmetry. The spin-dependent hopping elements are related by both the full symmetry of the molecule and the local symmetry of localized orbitals. For example, in the case of localized orbitals in a regular polygon that are invariant under the local symmetry group of the magnetic center,

$$P_{j,j+1;x} = \exp \left[i \frac{2\pi(j-k)}{n} \right] P_{k,k+1;x}, \quad (26)$$

with the convention that site $n+1$ coincides with site 1. In this case, there is only one free parameter that determines all of the P_x matrix elements. Therefore, the regular n -tagon molecule in the absence of external electric and magnetic fields can be described by a Hubbard model, with five independent parameters: U , t , and \mathbf{P}_{12} . In addition, the σ_v symmetry, if present will impose $\mathbf{P}_{12} = p \mathbf{e}_z$, thus reducing the number of free parameters to three.

B. Hubbard model of the spin triangle: Direct exchange

In this section we give a brief description of the Hubbard model for a triangular molecule with D_{3h} symmetry. In this model we assume only direct coupling between the magnetic centers, thus no bridge in-between. Even so, this simplified model catches the main features of the effective spin Hamiltonian and gives the microscopic mechanisms for the spin-electric coupling. The Hamiltonian describing the electrons in the triangular molecule reads

$$H_H = \left[\sum_{i,\sigma} c_{i\sigma}^\dagger (t + i\sigma\lambda_{SO}) c_{i+1,\sigma} + \text{H.c.} \right] + \sum_{i,\sigma} \left(\epsilon_0 n_{i\sigma} + \frac{1}{2} U n_{i\sigma} n_{i\bar{\sigma}} \right), \quad (27)$$

where $\lambda_{SO} \equiv p = \mathbf{P}_{ij} \cdot \mathbf{e}_z$ is the spin-orbit parameter (only one), ϵ_0 is the on-site orbital energy, and U is the on-site Coulomb repulsion energy. As stated before, typically $\lambda_{SO}, |t| \ll U$, which allows for a perturbative treatment of the hopping and spin-orbit Hamiltonians. These assumptions agree well with the numerical calculations performed in Ref. 59.

The perturbation theory program involves the unperturbed states of the system. The first set of unperturbed states are the one-electron states

$$|\phi_i^\sigma\rangle = c_{i\sigma}^\dagger |0\rangle, \quad (28)$$

while the three-electron states split in two categories: (i) the singly occupied site states

$$|\psi_k^\sigma\rangle = \prod_{j=1}^3 c_{j\sigma_j}^\dagger |0\rangle, \quad (29)$$

with $\sigma_j = \sigma$ for $j \neq k$ and $\sigma_j = \bar{\sigma}$, for $j = k$, and (ii) the double-occupied sites

$$|\psi_{kp}^\sigma\rangle = c_{k\uparrow}^\dagger c_{k\downarrow}^\dagger c_{p\sigma}^\dagger |0\rangle, \quad (30)$$

with $k=1,2,3$ and $p \neq k$. The states $|\psi_k^\sigma\rangle$ and $|\psi_{kp}^\sigma\rangle$ span the subspaces with $M=1/2$ and $M=-1/2$ for $\sigma=\uparrow$ and $\sigma=\downarrow$, respectively.

The states in Eqs. (28)–(30) are degenerate with energies $E=\epsilon_0$, $E=3\epsilon_0$, and $E=3\epsilon_0+U$, respectively. Note that these state are eigenstates of the Hamiltonian in Eq. (27) only in the absence of tunneling and SOI.

The above defined states are not yet adapted to the symmetry of the system, i.e., they are not basis states of the corresponding irreducible representations of D_{3h} point group. Finding these states is required by the fact that the symmetry of the molecule is made visible through the hopping and SOI terms in the Hubbard Hamiltonian. This is accomplished by using the projector operator formalism.⁴⁹ We obtain for the one-electron symmetry adapted states.

$$|\phi_{A'_1}^\sigma\rangle = \frac{1}{\sqrt{3}} \sum_{i=1}^3 |\phi_i^\sigma\rangle, \quad (31)$$

$$|\phi_{E'_\pm}^\sigma\rangle = \frac{1}{\sqrt{3}} \sum_{i=1}^3 \epsilon_{1,2}^{i-1} |\phi_i^\sigma\rangle, \quad (32)$$

where A'_2 and E'_\pm are one-dimensional and two-dimensional irreducible representations in D_{3h} , respectively. Similarly, the symmetry adapted states with the singly-occupied magnetic centers read

$$|\psi_{A'_2}^{1\sigma}\rangle = \frac{1}{\sqrt{3}} \sum_{i=1}^3 |\psi_i^\sigma\rangle, \quad (33)$$

$$|\psi_{E'_\pm}^{1\sigma}\rangle = \frac{1}{\sqrt{3}} \sum_{i=1}^3 \epsilon_{1,2}^{i-1} |\psi_i^\sigma\rangle, \quad (34)$$

while the symmetry adapted states of the doubly-occupied magnetic centers read

$$|\psi_{A'_{1,2}}^{2\sigma}\rangle = \frac{1}{\sqrt{6}} \sum_{i=1}^3 (|\psi_{i1}^\sigma\rangle \pm |\psi_{i2}^\sigma\rangle), \quad (35)$$

$$|\psi_{E'_{\pm 1}}^{2\sigma}\rangle = \frac{1}{\sqrt{6}} \sum_{i=1}^3 \epsilon_{1,2}^{i-1} (|\psi_{i1}^\sigma\rangle + |\psi_{i2}^\sigma\rangle), \quad (36)$$

$$|\psi_{E'_{\pm 2}}^{2\sigma}\rangle = \frac{1}{\sqrt{6}} \sum_{i=1}^3 \epsilon_{1,2}^{i-1} (|\psi_{i1}^\sigma\rangle - |\psi_{i2}^\sigma\rangle). \quad (37)$$

The tunneling and SOI mixes the singly-occupied and doubly-occupied states. Since both the tunneling and SOI terms in the Hubbard Hamiltonian transform as the totally symmetric irreducible representation A'_1 in D_{3h} , only states transforming according to the same irreducible representations Γ mix. We obtain the perturbed states in first order in t/U and λ_{SO} ,

$$|\Phi_{A'_2}^{1\sigma}\rangle \equiv |\psi_{A'_2}^{1\sigma}\rangle, \quad (38)$$

$$|\Phi_{E'_\pm}^{1\sigma}\rangle \equiv |\psi_{E'_\pm}^{1\sigma}\rangle + \frac{(\bar{\epsilon} - 1)(t \pm \sigma\lambda_{SO})}{\sqrt{2}U} |\psi_{E'_{\pm 1}}^{2\sigma}\rangle + \frac{3\epsilon(t \pm \sigma\lambda_{SO})}{\sqrt{2}U} |\psi_{E'_{\pm 2}}^{2\sigma}\rangle. \quad (39)$$

Doubly-occupied states become high in energy when $|t|/U, \lambda_{SO}/U \ll 1$. In this limit, the orbital states are quenched into singly-occupied localized atomic orbitals, and low-energy behavior is determined by spin and described by a spin Hamiltonian. In this limit the states in Eq. (34) are exactly the same chiral states in the spin Hamiltonian, i.e., $|\psi_{E'_\pm}^{1\sigma}\rangle \equiv |\psi_{\sigma}^{(1,2)}\rangle$ and $|\psi_{A'_2}^{1\sigma}\rangle \equiv |\psi_{\sigma}^{(0)}\rangle$. The probability of finding two electrons at the same site decays as $|t|/U$. The lowest energy states have total spin $S=1/2$ and the chirality $C_z = \pm 1$, and the fluctuations of chirality $\Delta C_z = \sqrt{\langle C_z^2 \rangle - \langle C_z \rangle^2}$ in the eigenstates vanish, see Fig. 5. The chiral states emerge as the eigenstates in the large- U limit, when the system is well described by the spin Hamiltonian:

The coupling of the molecule to an external electric field \mathbf{E} takes place via two mechanisms. The first one implies modification of the on-site single particle energies ϵ_0 and leads to the following electric-dipole coupling Hamiltonian:

$$H_{e-d}^0 = -e \sum_{\sigma} \frac{E_y a}{\sqrt{3}} c_{1\sigma}^\dagger c_{1\sigma} - \frac{a}{2} \left(\frac{E_y}{\sqrt{3}} + E_x \right) c_{2\sigma}^\dagger c_{2\sigma} + \frac{a}{2} \left(E_x - \frac{E_y}{\sqrt{3}} \right) c_{3\sigma}^\dagger c_{3\sigma}, \quad (40)$$

with a being the geometrical distance between the magnetic ions and $E_{x,y}$ the in-plane components of the electric field.

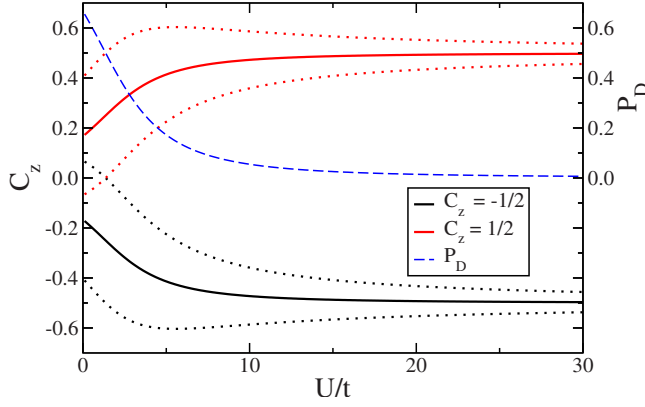


FIG. 5. (Color online) Spin Hamiltonian limit. Expectation values of chirality $\langle C_z \rangle$ (full lines) and their bounds of uncertainty $\langle C_z \rangle \pm \Delta C_z$ (dotted lines), see text, in the low-energy states of the Hubbard model as a function of the on-site repulsion U at the fixed hopping matrix element $t=1$ (left scale). The dashed line shows dependence of the double occupancy probability P_D in the ground state on the right scale. The spin Hamiltonian description becomes accurate in the $U \rightarrow \infty$ limit. The approach to this limit is slow, and the double occupancy probability is proportional to t/U .

The second mechanism is due to modification of the hopping parameters t_{ii+1} in electric field and gives

$$H_{e-d}^1 = \sum_{i,\sigma} t_{ii+1}^E c_{i\sigma}^\dagger c_{i+1\sigma} + \text{H.c.}, \quad (41)$$

where $t_{ii+1}^E = \langle \phi_{i\sigma} | -e\mathbf{r} \cdot \mathbf{E} | \phi_{i+1\sigma} \rangle$ are new hopping parameters induced solely by the electric field \mathbf{E} , and $\Phi_{i\sigma}$ are the Wannier states localized on the magnetic centers. We can write the \mathbf{E} -induced hoppings as $t_{ii+1}^E = \sum_{q=x,y,z} q_{ii+1} E_q$, with $q_{ii+1} = -\langle \phi_{i\sigma} | eq | \phi_{i+1\sigma} \rangle$ being electric dipole matrix elements between the i and $i+1$ ions. These matrix elements are not all independent, symmetry alone reducing drastically the number of independent electric dipole parameters. In order to find suitable independent free parameters, we switch from the description in terms of localized Wannier orbitals $\Phi_{i\sigma}$ to the description in terms of symmetry adapted states, namely from q_{ii+1} to $q_{\Gamma\Gamma'} = \langle \phi_{\Gamma\sigma} | q | \phi_{\Gamma'\sigma} \rangle$, where $\Gamma = A'_1, E'_\pm$. In the basis of symmetry adapted states, the components $q_{\Gamma\Gamma'}$ satisfy a number of relations. In particular, we find

$$\langle \phi_{A'_1}^\sigma | x | \phi_{A'_1}^\sigma \rangle = \langle \phi_{A'_1}^\sigma | y | \phi_{A'_1}^\sigma \rangle = \langle \phi_{E'_+}^\sigma | x | \phi_{E'_+}^\sigma \rangle \equiv 0, \quad (42)$$

$$\langle \phi_{E'_-}^\sigma | x | \phi_{E'_-}^\sigma \rangle = \langle \phi_{E'_+}^\sigma | y | \phi_{E'_+}^\sigma \rangle = \langle \phi_{E'_-}^\sigma | y | \phi_{E'_-}^\sigma \rangle \equiv 0, \quad (43)$$

$$\langle \phi_{E'_+}^\sigma | x | \phi_{E'_-}^\sigma \rangle = -i \langle \phi_{E'_+}^\sigma | y | \phi_{E'_-}^\sigma \rangle \equiv -d_{EE}/e, \quad (44)$$

$$\begin{aligned} \langle \phi_{A'_1}^\sigma | x | \phi_{E'_+}^\sigma \rangle &= \langle \phi_{A'_1}^\sigma | x | \phi_{E'_-}^\sigma \rangle = -i \langle \phi_{A'_1}^\sigma | y | \phi_{E'_+}^\sigma \rangle = i \langle \phi_{A'_1}^\sigma | y | \phi_{E'_-}^\sigma \rangle \\ &\equiv -d_{AE}/e. \end{aligned} \quad (45)$$

These relations reduce the number of free coupling constants to two, namely, d_{EE} and d_{AE} .

It is instructive to write first the relation between the second quantized operators $c_{i\sigma}^\dagger (c_{i\sigma})$ and $c_{\Gamma\sigma}^\dagger (c_{\Gamma\sigma})$, which create

(annihilate) electrons in localized and symmetry adapted states, respectively,

$$\begin{pmatrix} c_{1\sigma}^\dagger \\ c_{2\sigma}^\dagger \\ c_{2\sigma}^\dagger \end{pmatrix} = \frac{1}{\sqrt{3}} \begin{pmatrix} 1 & 1 & \epsilon \\ 1 & \bar{\epsilon} & \bar{\epsilon} \\ 1 & \epsilon & 1 \end{pmatrix} \begin{pmatrix} c_{A'_1\sigma}^\dagger \\ c_{E'_+\sigma}^\dagger \\ c_{E'_-\sigma}^\dagger \end{pmatrix}. \quad (46)$$

With these expressions at hand, we can write the electric dipole Hamiltonian together with the spin-orbit Hamiltonian in the following form:

$$\begin{aligned} H_{e-d}^0 &= \frac{-iea\sqrt{3}}{2} \sum_{\sigma} (\bar{E} c_{E'_+\sigma}^\dagger c_{A'_1\sigma} - \epsilon E c_{E'_-\sigma}^\dagger c_{A'_1\sigma} + \epsilon \bar{E} c_{E'_-\sigma}^\dagger c_{E'_+\sigma}) \\ &+ \text{H.c.}, \end{aligned} \quad (47)$$

$$\begin{aligned} H_{e-d}^1 &= \sum_{\sigma} d_{AE} (\bar{E} c_{A'_1\sigma}^\dagger c_{E'_+\sigma} - E c_{A'_1\sigma}^\dagger c_{E'_-\sigma}) + \bar{E} d_{EE} c_{E'_+\sigma}^\dagger c_{E'_-\sigma} \\ &+ \text{H.c.}, \end{aligned} \quad (48)$$

$$H_{SO} = \sqrt{3}\lambda_{SO} \sum_{\sigma} \sigma (c_{E'_-\sigma}^\dagger c_{E'_-\sigma} - c_{E'_+\sigma}^\dagger c_{E'_+\sigma}), \quad (49)$$

where $E = E_x + iE_y$ ($\bar{E} = E_x - iE_y$). The symmetry adapted states can also be expressed in terms of the symmetry adapted operators c_{Γ}^\dagger . The expressions for these states are shown in Appendix A. Using these states, we can compute all the matrix elements corresponding to the electric dipole and SOI Hamiltonian, respectively. The explicit form of these matrix elements can be found in Appendix B.

We now compute the electric dipole matrix elements between the perturbed chiral states of the E_{\pm} symmetry. The question is to what order in t/U and/or $eEa(d_{EE}, d_{AE})/U$ we want to do it. We use the relations $|ea| \gg d_{EE}, d_{AE}$, which hold in the case of localized orbitals. This leads us to the following matrix element of the electric dipole in the ground state:

$$|\langle \Phi_{E'_-}^{1\sigma} | H_{e-d}^0 | \Phi_{E'_+}^{1\sigma} \rangle| \propto \left| \frac{t^3 eEa}{U^3} \right|, \quad (50)$$

$$|\langle \Phi_{E'_-}^{1\sigma} | H_{e-d}^1 | \Phi_{E'_+}^{1\sigma} \rangle| \approx \left| \frac{4t}{U} Ed_{EE} \right|. \quad (51)$$

We now relate the SOI matrix elements to the DM vectors in the effective spin Hamiltonian. From Eq. (49) we get

$$\langle \Phi_{E'_\pm}^{1\sigma} | H_{SO} | \Phi_{E'_\pm}^{1\sigma} \rangle = \pm \frac{5\sqrt{3}\lambda_{SO}t}{2U} \text{sgn}(\sigma), \quad (52)$$

In the same time, in D_{3h} symmetry, the DM term reads

$$H_{SO} = \frac{iD_z}{2} \sum_{i=1}^3 (s_+^i s_-^{i+1} - s_-^i s_+^{i+1}), \quad (53)$$

allowing us to make the following identification:

$$D_z \equiv \frac{5\lambda_{\text{SO}t}}{U}. \quad (54)$$

We see that this SOI term acts exactly as the ‘‘microscopic’’ SOI derived before: it splits the chiral states, but it does not mix them.

The Hubbard model with spin-orbit coupling can reproduce the energy-level structure of the spin Hamiltonian. In the limit of strong on-site repulsion $|t|/U \ll 1$, the atomic orbitals in the triangle vertices are occupied by one electron each. The lowest energy manifold consists of four states with the total spin $S=1/2$. These states are split from the next four-level $S=3/2$ manifold by a gap of the order of t^2/U .

C. Superexchange in molecular bonds

In this section, we use the Hubbard model to deduce the dependence of the spin Hamiltonian of MNs on the external electric fields in the case where the coupling between magnetic sites is mediated by a nonmagnetic bridge. In particular, we study how the parameters of the effective spin Hamiltonian depend on the hopping matrix elements that are modified by the presence of an electric field. The spins in molecular nanomagnets are localized at the magnetic centers and interact through the long bridges of nonmagnetic atoms. In addition, we do not expect that these orbitals deform in the electric field. Therefore, we expect that the superexchange mechanism through the bridge is more significant than the direct exchange. This method was successfully applied in the studies of strongly correlated electrons, like cuprates⁵⁶ and multiferroics.⁵⁸

In order to describe the magnetic coupling, we consider a pair of sites corresponding to the magnetic centers and a bridge site. Since the direct overlap of the orbitals localized on the magnetic centers is small, we set the direct hopping between the magnetic centers to zero but allow for the hopping of electrons between the magnetic sites and the bridge site. This hopping gives rise to superexchange interaction between the spins on the magnetic sites.⁵⁴ In the limit of strong on-site repulsions, the effective Hamiltonian in the lowest energy sector of the bond corresponds to a spin Hamiltonian where the coupling strengths are determined by the Hubbard model parameters. This correspondence provides an intuitive picture of the mechanism that leads to the interaction between the spins. It also allows us to infer the properties of the molecule that lead to a strong spin-electric coupling, e.g., the delocalization of the orbitals and their local symmetry.

The Hubbard Hamiltonian of the bond is given by

$$H_b = \sum_{i,\alpha\beta} \left[c_{i\alpha}^\dagger \left(t_i \delta_{\alpha\beta} + \frac{i\mathbf{P}_i}{2} \cdot \boldsymbol{\sigma}_{\alpha\beta} \right) b_\beta + \text{H.c.} \right] + U_1(n_1) + U_2(n_2) + U_b(n_b), \quad (55)$$

where the indices 1 and 2 refer to the magnetic sites, and b refers to the bridge site. We derive the spin Hamiltonian by fourth-order Schrieffer-Wolff transformation of the Hamiltonian H_b .

The Schrieffer-Wolff transformation⁶⁵ of the bond Hamiltonian $H_b = H_0 + H_{\text{tun}}$, where the unperturbed Hamiltonian

$H_0 = U_1(n_1) + U_2(n_2) + U_b(n_b)$ produces an effective low energy Hamiltonian H_{12} that approximately describes the low-energy dynamics of the bond. The effective Hamiltonian is

$$H_{12} = \mathcal{P} e^S H_b e^{-S} \mathcal{P}, \quad (56)$$

where the antiunitary operator S is chosen so that the low-energy space of H_0 is decoupled from the high-energy space. This operator is found iteratively, $S = S^{(1)} + S^{(2)} + \dots$ so that the n th order transformation $S^{(n)}$ removes the terms that couple the low- and high-energy states up to order n . The projector \mathcal{P} projects to the low-energy states. In our system, the lowest order Schrieffer-Wolff transformation that gives a nontrivial contribution to the low-energy spin Hamiltonian is of fourth order, and the operator S is approximated as $S \approx \sum_{n=1}^4 S^{(n)}$.

The unperturbed Hamiltonian, $H_0 = U_1 + U_2 + U_b$, describes localized electrons, and the hopping H_{tun} acts as perturbation. The low-energy subspace of the unperturbed Hamiltonian is spanned by the states in which the magnetic ions are singly occupied, and the bridge is doubly occupied. The lowest-order terms that give rise to a nontrivial spin Hamiltonian, in the limit $|t|, |\mathbf{P}| \ll U$, are of the fourth order in t and \mathbf{P} .

The resulting interaction of the spins includes an isotropic exchange of strength J , a Dzyalozhinsky-Moriya interaction described by a vector \mathbf{D} , and an anisotropic exchange term described by a second rank symmetric traceless tensor $\boldsymbol{\Gamma}$,⁶⁶

$$H_{12} = JS_1 \cdot S_2 + \mathbf{D} \cdot (\mathbf{S}_1 \times \mathbf{S}_2) + \mathbf{S}_1 \cdot \boldsymbol{\Gamma} \mathbf{S}_2. \quad (57)$$

Quite generally the interaction between two spins up to second order in \mathbf{P}_{12} can be represented as an isotropic exchange of rotated spins.⁵⁶ However, since the frustration in the triangle is strong, it is a good approximation to take only the Dzyalozhinsky-Moriya interaction into account for the weak spin-orbit coupling, $|\mathbf{P}_{12}| \ll |t_{12}|$ when describing a full molecule.

In a bond with a single bridge site, the largest possible symmetry is C_{2v} . We introduce Cartesian coordinates with the x axis pointing from the magnetic center 1 to 2, y axis lying in the bond plane and pointing toward the bridge site, and the z axis normal to the bond plane (Fig. 6). The elements of the C_{2v} symmetry group are then rotation $R_{y,\pi}$ by π about the y axis, reflection σ_v in the yz plane, and reflection σ_h in the xy plane. Each of these symmetry operations imposes constraints on the parameters of H_b . In the case of localized orbitals that remain invariant under the local symmetries of their respective sites, the constraints resulting from the $R_{y,\pi}$ symmetry are

$$t_1 = t_2, \quad (58)$$

$$P_{x,1} = -P_{x,2}, \quad (59)$$

$$P_{y,1} = P_{y,2}, \quad (60)$$

$$P_{z,1} = -P_{z,2}. \quad (61)$$

The σ_v symmetry implies

$$t_1 = t_2, \quad (62)$$

$$P_{x,1} = P_{x,2}, \quad (63)$$

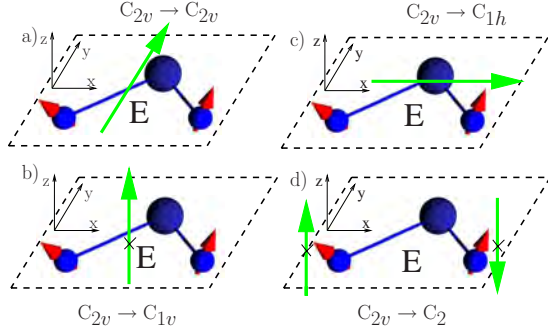


FIG. 6. (Color online) Geometry of the bond and reduction of symmetry. (a) Electric field \mathbf{E} in the y direction, leaves the C_{2v} symmetry unbroken. (b) An electric field \mathbf{E} in the z direction, normal to the bond plane, reduces the symmetry to $\{E, \sigma_v\}$. (c) An electric field \mathbf{E} in the x direction, along the line connecting the magnetic centers, reduces the symmetry to $\{E, \sigma_h\}$. (d) In an inhomogeneous staggered electric field \mathbf{E} , the reduced symmetry group is $\{E, R_y, \pi\}$.

$$P_{y,1} = -P_{y,2}, \quad (64)$$

$$P_{z,1} = -P_{z,2}, \quad (65)$$

and the σ_h symmetry implies

$$\mathbf{P}_1 = -\mathbf{P}_2 = p\mathbf{e}_z. \quad (66)$$

In the perturbative calculation of the effective spin Hamiltonian parameters, these constraints reproduce the Dzyalozhinsky-Moriya rules. We do not deal with the symmetry of on-site energies $U_{1,2,b}$ in any detail since they do not affect the spin Hamiltonian at this level of approximation.

D. Electric field along y

In the electric field pointing along the y axis, the point group symmetry of the bridge remains C_{2v} , and all of the constraints (59)–(66) hold. The fourth-order Schrieffer-Wolff transformation then gives the interaction between the spins on magnetic centers of form (57) with the parameters

$$J = \frac{1}{12U^3}(48t^4 - 40t^2p_z^2 + 3p_z^4), \quad (67)$$

$$\mathbf{D} = \frac{2}{U^3}tp_z(4t^2 - p_z^2)\mathbf{e}_z, \quad (68)$$

$$\Gamma_{xx} = \Gamma_{yy} = -\frac{1}{2}\Gamma_{zz} = -\frac{8}{3U^3}t^2p_z^2, \quad (69)$$

while all the off-diagonal elements of Γ vanish. Here, the parameters of the Hubbard model satisfy the symmetry constraints of the full C_{2v} , and

$$t_1 = t_2 = t, \quad (70)$$

$$\mathbf{P}_1 = -\mathbf{P}_2 = p_z\mathbf{e}_z. \quad (71)$$

We have introduced $U^3 = U_{c2}(2U_{c2} - U_{b2})(U_{b1} - U_{b2} + U_{c2})^2 / (4U_{c2} - U_{b2})$, where the on-site repulsions are U_{b2} for

the doubly occupied bridge, U_{b1} for the singly occupied bridge, and U_{c2} for the doubly occupied magnetic center. The parameter U describes the energy cost of leaving the manifold of states with the minimal energy of Coulomb repulsion. We assume that the lowest energy charge configuration corresponds to a doubly occupied bridge, so that $U_{b2} < U_{b1}$.

In first order, the variations in the spin-Hamiltonian parameters resulting from the modification of the Hubbard model parameters are

$$\delta J = \frac{1}{3U^3}[(48t^3 - 20tp_z^2)\delta t + (-20t^2p_z + 3p_z^3)\delta p_z], \quad (72)$$

$$\delta D_z = \frac{2}{U^3}[(12t^2p_z - p_z^3)\delta t + (4t^3 - 3tp_z^2)\delta p_z], \quad (73)$$

$$\delta \Gamma_{xx} = \delta \Gamma_{yy} = -\frac{\delta \Gamma_{zz}}{2} = -\frac{16tp_z}{3U^3}(p_z\delta t + t\delta p_z). \quad (74)$$

Electric field modifies the orbitals and therefore the overlaps between them that determine the hopping parameters. We consider the case where the variations δt and δp_z are linear in the field intensity E_y : $\delta t = \kappa_t E_y$, $\delta p_z = \kappa_{p_z} E_y$. We will not discuss the effect of variations in the on-site energies U in any details since their only effect in the fourth-order perturbation is a rescaling of all the spin Hamiltonian parameters by $U^3/(U + \delta U)^3$.

We stress that these linear modifications of the hopping parameters are characteristic for the C_{2v} symmetry. If the electric field is oriented differently and thus lowers the system symmetry (see below) first-order increments are not allowed, and the spin-electric coupling is at least a second-order effect in the electric field. The modification of the orbitals includes the energy scale of splitting of the atomic orbitals in the molecular field. We have assumed earlier that the splitting of the orbitals localized on the magnetic centers is large, and the dominant source of the spin-electric coupling is the modification of the bridge orbital. Therefore, the key criterion for strong spin-electric coupling is the presence of bridge orbitals that are weakly split in the molecular field. If, in addition, we assume that the modification is a property of the bond alone, and not of the entire molecule, the κ parameters can be determined in an *ab initio* calculations on a smaller collection of atoms.

In the limit of weak spin-orbit coupling, $|t| \gg |p_z|$, the main effect of the electric fields is a change of J , leading to our symmetry-based results, see Eq. (15). In particular, the d parameter of the symmetry analysis is

$$d = \frac{4}{U^3}[(48t^3 - 20tp_z^2)\kappa_t + (-20t^2p_z + 3p_z^3)\kappa_{p_z}]. \quad (75)$$

In this case, the Dzyalozhinsky-Moriya vector \mathbf{D} is constrained to point in the z direction, $\mathbf{D} = D\mathbf{e}_z$. The model suggests that the dominant effect of the electric field in the molecules with dominant Heisenberg exchange ($J \gg |\mathbf{D}|$) is modification of the isotropic exchange constants J , and

$$\frac{|\delta\mathbf{D}|}{|\delta J|} \sim \frac{|\mathbf{D}|}{|J|}, \quad (76)$$

so that the modification of the Dzyalozhinsky-Moriya vector $\mathbf{D} \rightarrow \mathbf{D} + \delta\mathbf{D}$ is weaker. However, in the molecules in which the modifications of J are inefficient in inducing the spin-electric coupling, as, for example, in the spin-1/2 pentagon, the modifications of \mathbf{D} may eventually provide the main contribution to the spin-electric coupling.

Electric field pointing in a generic direction breaks the C_{2v} symmetry of the bridge and allows further modification of the Hubbard and spin Hamiltonian parameters that do not obey all the symmetry constraints in Eqs. (58)–(66). With the relaxed constraints, both the direction and intensity of $\mathbf{P}_{1,2}$, as well as the spin-independent hoppings $t_{1,2}$ become field dependent. This observation can be used in the search for molecules that show strong spin-electric coupling. The energy cost of changing the distance between the localized orbitals may be significantly higher than the cost of modifying the shape of the bridge orbital. In order to investigate this dependence, we study the effective spin Hamiltonian description of a bridge with all possible residual symmetries.

1. Residual σ_v symmetry

An electric field $\mathbf{E} = E\mathbf{e}_z$ normal to the bond's plane reduces the initial C_{2v} symmetry down to $\{E, \sigma_v\}$. This reduction of the symmetry also happens when a molecule is deposited on the surface parallel to the bond plane. While the constraints in Eq. (66) hold, this reduction in symmetry implies the appearance of nonzero in-plane components of $\mathbf{P}_{1,2}$. We parametrize the most general Hubbard model parameters $t_{1,2}$ and $\mathbf{P}_{1,2}$ consistent with the symmetry as

$$t_1 = t_2 = t, \quad (77)$$

$$P_{1,x} = P_{2,x} = p_{xy} \cos \phi, \quad (78)$$

$$P_{1,y} = -P_{2,y} = p_{xy} \sin \phi, \quad (79)$$

$$P_{1,z} = -P_{2,z} = p_z. \quad (80)$$

The effective low energy spin Hamiltonian, derived by Schrieffer-Wolff transformation up to fourth order in t/U , and $|\mathbf{P}|/U$ is given by Eq. (57), with the nonzero parameters,

$$J = \frac{1}{12U^3} [p_{xy}^4 - 2p_{xy}^2 p_z^2 + 3p_z^4 - 8t^2(p_{xy}^2 + 5p_z^2) + 48t^4 - 8p_{xy}^2(p_z^2 - 4t^2)\cos 2\phi + 2p_{xy}^4 \cos 4\phi], \quad (81)$$

$$D_y = -\frac{p_{xy}}{U^3} (p_z \cos \phi + 2t \sin \phi) (-p_z^2 + 4t^2 + p_{xy}^2 \cos 2\phi), \quad (82)$$

$$D_z = -\frac{1}{2U^3} (4tp_z - p_{xy}^2 \sin 2\phi) (p_z^2 - 4t^2 - p_{xy}^2 \cos 2\phi), \quad (83)$$

$$\Gamma_{xx} = -\frac{1}{6U^3} [p_{xy}^2(1 - \cos 2\phi) + 2p_z^2][8t^2 + p_{xy}^2(1 + \cos 2\phi)], \quad (84)$$

$$\Gamma_{yy} = \frac{1}{12U^3} \{-p_{xy}^4 + 8p_{xy}^2 p_z^2 + 32t^2(p_{xy}^2 - p_z^2) + p_{xy}^2[8(p_z^2 - 4t^2)\cos 2\phi + p_{xy}^2 \cos 4\phi + 48tp_z \sin 2\phi]\}, \quad (85)$$

$$\Gamma_{yz} = \Gamma_{zy} = \frac{p_{xy}}{U^3} (p_z \cos \phi + 2t \sin \phi) (-4tp_z + p_{xy}^2 \sin 2\phi) \quad (86)$$

$$\Gamma_{zz} = -\Gamma_{xx} - \Gamma_{yy}. \quad (87)$$

In the lowest order in spin-orbit coupling the spin interaction consists of the isotropic exchange with $J \approx 4t^4/U^3$, and the Dzyalozhinsky-Moriya interaction with $\mathbf{D} \approx -8t^3(p_{xy} \sin \phi \mathbf{e}_y + p_z \mathbf{e}_z)/U^3$.

As a matter of principle, the spin-orbit coupling mediated hopping \mathbf{P} does not have to be much weaker than the spin-independent hopping t . In this case, all the nonzero terms in Eqs. (81)–(87) are of comparable size, and the variation in spin Hamiltonian with the angle ϕ becomes significant. Note that the angle ϕ describes the directions of spin-orbit coupling induced hopping parameters $\mathbf{P}_{1,2}$, and that it is not directly connected to the bond angle between the magnetic sites and the bridge site. However, for the bridge orbital without azimuthal symmetry, the angle ϕ does depend on the bond angle. For the molecules in which the full symmetry allows only for the spin-electric coupling mediated by the spin-orbit interaction, this effect is important.

With these assumptions, the dependence of the effective spin Hamiltonian on p_{xy} suggests that the strength of induced in-plane Dzyalozhinsky-Moriya vector will be sensitive to the angle ϕ that is determined by the angular dependence of the bridge and magnetic center orbitals. In turn, for a fixed symmetry of the bridge orbital, this dependence directly translates into the dependence of the spin-electric coupling constant on the bridge bond angle.

In the presence of electric field $\mathbf{E} = E\mathbf{e}_z$, the hopping parameters will change from their initial values that satisfy the constraints implied by the C_{2v} symmetry, into a set of values that satisfy those implied by σ_v only. The resulting change in the spin-Hamiltonian parameters reads

$$\delta J = \frac{1}{3U^3} [4t_0(12t_0^2 - 5p_{z0}^2)\delta t + p_{z0}(-20t_0^2 + 3p_{z0}^2)\delta p_z], \quad (88)$$

$$\delta D_y = -\frac{1}{U^3} (4t_0^2 - p_{z0}^2) (2t_0 \sin \phi + p_{z0} \cos \phi) \delta p_{xy}, \quad (89)$$

$$\delta D_z = \frac{2}{U^3} [p_{z0}(12t_0^2 - p_{z0}^2)\delta t + t_0(4t_0^2 - 3p_{z0}^2)\delta p_z], \quad (90)$$

$$\delta\Gamma_{xx} = \delta\Gamma_{yy} = -\frac{1}{2}\delta\Gamma_{zz} = -\frac{16}{3U^3}t_0p_{z0}(p_{z0}\delta t + t_0\delta p_z), \quad (91)$$

$$\delta\Gamma_{yz} = \delta\Gamma_{zy} = -\frac{4}{U^3}t_0p_{z0}(2t_0 \sin \phi + p_{z0} \cos \phi)\delta p_{xy}. \quad (92)$$

The σ_v -symmetric variations in Hubbard parameters occur when an external electric field is applied along the z direction to a C_{2v} symmetric bond. Again, the variations in the parameters is generically linear in the field strength, $\delta t = \kappa_{t,\sigma v}E_z$, $\delta p_{xy} = \kappa_{p_{xy},\sigma v}E_z$, and $\delta p_z = \kappa_{p_z,\sigma v}E_z$, where the κ parameters depend on the modification of the bridge orbital in the electric field. As opposed to the case of the field along the y direction that maintains the bonds C_{2v} symmetry, the κ parameters for the field along the z axis vanish in zero field since the z component of a vector has no matrix elements between the relevant C_{2v} -symmetric states. The linear expansion is valid when the field is strong enough to distort the bridge orbital. Alternatively, the expansion is valid for a bond with lower symmetry in zero electric field, e.g., when the bond is close to a surface.

2. Residual σ_h symmetry

In an electric field that lies in plane of the bond, with $\mathbf{E} \parallel \hat{\mathbf{x}}$, the only residual symmetry transformation is the reflection about the xy plane (σ_h). Within this reduced symmetry, the two magnetic sites are no longer equivalent, but the spin-dependent hopping parameters $\mathbf{P}_{1,2}$ still point along the z axis,

$$t_1 \neq t_2, \quad \mathbf{P}_1 = p_1\mathbf{e}_z \neq p_2\mathbf{e}_z = \mathbf{P}_2. \quad (93)$$

In the fourth order in hopping parameters t and \mathbf{P} , the resulting low energy spin Hamiltonian is again given by Eq. (57), with the following nonzero coupling constants:

$$J = \frac{1}{12U^3}[32t_1t_2p_{1z}p_{2z} - 4(t_1^2p_{2z}^2 + t_2^2p_{1z}^2) + 48t_1^2t_2^2 + 3p_{1z}^2p_{2z}^2], \quad (94)$$

$$\mathbf{D} = -\frac{1}{U^3}(t_1p_{2z} - t_2p_{1z})(4t_1t_2 + p_{1z}p_{2z})\mathbf{e}_z, \quad (95)$$

$$\Gamma_{xx} = \Gamma_{yy} = -\frac{\Gamma_{zz}}{2} = -\frac{2}{3U^3}(t_1p_{2z} - t_2p_{1z})^2. \quad (96)$$

Similar to the case of full C_{2v} symmetry, the spin Hamiltonian consists of the isotopic exchange J , Dzyalozhinsky-Moriya vector $\mathbf{D} = D_z\hat{\mathbf{z}}$ normal to the bond plane, and diagonal tensor Γ isotropic in the bond plane ($\Gamma_{xx} = \Gamma_{yy}$). We stress that the dependence of the effective spin Hamiltonian parameters on those entering the spin Hubbard Hamiltonian is different for these two symmetries, and so is the response to the applied electric field. On one hand, the C_{2v} preserving electric field induces the transitions in the lowest-energy multiplet in the lowest order. On the other hand, the electric field

that reduces the bond symmetry to $\{E, \sigma_h\}$ does not alter the coupling of spins in the lowest order since the deformation of the molecule requires some coupling to the field.

As in previous case, we expand the σ_h symmetric spin Hamiltonian around the C_{2v} symmetric case. We introduce a perturbation of the parameters Hubbard parameters in the electric field consistent with the residual symmetry: $t_1 = t_0 + \delta t_1$, $t_2 = t_0 + \delta t_2$, $p_{1z} = p_{z0} + \delta p_{1z}$, and $p_{2z} = -p_{z0} + \delta p_{2z}$. As a consequence, the spin Hamiltonian parameters are incremented by

$$\delta J = \frac{1}{6U^3}[4t_0(12t_0^2 - 5p_{z0}^2)(\delta t_1 + \delta t_2) + p_{z0}(-20t_0^2 + 3p_{z0}^2) \times (\delta p_{1z} - \delta p_{2z})], \quad (97)$$

$$\delta D_z = \frac{1}{U^3}[p_{z0}t_0(12t_0 - p_{z0})(\delta t_1 + \delta t_2) + t_0(4t_0^3 - 3p_{z0}^2)(\delta p_{1z} - \delta p_{2z})], \quad (98)$$

$$\delta\Gamma_{xx} = \delta\Gamma_{yy} = -\frac{\delta\Gamma_{zz}}{2} = -\frac{8}{3U^3}t_0p_{z0}[p_{z0}(\delta t_1 + \delta t_2) + t_0(\delta p_{1z} - \delta p_{2z})]. \quad (99)$$

As for the case of σ_v residual symmetry, there is no spin-electric effect of the first order in electric field, and the crucial condition for coupling to the electric field in this direction is weak splitting of the bridge orbitals in the molecular field.

3. Residual $R_{y,\pi}$ symmetry

Reduction in the symmetry of the bond, from the full C_{2v} to the group $\{E, R_{y,\pi}\}$, does not occur for any vector perturbation. In terms of electric fields, this reduction in the symmetry would correspond to an inhomogeneous electric field that points in the \mathbf{e}_z direction at the position of one of the magnetic centers, and in the $-\mathbf{e}_z$ direction at the position of the other. This symmetry breaking can also happen when the localized orbitals on the magnetic centers have lobes of opposite signs extending in the z direction and oriented opposite to each other.

The most general Hubbard model parameters consistent with the residual symmetry are

$$t_1 = t_2 = t, \quad (100)$$

$$P_{1x} = -P_{2x} = p_{xy} \cos \phi, \quad (101)$$

$$P_{1y} = P_{2y} = p_{xy} \sin \phi, \quad (102)$$

$$P_{1z} = P_{2z} = p_z. \quad (103)$$

After the fourth-order Schrieffer-Wolff transformation, the effective low-energy spin Hamiltonian has form (57) with nonzero parameters,

$$J = \frac{1}{12U^3}(p_{xy}^4 - 2p_{xy}^2p_z^2 + 3p_z^4 - 8t^2(p_{xy}^2 + 5p_z^2) + 48t^2 + 8p_{xy}^2(p_z^2 - 4t^2)\cos 2\phi + 2p_{xy}^4\cos 4\phi), \quad (104)$$

$$D_x = \frac{1}{U^3} p_{xy} (-2t \cos \phi + p_z \sin \phi) (p_z^2 - 4t^2 + p_{xy}^2 \cos 2\phi), \quad (105)$$

$$D_z = -\frac{1}{2U^3} (4tp_z + p_{xy}^2 \sin 2\phi) (p_z^2 - 4t^2 + p_{xy}^2 \cos 2\phi), \quad (106)$$

$$\begin{aligned} \Gamma_{xx} = & \frac{1}{12U^3} (-p_{xy}^4 + 8p_{xy}^2 p_z^2 + 32t^2 (p_{xy}^2 - p_z^2) \\ & + p_{xy}^2 [-8(p_z^2 - 4t^2) \cos 2\phi + p_{xy}^2 \cos 4\phi \\ & - 48tp_z \sin 2\phi]), \end{aligned} \quad (107)$$

$$\Gamma_{zx} = \Gamma_{xz} = \frac{1}{U^3} p_{xy} (2t \cos \phi - p_z \sin \phi) (4tp_z + p_{xy}^2 \sin 2\phi), \quad (108)$$

$$\Gamma_{yy} = \frac{1}{6U^3} [p_{xy}^2 (1 + \cos 2\phi) + 2p_z^2] [p_{xy}^2 (-1 + \cos 2\phi) - 8t^2], \quad (109)$$

$$\begin{aligned} \Gamma_{zz} = -\Gamma_{xx} - \Gamma_{yy} = & -\frac{1}{6U^3} \{-p_{xy}^4 + 2p_{xy}^2 p_z^2 + 8t^2 (p_{xy}^2 - 4p_z^2) \\ & + p_{xy}^2 [-2(p_z^2 - 4t^2) \cos 2\phi + p_{xy}^2 \cos 4\phi - 24tp_z \sin 2\phi]\}. \end{aligned} \quad (110)$$

The expansion from the C_{2v} symmetric case gives (see the discussion of the σ_v residual symmetry in Sec. III D 1,

$$\delta J = \frac{1}{3U^3} [4t_0 (12t_0^2 - 5p_{z0}^2) \delta t + p_{z0} (-20t_0^2 + 3p_{z0}^2) \delta p_z], \quad (111)$$

$$\delta D_x = \frac{1}{U^3} (4t_0^2 - p_{z0}^2) (2t_0 \cos \phi_0 - p_{z0} \sin \phi_0) \delta p_{xy}, \quad (112)$$

$$\delta D_z = \frac{2}{U^3} [p_{z0} (12t_0^2 - p_{z0}^2) \delta t + t_0 (4t_0^2 - 3p_{z0}^2) \delta p_{z0}], \quad (113)$$

$$\delta \Gamma_{xx} = \delta \Gamma_{yy} = -\frac{1}{2} \delta \Gamma_{zz} = -\frac{16}{3U^3} p_{z0} t_0 (p_{z0} \delta t + t_0 \delta p_z), \quad (114)$$

$$\delta \Gamma_{zx} = \delta \Gamma_{xz} = \frac{4}{U^3} t_0 p_{z0} (2t_0 \cos \phi_0 - p_{z0} \sin \phi_0) \delta p_{xy}. \quad (115)$$

As in the case of σ_v symmetry, the resulting interaction of the spins on magnetic centers becomes dependent on the

angle ϕ between the two \mathbf{P} parameters. This dependence is pronounced in the case of strong spin-orbit coupling and can lead to the dependence of spin-electric effects on both the geometry of the bond and the shape of the bridge orbital.

E. Bond modification and symmetries

Spin-electric coupling induced by the superexchange through bridge atoms depends on the symmetry of the bridge and the direction of the electric field. This symmetry reflects on the resulting coupling of spins in an MN. In this section, we combine the results of the Hubbard model study of the individual bonds with the previous symmetry considerations and provide rough estimates of the most promising spin-electric coupling mechanism in the triangular and pentagonal molecules.

The spin-electric coupling via superexchange is most sensitive to the electric fields that does not break the initial C_{2v} local symmetry of the bond. This symmetry corresponds to the electric field that lies in the plane of the molecule and normal to the bond. All the other couplings require modification of the bridge orbitals and are suppressed by a factor $d|\mathbf{E}|/U_d$, where U_d is on-site repulsion on the bridge. Assuming that this repulsion is strong, we can model the spin electric coupling as a set of modifications of the spin interactions δH_{jj+1} between the neighboring magnetic centers, with $\|\delta H_{jj+1}\| \propto |E_{\perp}^{\text{bond}}|$, where E_{\perp}^{bond} is the projection of the electric field normal to the bond and lying in the molecule's plane.

In the triangle, the strongest effects of electric field is modification of exchange couplings $\delta J_{jj+1} = \delta J_0 \cos(2j\pi/3 + \theta_0)$, where the angle θ_0 describes the orientation of the in-plane component of the electric field, and δJ_0 is a molecule-dependent constant. This modification leads to a specific coupling of the in-plane components of chirality to the electric field $H_{e-d}^{\text{eff}} = d\mathbf{E}' \cdot \mathbf{C}_{\parallel}$, see Eq. (7). Other types of coupling are suppressed either due to weaker influence of electric field on the bonds or due to the symmetry of the molecule. If the spin-electric coupling is mediated by the spin-orbit interaction, the suppression is by a factor of the order $|\mathbf{D}|/J$, and if the coupling is mediated by electric field, the suppression factor is $d|\mathbf{E}|/J$. Assuming the simplest case, the modification of exchange coupling is the most promising mechanism for spin-electric coupling in triangular molecules.

In the pentagons, the modification of spin-spin interaction δH_{jj+1} preferred by the superexchange mechanism is inefficient in inducing the spin-electric coupling of the molecule. The pattern δJ_{jj+1} of exchange coupling constants induced by an external electric field does not couple the states within the lowest energy manifold. In order to couple the spins in the pentagon to an external field, another mechanism is needed. The modification of the Dzyalozhinsky-Moriya vectors $\delta D_{jz} = \delta D_{z0} \cos(2j\pi/5 + \theta_0)$, where δD_{z0} is a molecule-dependent constant, and θ_0 describes the orientation of the in-plane component of the electric field, are preferred by the superexchange bridge model. In the symmetry analysis, we have found that this form of modification of spin-orbit coupling does not induce spin-electric coupling. The same applies to the modifications of in-plane components $D_{jj+1,x(y)}$.

The main effect that gives rise to spin-electric coupling is the modification of the exchange interactions δJ_{jj+1} in the presence of the original spin-orbit interaction $D_{jj+1,z}$. Compared to a triangle composed out of identical bonds, this interaction will be weaker by a factor of $|\mathbf{D}_{jj+1}|/J_{jj+1}$.

In summary, within our model of the superexchange-mediated spin-electric coupling, the most promising candidates for the spin manipulation via electric field are triangular molecules. In pentagons, the best candidates are molecules with strong spin-orbit interaction, and weakly split bridge orbitals.

IV. EXPERIMENTAL SIGNATURES OF THE SPIN-ELECTRIC COUPLING

Coherent quantum control of spins in an MN using electric fields can be achieved by resonant driving of the transitions between the chirality eigenstates.⁴² At present, however, little is known about the effects of electric fields on the spin states of molecular magnets. As a preliminary step, it is thus useful to identify possible signatures of such a coupling that are observable in the experiments routinely used to characterize these systems.

In this section, we study the ways in which the spin-electric coupling can be detected in electron spin resonance (ESR), in nuclear magnetic resonance (NMR), and in the thermodynamic measurement of an MN.

A. Electron spin resonance

ESR investigates transitions between states belonging to a given S multiplet and having different spin projections M along the magnetic field direction.⁶⁷ This technique provides information on the anisotropies of the spin system, as well as on the chemical environment, and the spin dynamics.²⁹ In the following, we show how the effects of an external electric field can show up in the ESR spectra of antiferromagnetic spin rings by affecting both the frequency and the oscillator strength of the transitions.

1. Triangle of $s=1/2$ spins

We start by considering the simplest case of interest, namely, that of a triangle of $s=1/2$ spins with D_{3h} symmetry. The lowest energy eigenstates of the spin triangle, given in Eq. (3) form an $S=1/2$ quadruplet. The effective Hamiltonian H_{eff} of the molecule in the presence of electric and magnetic fields within this quadruplet is given by Eq. (15).

We first consider the case of a static magnetic field perpendicular to the molecule's plane ($\mathbf{B} \parallel \hat{\mathbf{z}}$). The eigenvalues of H_{eff} are then given by

$$\lambda_{\sigma}^{\alpha} = \sigma[\mathcal{B} + \alpha(\Delta_{\text{SO}}^2 + \mathcal{E}^2)^{1/2}], \quad (116)$$

where $\mathcal{E} \equiv d|\mathbf{E} \times \hat{\mathbf{z}}|$, $\mathcal{B} = \mu_B \sqrt{g_{\parallel}^2 B_z^2 + g_{\perp}^2 B_{\perp}^2}$, $\sigma = \pm 1/2$ is the eigenvalue of S_z , and $\alpha = \pm 1$ is the eigenstate chirality in the limit of vanishing electric field. In fact, $|\lambda_{\sigma}^{\alpha}\rangle_{\mathcal{E}=0}$ coincides with $|\alpha, \sigma\rangle$ up to a phase factor. In the presence of electric field, the eigenstates read

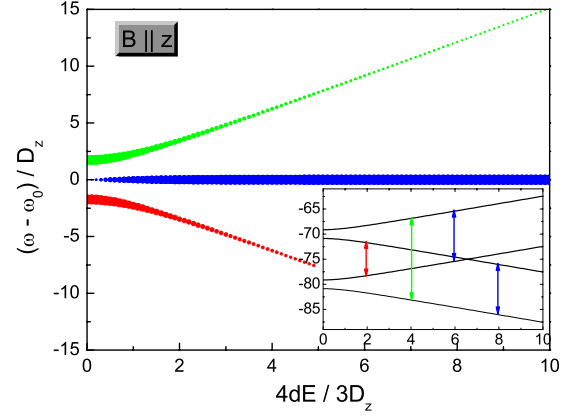


FIG. 7. (Color online) Energy (ω) of the ESR transitions in a triangle of $s=1/2$ spins as a function of the applied electric field \mathbf{E} that lies in the molecule's plane so that $d|\mathbf{E}|=dE=\mathcal{E}$. The magnetic field is $\mathbf{B} \parallel \hat{\mathbf{z}}$ and $\omega_0 = g\mu_B B$, see Eqs. (120) and (121). The diameter of the circles is proportional to the transition amplitudes $|\langle \alpha | S_x | \alpha' \rangle|$, Eqs. (118) and (119). Here, $|\alpha\rangle$ are the eigenstates of H in the lowest energy $S=1/2$ multiplet. Inset: eigenvalues (in units of D_z) as a function of $\mathcal{E} = d|\mathbf{E}_{\parallel}|$, in units $3D_z/4$.

$$|\lambda_{\sigma}^{\alpha}\rangle = \{2\sigma[\Delta_{\text{SO}} + \alpha(\mathcal{E}^2 + \Delta_{\text{SO}}^2)^{1/2}] + 1, \sigma\rangle + \mathcal{E}e^{-i\theta}|-1, \sigma\rangle\}/D^{\alpha}, \quad (117)$$

where $D^{\alpha} = \{\mathcal{E}^2 + [\Delta_{\text{SO}} + \alpha(\mathcal{E}^2 + \Delta_{\text{SO}}^2)^{1/2}]^2\}^{1/2}$.

Electron spin resonance induces transitions between such eigenstates. The transition amplitudes are given by the absolute values of matrix elements of x component of the total spin, taken between the states that the transition connects,

$$\langle \lambda_{-1/2}^{\alpha} | S_x | \lambda_{+1/2}^{-\alpha} \rangle = -\mathcal{E}^2/D^{+1}D^{-1}, \quad (118)$$

$$\langle \lambda_{-1/2}^{\alpha} | S_x | \lambda_{+1/2}^{\alpha} \rangle = \frac{\Delta_{\text{SO}}[\Delta_{\text{SO}} + \alpha(\mathcal{E}^2 + \Delta_{\text{SO}}^2)^{1/2}]}{(D^{\alpha})^2}. \quad (119)$$

The corresponding frequencies are given by

$$\lambda_{+1/2}^{\alpha} - \lambda_{-1/2}^{-\alpha} = \mathcal{B}, \quad (120)$$

$$\lambda_{+1/2}^{\alpha} - \lambda_{-1/2}^{\alpha} = \mathcal{B} + \alpha(\mathcal{E}^2 + \Delta_{\text{SO}}^2)^{1/2}. \quad (121)$$

As an illustrative example, we plot the frequencies and amplitudes of the ESR transitions as a function of the electric field (Fig. 7). While for $\mathcal{E}=0$, these transitions can only take place between states of equal C_z (red and green symbols online, transitions with the larger amplitude at low fields, in the figure and in the inset), the electric field mixes states of opposite chirality, thus transferring oscillator strength to two further transitions, whose frequencies are independent of \mathcal{E} (blue symbols online, constant frequency transition in the figure). In the limit $dE \gg D_z$, the eigenstates of the spin Hamiltonian tend to coincide with those of S_{12}^2 , and ESR transitions take place between states of equal S_{12} . While the eigenstates depend on the in-plane orientation of the electric field, no such dependence is present in the frequencies and oscillator strength of the ESR transitions. Besides, these quantities are independent of the exchange coupling J and

depend on the value of the applied magnetic field only through an additive constant (ω_0).

The dependence of the ESR spectrum on the applied electric field is qualitatively different if the static magnetic field is applied in-plane (e.g., $\mathbf{B} \parallel \hat{\mathbf{x}}$ and the oscillating field oriented along $\hat{\mathbf{z}}$). In this case, the eigenvalues of H_{eff} are

$$\mu_{\sigma}^{\alpha} = \alpha \sigma [\Delta_{\text{SO}}^2 + (\mathcal{E} + \alpha \mathcal{B})^2]^{1/2}, \quad (122)$$

where $\sigma = \pm 1/2$ is the value of $\langle S_x \rangle$ in the limit of large magnetic field ($\mathcal{B} \gg \mathcal{E}, \Delta_{\text{SO}}$) and $\alpha = \pm 1$. The corresponding eigenstates read

$$\begin{aligned} |\mu_{\sigma}^{\alpha}\rangle = & \{e^{i\theta}(\Delta_{\text{SO}} + \mu_{\sigma}^{\alpha})[|+1, +1/2\rangle - |-1, -1/2\rangle] \\ & + (\mathcal{B} + \alpha \mathcal{E})[|+1, -1/2\rangle - |-1, +1/2\rangle]\} / D_{\sigma}^{\alpha}, \end{aligned} \quad (123)$$

where

$$D_{\sigma}^{\alpha} = \sqrt{2} [(\Delta_{\text{SO}} + \mu_{\sigma}^{\alpha})^2 + (\mathcal{B} + \alpha \mathcal{E})^2]^{1/2}. \quad (124)$$

The expectation values of the total spin along the magnetic field for each of the above eigenstates are given by the following expressions

$$\langle \mu_{\sigma}^{\alpha} | S_x | \mu_{\sigma}^{\alpha} \rangle = 2 [(\Delta_{\text{SO}} + \mu_{\sigma}^{\alpha})(\mathcal{B} - \alpha \mathcal{E})] / (D_{\sigma}^{\alpha})^2, \quad (125)$$

which are independent of the in-plane direction of the electric field. The ESR transitions between such eigenstates induced by a magnetic field that oscillates along the z direction are given by the expressions

$$\begin{aligned} \langle \mu_{\sigma}^{\alpha} | S_z | \mu_{\sigma'}^{-\alpha} \rangle &= \frac{(\Delta_{\text{SO}} + \mu_{\sigma}^{\alpha})(\Delta_{\text{SO}} + \mu_{\sigma'}^{-\alpha}) + (\mathcal{E}^2 - \mathcal{B}^2)}{D^{\alpha} D^{-\alpha}}, \\ \langle \mu_{\sigma}^{\alpha} | S_z | \mu_{\sigma'}^{\alpha} \rangle &= 0. \end{aligned} \quad (126)$$

Therefore, the application of the electric field shifts the energy of the transitions between states of opposite α , thus removing their degeneracy; however, unlike the case $\mathbf{B} \parallel \hat{\mathbf{z}}$, it does not increase the number of allowed transitions.

In the case of tilted magnetic fields, the dependence of the ESR spectrum on the applied electric field presents qualitatively different features (Fig. 8). In particular, the spectrum is dominated by two pairs of degenerate transitions that anticross as a function of the electric field. Away from the anticrossing, the transitions with the largest oscillator strength display frequency dependence on the electric field.

2. Pentagons of $s=1/2$ spins

Triangles of $s=3/2$ spins (not shown here) display the same qualitative behavior as the one discussed above. In contrast, chains including an odd number $N > 3$ spins behave differently. This is mainly due to the fact that the spin-electric coupling δH does not couple directly the four eigenstates of H belonging to the lowest $S=1/2$ multiplet: such coupling only takes place through mixing with the higher $S=1/2$ multiplet. As a consequence, the effects of the spin-electric coupling tend to be weaker as compared to the case of the triangle; besides, unlike the above case of the spin

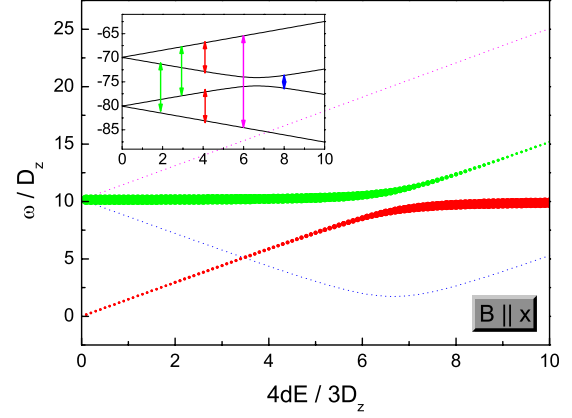


FIG. 8. (Color online) Energy (ω) of the ESR transitions in a triangle of $s=1/2$ spins as a function of the applied in-plane electric field \mathbf{E} so that $d|\mathbf{E}|=dE=\mathcal{E}$, and in the presence of the in-plane magnetic field $\mathbf{B} \parallel \hat{\mathbf{x}}$. The diameter of the circles is proportional to $|\langle \alpha | S_z | \alpha' \rangle|$, Eqs. (120) and (121). The states $|\alpha\rangle$ are the eigenstates of H in the lowest $S=1/2$ multiplet. Inset: eigenvalues (in units of D_z) as a function of $d|\mathbf{E}_{\parallel}|=\mathcal{E}$, in units $3D_z/4$.

triangle, they depend on the exchange coupling J . Illustrative numerical results are shown in Figs. 9 and 10 for the cases of a perpendicular and in-plane magnetic field, respectively. In the former case, both the frequencies and amplitude of the ESR transitions are hardly affected by the electric field in the same range of physical parameters considered in Fig. 7. In the case of an in-plane magnetic field, instead, a relatively small shift in the transition energies is accompanied by a strong transfer of the oscillator strength for values of the spin-electric coupling exceeding the Dzyalozhinsky-Moriya coupling constant.

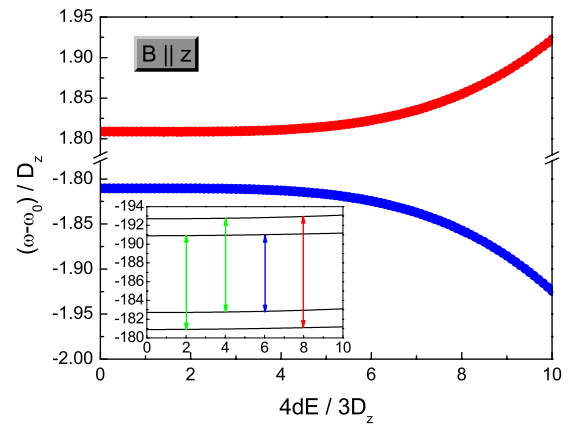


FIG. 9. (Color online) Energy (ω) of the ESR transitions in a pentagon of $s=1/2$ spins as a function of the electric field applied in the molecule's plane $d|\mathbf{E}|=dE=\mathcal{E}$. The Zeeman splitting, $\omega_0 = g\mu_B B$ is set by the magnetic field $\mathbf{B} \parallel \hat{\mathbf{z}}$, orthogonal to the molecule's plane. The considered transitions are those between eigenstates ($|\alpha\rangle$) belonging to the $S=1/2$ multiplet of the spin Hamiltonian (figure inset). Unlike the case of the spin triangle, these are coupled to each other by the electric field via eigenstates belonging to other multiplets, and therefore depends also on the exchange constant J (here $J/\Delta_{\text{SO}}=100$). The diameter of the circles is proportional to $|\langle \alpha | S_x | \alpha' \rangle|$, and therefore to the transition amplitude.

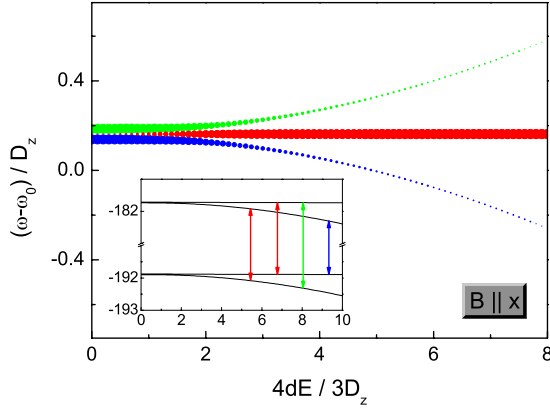


FIG. 10. (Color online) Energy (ω) of the ESR transitions in a pentagon of $s=1/2$ spins as a function of the applied in-plane electric field \mathbf{E} so that $d|\mathbf{E}|=dE=\mathcal{E}$. The Zeeman splitting is set by an in-plane magnetic field $\mathbf{B}\parallel\hat{x}$, and $\omega_0=g\mu_B B$. The considered transitions are those between eigenstates ($|\alpha\rangle$) belonging to the $S=1/2$ multiplet of the spin Hamiltonian (figure inset). Unlike the case of the spin triangle, these are coupled to each other by the electric field via eigenstates belonging to other multiplets and therefore depends also on the exchange constant J (here $J/\Delta_{SO}=100$). The diameter of the circles is proportional to $|\langle\alpha|S_z|\alpha'\rangle|$, and therefore to the transition amplitude.

B. Nuclear magnetic resonance

The spin-electric Hamiltonian δH_0 modifies nonuniformly the superexchange couplings between neighboring spins. This might not affect the projection of the total spin (as in the case $\mathbf{B}\parallel\hat{z}$, see above), but it generally affects the moment distribution within the spin chain. Such effect can be investigated through experimental techniques that act as local probes in molecular nanomagnets, such as NMR (Ref. 68) or x-ray absorption.⁶⁹ In NMR, the expectation value of a given spin within the cluster can be inferred through the frequency shift induced on the transitions of the corresponding nucleus. The shift in the nuclear resonance frequency for the nucleus of the i -th magnetic ion is $\Delta\nu=\gamma A\langle s_{z,i}\rangle$, where A is the contact hyperfine interaction constant at the nuclear site. The constant of proportionality A depends on the spin density at the position of the nucleus and can be extracted from the experiment by considering the polarized ground state $M=S$ at high magnetic fields.⁶⁸ As in the case of ESR, the dependence of the NMR spectra on the applied electric field qualitatively depends on the orientation of the static magnetic field \mathbf{B} with respect to the molecule. Unlike the case of ESR, however, it also depends on the in-plane orientation of the electric field, i.e., on the way in which the \mathbf{E} breaks the symmetry of the molecule.

1. Spin triangles

Let us start by considering a spin $s=1/2$ triangle, with a magnetic field applied perpendicular to the molecule plane ($\mathbf{B}\parallel\hat{z}$). In this case, the distribution of the spin projection along z is given by the following expression:

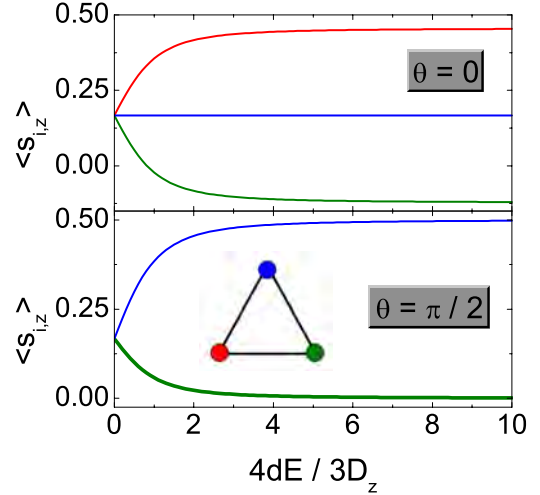


FIG. 11. (Color online) Expectation values of the z component of $s=1/2$ spins in a triangular molecule as a function of applied electric field. The magnetic field is perpendicular to the ring plane ($\mathbf{B}\parallel\hat{z}$); the electric field is parallel and perpendicular to \mathbf{r}_{12} in the upper and lower panel, respectively. In the electric field along one of the bonds (lower panel), the spins that lie on that bond have the same out-of-plane projections. The shadings (colors online) denote the different spins.

$$\langle\lambda_\sigma^\alpha|s_{i,z}|\lambda_\sigma^\alpha\rangle=\sigma/3+f_\sigma^\alpha(\mathcal{E})\cos[\theta+\pi(5/3-i)], \quad (127)$$

where

$$f_\sigma^\alpha(\mathcal{E})\equiv\frac{4\sigma\mathcal{E}[\Delta_{SO}+\alpha(\Delta_{SO}^2+\mathcal{E}^2)^{1/2}]}{3(D^\alpha)^2}. \quad (128)$$

Here, the expressions of the eigenstates $|\lambda_\sigma^\alpha\rangle$ and of D^α are given in Sec. IV A. For $E=0$, the three spins are equivalent and $\langle\lambda_{\pm 1/2}^\alpha|s_{i,z}|\lambda_{\pm 1/2}^\alpha\rangle=\pm 1/6$. If the electric field is finite and oriented along one of the triangle sides (e.g., $\mathbf{E}\parallel\mathbf{r}_{12}$, corresponding to $\theta=0$), then expectation values along z of spins 1 and 2 undergo opposite shifts, whereas that of spin 3 is left unchanged: $\Delta_{\mathbf{E}}\langle s_{1,z}\rangle=-\Delta_{\mathbf{E}}\langle s_{2,z}\rangle$, where $\Delta_{\mathbf{E}}\langle s_{i,z}\rangle\equiv\langle s_{i,z}\rangle_{\mathbf{E}}-\langle s_{i,z}\rangle_{\mathbf{E}=0}$. This is shown in Fig. 11 for the ground state of the spin Hamiltonian, but the above relations hold for any of the four eigenstates $|\lambda_\sigma^\alpha\rangle$ belonging to the $S=1/2$ quadruplet. If the NMR frequency shifts $\Delta\nu_i$ are larger than the corresponding line widths, the single line at $\mathbf{E}=0$ splits into three equispaced lines, with intensity ratios 1:1:1. If, instead, the electric field is applied along a symmetry plane of the triangle (e.g., $\mathbf{E}\perp\mathbf{r}_{12}$, corresponding to $\theta=\pi/2$), spins 1 and 2 remain equivalent and their magnetic moments display the same electric field dependence, while the shift of the third one is opposite in sign and twice as large in absolute value: $\Delta_{\mathbf{E}}\langle s_{1,z}\rangle=\Delta_{\mathbf{E}}\langle s_{2,z}\rangle=-\Delta_{\mathbf{E}}\langle s_{3,z}\rangle/3$. The intensity ratios of the two NMR lines are, correspondingly, 1:2. The expectation values for the remaining eigenstates can be derived by the following equations: $\Delta_{\mathbf{E}}\langle\lambda_{-1/2}^\alpha|s_{i,z}|\lambda_{-1/2}^\alpha\rangle=-\Delta_{\mathbf{E}}\langle\lambda_{+1/2}^\alpha|s_{i,z}|\lambda_{+1/2}^\alpha\rangle$ and $\langle\lambda_1^1|s_{i,z}|\lambda_1^1\rangle=-\Delta_{\mathbf{E}}\langle\lambda_\sigma^{-1}|s_{i,z}|\lambda_\sigma^{-1}\rangle$. Therefore, at finite temperature, the shifts in the expectation values of the three spins are given by

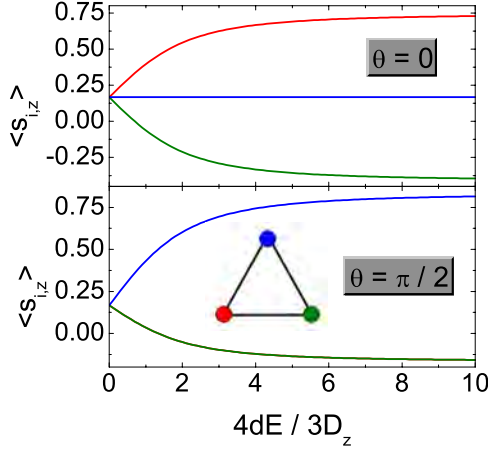


FIG. 12. (Color online) Expectation values of the z component of $s=3/2$ spins in a triangular molecule as a function of applied electric field. The magnetic field is perpendicular to the ring plane ($\mathbf{B} \parallel \hat{z}$); the electric field is parallel and perpendicular to \mathbf{r}_{12} in the upper and lower panels, respectively. The shadings denote the different spins.

$$\frac{\Delta_{\mathbf{E}} \langle s_{i,z} \rangle}{\Delta_{\mathbf{E}} \langle \lambda_{-1/2}^+ | s_{i,z} | \lambda_{-1/2}^+ \rangle} = \frac{\sum_{\alpha} \alpha \cosh\left(\frac{\lambda_{-1/2}^{\alpha}}{k_B T}\right)}{\sum_{\alpha} \cosh\left(\frac{\lambda_{-1/2}^{\alpha}}{k_B T}\right)}. \quad (129)$$

If the field is oriented along the molecule plane ($\mathbf{B} \parallel \hat{x}$), the expectation value of the three spins corresponding to each of the eigenstates are given by the following expressions:

$$\langle \mu_{\sigma}^{\alpha} | s_{i,x} | \mu_{\sigma}^{\alpha} \rangle = g_{\sigma}^{\alpha}(\mathcal{E}) + (1/3)\cos(\theta - 2i\pi/3), \quad (130)$$

where

$$g_{\sigma}^{\alpha}(\mathcal{E}) \equiv \frac{2}{3} \frac{(\Delta_{SO} + \mu_{\sigma}^{\alpha})(\mathcal{B} + \alpha\mathcal{E})}{(D^{\alpha})^2}. \quad (131)$$

If the magnetic field is parallel to the triangle plane, the in-plane electric field can modify the total spin expectation value along \mathbf{B} . The changes that \mathbf{E} induces in the magnetization distribution within the triangle at zero temperature are less varied than in the previous case (Fig. 11). In fact, the magnitude of the $\Delta_{\mathbf{E}} \langle s_{i,z} \rangle$ is much smaller, and all the spins undergo shifts of equal sign and slope. The NMR line, which is slitted into three lines already for $\mathbf{E}=0$, is rigidly shifted by the applied electric field.

If the triangle is formed by half-integer spins $s > 1/2$, an analogous dependence of the expectation values $\langle s_{i,z} \rangle$ on the electric field is found. As an illustrative example, we report in Fig. 12 the case of $s=3/2$.

2. Pentagon of $s=1/2$ spins

Spin chains consisting of an odd number of half-integer spins present analogous behaviors but also meaningful differences with respect to the case of the spin triangle. In particular, the spin-electric Hamiltonian δH_0 does not couple states belonging to the lowest $S=1/2$ quadruplet directly

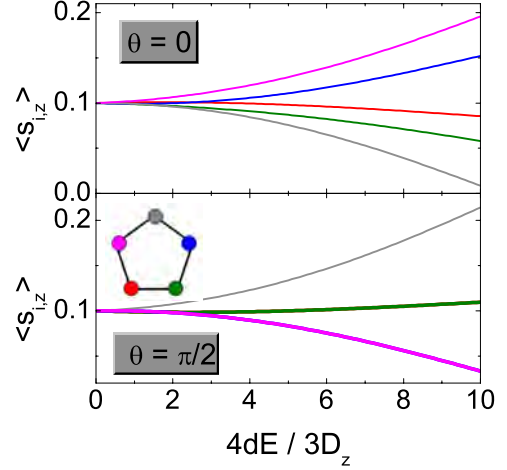


FIG. 13. (Color online) Expectation values of the z component of $s=1/2$ spins in a pentagon as a function of applied electric field. The magnetic field is perpendicular to the ring plane ($\mathbf{B} \parallel \hat{z}$); the electric field is parallel ($\theta=0$) and perpendicular ($\theta=\pi/2$) to \mathbf{r}_{12} in the upper and lower panel, respectively. The shadings (colors online) denote the different spins.

(i.e., matrix elements $\langle i | \delta H_0 | j \rangle = 0$ for $i, j \leq 4$); these couplings are mediated by states belonging to higher $S=1/2$ multiplets that are higher in energy by a quantity $\sim J$. Therefore, the effect of the electric field tends to be significantly smaller than in the case of a triangle with equal D_z and \mathcal{E} (see Fig. 13) and depends also on the exchange coupling J .

C. Magnetization, polarization, and susceptibilities

The spin-electric coupling shifts the energy eigenvalues of the nanomagnet, thus affecting thermodynamic quantities, such as magnetization, polarization, and susceptibilities. In the following, we compute these quantities in the case of the $s=1/2$ spin triangle as a function of the applied magnetic and electric fields. Under the realistic assumption that the exchange splitting J is the largest energy scale in the spin Hamiltonian, and being mainly interested in the low-temperature limit, we restrict ourselves to the $S=1/2$ quadruplet, and use the effective Hamiltonian H_{eff} in Eq. (21).

The eigenenergies of the lowest $S=1/2$ sector in the presence of electric and magnetic fields are

$$E_{\alpha,\gamma} = \alpha\gamma \sqrt{\mathcal{B}^2 + \Delta_{SO}^2 + \mathcal{E}^2 + 2\gamma E_0^2}, \quad (132)$$

with $\mathcal{B} = \mu_B \sqrt{g_{\parallel}^2 H_{\parallel}^2 + g_{\perp}^2 H_{\perp}^2}$, $E_0 = [(\mathcal{B}_z \Delta_{SO})^2 + (\mathcal{B}\mathcal{E})^2]^{1/4}$, and $\mathcal{B}_z = \mu_B g_{\parallel} H_{\parallel}$. Note that these energies are the generalization of the ones in the previous section, which were valid for in-plane magnetic field only, and that the magnetic field $B_i \equiv \mu_0 H_i$, with $i=x, y, z$. The partition function for N identical and noninteracting molecules is $Z = Z_1^N$, with $Z_1 = \sum_{\alpha,\gamma} \exp(-\beta E_{\alpha,\gamma})$ being the partition function for one molecule, and $\beta = 1/(k_B T)$. The free energy reads

$$F \equiv -1/\beta \ln Z = -N k_B T \ln \left[2 \sum_{\gamma} \cosh(\beta E_{\gamma}) \right], \quad (133)$$

with $E_{\gamma} \equiv E_{1/2,\gamma}$. From this, we can derive different thermodynamic quantities like the magnetization $M_i = -\partial F / \partial H_i$, the

electric polarization $P_i = -\partial F / \partial E_i$, the heat capacity $C = -\partial / \partial T (\partial \ln(Z) / \partial \beta)$, and the corresponding susceptibilities: $\chi_{E_i E_j} = \partial P_i / \partial E_j = \partial^2 F / \partial E_i \partial E_j$ —the *electric* susceptibility, $\chi_{B_i B_j} = \partial M_i / \partial H_j = \partial^2 F / \partial H_i \partial H_j$ —the *spin* susceptibility, and $\chi_{E_i B_j} = \partial P_i / \partial M_j = \partial^2 F / \partial E_i \partial H_j$ —the *spin-electric* susceptibility. For the electric polarization components P_i we get

$$P_i = \frac{Nd\mathcal{E}_i}{4 \sum_{\gamma=\pm 1} \cosh(\beta E_\gamma)} \sum_{\gamma=\pm 1} \frac{\sinh(\beta E_\gamma)}{E_\gamma} \times \left(1 + \gamma \frac{\mathcal{B}^2}{E_0^2}\right) (1 - \delta_{i,z}), \quad (134)$$

while for the magnetization components M_i we get

$$M_i = \frac{Ng_i \mu_B \mathcal{B}_i}{2 \sum_{\gamma=\pm 1} \cosh(\beta E_\gamma)} \sum_{\gamma=\pm 1} \frac{\sinh(\beta E_\gamma)}{E_\gamma} \times \left(1 + \gamma \frac{\Delta_{\text{SO}}^2 \delta_{i,z} + \mathcal{E}^2}{E_0^2}\right), \quad (135)$$

where again $i=x,y$. Making use of the above expressions, we can obtain the above defined susceptibilities

$$\chi_{E_i E_j} = \frac{P_i}{E_j} \delta_{ij} - \beta P_i P_j + \frac{Nd^4 E_i E_j}{2 \sum_{\gamma=\pm 1} \cosh(\beta E_\gamma)} \times \left[\sum_{\gamma=\pm 1} \frac{\beta E_\gamma \cosh(\beta E_\gamma) - \sinh(\beta E_\gamma)}{2E_\gamma^3} \left(1 + \gamma \frac{\mathcal{B}^2}{E_0^2}\right)^2 + \gamma \frac{\mathcal{B}^4 \sinh(\beta E_\gamma)}{E_0^6 E_\gamma} \right] = \chi_{E_i E_j}, \quad (136)$$

$$\chi_{B_i B_j} = \frac{M_i}{B_j} \delta_{ij} - \beta M_i M_j + \frac{Ng_i^2 g_j^2 B_i B_j}{2 \sum_{\gamma=\pm 1} \cosh(\beta E_\gamma)} \sum_{\gamma=\pm 1} \left[\frac{(\Delta_{\text{SO}}^2 \delta_{i,z} + \mathcal{E}^2)(\Delta_{\text{SO}}^2 \delta_{j,z} + \mathcal{E}^2) \sinh(\beta E_\gamma)}{E_0^6 E_\gamma} + \frac{\beta E_\gamma \cosh(\beta E_\gamma) - \sinh(\beta E_\gamma)}{2E_\gamma^3} \right] \times \left(1 + \gamma \frac{\Delta_{\text{SO}}^2 \delta_{i,z} + \mathcal{E}^2}{E_0^2}\right) \left(1 + \gamma \frac{\Delta_{\text{SO}}^2 \delta_{j,z} + \mathcal{E}^2}{E_0^2}\right) = \chi_{B_i B_j}, \quad (137)$$

$$\chi_{B_i E_j} = -\beta M_i P_j + \frac{Ng_i d^2 B_i E_j}{2 \sum_{\gamma=\pm 1} \cosh(\beta E_\gamma)} \sum_{\gamma=\pm 1} \left[\gamma \frac{(\Delta_{\text{SO}}^2 \delta_{i,z} + \mathcal{E}^2)(\Delta_{\text{SO}}^2 \delta_{j,z} + \mathcal{E}^2) \sinh(\beta E_\gamma)}{E_0^6 E_\gamma} + \frac{\beta E_\gamma \cosh(\beta E_\gamma) - \sinh(\beta E_\gamma)}{2E_\gamma^3} \right] \times \left(1 + \gamma \frac{\Delta_{\text{SO}}^2 \delta_{i,z} + \mathcal{E}^2}{E_0^2}\right) \left(1 + \gamma \frac{\mathcal{B}^2}{E_0^2}\right) (1 - \delta_{j,z}) = \chi_{B_i E_j}. \quad (138)$$

The polarization \mathbf{P} , magnetization \mathbf{M} , and susceptibilities χ , Eqs. (134)–(138), all depend on the spin-electric coupling constant d . In the following, we analyze the details of this dependence and identify the conditions suitable for extracting the value of d from the measurable quantities.

1. Polarization and magnetization

The in-plane polarization of the molecule as a function of the magnetic field is illustrated in Figs. 14 and 15. The polarization is a growing function of the magnetic field strength, and it gets reduced by the normal component of the field.

The low-temperature, $k_B T \ll \Delta_{\text{SO}}$, thermodynamic properties of a molecule with spin-electric coupling show a simple dependence on the strength of external electric and magnetic fields in the special cases of in-plane and out-of plane magnetic fields. We focus only on effects in leading orders in electric field under the realistic assumption that the electric dipole splitting is small compared to the SO splitting, i.e.,

$\mathcal{E} \ll \Delta_{\text{SO}}$. Also, we analyze two limiting cases: (i) $k_B T \ll \mathcal{E}$, i.e., low-temperature regime, and (ii) $k_B T \gg \mathcal{E}$, i.e., high temperature regime. However, we assume all temperatures (in both regimes) to satisfy $k_B T \ll \Delta_{\text{SO}}$ so that the spin-orbit split levels are well resolved. In the first case (i), we obtain for the polarization

$$P_i \approx \begin{cases} \frac{nd\mathcal{E}_i \mathcal{B}}{4\mathcal{E}\Delta_B} & \text{for } \mathcal{E} \ll \mathcal{B} \\ \frac{nd\Delta_{\text{SO}}^2 \mathcal{E}_i}{4\Delta_B^3} & \text{for } \mathcal{E} \gg \mathcal{B}, \end{cases} \quad (139)$$

while for the second situation (ii) we obtain

$$P_i = \frac{nd\Delta_{\text{SO}}^2 \mathcal{E}_i}{4\Delta_B^3} \left(1 + \frac{\mathcal{B}^2}{\Delta_{\text{SO}}^2} \beta \Delta_B\right), \quad (140)$$

with $\Delta_B = \sqrt{\mathcal{B}^2 + \Delta_{\text{SO}}^2}$ and $n=N/V$ the density of molecules in the crystal. We see that, for low temperatures, the electric

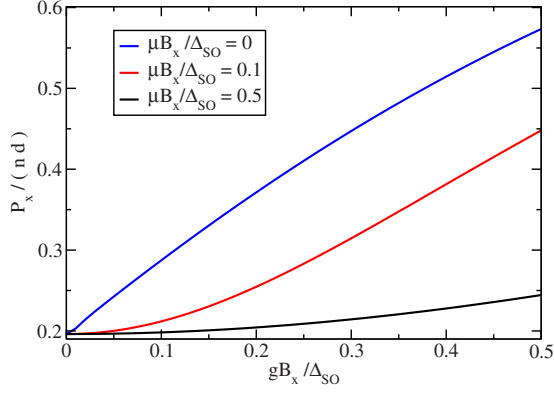


FIG. 14. (Color online) Electric polarization P_x (x component) in Eq. (134) as a function of the magnetic field in the x direction. The three lines correspond to various values of an additional external electric field in the z direction. The plot is for the temperature $k_B T = 0.001 \Delta_{SO}$, and the electric field $dE_x = 0.1 \Delta_{SO}$.

polarization P_i ranges from being independent of the magnitude of the electric field ($\mathcal{E} \ll \mathcal{B}$) to a linear dependence on the applied electric field E for large fields ($\mathcal{E} \gg \mathcal{B}$). Also, the polarization is strongly dependent on the magnetic field (linear in B) for low E fields, thus implying strong magnetoelectric response.

We now switch to the other special case, namely, when the external magnetic field is applied perpendicularly to the spin triangles. The electric polarization now reads

$$P_i = \frac{nd\mathcal{E}_i}{4\Delta_{\mathcal{E}}} \tanh(\beta\Delta_{\mathcal{E}}), \quad (141)$$

with $\Delta_{\mathcal{E}} = \sqrt{\Delta_{SO}^2 + \mathcal{E}^2}$. The polarization P_i does not depend on the magnetic field B , and there are no spin-electric effects present for this particular case.

Our results suggest that the spin-electric coupling can be detected by measuring the polarization of the crystal of triangular single molecule antiferromagnets that lie in parallel planes in the in-plane electric and magnetic fields.

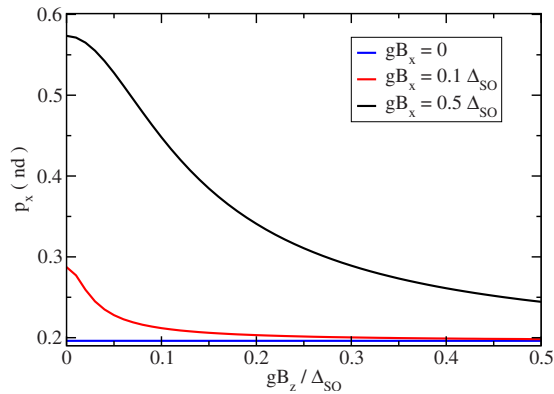


FIG. 15. (Color online) Electric polarization P_x (x component) in Eq. (134) as a function of the magnetic field in the z direction. The three lines correspond to various values of the external magnetic field in the x direction. The plot is for the temperature $k_B T = 0.001 \Delta_{SO}$, and the electric field $dE_x = 0.1 \Delta_{SO}$.

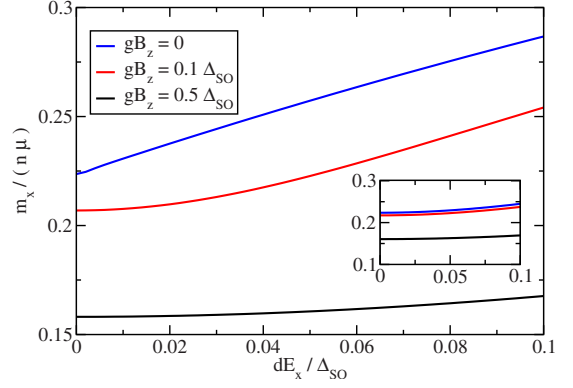


FIG. 16. (Color online) In-plane magnetization M_x in the x direction in Eq. (135) as a function of the electric field E_x in the x direction. The three lines correspond to a fixed value of an additional magnetic field in the z direction. The assumed temperature is $k_B T = 0.001 \Delta_{SO}$, while in the inset it is at higher temperature $k_B T = 0.1 \Delta_{SO}$.

The out-of plane component M_z of the molecule's magnetization is rather insensitive to the electric fields since any effect of the applied in-plane electric field has to compete with the spin-orbit coupling induced zero-field splitting Δ_{SO} . Since we expect to find weak coupling to electric field and small coupling constant d , it would require very strong electric fields to achieve the regime $d|E| \sim \Delta_{SO}$. The in-plane components of magnetization M_x and M_y , on the other hand, show clear dependence on electric fields, Fig. 16. At low magnetic fields the in-plane component of polarization appears and grows with the strength of in-plane electric fields. However, the electric field dependence becomes less pronounced when an additional magnetic field is applied normal to the triangle's plane.

In the dependence of the magnetization on electric fields, and for the case of an in-plane magnetic field, we find the same two main regimes as in the study of the polarization: $\mathcal{E} \gg k_B T$ (i) and $\mathcal{E} \ll k_B T$ (ii). In the first case (i) we obtain

$$M_i \approx \frac{ng_i \mu_B \mathcal{B}_i}{4\Delta_{\mathcal{B}}} \left(1 + \frac{\mathcal{E} \Delta_{SO}^2}{\mathcal{B} \Delta_{\mathcal{B}}^2} \right), \quad (142)$$

while for the second case (ii) we get

$$M_i = \frac{ng_{\perp} \mu_B \mathcal{B}_i}{4\Delta_{\mathcal{B}}} \left[1 - \frac{3\mathcal{E}^2 \Delta_{SO}^2}{2\Delta_{\mathcal{B}}^4} \left(1 - \frac{\beta \Delta_{\mathcal{B}}}{3} \right) \right]. \quad (143)$$

The magnetization shows a strong dependence on the electric field E , especially for $\mathcal{E} \gg \mathcal{B}$ where this is linear in E field. For low electric fields, however, the magnetization shows only a weak dependence on the electric field, both at low and high temperatures.

For the magnetization (along z) in the presence of a perpendicular (also along z) magnetic field we obtain

$$M_z = \frac{ng_z \mu_B}{4} \tanh(\beta \mathcal{B}), \quad (144)$$

which is manifestly independent of the spin-electric coupling constant d .

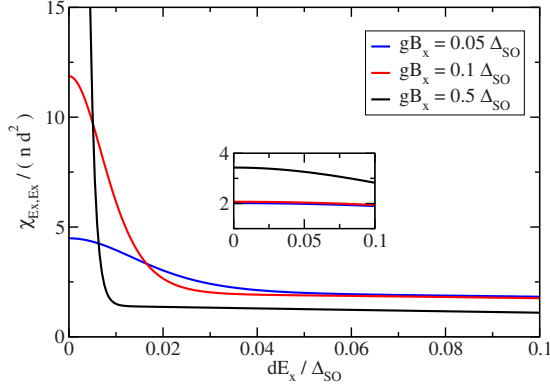


FIG. 17. (Color online) Electric susceptibility (xx component), Eq. (136), as a function of the electric field in x direction. The three lines correspond to various values of the external magnetic field in the x direction. The plot is for the temperature $k_B T = 0.001 \Delta_{SO}$. In the inset, the same quantity is plotted at a higher temperature, $k_B T = 0.1 \Delta_{SO}$.

2. Susceptibilities

The effects of spin-electric coupling on the polarization of a molecule show up in the electric susceptibility and the spin-electric susceptibility. In Figs. 17 and 18, we plot the xx and xy components of the electric susceptibility tensor as a function of electric field for various strengths and orientations of an additional magnetic field. Both susceptibilities show a high peak in the region of weak electric fields that is suppressed by in-plane magnetic fields. The peaks are pronounced at low temperatures and vanish as the temperature exceeds the splitting of the two lowest-energy levels, $k_B T \gg d|\mathbf{E}_{\parallel}|$.

In the case of in-plane magnetic field, and weak coupling to the electric field $d|\mathbf{E}| \ll \Delta_{SO}$, we can calculate the electric $\chi_{E_i E_j}$ and spin-electric $\chi_{E_i B_j}$ susceptibilities in the two limiting cases (i) and (ii) defined above, with $i=x, y$. For the electric susceptibility we obtain

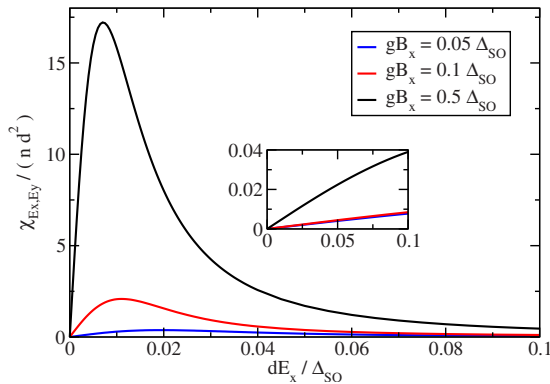


FIG. 18. (Color online) Electric susceptibility (xy component), Eq. (136), as a function of the electric field in x direction. The three lines correspond to various values of the external magnetic field in the x direction. The plot is for the temperature $k_B T = 0.001 \Delta_{SO}$. In the inset the same quantity is plotted at a higher temperature $k_B T = 0.1 \Delta_{SO}$.

$$\chi_{E_i E_j} \approx \begin{cases} \frac{nd^2 \mathcal{B}(\mathcal{E}^2 \delta_{ij} - \mathcal{E}_i \mathcal{E}_j)}{4\mathcal{E}^3 \Delta_B} & \text{for } \mathcal{E} \ll \mathcal{B} \\ \frac{nd^2 \Delta_{SO}^2 \delta_{ij}}{4\Delta_B^3} & \text{for } \mathcal{E} \gg \mathcal{B} \end{cases} \quad (145)$$

in the first case (i), and

$$\chi_{E_i E_j} \approx \frac{nd \Delta_{SO}^2 \delta_{ij}}{4\Delta_B^3} \left(1 + \frac{\mathcal{B}^2}{\Delta_{SO}^2} \beta \Delta_B \right). \quad (146)$$

in the second case (ii). We see that for low E fields, the electric susceptibility $\chi_{E_i E_j}$ depends strongly on the applied electric field, and even vanishes if the field is applied, say, along the x or y directions. For large E fields instead, the electric susceptibility becomes independent of the electric field itself and, for low magnetic fields (i.e., for $\mathcal{B} \ll \Delta_{SO}$) this reduces to a constant value $\chi_{E_i E_j} = \delta_{ij} n d^2 / 4 \Delta_{SO}$. At finite (large) temperatures the electric susceptibility is still independent of the electric field, but it is enhanced by thermal effects $\sim 1/T$.

For the electric susceptibilities $\chi_{E_i E_j}$ in perpendicular magnetic field, we obtain

$$\chi_{E_i E_j} = \frac{nd^2}{4\Delta_{\mathcal{E}}} \left(\delta_{ij} - \frac{\mathcal{E}_i \mathcal{E}_j}{\Delta_{\mathcal{E}}} \right), \quad (147)$$

where we assumed $\Delta_{SO} \gg k_B T$, as in the previous section. As expected, there is no dependence of $\chi_{E_i E_j}$ on the B field, and for vanishing electric field the electric susceptibility reduces to a constant $\chi_{E_i E_j} = \delta_{ij} n d^2 / 4 \Delta_{SO}$.

The quantity of most interest in the present spin system is the spin-electric susceptibility $\chi_{E_i B_j}$, i.e., the magnetic response (electric response) in electric fields (magnetic fields). The nonzero spin-electric susceptibility allows for the electric control of magnetization and magnetic control of polarization in the crystals of triangular MNs, even in the case when the coupling between the molecules is negligible. In addition, $\chi_{E_i B_j}$ is nonzero only in the presence of spin-electric coupling, i.e., when $d \neq 0$.

The spin-electric susceptibility shows a characteristic peak in weak electric fields which vanishes in an external magnetic field, see Figs. 19 and 20. The peak in the diagonal xx component, $\chi_{E_x B_x}$, moves toward the higher electric fields and broadens as the magnetic field B_x increases. The peak in the off-diagonal component $\chi_{E_x B_z}$, on the other hand, shifts toward the lower electric fields and narrows as the in-plane magnetic field increases. Both peaks disappear at high temperatures, $k_B T \gg \Delta_{SO}$.

For in-plane magnetic fields and weak spin-electric coupling the spin-electric susceptibility $\chi_{E_i B_j}$ is

$$\chi_{E_i B_j} \approx \frac{nd g_j \mu_B \mathcal{E}_i B_j \Delta_{SO}^2}{4\mathcal{E} \mathcal{B} \Delta_B^3} \quad (148)$$

for the low temperature case (i), while for the second case (ii) we obtain

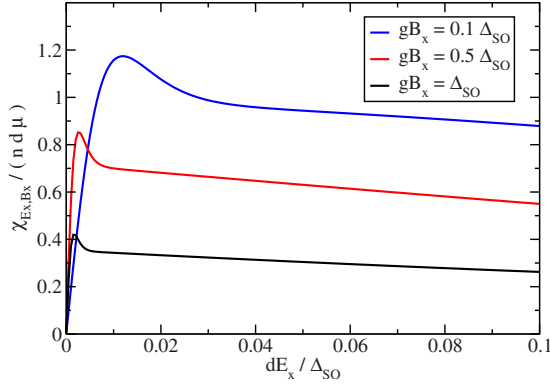


FIG. 19. (Color online) Linear magnetoelectric tensor (xx component) in Eq. (138) as a function of the electric field in the x direction. The three lines correspond to various values of the external magnetic field in the x direction. The plot is for the temperature $k_B T = 0.001 \Delta_{SO}$.

$$\chi_{E_i B_j} \approx -\frac{3n\Delta_{SO}^2 d g_j \mu_B \mathcal{E}_i \mathcal{B}_j}{4\Delta_B^5} \left(1 - \frac{\beta \Delta_B}{3}\right). \quad (149)$$

By inspecting the above expression, we can infer that for low temperatures and low E fields the spin-electric susceptibility shows no dependence on the absolute value of the electric field E and only a weak dependence on the applied magnetic field B . Moreover, when both fields are applied along one special direction, say, along x , and assuming also $B \ll \Delta_{SO}$, the spin-electric susceptibility becomes $\chi_{E_x B_x} = n d g_i \mu_B / 4 \Delta_{SO}$, i.e., it reaches a constant value. The finite temperature expression shows that the spin-electric response is reduced, as opposed to the electric response where temperature increases the response. Thus, for strong spin-electric response one should probe the spin system at low temperatures ($k_B T \ll \Delta_{SO}$) (Fig. 21).

The diagonal out-of-plane component of the magnetic susceptibility, $\chi_{B_z B_z}$, in the presence of an external magnetic field in the x direction decays strongly in the applied electric

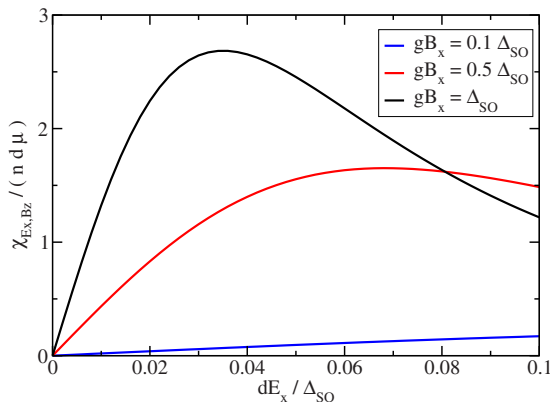


FIG. 20. (Color online) Linear magnetoelectric tensor (xz component) in Eq. (138) as a function of the electric field in the x direction. The three lines correspond to various values of the external electric field in the x direction. The plot is for the temperature $k_B T = 0.001 \Delta_{SO}$.

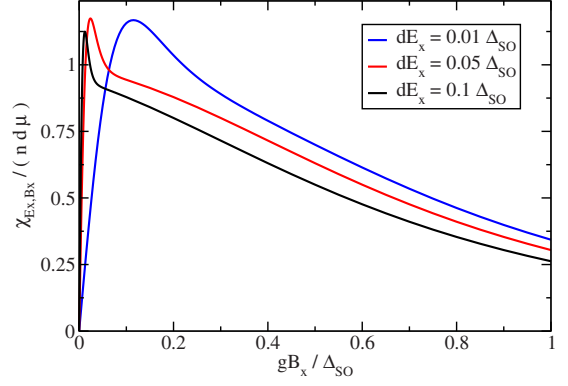


FIG. 21. (Color online) Linear magnetoelectric tensor (xx component) in Eq. (138) as a function of the magnetic field in the x direction. The three lines correspond to various values of the external electric field in the x direction. The plot is for the temperature $k_B T = 0.001 \Delta_{SO}$.

field along the x direction, Fig. 22. In electric fields, the $\chi_{B_x B_x}$ component shows a peak that is reduced by the application of the magnetic field in the x direction, Fig. 23.

We can derive the magnetic susceptibilities in the two regimes. In the first case (i) we obtain (assuming now only linear effects in E field)

$$\chi_{B_i B_j} = \frac{n g_{\perp}^2 \mu_B^2}{2\Delta_B} \left[\delta_{ij} - \frac{\mathcal{B}_i \mathcal{B}_j}{\Delta_B^2} + \frac{\mathcal{E} \Delta_{SO}^2}{\mathcal{B} \Delta_B^2} \left(\delta_{ij} - \frac{(3\mathcal{B}^2 + \Delta_B^2) \mathcal{B}_i \mathcal{B}_j}{\mathcal{B}^2 \Delta_B^2} \right) \right], \quad (150)$$

with $i, j = x, y$, while

$$\chi_{B_z B_z} = \frac{n g_z^2 \mu_B^2 \Delta_{SO}^2}{2\Delta_B \mathcal{B} \mathcal{E}} \quad (151)$$

for $\mathcal{B}_z \Delta_{SO} \ll \mathcal{B} \mathcal{E}$. At low temperatures the in-plane magnetic susceptibility shows a linear dependence on the applied electric field E , thus allowing for a simple estimate of the electric dipole parameter d from magnetic measurements. Note that

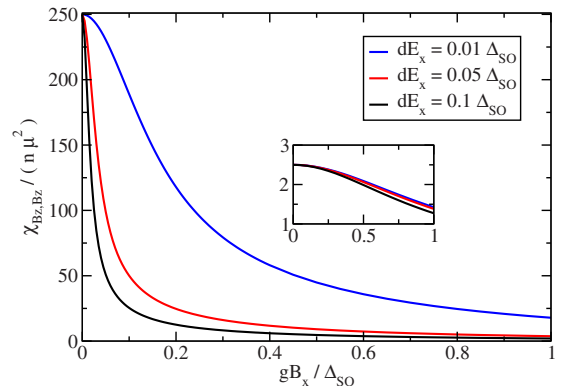


FIG. 22. (Color online) Magnetic susceptibility (zz component) in Eq. (137) as a function of the magnetic field in the x direction. The three lines correspond to various values of the external electric field in the x direction. The plot is for the temperature $k_B T = 0.001 \Delta_{SO}$. The inset represents the same quantity at a higher temperature $k_B T = 0.1 \Delta_{SO}$.

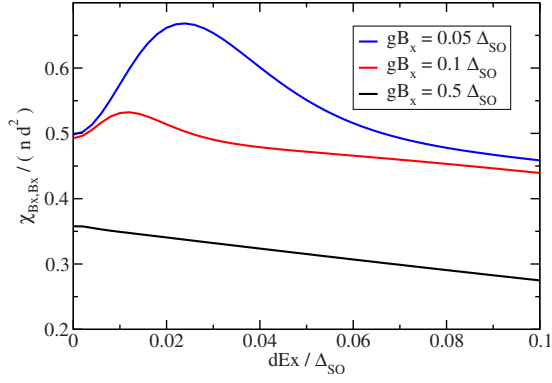


FIG. 23. (Color online) Magnetic susceptibility (xx component), Eq. (137) as a function of the electric field in the x direction. The three lines correspond to various values of the additional magnetic field in the z direction. The plot is for the temperature $k_B T = 0.001 \Delta_{SO}$.

for strong electric fields ($\mathcal{E} \gg B$), the magnetic susceptibility can vanish since the magnetization does not depend on the magnetic field anymore. However, such a regime would not help to identify the electric dipole coupling strength d from susceptibility measurements directly. The perpendicular magnetic susceptibility shows a strong electric field dependence $\chi_{B_z, B_z} \sim \mathcal{E}^{-1}$ and can be used as an efficient probe for extracting the electric dipole parameter d . In the second case (ii) we obtain

$$\chi_{B_i B_j} = \frac{ng_z^2 \mu_B^2}{2\Delta_B} \left[\delta_{ij} - \frac{B_i B_j}{\Delta_B^2} - \frac{\mathcal{E}^2 \Delta_{SO}^2}{\Delta_B^4} \left(\frac{3}{2} \left(\delta_{ij} + \frac{B_i B_j}{\Delta_B^2} \right) - \beta \Delta_B \left(\delta_{ij} + \frac{4B_i B_j}{\Delta_B^2} \right) \right) \right], \quad (152)$$

when $i, j = x, y$, and

$$\chi_{B_z B_z} = \frac{ng_z^2 \mu_B^2 B^2}{2\Delta_B^3} \left(1 + \beta \Delta_B \frac{\Delta_{SO}^2}{B^2} \right). \quad (153)$$

The magnetic response increases with temperature. Also, in this limit the dependence of the magnetic susceptibility on the applied electric field is rather weak ($\chi_{B_i B_j}(\mathcal{E}) \sim \mathcal{E}^2$), thus this regime is also not suitable for observing spin-electric effects.

For the magnetic susceptibility in the perpendicular magnetic field we find

$$\chi_{B_z B_z} = \frac{\beta ng_z^2 \mu_B^2}{4} \operatorname{sech}(\beta B), \quad (154)$$

while for the in-plane magnetic susceptibility $\chi_{B_{x(y)B_{x(y)}}$ we obtain

$$\chi_{B_{x(y)B_{x(y)}}} = \frac{ng_z^2 \mu_B^2 \Delta_{SO}}{2(B^2 - \Delta_{SO}^2)} \left[\frac{B}{\Delta_{SO}} \left(1 - \frac{\mathcal{E}^2}{B^2} \right) \tanh(\beta B) - 1 \right] \quad (155)$$

in the limit $B, k_B T \ll \Delta_{SO}$. We mention that for B perpendicular to the molecular plane there is no electric field E (mag-

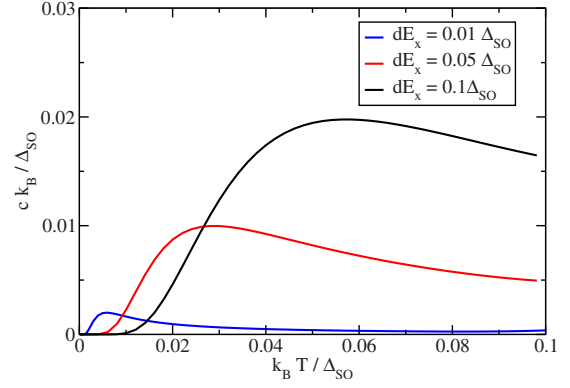


FIG. 24. (Color online) Heat capacity, Eq. (156), as a function of temperature in various electric fields.

netic field B) dependence of the magnetization M_i (electric polarization P_i). Thus, in order to see spin-electric effects one needs to apply magnetic fields which have nonzero in-plane components.

D. Heat capacity

Next we investigate the dependence of the heat capacity on the applied electric and magnetic fields in different regimes. The heat capacity is defined as $C = -\partial/\partial T(\partial \ln(Z)/\partial \beta)$ so that we obtain

$$C = \frac{Nk_B \beta^2}{4} \sum_{p=\pm 1} \frac{(E_1 + pE_{-1})^2}{\cosh^2 \left[\frac{\beta(E_1 + pE_{-1})}{2} \right]}. \quad (156)$$

We consider the cases of perpendicular B field and in-plane B field in the limit $\Delta_{SO} \gg k_B T$. In the first case, i.e., for $B \parallel z$ we obtain

$$C \approx Nk_B \beta^2 \begin{cases} \Delta_{SO}^2 e^{-2\beta \Delta_{SO}} + B^2 e^{-2\beta B}, & B \gg k_B T \\ \Delta_{SO}^2 e^{-2\beta \Delta_{SO}} + \frac{B^2}{4}, & B \ll k_B T. \end{cases} \quad (157)$$

The heat capacity C shows a quadratic dependence on the applied electric field for the entire range of E -field strengths. On the other hand, the magnetic field dependence of C is nonmonotonic and shows a maximum for some finite B -field strength $B_{\max} \approx k_B T$. In the second situation, i.e., for $B \perp z$ we get

$$C \approx Nk_B \beta^2 \begin{cases} \frac{B^2 \mathcal{E}^2}{\Delta_B^2} e^{-2(\beta B \mathcal{E} / \Delta_B)} + \Delta_B^2 e^{-2\beta \Delta_B}, & \mathcal{E} \gg k_B T \\ \frac{B^2 \mathcal{E}^2}{4\Delta_B^2}, & \mathcal{E} \ll k_B T. \end{cases} \quad (158)$$

As in the previous case, the dependence of the heat capacity C is linear in E field for low E fields. However, for large E fields the dependence is nonmonotonic and thus shows a maximum for some finite electric field strength $\mathcal{E}_{\max} \approx k_B T$.

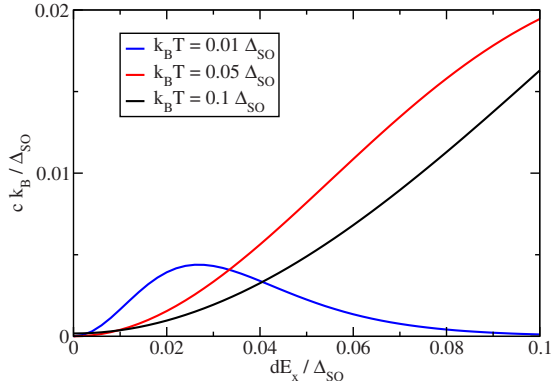


FIG. 25. (Color online) Heat capacity, Eq. (156), at low temperature as a function of external electric field.

Note that in this case also the dependence on the magnetic field is nonmonotonic, and thus we obtain a second maximum for $B_{\max} \simeq k_B T$. The effects of the spin-electric coupling on the heat capacity are illustrated in Figs 24 and 25. We can conclude from the above expressions that the strongest dependence of the heat capacity on the electric field is when the magnetic field is applied in plane, and then it is mostly quadratic.

For the derivation of all the thermodynamic quantities presented in the previous sections, we have restricted ourselves to the contributions arising from only the lowest four states, even though the spin system spans eight states in total. This description is valid if the splitting between the energies of $S=1/2$ and $S=3/2$ states is much larger than the temperature $k_B T$. This splitting varies strongly with the applied magnetic field for $B=3J/4$ one of the $S=3/2$ states ($M=-3/2$) crossing the $M=1/2$ of the $S=1/2$ states and, even more, for $B>3J/2$ the $M=-3/2$ becomes the spin system ground states. Thus, for large magnetic fields our effective description in terms of only the $S=1/2$ states breaks down and one have to reconsider the previous quantities in this limit.

V. CONCLUSIONS

Electric fields can be applied at very short spatial and temporal scales, which makes them preferable for quantum information processing applications over the more standard magnetic fields. Molecular nanomagnets, while displaying rich quantum dynamics, have not yet been shown to respond to electric fields in experiments. We have investigated theoretically the possibility of spin-electric coupling in molecular nanomagnets using symmetry analysis and found that the spin-electric coupling is possible in antiferromagnetic ground-state manifolds of spin-1/2 and spin-3/2 triangles, as well as in spin-1/2 pentagon. The spin-electric coupling in the triangle can exist even in the absence of spin-orbit coupling, while the coupling in the pentagon requires the spin-orbit interaction in the molecule. We have characterized the form of the spin-electric coupling in all of these molecules and presented the selection rules for the transitions between the spin states induced by electric fields.

While the symmetry can predict the presence or absence of the spin-electric coupling, it cannot predict the size of the

corresponding coupling constant. In order to find a molecule suitable for electric manipulation, it is necessary to have an estimate of the spin-electric coupling strength. For this purpose, we have described the molecular nanomagnets in terms of the Hubbard model and related the coupling constants of the symmetry-based models to the hopping and on-site energy parameters of the Hubbard model. We have found that the modification of the Hubbard model parameters due to the electric field produces a spin-electric coupling of the same form as predicted by the symmetry analysis. However, within the Hubbard model, the coupling constants have a clear and intuitive meaning in terms of the hopping and on-site energies of the localized electrons. We have also studied the superexchange interaction of the spins on the magnetic centers through the bridge. If we assume that the interaction of the localized spins is a property of the bridge alone, the spin-electric coupling can be calculated by *ab initio* analysis of the bridge alone, and not of the entire molecule.

Finally, we analyzed the role of spin-electric coupling in standard experimental setups typically used for the characterization of molecular nanomagnets. We find that the spin-electric coupling can be detected in the ESR and NMR spectra that probe the local spins. Also, thermodynamic quantities, like the polarization, magnetization, linear magnetoelectric effect, and the specific heat, show signatures of spin-electric coupling in the triangular molecules. Thus, our results set a path toward finding suitable molecules that exhibit spin-electric effects and how they can be identified experimentally.

In this work, we have focused on the spin rings with an odd number of magnetic centers (odd spin rings), whose low-energy spectrum is dominated by frustration effects. The odd spin rings, due to frustration, possess a fourfold degenerate ground state multiplet, which can be split by electric fields. As opposed to the odd spin rings, the ground states of even-spin rings is usually a nondegenerate $S=0$ state, separated from the higher energy states by a gap of the order of exchange coupling J . Coupling of the electric field to these states can thus proceed only via excited states, and the coupling strength is reduced by $d|E|/J$. Similarly, in odd-spin rings where the spin frustration is removed by a lowered symmetry, the ground-state multiplet consists of an $S=1/2$ Kramers doublet, which cannot be split by electric fields. Therefore, the odd spin rings with equivalent magnetic centers seem to be the most suitable candidates for observing the spin-electric coupling and using it for quantum control of spins.

ACKNOWLEDGMENTS

We thank M. Affronte and V. Bellini for useful discussions. We acknowledge financial support from the Swiss NSF, the NCCR Nanoscience Basel, the Italian MIUR under FIRB Contract No. RBIN01EY74, the EU under ‘‘MagMaNet’’ and ‘‘MolSpinQIP,’’ and the Italian CNR under the Short Term Mobility Program 2010.

APPENDIX A: SPIN STATES IN TERMS OF THE c_{Γ}^{\dagger} OPERATORS

In this appendix, we show the expressions for the three-electron symmetry-adapted states $|\psi_{\Gamma}^{i,\sigma}\rangle$ in Eqs. (29) and (37)

in terms of the symmetry adapted creation operators $c_{\Gamma,\sigma}^\dagger$. Making use of Eq. (46) we obtain

$$|\psi_{A_2}^{1\sigma}\rangle = \frac{i\epsilon}{\sqrt{3}}(c_{A_1\sigma}^\dagger c_{E_+\sigma}^\dagger c_{E_-\sigma}^\dagger + c_{E_+\sigma}^\dagger c_{E_-\sigma}^\dagger c_{A_1\sigma}^\dagger - c_{E_-\sigma}^\dagger c_{E_+\sigma}^\dagger c_{A_1\sigma}^\dagger)|0\rangle, \quad (\text{A1})$$

$$|\psi_{E_+}^{1\sigma}\rangle = \frac{i}{\sqrt{3}}(c_{A_1\sigma}^\dagger c_{A_1\sigma}^\dagger c_{E_+\sigma}^\dagger + \epsilon c_{E_+\sigma}^\dagger c_{E_+\sigma}^\dagger c_{E_-\sigma}^\dagger + \bar{\epsilon} c_{E_-\sigma}^\dagger c_{E_-\sigma}^\dagger c_{A_1\sigma}^\dagger)|0\rangle, \quad (\text{A2})$$

$$|\psi_{E_-}^{1\sigma}\rangle = \frac{i}{\sqrt{3}}(c_{A_1\sigma}^\dagger c_{A_1\sigma}^\dagger c_{E_-\sigma}^\dagger + \epsilon c_{E_-\sigma}^\dagger c_{E_-\sigma}^\dagger c_{E_+\sigma}^\dagger + \bar{\epsilon} c_{E_+\sigma}^\dagger c_{E_+\sigma}^\dagger c_{A_1\sigma}^\dagger)|0\rangle, \quad (\text{A3})$$

$$|\psi_{A_1}^{2\sigma}\rangle = \frac{\sigma\epsilon}{\sqrt{2}}(c_{E_+\sigma}^\dagger c_{A_1\sigma}^\dagger c_{E_-\sigma}^\dagger + c_{E_-\sigma}^\dagger c_{A_1\sigma}^\dagger c_{E_+\sigma}^\dagger)|0\rangle, \quad (\text{A4})$$

$$|\psi_{A_2}^{2\sigma}\rangle = -\frac{i\sigma\epsilon}{\sqrt{6}}(2c_{A_1\sigma}^\dagger c_{E_+\sigma}^\dagger c_{E_-\sigma}^\dagger + c_{E_+\sigma}^\dagger c_{A_1\sigma}^\dagger c_{E_-\sigma}^\dagger - c_{E_-\sigma}^\dagger c_{A_1\sigma}^\dagger c_{E_+\sigma}^\dagger) \times |0\rangle, \quad (\text{A5})$$

$$|\psi_{E_+}^{2\sigma}\rangle = \frac{\sigma}{\sqrt{2}}(\bar{\epsilon} c_{A_1\sigma}^\dagger c_{A_1\sigma}^\dagger c_{E_+\sigma}^\dagger + \epsilon c_{E_-\sigma}^\dagger c_{A_1\sigma}^\dagger c_{E_-\sigma}^\dagger)|0\rangle, \quad (\text{A6})$$

$$|\psi_{E_-}^{2\sigma}\rangle = \frac{\sigma}{\sqrt{2}}(\bar{\epsilon} c_{A_1\sigma}^\dagger c_{A_1\sigma}^\dagger c_{E_-\sigma}^\dagger + \epsilon c_{E_+\sigma}^\dagger c_{A_1\sigma}^\dagger c_{E_+\sigma}^\dagger)|0\rangle, \quad (\text{A7})$$

$$|\psi_{E_+}^{2\sigma}\rangle = \frac{i\sigma\bar{\epsilon}}{\sqrt{6}}(c_{A_1\sigma}^\dagger c_{A_1\sigma}^\dagger c_{E_+\sigma}^\dagger - \bar{\epsilon} c_{E_-\sigma}^\dagger c_{A_1\sigma}^\dagger c_{E_-\sigma}^\dagger - 2\epsilon c_{E_+\sigma}^\dagger c_{E_+\sigma}^\dagger c_{E_-\sigma}^\dagger) \times |0\rangle, \quad (\text{A8})$$

$$|\psi_{E_-}^{2\sigma}\rangle = \frac{i\sigma\bar{\epsilon}}{\sqrt{6}}(c_{A_1\sigma}^\dagger c_{A_1\sigma}^\dagger c_{E_-\sigma}^\dagger - \bar{\epsilon} c_{E_+\sigma}^\dagger c_{A_1\sigma}^\dagger c_{E_+\sigma}^\dagger - 2\epsilon c_{E_-\sigma}^\dagger c_{E_-\sigma}^\dagger c_{E_+\sigma}^\dagger) \times |0\rangle, \quad (\text{A9})$$

where σ stands above for sign(σ).

APPENDIX B: H_{SO} , $H_{\text{e-d}}^0$, AND $H_{\text{e-d}}^1$ MATRIX ELEMENTS

For the SOI matrix elements we obtain

$$\langle \psi_{A_1}^{2\sigma} | H_{\text{SO}} | \psi_{A_2}^{1\sigma} \rangle = \frac{2i\lambda_{\text{SO}}}{\sqrt{2}} \sigma, \quad (\text{B1})$$

$$\langle \psi_{E_\pm}^{2\sigma} | H_{\text{SO}} | \psi_{E_\pm}^{1\sigma} \rangle = \pm \frac{i\bar{\epsilon}\lambda_{\text{SO}}}{\sqrt{2}} \sigma, \quad (\text{B2})$$

$$\langle \psi_{E_\pm}^{2\sigma} | H_{\text{SO}} | \psi_{E_\pm}^{1\sigma} \rangle = \pm \frac{\sqrt{3}\epsilon\lambda_{\text{SO}}}{\sqrt{2}} \sigma, \quad (\text{B3})$$

$$\langle \psi_{A_1}^{2\sigma} | H_{\text{SO}} | \psi_{A_2}^{2\sigma} \rangle = -\sigma 2\lambda_{\text{SO}}, \quad (\text{B4})$$

$$\langle \psi_{E_\pm}^{2\sigma} | H_{\text{SO}} | \psi_{E_\pm}^{2\sigma} \rangle = \pm \sigma \frac{\sqrt{3}}{2} \lambda_{\text{SO}}, \quad (\text{B5})$$

$$\langle \psi_{E_\pm}^{2\sigma} | H_{\text{SO}} | \psi_{E_\pm}^{2\sigma} \rangle = \pm \frac{i\lambda_{\text{SO}}}{2} \sigma, \quad (\text{B6})$$

$$\langle \psi_{E_\pm}^{2\sigma} | H_{\text{SO}} | \psi_{E_\pm}^{2\sigma} \rangle = \mp \sigma \frac{\sqrt{3}}{2} \lambda_{\text{SO}}, \quad (\text{B7})$$

while the remaining terms are equal to zero. For the electric dipole matrix elements we obtain

$$\langle \psi_{E_-}^{2\sigma} | H_{\text{e-d}}^0 | \psi_{E_+}^{2\sigma} \rangle = \frac{a}{2}((\bar{\epsilon}-1)E_x + \epsilon\sqrt{3}E_y), \quad (\text{B8})$$

$$\langle \psi_{E_-}^{2\sigma} | H_{\text{e-d}}^0 | \psi_{E_+}^{2\sigma} \rangle = \frac{a}{2}\left(\epsilon E_x + \frac{1-\bar{\epsilon}}{\sqrt{3}}E_y\right), \quad (\text{B9})$$

$$\langle \psi_{E_-}^{2\sigma} | H_{\text{e-d}}^0 | \psi_{E_+}^{2\sigma} \rangle = -\frac{a}{2}\left(\epsilon E_x + \frac{1-\bar{\epsilon}}{\sqrt{3}}E_y\right), \quad (\text{B10})$$

$$\langle \psi_{E_-}^{2\sigma} | H_{\text{e-d}}^0 | \psi_{E_+}^{2\sigma} \rangle = -\frac{a}{2}((\bar{\epsilon}-1)E_x + \epsilon\sqrt{3}E_y), \quad (\text{B11})$$

$$\langle \psi_{E_-}^{1\sigma} | H_{\text{e-d}}^1 | \psi_{E_+}^{2\sigma} \rangle = -\frac{i\epsilon E}{\sqrt{6}}(\epsilon d_{EE}^* - 2\bar{\epsilon}d_{AE}^* - d_{AE}), \quad (\text{B12})$$

$$\langle \psi_{E_+}^{1\sigma} | H_{\text{e-d}}^1 | \psi_{E_-}^{2\sigma} \rangle = \frac{i\bar{\epsilon}E}{\sqrt{6}}(\epsilon d_{EE} + 2\bar{\epsilon}d_{AE}^* + d_{AE}), \quad (\text{B13})$$

$$\langle \psi_{E_-}^{1\sigma} | H_{\text{e-d}}^1 | \psi_{E_+}^{2\sigma} \rangle = \frac{\epsilon E}{\sqrt{2}}(\epsilon d_{EE}^* + d_{AE}), \quad (\text{B14})$$

$$\langle \psi_{E_+}^{1\sigma} | H_{\text{e-d}}^1 | \psi_{E_-}^{2\sigma} \rangle = -\frac{\bar{\epsilon}E}{\sqrt{2}}(\epsilon d_{EE} - d_{AE}), \quad (\text{B15})$$

$$\langle \psi_{E_-}^{1\sigma} | H_{\text{e-d}}^1 | \psi_{E_+}^{1\sigma} \rangle = 0. \quad (\text{B16})$$

- ¹D. Gatteschi, R. Sessoli, and J. Villain, *Molecular Nanomagnets* (Oxford University Press, Oxford, 2006).
- ²D. Gatteschi and R. Sessoli, *Angew. Chem., Int. Ed.* **42**, 268 (2003).
- ³M. Leuenberger and D. Loss, *Nature (London)* **410**, 789 (2001).
- ⁴E. M. Chudnovsky and L. Gunther, *Phys. Rev. Lett.* **60**, 661 (1988).
- ⁵D. D. Awschalom, J. F. Smyth, G. Grinstein, D. P. DiVincenzo, and D. Loss, *Phys. Rev. Lett.* **68**, 3092 (1992).
- ⁶R. Sessoli, D. Gatteschi, A. Caneschi, and M. A. Novak, *Nature (London)* **365**, 141 (1993).
- ⁷L. Thomas, F. Lioni, R. Ballou, D. Gatteschi, R. Sessoli, and B. Barbara, *Nature (London)* **383**, 145 (1996).
- ⁸J. R. Friedman, M. P. Sarachik, J. Tejada, and R. Ziolo, *Phys. Rev. Lett.* **76**, 3830 (1996).
- ⁹W. Wernsdorfer, E. Bonet Orozco, K. Hasselbach, A. Benoit, D. Maily, O. Kubo, H. Nakano, and B. Barbara, *Phys. Rev. Lett.* **79**, 4014 (1997).
- ¹⁰J. Tejada, X. X. Zhang, E. del Barco, J. M. Hernández, and E. M. Chudnovsky, *Phys. Rev. Lett.* **79**, 1754 (1997).
- ¹¹E. del Barco, A. D. Kent, E. M. Rumberger, D. N. Hendrickson, and G. Christou, *Phys. Rev. Lett.* **91**, 047203 (2003).
- ¹²D. Gatteschi, A. Caneschi, L. Pardi, and R. Sessoli, *Science* **265**, 1054 (1994).
- ¹³C. Sangregorio, T. Ohm, C. Paulsen, R. Sessoli, and D. Gatteschi, *Phys. Rev. Lett.* **78**, 4645 (1997).
- ¹⁴D. Gatteschi, R. Sessoli, and A. Cornia, *Chem. Commun. (Cambridge)* (2000) 725.
- ¹⁵A. Chiolero and D. Loss, *Phys. Rev. Lett.* **80**, 169 (1998).
- ¹⁶F. Meier and D. Loss, *Phys. Rev. Lett.* **86**, 5373 (2001).
- ¹⁷M. N. Leuenberger and D. Loss, *Phys. Rev. B* **61**, 12200 (2000).
- ¹⁸I. Chiorescu, W. Wernsdorfer, A. Müller, H. Bögge, and B. Barbara, *Phys. Rev. Lett.* **84**, 3454 (2000).
- ¹⁹I. Chiorescu, W. Wernsdorfer, A. Müller, H. Bögge, and B. Barbara, *J. Magn. Magn. Mater.* **221**, 103 (2000).
- ²⁰O. Waldmann, R. Koch, S. Schromm, P. Müller, I. Bernt, and R. W. Saalfrank, *Phys. Rev. Lett.* **89**, 246401 (2002).
- ²¹D. Loss, D. P. DiVincenzo, and G. Grinstein, *Phys. Rev. Lett.* **69**, 3232 (1992).
- ²²M. N. Leuenberger and D. Loss, *Phys. Rev. B* **61**, 1286 (2000).
- ²³M. N. Leuenberger, F. Meier, and D. Loss, *Monatsch. Chem.* **134**, 217 (2003).
- ²⁴W. Wernsdorfer and R. Sessoli, *Science* **284**, 133 (1999).
- ²⁵M. N. Leuenberger and D. Loss, *Phys. Rev. B* **63**, 054414 (2001).
- ²⁶G. González and M. N. Leuenberger, *Phys. Rev. Lett.* **98**, 256804 (2007).
- ²⁷G. González, M. N. Leuenberger, and E. R. Mucciolo, *Phys. Rev. B* **78**, 054445 (2008).
- ²⁸F. Troiani, A. Ghirri, M. Affronte, S. Carretta, P. Santini, G. Amoretti, S. Piligkos, G. Timco, and R. E. P. Winpenny, *Phys. Rev. Lett.* **94**, 207208 (2005).
- ²⁹A. Ardavan, O. Rival, J. J. L. Morton, S. J. Blundell, A. M. Tyryshkin, G. A. Timco, and R. E. P. Winpenny, *Phys. Rev. Lett.* **98**, 057201 (2007).
- ³⁰S. Carretta, P. Santini, G. Amoretti, F. Troiani, and M. Affronte, *Phys. Rev. B* **76**, 024408 (2007).
- ³¹F. Meier, J. Levy, and D. Loss, *Phys. Rev. B* **68**, 134417 (2003).
- ³²J. Lehmann, A. Gaita-Ariño, E. Coronado, and D. Loss, *Nat. Nanotechnol.* **2**, 312 (2007).
- ³³G. A. Timco *et al.*, *Nat. Nanotechnol.* **4**, 173 (2008).
- ³⁴A. Candini *et al.*, *Phys. Rev. Lett.* **104**, 037203 (2010).
- ³⁵H. B. Heersche, Z. de Groot, J. A. Folk, H. S. J. van der Zant, C. Romeike, M. R. Wegewijs, L. Zobbi, D. Barreca, E. Tondello, and A. Cornia, *Phys. Rev. Lett.* **96**, 206801 (2006).
- ³⁶K. Osorio, Edgar A. amd Moth-Poulsen, H. S. J. van der Zant, J. Paaske, P. Hedegrd, K. Flensberg, J. Bendix, and T. Bjrnholm, *Nano Lett.* **10**, 105 (2010).
- ³⁷C. Romeike, M. R. Wegewijs, and H. Schoeller, *Phys. Rev. Lett.* **96**, 196805 (2006).
- ³⁸C. Romeike, M. R. Wegewijs, W. Hofstetter, and H. Schoeller, *Phys. Rev. Lett.* **96**, 196601 (2006).
- ³⁹M. N. Leuenberger and E. R. Mucciolo, *Phys. Rev. Lett.* **97**, 126601 (2006).
- ⁴⁰L. Michalak, C. M. Canali, M. R. Pederson, M. Paulsson, and V. G. Benza, *Phys. Rev. Lett.* **104**, 017202 (2010).
- ⁴¹F. Troiani, M. Affronte, S. Carretta, P. Santini, and G. Amoretti, *Phys. Rev. Lett.* **94**, 190501 (2005).
- ⁴²M. Trif, F. Troiani, D. Stepanenko, and D. Loss, *Phys. Rev. Lett.* **101**, 217201 (2008).
- ⁴³C. F. Hirjibehedin, C. P. Lutz, and A. J. Heinrich, *Science* **312**, 1021 (2006).
- ⁴⁴A. C. Bleszynski-Jayich, L. E. Fröberg, M. T. Björk, H. J. Trodahl, L. Samuelson, and R. M. Westervelt, *Phys. Rev. B* **77**, 245327 (2008).
- ⁴⁵V. Srinivasa, J. Levy, and C. S. Hellberg, *Phys. Rev. B* **76**, 094411 (2007).
- ⁴⁶V. Srinivasa and J. Levy, *Phys. Rev. B* **80**, 024414 (2009).
- ⁴⁷A. I. Popov, D. I. Plokhov, and A. K. Zvezdin, *EPL* **87**, 67004 (2009).
- ⁴⁸L. N. Bulaevskii, C. D. Batista, M. V. Mostovoy, and D. I. Khomskii, *Phys. Rev. B* **78**, 024402 (2008).
- ⁴⁹B. S. Tsukerblat, *Group Theory in Chemistry and Spectroscopy: A Simple Guide to Advanced Usage* (Dover, New York, 2006).
- ⁵⁰V. Bellini, A. Olivieri, and F. Manghi, *Phys. Rev. B* **73**, 184431 (2006).
- ⁵¹K.-Y. Choi, Y. H. Matsuda, H. Nojiri, U. Kortz, F. Hussain, A. C. Stowe, C. Ramsey, and N. S. Dalal, *Phys. Rev. Lett.* **96**, 107202 (2006).
- ⁵²P. A. Angaridis, P. Baran, R. Boča, F. Cervantes-Lee, W. Haase, G. Mezel, R. G. Raptis, and R. Werner, *Inorg. Chem.* **41**, 2219 (2002).
- ⁵³N. Baadji, M. Piacenza, T. Tugsuz, F. D. Sala, G. Maruccio, and S. Sanvito, *Nature Mater.* **8**, 813 (2009).
- ⁵⁴T. Moriya, *Phys. Rev. Lett.* **4**, 228 (1960).
- ⁵⁵L. Shekhtman, O. Entin-Wohlman, and A. Aharony, *Phys. Rev. Lett.* **69**, 836 (1992).
- ⁵⁶T. Yildirim, A. B. Harris, O. Entin-Wohlman, and A. Aharony, *Phys. Rev. Lett.* **73**, 2919 (1994).
- ⁵⁷I. A. Sergienko and E. Dagotto, *Phys. Rev. B* **73**, 094434 (2006).
- ⁵⁸S. Dong, K. Yamauchi, S. Yunoki, R. Yu, S. Liang, A. Moreo, J.-M. Liu, S. Picozzi, and E. Dagotto, *Phys. Rev. Lett.* **103**, 127201 (2009).
- ⁵⁹A. V. Postnikov, J. Kortus, and M. R. Pederson, *Phys. Status Solidi B* **243**, 2533 (2006).
- ⁶⁰M. I. Belinsky, *Chem. Phys.* **361**, 137 (2009).
- ⁶¹M. I. Belinsky, *Chem. Phys.* **361**, 152 (2009).
- ⁶²N. E. Bonesteel, T. M. Rice, and F. C. Zhang, *Phys. Rev. Lett.* **68**, 2684 (1992).
- ⁶³J. M. Clemente-Juan, E. Coronado, A. Gaita-Arino, C. Gimenez-

- Saiz, H.-U. Gudel, A. Sieber, R. Bircher, and H. Mutka, *Inorg. Chem.* **44**, 3389 (2005).
- ⁶⁴J. Luzon, K. Bernot, I. J. Hewitt, C. E. Anson, A. K. Powell, and R. Sessoli, *Phys. Rev. Lett.* **100**, 247205 (2008).
- ⁶⁵R. Winkler, *Spin-Orbit Coupling Effects in Two-Dimensional Electron and Hole Systems* (Springer-Verlag, Berlin, 2003).
- ⁶⁶T. Moriya, *Phys. Rev.* **120**, 91 (1960).
- ⁶⁷A. Bencini and D. Gatteschi, *EPR of Exchange Coupled Systems* (Springer-Verlag, Berlin, 1989).
- ⁶⁸E. Micotti, Y. Furukawa, K. Kumagai, S. Carretta, A. Lascialfari, F. Borsa, G. A. Timco, and R. E. P. Winpenny, *Phys. Rev. Lett.* **97**, 267204 (2006).
- ⁶⁹A. Ghirri, G. Lorusso, F. Moro, F. Troiani, V. Corradini, C. Muryn, F. Tuna, G. Timco, R. E. P. Winpenny, and M. Affronte, *Phys. Rev. B* **79**, 224430 (2009).

Current-conserving Aharonov-Bohm interferometry with arbitrary spin interactionsMinchul Lee¹ and Dimitrije Stepanenko²¹*Department of Applied Physics, College of Applied Science, Kyung Hee University, Yongin 446-701, Korea*²*Department of Physics, University of Basel, Klingelbergstrasse 82, CH-4056 Basel, Switzerland*

(Received 24 August 2011; revised manuscript received 4 January 2012; published 21 February 2012)

We propose a general scattering-matrix formalism that guarantees the charge conservation at junctions between conducting arms with arbitrary spin interactions. By using our formalism, we find that the spin-flip scattering can happen even at nonmagnetic junctions if the spin eigenstates in arms are not orthogonal, which has been missed in previous similar studies. We apply our formalism to the Aharonov-Bohm interferometer consisting of an n -type semiconductor ring with both the Rashba spin-orbit coupling and the Zeeman splitting. We discuss the characteristics of the interferometer as a conditional (unconditional) spin switch in the weak (strong) -coupling limit.

DOI: [10.1103/PhysRevB.85.075316](https://doi.org/10.1103/PhysRevB.85.075316)

PACS number(s): 73.63.-b, 73.23.-b, 71.70.Ej, 03.65.Vf

I. INTRODUCTION

Coherent transport of electrons through mesoscopic rings or structures with nontrivial geometries has been extensively investigated both theoretically^{1–22} and experimentally^{23–28} in recent decades. The studies have aimed at exploring the quantum interference in solid-state circuits and also revolutionizing electronic devices in such a way as to exploit the quantum effects. At the heart of the studies of mesoscopic rings, there are two hallmarks of quantum coherence: the Aharonov-Bohm²⁹ (AB) and Aharonov-Casher³⁰ (AC) effects. These two effects are related to geometric phases due to the coupling of a charge to a magnetic flux and of a spin degree of freedom to an electric field via spin-orbit coupling (SOC), respectively. Since the AB oscillations in conductance through normal-metal rings were revealed,¹ it has been found that the effects can lead to diverse quantum interference phenomena such as conductance fluctuations,²³ persistent charge and spin currents,^{2,4} the AB effect for excitons,⁶ the mesoscopic Kondo effect,⁷ spin switching,^{8,12} spin filtering,¹⁵ and the spin Hall effect.²⁰ From a practical point of view, the quantum coherent phenomena in mesoscopic rings, especially using the spin degrees of freedom, have been applied to the fast-growing field of spintronics^{31,32} and are now known to provide the easy-to-control devices that generate, manipulate, and detect the spin-dependent current or signal.

Mesoscopic rings fabricated in semiconductors offer the intriguing possibility to study simultaneously the AB and AC effects because of the SOC naturally present in crystals. The SOC itself can have various forms in different materials, leading to diverse current oscillations.^{12,26,27} In addition, the strength of the SOC can be controlled by tuning a backgate voltage to the device.³³ Among various forms of SOC, the Rashba SOC, originating from the broken structural inversion symmetry, is linear in momentum and easy to analyze. The studies of spin interference^{9,12} subject to the Rashba SOC have shown that the Rashba coupling strength can modulate the unpolarized current, suggesting the possibility of all-electrical spintronic devices. Recently, a number of experimental^{26,27} and theoretical^{18,20,21} studies have investigated transport of heavy holes in rings, whose SOC is cubic in momentum. In the presence of external magnetic fields, the Zeeman splitting

is operative together with the SOC and its effect should be taken into account.^{5,8,10,14,17}

The general framework for the theoretical studies of the mesoscopic transport relies on the Landauer approach,³⁴ in which the tunneling between conduction modes in electrodes and mesoscopic systems can be described in terms of a scattering matrix. The scattering matrix relates the amplitudes and phases of the outgoing and incoming modes at a coherent scatterer. While the explicit form of the scattering matrix depends on the details of the physical nature of the scatterer, there is an essential constraint on it, namely the charge-current conservation. This conservation constraint should be fulfilled naturally as long as the scattering matrix is obtained by directly solving the Schrödinger equation containing the scatterer. However, the exact solution is available only in few simple cases or by numerical methods, so special caution is necessary when building up the correct scattering matrix in any other way. A problem is that the guarantee of the charge-current conservation looks less obvious if the charge transport is entangled with the spin degrees of freedom, which may be affected by the scatterer and/or the spin-dependent interactions.

We have found that this conservation problem can arise even in a simple and well-studied case, namely the AB interferometry formed by a semiconductor ring with both the Rashba SOC and the Zeeman splitting present. In this case, the ring modes form nonorthogonal spin textures; the spins of the modes at the same energy are not orthogonal to each other at any point in the ring. No shared single spin axis exists, and the connection between the lead and ring modes whose spins cannot be ever aligned in parallel then becomes a nontrivial problem; a spin mixing arises. We will argue in the text that any previous theoretical studies considering both the effect of the Rashba SOC and the Zeeman splitting have failed to satisfy the charge-current conservation unless the whole system is solved exactly by, for example, numerical methods.

Our goal in this work is to find a general theoretical formalism that guarantees the charge-current conservation at the lead-ring junctions by its own way of constructing the scattering matrix in the presence of arbitrary spin interactions in the ring. We treat the problem by introducing artificial

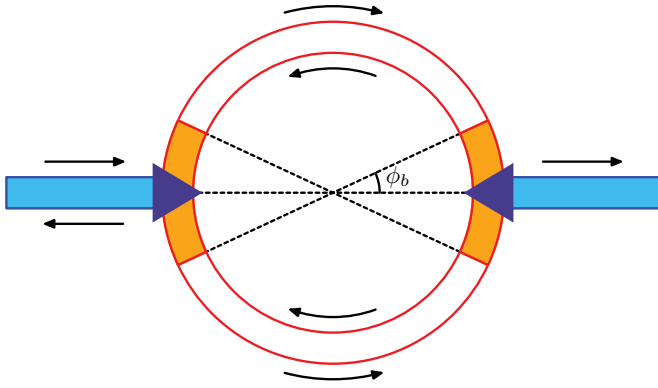


FIG. 1. (Color online) Schematic diagram of the buffered Aharonov-Bohm interferometer. The upper and low arms of the ring are connected to the junctions through buffers whose angular size is given by ϕ_b .

buffer regions free of spin interactions in the vicinity of every junction, as shown in Fig. 1. The spin-mixing effect is then taken care of at the interfaces between the buffers and the spinful regions in a standard way. Finally, the original system is recovered in the limit of vanishing buffers. By using our formalism, we first recover the known results in the case of orthogonal spin textures and interpret the role of buffers. Secondly, we apply our formalism to the n -type semiconductor ring with both the Rashba SOC and the Zeeman splitting. We find that (i) our formalism truly guarantees the charge-current conservation at every junction, giving rise to correct predictions; (ii) the spin-flip scattering can happen even if the junctions are defined as nonmagnetic, which cannot be observed in any previous studies; (iii) the ring interferometer can act as a conditional (unconditional) spin switch in the weak (strong) -coupling regimes if some conditions are met. Although similar studies have been done in recent decades, our analysis is, to the best of our knowledge, the first one that strictly guarantees the charge-current conservation and treats the Rashba SOC and the Zeeman splitting on an equal footing.

Our paper is structured as follows. In Sec. II, previous studies are summarized, and our formalism is introduced and derived in detail. The case of orthogonal spin texture is treated within our formalism in Sec. III. Section IV is devoted to the study of a case of nonorthogonal spin states in which both the Rashba SOC and the Zeeman splitting are taken into account. Finally, we conclude and summarize in Sec. V.

II. GENERAL FORMALISM TO BUILD A CURRENT-CONSERVING SCATTERING MATRIX

A. Limitations of previous studies

The scattering in the mesoscopic system is frequently characterized in terms of the scattering matrix, which defines the amplitudes and phases of the scattered states relative to the injected states. The scattering matrix depends on the details of the system but is constrained by the laws of conservation. The most important properties that the scattering matrix obeys are the charge-current conservation, if there is neither a source nor a sink in the scatterer, and the spin-current

conservation, if the scatterer is nonmagnetic. The conservation conditions, together with some symmetry-based arguments, greatly simplify the form of the scattering matrix so that it can be described by a few parameters. For example, the most frequently used scattering matrix at the lead-ring junction is controlled by a single parameter ϵ that is varied between 0 (no tunneling) and 1/2 (perfect tunneling), being expressed as

$$\begin{bmatrix} \tilde{r} \\ \tilde{u}^{\text{out}} \\ \tilde{d}^{\text{out}} \end{bmatrix} = \begin{bmatrix} -\zeta p & \sqrt{\epsilon} & \sqrt{\epsilon} \\ \sqrt{\epsilon} & \frac{\zeta}{2}(p-1) & \frac{\zeta}{2}(1+p) \\ \sqrt{\epsilon} & \frac{\zeta}{2}(1+p) & \frac{\zeta}{2}(p-1) \end{bmatrix} \begin{bmatrix} \tilde{s} \\ \tilde{u}^{\text{in}} \\ \tilde{d}^{\text{in}} \end{bmatrix}, \quad (1)$$

with $p \equiv \sqrt{1-2\epsilon}$ and $\zeta = \pm 1$. The scattering matrix connects the flux-normalized amplitudes (\tilde{s} , \tilde{u}^{in} , \tilde{d}^{in}) of incoming waves from the lead, upper, and lower arms of the ring to those (\tilde{r} , \tilde{u}^{ou} , \tilde{d}^{ou}) of the outgoing waves. Here the scattering to and from the upper and lower arms is assumed to be symmetric.

This simple construction of the scattering matrix can be extended further to the magnetic case in which spin-dependent interactions exist in the arms. In the presence of the Zeeman splitting, one can treat the scattering of spin up and down separately, each of which is described by the simple scattering matrix mentioned before. For the case of linear-in-momentum SOC such as the Rashba SOC, one can identify a common spin polarization axis at the junction so that spin-separate treatment¹¹ is still possible. In the perfect tunneling limit, the scattering matrix can be derived analytically by applying Griffith's boundary condition^{3,11} at the lead-ring junctions, which demands that the wave function is continuous and that the spin-current density is conserved. Here the second boundary condition is merely the charge-current conservation for each spin. In this way, the charge-current conservation is satisfied. It should be noted that here the spin-separate treatment is possible because all the arms meeting at a junction share a single spin polarization axis and the spin is conserved in the scattering at the junction.

However, the latter assumption is quite fragile and generally fails in the presence of general spin-dependent interactions in the arms. The simple cases in which it can happen are the n -type semiconductor ring with both the Rashba SOC and the Zeeman splitting, and the p -type semiconductor ring with cubic-in-momentum SOC.²¹ As will be shown in Sec. IV, the ring eigenstates turn out to be neither parallel nor orthogonal to each other in the spin space at all, denying a common spin polarization axis. The scattering into the ring then involves all the spin states, preventing the commonly used spin-separate treatment. The extended Griffith's boundary condition, applying both the charge- and spin-current conservation, would not succeed in this case because in the nonorthogonal spin texture, as will be shown in our calculations, the spin current is not conserved at junctions in general: spin is no longer a good quantum number.

The previous studies considering the effect of both the Rashba SOC and the Zeeman splitting have dealt with this situation by using various methods: the transfer-matrix method accompanied with wave-function matching,^{5,8,10} the perturbative approach,¹⁴ the path-integral approach,¹⁷ and numerical calculations based on tight-binding models.^{13,16,22} Among them, it is only the numerical methods^{13,16,22} that fulfill the charge-current conservation. In this approach,

the Schrödinger equation projected into the tight-binding model is numerically solved so that the obtained electronic transport should automatically satisfy the conservation law. The numerical approach is exact and can provide solutions even when no analytical solution is available. However, it is less adequate in capturing the qualitative understanding of the scattering processes taking place at junctions: The tight-binding model to which the numerical methods resort suffers from the finite-lattice-size effect, so it may not clearly clarify the role of the scattering at the junctions.

The perturbative and the path-integral approaches are, in principle, approximate methods so that the conservation is not strictly enforced. In Ref. 14, while the Rashba SOC is taken exactly, the Zeeman splitting is added as a perturbation without any consideration of conservation. The path-integral formalism used in Ref. 17 may be conceptually useful to interpret the result in terms of phases or winding numbers. However, it is limited by its semiclassical treatment.

A few groups^{5,8,10} have performed serious studies on the AB interferometry in the presence of the nonorthogonal spin texture by exploiting the transfer-matrix method. The transport is described by a flux-normalized transfer matrix that relates the amplitudes within each arm of the ring from one junction to the other junction. In obtaining the transfer matrix, they have taken into account the state dependence of the propagation velocities and the nonorthogonality of the spin states. However, there are problems with regard to their treatment of lead-ring scattering at junctions. First, they have assumed that there is no spin-flip scattering at lead-ring junctions at all, and they defined the scattering matrix on the assumption by hand. As our theory reveals, however, this is generally not the case in the presence of arbitrary spin interaction in the ring. Secondly, they determine the relation between the lead and the ring modes solely by the wave-function matching. From their assumption, the scattering matrix for each spin is defined with respect to the spin-polarized states along the z axis, adopting the spin-separate treatment. The amplitudes of the nonorthogonal ring eigenstates are then determined via the continuity of the wave function with the injected state obtained by the scattering matrix. Considering that the scattering matrix in the form of Eq. (1) should be defined with respect to the coefficients of *flux-normalized modes*, this wave-function matching does not fulfill the charge-current conservation at all. The mode dependence of the propagation velocity is not reflected in the construction of the scattering matrix. No unitarity property of the scattering matrix with respect to the flux-normalized lead and ring modes is guaranteed. Hence, in their works the conservation at each junction is not checked, while strangely the total source-to-drain transport through the ring seems to obey the conservation law. We suspect that their final results might be wrong since the charge-current conservation is not strictly enforced at each junction.

B. Buffered structure

One can then issue several questions. Is there a general framework to build the spin-dependent scattering matrix that guarantees satisfying the conservation laws by construction? What is the smallest number of controlling parameters required to describe the scattering in the presence of arbitrary spin-

dependent interactions? Can the spin-flip scattering happen even if the scatterer itself is nonmagnetic?

In order to answer these questions, we propose a general formalism to build up a consistent (spin-dependent) scattering matrix for arbitrary spin interaction. The key idea of our method is to insert artificial buffer regions between the scatter and arms, as depicted in Fig. 1. The buffer regions are assumed to be free of any spin-dependent interaction. Hence, the scattering between buffer regions can be described by the simple spin-separate scattering matrix. The complexity due to the spin-dependent interaction results in its effect at interfaces between buffers and arms. The wave functions at interfaces are matched in a systematic way by using the continuity of the wave function and its current density. This wave matching, together with the scattering matrix between buffer states, leads one to find the scattering matrix between states of arms. The size of artificial buffers is then shrunk to zero in order to recover the original configuration. The shrinking does not remove all the effects of buffers because the effect of scattering at buffer-arm interfaces still remains. In the end, the scattering matrix connecting states of arms is constructed.

The advantages of our methods are listed as follows: (i) The scattering matrix obtained guarantees that the conservation laws will be satisfied. This is because the scattering between buffer states and the scattering at buffer-arm interfaces are set up to conserve the charge and spin currents. (ii) It systematically identifies the minimal set of controlling parameters that the scatterer can have. (iii) It provides a reasonable explanation for the effect of spin interactions in arms on the spin-dependent (possibly spin-flip) scattering even when the scatterer itself is nonmagnetic.

In the following sections, we build up our formalism, especially focusing on the AB interferometer shown in Fig. 1. The system consists of two leads and one ring. Each part is assumed to be narrow enough to be regarded as a one-dimensional conductor with a single transverse mode. The scattering matrix between the lead and the ring then becomes a 6×6 matrix. We will construct a general scattering matrix for a ring with arbitrary spin interaction. Our formalism, however, is quite general and can be applied to mesoscopic circuits with any geometry.

C. Arms: Lead part

The leads are composed of normal conductors directed along the x direction. They are free of any magnetic interaction, and their Hamiltonians read

$$H_{\text{lead}} = \frac{p_x^2}{2m_0^*} + U_0, \quad (2)$$

where m_0^* is the effective mass of electrons in the leads and U_0 is the minimum energy of the transverse mode. Thanks to the spin degeneracy, the spin polarization axis of eigenstates can be chosen arbitrarily. Eigenstates of the leads with the eigenenergy E are then given by

$$e^{\pm iqx} \chi_{\ell\mu}, \quad (3)$$

with the wave number $q = \sqrt{2m_0(E - U_0)}/\hbar$ and the spinors

$$\chi_{\ell+} = \begin{bmatrix} e^{-i\varphi_\ell/2} \cos \vartheta_\ell \\ e^{+i\varphi_\ell/2} \sin \vartheta_\ell \end{bmatrix}, \quad \chi_{\ell-} = \begin{bmatrix} -e^{-i\varphi_\ell/2} \sin \vartheta_\ell \\ e^{+i\varphi_\ell/2} \cos \vartheta_\ell \end{bmatrix}. \quad (4)$$

Here $\mu = \pm$ is the spin index and $\ell = L, R$ is the lead index. The angles $(\vartheta_\ell, \varphi_\ell)$ define the spin-polarization axis for the injection from the left lead ($\ell = L$) and the spin detection axis in the right lead ($\ell = R$), respectively. In terms of coefficients of injected (s_μ), reflected (r_μ), and transmitted (t_μ) waves, the general wave functions in the leads are given by

$$\begin{aligned} \Psi_L(x) &= \sum_\mu [s_\mu e^{iqx} + r_\mu e^{-iqx}] \chi_{L\mu} \\ &= \mathcal{U}_L(e^{iqx}s + e^{-iqx}r), \end{aligned} \quad (5a)$$

$$\Psi_R(x) = \sum_\mu t_\mu e^{iqx} \chi_{R\mu} = \mathcal{U}_R e^{iqx} t, \quad (5b)$$

where

$$s \equiv \begin{bmatrix} s_+ \\ s_- \end{bmatrix}, \quad r \equiv \begin{bmatrix} r_+ \\ r_- \end{bmatrix}, \quad t \equiv \begin{bmatrix} t_+ \\ t_- \end{bmatrix} \quad (6)$$

and

$$\mathcal{U}_\ell \equiv \begin{bmatrix} e^{-i\varphi_\ell/2} \cos \vartheta_\ell & -e^{-i\varphi_\ell/2} \sin \vartheta_\ell \\ e^{+i\varphi_\ell/2} \sin \vartheta_\ell & e^{+i\varphi_\ell/2} \cos \vartheta_\ell \end{bmatrix}. \quad (7)$$

The group velocities of the eigenstates are $\pm v_0 \equiv \pm \hbar q / m_0$, and the charge-current densities in the leads are

$$J_L = v_0 \sum_\mu (|s_\mu|^2 - |r_\mu|^2), \quad J_R = v_0 \sum_\mu |t_\mu|^2. \quad (8)$$

D. Arms: Ring part

The ring can be either of a normal conductor, an n -type semiconductor, or a p -type semiconductor. It is narrow enough that the radial dimension is constant with the radius ρ_0 and the degree of freedom is solely described by the azimuthal angle ϕ . We assume that an external magnetic field \mathbf{B} is applied so that the ring encloses a magnetic flux Φ , or the dimensionless flux $f = \Phi/\Phi_0$ with the flux quantum $\Phi_0 = hc/e$, and the spin splitting arises due to the Zeeman term,

$$H_Z = \frac{g^* \mu_B}{2} \boldsymbol{\sigma} \cdot \mathbf{B}, \quad (9)$$

where g^* is the Landé g factor, μ_B is the Bohr magneton, and $\boldsymbol{\sigma}$ is the Pauli matrices. For semiconductor rings, an appropriate SOC, H_{SO} , is operative [see Eq. (52) for the Rashba SOC]. The ring Hamiltonian is then given by

$$H_{\text{ring}} = E_0(-i\partial_\phi - f)^2 + H_{SO} + \frac{g^* \mu_B}{2} \boldsymbol{\sigma} \cdot \mathbf{B}, \quad (10)$$

with

$$E_0 = \frac{\hbar^2}{2m^* \rho_0^2}, \quad (11)$$

where m^* is the effective mass in the ring. In general, the Hamiltonian has four eigenstates labeled by the spin index $\mu = \pm$ and the propagation direction $\varrho = +$ (counterclockwise) and $-$ (clockwise) at a given energy E . Each eigenstate is

endowed with a wave number k_μ^ϱ , the solution of the dispersion relation [see Eq. (54), for example]. The wave number can be a real (propagating state) or a complex number (evanescent wave). The general form of the eigenstates is then written as

$$\phi_\mu^\varrho(\phi) = e^{i(k_\mu^\varrho + f)\phi} \begin{bmatrix} a_\mu^\varrho(\phi) \\ b_\mu^\varrho(\phi) \end{bmatrix} \quad (12)$$

[compare with Eq. (53), for example]. In terms of coefficients u_μ^ϱ for the upper arm (U) and d_μ^ϱ for the lower arm (D), the ring wave functions are given by

$$\Psi_U(\phi) = \sum_{\mu\varrho} u_\mu^\varrho \phi_\mu^\varrho(\phi) = \sum_{\varrho} \mathcal{U}^\varrho(\phi) \mathcal{K}^\varrho(\phi) u^\varrho, \quad (13a)$$

$$\Psi_D(\phi) = \sum_{\mu\varrho} d_\mu^\varrho \phi_\mu^\varrho(\phi) = \sum_{\varrho} \mathcal{U}^\varrho(\phi) \mathcal{K}^\varrho(\phi) d^\varrho, \quad (13b)$$

where

$$u^\varrho \equiv \begin{bmatrix} u_+^\varrho \\ u_-^\varrho \end{bmatrix}, \quad d^\varrho \equiv \begin{bmatrix} d_+^\varrho \\ d_-^\varrho \end{bmatrix} \quad (14)$$

and

$$\mathcal{U}^\varrho(\phi) \equiv \begin{bmatrix} a_+^\varrho(\phi) & a_-^\varrho(\phi) \\ b_+^\varrho(\phi) & b_-^\varrho(\phi) \end{bmatrix}, \quad \mathcal{K}^\varrho(\phi) \equiv e^{if\phi} \begin{bmatrix} e^{ik_+^\varrho\phi} & 0 \\ 0 & e^{ik_-^\varrho\phi} \end{bmatrix}. \quad (15)$$

The group velocity of each eigenstate, ϱv_μ^ϱ , is given by the expectation value $\langle \phi_\mu^\varrho | v_\phi | \phi_\mu^\varrho \rangle$ of the velocity operator v_ϕ . Note that the SOC affects the velocity operator, and in general the energy eigenstate is not the eigenstate of the velocity operator. If the time-reversal symmetry is not broken, the relations $v_+^+ = v_-^-$ and $v_+^- = v_-^+$ hold generally no matter what the SOC is. In terms of the group velocities, the charge-current densities in the ring are expressed as

$$J_U = \sum_\mu (v_\mu^+ |u_\mu^+|^2 - v_\mu^- |u_\mu^-|^2), \quad (16a)$$

$$J_D = \sum_\mu (v_\mu^+ |d_\mu^+|^2 - v_\mu^- |d_\mu^-|^2) \quad (16b)$$

for the upper and lower arms, respectively. For later use, we define the action of the velocity operator on the wave function,

$$v_\phi \Psi_U(\phi) = \sum_{\varrho} \varrho \mathcal{V}^\varrho(\phi) \mathcal{K}^\varrho(\phi) u^\varrho, \quad (17a)$$

$$v_\phi \Psi_D(\phi) = \sum_{\varrho} \varrho \mathcal{V}^\varrho(\phi) \mathcal{K}^\varrho(\phi) d^\varrho, \quad (17b)$$

where the 2×2 matrix $\mathcal{V}^\varrho(\phi)$ depends on the details of the system [see Eq. (60b), for example].

E. Buffers

In our formalism, no buffer region is inserted between the leads and the junctions. This is because the leads, just like the buffers, are free of spin-dependent interactions and the scattering at the interface between the lead and the buffer becomes trivial. On the other hand, as shown in Fig. 1, the buffer regions are inserted between the junctions and the ring arms. In the AB interferometer, therefore, four buffer regions with the same angular size ϕ_b are defined in the both sides of upper and lower arms. Having the junctions at the angles ϕ_L and $\phi_R = 0$, the interfaces between the buffers and the arms

are located at $\phi_{UR} = \phi_b$, $\phi_{UL} = \phi_L - \phi_b$, $\phi_{DL} = \phi_L + \phi_b$, and $\phi_{DR} = 2\pi - \phi_b$. Since the buffers are free of any spin-dependent interactions, the Hamiltonian in buffers reads

$$H_{\text{buffer}} = E_0(-i\partial_\phi - f)^2 + U_b, \quad (18)$$

where U_b is the offset in the band bottom with respect to the ring part. With no spin interaction, we are free to choose the spin polarization axes in them, and the axis of each buffer is chosen to be that of the nearest-neighboring lead. Eigenstates of the buffers with the energy E , labeled by μ and ϱ , are then given by

$$e^{i(\varrho\kappa+f)\phi} \chi_{\ell\mu}, \quad (19)$$

with the wave number $\kappa = \sqrt{(E - U_b)/E_0}$ and the nearby-lead index ℓ . By defining the coefficients $u_{\ell\mu}^{\varrho}$ for the upper buffers close to the side ℓ , and $d_{\ell\mu}^{\varrho}$ for the lower buffers close to the side ℓ , the buffer wave functions are written as

$$\Psi_{U\ell}(\phi) = \sum_{\mu\varrho} u_{\ell\mu}^{\varrho} e^{i(\varrho\kappa+f)(\phi-\phi_\ell)} \chi_{\ell\mu} = \sum_{\varrho} \mathcal{U}_\ell \mathcal{K}_b^{\varrho}(\phi) u_\ell^{\varrho}, \quad (20a)$$

$$\Psi_{D\ell}(\phi) = \sum_{\mu\varrho} d_{\ell\mu}^{\varrho} e^{i(\varrho\kappa+f)(\phi-\phi_\ell)} \chi_{\ell\mu} = \sum_{\varrho} \mathcal{U}_\ell \mathcal{K}_b^{\varrho}(\phi) d_\ell^{\varrho}, \quad (20b)$$

where

$$u_\ell^{\varrho} \equiv \begin{bmatrix} u_{\ell+}^{\varrho} \\ u_{\ell-}^{\varrho} \end{bmatrix}, \quad d_\ell^{\varrho} \equiv \begin{bmatrix} d_{\ell+}^{\varrho} \\ d_{\ell-}^{\varrho} \end{bmatrix}, \quad (21)$$

and

$$\mathcal{K}_b^{\varrho} \equiv e^{i(\varrho\kappa+f)(\phi-\phi_\ell)} \begin{bmatrix} 1 & 0 \\ 0 & 1 \end{bmatrix}. \quad (22)$$

The group velocities of the eigenstates are simply given by $\pm v_b \equiv \pm \hbar\kappa/m\rho_0$, which is the eigenvalue of the velocity operator $v_\phi = (\hbar/m\rho_0)(-i\partial_\phi - f)$, and the charge-current densities in the buffers are

$$J_{U\ell} = v_b \sum_{\mu} (|u_{\ell\mu}^+|^2 - |u_{\ell\mu}^-|^2), \quad (23a)$$

$$J_{D\ell} = v_b \sum_{\mu} (|d_{\ell\mu}^+|^2 - |d_{\ell\mu}^-|^2), \quad (23b)$$

for the upper and lower buffers, respectively. For later use, we define the wave function applied by the velocity operator,

$$v_\phi \Psi_{U\ell}(\phi) = v_b \mathcal{U}_\ell (\mathcal{K}_b^+ u_\ell^+ - \mathcal{K}_b^- u_\ell^-), \quad (24a)$$

$$v_\phi \Psi_{D\ell}(\phi) = v_b \mathcal{U}_\ell (\mathcal{K}_b^+ d_\ell^+ - \mathcal{K}_b^- d_\ell^-). \quad (24b)$$

F. Lead-buffer scattering matrices

With the buffered structure, the scattering at the junctions connects the states in the leads and the buffers. Since both the leads and the buffers have no magnetic interaction, the conventional scattering matrix can be defined to describe the scattering at the junctions. The reasonable conditions¹ for the scattering matrix are that (i) no spin flip takes place, (ii) the scatterings from and to the upper and lower arms are the same, (iii) no phase shift is acquired, and (iv) the charge current is conserved. The first condition makes the scattering matrix diagonal in the spin space, and due to the second condition the scattering matrix with respect to the normalized flux is

symmetric in the exchange between the upper and lower arms. The most general lead-buffer scattering matrix satisfying the above conditions is then¹

$$\mathcal{S} = \begin{bmatrix} \mathcal{S}_{11} & \mathcal{S}_{12} \\ \mathcal{S}_{21} & \mathcal{S}_{22} \end{bmatrix} = \begin{bmatrix} \mathcal{S}_{0,11} \otimes \sigma_0 & \mathcal{S}_{0,12} \otimes \sigma_0 \\ \mathcal{S}_{0,21} \otimes \sigma_0 & \mathcal{S}_{0,22} \otimes \sigma_0 \end{bmatrix}, \quad (25)$$

with

$$\mathcal{S}_{0,11} = -\zeta \sqrt{1-2\epsilon}, \quad (26a)$$

$$\mathcal{S}_{0,12} = \sqrt{\frac{v_b}{v_0}} \epsilon [1 \ 1], \quad (26b)$$

$$\mathcal{S}_{0,12} = \sqrt{\frac{v_0}{v_b}} \epsilon \begin{bmatrix} 1 \\ 1 \end{bmatrix}, \quad (26c)$$

$$\mathcal{S}_{0,22} = \begin{bmatrix} \frac{\zeta}{2}(\sqrt{1-2\epsilon}-1) & \frac{\zeta}{2}(1+\sqrt{1-2\epsilon}) \\ \frac{\zeta}{2}(1+\sqrt{1-2\epsilon}) & \frac{\zeta}{2}(\sqrt{1-2\epsilon}-1) \end{bmatrix}, \quad (26d)$$

with $\zeta = \pm 1$. The submatrices $\mathcal{S}_{0,11}$, $\mathcal{S}_{0,12}$, $\mathcal{S}_{0,21}$, and $\mathcal{S}_{0,22}$ describe the lead-to-lead, arm-to-lead, lead-to-arm, and arm-to-arm scatterings, respectively. Here the controlling parameter ϵ varies from 0 (perfect transmission) to 1/2 (complete decoupling), and σ_0 is a 2×2 identity matrix in the spin space, indicating the absence of spin-flip scattering. Throughout this paper, we choose $\zeta = +1$ considering the case of phase-conserving scattering between upper and lower arms.

Assuming that both junctions have the same scattering matrix, one can set up linear equations for the coefficients of lead and buffer states: at the left junction,

$$r = \mathcal{S}_{11}s + \mathcal{S}_{12}c_L^{\leftarrow}, \quad (27a)$$

$$c_L^{\leftarrow} = \mathcal{S}_{12}s + \mathcal{S}_{22}c_L^{\leftarrow}, \quad (27b)$$

and at the right junction,

$$t = \mathcal{S}_{12}c_R^{\rightarrow}, \quad (28a)$$

$$c_R^{\rightarrow} = \mathcal{S}_{22}c_R^{\rightarrow}, \quad (28b)$$

where the left- and right-moving buffer states are defined as

$$c_\ell^{\leftarrow} \equiv \begin{bmatrix} u_\ell^+ \\ d_\ell^- \end{bmatrix} = \begin{bmatrix} u_{\ell+}^+ \\ u_{\ell-}^+ \\ d_{\ell+}^- \\ d_{\ell-}^- \end{bmatrix}, \quad c_\ell^{\rightarrow} \equiv \begin{bmatrix} u_\ell^- \\ d_\ell^+ \end{bmatrix} = \begin{bmatrix} u_{\ell+}^- \\ u_{\ell-}^- \\ d_{\ell+}^+ \\ d_{\ell-}^+ \end{bmatrix}, \quad (29)$$

respectively.

Note that the form of the scattering matrix guarantees the charge- and spin-current conservation by construction.

G. Lead-arm scattering matrices

Now we derive the scattering matrix connecting the lead states and the ring states. To do that, we need to find out the linear relations between the buffer states and the ring states. The relations are to be determined from the boundary conditions at the buffer-arm interfaces by using the continuity of wave function $\Psi(\phi)$ and the current conservation. The latter condition can be reformulated in terms of the continuity of $H(\phi)\Psi(\phi)$, where $H(\phi)$ is the total ring Hamiltonian for both the buffer and arm regions in the ring. The ring Hamiltonian takes into account the discontinuous change of the spin-dependent terms at the interfaces. As long as the

SOC is composed of the linear and/or second orders of the momentum operator, the continuity of $H(\phi)\Psi(\phi)$ leads to the continuity of $v_\phi\Psi(\phi)$. Now we apply the boundary conditions at four interfaces. By using Eqs. (13) and (20), the continuity of the wave function, $\Psi_U(\phi_{U\ell}) = \Psi_{U\ell}(\phi_{U\ell})$ and $\Psi_D(\phi_{D\ell}) = \Psi_{D\ell}(\phi_{D\ell})$, at the interfaces gives rise to

$$\sum_{\ell} \mathcal{U}^e(\phi_{U\ell}) \mathcal{K}^e(\phi_{U\ell}) u^e = \mathcal{U}_\ell \sum_{\ell} \mathcal{K}_b^e(\phi_{U\ell}) u_\ell^e, \quad (30a)$$

$$\sum_{\ell} \mathcal{U}^e(\phi_{D\ell}) \mathcal{K}^e(\phi_{D\ell}) d^e = \mathcal{U}_\ell \sum_{\ell} \mathcal{K}_b^e(\phi_{D\ell}) d_\ell^e. \quad (30b)$$

The second continuity conditions, $v_\phi\Psi_U(\phi_{U\ell}) = v_\phi\Psi_{U\ell}(\phi_{U\ell})$ and $v_\phi\Psi_D(\phi_{D\ell}) = v_\phi\Psi_{D\ell}(\phi_{D\ell})$, together with Eqs. (17) and (24), lead to

$$\sum_{\ell} \varrho \mathcal{V}^e(\phi_{U\ell}) \mathcal{K}^e(\phi_{U\ell}) u^e = v_b \mathcal{U}_\ell \sum_{\ell} \varrho \mathcal{K}_b^e(\phi_{U\ell}) u_\ell^e, \quad (31a)$$

$$\sum_{\ell} \varrho \mathcal{V}^e(\phi_{D\ell}) \mathcal{K}^e(\phi_{D\ell}) d^e = v_b \mathcal{U}_\ell \sum_{\ell} \varrho \mathcal{K}_b^e(\phi_{D\ell}) d_\ell^e. \quad (31b)$$

It is straightforward to solve the equations for the coefficients of the buffer states:

$$u_\ell^e = [\mathcal{K}_b^e(\phi_{U\ell})]^{-1} \sum_{\ell'} \mathcal{Z}_\ell^{e\ell'}(\phi_{U\ell}) \mathcal{K}^{\ell'}(\phi_{U\ell}) u^{\ell'}, \quad (32a)$$

$$d_\ell^e = [\mathcal{K}_b^e(\phi_{D\ell})]^{-1} \sum_{\ell'} \mathcal{Z}_\ell^{e\ell'}(\phi_{D\ell}) \mathcal{K}^{\ell'}(\phi_{D\ell}) d^{\ell'}, \quad (32b)$$

with

$$\mathcal{Z}_\ell^{e\ell'}(\phi) \equiv \mathcal{U}_\ell^{-1} \frac{\mathcal{U}^{\ell'}(\phi) + \varrho \mathcal{V}^{\ell'}(\phi)/v_b}{2}. \quad (33)$$

Once the relations between coefficients of the buffer and the ring states are set up, it is time to shrink the buffers by setting $\phi_b \rightarrow 0$. The buffer propagating matrices, \mathcal{K}_b^e , become the identity matrix just because of the zero propagating distance. Here some caution should be taken with regard to the limit values of the interface points. The left interfaces go to the single point, $\phi_{UL}, \phi_{DL} \rightarrow \phi_L \equiv \phi_L^\pm$, while the limit values of the right interfaces are different, $\phi_{UR} \rightarrow 0 \equiv \phi_R^+$ and $\phi_{DR} \rightarrow 2\pi \equiv \phi_R^-$.

Combining Eqs. (27), (28), and (32), one can build linear equations for the coefficients of lead and ring states, which are similar to Eqs. (27) and (28): at the left junction,

$$r = \mathcal{S}_{L,11}s + \mathcal{S}_{L,12}\mathcal{K}_L^{\leftarrow}c^{\leftarrow}, \quad (34a)$$

$$\mathcal{K}_L^{\rightarrow}c^{\rightarrow} = \mathcal{S}_{L,12}s + \mathcal{S}_{L,22}\mathcal{K}_L^{\leftarrow}c^{\leftarrow}, \quad (34b)$$

and at the right junction,

$$t = \mathcal{S}_{R,12}\mathcal{K}_R^{\rightarrow}c^{\rightarrow}, \quad (35a)$$

$$\mathcal{K}_R^{\leftarrow}c^{\leftarrow} = \mathcal{S}_{R,22}\mathcal{K}_R^{\rightarrow}c^{\rightarrow}, \quad (36a)$$

where the left- and right-moving ring states and the propagating matrices are defined as

$$c^{\leftarrow} \equiv \begin{bmatrix} u^+ \\ d^- \end{bmatrix} = \begin{bmatrix} u_+^+ \\ u_-^+ \\ d_+^- \\ d_-^- \end{bmatrix}, \quad c^{\rightarrow} \equiv \begin{bmatrix} u^- \\ d^+ \end{bmatrix} = \begin{bmatrix} u_+^- \\ u_-^- \\ d_+^+ \\ d_-^+ \end{bmatrix}, \quad (36)$$

and

$$\mathcal{K}_\ell^{\leftarrow} \equiv \begin{bmatrix} \mathcal{K}^+(\phi_\ell^+) & \\ & \mathcal{K}^-(\phi_\ell^-) \end{bmatrix}, \quad \mathcal{K}_\ell^{\rightarrow} \equiv \begin{bmatrix} \mathcal{K}^-(\phi_\ell^+) & \\ & \mathcal{K}^+(\phi_\ell^-) \end{bmatrix}, \quad (37)$$

respectively. The lead-ring scattering matrices

$$\mathcal{S}_\ell = \begin{bmatrix} \mathcal{S}_{\ell,11} & \mathcal{S}_{\ell,12} \\ \mathcal{S}_{\ell,21} & \mathcal{S}_{\ell,22} \end{bmatrix} \quad (38)$$

are then given by

$$\mathcal{S}_{\ell,11} = \mathcal{S}_{11} + \mathcal{S}_{12}\mathcal{Q}_\ell^-(\mathcal{Q}_\ell^+ - \mathcal{S}_{22}\mathcal{Q}_\ell^-)^{-1}\mathcal{S}_{21}, \quad (39a)$$

$$\mathcal{S}_{\ell,12} = \mathcal{S}_{12}[\mathcal{P}_\ell^+ + \mathcal{Q}_\ell^-(\mathcal{Q}_\ell^+ - \mathcal{S}_{22}\mathcal{Q}_\ell^-)^{-1}(\mathcal{S}_{22}\mathcal{P}_\ell^+ - \mathcal{P}_\ell^-)], \quad (39b)$$

$$\mathcal{S}_{\ell,21} = (\mathcal{Q}_\ell^+ - \mathcal{S}_{22}\mathcal{Q}_\ell^-)^{-1}\mathcal{S}_{21}, \quad (39c)$$

$$\mathcal{S}_{\ell,22} = (\mathcal{Q}_\ell^+ - \mathcal{S}_{22}\mathcal{Q}_\ell^-)^{-1}(\mathcal{S}_{22}\mathcal{P}_\ell^+ - \mathcal{P}_\ell^-), \quad (39d)$$

with

$$\mathcal{P}_L^e \equiv \begin{bmatrix} \mathcal{Z}_L^{e+}(\phi_L) & \\ & \mathcal{Z}_L^{e-}(\phi_L) \end{bmatrix}, \quad \mathcal{Q}_L^e \equiv \begin{bmatrix} \mathcal{Z}_L^{e-}(\phi_L) & \\ & \mathcal{Z}_L^{e+}(\phi_L) \end{bmatrix}, \quad (40a)$$

$$\mathcal{P}_R^e \equiv \begin{bmatrix} \mathcal{Z}_R^{e-}(\phi_R^+) & \\ & \mathcal{Z}_R^{e+}(\phi_R^-) \end{bmatrix}, \quad \mathcal{Q}_R^e \equiv \begin{bmatrix} \mathcal{Z}_R^{e+}(\phi_R^+) & \\ & \mathcal{Z}_R^{e-}(\phi_R^-) \end{bmatrix}. \quad (40b)$$

From Eqs. (39) and (40), a few immediate general features of the scattering matrix can be discussed: (i) In general, the matrices $\mathcal{Z}_\ell^{e\ell'}$ are not spin diagonal. This means that the lead-ring scattering matrices are not diagonal in the spin basis even if we start with the assumption that the junction itself does not invoke the spin-flip scattering. For example, the spin up injected from the lead can be reflected into the spin down for any spin injection axis. This is not because the junction is a magnetic scatterer but rather because of spin-dependent interaction in the ring. The magnetic property in the arms of the ring can invoke the spin-dependent scattering at the junctions.

(ii) The buffer effect remains. The lead-ring scattering matrix has two controlling parameters: ϵ and U_b . The latter parameter enters into the scattering matrix in terms of the buffer group velocity v_b . The velocity v_b appears in the scattering matrix in two ways: in the overall factor $\sqrt{v_b/v_0}$ of \mathcal{S}_{12} and \mathcal{S}_{21} [see Eq. (26)] and in the matrices $\mathcal{Z}_\ell^{e\ell'}$ [see Eq. (33)]. The overall factor $\sqrt{v_b/v_0}$ appears in $\mathcal{S}_{\ell,ij}$ in the same way as in \mathcal{S}_{ij} and does not affect the spin-dependent scattering discussed above. On the other hand, v_b in the matrices $\mathcal{Z}_\ell^{e\ell'}$ can tune magnitudes of its off-diagonal components. Therefore, we can draw a conclusion that at least two parameters for junctions, here ϵ and U_b , are necessary to specify and control the spin-dependent scattering due to arbitrary spin-dependent interaction in arms.

We would like to emphasize that the scattering matrix, Eq. (39), is the only solution that guarantees the conservation of the charge and spin currents at junctions under our symmetric assumptions. Since we have used the simplest buffer structure that introduces only one additional parameter, more complexity, if necessary, can be introduced into the scattering matrix by allowing additional interactions in the buffer. Here

we introduce the minimal scattering matrix working properly in the presence of general SOC.

H. Reflection and transmission coefficients

It is now quite straightforward to solve Eqs. (34) and (35) in order to obtain the spin-resolved reflection and transmission coefficients in terms of the lead-ring scattering matrix $\mathcal{S}_{\ell,ij}$:

$$t = \mathcal{S}_{R,12}(\mathcal{K}^{\rightarrow} \mathcal{F} - \mathcal{S}_{L,22} \mathcal{K}^{\leftarrow} \mathcal{F} \mathcal{S}_{R,22})^{-1} \mathcal{S}_{L,21} s, \quad (41a)$$

$$r = [\mathcal{S}_{L,11} + \mathcal{S}_{L,12} \mathcal{K}^{\leftarrow} \mathcal{F} \mathcal{S}_{R,22} \times (\mathcal{K}^{\rightarrow} \mathcal{F} - \mathcal{S}_{L,22} \mathcal{K}^{\leftarrow} \mathcal{F} \mathcal{S}_{R,22} t)^{-1} \mathcal{S}_{L,21}] s, \quad (41b)$$

with

$$\mathcal{K}^{\leftarrow} = \text{diag}(e^{ik_{+}^{\leftarrow} \phi_L}, e^{ik_{-}^{\leftarrow} \phi_L}, e^{-ik_{+}^{\leftarrow} (2\pi - \phi_L)}, e^{-ik_{-}^{\leftarrow} (2\pi - \phi_L)}), \quad (42a)$$

$$\mathcal{K}^{\rightarrow} \equiv \text{diag}(e^{ik_{+}^{\rightarrow} \phi_L}, e^{ik_{-}^{\rightarrow} \phi_L}, e^{-ik_{+}^{\rightarrow} (2\pi - \phi_L)}, e^{-ik_{-}^{\rightarrow} (2\pi - \phi_L)}), \quad (42b)$$

$$\mathcal{F} \equiv \text{diag}(e^{if \phi_L}, e^{if \phi_L}, e^{-if (2\pi - \phi_L)}, e^{-if (2\pi - \phi_L)}). \quad (42c)$$

Note that the overall factors $\sqrt{v_b/v_0}$ in $\mathcal{S}_{\ell,12}$ and $\mathcal{S}_{\ell,21}$ are canceled out in the reflection and transmission coefficients. Therefore, the velocity in the leads does not affect the coefficients at all.

Below we calculate the transmission amplitudes $T_{\mu\mu'} = |t_{\mu\mu'}|^2$, and by using them the charge conductance

$$G = \frac{e^2}{h} \sum_{\mu\mu'} T_{\mu\mu'} \quad (43)$$

and the current polarization

$$P = \frac{1}{2} \sum_{\mu\mu'} \mu T_{\mu\mu'} \quad (44)$$

with respect to the unpolarized input current are obtained.

III. ORTHOGONAL SPIN STATES

Before proceeding to study the case in which our formalism is indispensable, we apply it to the simple cases in which the spin-separate treatment is possible. As mentioned in the preceding section, the spin-separate treatment can be used when the ring is of the normal conductor, or has the linear-in-momentum SOC such as Rashba SOC, or has the Zeeman splitting only. What is in common in all the cases is that the group velocity and the spin matrix are direction-independent, $v_{\mu}^{\leftarrow} = v_{\mu}$ and $\mathcal{U}^{\leftarrow}(\phi) = \mathcal{U}(\phi)$, and that the energy eigenstates are also the eigenstates of the corresponding velocity operator,

$$v_{\phi} \varphi_{\mu}^{\leftarrow}(\phi) = \varrho v_{\mu} \varphi_{\mu}^{\leftarrow}(\phi) \quad (45)$$

($v_{+} \neq v_{-}$ only when the Zeeman splitting is finite). Then the matrix $\mathcal{V}^{\rho}(\phi)$ in Eq. (17) is simply given by

$$\mathcal{V}^{\rho}(\phi) = \mathcal{U}(\phi) \begin{bmatrix} v_{+} & 0 \\ 0 & v_{-} \end{bmatrix}. \quad (46)$$

Accordingly, the matrices $\mathcal{Z}_{\ell}^{\varrho\varrho'}(\phi)$ are simplified to

$$\mathcal{Z}_{\ell}^{\varrho\varrho'}(\phi) = [\mathcal{U}_{\ell}^{-1} \mathcal{U}(\phi)] \begin{bmatrix} z_{+}^{\varrho} & 0 \\ 0 & z_{-}^{\varrho} \end{bmatrix} \quad (47)$$

with

$$z_{\mu}^{\varrho} \equiv \frac{1 + \varrho v_{\mu}/v_b}{2}. \quad (48)$$

By setting $\mathcal{U}_{\ell} = \mathcal{U}(\phi_{\ell})$ [note that $\mathcal{U}(\phi_{R}^{\leftarrow})$ and $\mathcal{U}(\phi_{R}^{\rightarrow})$ usually differ only up to the overall phase factor], the matrices $\mathcal{Z}_{\ell}^{\varrho\varrho'}(\phi_{\ell})$ become spin diagonal, and consequently we recover the spin-separate lead-ring scattering matrix. For each spin component, the lead-ring scattering matrix for spin μ can be expressed as

$$\mathcal{S}_{\ell\mu,11} = \mathcal{S}_{\mu,11} + \mathcal{S}_{\mu,12} z_{\mu}^{\leftarrow} (z_{\mu}^{\leftarrow} - z_{\mu}^{\leftarrow} \mathcal{S}_{\mu,22})^{-1} \mathcal{S}_{\mu,21}, \quad (49a)$$

$$\mathcal{S}_{\ell\mu,12} = \mathcal{S}_{\mu,12} [z_{\mu}^{\leftarrow} + z_{\mu}^{\leftarrow} (z_{\mu}^{\leftarrow} - z_{\mu}^{\leftarrow} \mathcal{S}_{\mu,22})^{-1} (z_{\mu}^{\leftarrow} \mathcal{S}_{\mu,22} - z_{\mu}^{\leftarrow})], \quad (49b)$$

$$\mathcal{S}_{\ell\mu,21} = (z_{\mu}^{\leftarrow} - z_{\mu}^{\leftarrow} \mathcal{S}_{\mu,22})^{-1} \mathcal{S}_{\mu,21}, \quad (49c)$$

$$\mathcal{S}_{\ell\mu,22} = (z_{\mu}^{\leftarrow} - z_{\mu}^{\leftarrow} \mathcal{S}_{\mu,22})^{-1} (z_{\mu}^{\leftarrow} \mathcal{S}_{\mu,22} - z_{\mu}^{\leftarrow}). \quad (49d)$$

The buffer effect due to the velocity mismatch at buffer-ring interfaces still remains in the above expressions. However, one can recover the original form of the scattering matrix by redefining the controlling parameter ϵ . In other words, one can easily prove that the above scattering matrix can be rewritten as

$$\mathcal{S}_{\ell\mu,ij}(\epsilon, U_b) = \mathcal{S}_{ij}(\epsilon'_{\mu}) \quad (50)$$

with

$$\epsilon'_{\mu}(\epsilon, U_b) = \frac{(v_{\mu}/v_b)\epsilon}{(z_{\mu}^{\leftarrow} + \zeta z_{\mu}^{\leftarrow} \sqrt{1 - 2\epsilon})^2}. \quad (51)$$

Note that $0 \leq \epsilon'_{\mu} \leq 1/2$ for $0 \leq \epsilon \leq 1/2$ and $0 < v_b < \infty$, as expected. This implies that in the cases in which the spin-separate treatment is possible, the only role of the buffer is to renormalize the tunneling parameter ϵ through Eq. (51). Hence the buffer is unnecessary and the junction can be characterized by a single parameter ϵ'_{μ} of arbitrary values. However, our formalism reveals the possible origin of spin-dependent values for ϵ'_{μ} . The difference between ϵ'_{μ} for two spins is due to different group velocity v_{μ} in the ring and the consequent difference in the magnitude of velocity mismatch at the junction. Even though it is convention in the literature to define the same value of ϵ for two spins, it is more physically correct to have different tunneling parameters for two spin components, as shown in our formalism.

IV. NONORTHOGONAL SPIN STATES

As an application of our formalism, we consider the n -type semiconductor ring with both the Rashba SOC and the Zeeman splitting. First, we set up the lead-arm scattering matrix in this case and then examine the features of the scattering matrix. After that, the spin-resolved transport through the ring is investigated.

A. Setup of the scattering matrix

The Rashba SOC in the ring geometry is given by

$$H_{\text{SO}} = \frac{\alpha}{\rho_0} \left[(\sigma_x \cos \phi + \sigma_y \sin \phi) \left(-i \frac{\partial}{\partial \phi} - f \right) + \frac{i}{2} (\sigma_x \sin \phi - \sigma_y \cos \phi) \right]. \quad (52)$$

It is straightforward to calculate the eigenstates of the ring Hamiltonian, Eq. (10), and we obtain four eigenstates,³⁵

$$\varphi_+^e(\phi) = e^{i(k_+^e + f)\phi} \begin{bmatrix} e^{-i\phi/2} \cos \frac{\theta_+^e}{2} \\ e^{+i\phi/2} \sin \frac{\theta_+^e}{2} \end{bmatrix}, \quad (53a)$$

$$\varphi_-^e(\phi) = e^{i(k_-^e + f)\phi} \begin{bmatrix} -e^{-i\phi/2} \sin \frac{\theta_-^e}{2} \\ e^{+i\phi/2} \cos \frac{\theta_-^e}{2} \end{bmatrix}, \quad (53b)$$

where the wave numbers are the solutions of

$$\frac{E}{E_0} = [k_\mu^e]^2 + \mu \sqrt{(\gamma_Z - k_\mu^e)^2 + (\gamma_R k_\mu^e)^2} + \frac{1}{4} \quad (54)$$

with dimensionless constants

$$\gamma_Z \equiv \frac{g^* \mu_B B / 2}{E_0} \quad \text{and} \quad \gamma_R \equiv \frac{\alpha / \rho_0}{E_0}. \quad (55)$$

Here $E_+(\gamma_R, \gamma_Z)$ is the energy bottom of the upper spin branch ($\mu = +$), and the angles are defined via

$$\cos \theta_\mu^e = \frac{\gamma_Z - k_\mu^e}{\sqrt{(\gamma_Z - k_\mu^e)^2 + (\gamma_R k_\mu^e)^2}}, \quad (56a)$$

$$\sin \theta_\mu^e = \frac{\gamma_R k_\mu^e}{\sqrt{(\gamma_Z - k_\mu^e)^2 + (\gamma_R k_\mu^e)^2}}. \quad (56b)$$

Note that the spin textures of the eigenstates are all crownlike as in the Rashba SOC-only case: The effective magnetic

field for each eigenstate has the radial and z -directional components whose relative strength is determined by the angle θ_μ^e . However, in this case, the angles θ_μ^e are all different, which may lead to complicated (energy-dependent) spin precession along the ring. On the reversal of the Zeeman splitting, Eqs. (54) and (56) guarantee the following relations:

$$k_\mu^e(\gamma_Z) = -k_\mu^e(-\gamma_Z) \quad \text{and} \quad \theta_\mu^e(\gamma_Z) = \theta_\mu^e(-\gamma_Z) + \mu\pi. \quad (57)$$

Both the parameters γ_Z and f are proportional to the magnetic field B , and their ratio is fixed to

$$\frac{\gamma_Z}{f} = g^* \frac{m^*}{m}, \quad (58)$$

where m is the electron mass in vacuum. In solids, the effective mass of electrons can be much smaller than its raw value. So the dimensionless flux f can vary over successive integers with a negligible change in γ_Z .

In order to build the lead-ring scattering matrices, Eq. (39), one needs to construct the appropriate matrices $\mathcal{U}^\rho(\phi)$ and $\mathcal{V}^\rho(\phi)$. By using the above eigenstates and the velocity operator,

$$v_\phi = \frac{\hbar}{m\rho_0} \left(-i \frac{\partial}{\partial \phi} - f \right) + \frac{\alpha}{\hbar} (\sigma_x \cos \phi + \sigma_y \sin \phi), \quad (59)$$

the matrices for the n -type semiconductor ring are found to be

$$\mathcal{U}^\rho(\phi) = \begin{bmatrix} e^{-i\phi/2} \cos \frac{\theta_+^e}{2} & -e^{-i\phi/2} \sin \frac{\theta_+^e}{2} \\ e^{+i\phi/2} \sin \frac{\theta_+^e}{2} & e^{+i\phi/2} \cos \frac{\theta_+^e}{2} \end{bmatrix}, \quad (60a)$$

$$\mathcal{V}^\rho(\phi) = \frac{\hbar}{m\rho_0} \left(\begin{bmatrix} k_+^e e^{-i\phi/2} \cos \frac{\theta_+^e}{2} & -k_-^e e^{-i\phi/2} \sin \frac{\theta_+^e}{2} \\ k_+^e e^{+i\phi/2} \sin \frac{\theta_+^e}{2} & k_-^e e^{+i\phi/2} \cos \frac{\theta_+^e}{2} \end{bmatrix} + \frac{1}{2 \cos \theta_R} \begin{bmatrix} -e^{-i\phi/2} \cos \frac{2\theta_R - \theta_+^e}{2} & -e^{-i\phi/2} \sin \frac{2\theta_R - \theta_+^e}{2} \\ -e^{+i\phi/2} \sin \frac{2\theta_R - \theta_+^e}{2} & e^{+i\phi/2} \cos \frac{2\theta_R - \theta_+^e}{2} \end{bmatrix} \right), \quad (60b)$$

with the Rashba angle θ_R defined via

$$\cos \theta_R \equiv -\frac{1}{\sqrt{1 + \gamma_R^2}} \quad \text{and} \quad \sin \theta_R \equiv \frac{\gamma_R}{\sqrt{1 + \gamma_R^2}}. \quad (61)$$

These matrices enter into Eq. (33) and determine the lead-arm scattering matrices in Eq. once the injection and detection spin axes are fixed through \mathcal{U}_ℓ .

For a closed ring, the single-valued condition quantizes the ring levels:

$$n = k_\mu^e(E) + f - \frac{1}{2}, \quad (62)$$

where n is any integer.

B. Lead-arm scattering matrix

In this subsection, we examine the matrix elements of the lead-arm S matrix, Eq. (39), in the presence of both the Rashba

SOC and Zeeman terms. For later use, the matrix elements of the S matrix for the left junction ($\ell = L$) are called

$$\mathcal{S}_{L,11} = \begin{bmatrix} r_{++} & r_{+-} \\ r_{-+} & r_{--} \end{bmatrix} \quad \text{and} \quad \mathcal{S}_{L,21} = \begin{bmatrix} t_{u++} & t_{u+-} \\ t_{u-+} & t_{u--} \\ t_{d++} & t_{d+-} \\ t_{d-+} & t_{d--} \end{bmatrix}. \quad (63)$$

First, we focus on the spin-flip scattering taking place in the lead side. Figure 2 shows the dependence of the reflection amplitudes $|r_{\mu\mu'}|^2$ on U_b for different values of γ_Z , with γ_R being fixed at a finite value. In the absence of the Zeeman splitting ($\gamma_Z = 0$), we obtain $|r_{++}|^2 = |r_{--}|^2$ and $|r_{+-}|^2 = |r_{-+}|^2 = 0$, as expected. We numerically confirmed that this is true regardless of the polarization axis ($\vartheta_\ell, \phi_\ell$), the Rashba SOC strength γ_R , the junction parameters ϵ , and U_b . That is, no spin-flip reflection takes place when only the Rashba SOC exists. In this case, the role of U_b is to simply renormalize ϵ [see Eq. (51)] as displayed in Figs. 2(a) and 2(b): The perfect

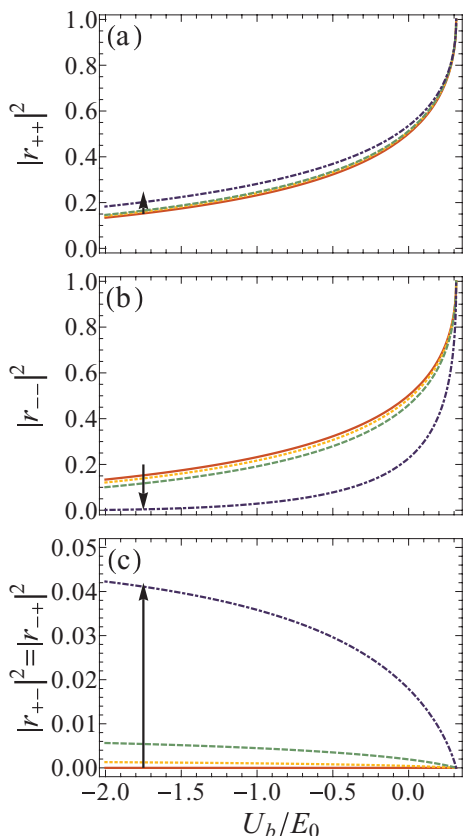


FIG. 2. (Color online) Reflection amplitudes as functions of U_b ($\leq E$) for different values of γ_Z : 0 (solid), $\gamma_R/2$ (dotted), γ_R (dashed), and $2\gamma_R$ (dot-dashed). Here we set $\epsilon = 1/4$, $\gamma_R = 0.1$, and $E = 1.02 \times E_+$ ($\gamma_R = 0.1, \gamma_Z = 0.2$). The spin polarization in the lead is set to be along the x axis: $(\vartheta_L, \varphi_L) = (\pi/2, 0)$. The arrows indicate the trend with increasing γ_Z .

transmission can happen at some values of U_b even though $\epsilon = 1/4 < 1/2$ is used.

On the other hand, the spin-conserving feature of the reflection is no longer valid as soon as the Zeeman splitting is switched on. Figure 2(c) clearly shows that the spin-flip reflection occurs for finite values of γ_Z , and its amplitude, $|r_{+-}|^2 = |r_{-+}|^2$, increases with γ_Z . The spin-flip reflection depends sensitively on the incident energy E and the polarization axis $(\vartheta_\ell, \varphi_\ell)$ as well as U_b , as can be seen in Fig. 3. It modulates with the spin-polarization axis in the lead, and more importantly, decreases rapidly with increasing E . Although the amplitude of spin-flip scattering can be considerably large near the band bottom, E_+ , it becomes negligibly small with the incident energy E well above the band bottom. This explains why the previous works^{5,8,10} could not see the breakdown of the current conservation with their wrong S matrix: Unless the energy is close to the band bottom, the spin-flip scattering makes quite a small contribution to the total current. However, its presence, although small, is important to fulfill both the current conservation and the correct matching of the wave function.

Figure 4 displays the transmission amplitudes $|t_{u\mu+}|^2$ and $|t_{d\mu+}|^2$ as functions of U_b for spin $\mu = +$ injection from the lead. In the absence of the Zeeman splitting, $|t_{u++}|^2 = |t_{d-+}|^2$

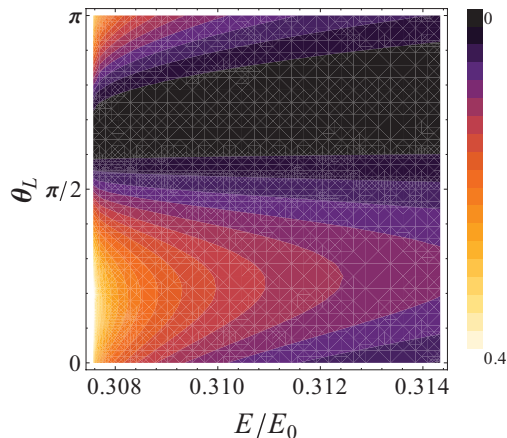


FIG. 3. (Color online) Contour plot of spin-flip reflection amplitude $|r_{+-}|^2$ as a function of E and ϑ_L . Here we set $\epsilon = 1/2$, $U_b = 0$, $\gamma_R = 0.1$, $\gamma_Z = 2\gamma_R$, $\varphi_L = 0$. The energy ranges from E_+ ($\gamma_R = 0.1, \gamma_Z = 0.2$) to $1.02E_+$ ($\gamma_R = 0.1, \gamma_Z = 0.2$).

and $|t_{u-+}|^2 = |t_{d++}|^2$ hold no matter what values the other parameters have. Similar relations can be found for spin-injection as well. This is because the eigenstates $\varphi_+(\phi)$ and $\varphi_-(\phi)$ make time-reversal pairs with $\varphi_-(\phi)$ and $\varphi_+(\phi)$, respectively. However, the introduction of finite Zeeman splitting breaks the time-reversal symmetry of the system, and the balance between the transmission coefficients is gone. The transmission amplitudes for different μ and ϱ behave differently with increasing γ_Z because the group velocities v_μ^{ϱ} are all different, and the spin overlaps between the injected wave and the eigenstates also become different from each other. Note that the transmission amplitudes are not necessarily smaller than 1 since it is the current, not the tunneling coefficient, that satisfies the unitary condition.

As proposed in our formalism, the charge-current conservation, $J_L + J_U - J_D = 0$, is well satisfied, as shown in Fig. 5. Interestingly, the time-reversal breaking and its consequences on the transmission amplitudes do not invalidate the symmetric scattering to two arms imposed on the raw S matrix, Eq. (26). As can be seen from Fig. 5, the normalized currents in both

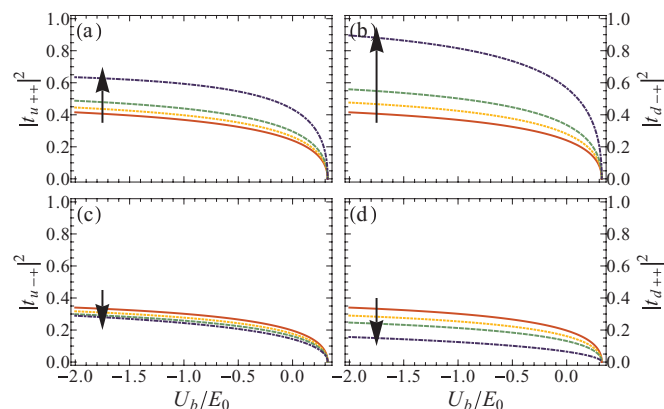


FIG. 4. (Color online) Transmission amplitudes $|t_{u\mu+}|^2$ and $|t_{d\mu+}|^2$ as function of U_b for spin $\mu = +$ injection from the lead. Values of parameters and plot styles are the same as in Fig. 2 except $E = 1.05 \times E_+$ ($\gamma_R = 0.1, \gamma_Z = 0.2$).

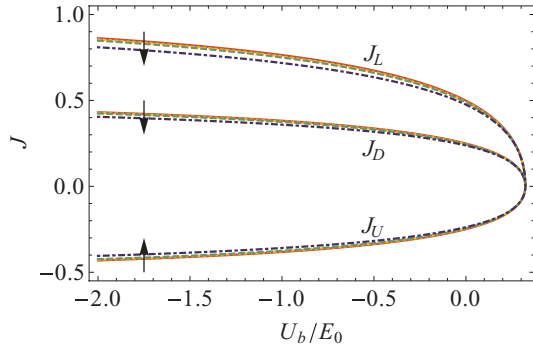


FIG. 5. (Color online) Charge currents, J_L , J_U , and J_D , as functions of U_b with respect to a unit spin + polarized current ($v_0 = 1$) from the lead. Values of parameters and plot styles are the same as in Fig. 4.

arms are observed to always satisfy $J_U = -J_D$. One would guess that the imbalances in the transmission amplitudes (see Fig. 4) and nonorthogonality of the eigenstates lead to the asymmetry between the scatterings at upper and lower buffer-arm interfaces. However, our calculations show that the symmetry of the junction remains untouched based on the fact that the raw S matrix is symmetric and the upper and lower arms are identical.

Finally, we extract the effective spin-dependent control parameters ϵ_μ from

$$\epsilon_\mu \equiv \frac{1 - \sum_{\mu'} |r_{\mu'\mu}|^2}{2} \quad (64)$$

as a function of ϵ and U_b in Fig. 6. As expected, ϵ_μ depends sensitively on U_b , and is spin-dependent: $\epsilon_+ \neq \epsilon_-$. Moreover, it also depends on the ring property, such as the strength of the Rashba SOC and the Zeeman term, so that, in contrast to the conventional scattering theory, the scattering at a junction is not determined solely by the junction itself but is affected by the arm properties as wells.

C. Aharonov-Bohm interferometry

In this subsection, we investigate the charge and spin transport through the Aharonov-Bohm-type interferometer in the presence of both the Rashba SOC and Zeeman terms. We divide the study into two regimes: weak- and strong-coupling limits. In the weak-coupling regime where the effective control parameters ϵ_μ are small, the transport features the quantized levels in the ring, while in the strong-coupling regime the interference between the eigenstates is important.

1. Weak-coupling limit

Figure 7 shows a typical dependence of the charge conductance G on f and γ_Z in the weak-coupling limit with $\epsilon = 0.15$ and $U_b = 0$. The high transmission (the bright lines) occurs when the quantization condition, Eq. (62), is satisfied. Here the resonant tunneling via the quantized ring levels boosts the transmission. This boosting is not affected by the choice of the spin-polarization axis in the leads. Exactly the same charge conductance is obtained by taking the spin-polarization axis along the z axis instead of the x axis used in Fig. 7. The conductance plot is symmetric with respect to the point

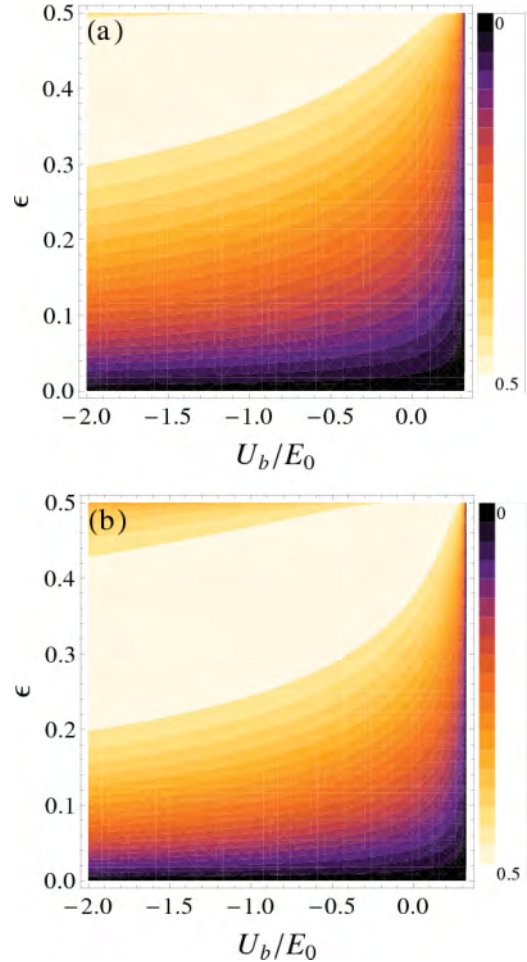


FIG. 6. (Color online) Contour plots of effective control parameters ϵ_+ (a) and ϵ_- (b) as functions of ϵ and U_b for $\gamma_R = 0.1$, $\gamma_Z = 2\gamma_R$, $E = 1.05 \times E_+$ ($\gamma_R = 0.1$, $\gamma_Z = 0.2$), and $(\vartheta_L, \varphi_L) = (\pi/2, 0)$.

(f, γ_Z) = (0, 0), which is attributed to the relations in Eq. (57). In addition, the resonance lines exhibit the anti-crossing-like behavior, which is absent in the quantized levels themselves, Eq. (62). The anticrossing behavior originates from the Fano-like antiresonance between two degenerate ring states whose spin polarizations are rather parallel, leading to large overlap between their wave functions. In this case, the injected state with any spin polarization has almost the same overlaps with the degenerate ring states, resulting in destructive interference between them in the transmitted state. This happens mostly when the time-reversal pair states $(\varphi_+^+, \varphi_-^-)$ or $(\varphi_+^-, \varphi_-^+)$ cross, as seen in Fig. 7, and less frequently when the counterpropagating pair states $(\varphi_+^+, \varphi_-^-)$ or $(\varphi_+^-, \varphi_-^+)$ do. For the pairs $(\varphi_+^+, \varphi_-^+)$ or $(\varphi_+^-, \varphi_-^-)$, their spin polarizations are almost orthogonal to each other so that the transport through each state is almost independent of that through the other, and their transmission amplitudes are simply additive.

In Fig. 8(a), the charge conductance is calculated as a function of external magnetic field B or the normalized flux f by taking into account the linear relation, Eq. (58), between γ_Z and f with the ratio $g^*m^*/m = 0.1$, which is indicated by the white lines in Fig. 7. The charge conductance clearly exhibits four (or three) peaks as the magnetic flux is increased by one flux quantum Φ_0 . The accidental degeneracy in the ring

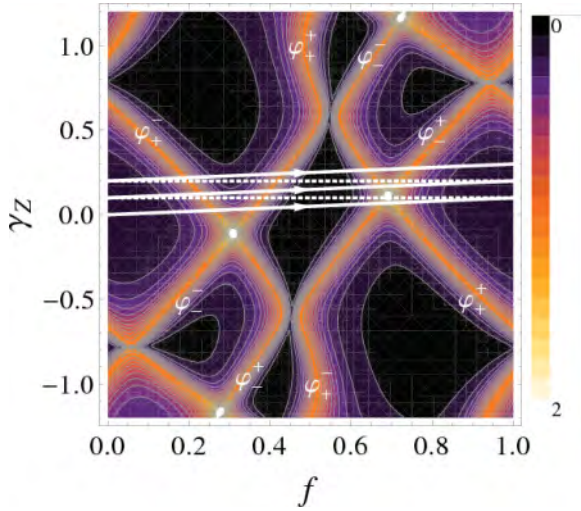


FIG. 7. (Color online) Contour plot of charge conductance G in units of e^2/h as a function of f and γ_Z in the weak-coupling limit with $\epsilon = 0.15$ and $U_b = 0$. Here we have used $\gamma_R = 0.4$ and $E = 2E_+(\gamma_R = 0.4, \gamma_Z = 0.8)$. The white lines follow the linear relation between f and γ_Z : $\gamma_Z = 0.1 \times f$.

levels enhances the conductance further, while it is still smaller than the two-channel maximum value $2e^2/h$. The fluctuations in the peak heights are mainly due to the variation of the spin-polarization axis of the ring eigenstates at junctions.

Each ring eigenstate, having the crownlike spin texture, brings about the spin-flip transport as shown in Figs. 8(b) and 8(c). While the peaks in the spin-flip transmission amplitudes (solid lines) are located at the same positions as those in the charge conductance, they alternate between T_{+-} and T_{-+} :

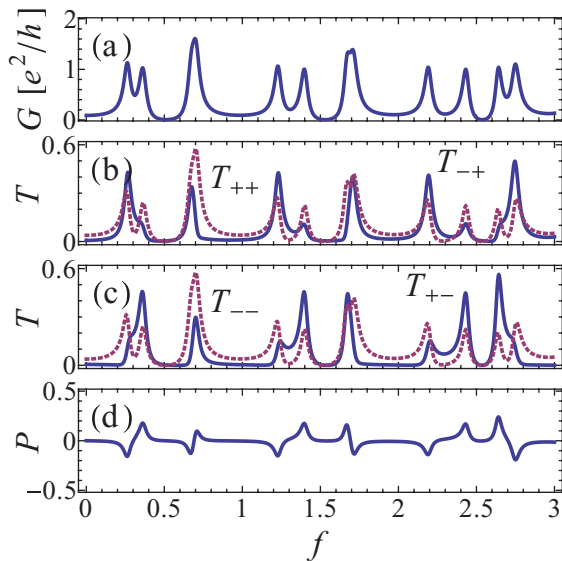


FIG. 8. (Color online) (a) Charge conductance G , (b,c) spin-conserving transmission amplitudes T_{++} , T_{--} (dotted lines), and spin-flip transmission amplitudes T_{+-} , T_{-+} (solid lines), and (d) current polarization as functions of f along the white lines in Fig. 7 with $\gamma_Z = 0.1 \times f$. Here the polarization axis of two leads is chosen to align with the positive x axis: $(\vartheta_\ell, \varphi_\ell) = (\pi/2, 0)$. Values of other parameters are the same as in Fig. 7.

the $\mu = +$ level gives rise to the enhancement of T_{-+} and the $\mu = -$ level to that of T_{+-} . This level dependence is easily understood from the fact that the spin polarization of the $\mu = +$ ($-$) level has an inward (outward) radial component. Since the tilt angle ϑ_μ^0 varies between 0 and π , however, the spin-flip amplitudes also fluctuate. In addition, each level also makes a comparable contribution to the spin-conserving transmissions, $T_{++} = T_{--}$ (dotted lines), which follow the behavior of the charge conductance. These spin-dependent transmissions enable the unpolarized current input to generate the spin-polarized current. As seen in Fig. 8(d), the current polarization P exhibits peaks and valleys whenever the spin-flip transmission is enhanced. However, since the spin blocking or the spin flip occur only partially, its magnitude is usually much smaller than $1/2$.

In order to achieve the complete spin polarization or spin flip, the lead spin axis should be set to align with the (energy-dependent) spin polarization of the level at the junction. However, the arbitrary tuning of the spin polarization of the lead is not easy to implement. Instead, one can adjust the spin polarization of the ring level to the predefined spin axis of the lead by tuning the external magnetic field. The formulas for the tilt angle, Eq. (56), show that a special adjustment, $k_\mu^0 = \gamma_Z$, yields $\theta_\mu^0 = \pm\pi/2$, setting the spin-polarization axis of the arm state at junctions along the x direction. The adjustment requires the energy

$$\frac{E}{E_0} = \gamma_Z^2 + |\gamma_Z \gamma_R| + \frac{1}{4} \quad (65)$$

(here $\mu = +$ is chosen) and the quantization condition

$$n = \gamma_Z + f - \frac{1}{2}. \quad (66)$$

From Eq. (66), together with Eq. (58), the candidates for the magnetic field B or the normalized Zeeman splitting γ_Z are suggested, and the energy is then determined through Eq. (65). Figure 9 displays the variation of transmission amplitudes with $n = 6$ in Eq. (66). At the point 1 ($f = f_1$), the two conditions, Eqs. (65) and (66), are exactly satisfied with $k_+^0 = \gamma_Z$ so that T_{+-} is almost at its maximum and the other amplitudes are negligible. Hence, the *conditional spin switch* is embodied: the spin $+$ is completely blocked while spin $-$ is completely flipped. At the same time, the maximal current polarization shown in Fig. 9(c) indicates that it can also work as the perfect spin polarizer for unpolarized injection. The opposite spin switch that flips spin $+$ to $-$ can be implemented by reversing the direction of the external magnetic field so that the two conditions are satisfied with $k_-^0 = \gamma_Z < 0$. Note that the behavior as the perfect spin switch or spin polarizer appears at $f \approx f_1 \pm 1$ (points 2 and 3) as well. This is due to the small ratio $g^*m^*/m = 0.1$ used in calculations: γ_Z does not change so much for a few periods of f so that the conditions, Eqs. (65) and (66), are approximately satisfied at several values of f .

The spin flip occurring at the junction discussed in the preceding section would spoil the spin switch efficiency by inducing the tunneling to the other spin branch, and the spin tunneling cannot be determined only by the spin texture of the levels in the ring. However, we numerically confirmed that the observed spin-switch functionality is immune to the variation of ϵ and U_b as long as the effective control parameters ϵ_μ are small enough. In fact, the spin flip is very weak if the injection

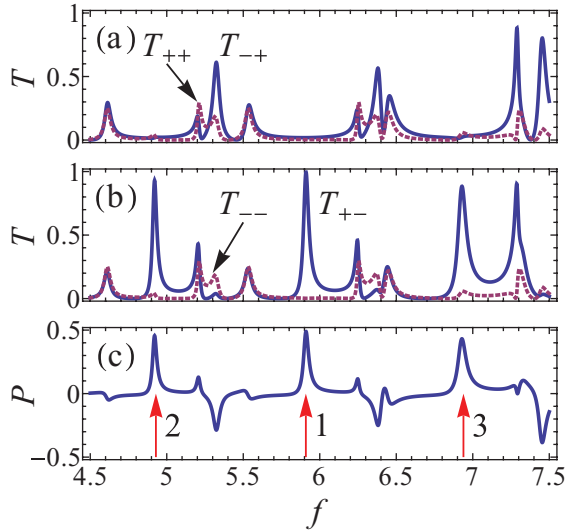


FIG. 9. (Color online) (a),(b) Spin-conserving transmission amplitudes T_{++} , T_{--} (dotted lines) and spin-flip transmission amplitudes T_{-+} , T_{+-} (solid lines), and (c) current polarization as functions of f with the relation $\gamma_Z = 0.1 \times f$. The condition $k_+^z = \gamma_Z$ is exactly satisfied at the point 1, and the energy E is given by Eq. (65) with respect to the solutions of Eq. (66) for $n = 6$. Here we have used $\epsilon = 0.1$, $U_b = 0$, and $\gamma_R = 0.4$. The red arrows indicates the points (1,2,3) where the spin switch is close to its maximum.

energy is well above the band bottom E_+ (see Fig. 3). This is the case for Eq. (65) as long as γ_R is large enough. One can then safely use the usual analysis of spin transport based on the spin precession in the ring with no spin flip at the junctions.

2. Strong-coupling limit

Figure 10 shows the evolution of the charge conductance G as the lead-ring junction gets more transparent. The resonance feature due to the ring level, in spite of getting smeared out with increasing ϵ , is still visible up to $\epsilon \sim 0.4$. For larger values of $\epsilon \gtrsim 0.4$, the conductance peak position does not follow the quantization condition, Eq. (62), any longer, and instead every four consecutive peaks in a period of f are merged to a single one that is located close to $f = n\pi$. In addition, a dip is formed between them. The dip appears between the time-reversal pair states if they are in succession, as can be seen in Figs. 10 (a), 10(c), and 10(d). Interestingly, the anti-crossing-like behavior can be intensified as ϵ increases, as seen in Fig. 10(c), if the pair states are close to each other in the weak-coupling limit. In this case, the transparent junction enhances the destructive interference between two resonant levels. The dip can also be formed in other places if the time-reversal pair is not in succession [see Fig. 10(b)]. In this case, the dip is less prominent, implying the destructive interference is not strong enough.

The charge transport in the strong-coupling limit ($\epsilon \sim 1/2$), as seen in Fig. 11, clearly exhibits the well-known AB oscillations as the magnetic flux is varied. In addition, the Zeeman splitting γ_Z , increasing linearly with f , superposes line-shaped patterns upon the AB oscillations along which the conductance is suppressed. This suppression is due to the localization effect in the ring. To put it simply, consider

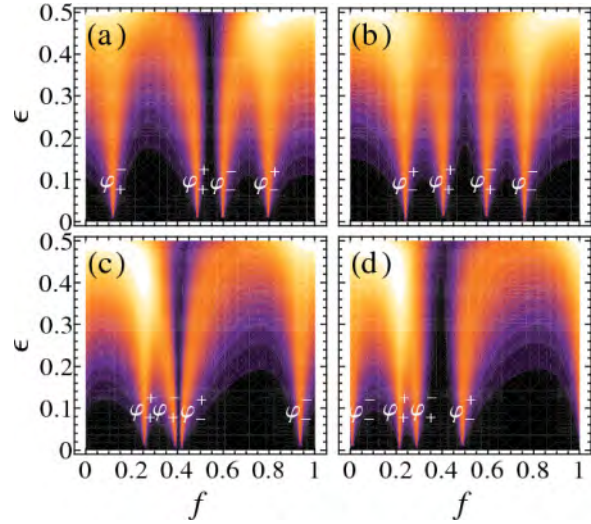


FIG. 10. (Color online) Contour plots of charge conductance G in units of e^2/h as a function of f and ϵ for (a) $\gamma_R = \gamma_Z = 0.4$ and $E = 2E_+(\gamma_R = 0.4, \gamma_Z = 0.8)$ (refer to Fig. 7) and (b),(c),(d) $\gamma_R = 0.6$ and $E = 2E_+(\gamma_R = 0.6, \gamma_Z = 1.3)$ with $\gamma_Z = 0$ (b), 0.7 (c), and 1 (d). Here we have used $U_b = 0$, and the color scale is the same as in Fig. 7.

the Rashba-free system. The analytical expression for the spin-dependent transmission amplitude is then available:

$$T_\mu = \frac{4\epsilon'_\mu{}^2 \cos^2 \pi f \sin^2 \pi \tilde{k}_\mu}{|\epsilon'_\mu e^{2\pi i \tilde{k}_\mu} - \cos 2\pi \tilde{k}_\mu + \left(\frac{1-p_\mu}{2}\right)^2 + \left(\frac{1+p_\mu}{2}\right)^2 \cos 2\pi f|^2}, \quad (67)$$

with ϵ'_μ given by Eq. (51), $p_\mu = \sqrt{1 - 2\epsilon'_\mu}$, and $\tilde{k}_\mu = \sqrt{E/E_0 - \mu\gamma_Z}$. The transmission vanishes not only when $f = n + 1/2$ but also when $\tilde{k}_\mu = n$, where n is an integer. The latter condition means that the wave in the ring forms the standing wave so that the state is localized and does not contribute to the transport. Hence the conductance suppression happens at $E/E_0 = n^2 + \mu\gamma_Z$, making spin-dependent dark lines in the charge conductance (see Fig. 11). The Rashba SOC, present in our system but rather small, makes a perturbative coupling between spin-+ and -- states, inducing the anticrossing of

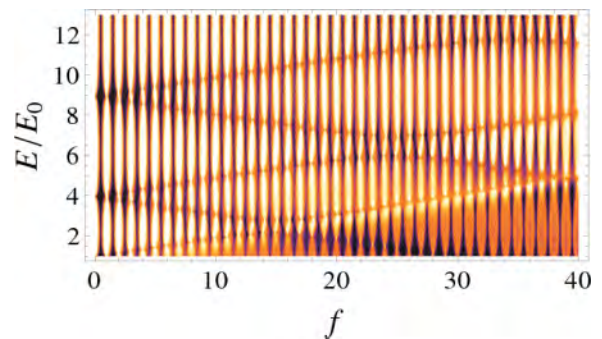


FIG. 11. (Color online) Contour plot of charge conductance G in units of e^2/h as a function of f and E/E_0 in the strong-coupling limit ($\epsilon = 1/2$). We have used $U_b = 0$ and $\gamma_R = 0.4$ and the Zeeman splitting γ_Z increases linearly with f : $\gamma_Z = 0.1 \times f$. The color scale is the same as in Fig. 7.

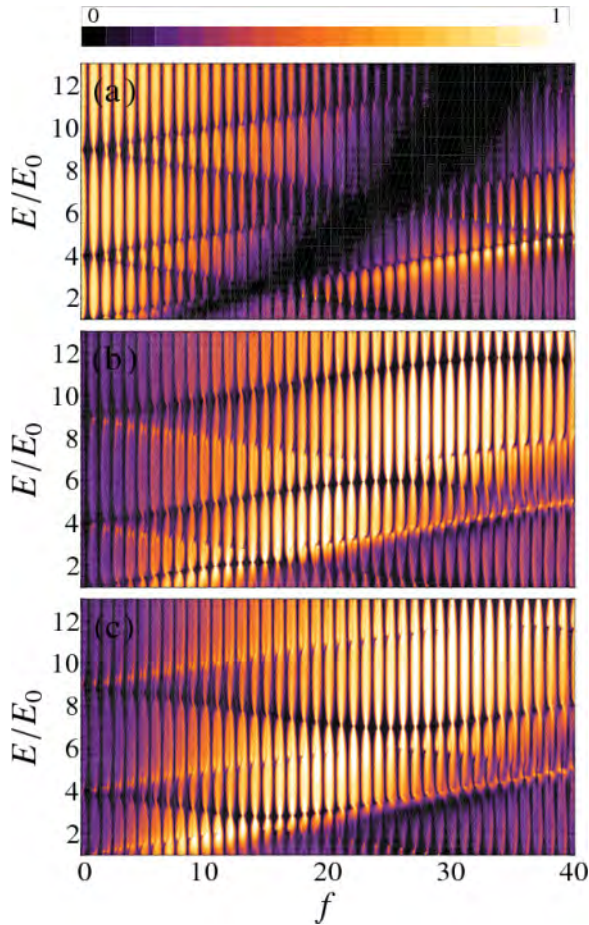


FIG. 12. (Color online) Contour plot of (a) spin-conserving transmission amplitudes $T_{++} = T_{--}$ and (b),(c) spin-flip transmission amplitudes T_{-+} (b) and T_{+-} (c) as functions of f and E/E_0 in the strong-coupling limit ($\epsilon = 1/2$). Here the polarization axis of two leads is chosen to align with the positive x axis: $(\vartheta_\ell, \varphi_\ell) = (\pi/2, 0)$. Values of other parameters are the same as in Fig. 11.

dark lines that would be degenerate otherwise. Finally, one can notice that in the lower right corner of Fig. 11 (under the line $E/E_0 = 1 + \gamma_Z$), the charge conductance is quite suppressed; the maximum is reduced by half, reaching e^2/h , not $2e^2/h$. This is because in this region $E < E_+$ so that only the spin- $-$ channel is open. The spin- $+$ channel exists in the evanescent waves whose contribution decreases exponentially with $E_+ - E$.

The spin transport in the strong-coupling limit is examined in Fig. 12. Similarly to the charge conductance, the spin-dependent transmissions feature the AB oscillations and the localization-induced dark line patterns. In addition, they also exhibit a global modulation of the height of the AB peaks. Interestingly, the modulation patterns are in opposite trends between spin-conserving transmissions (T_{++} and T_{--}) and spin-flip transmissions (T_{+-} and T_{-+}): when the spin-conserving transmissions are strong, the spin-flip transmissions are weak, and vice versa. This opposing behavior is clearly displayed in Fig. 13, where the charge and spin transmissions are calculated at a given injection energy, $E = 9E_0$. This global modulation of spin-dependent transmission is surely related to the variation of γ_Z with f : $\gamma_Z = 0.1 \times f$ is used here.

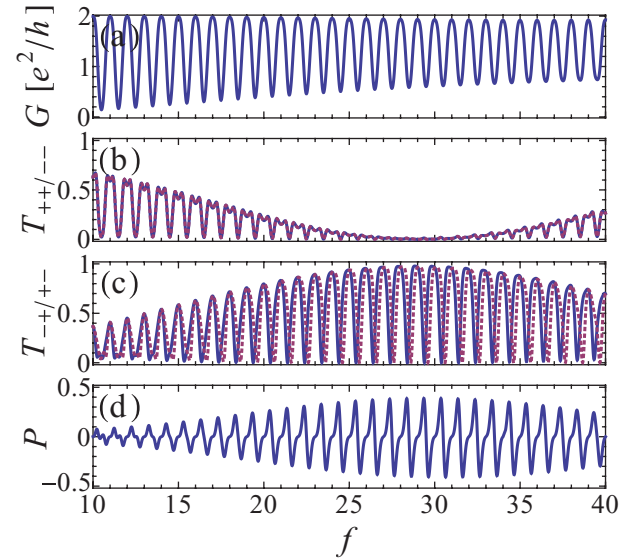


FIG. 13. (Color online) (a) Charge conductance G , (b) spin-conserving transmission amplitudes T_{++} (solid line), T_{--} (dotted line), (c) spin-flip transmission amplitudes T_{-+} (solid line), T_{+-} (dotted line), and (d) current polarization as functions of f along the $E = 9E_0$ line in Fig. 12. Here the polarization axis of two leads is chosen to align with the positive x axis: $(\vartheta_\ell, \varphi_\ell) = (\pi/2, 0)$. Values of other parameters are the same as in Fig. 12.

Subsequently, the nonadiabatic geometric phase connected to the Rashba SOC and the Zeeman splitting varies gradually and changes the interference between the ring modes, resulting in the modulation of the spin-dependent transmission. With the total charge transmission unchanged so much, the decrease of the spin-conserving transmission then accompanies the enhancement of the spin-flip transmission. Hence, in the regime of parameters where the spin-conserving transmissions are negligible, an *unconditional spin switch* is implemented: the injected spin $+$ is switched to the spin $-$ and vice versa. As can be seen in Figs. 12 and 13, the parameter regime for the system to act as a good spin switch is quite wide: the working condition encloses several periods of f and a wide range of energy. It is attributed to the slow variation of the geometrical phase with f . Finally, this system can also behave as a good spin polarizer for unpolarized current injection, as seen in Fig. 13(d). Since the maxima of T_{-+} and T_{+-} are off the synchronization, the current polarization oscillates strongly between -0.4 and 0.4 . The polarization of spin current can then be easily tuned by changing the magnetic flux by the half-flux quantum $\Phi_0/2$.

In fact, there is a prior numerical study that also investigated the effect of both the Rashba SOC and the Zeeman splitting in the strong-coupling limit by using the nonequilibrium Green's function formalism based on the tight-binding model.²² However, using rather small values of the magnetic field, $-3 \leq f \leq 3$, the Zeeman splitting could not have any noticeable effect in the study: Note that the value of g^*m^*/m is small in usual semiconductors [see Eq. (58)], so we have varied f over a wide range. Hence we believe that our study is the first analysis that has considered both the Rashba SOC and the Zeeman splitting on an equal footing.

V. DISCUSSION AND CONCLUSION

We have proposed a general scattering-matrix formalism that naturally guarantees the charge conservation through a quantum ring with arbitrary spin-dependent interactions. To this end, we insert artificial SOC-free buffers in the vicinity of every junction and solve the system Hamiltonian in a standard way. The original problem is recovered by shrinking the size of the buffers to zero, while the effect of the buffers still remains. It is found that as long as the ring has nonorthogonal spin textures the spin-flip scattering can happen even if the junction itself is nonmagnetic. In the case of an n -type semiconductor with both the Rashba SOC and the Zeeman splitting, the finite spin-flip scattering and the conservation of charge current are numerically confirmed. In addition, it is found that the interplay of the AB and AC effects, in the presence of the Zeeman splitting, enables the ring interferometer to act as a conditional (unconditional) spin switch in the weak (strong)-coupling limit.

It should be noted that our formalism is not restricted to the structure of the AB interferometer used in this paper. The technique of inserting artificial buffers and shrinking them

to zero can be applied to any network of semiconductors with arbitrary SOC. As stated above, the merit of our formalism is that the charge-current conservation at junctions is guaranteed as long as the interfaces between buffers and the spin-dependent regions are treated correctly.

While in our study we focus on the simplest scattering matrix by minimizing the number of physical parameters for buffers, the scattering matrix can be generalized by introducing some spin-dependent coupling into the buffers in a controlled way. The extended form of the scattering matrix may give us a clue about the general structure of the scattering matrix connecting any spin-dependent channels with a single constraint: the charge-current conservation. It would be interesting to find out the general form of the scattering matrix based only on the conservation laws without relying on the specific model, such as buffers.

ACKNOWLEDGMENTS

This work was supported by grants from the Kyung Hee University Research Fund (KHU-20090742).

-
- ¹M. Büttiker, Y. Imry, and M. Y. Azbel, *Phys. Rev. A* **30**, 1982 (1984).
- ²D. Loss, P. Goldbart, and A. V. Balatsky, *Phys. Rev. Lett.* **65**, 1655 (1990).
- ³J.-B. Xia, *Phys. Rev. B* **45**, 3593 (1992).
- ⁴D. Loss and P. M. Goldbart, *Phys. Rev. B* **45**, 13544 (1992).
- ⁵Y.-S. Yi, T.-Z. Qian, and Z.-B. Su, *Phys. Rev. B* **55**, 10631 (1997).
- ⁶R. A. Römer and M. E. Raikh, *Phys. Rev. B* **62**, 7045 (2000).
- ⁷K. Kang and S.-C. Shin, *Phys. Rev. Lett.* **85**, 5619 (2000).
- ⁸D. Frustaglia, M. Hentschel, and K. Richter, *Phys. Rev. Lett.* **87**, 256602 (2001).
- ⁹F. E. Meijer, A. F. Morpurgo, and T. M. Klapwijk, *Phys. Rev. B* **66**, 033107 (2002).
- ¹⁰M. Hentschel, H. Schomerus, D. Frustaglia, and K. Richter, *Phys. Rev. B* **69**, 155326 (2004).
- ¹¹B. Molnár, F. M. Peeters, and P. Vasilopoulos, *Phys. Rev. B* **69**, 155335 (2004).
- ¹²D. Frustaglia and K. Richter, *Phys. Rev. B* **69**, 235310 (2004).
- ¹³S. Souma and B. K. Nikolić, *Phys. Rev. B* **70**, 195346 (2004).
- ¹⁴X. F. Wang and P. Vasilopoulos, *Phys. Rev. B* **72**, 165336 (2005).
- ¹⁵M. Lee and C. Bruder, *Phys. Rev. B* **73**, 085315 (2006).
- ¹⁶B. K. Nikolić, L. P. Zárbo, and S. Souma, *Phys. Rev. B* **73**, 075303 (2006).
- ¹⁷P. Lucignano, D. Giuliano, and A. Tagliacozzo, *Phys. Rev. B* **76**, 045324 (2007).
- ¹⁸A. A. Kovalev, M. F. Borunda, T. Jungwirth, L. W. Molenkamp, and J. Sinova, *Phys. Rev. B* **76**, 125307 (2007).
- ¹⁹M. Pletyukhov and U. Zülicke, *Phys. Rev. B* **77**, 193304 (2008).
- ²⁰M. F. Borunda, X. Liu, A. A. Kovalev, X.-J. Liu, T. Jungwirth, and J. Sinova, *Phys. Rev. B* **78**, 245315 (2008).
- ²¹D. Stepanenko, M. Lee, G. Burkard, and D. Loss, *Phys. Rev. B* **79**, 235301 (2009).
- ²²V. Moldoveanu and B. Tanatar, *Phys. Rev. B* **81**, 035326 (2010).
- ²³C. P. Umbach, S. Washburn, R. B. Laibowitz, and R. A. Webb, *Phys. Rev. B* **30**, 4048 (1984).
- ²⁴R. A. Webb, S. Washburn, C. P. Umbach, and R. B. Laibowitz, *Phys. Rev. Lett.* **54**, 2696 (1985).
- ²⁵T. Bergsten, T. Kobayashi, Y. Sekine, and J. Nitta, *Phys. Rev. Lett.* **97**, 196803 (2006).
- ²⁶B. Habib, E. Tutuc, and M. Shayegan, *Appl. Phys. Lett.* **90**, 152104 (2007).
- ²⁷B. Grbić, R. Leturcq, T. Ihn, K. Ensslin, D. Reuter, and A. D. Wieck, *Phys. Rev. Lett.* **99**, 176803 (2007).
- ²⁸F. Qu, F. Yang, J. Chen, J. Shen, Y. Ding, J. Lu, Y. Song, H. Yang, G. Liu, J. Fan, Y. Li, Z. Ji, C. Yang, and L. Lu, *Phys. Rev. Lett.* **107**, 016802 (2011).
- ²⁹Y. Aharonov and D. Bohm, *Phys. Rev.* **115**, 485 (1959).
- ³⁰Y. Aharonov and A. Casher, *Phys. Rev. Lett.* **53**, 319 (1984).
- ³¹S. A. Wolf, D. D. Awschalom, R. A. Buhrman, J. M. Daughton, S. von Molnár, M. L. Roukes, A. Y. Chtchelkanova, and D. M. Treger, *Science* **294**, 1488 (2001).
- ³²I. Zutic, J. Fabian, and S. Das Sarma, *Rev. Mod. Phys.* **76**, 323 (2004).
- ³³J. Nitta, T. Akazaki, H. Takayanagi, and T. Enoki, *Phys. Rev. Lett.* **78**, 1335 (1997).
- ³⁴S. Datta, *Electronic Transport in Mesoscopic Systems* (Cambridge University Press, Cambridge, 1995).
- ³⁵The solution, Eq. (53), is valid when the energy E is such that both of the spin branch solutions are involved. Otherwise, all four eigenstates belong to the lower spin branch.

Singlet-triplet splitting in double quantum dots due to spin-orbit and hyperfine interactionsDimitrije Stepanenko,¹ Mark Rudner,² Bertrand I. Halperin,² and Daniel Loss¹¹*Department of Physics, University of Basel, Klingelbergstrasse 82, CH-4056 Basel, Switzerland*²*Department of Physics, Harvard University, 17 Oxford St., Cambridge, Massachusetts 02138, USA*

(Received 8 December 2011; published 16 February 2012)

We analyze the low-energy spectrum of a two-electron double quantum dot under a potential bias in the presence of an external magnetic field. We focus on the regime of spin blockade, taking into account the spin-orbit interaction and hyperfine coupling of electron and nuclear spins. Starting from a model for two interacting electrons in a double dot, we derive an effective two-level Hamiltonian in the vicinity of an avoided crossing between singlet and triplet levels, which are coupled by the spin-orbit and hyperfine interactions. We evaluate the level splitting at the anticrossing, and show that it depends on a variety of parameters including the spin-orbit coupling strength, the orientation of the external magnetic field relative to an internal spin-orbit axis, the potential detuning of the dots, and the difference between hyperfine fields in the two dots. We provide a formula for the splitting in terms of the spin-orbit length, the hyperfine fields in the two dots, and the double dot parameters such as tunnel coupling and Coulomb energy. This formula should prove useful for extracting spin-orbit parameters from transport or charge sensing experiments in such systems. We identify a parameter regime where the spin-orbit and hyperfine terms can become of comparable strength, and discuss how this regime might be reached.

DOI: [10.1103/PhysRevB.85.075416](https://doi.org/10.1103/PhysRevB.85.075416)

PACS number(s): 73.21.La, 03.67.Lx, 73.63.Kv, 73.23.-b

I. INTRODUCTION

Electron spins in gated quantum dots have been extensively studied for their possible use in quantum information processing.¹⁻³ In this context, the main interest lies in the study of coherent quantum evolution of electron spins in a network of coupled quantum dots in the presence of external magnetic fields. A double quantum dot (DQD) populated by two electrons is the smallest such network in which all of the steps necessary for quantum computation can be demonstrated. In addition, a DQD can host encoded two-spin qubits that require less resources for control than the single-electron spins in quantum dots. In DQDs, the spins can be manipulated exclusively by electric fields in the presence of a constant magnetic field, taking advantage of the spin orbit and/or nuclear hyperfine interactions.^{2,4-13}

Requirements for the precise control of spin qubits have prompted the detailed study of the interactions of electron spins in quantum dots. The DQDs give experimental access to the coherent spin dynamics. Studies of transport through DQDs in the spin-blockade regime¹⁴ have been particularly useful for probing the electron and nuclear spin dynamics. In this regime, charge transfer between the two dots of a DQD can take place only when the electrons form a singlet state with total spin zero. This allows weak spin-non-conserving interactions to be studied via charge sensing¹⁵ or by charge transport measurements,^{14,16} even in the presence of much stronger spin-conserving interactions. The most important spin-non-conserving interactions are the spin-orbit interaction and the hyperfine interaction between the electron spins and a collection of nuclear spins inside the DQD.¹⁷

In this work, we investigate the hyperfine- and spin-orbit-mediated coupling between electronic singlet and triplet spin states of a DQD in the spin-blockade regime. We show that the spin-orbit and hyperfine contributions to this splitting can be tuned by a number of parameters. We derive an explicit formula that gives this splitting as a function of a homogeneous external

magnetic field and the detuning between the ground-state energies of the dots in a DQD. These parameters can be varied in an experiment. In addition, the splitting depends on the spin-orbit coupling interaction and the inhomogeneous nuclear Overhauser field as well as on the dot parameters such as the hopping amplitude between the dots in a DQD, Coulomb repulsion between the electrons, and the direct exchange interaction. Further, we describe how the dependence of the singlet-triplet splitting on these parameters might be used to extract the intrinsic strengths of the spin-orbit and hyperfine couplings from charge sensing measurements in which the DQD is swept through a singlet-triplet level crossing in the presence of spin-orbit interaction and a fluctuating nuclear field.

Recently, it was predicted that the angular momentum transferred between electron and nuclear spins in both dc transport¹⁸ and Landau-Zener-type gate sweep experiments^{19,20} can show extreme sensitivity to the ratio of spin-orbit and hyperfine couplings. Our result gives an explicit dependence of this ratio on the detuning and external magnetic field, thus showing how all regimes can potentially be reached.

The paper is organized as follows. In Sec. II, we introduce a model of a DQD, and describe its energy levels as a function of detuning. In Sec. III, we find the matrix elements of the spin-orbit interaction in the space of relevant low-energy states. In Sec. IV, we study the orbital and spin structure of the singlet and triplet states, which nominally intersect for particular combinations of the DQD potential detuning and external magnetic field. In Sec. V, we define an effective Hamiltonian that describes the action of the spin-orbit and hyperfine couplings in the corresponding two-level subspace. Then, in Sec. VI, we study the dependence of the resulting singlet-triplet splitting on external parameters and show how this dependence can be used to extract the spin-orbit interaction strength and the size of Overhauser field fluctuations from charge sensing measurements. In Sec. VII, we discuss how the DQD can be tuned between the regimes of spin-orbit-dominated splitting

and the hyperfine-dominated splitting. Finally, we summarize our results in Sec. VIII.

II. MODEL HAMILTONIAN FOR DOUBLE QUANTUM DOTS

In a DQD, electrons are confined near the minima of a double-well potential V_{DQD} , created by electrical gating of a two-dimensional electron gas (2DEG) in, for example, GaAs, see Fig. 1. For the case of a deep potential, we treat the two local minima of the double-well as isolated harmonic wells with ground-state wave functions $\varphi_{1,2}$. In order to define an orthonormal basis of single-particle states for building up the two-electron states of the DQD, we form the Wannier orbitals Φ_L and Φ_R , centered in the left and right dots, respectively:²¹

$$\Phi_{L,R} = \frac{1}{\sqrt{1-2sg+g^2}}(\varphi_{1,2} - g\varphi_{2,1}), \quad (1)$$

where $s = \langle \varphi_1 | \varphi_2 \rangle = \exp[-(a/a_B)^2]$ is the overlap of the harmonic oscillator ground-state wave functions of the two wells, $a_B = \sqrt{\hbar/m\omega_0}$ is the Bohr radius of a single quantum dot, $\hbar\omega_0$ is the single-particle level spacing, and $2a = l$ is the interdot distance. The mixing factor of the Wannier states is $g = (1 - \sqrt{1-s^2})/s$.

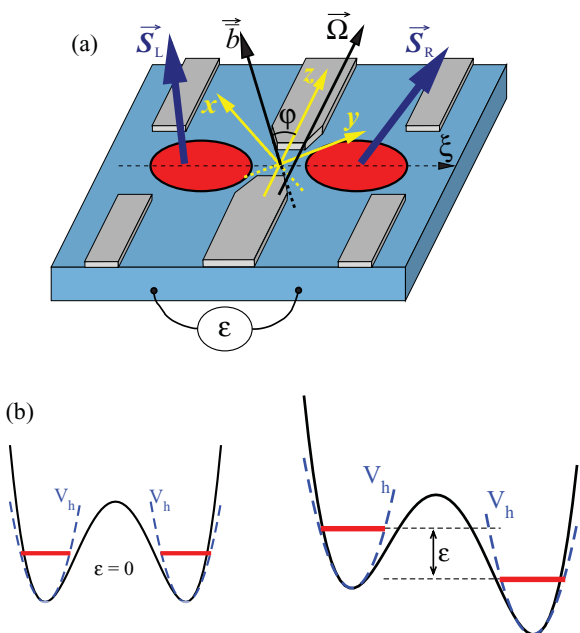


FIG. 1. (Color online) (a) Double quantum dot model and the coordinate system. \mathbf{S}_L and \mathbf{S}_R denote the spin 1/2 of the electron in the right and in the left quantum dots, respectively. The dots lie in the ξz plane and are tunnel-coupled along the ξ direction (perpendicular to the z axis). They can be detuned by the externally applied voltage ε/e . The spin-orbit field $\mathbf{\Omega}$ points along the z axis, defining the first quantization axis for the triplet states $|T_{z,\pm}\rangle$ and $|T_{z0}\rangle$ (see main text). The effective magnetic sum field $\mathbf{\bar{b}}$ defines the second quantization axis for the triplet states $|T_{\pm}\rangle$ and $|T_0\rangle$. We choose the mutually orthogonal axes x, y, z so that $\mathbf{\bar{b}}$ lies in the xz plane. (b) Effect of detuning on the quantum dot levels. At zero detuning $\varepsilon = 0$, an electron has the same energy on the left and right quantum dots. For nonzero detuning, the energy of an electron on the left dot is ε higher than the energy of an electron on the right dot.

The two electrons in the DQD are coupled by the Coulomb interaction,

$$C = \frac{1}{4\pi\kappa} \frac{e^2}{|\mathbf{r}_1 - \mathbf{r}_2|}, \quad (2)$$

where \mathbf{r}_1 (\mathbf{r}_2) is the position of electron 1 (2) and κ is the dielectric constant of the host material. In this work, we consider the regime where the single-particle level spacing is the largest energy scale, in particular larger than the Coulomb repulsion, $\hbar\omega_0 \gg e^2/(4\pi\kappa a)$. In this case, and assuming that the hyperfine and spin-orbit interactions are also weak, single-particle orbital excitations can be neglected. Therefore the relevant part of the two-electron Hilbert space is approximately spanned by Slater determinants involving the Wannier orbitals $\Phi_{L,R}$. Including spin, and using second quantization notation where c_L^\dagger (c_R^\dagger) creates an electron in the Wannier state Φ_L (Φ_R), we define the two-electron basis states:

$$|(2,0)S\rangle = c_{L\uparrow}^\dagger c_{L\downarrow}^\dagger |0\rangle, \quad (3)$$

$$|(0,2)S\rangle = c_{R\uparrow}^\dagger c_{R\downarrow}^\dagger |0\rangle, \quad (4)$$

$$|(1,1)S\rangle = \frac{1}{\sqrt{2}}(c_{L\uparrow}^\dagger c_{R\downarrow}^\dagger - c_{L\downarrow}^\dagger c_{R\uparrow}^\dagger) |0\rangle, \quad (5)$$

$$|T_+\rangle = c_{L\uparrow}^\dagger c_{R\uparrow}^\dagger |0\rangle, \quad (6)$$

$$|T_0\rangle = \frac{1}{\sqrt{2}}(c_{L\uparrow}^\dagger c_{R\downarrow}^\dagger + c_{L\downarrow}^\dagger c_{R\uparrow}^\dagger) |0\rangle, \quad (7)$$

$$|T_-\rangle = c_{L\downarrow}^\dagger c_{R\downarrow}^\dagger |0\rangle. \quad (8)$$

The orbital parts of the basis states with single occupancy in each well, i.e., the spin singlet $|(1,1)S\rangle$ and the spin triplet $|T_{0,\pm}\rangle$, are given by

$$\Psi_{\pm}^s(\mathbf{r}_1, \mathbf{r}_2) = \frac{1}{\sqrt{2}}[\Phi_L(\mathbf{r}_1)\Phi_R(\mathbf{r}_2) \pm \Phi_R(\mathbf{r}_1)\Phi_L(\mathbf{r}_2)], \quad (9)$$

while the orbital parts of the two states $|(2,0)S\rangle$ and $|(0,2)S\rangle$ with double occupation of the left and right wells, respectively, are given by

$$\Psi_{L,R}^d(\mathbf{r}_1, \mathbf{r}_2) = \Phi_{L,R}(\mathbf{r}_1)\Phi_{L,R}(\mathbf{r}_2). \quad (10)$$

The orbital functions Ψ_{\pm}^s and $\Psi_{L,R}^d$ are symmetric under exchange of particles, and therefore must be associated with the antisymmetric singlet spin wave function (total spin $S = 0$), while Ψ_{\pm}^s is antisymmetric under exchange, and is associated with the symmetric triplet spin wave function (total spin $S = 1$).

The electrostatic gates that create the potential V_{DQD} can, in addition, tune the energies of the electrons in the potential minima by creating an additional bias potential V_{bias} . We model this bias as a simple detuning ε , which gives an energy difference for an electron occupying the left or the right dot,

$$\varepsilon = \langle \Phi_L | eV_{\text{bias}} | \Phi_L \rangle - \langle \Phi_R | eV_{\text{bias}} | \Phi_R \rangle. \quad (11)$$

In the symmetric case, $\varepsilon = 0$, the voltages on the electrostatic gates are set so that, in the absence of electron-electron interactions, an electron would have the same energy in either well. The Coulomb repulsion (2) penalizes the states $|(0,2)S\rangle$

and $|(2,0)S\rangle$ with double occupation of either well by an amount U , given by

$$U = \langle \Psi_{L,R}^d | C | \Psi_{L,R}^d \rangle. \quad (12)$$

Therefore, for a symmetric potential, $\varepsilon \approx 0$, the lowest energy states of two electrons will be primarily comprised of singly occupied orbitals. When the detuning is large enough to overcome the on-site electron-electron repulsion in one well, $|\varepsilon| > U$, the doubly occupied state with both electrons on the dot with lower potential becomes the ground state. Varying the gate voltages to increase the detuning from large and negative to large and positive values then tunes the occupation numbers of the two dots in the ground state of the DQD through the sequence $(2,0) \rightarrow (1,1) \rightarrow (0,2)$. Since the states with the charge configurations $(2,0)$ and $(0,2)$ are singlets, while those with the $(1,1)$ charge configuration can be either singlet or triplet, the measurement of charge as a function of detuning can reveal the spin states.

The strong spin-independent terms, i.e. the confinement potential V_{DQD} , Coulomb repulsion C , and the kinetic energy are, at low energies and in the limit of tight confinement, described by the matrix elements between Slater-determinant-type states in which the two electrons are loaded into some combination of the Wannier orbitals [see Eq. (12) and Ref. 21]:

$$t = \langle \Phi_{L,R} | h_{1,2}^0 | \Phi_{R,L} \rangle - \frac{1}{\sqrt{2}} \langle \Psi_+^s | C | \Psi_{L,R}^d \rangle, \quad (13)$$

$$V_{\pm} = \langle \Psi_{\pm}^s | C | \Psi_{\pm}^s \rangle, \quad (14)$$

$$X = \langle \Psi_{L,R}^d | C | \Psi_{R,L}^d \rangle. \quad (15)$$

Here, we have used $h_{1,2}^0 = H_{\text{osc}} + V_{\text{DQD}}(\mathbf{r}) - V_h(\mathbf{r} \mp a\mathbf{e}_x)$ to label the part of Hamiltonian that includes the kinetic energy T and the harmonic part of the potential V_{DQD} near the dot centers. The dots are displaced by $\pm a$ along the axis with the unit vector \mathbf{e}_x , see Fig. 1. Thus $h_{1,2}^0 - H_{\text{osc}}$ describes the tunneling due to the mismatch between the true double-dot potential V_{DQD} and the potential of the harmonic wells.²¹ The matrix element X describes coordinated hopping of two electrons from one quantum dot to the other, t is the renormalized single-electron hopping amplitude between the two dots, which includes contributions of both the single-particle tunneling amplitude and the Coulomb interaction, and V_+ (V_-) is the Coulomb energy in the singlet (triplet) state with one electron in each well.

The confinement potential V_{DQD} , the Coulomb interaction C , and the detuning ε provide the largest energy scales in a DQD. These terms add up to the spin-independent Hamiltonian $H_0 = T + V_{\text{DQD}} + C + V_{\text{bias}}$, which within the space of the six lowest-energy dot orbitals, using the basis defined in Eqs. (3)–(8), is represented by

$$H_0 = \begin{pmatrix} H_{\text{SS}} & 0 \\ 0 & H_{\text{TT},0} \end{pmatrix}, \quad (16)$$

where the singlet Hamiltonian in the basis $|(0,2)S\rangle, |(2,0)S\rangle, |(1,1)S\rangle$ is

$$H_{\text{SS}} = \begin{pmatrix} U - \varepsilon & X & -\sqrt{2}t \\ X & U + \varepsilon & -\sqrt{2}t \\ -\sqrt{2}t & -\sqrt{2}t & V_+ \end{pmatrix}, \quad (17)$$

and the triplet Hamiltonian is diagonal, $H_{\text{TT},0} = V_-$.

In addition to the terms described above, there are three sources of spin-dependent interactions: Zeeman coupling to an external magnetic field, hyperfine coupling between electron spins and nuclear spins in a quantum dot, and the spin-orbit interaction. For now, we neglect the spin-orbit interaction, and analyze it in detail in the next section.

The direct coupling of the electron spins to a uniform external magnetic field \mathbf{B} is described by the Zeeman term

$$H_Z = -\mu_e \mathbf{B} \cdot \bar{\mathbf{g}} \cdot (\mathbf{S}_L + \mathbf{S}_R), \quad (18)$$

where $\bar{\mathbf{g}}$ is the electron g tensor and μ_e is the electron magnetic moment. The g tensor can show significant anisotropy in the quantum wells. The Fermi contact hyperfine interaction between electron and nuclear spins reads

$$H_{\text{nuc}} = \sum_i \mathbf{h}_i \cdot \mathbf{S}_i, \quad (19)$$

where \mathbf{h}_i , $i = L, R$, is the Overhauser field of the quantum dot i , given by²²

$$\mathbf{h}_i = \sum_j A_j |\Psi_i(\mathbf{R}_j)|^2 \mathbf{I}_j. \quad (20)$$

Here, A_j is the hyperfine coupling constant for the nuclear species at site j , with typical size of the order of $90 \mu\text{eV}$ for GaAs,²³ Ψ_i is the electron orbital envelope wave function in the right ($i = R$) and left ($i = L$) dots, \mathbf{R}_j is the position of the j th nucleus in the quantum dot, and \mathbf{I}_j is the corresponding nuclear spin.

Because the Zeeman and hyperfine interactions, Eqs. (18) and (19), have similar forms, we combine them into effective fields that acts on the electron spin in each dot:

$$H_{\text{nuc}} + H_Z = -\mathbf{b}_L \cdot \mathbf{S}_L - \mathbf{b}_R \cdot \mathbf{S}_R. \quad (21)$$

The effective fields $\mathbf{b}_{L,R} = \mu_e \mathbf{B}_{L,R} \cdot \bar{\mathbf{g}} - \mathbf{h}_{L,R}$ include the contributions of the external and Overhauser fields, with all coupling constants absorbed in the field definitions. The energy levels arising from the spin-conserving Hamiltonian (16), along with coupling to a uniform effective field (21) with $\mathbf{b}_L = \mathbf{b}_R$, are shown in the left panel of Fig. 2.

Below, we will be interested in transitions that change the total spin of the pair of electrons in the DQD. To facilitate the discussion, we separate the total field into a sum field $\bar{\mathbf{b}} = (\mathbf{b}_L + \mathbf{b}_R)/2$ and a difference field $\delta\mathbf{b} = (\mathbf{b}_L - \mathbf{b}_R)/2$:

$$H_{\text{nuc}} + H_Z = -\bar{\mathbf{b}} \cdot (\mathbf{S}_L + \mathbf{S}_R) - \delta\mathbf{b} \cdot (\mathbf{S}_L - \mathbf{S}_R). \quad (22)$$

The symmetric component $\bar{\mathbf{b}}$ conserves the magnitude of the total spin, $[\bar{\mathbf{b}} \cdot (\mathbf{S}_L + \mathbf{S}_R), (\mathbf{S}_L + \mathbf{S}_R)^2] = 0$, while the antisymmetric component $\delta\mathbf{b}$ does not. We include the spin-conserving field $\bar{\mathbf{b}}$ into the unperturbed Hamiltonian, and define

$$H_{\text{TT}} = H_{\text{TT},0} - \bar{\mathbf{b}} \cdot (\mathbf{S}_L + \mathbf{S}_R). \quad (23)$$

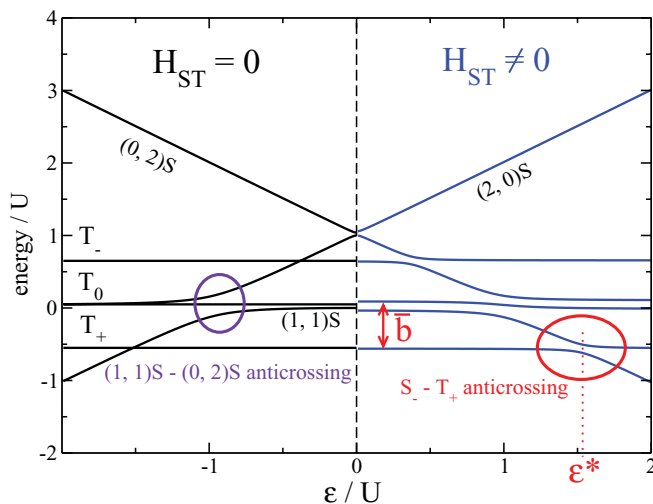


FIG. 2. (Color online) Energy levels of the double quantum dot system obtained from exact numerical diagonalization of H given in Eq. (30) and plotted as a function of the detuning ε measured in units of the Coulomb on-site repulsion energy U . Of particular interest here are the crossings and anticrossings of singlet and triplet states due to spin-orbit and hyperfine interactions. For $H_{ST} = 0$ [see Eq. (42)], i.e., vanishing singlet-triplet mixing (left-hand side of plot), the parameter values chosen are $(U, t, p, X, V_-, V_+, \bar{b}, \delta b_y, \delta \mathbf{b} \cdot \mathbf{e}, \delta \mathbf{b} \cdot \mathbf{e}', \varphi) = (1, 0.1, 0, 0, 0.05, 0.04, 0.3, 0, 0, 0, 0)$. In this case, the singlets $|(1, 1)S\rangle$ and $|(0, 2)S\rangle$ anticross (left oval) and a finite gap opens, whereas the singlets and triplets only cross (no gap). For $H_{ST} \neq 0$, additional gaps open (right-hand side of plot), in particular, at the lower singlet-triplet anticrossing around $\varepsilon = \varepsilon^*$ (right oval) with an energy splitting Δ_{ST} that depends on magnetic field, detuning, spin-orbit, and hyperfine interactions (see main text and figures below). The singlet S_- is a superposition of $|(1, 1)S\rangle$ and $|(0, 2)S\rangle$ [see Eq. (37)]. The parameter values chosen for the right plot are $(U, t, p, X, V_-, V_+, \bar{b}, \delta b_y, \delta \mathbf{b} \cdot \mathbf{e}, \delta \mathbf{b} \cdot \mathbf{e}', \varphi) = (1, 0.1, 0.01, 0, 0.05, 0.04, 0.3, 0.02, 0.02, 0.01, \pi/2)$.

Below, we will investigate the role of the Overhauser fields in causing spin transitions near a singlet-triplet level crossing in a two-electron DQD. While the external magnetic field \mathbf{B} is a classical variable, the Overhauser fields $\mathbf{h}_{L,R}$ are, in principle, quantum operators that involve a large number of nuclear spins, see Eq. (20). Hyperfine-induced electron spin transitions may be accompanied by nuclear spin flips, and the dynamical, quantum nature of the Overhauser field may be important. However, due to the large number of nuclear spins, the time scale for the Overhauser fields $\mathbf{h}_{L,R}$ to change appreciably can be much longer than the time spent near the avoided crossing where spin transitions are possible. Thus we will treat the fields $\bar{\mathbf{b}}$ and $\delta \mathbf{b}$ as quasistatic classical variables, and include a discussion of the averaging that occurs due to nuclear Larmor precession and statistical (thermal) fluctuations.

III. SPIN-ORBIT INTERACTION

In addition to the external and hyperfine fields, electron spins in a DQD are also influenced by orbital motion due to the spin-orbit interaction. Here, we describe how the bulk spin-orbit coupling of the 2DEG is manifested in the confined DQD system. In GaAs quantum wells, the spin-orbit interaction is caused by the inversion asymmetry of the interface that forms

the quantum well^{24–26} and the inversion asymmetry of host material.²⁷ With the 2DEG being much thinner than the lateral quantum dot dimensions, both spin-orbit interactions are linear in the in-plane momenta of the confined electrons, and together are given by

$$H_{SO} = \alpha(p_x \sigma_y - p_y \sigma_x) + \beta(-p_x \sigma_x + p_y \sigma_y), \quad (24)$$

where the Rashba and Dresselhaus spin-orbit interaction constants α and β , respectively, depend on the thickness and shape of the confinement in the growth direction and on the material properties of the heterostructure in which the 2DEG is fabricated. This form of spin-orbit coupling appears in a quantum well fabricated in the (001) plane of GaAs crystal, and the x' and y' axes point along the crystallographic directions [100] and [010], respectively.

Within the space of low-energy single-electron orbitals in the DQD, the action of the spin-orbit interaction can be expressed in terms of a spin-orbit field Ω ,

$$H_{SO} = \frac{i}{2} \Omega \cdot \sum_{\alpha, \beta = \uparrow \downarrow} (c_{L\alpha}^\dagger \sigma^{\alpha\beta} c_{R\beta} - \text{H.c.}), \quad (25)$$

where the field

$$i\Omega = \langle \Phi_L | p_\xi | \Phi_R \rangle \mathbf{a}_\Omega \quad (26)$$

depends on the orientation of the dots with respect to crystallographic axes through the vector \mathbf{a}_Ω .^{28–30} For a 2DEG in the (001) plane, \mathbf{a}_Ω is given by

$$\mathbf{a}_\Omega = (\beta - \alpha) \cos \theta \mathbf{e}_{[100]} + (\beta + \alpha) \sin \theta \mathbf{e}_{[110]}, \quad (27)$$

where the angle between the \mathbf{e}_ξ direction and the [110] crystallographic axis is denoted by θ . The matrix element of p_ξ , the momentum component along the ξ direction that connects the two dots, see Fig. 1, is taken between the corresponding Wannier orbitals, and it depends on the envelope wave function and the double dot binding potential. The spin-orbit field Ω accounts for the spin rotation when the electron hops between the dots. Therefore the spin-orbit interaction enables transitions between triplet states with single occupation of each well, to the singlet states with double occupation of either the left or the right well.

The matrix element in Eq. (26) can be calculated explicitly in a model potential,^{21,28} giving

$$\Omega = \frac{4t}{3} \frac{l}{\Lambda_{SO}} \frac{\mathbf{a}_\Omega}{|\mathbf{a}_\Omega|}, \quad (28)$$

where l is the interdot distance. The numerical prefactor is model dependent, but the dependence on other parameters is generic. The hopping amplitude t , and the interdot separation l depend on the geometry of the double dot system, whereas the spin-orbit length Λ_{SO} is determined by material properties (Rashba and Dresselhaus spin-orbit strength) and by the orientation of the DQD with respect to the crystallographic axes. In particular, if the 2DEG lies in the (001) plane, it is given by

$$\frac{1}{\Lambda_{SO}} = \sqrt{\left(\frac{\cos \theta}{\lambda_-}\right)^2 + \left(\frac{\sin \theta}{\lambda_+}\right)^2}, \quad (29)$$

where $\lambda_{\pm} = \hbar/[m^*(\beta \pm \alpha)]$,³¹ with m^* being the effective band mass of the electron. In the special case $\beta = 0$, $\theta = 0$, this definition reduces to the Rashba spin-orbit length $\Lambda_{\text{SO}}|_{\beta=\theta=0} = \lambda_{\text{SO}} = \hbar/m^*\alpha$.

One of the main goals in the following is to derive the dependence of the energy splitting at the anticrossing between the lowest-energy electron spin triplet and singlet states (see Fig. 2, $S_- - T_+$ anticrossing) in terms of this spin-orbit length Λ_{SO} . Detailed understanding of this dependence may then be used to extract the value of Λ_{SO} , e.g., from measurements of the singlet-triplet transition probability in gate-sweep experiments.

Within the model used above for explicit calculation, the components of Ω are real, even in the presence of magnetic fields. This is due to the high symmetry of the ground-state orbitals of the quantum dot in the model, and remains true even after the replacement $p_{\xi} \rightarrow p_{\xi} - (e/c)A_{\xi}$ in the spin-orbit Hamiltonian H_{SO} (24). However, this fact is not essential for the physics described below.

IV. SINGLET-TRIPLET TRANSITIONS AND THE CHOICE OF SPIN QUANTIZATION AXIS

Transitions between singlet and triplet states can be mediated by the spin-orbit interaction or by an inhomogeneous effective magnetic field (external plus hyperfine), $\delta\mathbf{b}$. In Ref. 19, it was shown that the transfer of angular momentum between electrons and the nuclei strongly depends on the relative size and phase of the electron spin-flip matrix elements induced by spin-orbit interaction and by the difference of the Overhauser fields in the two dots. Using our model of a detuned DQD, we will study these matrix elements in the following in detail and in particular focus on the singlet-triplet level splitting, see Fig. 2, right panel.

The homogeneous field $\bar{\mathbf{b}}$ acts only within the spin-triplet subspace, while the inhomogeneous field $\delta\mathbf{b}$ mixes singlet $S = 0$ and triplet $S = 1$ states. Representing the total Hamiltonian in the basis $\{|(0,2)S\rangle, |(2,0)S\rangle, |(1,1)S\rangle, |T_{z+}\rangle, |T_{z0}\rangle, |T_{z-}\rangle\}$, where the z axis is taken along Ω , see Fig. 1, we find

$$H = \begin{pmatrix} U - \varepsilon & X & -\sqrt{2}t & 0 & -i\sqrt{2}\Omega & 0 \\ X & U + \varepsilon & -\sqrt{2}t & 0 & -i\sqrt{2}\Omega & 0 \\ -\sqrt{2}t & -\sqrt{2}t & V_+ & -\sqrt{2}(\delta b_x - i\delta b_y) & 2\delta b_z & \sqrt{2}(\delta b_x + i\delta b_y) \\ 0 & 0 & -\sqrt{2}(\delta b_x + i\delta b_y) & V_- + 2\bar{b}_z & \bar{b}_x\sqrt{2} & 0 \\ i\sqrt{2}\Omega & i\sqrt{2}\Omega & 2\delta b_z & \bar{b}_x\sqrt{2} & V_- & \bar{b}_x\sqrt{2} \\ 0 & 0 & \sqrt{2}(\delta b_x - i\delta b_y) & 0 & \bar{b}_x\sqrt{2} & V_- - 2\bar{b}_z \end{pmatrix}. \quad (30)$$

The Hamiltonian (30) is the starting point for all of our further calculations. Our results will show the dependence of the singlet-triplet splitting on the parameters that enter H . This Hamiltonian describes a double quantum dot with a single orbital per dot, i.e., in the Hund-Mulliken approximation, and it is valid as long as the dot quantization energy is the largest energy scale in the problem. It can be applied to double quantum dots of various kinds, for example, gated lateral or vertical dots in III-V semiconductor materials, quantum dots in nanowires, or self-assembled quantum dots. We illustrate the spectrum of H in Fig. 2, for a set of parameters that emphasizes anticrossings of the levels. The spectrum is obtained by exact diagonalization of H , and it is given as a function of detuning ε . For other types of quantum dots, the parameter values would change, but the overall structure of the spectrum remains the same.

V. EFFECTIVE HAMILTONIAN NEAR THE SINGLET-TRIPLET ANTICROSSING

In the limit of large detuning, $|\varepsilon| \gg U, V_+, V_-, |\bar{\mathbf{b}}|$, the ground state is a spin singlet with both electrons in either the left or right dot, depending on whether $\varepsilon > 0$ or $\varepsilon < 0$. In the region of weak detuning, the ground state has one electron in each of the dots. For a sufficiently strong sum field,

$|\bar{\mathbf{b}}| > U - V_+$, the singlet ground state exhibits an avoided level crossing with the lowest-energy triplet state, i.e., the $S = 1$ state oriented along $\bar{\mathbf{b}}$, see Fig. 1, at a detuning where the potential energy gained by the singlet's double occupancy of the lower well compensates the Zeeman energy gained by the spin-polarized triplet. Here, the residual splitting is determined by the spin nonconserving interactions. The behavior near this anticrossing has been the focus of many recent studies on the interaction of electron spins with the nuclei.^{11,32-35} The role of spin-orbit interaction has received less attention than that of the nuclei, and will be analyzed in the following sections.

The orbital structure of the levels near the anticrossing is determined by the spin-independent interactions and by the direction and amplitude of the sum field $\bar{\mathbf{b}}$. The singlet subspace acted on by the Hamiltonian (17) includes a state with single occupation of the two dots and two states, which feature double occupation of either the left or the right dot. Generically, the state that takes part in the anticrossing includes amplitudes of all three singlet states. However, because $U \gg J$, where $J \approx 4t^2/(U - V_+) \sim 0.01\text{--}0.1$ meV is the splitting between the lowest-energy triplet and the lowest-energy singlet state, and $U \sim 1$ meV, admixture of at least one of the singlets will always be suppressed at the anticrossing by a large energy denominator (note that $t \approx 0.01\text{--}0.1$ meV $\ll U - V_+$).

Let us now construct the effective Hamiltonian that acts in the two-level subspace spanned by the levels near the anticrossing. First, the spin-conserving part of the full (6×6) Hamiltonian reads

$$H_{\text{sc}} = \begin{pmatrix} H_{\text{SS}} & 0 \\ 0 & H_{\text{TT}} \end{pmatrix}, \quad (31)$$

where the block H_{SS} acts in the singlet subspace, H_{TT} acts in the triplet subspace, and the off-diagonal blocks vanish due to spin conservation.

Explicitly, the block H_{SS} is given by Eq. (17) in the basis Eqs. (3)–(8). The triplet block H_{TT} is given in Eq. (23). Since $U \gg t \gg X$ in a typical quantum dot, the state at the anticrossing can include significant contributions from at most two out of three basis singlets. We will consider the anticrossing at positive values of the detuning ε (the anticrossing at negative voltage is analogous) so that the $|(2,0)S\rangle$ state with the energy $U + \varepsilon$ is far detuned from the other two singlets. The remaining two singlets can be close in energy. In order to include the possibility of near degeneracy, we will introduce a mixing angle ψ that parametrizes the hybridization of the $|(0,2)S\rangle$ and $|(1,1)S\rangle$ states. In the restricted subspace of these hybridized states, the singlet Hamiltonian reads:

$$H_{\text{t}} = \frac{U - \varepsilon + V_+}{2} + \boldsymbol{\tau} \cdot \mathbf{n} \sqrt{\frac{(U - \varepsilon - V_+)^2}{4} + 2t^2}, \quad (32)$$

$$H_{\text{SS}} = \begin{pmatrix} U + \varepsilon & X \cos \psi - \sqrt{2}t \sin \psi & -X \sin \psi - \sqrt{2}t \cos \psi \\ X \cos \psi - \sqrt{2}t \sin \psi & E_{S+} & 0 \\ -X \sin \psi - \sqrt{2}t \cos \psi & 0 & E_{S-} \end{pmatrix}, \quad (35)$$

where

$$E_{S\pm} = \frac{U - \varepsilon + V_+}{2} \pm \sqrt{(U - \varepsilon - V_+)^2/4 + 2t^2} \quad (36)$$

are the eigenvalues of H_{SS} in the spin-conserving sector. The basis vectors used here are the far-detuned singlet $|(2,0)S\rangle$ [see Eq. (3)] and the singlets $|S_{\pm}\rangle$ defined by

$$|S_+\rangle = \sin \psi |(1,1)S\rangle - \cos \psi |(0,2)S\rangle, \quad (37)$$

$$|S_-\rangle = \cos \psi |(1,1)S\rangle + \sin \psi |(0,2)S\rangle. \quad (38)$$

In the limit $U \gg t$, $|S_{\pm}\rangle$ become eigenstates of H_{SS} with energies $E_{S\pm}$ given in Eq. (36).

While the mixing of orbital states belonging to singlets does not affect the triplet Hamiltonian H_{TT} , it will change the form of coupling between the singlet and triplet states near the anticrossing. In the following, we first diagonalize the triplet sector in order to find the explicit form of the triplet state at the anticrossing, and then find the effective Hamiltonian of the singlet-triplet coupling.

The triplets are Zeeman split by the sum-field $\bar{\mathbf{b}}$. We have chosen the z axis of spin quantization so that the spin-orbit interaction couples $|(0,2)S\rangle$ and $|(2,0)S\rangle$ to the $|S = 1, S_z = 1\rangle$

where $\boldsymbol{\tau} = (\tau_x, \tau_y, \tau_z)$ is the vector of Pauli matrices. The pseudospin $\boldsymbol{\tau}$ describes the components of the anticrossing singlet state, $|\tau_z = 1\rangle = |(1,1)S\rangle$, $|\tau_z = -1\rangle = |(0,2)S\rangle$, within the approximation that we neglect the remaining $|(2,0)S\rangle$ component (this is valid when $|t/U| \ll 1$). In this case, $\mathbf{n} = \mathbf{e}_z \cos 2\psi + \mathbf{e}_x \sin 2\psi$ is a unit vector parametrized by the mixing angle ψ that describes the relative size of mixing and splitting of τ_z eigenstates. Note that the y component of \mathbf{n} vanishes due to the choice of phases in the quantum dot ground states, which guarantees that the spin-independent hopping matrix element t is purely real. We remark again that in our DQD setup the hopping matrix element t stays real even in the presence of magnetic fields.²¹ The mixing angle of the doubly and singly occupied states at the $S = 0$ anticrossing, $|(0,2)S\rangle$ and $|(1,1)S\rangle$, respectively, is defined by

$$\cos 2\psi = \frac{U - V_+ - \varepsilon}{\sqrt{(U - V_+ - \varepsilon)^2 + 8t^2}}, \quad (33)$$

$$\sin 2\psi = \frac{2\sqrt{2}t}{\sqrt{(U - V_+ - \varepsilon)^2 + 8t^2}}. \quad (34)$$

In the basis of eigenstates of Eq. (32), the singlet Hamiltonian H_{SS} is given by

state. We will now diagonalize the triplet part of the spin-conserving Hamiltonian, given by

$$H_{\text{TT}} = V_- + 2\bar{b} \begin{pmatrix} -\cos \varphi & \frac{1}{\sqrt{2}} \sin \varphi & 0 \\ \frac{1}{\sqrt{2}} \sin \varphi & 0 & \frac{1}{\sqrt{2}} \sin \varphi \\ 0 & \frac{1}{\sqrt{2}} \sin \varphi & \cos \varphi \end{pmatrix}, \quad (39)$$

where we have used $\bar{b} = |\bar{\mathbf{b}}|$, $\cos \varphi = \bar{b}_z/\bar{b}$, and $\sin \varphi = \bar{b}_x/\bar{b}$ (see Fig. 1). The unitary transformation $U_{\text{t}} H_{\text{TT}} U_{\text{t}}^\dagger$ that diagonalizes H_{TT} is

$$U_{\text{t}} = \begin{pmatrix} \cos^2 \frac{\varphi}{2} & -\frac{1}{\sqrt{2}} \sin \varphi & \sin^2 \frac{\varphi}{2} \\ -\frac{1}{\sqrt{2}} \sin \varphi & -\cos \varphi & \frac{1}{\sqrt{2}} \sin \varphi \\ \sin^2 \frac{\varphi}{2} & \frac{1}{\sqrt{2}} \sin \varphi & \cos^2 \frac{\varphi}{2} \end{pmatrix}. \quad (40)$$

We denote the basis states by $|T_+\rangle$, $|T_0\rangle$, and $|T_-\rangle$, where, now, the quantization axis is given by the sum field $\bar{\mathbf{b}}$.

With the diagonalization of the triplet block of the spin-conserving Hamiltonian and the preceding approximate diagonalization of the spin-conserving singlet Hamiltonian (35), we are able to describe the spin-conserving interaction near the anticrossing in a convenient form. We will use $|S_-\rangle$ and $|T_+\rangle$ as basis vectors, and study the effective Hamiltonian

in the vicinity of the anticrossing that can emerge from spin-nonconserving interactions.

The full Hamiltonian is

$$H = H_{\text{sc}} + H_{\text{SO}} - \delta \mathbf{b} \cdot (\mathbf{S}_L - \mathbf{S}_R), \quad (41)$$

and in block form reads

$$H = \begin{pmatrix} H_{\text{SS}} & H_{\text{ST}} \\ H_{\text{TS}} & H_{\text{TT}} \end{pmatrix}. \quad (42)$$

The diagonal blocks H_{SS} and H_{TT} give the spin-conserving part, denoted by H_{sc} , while the off-diagonal blocks H_{ST} and $H_{\text{TS}} = H_{\text{ST}}^\dagger$ induce singlet-triplet transitions. In the basis $[|(2,0)S\rangle, |S_+\rangle, |S_-\rangle, |T_+\rangle, |T_0\rangle, |T_-\rangle]$, the diagonal blocks take

a simple form. The singlet block is H_{SS} given in Eq. (35). The triplet block H_{TT} is diagonal and reads

$$H_{\text{TT}} = \text{diag}(V_- - |\bar{\mathbf{b}}|, V_-, V_- + |\bar{\mathbf{b}}|), \quad (43)$$

where we used that $|T_+\rangle$ is the lowest-energy triplet.

The effective Hamiltonian near the anticrossing is determined by the spin-conserving terms $t, U, X, \varepsilon, \bar{\mathbf{b}}$, and by the spin-non-conserving terms Ω , arising from spin-orbit coupling, and $\delta \mathbf{b}$, the effective difference field. All these interactions can be treated perturbatively in dots with weak overlap of the orbitals. The off-diagonal terms are denoted by $H_{\text{ST}} = H_{\text{ST}}^{\text{SO}} + H_{\text{ST}}^{\delta \mathbf{b}}$, and $H_{\text{TS}} = H_{\text{ST}}^\dagger$, where

$$H_{\text{ST}}^{\text{SO}} = i\Omega \begin{pmatrix} -\sin \varphi & -\sqrt{2} \cos \varphi & \sin \varphi \\ \cos \psi \sin \varphi & \sqrt{2} \cos \psi \cos \varphi & -\cos \psi \sin \varphi \\ -\sin \psi \sin \varphi & -\sqrt{2} \sin \psi \cos \varphi & \sin \psi \sin \varphi \end{pmatrix}, \quad (44)$$

$$H_{\text{ST}}^{\delta \mathbf{b}} = \begin{pmatrix} 0 & 0 & 0 \\ \sqrt{2}(i\delta b_y + \delta \mathbf{b} \cdot \mathbf{e}') \sin \psi & 2(\delta \mathbf{b} \cdot \mathbf{e}) \sin \psi & \sqrt{2}(i\delta b_y - \delta \mathbf{b} \cdot \mathbf{e}') \sin \psi \\ \sqrt{2}(i\delta b_y + \delta \mathbf{b} \cdot \mathbf{e}') \cos \psi & 2(\delta \mathbf{b} \cdot \mathbf{e}) \cos \psi & \sqrt{2}(i\delta b_y - \delta \mathbf{b} \cdot \mathbf{e}') \cos \psi \end{pmatrix}, \quad (45)$$

where the unit vector

$$\mathbf{e} = \mathbf{e}_x \sin \varphi + \mathbf{e}_z \cos \varphi \quad (46)$$

points in the direction of the homogeneous field $\bar{\mathbf{b}}$, and the vector

$$\mathbf{e}' = -\mathbf{e}_x \cos \varphi + \mathbf{e}_z \sin \varphi \quad (47)$$

lies in the xz plane, which contains Ω and $\bar{\mathbf{b}}$ and points in the direction normal to $\bar{\mathbf{b}}$.

In the vicinity of the anticrossing, the DQD behaves as an effective two-level system, with the dynamics described by an effective Hamiltonian denoted by H_{cr} . Up to first order in spin-non-conserving interactions and, after neglecting the high-energy state $|(2,0)S\rangle$, we find

$$H_{\text{cr}}^{(1)} = \begin{pmatrix} E_{S-} & H_{34} \\ H_{43} & E_{T+} \end{pmatrix}, \quad (48)$$

where $H_{34} = \langle S_- | H | T_+ \rangle$ is the matrix element of H , Eq. (42), between the anticrossing states, and $E_{T+} = V_- - \bar{b}$.

VI. SINGLET-TRIPLET SPLITTING AT THE ANTICROSSING

The singlet-triplet splitting Δ_{ST} at the $S_- - T_+$ anticrossing, see Fig. 2, can be accessed in the spin blockade regime by transport measurements or by charge sensing. This splitting gives valuable information about the properties of the quantum dots and the nuclear polarization. The splitting Δ_{ST} was used in the interpretation of both transport^{15,36} and charge sensing¹⁵ measurements in double quantum dots, where it was attributed to the effects of hyperfine interaction. The anisotropy in the splitting between the singlet and triplet two-electron states in

an isolated quantum dot^{37,38} was successfully explained as a consequence of spin-orbit interaction. Similarly, the effects of both the spin-orbit interaction and the hyperfine coupling were measured in double quantum dots fabricated in InAs nanowires.^{17,39} However, a systematic study of the dependence of singlet-triplet splitting on gate voltages and magnetic field strength and direction was not undertaken. When such a study is performed, our predictions for these dependencies, derived from the model (30) can be checked against experimental results, and may be used to extract information about spin-orbit and hyperfine fields.

We shall derive now explicit expressions for Δ_{ST} in terms of the experimentally relevant quantities ε , $\bar{\mathbf{b}}$, $\delta \mathbf{b}$, and Ω . We proceed by perturbation expansion in H_{ST} , t/U , and X/U . First, we focus on the first-order contributions and, afterward, address the higher-order corrections, which become relevant around the points where the leading contributions can be tuned to zero by the control parameters.

As the DQD detuning ε is varied with other parameters held fixed, there is a special value ε^* where the energy E_{S-} of the lowest singlet, Eq. (36), becomes equal to the energy $E_{T+} = V_- - \bar{b}$ of the triplet $|T_+\rangle$, Eq. (43). The detuning at which this crossing occurs is controlled by the amplitude \bar{b} of the sum field, as well as the tunnel coupling t . For the unperturbed case, described by H_0 , ε^* is the solution of the equation

$$E_{S-}(\varepsilon^*) = V_- - \bar{b}. \quad (49)$$

When the spin-non-conserving interactions are taken into account, the crossing of singlet ($S = 0$) and triplet ($S = 1$) states is avoided due to state mixing (hybridization).

Up to first order in H_{ST} , t/U , and X/U , the splitting follows from Eq. (48) and reads

$$\Delta_{ST}(\varepsilon, \bar{b}, \varphi) = 2\sqrt{|H_{34}|^2 + (E_{S-} - E_{T+})^2}. \quad (50)$$

For a fixed value of \bar{b} , the splitting attains its minimum value Δ_{ST}^* at ε^* ,

$$\Delta_{ST}^* \equiv \Delta_{ST}(\varepsilon^*(\bar{b}), \bar{b}, \varphi) = \min_{\varepsilon} \Delta_{ST}(\varepsilon, \bar{b}, \varphi), \quad (51)$$

where ε^* implicitly depends on \bar{b} , as well as other DQD parameters. From Eqs. (44), (45), and (48), the splitting is equal to $2|H_{34}|$,

$$\Delta_{ST}^* = 2|-i\Omega \sin \varphi \sin \psi + \sqrt{2}(\delta \mathbf{b} \cdot \mathbf{e}' + i\delta b_y) \cos \psi|. \quad (52)$$

Note that Δ_{ST}^* contains contributions from both the spin-orbit coupling and the difference field $\delta \mathbf{b}$. The relative importance of each of the two terms depends on the detuning ε^* through the mixing angle ψ , as well as on the geometry through the angle φ between the effective field $\bar{\mathbf{b}}$ and the spin-orbit field Ω . When varying the detuning ε from large to small values, ψ decreases from $\psi \approx \pi/2$ at strong detuning, $\varepsilon \gg U - V_+$, to $\psi \approx 0$ at $|\varepsilon| \ll t$. For a mixing angle $\psi \approx \pi/2$, the contribution to Δ_{ST}^* coming from the spin-orbit interaction dominates the one from the difference field, and vice versa for $\psi \approx 0$.

Reaching the $\psi \approx 0$ regime requires weak magnetic fields, i.e., $\bar{b} \ll t$, and in this case, the energy splittings between the triplet states are not large enough to warrant the use of the simple model for a two-level anticrossing. On the other hand, reaching the regime with $\psi \approx \pi/2$ requires that the detuning ε^* at which $|S_- \rangle$ and $|T_+ \rangle$ anticross is far away from ε_{12} , the detuning at the anticrossing of $|(1,1)S \rangle$ and $|(0,2)S \rangle$ singlets, see Fig. 2. The width of the $|(1,1)S \rangle - |(0,2)S \rangle$ anticrossing is of the order t , so the requirement is $|\varepsilon^* - \varepsilon_{12}| \gg t$. Therefore the Zeeman energy of $|T_+ \rangle$ must be larger than t , so $|\mu_e \mathbf{B} \cdot \bar{\mathbf{g}}| \gg t$, which gives $B \gg 0.2$ T for typical values $t \sim 10 \mu\text{eV}$ and $|g| = 0.4$.

These considerations show that, at least in principle, the relative strengths of the spin-orbit and hyperfine contributions to the singlet-triplet coupling can be tuned through a wide range of values using a combination of gate voltages and magnetic field strength and direction. What do we expect for typical GaAs dots? Using a value of 3–5 mT for the random hyperfine field (see, e.g., Ref. 2 and references therein), and an isotropic electron g factor $|g| = 0.4$, we estimate $|\delta b| \approx 70$ – 120 neV. For the spin-orbit coupling Ω , see Eq. (28), using $t = 10 \mu\text{eV}$, an interdot separation $l = 50$ nm, and a spin-orbit length Λ_{SO} in the range 6– $30 \mu\text{m}$ (see, e.g., Refs. 10 and 40), we find $|\Omega| \approx 20$ – 110 neV. Parameters may vary from device to device, but it appears that the spin-orbit and hyperfine couplings are generally of similar orders of magnitude, with the spin-orbit coupling typically a few times weaker. Thus adjustments of the matrix elements over a reasonable range of ψ may be sufficient to explore both the hyperfine and spin-orbit dominated regimes. Similar analysis can be performed for devices in other materials, such as InAs or InSb nanowires, where the natural balance between hyperfine and spin-orbit couplings may shift.

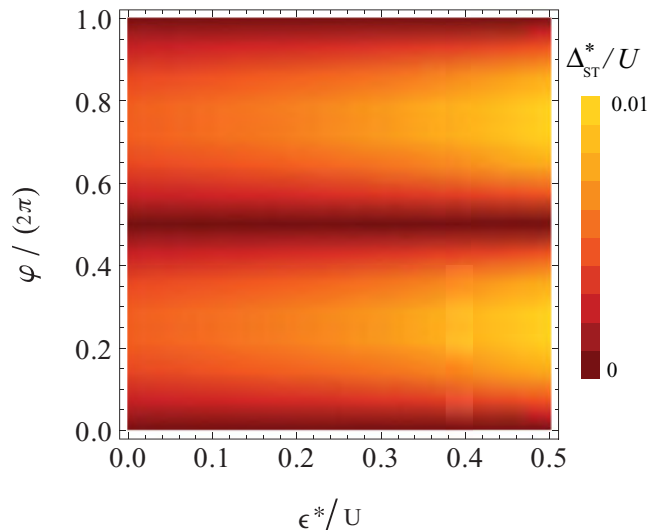


FIG. 3. (Color online) Singlet-triplet level splitting $\Delta_{ST}^* = \Delta_{ST}(\varepsilon^*, \bar{b}, \varphi)$, Eq. (52), for $\delta \mathbf{b} = 0$ (no nuclear field), as a function of the detuning ε^* at which the crossing occurs (cf. Fig. 2) and of the angle φ between the spin-orbit field Ω and the magnetic sum field $\bar{\mathbf{b}}$ (cf. Fig. 1). Parameters used for this plot are $U = 1$, $t = 0.01$, $V_+ = 0.75$, $\delta \mathbf{b} = 0$.

A. Singlet-triplet splitting Δ_{ST}^* for $\delta \mathbf{b} = 0$

Let us first consider the special case of vanishing difference field, $\delta \mathbf{b} = 0$, and finite uniform field, $\bar{\mathbf{b}} \neq 0$. In this case, the splitting depends not only on Ω but also on the detuning at the minimal splitting ε^* , which itself is implicitly determined by the sum field amplitude \bar{b} . The geometry of the system enters through the angle φ between \bar{b} and the spin-orbit field Ω . In Fig. 3, we show a plot of the level splitting $\Delta_{ST}(\varepsilon^*, \bar{b}, \varphi)$, given in Eq. (52) as a function of its variables and for $\delta \mathbf{b} = 0$.

At any fixed angle $\varphi \neq 0$, Δ_{ST}^* shows a dependence on the detuning ε^* at the anticrossing due to the mixing of $|(0,2)S \rangle$, which is coupled to $|T_+ \rangle$ via the spin-orbit interaction, and $|(1,1)S \rangle$, which does not couple to $|T_+ \rangle$ via spin-orbit coupling in the first order, see Fig. 4. At large values of detuning, $\varepsilon^* \gg U - V_+$, the splitting reaches a saturation value of $2\Omega \sin \varphi$. For typical GaAs quantum dots, reaching this regime requires strong magnetic fields of $|\mu_e \mathbf{B} \cdot \bar{\mathbf{g}}| \gg t$. At lower values of the detuning $\varepsilon < U - V_+$, the mixing of the singlet $|(1,1)S \rangle$ becomes significant, and the spin-orbit coupling value Ω cannot be read off directly from the splitting.

The maximal splitting Δ_{ST}^* caused by spin-orbit interaction is $\Delta_{ST}^* = 2\Omega |\sin \varphi|$ for $\psi = \pi/2$. From Eqs. (28) and (29), we find that Ω is set by the material properties [Dresselhaus (β) and Rashba (α) spin-orbit interactions] and the geometry of the dots. Assuming that the magnetic field is strong enough to separate the $|T_0 \rangle$ and $|T_- \rangle$ states from the anticrossing, $U \gg \bar{b} \gg t \gg |\delta \mathbf{b}|$, the maximal splitting is ($|\sin \psi| = 1$)

$$\Delta_{ST}^* = \frac{4t}{3} \frac{l}{\Lambda_{SO}} |\sin \varphi| \quad (\delta \mathbf{b} = 0), \quad (53)$$

where l is the interdot distance. The numeric factor (of order unity) is nonuniversal and depends on the specific dot geometry. Formula (53) is one of the main results of this paper. It provides a simple but useful relation between quantities that

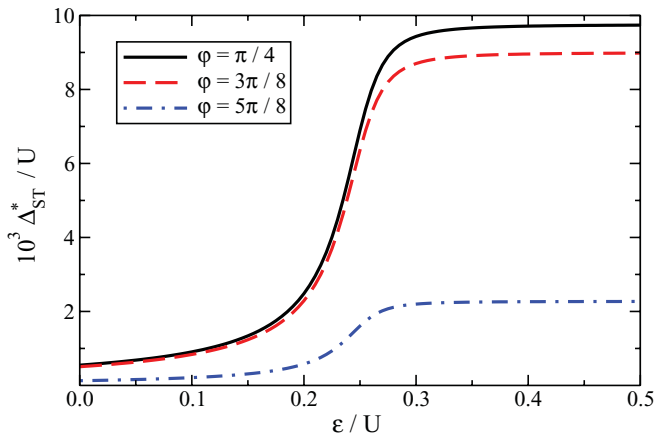


FIG. 4. (Color online) Singlet-triplet level splitting $\Delta_{ST}^* = \Delta_{ST}(\varepsilon^*, \bar{b}, \varphi)$, Eq. (52), for $\delta\mathbf{b} = 0$ (no nuclear polarization), as a function of the detuning ε^* at which the crossing occurs (see Fig. 2) and of the angle φ between the spin-orbit field $\mathbf{\Omega}$ and the magnetic sum field $\bar{\mathbf{b}}$ (see Fig. 1). At small detuning $\varepsilon^* < t$, the splitting becomes rather small, while it saturates at large detuning $\varepsilon^* > U$. The saturation value is $\propto |\sin \varphi|$, shown for $\varphi = \pi/4$ (full line), $\varphi = 3\pi/8$ (dashed line), and $\varphi = 5\pi/8$ (dashed-dotted line). Parameters used for this plot are $U = 1$, $t = 0.01$, $V_+ = 0.75$, $\delta\mathbf{b} = 0$.

can be determined experimentally, such as Δ_{ST}^* , t , l , and φ , and a quantity of interest—the spin-orbit length Λ_{SO} . This relation could allow the strength of spin-orbit coupling to be measured experimentally,^{17,35} though the geometry and detuning-dependence must be carefully taken into account in order to obtain an accurate estimate.

Let us remark here briefly on the special case of zero detuning, i.e., $\varepsilon = 0$ and weak magnetic fields. In this case, the splitting is not described by our calculations, which require sufficiently large separation of the triplets in energy. However, in a slightly different system—a single quantum dot containing two electrons—singlet-triplet coupling, which is forbidden by time-reversal symmetry, can be generated by applying a magnetic field, $\Delta_{ST}^* \approx (a_B/\lambda_{SO})E_Z$.³¹ This case cannot be recovered from our DQD model with one orbital per site. Indeed, here, we have seen that in weak fields, $\bar{b} \ll t$, the coupling of the two states with single occupation in each well $|(1,1)S\rangle$ and $|T_+\rangle$ due to the spin-orbit interaction involves doubly occupied states that are higher in energy due to the on-site repulsion. On the other hand, for a pair of electrons in a single quantum dot, the on-site repulsion is approximately the same for both states, singlet and triplet. We note that for DQDs in weak fields, the Zeeman energy E_Z , occurring in the splitting for a single dot,³¹ gets replaced by the exchange energy J if the mixing of triplets due to $\delta\mathbf{b} \neq 0$ is neglected.

B. Singlet-triplet splitting Δ_{ST}^* for $\delta\mathbf{b} \neq 0$

In addition to spin-orbit coupling of the anticrossing triplet to $|(0,2)S\rangle$, the anticrossing triplet is coupled to the singlet $|(1,1)S\rangle$ through the difference field $\delta\mathbf{b}$. The previous considerations show that the contributions from the difference field $\delta\mathbf{b}$ to the splitting cannot be neglected for angles $\varphi \sim 0, \pi$, or for field strengths where $\varepsilon^* < U - V_+$, which is often the case. Therefore we now discuss the splitting in the presence

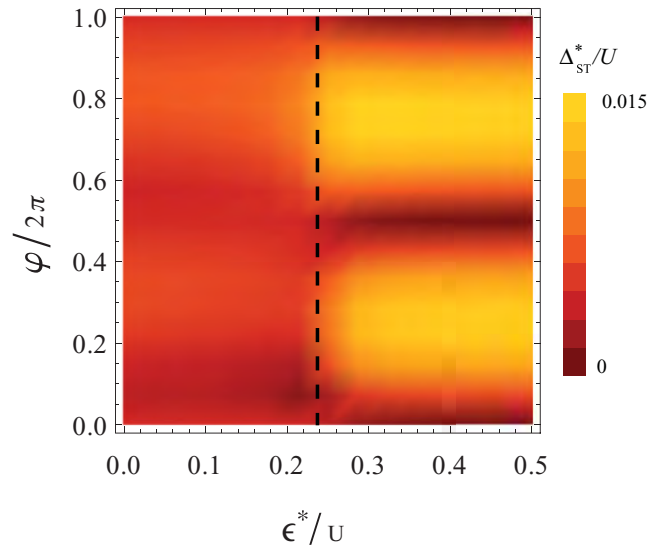


FIG. 5. (Color online) The same plot of the singlet-triplet splitting as in Fig. 3 except for finite nuclear polarization chosen to be $\delta\mathbf{b} = (-0.0006, 0.0008, 0.0012)$. In the strong detuning regime, $\varepsilon^* > U - V_+$, on the right-hand side of the plot, the splitting is determined by spin-orbit interaction, $v_{SO} > v_{HF}$, and resembles the same area in Fig. 3. In the weak detuning regime, $\varepsilon^* < U - V_+$, on the left-hand side of the plot, the hyperfine interaction increases the splitting. The regime with similar strengths of the interactions, $v_{SO} \sim v_{HF}$ can be identified in the region $\varepsilon^* \approx U - V_+ = 0.25U$. For ε^* on the left-hand side of the vertical dashed line, and $\varphi \approx 0, \pi$, the splitting is dominated by hyperfine interaction, $v_{HF} > v_{SO}$. Near the dotted line, and for the angles $\varphi \approx \pi/2, 3\pi/2$ the sizes of spin-orbit and hyperfine interactions are similar, $v_{SO} \approx v_{HF}$.

of both, the spin-orbit field $\mathbf{\Omega}$ and $\delta\mathbf{b}$. The splitting Δ_{ST}^* as a function of detuning ε^* and direction of $\bar{\mathbf{b}}$ is shown in Fig. 5.

When both sources of splitting are present, generically, the gap Δ_{ST}^* remains open. The spin-orbit contribution to Eq. (52) is always purely imaginary, while the $\delta\mathbf{b}$ contribution has both a real part, coming from the component lying in the xz plane, and an imaginary part, coming from the perpendicular component δb_y . For any fixed value of the spin-orbit coupling strength, closing the gap would require fine tuning of $\delta\mathbf{b}$, both in amplitude and direction. As a function of the direction of $\bar{\mathbf{b}}$ the contributions to Δ_{ST}^* compete, and, in addition, the relative size of the competing terms will change as a function of ε^* . Indeed, the spin-orbit term is strongest at large detuning $\varepsilon^* \gg U - V_+$, while the difference-field term becomes significant at small detuning $\varepsilon^* \sim t$. This competition affects the form of the φ -dependent splitting, see Fig. 6.

In the limit $|\mathbf{\Omega} \sin \psi| \ll |\delta\mathbf{b} \cos \psi|$, the splitting Δ_{ST}^* is caused mostly by the inhomogeneous field. In this case, the splitting is proportional to the size of component $\delta\mathbf{b}_\perp = \delta\mathbf{b} - \mathbf{e}(\delta\mathbf{b} \cdot \mathbf{e})$ of $\delta\mathbf{b}$, which is normal to the homogeneous field $\bar{\mathbf{b}} = |\bar{\mathbf{b}}|\mathbf{e}$. With the leading spin-orbit coupling correction, the splitting is [see Eq. (52)]

$$\Delta_{ST}^* = 2\sqrt{2}|\delta\mathbf{b}_\perp \cos \psi| - \frac{2\Omega\delta b_y \sin \psi \cos \psi}{|\delta\mathbf{b}_\perp \cos \psi|}. \quad (54)$$

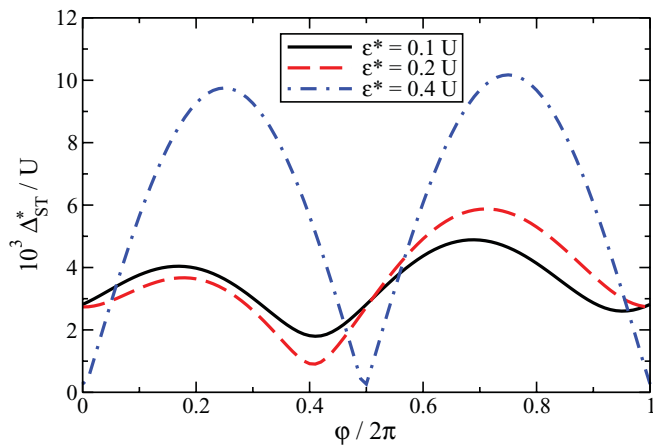


FIG. 6. (Color online) First-order singlet-triplet splitting $\Delta_{ST}^* = \Delta_{ST}(\varepsilon^*, \bar{b}, \varphi)$, Eq. (52), for finite nuclear polarization $\delta \mathbf{b} \neq 0$, plotted as a function of the angle φ (see Fig. 1), for various detunings ε^* (see Fig. 2). The parameters used for the plot are $U = 1$, $t = 0.01$, $V_+ = 0.75$, $V_- = 0.74$, $\Omega = 0.005$, and $\delta \mathbf{b} = (-0.0006, 0.0008, 0.0012)$. The curves correspond to $\varepsilon^* = 0.1$ (full line), $\varepsilon^* = 0.2$ (dashed), $\varepsilon^* = 0.4$ (dashed-dotted). In the strong detuning regime (dashed-dotted line), the angular dependence reflects the $|\sin \varphi|$ dependence of the spin-orbit term [see Eq. (53)]. The regime of weaker detuning (full and dashed line) shows the hyperfine effects.

C. Measuring the singlet-triplet coupling

The singlet-triplet coupling Δ_{ST}^* is manifested experimentally, for example, in the spin flip probability when the system is taken through the level crossing during a time-dependent gate sweep.⁴¹ In such experiments, the system is initialized to its ground state at large ε , the (0,2) singlet. When ε is then ramped to take the system through the singlet-triplet crossing, the two-electron spin state may change with a probability determined by a combination of the coupling Δ_{ST}^* and the sweep rate. The final spin state can then be read out by quickly ramping back to large ε where the singlet and triplet states have discernibly different charge distributions, which can be detected by a nearby charge sensor.

Even with single-shot spin detection,¹¹ determining the spin-flip probability requires building up statistics over many experimental runs. Within each run, the parameters in Eq. (52) may be considered fixed. However, the hyperfine field components are, in general, *a priori* unknown: under typical experimental conditions, the temperature is high compared with all intrinsic energy scales within the nuclear spin system, and the equilibrium state is nearly completely random. Depending on the measurement time scale, the nuclear fields on subsequent experimental runs may either remain constant or may change. While the correlation time for the longitudinal component of the nuclear field (parallel to the external field) may be quite long, the transverse components change on the time scale of nuclear Larmor precession, which for moderate fields of a few hundred milli Tesla can reach the submicrosecond timescale. The coherence time associated with this precession may reach several hundred microseconds to one millisecond.

Let $P(\Delta_{ST}^*)$ be the probability that the system makes a transition to the triplet state in a single sweep, when the value

of Δ_{ST}^* is specified. In an experiment where measurements of the singlet and triplet fractions are averaged over a time long compared to all nuclear spin relaxation times, one obtains an averaged probability $\langle P(\Delta_{ST}^*) \rangle$, where $\langle A \rangle$ denotes the mean value of quantity A , averaging over a Gaussian distribution of $\delta \mathbf{b}$, while other parameters such as B, t, \bar{b}, ϕ , and the sweep rate are held fixed. If the measurements are averaged over a shorter period, which is long compared to the time for phase relaxation of the nuclear spins, but short compared to the longitudinal relaxation times, then the Gaussian average should be taken only over the transverse components of $\delta \mathbf{b}$, while the component parallel to the applied magnetic field is held fixed.

When the sweep rate through the S-T transition is rapid, the probability $P(\Delta_{ST}^*)$ should be proportional to $(\Delta_{ST}^*)^2$, so an average value of $P(\Delta_{ST}^*)$ will measure the mean value of $(\Delta_{ST}^*)^2$. For lower values of the sweep rate, P will have corrections due to $(\Delta_{ST}^*)^4$, etc. Therefore measurements of the averaged value $\langle P(\Delta_{ST}^*) \rangle$ for a wide range of sweep rates should, in principle, yield average values of all powers of $(\Delta_{ST}^*)^2$, and thus allow one to deduce the probability distribution for $(\Delta_{ST}^*)^2$. Here, we concentrate on the mean value of $(\Delta_{ST}^*)^2$, and discuss predictions for this mean value as a function of the parameters B, ϕ , and t .

We illustrate the dependence of $\langle (\Delta_{ST}^*)^2 \rangle$ on the angle φ and mixing ψ in Figs. 7 and 8. The dependence of the splitting on the angle φ , inherent in the nonaveraged splitting, see Eq. (52), remains visible when the splitting is dominated by spin-orbit interaction. As expected, the dependence of the splitting on the angle φ , Fig. 7, is most visible in the case of weak fluctuations of $\delta \mathbf{b}$, i.e., for weak hyperfine coupling. In addition, the angular dependence is more pronounced for larger mixing angles, since the spin-orbit-induced splitting depends on $\Omega \sin \psi$ (see Fig. 8).

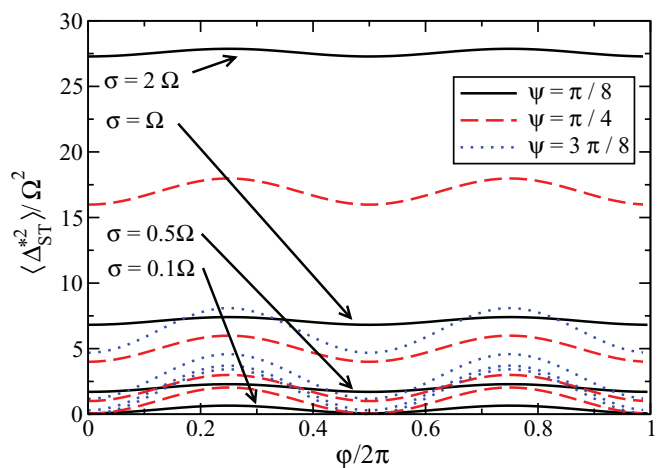


FIG. 7. (Color online) Square of the splitting $\langle \Delta_{ST}^{*2} \rangle$, Eq. (52), averaged over Gaussian fluctuations of $\delta \mathbf{b}$ with zero mean and standard deviation σ . The plots show the dependence of $\langle \Delta_{ST}^{*2} \rangle$ on the angle φ for various mixing angles ψ . We have assumed isotropic Gaussian fluctuations with a standard deviation σ . Plots are for the values $\sigma/\Omega = 0.1, 0.5, 1, 2$ and illustrate the effects of various strengths of fluctuations. The curves are found by numerical averaging over the fields $\delta \mathbf{b}$.

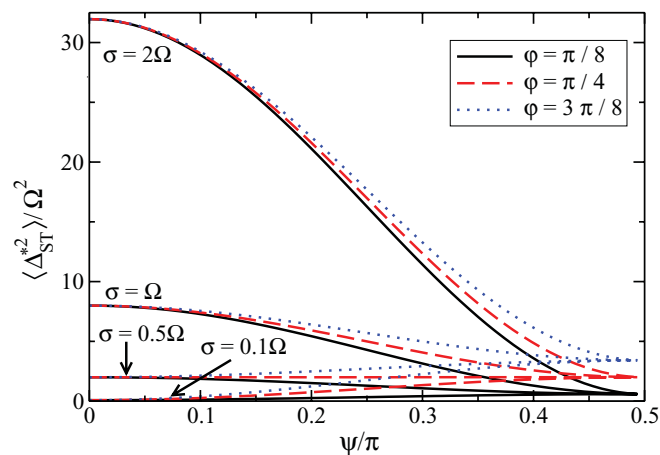


FIG. 8. (Color online) Average square of the splitting $\langle \Delta_{ST}^{*2} \rangle$, in the fluctuating nuclear field $\delta \mathbf{b}$. The parameters are chosen as in Fig. 7, and we illustrate the dependence on the mixing angle ψ .

The fluctuating difference field, besides changing the average $\langle (\Delta_{ST}^*)^2 \rangle$, introduces noise in the splitting. We find that the standard deviation σ_Δ of the splitting, in the limit of weak fluctuations $|\Omega \sin \varphi \sin \psi| \gg \sigma$ is

$$\sigma_{\Delta,G} = 2\sigma |\cos \psi|, \quad (55)$$

so that it also shows dependence on the mixing angle ψ .

Fluctuations in $\delta \mathbf{b}$ smear the splitting at the anticrossing Δ_{ST}^* . The average value and noise in the splitting can be used to measure the strengths of spin-orbit coupling Ω and the hyperfine field $\delta \mathbf{b}$. The relative size of fluctuations in Δ_{ST}^* , as a function of φ , has minima at $\varphi \approx \pi/2, 3\pi/2$.

D. Higher-order corrections

So far, our analysis of the $|S_- \rangle - |T_+ \rangle$ anticrossing was based on the assumption that the largest contribution to the splitting Δ_{ST}^* , Eq. (52), results from the direct coupling of the two states via H_{ST}^{SO} and $H_{ST}^{\delta \mathbf{b}}$. However, if the detuning ε^* is not large enough to make the influence of the levels that are energetically further away from the anticrossing completely negligible, higher-order terms that describe virtual transitions to such higher levels, and thus involve more than one transition between the singlets and the triplets, become important.

To study this regime, we derive an effective Hamiltonian in the vicinity of the anticrossing by a second-order Schrieffer-Wolff (SW) transformation.^{42,43} We divide the Hilbert space of the DQD into a relevant part that includes the anticrossing states, and an auxiliary part that contains the remaining four states. The time-independent perturbation series is then performed in powers of the spin-non-conserving interactions. The spin-conserving Hamiltonian H_{sc} (31) is taken as the unperturbed part, while $H - H_{sc}$ is the perturbation. In reordering the basis, we choose the crossing states $|S_- \rangle$ and $|T_+ \rangle$ of H_{sc} to be the first two basis states. Then, the Hamiltonian has a block-diagonal form denoted by

$$H = \begin{pmatrix} A & C \\ C^\dagger & B \end{pmatrix}, \quad (56)$$

where A is a 2×2 matrix that describes the anticrossing states, B is a 4×4 matrix of the states with energies far from the anticrossing, and the 2×4 matrix C represents the coupling between the subspaces controlled by A and B . In the basis $(|S_- \rangle, |T_+ \rangle, |T_0 \rangle, |T_- \rangle, |(2,0)S \rangle, |S_+ \rangle)$ with the two anticrossing levels at the positions 1 and 2, we can read off the blocks from Eq. (56):

$$A = \begin{pmatrix} E_{S_-} & -i\Omega_s \sin \psi + \sqrt{2}\delta_+ \cos \psi \\ i\Omega_s \sin \psi + \sqrt{2}\delta_- \cos \psi & E_{T_+} \end{pmatrix}, \quad (57)$$

$$B = \begin{pmatrix} V_- & 0 & i\sqrt{2}\Omega_c & -i\sqrt{2}\Omega_c \cos \psi + 2\delta \sin \psi \\ 0 & V_- + \bar{b} & -i\Omega_s & i\Omega_s \cos \psi - \sqrt{2}\delta_+ \sin \psi \\ -i\sqrt{2}\Omega_c & i\Omega_s & U + \varepsilon & -\sqrt{2}t \sin \psi - X \cos \psi \\ i\sqrt{2}\Omega_c \cos \psi + 2\delta \sin \psi & -i\Omega_s \cos \psi - \sqrt{2}\delta_- \sin \psi & -\sqrt{2}t \sin \psi - X \cos \psi & E_{S_+} \end{pmatrix}, \quad (58)$$

$$C = \begin{pmatrix} -i\sqrt{2}\Omega_c \sin \psi + 2\delta \cos \psi & i\Omega_s \sin \psi - \sqrt{2}\delta_- \cos \psi & -\sqrt{2}t \cos \psi + X \sin \psi & 0 \\ 0 & 0 & i\Omega_s & -i\Omega_s \cos \psi + \sqrt{2}\delta_- \sin \psi \end{pmatrix}, \quad (59)$$

where we have used the abbreviations $\delta = \delta \mathbf{b} \cdot \mathbf{e}$, $\delta_\pm = \delta \mathbf{b} \cdot \mathbf{e}' \pm i\delta b_y$, $\Omega_s = \Omega \sin \varphi$, $\Omega_c = \Omega \cos \varphi$, and the unit vectors \mathbf{e}' and \mathbf{e} are defined in Eqs. (46) and (47), respectively.

As a result of the SW transformation on Eq. (56), the off-diagonal block C is eliminated up to second order in C and the transformed block $A \xrightarrow{\text{SW}} A + \delta A$ becomes the Hamiltonian of an effective two-level system. Therefore the first-order Hamiltonian $H_{cr}^{(1)}$ from Eq. (48) is modified by second-order terms, $H_{cr} \xrightarrow{\text{SW}} H_{cr} + \delta A$, where δA is the second-order correction to A . The diagonal matrix elements δA_{11} and δA_{22} describe the renormalization of the energy levels, and their effect is to shift the detuning ε^* at which the anticrossing occurs. The explicit expressions of these corrections are

$$\begin{aligned} \delta A_{11} = & \frac{1}{E_{S_-} - V_-} [2(\Omega_c \sin \psi)^2 + 4\delta^2 \cos^2 \psi] + \frac{1}{E_{S_-} - U - \varepsilon} (\sqrt{2}t \cos \psi - X \sin \psi)^2 + \\ & + \frac{1}{E_{S_-} - V_- - \bar{b}} [2(\delta \mathbf{b} \cdot \mathbf{e}')^2 \cos^2 \psi + (\sqrt{2}\delta b_y \cos \psi + \Omega_s \sin \psi)^2], \end{aligned} \quad (60)$$

$$\delta A_{22} = \frac{1}{E_{T_+} - U - \varepsilon} \Omega_s^2 + \frac{1}{E_{T_+} - E_{S_+}} [(\Omega_s \cos \psi + \sqrt{2} \delta b_y \sin \psi)^2 + 2(\delta \mathbf{b} \cdot \mathbf{e}')^2 \sin^2 \psi], \quad (61)$$

$$\delta A_{12} = -\frac{i}{2} \Omega_s (\sqrt{2} t \cos \psi + X \sin \psi) \left(\frac{1}{E_{S_-} - U - \varepsilon} + \frac{1}{E_{T_+} - U - \varepsilon} \right). \quad (62)$$

In experiments that probe the electron spin dynamics, the most important terms are the off-diagonal ones, $\delta A_{12} = \delta A_{21}^*$. They lead to a modification of the first-order singlet-triplet splitting (51), i.e., $\Delta_{\text{ST}}^* \xrightarrow{\text{SW}} 2|H_{34} + \delta A_{12}|$. Thus, up to second-order, the splitting at the anticrossing becomes

$$\Delta_{\text{ST}}^* = 2 \left| -i\Omega \sin \varphi \left[\sin \psi - \left(\frac{t}{\sqrt{2}} \cos \psi - \frac{X}{2} \sin \psi \right) \left(\frac{1}{E_{S_-} - U - \varepsilon^*} + \frac{1}{E_{T_+} - U - \varepsilon^*} \right) \right] + \sqrt{2}(\delta \mathbf{b} \cdot \mathbf{e}' + i\delta b_y) \cos \psi \right|. \quad (63)$$

We see now that the new correction terms in Δ_{ST}^* become significant for weak detuning, when $\psi < \pi/2$, because the spin-independent tunneling contribution, which is $\propto \cos \psi$, can alter the first-order result, which is $\propto \sin \psi$. We compare the splitting in the second order, Eq. (63), with the first-order splitting and the result of exact numerical diagonalization of H , Eq. (30), in Fig. 9. The higher-order corrections are small, but they do become significant for the magnetic field normal to the spin-orbit parameter, $\varphi = \pi/2, 3\pi/2$, due to stronger effective strength $\Omega \sin \varphi$ of spin-orbit coupling. For other considered values of detuning, $\varepsilon^* = 0.1U$ and $\varepsilon^* = 0.2U$, the change of splitting is smaller than for the $\varepsilon^* = 0.4U$ case.

The limit $\psi = \pi/2$ requires strong magnetic fields, $B \sim 1$ T for a typical GaAs DQD. It is reasonable to assume that the experiments can be performed both in this limit and away from it, so that the dependence of Δ_{ST}^* on ψ can be probed. In materials with larger g factors such as InAs, InSb, SiGe, the limit is reached at lower fields. In addition, we have obtained similar results for a model DQD with $t = 0.1U$, $\Omega = 0.1t$,

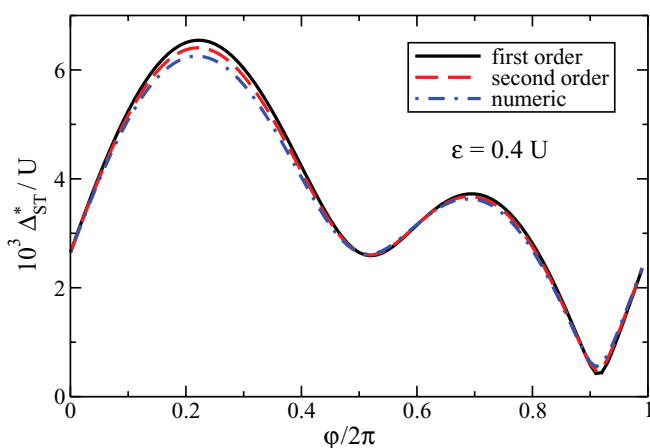


FIG. 9. (Color online) Comparison of the splitting Δ_{ST}^* obtained from the perturbation in first order (full line), Eq. (52), and in the second order (dashed line), Eq. (63), to the exact numerical result (dashed-dotted line), obtained by the direct numerical diagonalization of H , Eq. (30). The plots show the splitting Δ_{ST}^* as a function of the angle φ for the anticrossing at the detuning $\varepsilon^* = 0.4U$. The parameters used in this plot are $U = 1$, $t = 0.02$, $V_+ = 0.75$, $V_- = 0.74$, $\Omega = 0.005$, and $\delta \mathbf{b} = (-0.0006, 0.0008, 0.0012)$.

and $|\delta \mathbf{b}| \approx 0.5\Omega$ that describes a smaller DQD with more pronounced hopping.

VII. RATIO OF SPIN-ORBIT AND HYPERFINE TERMS

As pointed out before, the spin-non-conserving Hamiltonian in the vicinity of the anticrossing can be used to get experimental access to the spin-orbit interaction and nuclear polarization in the difference field $\delta \mathbf{b}$. Being a function of controllable parameters ε and $\bar{\mathbf{b}}$, this Hamiltonian can be altered by applying voltages to electrodes in the vicinity of the quantum dots, adjusting the strength of an external magnetic field, or changing the direction of the field.

The effect of the competition between spin-orbit- and hyperfine-induced spin flips on the efficiency of angular momentum transfer between electron and nuclear spins was recently studied theoretically, both in the context of dc transport experiments¹⁸ and in the context of gate-sweep experiments.^{19,20} References 18 and 19 revealed striking sensitivities of the polarization transfer efficiency on the ratio of spin-orbit and hyperfine coupling strengths. In those works, the coupling strengths were treated as phenomenological parameters. Here, we provide explicit expressions for them, and discuss how they can be tuned.

Following the notation of Ref. 19, we write

$$v_{\vartheta} = v_{\text{SO}} + e^{i\vartheta} v_{\text{HF}}, \quad (64)$$

where v_{SO} and v_{HF} stand for the transitions caused by spin-orbit and hyperfine interactions, respectively. Comparing with Eq. (48), we can identify v_{ϑ} with H_{34} . Then, adjusting the overall phase to make the spin-orbit part v_{SO} real, we identify in lowest order,

$$v_{\text{SO}} = |\Omega \sin \varphi \sin \psi|, \quad (65)$$

$$v_{\text{HF}} = |\cos \psi| \sqrt{(\delta \mathbf{b} \cdot \mathbf{e}')^2 + \delta b_y^2}, \quad (66)$$

$$\vartheta = \arctan \left[\frac{-\delta \mathbf{b} \cdot \mathbf{e}'}{\delta b_y} \right]. \quad (67)$$

The explicit expression for ϑ shows that the phase of the matrix element can be adjusted not only by changing the direction of $\delta \mathbf{b}$, but also by rotating the external magnetic field, which

changes \mathbf{e}' , and also controls the effective spin-orbit coupling strength.

Our results show that, in principle, it is possible to switch between the regimes of hyperfine-dominated and spin-orbit-dominated behaviors by changing the external magnetic field strength and direction. In the strong field regime, with the sum field $\bar{\mathbf{b}}$ being large, ε^* is also large, and thus the spin-orbit terms become dominant (ψ approaches $\pi/2$). This behavior is illustrated in Fig. 5. Note that the large values of ε^* require strong $\bar{\mathbf{b}}$ fields. On the other hand, switching to the regime $v_{\text{HF}} > v_{\text{SO}}$ is always possible by rotating the direction of the magnetic field so that it coincides with $\pm\mathbf{\Omega}/|\mathbf{\Omega}|$, giving $\varphi \approx 0$. In this case, the term v_{SO} is negligible and v_{HF} dominates the splitting. Higher-order corrections to the effective Hamiltonian at the anticrossing point do not alter this basic picture of the splitting, but they do change the values of the parameters ψ and φ at which the switching occurs.

The switching between the regimes dominated either by spin-orbit or by hyperfine interactions can potentially be achieved as follows. For the regime $v_{\text{SO}} > v_{\text{HF}}$, the sum field $\bar{\mathbf{b}}$ should point along the normal to the spin-orbit field $\mathbf{\Omega}$, see Eqs. (26) and (27), in order to maximize $|\sin\varphi|$. Also, the applied field should be as strong as possible, in order to maximize the amplitude of the singlet $|(0,2)S\rangle$ [contributing to the anticrossing singlet $|S_-\rangle$, see Eq. (37)]. On the other hand, the opposite regime, $v_{\text{HF}} > v_{\text{SO}}$, can be reached by orienting $\bar{\mathbf{b}}$ along $\mathbf{\Omega}$, and thus reaching $\sin\varphi = 0$. If $\sin\varphi = 0$ cannot be achieved, v_{SO} can be reduced by decreasing $\bar{\mathbf{b}}$ and thereby increasing the amplitude of the singlet state $|(1,1)S\rangle$ in the $|S_-\rangle$ singlet at the anticrossing.

VIII. CONCLUSIONS

We have derived an effective two-level Hamiltonian H_{cr} for a detuned two-electron double quantum dot in an external magnetic field. Our effective Hamiltonian describes the dynamics of the electron spins for the values of detuning $\varepsilon \approx \varepsilon^*$ close to the anticrossing of the lowest energy $S = 0$ and the lowest energy $S = 1$ state. We have shown how H_{cr} can be used in the interpretation of experiments that probe electron spin interactions by charge sensing and transport in the Coulomb blockade regime. The dependence of H_{cr} on the detuning and magnetic fields can also be used to switch the spin dynamics in a double quantum dot between the spin-orbit-dominated and the hyperfine-dominated regimes.

The spin dynamics at the anticrossing is governed by the spin-orbit and nuclear hyperfine interactions. In a double quantum dot, these two interactions act differently on the orbital electronic states. On one hand, the spin-orbit interaction causes hopping of an electron between the quantum dots

accompanied by a spin rotation, thus changing the occupation of the quantum dots. On the other hand, the nuclear hyperfine interaction acts as an inhomogeneous magnetic field, and causes spin rotations that are local to the dots, leaving the charge state unchanged. Due to this distinction, the detuning ε controls the relative strength of the two interactions in H_{cr} , in addition to the ratio $|\mathbf{\Omega}|/|\delta\mathbf{b}|$, or $|\mathbf{\Omega}|/\sigma$. In the limit of detuning much stronger than the on-site repulsion of the dots, $\varepsilon \gg U$, H_{cr} describes mostly the spin-orbit interaction, with negligible hyperfine effects. In the case of weaker detuning, the effective hyperfine interactions can be of the size comparable to the effective spin-orbit interactions.

In addition, we find that the orientations of both the double quantum dot and the external magnetic field, described in the H_{cr} by the spin-orbit field $\mathbf{\Omega}$ and the sum field $\bar{\mathbf{b}}$, influence the effective spin-orbit interaction. In particular, by having $\bar{\mathbf{b}}$ pointing along $\mathbf{\Omega}$, we can suppress the spin-orbit effects completely (in leading order).

The splitting of the anticrossing states is accessible to experiments. It can be calculated from H_{cr} , and we find the dependence of this splitting on detuning and the strength and direction of the sum field, $\Delta_{\text{ST}}(\varepsilon, \bar{\mathbf{b}}, \varphi)$. Of particular interest is the splitting of levels at the anticrossing. We calculate this quantity, $\Delta_{\text{ST}}^*(\varepsilon^*, \varphi)$ as a function of the detuning at the anticrossing point ε^* and the orientation of the sum field, given by the angle φ . Both the spin-orbit interaction strength and the inhomogeneity in the hyperfine coupling can be deduced by measuring the splitting and using our formulas for $\Delta_{\text{ST}}^*(\varepsilon^*, \varphi)$.

The relative strength of the spin-orbit and hyperfine terms in H_{cr} has a profound effect on the coupled dynamics of electron and nuclear spins. The value of the average angular momentum transfer to nuclear spins as an electron tunnels through a spin-blockaded DQD changes sharply as the interaction goes from the spin-orbit-dominated to the hyperfine-dominated regime. The spin-orbit interaction is dominant in the limit of strong detuning, $\varepsilon^* \gg U - V_{\pm}$. The regime dominated by nuclear hyperfine interaction is reached when the detuning is weaker $\varepsilon^* \lesssim t$ and the orientation of the sum field is along $\mathbf{\Omega}$. Using the dependencies of the matrix elements on gate voltages and magnetic field strength and orientation, it may be possible to tune between these two regimes *in situ*, thus enabling experiments to study their sensitive competition.

ACKNOWLEDGMENTS

We gratefully acknowledge helpful discussions with Izhar Neder. This work is partially supported by the Swiss NSF, NCCR Nanoscience, and QSIT, DARPA QuEST, and the Intelligence Advanced Research Projects Activity (IARPA) through the Army Research Office.

¹D. Loss and D. P. DiVincenzo, *Phys. Rev. A* **57**, 120 (1998).

²R. Hanson, L. P. Kouwenhoven, J. R. Petta, S. Tarucha, and L. M. K. Vandersypen, *Rev. Mod. Phys.* **79**, 1217 (2007).

³R. A. Žak, B. Röthlisberger, S. Chesi, and D. Loss, *Riv. Nuovo Cimento* **033**, 345 (2010).

⁴S. C. Benjamin, *Phys. Rev. A* **64**, 054303 (2001).

⁵J. Levy, *Phys. Rev. Lett.* **89**, 147902 (2002).

⁶L.-A. Wu and D. A. Lidar, *Phys. Rev. A* **66**, 062314 (2002).

⁷D. Stepanenko and N. E. Bonesteel, *Phys. Rev. Lett.* **93**, 140501 (2004).

- ⁸V. N. Golovach, M. Borhani, and D. Loss, *Phys. Rev. B* **74**, 165319 (2006).
- ⁹F. H. L. Koppens, C. Buizert, K. J. Tielrooij, I. T. Vink, K. C. Nowack, T. Meunier, L. P. Kouwenhoven, and L. M. K. Vandersypen, *Nature (London)* **442**, 766 (2006).
- ¹⁰K. C. Nowack, F. H. L. Koppens, Y. V. Nazarov, and L. M. K. Vandersypen, *Science* **318**, 1430 (2007).
- ¹¹C. Barthel, D. J. Reilly, C. M. Marcus, M. P. Hanson, and A. C. Gossard, *Phys. Rev. Lett.* **103**, 160503 (2009).
- ¹²S. Foletti, H. Bluhm, D. Mahalu, V. Umansky, and A. Yacoby, *Nat. Phys.* **5**, 903 (2009).
- ¹³S. Nadj-Perge, S. M. Frolov, E. P. A. M. Bakkers, and L. P. Kouwenhoven, *Nature (London)* **468**, 1084 (2010).
- ¹⁴K. Ono, D. G. Austing, Y. Tokura, and S. Tarucha, *Science* **297**, 1313 (2002).
- ¹⁵A. C. Johnson, J. R. Petta, C. M. Marcus, M. P. Hanson, and A. C. Gossard, *Phys. Rev. B* **72**, 165308 (2005).
- ¹⁶S. Tarucha, Y. Kitamura, T. Koder, and K. Ono, *Phys. Status Solidi B* **243**, 3673 (2006).
- ¹⁷S. Nadj-Perge, S. M. Frolov, J. W. W. van Tilburg, J. Danon, Y. V. Nazarov, R. Algra, E. P. A. M. Bakkers, and L. P. Kouwenhoven, *Phys. Rev. B* **81**, 201305 (2010).
- ¹⁸M. S. Rudner and L. S. Levitov, *Phys. Rev. B* **82**, 155418 (2010).
- ¹⁹M. S. Rudner, I. Neder, L. S. Levitov, and B. I. Halperin, *Phys. Rev. B* **82**, 041311 (2010).
- ²⁰A. Brataas and E. I. Rashba, *Phys. Rev. B* **84**, 045301 (2011).
- ²¹G. Burkard, D. Loss, and D. P. DiVincenzo, *Phys. Rev. B* **59**, 2070 (1999).
- ²²A. W. Overhauser, *Phys. Rev.* **92**, 411 (1953).
- ²³J. Schliemann, A. Khaetskii, and D. Loss, *J. Phys. Condens. Matter* **50**, R1809 (2003).
- ²⁴E. L. Rashba, *Sov. Phys. Solid State* (1960).
- ²⁵Y. Bychkov and E. Rashba, *J. Phys. C* **17**, 6039 (1984).
- ²⁶M. Dyakonov and V. Kachorovskii, *Sov. Phys. Semicond.* **20**, 110 (1986).
- ²⁷G. Dresselhaus, *Phys. Rev.* **100**, 580 (1955).
- ²⁸D. Stepanenko, N. E. Bonesteel, D. P. DiVincenzo, G. Burkard, and D. Loss, *Phys. Rev. B* **68**, 115306 (2003).
- ²⁹F. Baruffa, P. Stano, and J. Fabian, *Phys. Rev. Lett.* **104**, 126401 (2010).
- ³⁰F. Baruffa, P. Stano, and J. Fabian, *Phys. Rev. B* **82**, 045311 (2010).
- ³¹V. N. Golovach, A. Khaetskii, and D. Loss, *Phys. Rev. B* **77**, 045328 (2008).
- ³²D. J. Reilly, J. M. Taylor, J. R. Petta, C. M. Marcus, M. P. Hanson, and A. C. Gossard, *Science* **321**, 817 (2008).
- ³³D. J. Reilly, J. M. Taylor, E. A. Laird, J. R. Petta, C. M. Marcus, M. P. Hanson, and A. C. Gossard, *Phys. Rev. Lett.* **101**, 236803 (2008).
- ³⁴H. Bluhm, S. Foletti, D. Mahalu, V. Umansky, and A. Yacoby, *Phys. Rev. Lett.* **105**, 216803 (2010).
- ³⁵M. D. Schroer, K. D. Petersson, M. Jung, and J. R. Petta, *Phys. Rev. Lett.* **107**, 176811 (2011).
- ³⁶F. H. L. Koppens, J. A. Folk, J. M. Elzerman, R. Hanson, L. H. W. van Beveren, I. T. Vink, H. P. Tranitz, W. Wegscheider, L. P. Kouwenhoven, and L. M. K. Vandersypen, *Science* **309**, 1346 (2005).
- ³⁷D. M. Zumbühl, C. M. Marcus, M. P. Hanson, and A. C. Gossard, *Phys. Rev. Lett.* **93**, 256801 (2004).
- ³⁸J. Königmann, R. J. Haug, D. K. Maude, V. I. Fal'ko, and B. L. Altshuler, *Phys. Rev. Lett.* **94**, 226404 (2005).
- ³⁹A. Pfund, I. Shorubalko, K. Ensslin, and R. Leturcq, *Phys. Rev. Lett.* **99**, 036801 (2007).
- ⁴⁰D. M. Zumbühl, J. B. Miller, C. M. Marcus, K. Campman, and A. C. Gossard, *Phys. Rev. Lett.* **89**, 276803 (2002).
- ⁴¹J. R. Petta, J. M. Taylor, A. C. Johnson, A. Yacoby, M. D. Lukin, C. M. Marcus, M. P. Hanson, and A. C. Gossard, *Phys. Rev. Lett.* **100**, 067601 (2008).
- ⁴²J. R. Schrieffer and P. A. Wolff, *Phys. Rev.* **149**, 491 (1966).
- ⁴³S. Bravyi, D. P. DiVincenzo, and D. Loss, *Ann. Phys.* **326**, 2793 (2011).

Exchange-based CNOT gates for singlet-triplet qubits with spin-orbit interactionJelena Klinovaja,¹ Dimitrije Stepanenko,¹ Bertrand I. Halperin,² and Daniel Loss¹¹*Department of Physics, University of Basel, Klingelbergstrasse 82, CH-4056 Basel, Switzerland*²*Department of Physics, Harvard University, 17 Oxford St., 5 Cambridge, Massachusetts 02138, USA*

(Received 12 June 2012; published 13 August 2012)

We propose a scheme for implementing the CNOT gate over qubits encoded in a pair of electron spins in a double quantum dot. The scheme is based on exchange and spin-orbit interactions and on local gradients in Zeeman fields. We find that the optimal device geometry for this implementation involves effective magnetic fields that are parallel to the symmetry axis of the spin-orbit interaction. We show that the switching times for the CNOT gate can be as fast as a few nanoseconds for realistic parameter values in GaAs semiconductors. Guided by recent advances in surface codes, we also consider the perpendicular geometry. In this case, leakage errors due to spin-orbit interaction occur but can be suppressed in strong magnetic fields.

DOI: [10.1103/PhysRevB.86.085423](https://doi.org/10.1103/PhysRevB.86.085423)

PACS number(s): 73.21.La, 73.63.Kv, 85.35.Be

I. INTRODUCTION

Standard quantum computing¹ is based on encoding, manipulating, and measuring quantum information encoded in the state of a collection of quantum two-level systems, i.e., qubits. Spin-1/2 is an ideal implementation of a qubit since it is a natural two-level system, and every pure state of a spin-1/2 corresponds to a state of a qubit. For this reason, spins have been considered as carriers of quantum information in a variety of proposals.² The initial proposal³ called for spins in single-electron quantum dots electrically manipulated by the exchange interaction and local time-dependent Zeeman fields. A variety of other encoding schemes and manipulation techniques^{4–11} rely upon encoded qubits. In these schemes, the simplicity of qubit states and minimal number of physical carriers of quantum information are traded for less stringent requirements for experimental implementations. On one hand, the alternative setups protect from the most common types of errors by decoupling the computational degrees of freedom from the most common sources of noise, and therefore allow for longer gating times. On the other hand, in some alternative setups, the manipulation without fast switching of the local magnetic fields becomes possible.

The optimization in the encoding and manipulation protocols is always guided by the state of the art in the experiments. Recent results suggest that spin qubits can reside in a variety of material hosts with novel properties. Quantum dots in graphene¹² and carbon nanotubes¹³ are less susceptible to the decoherence due to nuclei and spin-orbit interaction. Spins in nanowires show very strong confinement in two spatial directions, and the gating is comparably simple.^{8,9} In hole systems, the carriers have distinct symmetry properties, and show coupling to the nuclear spins of a novel kind.¹⁴ Recently, the experiments in silicon¹⁵ have demonstrated coherent manipulation of spins similar to that achieved in the GaAs-based nanostructures. Within these hosts, the manipulation techniques that use exchange interaction, spatially inhomogeneous time-independent Zeeman splitting, and nuclear hyperfine interactions are within reach. Despite these developments, GaAs remains a promising route to spin qubits due to the highly advanced experimental techniques developed for this material.

Here, we study the implementation of the quantum gates on the encoded two-spin singlet-triplet (ST) qubits^{4,5,7,10,16,17} using resources that closely resemble those available in the current experimental setups. There, the application of the time-dependent electric fields through the gates fabricated into a structure¹¹ are preferred to time-dependent local magnetic fields. In addition, the nuclear spins^{7,16–19} and inhomogeneous magnetic fields^{20,21} are possible resources for spin control. In the setups based on semiconductors, the electrons or holes in the quantum dots are influenced by the spin-orbit interaction (SOI), which can contribute to the control.²²

In this work, we present a scheme for control of ST qubits which uses switching of the exchange interaction as a primary resource. We consider the scheme that is optimized for the application of quantum gates in the network of quantum dots. The construction of the CNOT gate uses pulses of the exchange interaction as the only parameter that is time dependent. The exchange interaction itself is not sufficient for the universal quantum computation over the ST qubits due to its high symmetry. The additional symmetry breaking is provided by nonuniform but static magnetic fields. These fields describe the influence both of magnetic fields, provided by the nearby magnets, and of the coupling to the nuclear spins in the host material via hyperfine interaction. Depending on the scheme used for the application of the quantum gates, the optimal geometry is either the one in which the magnetic fields point parallel to the axis of symmetry of the SOI or perpendicular to it.

One major problem in the realization of two-qubit quantum gates (in particular, we consider here the CNOT gate based on conditional phase gates) is the possibility of leakage errors where the spin states defining the logical qubit leave the computational space. These errors move the state of four spins from the 4-dimensional computational space of two qubits into some other portion of the 16-dimensional Hilbert space of four spin-1/2 particles. We consider two ways of addressing this problem. One scheme possesses the axial symmetry due to the fact that the SOI vector and magnetic fields are parallel. For this “parallel scheme,” we are able to construct a perfect CNOT gate, if we are able to control all the available parameters. Having in mind two-dimensional (2D) architectures, we also consider the CNOT gate between two



FIG. 1. (Color online) Parallel geometry: four quantum dots (yellow discs) aligned along the x axis in the presence of an external magnetic field \mathbf{B} that is applied parallel to the SOI vector $\boldsymbol{\beta}$ (red arrow), which must be perpendicular to the line of the dots and which we take to be the z direction. At each dot, there is a local magnetic field \mathbf{B}_i (blue arrows), also assumed to be parallel to \mathbf{B} , but with alternating orientations as indicated. The direction of \mathbf{B} defines the spin quantization axis. The dots are defined electrostatically by metallic gates (light green structures). Each dot contains a spin-1/2, and the exchange (J_{ij}) and the SOI-induced ($\boldsymbol{\beta}_{ij}$) interactions between the spins can be controlled by changing the electrostatic potential between the dots. The dots 1 and 2 (from left to right) define the first ST qubit, and the dots 3 and 4 the second ST qubit.

qubits in the case when the SOI vector and magnetic fields are perpendicular to each other. Here, we can not prevent the leakage out of the computational space, however, we show that it is suppressed by a ratio between the SOI and Zeeman energy coming from a strong external magnetic field. All our constructions assume that the controlled interactions are switched in time by rectangular pulses. Any deviations from this form of time dependence lead to additional corrections and affect the fidelity of the gate.

The paper is organized as follows. In Sec. II, we introduce the model for the double dots and effective Hamiltonians for field gradients and exchange and spin-orbit interactions. In Sec. III, we consider the parallel geometry and derive the CNOT gate via the conditional phase gates and swap gates, all based on exchange. There, we also give estimates for the switching times. The scheme for the perpendicular geometry is then addressed in Sec. IV, and we conclude in Sec. V.

II. EFFECTIVE MODEL

We consider in the following singlet-triplet qubits that are implemented by two electrons confined to a double-quantum-dot system^{4,5} (see Figs. 1 and 2). Such ST qubits have been realized successfully in several labs,²³ and single- and two-qubit operations have also been demonstrated recently.^{7,10,17,24} There are several schemes for the fundamental CNOT gate, which can be divided into two classes, schemes which make use of exchange interaction and schemes which do not, but

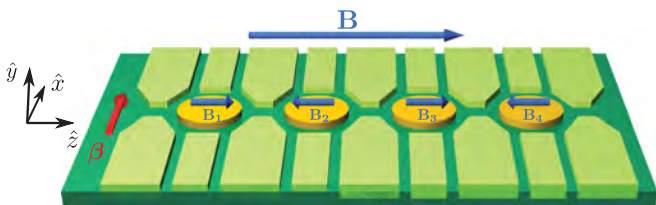


FIG. 2. (Color online) Perpendicular geometry: similar to the setup shown in Fig. 1, but with the difference that here the SOI vector $\boldsymbol{\beta}$ (red arrow) is *perpendicular* to the magnetic fields \mathbf{B} and \mathbf{B}_i , which define the spin quantization axis z .

instead rely on coupling of dipole moments.¹⁰ The latter schemes have the disadvantage to be rather slow and also to be affected by charge noise rather strongly. Here, we focus on exchange-based schemes specifically adapted to quantum dots in III-V semiconducting materials, which have the SOI, such as in GaAs or InAs quantum dots. Although the SOI is typically small compared to the level spacing of the dots, it needs to be taken into account in order to achieve high fidelities in gate operations.

We focus now on two such ST qubits and assume them to be encoded in four quantum dots that are arranged in a row (see Figs. 1 and 2). The external magnetic field \mathbf{B} is assumed to give the largest energy scale and determines the spin quantization axis z . The Hilbert space of four spin-1/2 is spanned by $2^4 = 16$ basis states. The total spin of the system is given by $\hat{\mathbf{S}} = \sum_{i=1}^4 \hat{\mathbf{S}}_i$, where $\hat{\mathbf{S}}_i$ is a spin-1/2 operator acting on the spin in a dot $i = 1, 2, 3, 4$. Due to axial symmetry, the z component \hat{S}^z becomes a good quantum number, and the eigenstates corresponding to $S^z = 0$ span a six-dimensional subspace. The singlet state of a qubit is defined as $|S\rangle = (|\downarrow\uparrow\rangle - |\uparrow\downarrow\rangle)/\sqrt{2}$ and the triplet state as $|T\rangle = (|\downarrow\uparrow\rangle + |\uparrow\downarrow\rangle)/\sqrt{2}$. We define the computational basis of the two ST qubits in this subspace as

$$\begin{aligned} |00\rangle &= |\downarrow\uparrow\downarrow\uparrow\rangle, & |11\rangle &= |\uparrow\downarrow\uparrow\downarrow\rangle, \\ |01\rangle &= |\downarrow\uparrow\uparrow\downarrow\rangle, & |10\rangle &= |\uparrow\downarrow\downarrow\uparrow\rangle, \end{aligned} \quad (1)$$

where $\{0, 1\}^{\otimes 2}$ denotes the ST qubit space, “ \uparrow ” and “ \downarrow ” denote states of the quantum-dot spins corresponding to the projection $S_i^z = \pm 1/2$ on the z axis. The remaining two states

$$|l_1\rangle = |\uparrow\uparrow\downarrow\downarrow\rangle, \quad |l_2\rangle = |\downarrow\downarrow\uparrow\uparrow\rangle \quad (2)$$

belong to the noncomputational leakage space. We note that the basis given in Eq. (1) is simply related to the common ST basis^{4,5} via rotations on the Bloch sphere (corresponding to a unitary basis transformation).

Aside from the externally applied magnetic field \mathbf{B} , we allow also for local magnetic fields \mathbf{B}_i that are constant in time (at least over the switching time of the gate). Such local fields can be generated, e.g., by nearby micromagnets²¹ or by the hyperfine field^{25–30} produced by the nuclear spins of the host material. In the latter case, in order to reach a high fidelity, it is important to perform a nuclear state narrowing,²⁵ i.e., to suppress the natural variance $\delta B_i \sim A/\sqrt{N} \sim 10$ mT to a smaller value, where N is the number of nuclear spins in the quantum dot, and A is the strength of the hyperfine coupling. In the ideal case, one should try to reach a limit where $|\mathbf{B}_i| \sim 50$ mT $\ll |\mathbf{B}|$ and the fluctuations in \mathbf{B}_i are much smaller than $|\mathbf{B}_i|$.

The magnetic fields \mathbf{B}_i are assumed to point along the external field \mathbf{B} so that they preserve the axial symmetry of the problem. However, the \mathbf{B}_i 's should have different values (to create field gradients between the dots), a simple scenario being local fields of opposite directions on neighboring dots (see Figs. 1 and 2). The corresponding Zeeman Hamiltonian is given by

$$H^B = \sum_{i=1}^4 (b + b_i) \hat{S}_i^z, \quad (3)$$

where the effective magnetic fields are defined in terms of energy as $b = g\mu_B B$ and $b_i = g\mu_B B_i$, respectively, with g being the electron g factor and μ_B the Bohr magneton.

The exchange interaction $J_{ij}(t)$ couples the electron spins of nearest-neighbor dots i and j and can be controlled electrostatically.^{7,21,23} If the tunnel barrier between the dots is high, we can treat them as independent. If the tunnel barrier is lowered and/or a detuning between the dots is applied, the two spins interact with each other, leading to an effective description in terms of a Heisenberg Hamiltonian^{3,22,31}

$$H^{ex} = J_{12}(t)\hat{\mathbf{S}}_1 \cdot \hat{\mathbf{S}}_2 + J_{23}(t)\hat{\mathbf{S}}_2 \cdot \hat{\mathbf{S}}_3 + J_{34}(t)\hat{\mathbf{S}}_3 \cdot \hat{\mathbf{S}}_4. \quad (4)$$

We assume that the magnetic field is sufficiently large compared to exchange energies, i.e., $J_{ij} \ll B$, to avoid admixture of triplets via the SOI (see the discussion of perpendicular geometry below).

We note that ideally it is best to switch the exchange J_{ij} by changing the corresponding interdot barrier height or distance, instead of detuning the double dot by a bias ϵ . Detuning is harmful for two reasons. First, detuning can admix other unwanted states [for example, $(0,2)S$ (see Fig. 2 in Ref. 22)]. To analyze the errors coming from detuning, one needs to go beyond the effective spin Hamiltonian and consider the microscopic model for the double dots, which includes Rashba and Dresselhaus SOI and inhomogeneous fields (see Ref. 22). Second, the control of J_{ij} via the tunnel barrier preserves the symmetry of the charge distribution in the double dot and thus, in particular, avoids the creation of dipole moments. In contrast, such dipole moments are unavoidable for detuning, and in the regime with $dJ_{ij}/d\epsilon \neq 0$ charge noise can enter most efficiently the qubit space, causing gate errors and decoherence of the ST qubits.²⁵ Thus, symmetric exchange switching is expected to be more favorable for achieving high gate fidelities.

Next, we account for the effects of spin-orbit interaction. Following Refs. 32–34, we model the SOI by a Dzyaloshinskii-Moriya (DM) term for two neighboring quantum dots [see, e.g., Eq. (1) in Ref. 33],

$$H_{ij}^{\text{SOI}} = \beta_{ij}(t) \cdot (\hat{\mathbf{S}}_i \times \hat{\mathbf{S}}_j), \quad (5)$$

where the SOI vector $\beta_{ij}(t)$ is perpendicular to the line connecting the dots. First, we consider a “parallel geometry” (see Fig. 1) where the SOI vectors β_{ij} are all parallel to each other and the magnetic fields \mathbf{B} and \mathbf{B}_j are assumed to be parallel to the SOI vectors. This preserves the axial symmetry of the spin system, and by definition, we choose the direction of \mathbf{B} to be the z axis. This leads to

$$H_{\parallel}^{\text{SOI}} = \sum_{i,j} \beta_{ij}(t) (\hat{S}_i^x \hat{S}_j^y - \hat{S}_i^y \hat{S}_j^x), \quad (6)$$

where the summation runs over neighboring dots i and j . The strength of the SOI, β_{ij} , depends on the distance between the dots as well as on the tunnel coupling between them. This allows us to assume that both $J_{ij}(t)$ and $\beta_{ij}(t)$ are switched on and off simultaneously.^{35–37}

We note here that both H^{ex} and $H_{\parallel}^{\text{SOI}}$, being axially symmetric interactions, preserve the z component of the total spin S^z . This means that our setup is protected from leakage to the subspace with $S^z \neq 0$. However, it is not protected from

the leakage to the noncomputational space given by Eq. (2). By a proper design of gates, this leakage can be minimized.

Alternatively, in a “perpendicular geometry” (see Fig. 2), the axis of the quantum dots is aligned parallel to the applied magnetic field, in the z direction. The SOI vector β_{ij} is perpendicular to this, and we take it to be in the x direction. The corresponding Hamiltonian becomes

$$H_{\perp}^{\text{SOI}} = \sum_{i,j} \beta_{ij}(t) (\hat{S}_i^y \hat{S}_j^z - \hat{S}_i^z \hat{S}_j^y). \quad (7)$$

Here, the SOI vector β_{ij} breaks the axial symmetry of the system, and the total spin S^z is no longer a good quantum number. As a consequence, leakage into the noncomputational space $S^z \neq 0$ is possible, in principle. However, this coupling involves higher-energy states and can thus be suppressed by choosing a sufficiently large magnetic field such that $\beta/B \ll 1$. In contrast, the SOI does not couple states within the computational space since the matrix elements of H_{\perp}^{SOI} between the states $|\downarrow\uparrow\rangle$ and $|\uparrow\downarrow\rangle$ vanish. We finally note that, similarly, a finite angle between the fields \mathbf{B} and \mathbf{B}_j leads to a leakage error of order $(\mathbf{B}_j)_{x,y}/B \ll 1$.

III. PARALLEL GEOMETRY

In this section, we concentrate on the parallel geometry (see Fig. 1). Using the axial symmetry of the problem we are able to construct a sequence of gate operations that implements the CNOT gate,¹ defined on the logical ST qubits given in Eq. (1) by $U_{\text{CNOT}}|a,b\rangle = |a, a \oplus b\rangle$, where $a, b = 0, 1$.

One important step in this construction is the implementation of the $\pi/4$ gate $U_{\pi/4}$ (see discussion below and Ref. 1). For this gate, we propose the following scheme consisting of four steps:

$$C_{23} \rightarrow (\pi_{12}, \pi_{34}) \rightarrow C_{23} \rightarrow (\pi_{12}, \pi_{34}), \quad (8)$$

where the conditional phase gate C_{23} exchange couples the dots 2 and 3 and adds a phase factor to the two ST qubits (see below). The swap gates π_{12} and π_{34} exchange spin states on the dots 1 and 2 and the dots 3 and 4, and can be performed in parallel.

A major issue in the implementation of $U_{\pi/4}$ is the avoidance of leakage errors during the coupling of qubits. To keep qubits in the computational space, operations on spins 2 and 3 must be constructed in such a way that the resulting gate is diagonal in the basis given by Eq. (1). This can be achieved in two ways. The first approach is to use strong pulses that lead to fast rotations around the Bloch sphere. The second approach is to use adiabatic pulses that are protected from the leakage to states with different energies.³⁸ However, the adiabaticity requires a longer pulse time. In this work, we focus on the first approach.

A. Conditional phase gate C_{23}

In this section, we describe the phase gate C_{23} involving the exchange and SOI interactions only between dots 2 and 3, while dots 1 and 4 are decoupled from dots 2 and 3, i.e., $J_{12} = J_{34} = 0$ and $\beta_{12} = \beta_{34} = 0$. In this case, the effective Hamiltonian is given by

$$H^C = H^B + H^{ex} + H_{\parallel}^{\text{SOI}} = H_1^C + H_{23}^C + H_4^C, \quad (9)$$

where we present it in block-diagonal form. The part of the Hamiltonian $H_i^C = (b + b_i)\hat{S}_i^z$ acts only on spins located at the dot $i = 1, 4$. The other part of the Hamiltonian H_{23}^C acts on spins located at the dots 2 and 3:

$$H_{23}^C = (b + b_2)\hat{S}_2^z + (b + b_3)\hat{S}_3^z + J_{23}\hat{S}_2 \cdot \hat{S}_3 + \beta_{23}(\hat{S}_2^x \hat{S}_3^y - \hat{S}_2^y \hat{S}_3^x). \quad (10)$$

Here, we assume a rectangular pulse shape for the exchange and spin-orbit interactions, and from now on we treat J_{23} and β_{23} as time-independent parameters. In this case, the unitary gate U^C is a simple exponential of the Hamiltonian

$$U^C = e^{-iH^C T_C} = e^{-iH_+^C T_C} e^{-iH_{23}^C T_C} e^{-iH_-^C T_C}. \quad (11)$$

The spins of dots 1 and 4 do not change in time apart from a phase factor coming from the corresponding magnetic field. In contrast, the spins of dots 2 and 3 change in time and acquire phases, as we describe next. For this, we express H_{23}^C as a matrix in the basis $\{|\uparrow\uparrow\rangle, |\uparrow\downarrow\rangle, |\downarrow\uparrow\rangle, |\downarrow\downarrow\rangle\}$:

$$\begin{pmatrix} H_+^C & 0 & 0 \\ 0 & H_0^C & 0 \\ 0 & 0 & H_-^C \end{pmatrix}, \quad (12)$$

where the block-diagonal form reflects the conservation of S^z . In the case of two parallel spins, the corresponding Hamiltonian is given by $H_{\pm}^C = J_{23}/4 \pm (b_2 + b_3)/2$, which just assigns a phase to the spins. In the case of antiparallel spins, the Hamiltonian H_0^C is given by

$$H_0^C = \frac{1}{2} \begin{pmatrix} -J_{23}/2 + \Delta b_{23} & J_{23} + i\beta_{23} \\ J_{23} - i\beta_{23} & -J_{23}/2 - \Delta b_{23} \end{pmatrix}, \quad (13)$$

where $\Delta b_{23} = b_2 - b_3$. Here, H_0^C describes the coupling between the states $|\uparrow\downarrow\rangle$ and $|\downarrow\uparrow\rangle$, which, in general, leads to leakage errors. This leakage can be prevented by choosing the pulse duration T_C in such a way that the corresponding unitary operator $U_0^C = \exp[-iH_0^C T_C]$ is diagonal in the basis $\{|\uparrow\downarrow\rangle, |\downarrow\uparrow\rangle\}$. It is more convenient to consider the evolution given by H_0^C on the Bloch sphere. For that, we rewrite H_0^C in terms of pseudospins,

$$H_0^C = -J_{23}/4 + (\tilde{J}_{23}/2) \mathbf{n}_{23} \cdot \boldsymbol{\tau}, \quad (14)$$

$$\tilde{J}_{23} = \sqrt{J_{23}^2 + \beta_{23}^2 + (\Delta b_{23})^2}, \quad (15)$$

$$\mathbf{n}_{23} = (J_{23}, -\beta_{23}, \Delta b_{23})/\tilde{J}_{23}, \quad (16)$$

where the unit vector \mathbf{n}_{23} defines the rotation axis on the Bloch sphere (see Fig. 3), and the pseudospin, acting on the states $\{|\uparrow\downarrow\rangle, |\downarrow\uparrow\rangle\}$, is described by the Pauli matrices $\boldsymbol{\tau}$. The north pole corresponds to $|\uparrow\downarrow\rangle$ and the south pole to $|\downarrow\uparrow\rangle$. The exchange interaction J_{23} , being the largest scale in H_0^C , forces \mathbf{n}_{23} to be aligned mostly along the x axis. If we neglect the SOI and any field gradients, the rotation on the Bloch sphere takes place in the yz plane. In the presence of SOI and field gradients, the rotation axis \mathbf{n}_{23} deviates from the x axis.

The unitary time evolution operator U_0^C corresponding to H_0^C takes the form

$$U_0^C = \exp(-iJ_{23}T_C/4)(\cos \alpha_C + i \mathbf{n}_{23} \cdot \boldsymbol{\tau} \sin \alpha_C), \quad (17)$$

where $\alpha_C = \tilde{J}_{23}T_C/2$. The duration of a pulse is determined by the condition that we obtain full rotations on the Bloch sphere

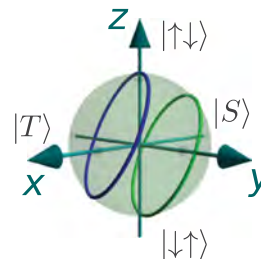


FIG. 3. (Color online) The Bloch sphere is defined with the north pole corresponding to $|\uparrow\downarrow\rangle$ and the south pole corresponding to $|\downarrow\uparrow\rangle$. The effect of the unitary evolution operator U_0^C [see Eq. (17)] on a state in the space $\{|\uparrow\downarrow\rangle, |\downarrow\uparrow\rangle\}$ is equivalent to the rotation on the Bloch sphere around the vector $J_{23}\mathbf{e}_x - \beta_{23}\mathbf{e}_y + \Delta b_{23}\mathbf{e}_z$. The conditional phase gate C_{23} corresponds to the full rotation on the Bloch sphere (shown by blue and green circles).

(see Fig. 3)

$$T_C = \frac{2\pi N_C}{\tilde{J}_{23}}, \quad (18)$$

where N_C is a positive integer. Note that deviations from Eq. (18) lead, again, to leakage errors.

As a result, the qubit states with parallel spins on dots 2 and 3 acquire the phases

$$\begin{aligned} \phi_{01} &= \frac{1}{2}(J_{23}/2 - b_1 + b_2 + b_3 - b_4)T_C, \\ \phi_{10} &= \frac{1}{2}(J_{23}/2 + b_1 - b_2 - b_3 + b_4)T_C, \end{aligned} \quad (19)$$

while the qubit states with antiparallel spins on dots 2 and 3 acquire the phases

$$\begin{aligned} \phi_{11} &= \frac{1}{2}(b_1 - b_4 - J_{23}/2)T_C + \pi N_C, \\ \phi_{00} &= \frac{1}{2}(-b_1 + b_4 - J_{23}/2)T_C + \pi N_C. \end{aligned} \quad (20)$$

Here, ϕ_{ab} corresponds to a phase acquired by a two-qubit state $|ab\rangle$. We note that phases produced by the magnetic field terms will be canceled during the second C_{23} pulse after the π pulses have been applied to the qubits.

B. Swap gates π_{12} and π_{34}

In this section, we discuss the swap gates π_{12} and π_{34} that exchange spin states between dots 1 and 2 and dots 3 and 4, respectively. The swap operation is a one-qubit operation, so dots 2 and 3 should be decoupled during the swap pulse, i.e., $J_{23} = 0$ and $\beta_{23} = 0$. The swap gate $\pi = (\pi_{12}, \pi_{34})$ is implemented, again, by a rectangular pulse and all parameters are assumed to stay constant during the switching process. This simplifies the unitary evolution operator

$$U^\pi = U_{12}^\pi U_{34}^\pi = e^{-iH_{12}^\pi T_\pi} e^{-iH_{34}^\pi T_\pi}. \quad (21)$$

Further, we focus on the first ST qubit (dots 1 and 2) and consider only π_{12} (π_{34} can be obtained analogously). We also note that since S^z is conserved separately for each qubit, the final state is always given by a linear combination of the states $|\downarrow\uparrow\rangle$ and $|\uparrow\downarrow\rangle$ on dots 1 and 2. Within this subspace, the effective Hamiltonian is given by

$$H_{12}^\pi = \frac{1}{2} \begin{pmatrix} -J_{12}/2 + \Delta b_{12} & J_{12} + i\beta_{12} \\ J_{12} - i\beta_{12} & -J_{12}/2 - \Delta b_{12} \end{pmatrix}, \quad (22)$$

or in pseudospin representation [see Eq. (14)]

$$H_{12}^{\pi} = -J_{12}/4 + (\tilde{J}_{12}/2) \mathbf{n}_{12} \cdot \boldsymbol{\tau}, \quad (23)$$

$$\tilde{J}_{12} = \sqrt{J_{12}^2 + \beta_{12}^2 + (\Delta b_{12})^2}, \quad (24)$$

$$\mathbf{n}_{12} = (J_{12}, -\beta_{12}, \Delta b_{12})/\tilde{J}_{12}, \quad (25)$$

where $\Delta b_{12} = b_1 - b_2$ and the Pauli matrix τ_i acts in the pseudospin space spanned by $|\uparrow\downarrow\rangle$ and $|\downarrow\uparrow\rangle$. Again, the unit vector \mathbf{n}_{12} defines the rotation axis. The corresponding unitary evolution operator reduces to the form

$$U_{12}^{\pi} = \exp(i J_{12} T_{\pi}/4)(\cos \alpha_{\pi} + i \mathbf{n}_{12} \cdot \boldsymbol{\tau} \sin \alpha_{\pi}), \quad (26)$$

where $\alpha_{\pi} = \tilde{J}_{12} T_{\pi}/2$.

The swap operation should exchange the states $|\uparrow\downarrow\rangle$ and $|\downarrow\uparrow\rangle$. In the absence of SOI and field gradients, the unitary evolution operator U_{12}^{π} corresponds to a rotation around the x axis ($\mathbf{n}_{12} = \mathbf{e}_x$) in the yz plane. At half the period, $T_{\pi}^0 = \pi/2\tilde{J}_{12}$, a state evolves from the north to the south pole and vice versa, i.e., $U_{12}^{\pi}|_{T_{\pi}^0} \propto \tau_x$.

However, in the presence of SOI and/or field gradients, the rotation axis \mathbf{n}_{12} is not aligned with \mathbf{e}_x (compare with Fig. 3), so the trajectory starting at the north (south) pole would never go exactly through the south (north) pole. The corresponding deviations lead to errors in the π_{12} gate on the order of $\sqrt{\Delta b_{12}^2 + \beta_{12}^2}/J_{12}$. This means that it is impossible to produce a perfect swap operation with only one single rectangular pulse. However, by applying a sequence of several rectangular pulses, it is still possible to produce a perfect π_{12} gate, as we demonstrate next.

Indeed, this goal can be achieved by the following three steps (see also Fig. 4). First, we switch on the exchange interaction J_{12} between the dots 1 and 2 (this also automatically switches on the SOI β_{12}). We assume J_{12} to be larger than Δb_{12} and/or β_{12} . The rotation axis \mathbf{n}_{12} in polar coordinates is given by

$$\mathbf{n}_{12} = (\sin \vartheta \cos \varphi, \sin \vartheta \sin \varphi, \cos \vartheta). \quad (27)$$

From now on, we work in the coordinate system in which the x axis points along $J_{12}\mathbf{e}_x - \beta_{12}\mathbf{e}_y$, so $\varphi = 0$ and $0 \leq \cos \vartheta = \Delta b_{12}/\tilde{J}_{12} \leq 1/\sqrt{2}$. The strength and the duration of the rectangular pulse is chosen in such a way that the rotation reaches the equator of the Bloch sphere. The initial and final vectors on the Bloch sphere are given by

$$\chi_i = (0, 0, 1), \quad (28)$$

$$\chi_f = [\cot \vartheta, \sqrt{\sin(2\vartheta - \pi/2)}/\sin \vartheta, 0], \quad (29)$$

allowing us to find the rotation angle $\alpha_{\pi}^{(a1)} = \pi/2 + \arcsin(\cot^2 \vartheta)$, and the corresponding pulse duration

$$T_{\pi}^{(a1)} = [\pi + 2 \arcsin(\cot^2 \vartheta)]/2\tilde{J}_{12}. \quad (30)$$

Second, after switching off exchange and spin-orbit interactions $J_{12} = 0$ and $\beta_{12} = 0$, the rotation takes place around the z axis in the equatorial plane, at a precession frequency determined by the field gradient Δb_{12} . The rotation angle becomes $\alpha_{\pi}^{(a2)} = 2[\pi - \arccos(\cot \vartheta)]$, and the pulse duration is given by

$$T_{\pi}^{(a2)} = \alpha_{\pi}^{(a2)}/\Delta b_{12}. \quad (31)$$

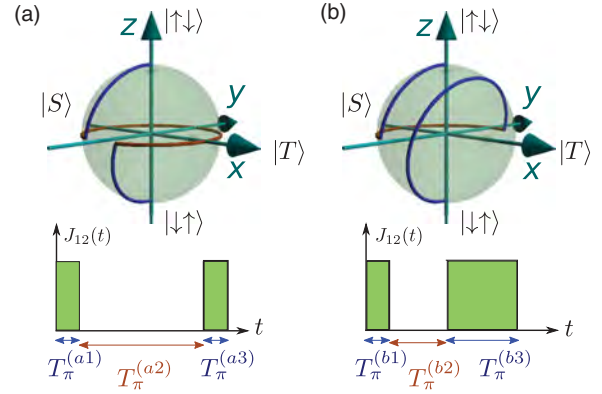


FIG. 4. (Color online) Two schemes for the swap gate $\pi_{12}: |\uparrow\downarrow\rangle \rightarrow |\downarrow\uparrow\rangle$, composed of three consecutive rotations on the Bloch sphere where the offset induced by Δb_{12} and β_{12} is fully compensated. (a) First, starting from the north pole, we turn on J_{12} and β_{12} to induce rotation around $J_{12}\mathbf{e}_x - \beta_{12}\mathbf{e}_y + \Delta b_{12}\mathbf{e}_z$ (upper blue arc) until we reach the equator where we turn off J_{12} and β_{12} . Second, we let the state precess around the z axis in the equatorial plane until the mirror point of the starting point on the equator is reached (brown arc). Third, we induce once more rotation around $J_{12}\mathbf{e}_x - \beta_{12}\mathbf{e}_y + \Delta b_{12}\mathbf{e}_z$ (lower blue arc) until we reach the south pole. Lower panel: associated rectangular gate pulses and switching times $T_{\pi}^{(a1,a2,a3)}$ for the three steps. (b) Alternative scheme where during the second step the state precesses along the equator until it reaches the point diametrically opposite to its starting point (brown arc).

Finally, we repeat the first step by applying a pulse of the same strength J_{12} (β_{12}) and during the same time $T_{\pi}^{(a3)} = T_{\pi}^{(a1)}$.

An alternative scheme (b) is presented in Fig. 4(b). During the second step, the state evolves on the Bloch sphere only over half of the equator, $\alpha_{\pi}^{(b2)} = \pi$, with the corresponding pulse duration $T_{\pi}^{(b2)} = \alpha_{\pi}^{(b2)}/\Delta b_{12}$. The duration of the third pulse is given by

$$T_{\pi}^{(b3)} = [3\pi - 2 \arcsin(\cot^2 \vartheta)]/2\tilde{J}_{12}. \quad (32)$$

The second step is the slowest one in these schemes, so the scheme (b) has an advantage over the scheme (a) by being faster as it requires less rotation on the equator. However, scheme (b) requires better control of parameters since $T_{\pi}^{(b1)} \neq T_{\pi}^{(b3)}$.

Here, we note that it is also possible to switch off the exchange coupling J_{12} not only on the equator, but also at any other point on the Bloch sphere. Moving away from the equator speeds up the gate performance, but demands greater precision in the tuning since the rotation proceeds along a smaller arc and in shorter time.

The scheme presented above confirms that it is possible to construct a perfect π swap gate even in the presence of the z component of the SOI vector β_{12} , or local field gradients Δb_{12} , by adjusting the pulse durations. The other two components of the SOI vector couple states of different total spin S^z , and thus cause leakage errors. Therefore, it is optimal to orient the magnetic fields (defining the spin quantization axis z) along the SOI vector β_{12} .

C. CNOT gate

After the execution of the four-step sequence given by Eq. (8), an initial qubit state is restored but with a phase factor [see Eqs. (19) and (20)]:

$$\begin{aligned}
 [00] &\xrightarrow{C_{23}} e^{i\phi_{00}}[00] \xrightarrow{(\pi_{12}, \pi_{34})} e^{i\phi_{00}}[11] \xrightarrow{C_{23}} e^{i(\phi_{11}+\phi_{00})}[11] \xrightarrow{(\pi_{12}, \pi_{34})} [00]e^{i(\phi_{11}+\phi_{00})}, \\
 [11] &\xrightarrow{C_{23}} e^{i\phi_{11}}[11] \xrightarrow{(\pi_{12}, \pi_{34})} e^{i\phi_{11}}[00] \xrightarrow{C_{23}} e^{i(\phi_{11}+\phi_{00})}[00] \xrightarrow{(\pi_{12}, \pi_{34})} [11]e^{i(\phi_{11}+\phi_{00})}, \\
 [01] &\xrightarrow{C_{23}} e^{i\phi_{01}}[01] \xrightarrow{(\pi_{12}, \pi_{34})} e^{i\phi_{01}}[10] \xrightarrow{C_{23}} e^{i(\phi_{01}+\phi_{10})}[10] \xrightarrow{(\pi_{12}, \pi_{34})} [01]e^{i(\phi_{01}+\phi_{10})}, \\
 [10] &\xrightarrow{C_{23}} e^{i\phi_{10}}[10] \xrightarrow{(\pi_{12}, \pi_{34})} e^{i\phi_{10}}[01] \xrightarrow{C_{23}} e^{i(\phi_{01}+\phi_{10})}[01] \xrightarrow{(\pi_{12}, \pi_{34})} [10]e^{i(\phi_{01}+\phi_{10})},
 \end{aligned} \tag{33}$$

with $\phi_{01} + \phi_{10} = -(\phi_{11} + \phi_{00}) = J_{23}T_C/2$, where we omit a trivial phase $2\pi N_C$. The total gate acting on the qubits as defined by Eq. (33) can be written in the compact form

$$e^{-i(J_{23}T_C/2)\sigma_1^x\sigma_2^x}, \tag{34}$$

where the Pauli matrix σ_1^j acts on the first ST qubit (formed by dots 1 and 2) and σ_2^j on the second one (formed by dots 3 and 4) with $j = x, y, z$. Choosing

$$T_C = \left(4\pi m - \frac{\pi}{2}\right) / J_{23}, \tag{35}$$

where m is a positive integer, we obtain the $\pi/4$ gate

$$U_{\pi/4} = e^{i\frac{\pi}{4}\sigma_1^x\sigma_2^x}. \tag{36}$$

Both Eqs. (18) and (35) should be satisfied simultaneously. For example, if $m = 1$ and $N_C = 2$, we get

$$T_C = \frac{\pi}{2} \sqrt{\frac{15}{\Delta b_{23}^2 + \beta_{23}^2}}, \tag{37}$$

$$J_{23} = \frac{7}{\sqrt{15}} \sqrt{\Delta b_{23}^2 + \beta_{23}^2}. \tag{38}$$

From this we can estimate the total switching time to perform the $\pi/4$ gate that is a sum of the switching times at each step [see Eq. (8)]. For the scheme discussed in Secs. III A and III B, the slowest part is given by the swap gates π_{12} and π_{34} , the switching time of which is limited by field gradients (due to nuclear spins^{7,16-19} and/or micromagnets^{20,21}), $|\Delta b_{12}| = |\Delta b_{34}| \approx 10$ mT, which corresponds to $T_\pi^{(b2)} \approx 10$ ns. The gate can be faster if the rotations around the z axis are performed not on the equator, but more closely to the poles. This allows us to decrease the switching time of the swap gate to 2 ns; however, this would require a more precise control over the pulses. The same trick can be used to decrease the switching time of the conditional phase gate C_{23} (compare Figs. 3 and 5). If field gradients larger than 10 mT are used, the switching rates will be proportionately larger.

Using the $\pi/4$ gate, we construct the controlled phase flip (CPF) gate $U_{\text{CPF}} = \text{diag}(1, 1, 1, -1)$ (see footnote¹³ in Ref. 3) as

$$U_{\text{CPF}} = U_{\pi/4} e^{-i\frac{\pi}{4}(\sigma_1^x + \sigma_2^x - 1)}. \tag{39}$$

Finally, we obtain the CNOT gate

$$U_{\text{CNOT}} = \begin{pmatrix} \mathbb{I} & 0 \\ 0 & \sigma_2^x \end{pmatrix} \tag{40}$$

by using the CPF gate and performing a basis rotation on qubit 2 (a single-qubit rotation by $\pi/2$ about the y axis),

$$U_{\text{CNOT}} = e^{i\frac{\pi}{4}\sigma_2^y} U_{\text{CPF}} e^{-i\frac{\pi}{4}\sigma_2^y}. \tag{41}$$

In summary, the full sequence of operations for the CNOT gate U_{CNOT} is given by

$$e^{i\frac{\pi}{4}\sigma_2^y} [(\pi_{12}\pi_{34})C_{23}(\pi_{12}\pi_{34})C_{23}] e^{-i\frac{\pi}{4}(\sigma_1^x + \sigma_2^x)} e^{-i\frac{\pi}{4}\sigma_2^y}. \tag{42}$$

We note again that this result has been derived under the assumption of rectangular pulse shapes. This is certainly an idealization, and in practice we expect deviations from this shape to cause errors for the gates and to affect the gate fidelity. The study of this issue, being very important for practical purposes, requires a separate investigation and is beyond the scope of this work.

IV. PERPENDICULAR GEOMETRY

In the previous section, we have discussed the parallel geometry for which we were able to construct a perfect CNOT gate under the assumption that we have a complete control over the parameters. The CNOT gate, together with single-qubit gates, allows us to simulate any other quantum gate and its implementation is a crucial step toward the realization of a quantum computer.¹ In a next step, many such elementary gates need to be connected into a large network. In recent years, the surface code³⁹ has emerged as one of the most promising platforms for this goal due to its large threshold of about 1% for fault-tolerant error correction.³⁹ This platform requires a

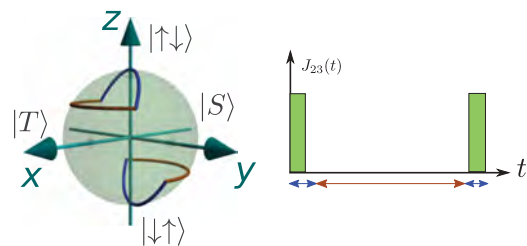


FIG. 5. (Color online) An alternative scheme for the conditional phase gate C_{23} (see also Fig. 3). Instead of the rotation with the pulse defined by Eqs. (18) and (35), we consider a sequence of three pulses. During the first and the third pulses (blue arcs), the state precesses quickly acquiring the $\pi/4$ phase [see Eq. (35)]. During the second pulse $J_{23} = 0$, the state precesses around the z axis over a shorter path than the one in Fig. 3. As a result, the switching is faster.

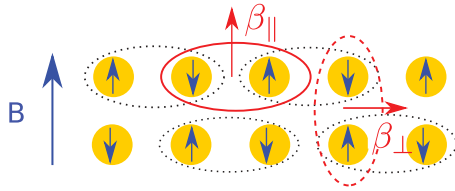


FIG. 6. (Color online) Schematic setup for 2D architecture. Two dots define an ST qubit (black dotted ellipses). An external magnetic field \mathbf{B} and local magnetic fields (blue arrows) are parallel. In the case of the coupling between two qubits from the same row (red solid ellipse), the SOI vector β_{\parallel} is parallel to the magnetic field \mathbf{B} , corresponding to the parallel geometry (see Fig. 1). In the case of coupling between two qubits from two neighboring rows (red dashed ellipse), the SOI vector β_{\perp} is perpendicular to the magnetic field \mathbf{B} , corresponding to the perpendicular geometry (see Fig. 2).

2D geometry and can be implemented in semiconductors of the type considered here.¹¹

The basic 2D scheme is illustrated in Fig. 6. There, we show an array of quantum dots where two neighboring dots in a given row represent one ST qubit. These quantum dots are embedded in a semiconductor where the SOI is of the same type in the entire structure. As a typical example, we mention Rashba and/or Dresselhaus SOI that both depend on the momentum of the electron. As a result, the direction of the SOI vector β is always perpendicular to the line along which two quantum dots are coupled by exchange interaction.²² Thus, for the coupling of two such qubits in the *same* row, the SOI vector β is parallel to the external magnetic field \mathbf{B} , so we can use the scheme designed for the parallel geometry in the previous section. In contrast, if we want to couple two qubits from *neighboring* rows, we should also consider a perpendicular geometry (see Figs. 1 and 6) in which the SOI vector β is perpendicular to the magnetic field \mathbf{B} .

This perpendicular geometry is characterized by several features. As was mentioned before, the axial symmetry in this case is broken by the SOI, leading to the coupling between computational ($S_z = 0$) and noncomputational ($S_z \neq 0$) space. If the magnetic field B is sufficiently large to split the triplet levels T_{\pm} far away from the computational space ($g\mu_B B \gg \beta$), we can neglect this leakage. We estimate for GaAs $B = 5 \text{ T} \approx 100 \mu\text{eV}/g\mu_B$. At the same time, the SOI does not couple states within the computational space, so for the realization of

the phase gate C_{23} and the swaps gates π_{12} and π_{34} , we can use the same scheme as in Sec. III only with $\beta = 0$.

V. CONCLUSIONS

We have studied the implementation of the CNOT gate for ST qubits in a model that is appropriate for current experiments.^{7,17,24} The setup consists of an array of quantum dots with controlled growth direction and the relative orientation of the dots. Pairs of neighboring dots build the ST qubits, where the quantization axis is determined by an externally applied magnetic field \mathbf{B} . Moreover, we introduce an inhomogeneity in magnetic fields \mathbf{B}_i by local micromagnets or by the hyperfine field. The resources used for time-dependent control are the exchange interaction $J_{ij}(t)$ and the SOI vector $\beta_{ij}(t)$.

If the SOI vector β is parallel to the external (\mathbf{B}) and local magnetic fields (\mathbf{B}_i), we are able to construct a perfect scheme for the CNOT gate based on the $\pi/4$ phase gate $U_{\pi/4}$, consisting of four basic steps. Two of the steps involve interaction of spins that belong to different qubits, and open the possibility of leakage errors. Under condition of total control over system parameters, we show that the leakage can be eliminated. In the other two steps, the tuning of exchange interaction enables perfect swap gates even in the presence of field gradients and SOI.

Motivated by recent results on the surface code, we shortly comment also on the 2D architecture. Here, we encounter a situation in which the SOI vector β and the magnetic fields \mathbf{B} and \mathbf{B}_i are perpendicular. In this case, the leakage to the noncomputational space with $S_z \neq 0$ is inevitable. However, it can be made very small as long as $\beta/g\mu_B B \ll 1$.

Depending on the pulsing scheme, the switching times for the conditional phase gate are shown to lie in the range 1–100 ns for typical GaAs parameters. Compared to the experimentally established decoherence times of about 250 μs ,¹⁷ this switching is sufficiently fast and shows that a CNOT gate based on exchange is a promising candidate for experimental realizations.

ACKNOWLEDGMENTS

We acknowledge discussions with A. Doherty, C. Marcus, I. Neder, and M. Rudner. This work is supported by IARPA/MQCO program, DARPA/QUEST program, the Swiss NSF, NCCR Nanoscience, and NCCR QSIT.

¹M. A. Nielsen and I. L. Chuang, *Quantum Computation and Quantum Information* (Cambridge University Press, Cambridge, UK, 2000).

²C. Kloeffel and D. Loss, [arXiv:1204.5917](https://arxiv.org/abs/1204.5917).

³D. Loss and D. P. DiVincenzo, *Phys. Rev. A* **57**, 120 (1998).

⁴J. Levy, *Phys. Rev. Lett.* **89**, 147902 (2002).

⁵S. C. Benjamin, *Phys. Rev. A* **64**, 054303 (2001).

⁶D. P. DiVincenzo, D. Bacon, J. Kempe, G. Burkard, and K. B. Whaley, *Nature (London)* **408**, 339 (2000).

⁷J. R. Petta, A. C. Johnson, J. M. Taylor, E. A. Laird, A. Yacoby, M. D. Lukin, C. M. Marcus, M. P. Hanson, and A. C. Gossard, *Science* **309**, 2180 (2005).

⁸M. Trif, V. N. Golovach, and D. Loss, *Phys. Rev. B* **75**, 085307 (2007).

⁹M. Trif, V. N. Golovach, and D. Loss, *Phys. Rev. B* **77**, 045434 (2008).

¹⁰M. D. Shulman, O. E. Dial, S. P. Harvey, H. Bluhm, V. Umansky, and A. Yacoby, *Science* **336**, 202 (2012).

- ¹¹L. Trifunovic, O. Dial, M. Trif, J. R. Wootton, R. Abebe, A. Yacoby, and D. Loss, *Phys. Rev. X* **2**, 011006 (2012).
- ¹²B. Trauzettel, D. V. Bulaev, D. Loss, and G. Burkard, *Nat. Phys.* **3**, 192 (2007).
- ¹³D. V. Bulaev, B. Trauzettel, and D. Loss, *Phys. Rev. B* **77**, 235301 (2008).
- ¹⁴J. Fischer, W. A. Coish, D. V. Bulaev, and D. Loss, *Phys. Rev. B* **78**, 155329 (2008).
- ¹⁵B. M. Maune, M. G. Borselli, B. Huang, T. D. Ladd, P. W. Deelman, K. S. Holabird, A. A. Kiselev, I. Alvarado-Rodriguez, R. S. Ross, A. E. Schmitz *et al.*, *Nature (London)* **481**, 344 (2012).
- ¹⁶A. C. Johnson, J. R. Petta, C. M. Marcus, M. P. Hanson, and A. C. Gossard, *Phys. Rev. B* **72**, 165308 (2005).
- ¹⁷H. Bluhm, S. Foletti, I. Neder, M. Rudner, D. Mahalu, V. Umansky, and A. Yacoby, *Nat. Phys.* **7**, 109 (2011).
- ¹⁸S. Tarucha, Y. Kitamura, T. Koder, and K. Ono, *Phys. Status Solidi B* **243**, 3673 (2006).
- ¹⁹H. Ribeiro, J. R. Petta, and G. Burkard, *Phys. Rev. B* **82**, 115445 (2010).
- ²⁰J. Baugh, Y. Kitamura, K. Ono, and S. Tarucha, *Phys. Rev. Lett.* **99**, 096804 (2007).
- ²¹R. Brunner, Y.-S. Shin, T. Obata, M. Pioro-Ladrière, T. Kubo, K. Yoshida, T. Taniyama, Y. Tokura, and S. Tarucha, *Phys. Rev. Lett.* **107**, 146801 (2011).
- ²²D. Stepanenko, M. Rudner, B. I. Halperin, and D. Loss, *Phys. Rev. B* **85**, 075416 (2012).
- ²³R. Hanson, L. P. Kouwenhoven, J. R. Petta, S. Tarucha, and L. M. K. Vandersypen, *Rev. Mod. Phys.* **79**, 1217 (2007).
- ²⁴C. Barthel, J. Medford, C. M. Marcus, M. P. Hanson, and A. C. Gossard, *Phys. Rev. Lett.* **105**, 266808 (2010).
- ²⁵W. A. Coish and D. Loss, *Phys. Rev. B* **70**, 195340 (2004).
- ²⁶A. Khaetskii, D. Loss, and L. Glazman, *Phys. Rev. B* **67**, 195329 (2003).
- ²⁷I. A. Merkulov, A. L. Efros, and M. Rosen, *Phys. Rev. B* **65**, 205309 (2002).
- ²⁸L. Cywiński, W. M. Witzel, and S. Das Sarma, *Phys. Rev. B* **79**, 245314 (2009).
- ²⁹R.-B. Liu, W. Yao, and L. Sham, *Adv. Phys.* **59**, 703 (2010).
- ³⁰S. Foletti, H. Bluhm, D. Mahalu, V. Umansky, and A. Yacoby, *Nat. Phys.* **5**, 903 (2009).
- ³¹G. Burkard, D. Loss, and D. P. DiVincenzo, *Phys. Rev. B* **59**, 2070 (1999).
- ³²N. E. Bonesteel, D. Stepanenko, and D. P. DiVincenzo, *Phys. Rev. Lett.* **87**, 207901 (2001).
- ³³G. Burkard and D. Loss, *Phys. Rev. Lett.* **88**, 047903 (2002).
- ³⁴D. Stepanenko, N. E. Bonesteel, D. P. DiVincenzo, G. Burkard, and D. Loss, *Phys. Rev. B* **68**, 115306 (2003).
- ³⁵L. Shekhtman, O. Entin-Wohlman, and A. Aharony, *Phys. Rev. Lett.* **69**, 836 (1992).
- ³⁶T. Yildirim, A. B. Harris, O. Entin-Wohlman, and A. Aharony, *Phys. Rev. Lett.* **73**, 2919 (1994).
- ³⁷F. Baruffa, P. Stano, and J. Fabian, *Phys. Rev. B* **82**, 045311 (2010).
- ³⁸A. Doherty *et al.* (unpublished).
- ³⁹D. S. Wang, A. G. Fowler, and L. C. L. Hollenberg, *Phys. Rev. A* **83**, 020302(R) (2011).

Hyperfine-induced decoherence in triangular spin-cluster qubits

Filippo Troiani,¹ Dimitrije Stepanenko,² and Daniel Loss²

¹*S3, Istituto Nanoscienze-CNR, via G. Campi 213/A, I-41100 Modena, Italy*

²*Department of Physics, University of Basel, Klingbergstrasse 82, CH-4056 Basel, Switzerland*

(Received 25 May 2012; published 17 October 2012)

We theoretically investigate hyperfine-induced decoherence in a triangular spin cluster for different qubit encodings. Electrically controllable eigenstates of spin chirality (C_z) show no appreciable decoherence up to $10^2 \mu\text{s}$, while a complete decoherence is estimated for the eigenstates of the total-spin projection (S_z) and of the partial spin sum (S_{12}) after $10 \mu\text{s}$. The robustness of chirality is due to its decoupling from both the total- and individual-spin components in the cluster. This results in a suppression of the effective interaction between C_z and the nuclear-spin bath. We finally estimate the reduction of the decoherence time scale for C_z , resulting from possible hyperfine contact terms or from the misalignment of the magnetic field.

DOI: [10.1103/PhysRevB.86.161409](https://doi.org/10.1103/PhysRevB.86.161409)

PACS number(s): 03.65.Yz, 03.67.Lx, 75.50.Xx

Introduction. Molecular nanomagnets represent a varied class of spin clusters, whose physical properties can be extensively engineered by chemical synthesis.¹ This makes them a potential alternative to other spin systems² for the implementation of spin-cluster qubits.^{3–5} While most of the attention has been so far focused on the use of the total-spin projection (S_z) as a computational degree of freedom (DOF), it has been recently realized that alternative encodings would enable the use of electric—rather than magnetic—fields for the qubit manipulation.⁶ In particular, transitions between states of opposite spin chirality [$C_z = (4/\sqrt{3})\mathbf{s}_1 \cdot \mathbf{s}_2 \times \mathbf{s}_3$] can be induced in antiferromagnetic triangles with Dzyaloshinskii-Moriya interaction. Spin-electric coupling constants compatible with ns gating times τ_g have been predicted by effective models^{6,7} and microscopic *ab initio* calculations,⁸ and might be possibly enhanced by suitable chemical substitutions.⁹

In order to assess the suitability of spin chirality for applications in quantum-information processing, its τ_g has to be contrasted with a characteristic decoherence time τ_d . At low temperatures, quantum coherence in molecular nanomagnets is limited by the coupling to the nuclear-spin environment, with typical values of τ_d in the microsecond range.^{10–12} All the existing literature is, however, concerned with linear superpositions of different S_z eigenstates. Here we theoretically investigate the dependence of hyperfine-induced decoherence on the qubit encoding within a prototypical spin-cluster qubit, consisting of an antiferromagnetic spin triangle. In particular, we consider three different DOFs, namely, S_z , C_z , and the partial spin sum S_{12} ($\mathbf{S}_{12} = \mathbf{s}_1 + \mathbf{s}_2$), whose value—as that of C_z —can be controlled through spin-electric coupling. Since the optimal candidate system has not been identified yet, we refer here to a prototypical molecular spin-cluster qubit, with a typical electron-spin Hamiltonian¹³ and bath of nuclear spins.¹⁴

Qubit encodings in the spin triangle. We consider a triangle of $1/2$ spins, with a dominant antiferromagnetic coupling and Zeeman interaction:

$$H_0 = J \sum_{i=1}^3 \mathbf{s}_i \cdot \mathbf{s}_{i+1} + g\mu_B \mathbf{B} \cdot \mathbf{S}. \quad (1)$$

An additional term H_1 determines the expression of the lowest eigenstates $|0\rangle$ and $|1\rangle$, belonging to the ground state $S = 1/2$

quadruplet. As discussed in the following, the robustness of the spin-cluster qubit with respect to hyperfine-induced decoherence strongly depends on the distinguishability between $|0\rangle$ and $|1\rangle$ in terms not only of total-spin orientation, but also of spin texture. Hereafter, we thus discuss these features in some detail in two relevant cases:

$$H_1^{C_z} = \frac{\Delta}{\sqrt{3}} \hat{\mathbf{z}} \cdot \sum_{i=1}^3 \mathbf{s}_i \times \mathbf{s}_{i+1}, \quad (2)$$

$$H_1^{S_{12}} = (J_{12} - J)\mathbf{s}_1 \cdot \mathbf{s}_2. \quad (3)$$

The term $H_1^{C_z}$ accounts for the Dzyaloshinskii-Moriya interaction.¹³ For an electron-spin Hamiltonian $H_e = H_0 + H_1^{C_z}$, the four lowest eigenstates can be labeled after the value of the spin chirality C_z , and the Dzyaloshinskii-Moriya term can be rephrased as $H_1^{C_z} = \Delta C_z S_z$.⁶ If the magnetic field is oriented parallel to the principal axis (z) of the molecule, the eigenstates $|C_z, S_z\rangle$ read $|\pm 1, +1/2\rangle = (|\downarrow\uparrow\uparrow\rangle + e^{\pm i2\pi/3}|\uparrow\downarrow\uparrow\rangle + e^{\mp i2\pi/3}|\uparrow\uparrow\downarrow\rangle)/\sqrt{3}$ and $|\pm 1, -1/2\rangle = \sigma_x^1 \sigma_x^2 \sigma_x^3 |\pm 1, +1/2\rangle$, where σ_x^i is the Pauli operator acting on \mathbf{s}_i . Both S_z and C_z commute with H_e , which makes them suitable as computational DOFs. In the first case, the logical states are

$$|0\rangle_{S_z} = |S_z = -1/2; C_z = +1\rangle,$$

$$|1\rangle_{S_z} = |S_z = +1/2; C_z = +1\rangle,$$

with spin expectation values [Fig. 1(a)]

$$\langle 1|s_{z,i}|1\rangle_{S_z} = -\langle 0|s_{z,i}|0\rangle_{S_z} = 1/6. \quad (4)$$

If the computational DOF is identified with spin chirality, the logical states are instead

$$|0\rangle_{C_z} = |C_z = +1; S_z = -1/2\rangle,$$

$$|1\rangle_{C_z} = |C_z = -1; S_z = -1/2\rangle,$$

and the expectation values of the three spins are independent on the qubit state [Fig. 1(a)],

$$\langle 1|s_{z,i}|1\rangle_{C_z} = \langle 0|s_{z,i}|0\rangle_{C_z} = -1/6. \quad (5)$$

As a result, $|0\rangle_{C_z}$ and $|1\rangle_{C_z}$ are indistinguishable in terms of total-spin projection and spin texture: They thus span an approximately decoherence-free subspace^{15–17} (see below). Such a condition is, however, not general. In fact, if the

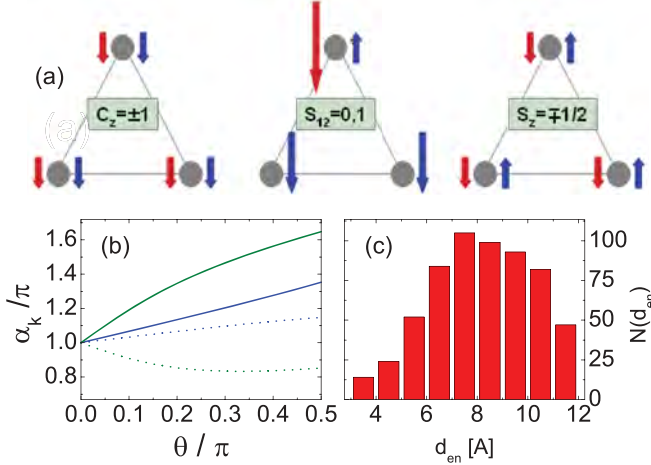


FIG. 1. (Color online) (a) Schematics of the local spin projections $\langle s_{z,i} \rangle$ in the spin triangle, corresponding to the $|0\rangle$ (red) and $|1\rangle$ (blue) states in the three considered qubit encodings. The logical states of the chirality qubit (C_z , left) have identical expectation values $\langle s_{z,i} \rangle$; this is not the case for the other two encodings (S_{12} and S_z). (b) Angle α_k between the vector $\langle \mathbf{S} \rangle$ and $\hat{\mathbf{z}}$ for the eigenstates $|0\rangle_{C_z}^\theta$ (blue) and $|1\rangle_{C_z}^\theta$ (green), for $\Delta/g\mu_B = 0.5$ (solid lines) and 2.0 (dotted). (c) Statistical distribution of the distances d_{en} between the $N_e = 3$ electron and the $N_n = 200$ nuclear spins with randomly generated positions.

applied magnetic field is tilted with respect to the z axis, $\mathbf{B} = B(\sin\theta\hat{\mathbf{x}} + \cos\theta\hat{\mathbf{z}})$, $\langle k|s_i|k\rangle_{C_z}^\theta$ (with $k = 0, 1$) are oriented along $\mathbf{B}'_k = (B_x, 0, B_z \pm \Delta/g\mu_B)$. Eigenstates of opposite chirality are thus characterized by different orientations of the spin expectation values [see Fig. 1(b)],

$$\langle k|s_{x,i}|k\rangle_{C_z}^\theta = \sin\alpha_k/6, \quad \langle k|s_{z,i}|k\rangle_{C_z}^\theta = \cos\alpha_k/6, \quad (6)$$

where $\alpha_k = \arctan[\frac{\chi B \sin\theta}{B \cos\theta + (-1)^k \Delta/g\mu_B}] + \pi$, $0 \leq \arctan \leq \pi$, and $\chi = \pm 1$ for $\Delta \gtrless Bg\mu_B$.

If no Dzyaloshinskii-Moriya interaction is present and one exchange coupling differs from the other two, the term $H_1^{C_z}$ is replaced by $H_1^{S_{12}}$ [Eq. (3)]. For $H_e = H_0 + H_1^{S_{12}}$, the four lowest eigenstates can be labeled after the partial sum of the first two spins, rather than the spin chirality, $|S_{12}, S_z\rangle$, where $S_{12} = 0, 1$. Their expressions read $|0, +1/2\rangle = (|\uparrow\downarrow\rangle - |\downarrow\uparrow\rangle)/\sqrt{2}$, $|1, +1/2\rangle = (|\uparrow\downarrow\rangle + |\downarrow\uparrow\rangle - 2|\uparrow\uparrow\rangle)/\sqrt{6}$, while $|S_{12}, -1/2\rangle = \sigma_x^1 \sigma_x^2 \sigma_x^3 |S_{12}, +1/2\rangle$. Choosing S_{12} as the computational DOF, one has

$$\begin{aligned} |0\rangle_{S_{12}} &= |S_{12} = 0; S_z = -1/2\rangle, \\ |1\rangle_{S_{12}} &= |S_{12} = 1; S_z = -1/2\rangle. \end{aligned}$$

As far as the spin expectation values are concerned, S_{12} represents an intermediate case between S_z and C_z . The qubit states have in fact identical values for the total spin, $\langle 0|\mathbf{S}|0\rangle_{S_{12}} = \langle 1|\mathbf{S}|1\rangle_{S_{12}}$, as C_z , but they strongly differ in terms of spin texture, as S_z [Fig. 1(a)]:

$$\langle 0|s_{z,i=1,2}|0\rangle_{S_{12}} = 0, \quad \langle 0|s_{z,3}|0\rangle_{S_{12}} = -1/2, \quad (7a)$$

$$\langle 1|s_{z,i=1,2}|1\rangle_{S_{12}} = -1/3, \quad \langle 1|s_{z,3}|1\rangle_{S_{12}} = 1/6. \quad (7b)$$

Nuclear spin and hyperfine interactions. The decoherence of the spin-cluster qubit is investigated by simulating the

coupled dynamics of electron and nuclear spins. The qubit and the nuclear environment are initialized respectively in the linear superposition $|\psi_e(0)\rangle = \frac{1}{\sqrt{2}}(|0\rangle + |1\rangle)$ and in the mixed state $\rho_n(0) = \sum_{\mathcal{I}} P_{\mathcal{I}} |\mathcal{I}\rangle \langle \mathcal{I}|$. Here, the expressions of $|0\rangle$ and $|1\rangle$ depend on H_1 , while $|\mathcal{I}\rangle = |m_1^{\mathcal{I}}, \dots, m_{N_n}^{\mathcal{I}}\rangle$ and $m_i^{\mathcal{I}}$ are the projections along the magnetic field direction of the N_n nuclear spins. In the pure-dephasing regime, each state $|\Psi_{\mathcal{I}}(0)\rangle = \frac{1}{\sqrt{2}}(|0\rangle + |1\rangle) \otimes |\mathcal{I}\rangle$ evolves into $|\Psi_{\mathcal{I}}(t)\rangle = \frac{1}{\sqrt{2}}(|0, \mathcal{I}_0\rangle + |1, \mathcal{I}_1\rangle)$, where $|\mathcal{I}_0\rangle$ ($|\mathcal{I}_1\rangle$) can be regarded as the state of the nuclear bath conditioned upon the qubit being in the $|0\rangle$ ($|1\rangle$) state. The degree of coherence in the reduced density matrix of the qubit, $\rho_e = \text{Tr}_n\{\sum_{\mathcal{I}} P_{\mathcal{I}} |\Psi_{\mathcal{I}}(t)\rangle \langle \Psi_{\mathcal{I}}(t)|\}$, is given by the so-called decoherence factor $r(t) = \sum_{\mathcal{I}} P_{\mathcal{I}} r_{\mathcal{I}}(t)$, with $r_{\mathcal{I}}(t) = \langle \mathcal{I}_1(t)|\mathcal{I}_0(t)\rangle$ and $\langle 0|\rho_e|1\rangle = r_{\mathcal{I}}/2$.

The nuclear-spin bath we consider consists of $N_n = 200$ hydrogens ($I = 1/2$), whose positions \mathbf{r}_p^n are randomly generated so as to reproduce typical values of the spin density and the electron-nuclear distances $d_{en} = |\mathbf{r}_i^e - \mathbf{r}_p^n|$, where \mathbf{r}_i^e are the positions of electron spins [Fig. 1(c)].¹⁸ The nuclear-spin Hamiltonian H_n includes Zeeman and dipole-dipole terms, $H_n = \hat{\mathbf{B}} \cdot \sum_p \omega_p \mathbf{I}_p + D_{nn} \sum_{p<q} (\mathbf{I}_p \cdot \mathbf{I}_q - 3(\mathbf{I}_p \cdot \hat{\mathbf{r}}_{pq})(\mathbf{I}_q \cdot \hat{\mathbf{r}}_{pq}))/r_{pq}^3$, where $D_{nn} = (\mu_0/4\pi)\mu_n^2\gamma_I^2$ and $\mathbf{r}_{pq} = \mathbf{r}_p^n - \mathbf{r}_q^n$. Electron and nuclear spins are coupled by dipole-dipole and contact interactions, $H_{en} = D_{en} \sum_i \sum_p [s_i \cdot \mathbf{I}_p - 3(s_i \cdot \hat{\mathbf{r}}_{ip})(\mathbf{I}_p \cdot \hat{\mathbf{r}}_{ip})]/r_{ip}^3 + \sum_i a_i s_i \cdot \mathbf{I}_{(i)}$, where $D_{en} = (\mu_0/4\pi)\mu_n\mu_e\gamma_I\gamma_e$ and $\mathbf{r}_{ip} = \mathbf{r}_i^e - \mathbf{r}_p^n$. The contact terms a_i , whose effect will be considered in the final part of this Rapid Communication, couples electron and nuclear spins belonging to the same magnetic center.

The dephasing arises from the qubit-state dependent dynamics of the nuclear bath, generated by an effective Hamiltonian \mathcal{H} . We use a two-step procedure^{19,20} to derive \mathcal{H} from the Hamiltonian $H = H_e + H_n + H_{en}$. We first replace in H the single-electron-spin operators $s_{\alpha,i}$ with their projection onto the $S = 1/2$ subspace, $s_p^\alpha \rightarrow \sum_{i,j=0}^3 \langle i|s_p^\alpha|j\rangle \sigma_{ij}$, where $\sigma_{ij} = |i\rangle\langle j|$ and $|i\rangle$ are the eigenstates of H_e . We then apply a Schrieffer-Wolff transformation to the projected Hamiltonian \mathcal{H} that removes from the Hamiltonian the terms that are off diagonal in the basis of electron-spin eigenstates $|i\rangle$,^{21,22} and finally neglect energy nonconserving terms (secular approximation). The resulting Hamiltonian reads $\mathcal{H} = \mathcal{H}^i + (|0\rangle\langle 0| - |1\rangle\langle 1|) \otimes \mathcal{H}^e$, where

$$\mathcal{H}^{\chi=i,e} = \sum_{p=1}^{N_n} \omega_p^\chi I_p^z + \sum_{p \neq q} (A_{pq}^\chi I_p^z I_q^z + B_{pq}^\chi I_p^+ I_q^-) \quad (8)$$

and $\hat{\mathbf{z}} \equiv \mathbf{B}/B$. Two-spin terms in the intrinsic Hamiltonian \mathcal{H}^i come from dipolar interactions between the nuclei. Those in the extrinsic Hamiltonian \mathcal{H}^e are mediated by virtual transitions between eigenstates of the electron-spin Hamiltonian: They thus depend quadratically on the hyperfine couplings D_{en} , while the dependence of ω_p^e is linear. The time evolution of the nuclear states $|\mathcal{I}_k\rangle$ is computed within the pair-correlation approximation, where the nuclear dynamics is traced back to independent flip-flop transitions between pairs of nuclear spins.^{21,23,24}

Hyperfine-induced decoherence. The fastest contribution to dephasing in the spin-cluster qubit is related to

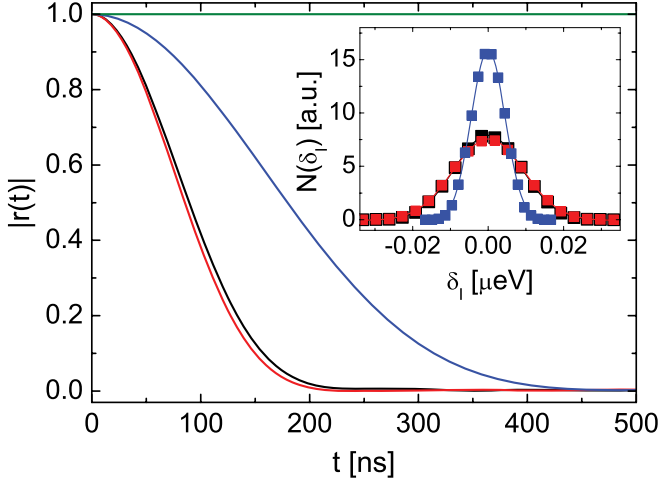


FIG. 2. (Color online) Time dependence of the decoherence factor r for the three qubit encodings: S_z (black), S_{12} (red), and C_z (green for $\theta = 0$ and blue for $\theta = \pi/8$). The curves are averaged over $N_{\mathcal{I}} = 5 \times 10^4$ randomly generated initial states $|\mathcal{I}\rangle$ of the nuclear bath. Inset: Statistical distribution (squares) of the parameter $\delta_{\mathcal{I}}$, and corresponding Gaussian fits (solid lines).

inhomogeneous broadening, and typically takes place on time scales that are much shorter than those characterizing the dynamics of the nuclear bath ($\tau_n \sim \hbar/|B_{pq}^k| \sim 10^2 \mu\text{s}$). Such a contribution results from the following renormalization of the energy gap between the states $|0\rangle$ and $|1\rangle$ induced by the hyperfine interaction: $\delta_{\mathcal{I}} = \sum_{k=0,1} (-1)^k \langle k, \mathcal{I} | \mathcal{H} | k, \mathcal{I} \rangle \simeq \sum_p \omega_p^e m_p^{\mathcal{I}}$. Being the nuclear spin bath initially in a mixture of states $|\mathcal{I}\rangle$, the decoherence factor evolves as $r(t \ll \tau_n) \simeq e^{-i(E_0 - E_1)t} \sum_{\mathcal{I}} P_{\mathcal{I}} e^{-i\delta_{\mathcal{I}} t}$, while $|\mathcal{I}_k(t \ll \tau_n)\rangle \simeq |\mathcal{I}\rangle$. In first order in H_{en} , $\delta_{\mathcal{I}}$ can be regarded as a function of the Overhauser field at the electron-spin sites,

$$\delta_{\mathcal{I}} \simeq \mu_B g \sum_i \mathbf{B}_{\text{hf}}^{\mathcal{I}}(\mathbf{r}_i^e) \cdot [\langle 0 | \mathbf{s}_i | 0 \rangle - \langle 1 | \mathbf{s}_i | 1 \rangle], \quad (9)$$

where $\mathbf{B}_{\text{hf}}^{\mathcal{I}}(\mathbf{r}_i^e) = D_{en} \sum_p m_p^{\mathcal{I}} [\hat{\mathbf{z}}' - 3(\hat{\mathbf{z}}' \cdot \hat{\mathbf{r}}_{ip}) \hat{\mathbf{r}}_{ip}] / r_{ip}^3$. In the case of the S_z qubit [see Eq. (4)], $\delta_{\mathcal{I}}^{S_z} \simeq -(\mu_B g / 3) \sum_i B_{\text{hf},z}^{\mathcal{I}}(\mathbf{r}_i^e)$. The statistical distribution $N(\delta_{\mathcal{I}}^{S_z})$ is reported in the inset of Fig. 2 (black squares) for 5×10^4 initial nuclear states $|\mathcal{I}\rangle$, randomly generated from a flat probability distribution $P_{\mathcal{I}} = 1/2^{N_n}$. $N(\delta_{\mathcal{I}}^{S_z})$ is well fitted by a Gaussian function (solid line), with $\sigma_{S_z} = 9.0$ neV. Correspondingly, the decay of $|r(t)|$ (black line in Fig. 2) is approximately Gaussian, and its characteristic time scale is 10^2 ns. In the case of the S_{12} qubit, the three electron spins are no longer equivalent, and $\delta_{\mathcal{I}}^{S_{12}} \simeq -(\mu_B g / 3) [2B_{\text{hf},z}^{\mathcal{I}}(\mathbf{r}_1^e) - B_{\text{hf},z}^{\mathcal{I}}(\mathbf{r}_2^e) - B_{\text{hf},z}^{\mathcal{I}}(\mathbf{r}_3^e)]$. However, the statistical distribution of $\delta_{\mathcal{I}}^{S_{12}}$ strongly resembles that of S_z (see the red squares in the figure inset, and the Gaussian fit with $\sigma_{S_{12}} = 9.4$ neV), and so does the time evolution of the decoherence factor (red curve in the main panel). In fact, since the distances d_{ee} between electron spins are larger than the smallest d_{en} [see Fig. 1(c)],¹⁸ the spatial fluctuations of the Overhauser field within the spin triangle are comparable to its average value. In spin clusters with larger d_{en}/d_{ee} ratios (not shown here), spatial fluctuations of $\mathbf{B}_{\text{hf}}(\mathbf{r})$ are relatively small.

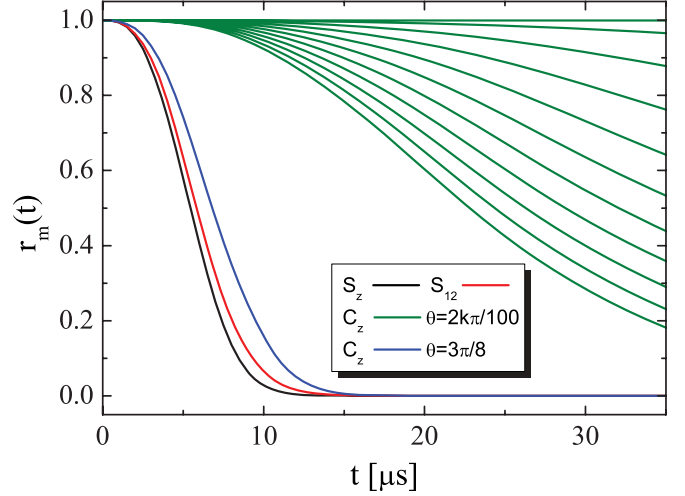


FIG. 3. (Color online) Time evolution of the decoherence factor r_m in the cases of the S_z (black) and S_{12} (red) DOFs. The case of chirality is displayed for small tilting angles $\theta = 2\pi k/100$, with k ranging from 0 (upper green curve) to 11 (lower green curves). All curves are averaged over 10^2 randomly generated initial conditions $|\mathcal{I}\rangle$; the spin Hamiltonian parameters are $\Delta = 1$ K, $B = 1$ T.

As a result, $\delta_{\mathcal{I}}^{S_{12}} \ll \delta_{\mathcal{I}}^{S_z}$, and the S_{12} qubit is less affected by inhomogeneous broadening than S_z .

In the case of the C_z qubit and for $\mathbf{B} \parallel \hat{\mathbf{z}}$, the Overhauser field does not renormalize the energy difference between the states $|0\rangle$ and $|1\rangle$ that have identical expectation values for all single-spin projections [Eqs. (5) and (9)]. The leading contribution to $\delta_{\mathcal{I}}^{C_z}$ is given by terms that are second order in the hyperfine Hamiltonian, $\delta_{\mathcal{I}}^{C_z} = \sum_{p \neq q} A_{pq}^e m_p^{\mathcal{I}} m_q^{\mathcal{I}}$, and its modulus is here five orders of magnitude smaller than that of $\delta_{\mathcal{I}}^{S_z}$ and $\delta_{\mathcal{I}}^{S_{12}}$. Correspondingly, no inhomogeneous broadening occurs in the considered time scale (green curve). For a tilted magnetic field ($\theta \neq 0$), states of opposite chirality have different expectation values $\langle \mathbf{s}_i \rangle$ [see Eq. (6)], and thus couple differently to the Overhauser field. The leading contribution to the renormalization of the energy difference reads $\delta_{\mathcal{I}}^{C_z}(\theta) \simeq (\mu_B g / 6) \sum_{k=0}^1 (-1)^k (\sin \alpha_k B_{\text{hf},x'}^{\mathcal{I}} + \cos \alpha_k B_{\text{hf},z'}^{\mathcal{I}})$, where $\mathbf{x}' \perp \mathbf{z}'$ and lies in the xz plane. The statistical distribution of $\delta_{\mathcal{I}}^{C_z}(\theta = \pi/8)$ and the resulting qubit dephasing are reported in Fig. 2 ($\sigma_{C_z} = 4.5$ neV, blue curve).

The nuclear-spin dynamics contributes to decoherence by correlating electron and nuclear spins. In order to single out this contribution, we compute the function $r_m(t) = \sum_{\mathcal{I}} P_{\mathcal{I}} |r_{\mathcal{I}}(t)|$. In the case of the S_z qubit, electron-nuclear correlations result in a decay of r_m in the μs time scale (Fig. 3, black curve). The decay is induced by the interplay of the dipolar interactions between the nuclei and of the term $\sum_p \omega_p^e I_p^z$, whose expectation value gives $\delta_{\mathcal{I}}^{S_z}$. A similar time dependence for r_m is obtained in the case of the S_{12} qubit (red curve). Here, the same terms in the effective Hamiltonian \mathcal{H} dominate, and have similar expectation values, $\delta_{\mathcal{I}}^{S_z} \simeq \delta_{\mathcal{I}}^{S_{12}}$ (see the inset of Fig. 2). This quantity ($\delta_{\mathcal{I}}^{C_z}$) is about five orders of magnitude smaller for the C_z qubit, if $\mathbf{B} \parallel \hat{\mathbf{z}}$. As a result, the dynamics of the nuclear bath is largely independent on the qubit state and no appreciable decoherence takes place for $t \lesssim 10^2 \mu\text{s}$ (upper green curve): On such a time scale the $|0\rangle$ and $|1\rangle$ states

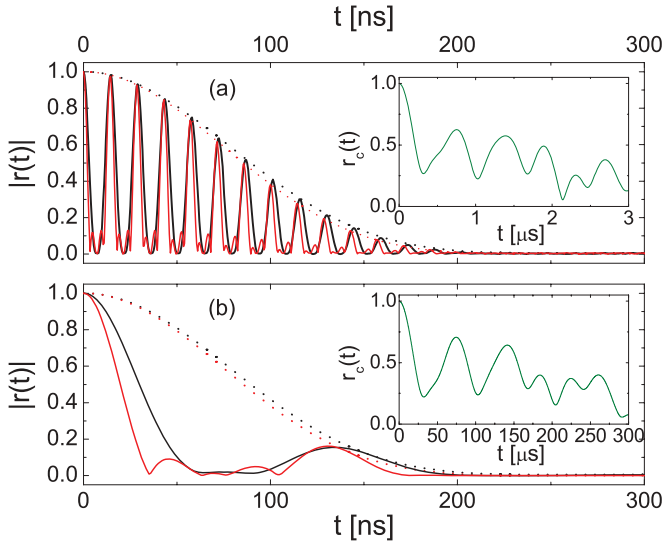


FIG. 4. (Color online) Time dependence of the decoherence factor in the presence of three additional nuclear spins ($N_n = 203$) localized at the electron-spin positions \mathbf{r}_i^e and coupled to the respective electron spins with a contact coupling (a) $a_p = 10$ mK or (b) $a_p = 1$ mK. The solid curves correspond to the cases S_z (black), S_{12} (red), and C_z (figure insets). The dotted lines represent the time dependence of r_m in the absence of the three nuclei with contact couplings.

thus define a decoherence-free subspace. However, $\delta_{\mathcal{T}}^{C_z}(\theta)$ and the decoherence rate rapidly increase for finite values of the tilting angle θ (lower green curves); for $\theta = 3\pi/8$ (blue), $r(t)$ approaches the curve corresponding to S_{12} and S_z .

We finally investigate the possible contribution to decoherence of the contact terms, resulting from the relatively strong coupling with the electron spins of few ($N_n^c \sim N_e \ll N_n$) nuclei. Here, the $N_n^c = N_e = 3$ additional nuclear spins

are localized at the electron-spin sites \mathbf{r}_i^e , and are assumed for simplicity identical to the remaining 200 nuclei. The inequivalence between the N_n^c and N_n^d nuclear spins, resulting from strong coupling of the former ones with the electron spins, warrants the factorization of the decoherence factor, $r(t) = r_c(t)r_d(t)$. The time evolution of $r_c(t)$ is reported in Fig. 4, for $a_p = 1$ and 10 mK [Figs. 4(a) and 4(b), respectively]. In the case of S_z (black curve) and S_{12} (red), r_c is responsible for the fast oscillations, while the decay is due to r_d (dotted lines). In the case of C_z , oscillations of the decoherence factor take place on a time scale which is much longer than that of S_z and S_{12} , but much shorter than the one that characterizes the contribution of the dipolar interactions (figure inset). The chirality qubit also presents a different dependence on the contact coupling constant a_i with respect to S_z and S_{12} . A comparison between the two panels shows in fact that the characteristic time scale of the oscillations in r_c is $\tau_d^c \sim \hbar/a_p$ for S_z and S_{12} , and $\tau_d^c \sim \hbar \delta_{ij}/a_p^2$ for C_z , where $\delta_{ij} \sim \min\{\Delta, g\mu_B B\}$ is the smallest difference between eigenvalues of H_e . The leading contributions of contact interaction to \mathcal{H} are thus quadratic in the hyperfine Hamiltonian for C_z , and linear for the other two DOFs.

In conclusion, we have shown that the nuclear-induced decoherence in a prototypical spin triangle strongly depends on the qubit encoding. In particular, no appreciable decoherence is found for the chirality qubit up to $10^2 \mu\text{s}$, due to the decoupling of C_z from both the total-spin orientation and the spin texture. The eigenstates of S_{12} are instead characterized by decoherence times comparable to those of the total-spin projection S_z , unless the distance between electron spins is strongly reduced with respect to the size of the nuclear bath.

We acknowledge financial support by PRIN of the Italian MIUR, by the Swiss NF, and by FP7-ICT project “ELFOS.”

¹D. Gatteschi, R. Sessoli, and J. Villain, *Molecular Nanomagnets* (Oxford University Press, Oxford, UK, 2007).

²See, e.g., C. Klocffel and D. Loss, arXiv:1204.5917.

³F. Meier, J. Levy, and D. Loss, *Phys. Rev. Lett.* **90**, 047901 (2003).

⁴F. Troiani, A. Ghirri, M. Affronte, S. Carretta, P. Santini, G. Amoretti, S. Piligkos, G. Timco, and R. E. P. Winpenny, *Phys. Rev. Lett.* **94**, 207208 (2005).

⁵J. Lehmann, A. Gaita-Ariño, E. Coronado, and D. Loss, *Nat. Nanotechnol.* **2**, 312 (2007).

⁶M. Trif, F. Troiani, D. Stepanenko, and D. Loss, *Phys. Rev. Lett.* **101**, 217201 (2008).

⁷M. Trif, F. Troiani, D. Stepanenko, and D. Loss, *Phys. Rev. B* **82**, 045429 (2010).

⁸M. F. Islam, J. F. Noss, C. M. Canali, and M. Pederson, *Phys. Rev. B* **82**, 155446 (2010).

⁹N. Baadji, M. Piacenza, T. Tugsuz, F. Della Sala, G. Maruccio, and S. Sanvito, *Nat. Mater.* **8**, 813 (2009).

¹⁰A. Ardavan, O. Rival, J. J. L. Morton, S. J. Blundell, A. M. Tyryshkin, G. A. Timco, and R. E. P. Winpenny, *Phys. Rev. Lett.* **98**, 057201 (2007).

¹¹S. Bertaina, S. Gambarelli, T. Mitra, B. Tsukerblat, A. Müller, and B. Barbara, *Nature (London)* **453**, 203 (2008).

¹²C. Schlegel, J. van Slageren, M. Manoli, E. K. Brechin, and M. Dressel, *Phys. Rev. Lett.* **101**, 147203 (2008).

¹³K.-Y. Choi, Y. H. Matsuda, H. Nojiri, U. Kortz, F. Hussain, A. C. Stowe, C. Ramsey, and N. S. Dalal, *Phys. Rev. Lett.* **96**, 107202 (2006).

¹⁴C. Schlegel, J. van Slageren, G. Timco, R. E. P. Winpenny, and M. Dressel, *Phys. Rev. B* **83**, 134407 (2011).

¹⁵P. Zanardi, and M. Rasetti, *Phys. Rev. Lett.* **79**, 3306 (1997).

¹⁶L.-M. Duan, and G. C. Guo, *Phys. Rev. Lett.* **79**, 1953 (1997).

¹⁷D.-A. Lidar, I. L. Chuang, and K. B. Whaley, *Phys. Rev. Lett.* **81**, 2594 (1998).

¹⁸The distance between any two electron spins is 5 Å. The nuclei are distributed in a sphere of radius $R = 10$ Å, with the constraints $|\mathbf{r}_i^n - \mathbf{r}_j^n| \geq 1.5$ Å and $|\mathbf{r}_i^n - \mathbf{r}_j^e| \geq 3$ Å.

¹⁹A. Szallas and F. Troiani, *Phys. Rev. B* **82**, 224409 (2010).

²⁰F. Troiani, V. Bellini, and M. Affronte, *Phys. Rev. B* **77**, 054428 (2008).

- ²¹W. Yao, R.-B. Liu, and L. J. Sham, *Phys. Rev. B* **74**, 195301 (2006).
- ²²W. A. Coish, J. Fischer, and D. Loss, *Phys. Rev. B* **77**, 125329 (2008).

- ²³W. M. Witzel, R. de Sousa, and S. Das Sarma, *Phys. Rev. B* **72**, 161306(R) (2005).
- ²⁴W. Yang and R.-B. Liu, *Phys. Rev. B* **78**, 085315 (2008).

The Florida State University

College of Arts and Sciences

has conferred upon

Dimitrie Stepanenko

the degree of

Doctor of Philosophy

in **Physics**

with all the rights, honors and privileges thereto appertaining

Witness the Seal of the University and the signatures

of its duly authorized officers hereunto affixed.

Given at Tallahassee, Florida, this fourth day of August,

in the year two thousand and five.


Peter B. Egan
Governor of the State of Florida


William W. Bennett
Governor, The Florida State University
Board of Trustees


Debra Austin
Chancellor, State University System




F. K. McRee
President of the University

George Lewis
Dean



УНИВЕРЗИТЕТ У БЕОГРАДУ

Адреса: Студентски трг 1, 11000 Београд, Република Србија
Тел.: 011 3207400; Факс: 011 2638818; Е-mail: officebu@rect.bg.ac.rs

Београд, 30.01.2012. године
Број: 06-613-7554/4-11
МЧБ

На основу члана 104. став 5. Закона о високом образовању ("Службени гласник РС", бр. 76/05, 100/07-аутентично тумачење и 97/08), члана 9. Правилника о признавању страних високошколских исправа ("Гласник Универзитета у Београду" бр. 129/06 и 145/08) и одлуке Комисије Универзитета за признавање страних високошколских исправа бр. 06-613-7554/3-11 од 02.11.2011. године, доносим

РЕШЕЊЕ

ПРИЗНАЈЕ СЕ високошколска исправа **The Florida State University, Талахаси, Флорида, САД**, од 12.08.2005. године, на којем је **Димитрије (Андрија) Степаненко** стекао образовање, као **диплома докторских академских студија (доктор наука – физичке науке)**.

Образложење

Универзитету у Београду и Физичком факултету обратио се Димитрије (Андрија) Степаненко, рођен 13.07.1974. године у Врању, Република Србија, захтевом за признавање дипломе The Florida State University, Талахаси, Флорида, САД, на којем је именовани стекао звање Doctor of Philosophy in Physics.

Стручни органи Факултета размотрили су све списе предмета и предложили Комисији Универзитета доношење одлуке, којом се предметна диплома признаје као диплома докторских студија (доктор физичких наука). Комисија је одлучила као у диспозитиву.

Са изложеног, одлучено је као у изреци овог решења.

ПОУКА О ПРАВНОМ ЛЕКУ:

Ово решење је коначно у управном поступку, па се против њега може покренути управни спор код Управног суда, у року од 30 дана од дана пријема решења.



РЕКТОР

Проф. др Бранко Ковачевић

THE FLORIDA STATE UNIVERSITY

COLLEGE OF ARTS AND SCIENCES

SYMMETRY AND CONTROL IN SPIN-BASED QUANTUM COMPUTING

By

DIMITRIJE STEPANENKO

A Dissertation submitted to the
Department of Physics
in partial fulfillment of the
requirements for the degree of
Doctor of Philosophy

Degree Awarded:
Summer Semester, 2005

The members of the Committee approve the dissertation of Dimitrije Stepanenko defended on June 10, 2005.

Nicholas E. Bonesteel
Professor Directing Thesis

Washington Mio
Outside Committee Member

Vladimir Dobrosavljević
Committee Member

Stephan von Molnar
Committee Member

Mark Riley
Committee Member

The Office of Graduate Studies has verified and approved the above named committee members.

To Andrija

ACKNOWLEDGEMENTS

It was unique privilege to spend my graduate school years working with my adviser and mentor, Professor Nick Bonesteel. The most important lessons he had taught me are that intuitive models and insights based on them are at least as important as the technical skills and that clarity and simplicity are necessary ingredients of every successful research.

People who contributed to research presented in this thesis, both directly and through the inspiring discussions are Nicholas Bonesteel and Layla Hormozi from the Florida State University, Kerwin Foster from the Dillard University, David DiVincenzo from the IBM T. J. Watson Research Center and Guido Burkard and Daniel Loss from the University of Basel.

I enjoyed the conversations about condensed matter physics with Professors Vladimir Dobrosavljević, Pedro Schlottmann and Stephan von Molnar that kept me aware that there are many interesting faces of every problem.

Darko, George, Kenny, Curt, Layla and John helped create an environment that made the long hours at the desk enjoyable. Sherry Tointigh and late Kate Caudill have shown a great deal of patience while dealing with my chaotic manner of handling paperwork, from the first day at FSU till the last signature on the last form.

I would like to thank Professor LJubiša Adamović, Vlatko, Snježana, Marko, Vlada, Dragana, Olan, Joe, Donnato, Cheryl, Eddy, Lucas, Ann, Myongshik, Kan, Balša, Ana, Ivana, Ćira, Aleksa, Ilka, Vincent and Patricia, Marjan, Boća and Dejan for their friendship and beautiful time spent together.

I am especially grateful to my mother Slavica and mother in law Vanja for being with my family and me when we needed help. Without their devotion and assistance, my time in graduate school would have been much longer.

My wife Jelena and son Andrija filled the years in graduate school with love and joy. I will always be thankful for their patience and understanding.

TABLE OF CONTENTS

List of Tables	vii
List of Figures	viii
Abstract	x
1. INTRODUCTION	1
1.1 Overview	2
1.2 Background on Quantum Computing	3
1.2.1 Classical Computers	3
1.2.2 Quantum Computers	7
1.2.3 Church-Turing Thesis	11
1.3 Physical Realizations	14
1.3.1 The Quantum Dot Quantum Computer	17
1.4 Spin-Orbit Coupling	21
1.5 Symmetry and Control	22
1.5.1 Reduction of the Effects of Spin-Orbit Coupling in Exchange Gates	24
1.5.2 Using Spin-Orbit Coupling Effects for Spin Control	26
1.6 Summary of Results	28
2. SPIN-ORBIT COUPLING AS A PROBLEM: REDUCING THE GATE ANISOTROPY	29
2.1 Reduction of Control Complexity	29
2.2 Isotropic Exchange	31
2.2.1 Simple Control	34
2.2.2 Universal Gate Set Using Isotropic Exchange	35
2.3 Anisotropy	37
2.4 Time Dependence, Interaction and the Gate	38
2.4.1 Control through Pulse Shaping	39
2.4.2 Voltage Control Program	40
2.5 Simplifications from Symmetry	42
2.6 Removal of First Order Anisotropy	44
2.6.1 Calculation of the Gate	44
2.6.1.1 Parity and Time Reversal	45
2.6.1.2 Time Reversal Symmetric Interactions and Time Symmetric Pulses	46
2.6.2 Perturbative Evaluation of the Gate	48
2.6.3 Local Symmetry	52
2.7 Summary of the Results	60

3. MICROSCOPIC DERIVATION OF SPIN INTERACTION	62
3.1 The Model of Quantum Dots Quantum Computer	64
3.1.1 Confinement to Two Dimensions	65
3.1.2 Confinement in Plane, from Two to Zero Dimensions	69
3.1.3 Control Mechanisms	71
3.2 Hund-Mulliken Approximation	74
3.2.1 Spin Orbit Coupling Hamiltonian	79
3.3 Axial Symmetry of the Effective Spin Interaction	84
3.4 Pulses of Hund-Mulliken Hamiltonian	86
3.4.1 Slightly asymmetric pulses	89
3.5 Robust CNOT	90
4. SPIN-ORBIT COUPLING AS A RESOURCE: USING THE GATE ANISOTROPY	95
4.1 Universal Gate Set Construction	96
4.1.1 Single Qubit Gates	100
4.1.2 Two Qubit Gates	103
4.2 Control Range	107
4.2.1 Control at Fabrication Level	108
4.2.2 Control through Time Dependence	116
4.3 Summary	122
APPENDIX A: Axially Symmetric Gate for CNOT Construction	124
APPENDIX B: Matrix Elements of Hund-Mulliken Hamiltonian	127
REFERENCES	129
BIOGRAPHICAL SKETCH	134

LIST OF TABLES

2.1 Behavior of gate parameters under parity (P) and time reversal (T). Quantities that are even(odd) under parity are of even(odd) order in spin interaction anisotropy. Gate parameters odd under time reversal vanish from the gates implemented by time-symmetric pulses.	45
3.1 Symmetry properties of the pulse parameters r and s , and gate parameters λ , α , β and γ under parity P and time reversal T	90

LIST OF FIGURES

1.1 Turing Machine	5
1.2 Universal Classical Logic Gates	6
1.3 Classical Circuit Model	7
1.4 Elements of Quantum Circuit Model	9
1.5 Universal Set of Quantum Gates	10
1.6 Quantum Circuit Complexity	11
1.7 Comparing Classical and Quantum Complexity	13
1.8 Quantum Dot Quantum Computer	18
1.9 Universal Quantum Gates Using Isotropic Exchange	20
2.1 Controlled Not Using Isotropic Exchange	36
2.2 Local Reference Frames	55
2.3 Constant Anisotropy Pulses	57
2.4 Loop and Local Reference Frames	58
2.5 Tree Topology	59
3.1 The Quantum Dot Quantum Computer	64
3.2 Band Bending	66
3.3 Voltage controlled gate	72
3.4 Isotropic Spin Interaction Strength	73
3.5 The Model Potential of Coupled Quantum Dots	75
3.6 Orbital Excitations and Failure Modes of a Spin Qubit	77
3.7 Zinc-Blende Crystal Structure	81
3.8 Precession and Hopping	83
3.9 Anisotropy in Spin Interaction	86
3.10 Time Dependent Hund-Mulliken Hamiltonian	89
3.11 Gate Hamiltonian	91
3.12 Robust CNOT	93
4.1 Range of Anisotropic Control	100

4.2 Sequence for pseudospin x rotation	101
4.3 Two-Spin Qubits	104
4.4 CNOT circuit	106
4.5 Angle of Electron Precession on Hopping	113
4.6 The Strength of Anisotropy	115
4.7 Decoherence for Slow Pulses	119
4.8 Double Occupancy for Fast Pulses	120
4.9 Control of Anisotropy Using the Pulse Shape	123

ABSTRACT

A promising proposal for quantum computation, due to Loss and DiVincenzo, is based on using electron spins in quantum dots as qubits — two-level systems which are the quantum analogues of classical bits. Two-qubit operations (quantum gates) are then carried out by switching on and off the exchange interaction between neighboring spins (i.e. “pulsing” the interaction).

This thesis presents a study of the effects of anisotropic corrections to the exchange interaction due to spin-orbit coupling on this scheme. It is shown that *time-symmetric pulsing* automatically eliminates some undesirable terms in the resulting quantum gates, and well-chosen pulse shapes can produce an effectively isotropic exchange gate which can be used for universal quantum computation. Deviations from perfect time-symmetric pulsing are then studied in the context of a microscopic model of GaAs quantum dots.

A new proposal for universal quantum computation which uses control of anisotropic corrections is then presented. In this proposal, the number of pulses required to carry out quantum gates scales as the inverse of a dimensionless measure of the degree of control. The size of this dimensionless “figure-of-merit” depends on (i) variation of anisotropy with interdot distance, and (ii) restrictions on the pulse duration due to decoherence for slow pulses and nonadiabatic transitions for fast pulses. Taking these constraints into account, the figure-of-merit is estimated for GaAs quantum dots and shown to be large enough to be useful for quantum computation.

CHAPTER 1

INTRODUCTION

A man provided with paper, pencil, and rubber, and subject to strict discipline, is in effect a universal Turing Machine.

Alan Turing

One of the most exciting current frontiers of science is the new field of quantum information and quantum computation. This excitement is due to the possibility of realizing a qualitatively new “quantum technology” which would be capable of performing various kinds of communication and computational tasks which no classical machine could do. The modern digital computer is certainly one of the great achievements of classical technology, and the realization of its quantum analogue, a “quantum computer”, is one of the main goals of this new field.

In a quantum computer, classical bits — the fundamental units of classical information which can take the values 0 or 1 — are replaced by two level quantum systems, or “qubits.” The Hilbert space of a single qubit is spanned by orthogonal basis states which play the role of a classical 0 and 1, and which by convention are denoted by the ket states $|0\rangle$ and $|1\rangle$. Classical logic gates that manipulate bits in a digital computer are then replaced by unitary operators acting on qubits, known as quantum gates. In analogy with classical computation, quantum computation is done by preparing a computer in an initial state, applying a sequence of quantum gates that change its state, and reading out the result of the computation by measuring the state of the qubits.

There is no question that the construction of a fully functioning quantum computer is a daunting task. Yet, remarkably, there does not seem to be any fundamental reason why one could not be built. One reason for optimism is the large number of proposals that have been made for realizing a quantum computer, spanning the fields of quantum optics, atomic

physics, and condensed-matter physics. This thesis is concerned with one such proposal — the quantum dot computer in which electron spins are used as qubits.

The topic of this thesis is manipulation of such spin qubits for quantum computation. The unifying theme is the use of symmetry as both a valuable source of insight into spin control and as a tool for the development of simple but powerful techniques for realizing quantum gates.

1.1 Overview

The topic of this thesis is the control of pairs of electron spins in coupled single electron quantum dots. In particular, we are concerned with the effect of anisotropic terms in the exchange interaction due to spin-orbit coupling on various quantum computing schemes. The original results presented here use symmetry as a guiding principle for designing simple solutions to the complex problem of complete control over spins using a limited influence on their interaction.

The strongest interaction between spin qubits in quantum dots is the Heisenberg-type isotropic exchange ($\mathbf{S}_1 \cdot \mathbf{S}_2$). In most proposals for quantum computers it has been assumed that this is in fact the exact form of the interaction between spins. This is why it is important to study the effects of anisotropic corrections — even if they are small, they lead to a *qualitative* change in the form of the interaction which can spoil various proposed quantum computing schemes.

In this thesis we show that symmetry based control can reduce the effects of deviations of the actual interaction from the purely isotropic form, making the anisotropy of quantum gates significantly smaller than the anisotropy of the underlying interaction. It is also shown that control over anisotropic corrections allows for their use as a resource for coherent control of spin, and a new scheme for universal quantum computation using this control is given.

The first chapter of the thesis provides a short overview of quantum computation aimed at putting the results of the thesis into a wider context. It points to the problems that are going to be treated in later chapters and gives a short review of the results.

The second chapter presents a scheme for reducing the influence of anisotropy in the spin interaction on quantum operations. In this chapter the anisotropy of the interaction

is treated a problem for quantum computing, and the perceived problem is solved using a novel time symmetry of the interaction, as well as shaping of pulses.

The third chapter deals with the microscopic basis of anisotropic coupling between spins, and deduces some of its general properties, again based on the symmetry of interaction and to a large extent independent of the interaction details.

Finally, in the fourth chapter the insights into symmetries of the spin interaction are used to devise a new scheme for quantum computation that uses anisotropy for spin control. The available range of control and estimates about the physical processes that constrain it suggest that control over anisotropic corrections through time dependence of classical control parameters can be a useful tool for the control of spins in GaAs quantum dots.

1.2 Background on Quantum Computing

Quantum computers and quantum information are fascinating subjects studied in the context of physics, computer science, mathematics, and technology. They are also interesting in the context of the more general inquiry about the nature of information. To understand the significance of quantum computing, it is useful to overview some of the basic concepts of computer science in the framework of more familiar classical computation.

1.2.1 Classical Computers

The idea of a machine that can perform computational tasks stems from the concept of formalization of knowledge. A body of knowledge is formalized when it is possible to devise a recipe for solving all the problems within its scope by simply following a universal set of instructions spelled out in an algorithm. Solving formalized problems does not involve any amount of genius or creativity. Machines are notoriously better than humans in following instructions, so the execution of algorithms can benefit from the use of machines. In a sense, all of science can be described as a creative effort to not only acquire, but also formalize knowledge about nature.

Accepting formalization, design of algorithms and delegation of non creative tasks to machines as a part of scientific practice, we are led to ask ourselves about the scope of this approach. This question was asked by David Hilbert in the form of a problem about the

formalization of mathematics, the famous Hilbert's Entscheidungsproblem [1]. This problem asked whether it is possible to decide if any given statement concerning arithmetic is true by following a predefined set of rules. Alan Turing [2] has demonstrated that such a set of rules does not exist. The same problem has been worked on and solved in an alternative fashion by the logician Alonso Church [3, 4].

Turing's solution to the Entscheidungsproblem not only solved an important problem in mathematics, but also opened a whole new area of research. After proving that it is impossible to solve all problems algorithmically, it is natural to ask which problems can be solved in this way. Answering that question motivated the introduction of a precise definition of an algorithmic solution to a problem.

The most important framework for studying algorithms is the Turing machine model of computation. A Turing machine is an abstract device that follows a set of instructions in order to solve a given problem. The precise definition of a Turing machine is given in [Fig.1.1], and it is a widely applicable model of all the processes that are governed by a set of instructions.

The Turing machine captures the essence of algorithmic solutions to computational problems. It also allows for quantification of the resources needed to perform a computational task, in the form of the instructions list length, the number of steps that are executed, or the length of the used portion of the tape. With a quantitative measure of the resources needed to execute a given program, it is possible to ask questions about the efficiency of algorithmic solutions to any given problem, and not just about their existence. Since the resources used in any run of the Turing machine explicitly depend only on the program being executed and the algorithm that is implemented, and only implicitly on the problem that is being solved, it is generically hard to find the resources necessary to solve a given problem. The study of resources required to produce a solution to a given problem as a function of the problem itself, rather than the employed algorithm, comes under the heading of "complexity theory" and it is one of the main topics of computer science.

An alternative to the Turing machine model of classical computation that will be more relevant for the discussion of quantum computing that follows is the so-called *classical circuit model*. In the classical circuit model, the state of a computer is specified by some number of bits — the fundamental units of classical information [5] [6]. A bit is a logical variable that

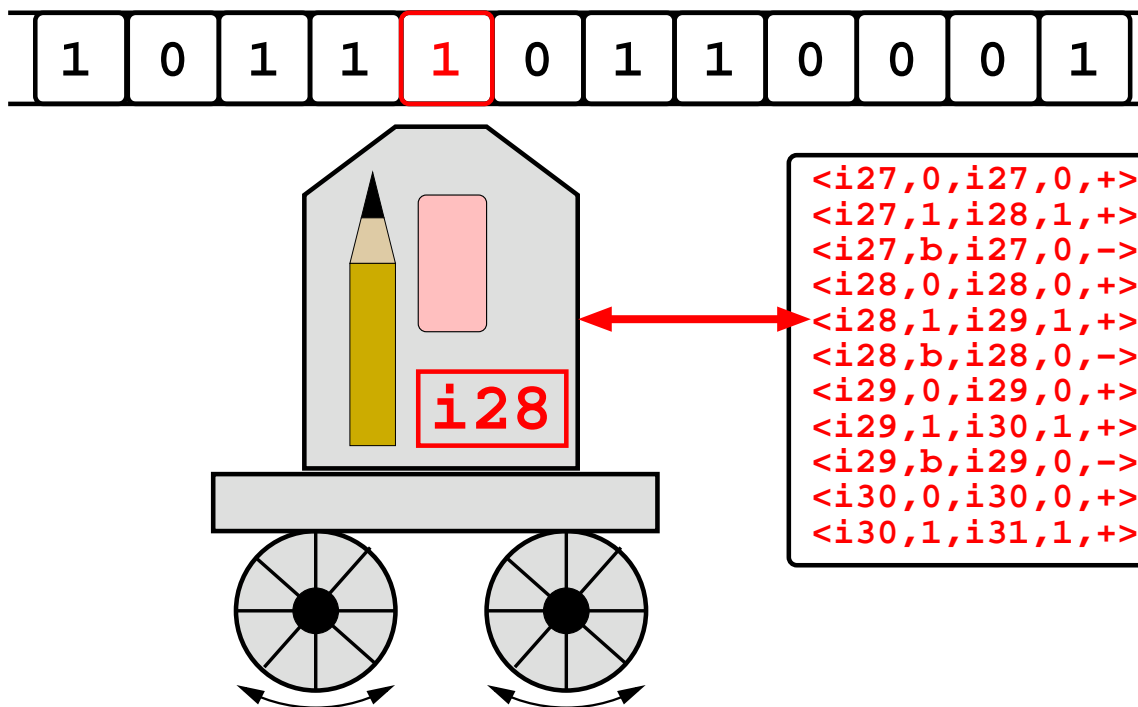


Figure 1.1. Illustration of the Turing machine. The Turing machine consists of an infinite tape with cells and a read write head. At any time the machine is in some internal state from a predefined set $\{i_1, i_2, \dots\}$. Each cell contains a symbol from a preselected alphabet, in this figure $\{0, 1\}$. Head moves along the tape and at each step it is over a single cell on the tape. At each steps it reads the symbol in the cell below it, reads an instruction and executes it. Instruction is a set of five objects, $\langle i_1, s_1, i_2, s_2, m \rangle$, where i_1, i_2 are internal states of the machine, s_1, s_2 are symbols from the alphabet and $m = \pm$ is the direction of motion of the head. Machine finds instruction for which i_1 is current internal state and s_1 is symbol on cell below the head. Than, it changes internal state to i_2 , writes the symbol s_2 in the cell and moves one cell in the direction m .

by convention takes values from the set $\{0, 1\}$ instead of more standard $\{\text{TRUE}, \text{FALSE}\}$. In the classical circuit model, every computation is represented by a set of logic gates acting on some number of bits. A logic gate f is defined by a Boolean function. It takes n bits in a state $i \in \{0, 1\}^n$ as the input and delivers m output bits in a state $o \in \{0, 1\}^m$, so that $o = f(i)$.

The usefulness of the Turing machine model is in its ability to quantify the resources needed to perform a given computational task. This quantification is also possible in the classical circuit model. To do this we must define what is known as a *universal set of logic*



Figure 1.2. Universal set of classical logic gates. One universal set of classical logic gates consists of a *NOR* and a *NOT* gate. In this figure, these gates are represented by truth tables and a symbol in classical circuit model.

gates. A universal set of gates is a small family of logic gates with few input and output bits that can be combined into circuits implementing any given logic gate with inputs and outputs of arbitrary size. The role of the elementary steps in a Turing machine operation is then played by the simple logic gates from a universal set.

An example of a universal set of gates are the *NOR* and *NOT* gates shown in [Fig. 1.2]. In this figure, and all similar diagrams, bits are represented by lines and gates are represented by their standard Boolean logic symbols, with time flowing from left to right. To quantify the computational resources in the circuit model, a classical circuit that represents a given computation is constructed from gates belonging to this universal set. The number of gates from the universal set used in this construction is then a measure of the resources needed to perform a computational task. It is a fundamental result that the complexity of any problem deduced within the classical circuit model (or any model of classical computation) is equal to its complexity in the Turing machine model. This fact allows us to talk about the complexity of a problem as a function of the problem itself, rather than as a function of both the problem and the model of computation used to evaluate its complexity.

One way in which the circuit model is more useful than the Turing machine model is that it suggests how we could actually build a computing device. If we could realize physical systems which are capable of represent bits, and carrying out a universal set of logic gates on these bits, then this system could serve as a computing device. For example, in a modern

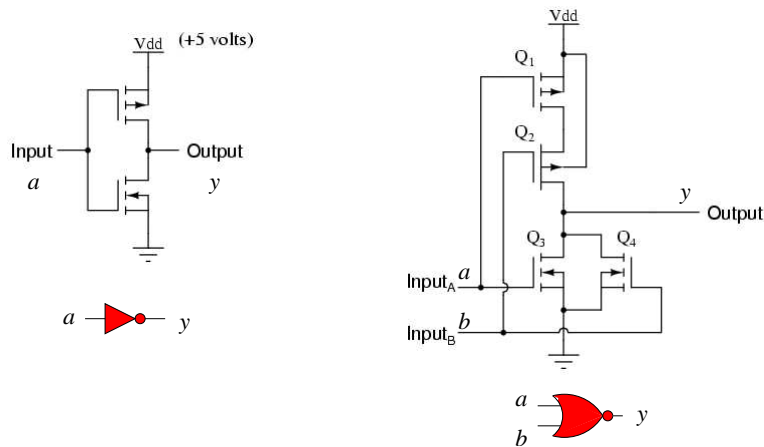


Figure 1.3. The classical circuit model of computation. The classical circuit model of computation is a direct abstraction of the actual electronics that performs computation in a digital electronic computer. The figure shows different levels of this abstraction. Electronic schemes on top produce a digital output as a function of digital input and can be represented by the symbols for *NOT* and *NOR* logical gates.

digital computer, bits correspond to voltages, and logic gates are carried out by transistor circuits, such as those shown in [Fig. 1.3].

We will see in the next section, that there is a quantum version of the classical circuit model which again allows for a quantitative measure of algorithmic complexity, and, as above, provides a guide for realizing such a “quantum computer” in a variety of physical systems.

1.2.2 Quantum Computers

The standard model of a quantum computer is the quantum circuit model, a quantum version of the classical circuit model described above. In the quantum circuit model, the elementary units of quantum information — the quantum analogue of the classical bit — is the quantum bit or *qubit*. A qubit is an abstract representation of a two-level quantum system with its state space spanned by logical basis states $|0\rangle$ and $|1\rangle$. A qubit that remains in one of its logical basis states throughout a quantum computation behaves exactly like a

classical bit. But, already at the level of its basic unit, quantum information shows some new properties, absent from the classical case.

Since the state of a qubit is quantum, it can exist in an arbitrary normalized superposition of the basis states, like $1/\sqrt{2}(|0\rangle + i|1\rangle)$. These states have a novel property that they are completely specified, but measurement in the computational basis gives either 0 or 1 with equal probability, like readout of a bit in a classical computer that can be in either the 0 or 1 states with equal probability. Even though the readout of the bit will have the same distribution of results as the measurement of a qubit in the computational basis, these two objects are different. The state of a probabilistic bit corresponds to its least specified state, while the state of a qubit is completely specified. The measurement of a qubit in this state in the computational basis, collapses its state into the state corresponding to the result of measurement. The quantum properties of a single two level system are the basis of the first practical application of quantum information in cryptography [7, 8].

Pairs of qubits can show even more novel features. For example, they can be in an *entangled* state, like $\frac{1}{\sqrt{2}}(|00\rangle + i|11\rangle)$. The results of measurements on a pair of qubits in such a state can show quantum correlations which are impossible to realize in any classical system [9], [10].

A quantum computer consists of a set of qubits that are manipulated in a controllable fashion. In the quantum circuit model, as in the classical circuit model, qubits are represented by lines, and operations on them are represented by so-called *quantum gates*. A quantum gate is a unitary operation that takes qubits in the input state and deliver them in an output state. These elements of a quantum circuit model are shown in [Fig. 1.4]. Each gate is specified by unitary transformation acting on the Hilbert space of the involved qubits. Computation begins with the preparation of a set of qubits into some initial state, typically $|00\dots 0\rangle$, continues with the application of a predetermined sequence of quantum gates, and finishes with a set of measurements of the qubit states. The result of the computation is then deduced from the results of this final measurement.

In passing we note that the quantum circuit model is not the only model of quantum computation. The most important alternative models are adiabatic quantum computation due to Farhi [11], and the one-way quantum computer of Raussendorf, Browne and Briegel [12]. The important point about all of these models, including the quantum circuit model,

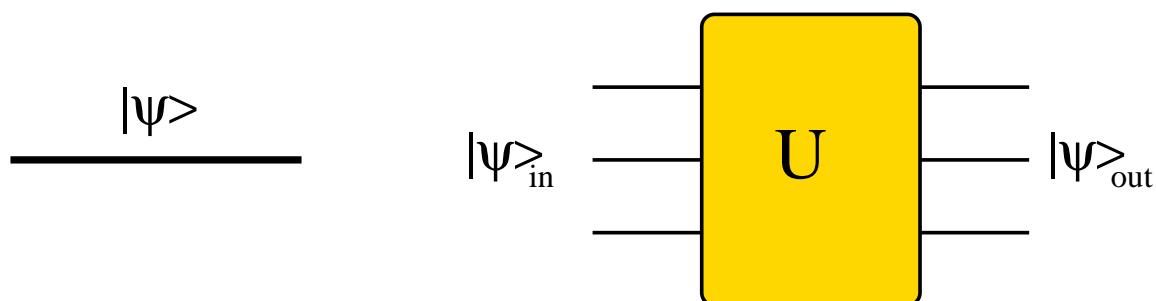


Figure 1.4. Elements of the quantum circuit model of quantum computation. In quantum circuit model a qubit is represented with a line. Gate is a box that takes some number of qubits (three in this figure) as an input and deliver the same number of qubits as an output. The state of qubits at the output is related to the state of qubits at the input through a unitary transformation that specifies the gate.

is that they are based on physical systems that undergo controlled evolution corresponding to the computing process. They are in principle realizable and reflect very concrete ideas about a real physical computer.

One of the earliest triumphs of quantum computing was DiVincenzo’s proof that gates acting on single qubits or pairs of qubits are sufficient for application of an arbitrary unitary evolution to any set of qubits [13]. The importance of this proof lies in the fact that it shows that control over single-body and two-body interactions is sufficient for the complete control over a set of qubits of arbitrary size. These two types of interaction are also the only types that can be controlled within reasonable assumptions about the obstacles that are present in realistic quantum systems.

We can now introduce the quantum analogue to the universal set of logic gates described in the previous section for classical computers. As in that case, there are many choices. The standard choice for a universal set of quantum gates consists of all possible single qubit operations and the so-called controlled not (CNOT) gate [Fig.1.5].

The CNOT gate is a two-qubit gate defined by its action on the computational basis of the qubits. In the basis

$$\{|00\rangle, |01\rangle, |10\rangle, |11\rangle\}, \quad (1.1)$$

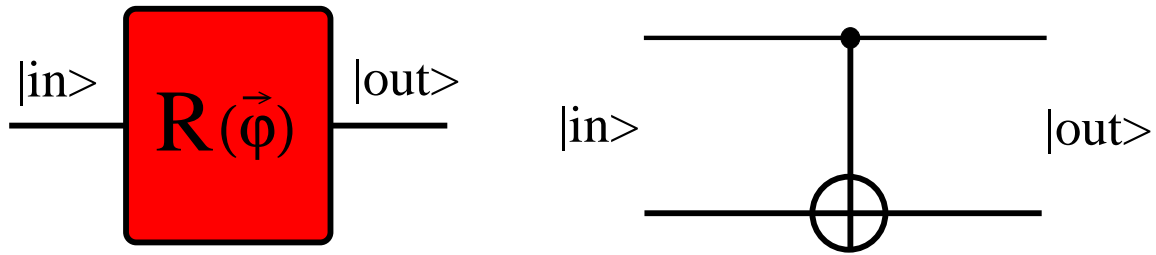


Figure 1.5. A universal set of quantum gates. An important universal set of gates consists of all unitary gates acting on a single qubit and the controlled not (CNOT) gate acting on a pair of qubits. If we attach pseudospin labels to qubit states $|0\rangle \equiv |\uparrow\rangle$ and $|1\rangle \equiv |\downarrow\rangle$, every single qubit gate corresponds to a unique rotation. In this sense, single qubit gate can be labeled $R(\phi)$ and parametrized by a vector ϕ , where the rotation axis is $\hat{\phi}$ and the rotation angle is ϕ . Action of a CNOT gate on logical basis is to flip (NOT operation) the state of target qubit if the state of control qubit is $|1\rangle$ and do nothing if the state of control qubit is $|0\rangle$. In the figure, control qubit is above target qubit. Action on all other input states is given by linearity of transformation.

where $|ab\rangle \equiv |a\rangle \otimes |b\rangle$ is a product state with both qubits in computational basis states, the matrix representation of a CNOT gate is

$$CNOT = \begin{bmatrix} 1 & 0 & 0 & 0 \\ 0 & 1 & 0 & 0 \\ 0 & 0 & 0 & 1 \\ 0 & 0 & 1 & 0 \end{bmatrix}. \quad (1.2)$$

Its action is thus to flip the logical state of the second (target) qubit if the first (control) qubit is in the $|1\rangle$ state and to do nothing to the target qubit if the control qubit is in the $|0\rangle$ state. The action of this gate on a general input state then follows from linearity.

Like the universal set of classical logic gates, a universal set of quantum gates allows for quantification of resources needed to perform a given quantum computation. The complex unitary transformation corresponding to a given quantum computation can be reduced to the application of a series of gates from a universal set, and the number of gates is then a measure of the resources used in the process, as illustrated in [Fig.1.6].

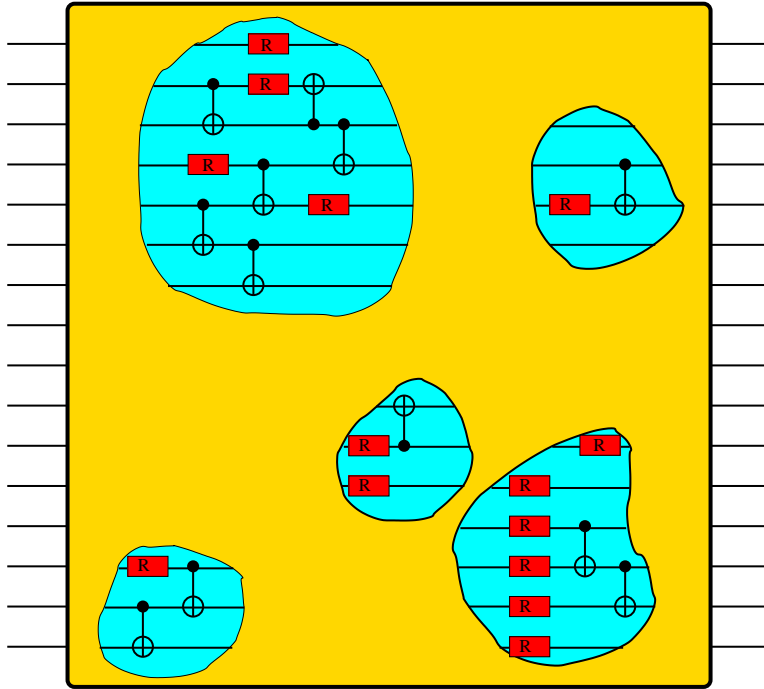


Figure 1.6. Complexity of a quantum gate is measured by the number of quantum gates from a universal set necessary to implement it.

1.2.3 Church-Turing Thesis

We have seen that both the Turing machine and circuit model of classical computation provide a way to quantify the resources needed to carry out a given computation. For quantum computation, resources are quantified using the quantum circuit model. In all three cases, the complexity of a problem is measured by the resources a model machine must use to solve it.

A key assumption of computational complexity theory is that complexity measures defined using different models of computation are essentially equal in the sense that any model of computation can be simulated within any other model of computation with at most a polynomial overhead. This assumption is usually referred to as the Church-Turing thesis. It is only because of the Church-Turing thesis that we can talk about the complexity of any given problem rather than the complexity of a problem in the context of some model of computation.

The Church-Turing thesis is proved to be true for all classical models of computation known to date that are, at least in principle, physically realizable. Quantum computers are the only possible exception. Quantum computing is in fact the model of computation that presents the most credible challenge to the Church-Turing thesis.

It should first be noted that a quantum computer is at least as powerful as any machine that can be described in the classical circuit model. If qubits are kept in their logical basis states throughout the computation then the quantum computer is equivalent to a reversible classical circuit, which is in turn equivalent to ordinary classical circuits, as shown by Fredkin and Toffoli [14]. It follows that any task that can be completed on a classical computer can be completed at least as efficiently on a quantum computer.

In fact, algorithms for a quantum computer that are more efficient than any algorithm for a classical computer exist and prove that a quantum computer is *more* powerful than a classical computer. However, it is not known whether the extra power of a quantum computers is significant in the sense of Church-Turing thesis. To illustrate the precise relation between the computational powers of classical and quantum computers, it is useful to consider two of the best known quantum algorithms — Grover’s search algorithm [15] and the famous Shor’s algorithm for factoring [16].

Grover’s algorithm performs a search of an unstructured database of size N for a tagged element and retrieves the tagged element with certainty after accessing the database only $O(\sqrt{N})$ times. The best classical algorithm must access the database $O(N)$ times to discover the tagged element with certainty. This proves that quantum computers are more powerful than classical ones, but here the improvement is insignificant in the sense of the Church-Turing thesis, because the achieved improvement is only polynomial.

The algorithm that led to a true explosion of interest in quantum computing is Shor’s factoring algorithm. This algorithm factors an N digit composite integer into its prime factors using $O(N^3)$ quantum gates. This is to be contrasted with the best known classical factoring algorithm which uses $O(\exp(N^{1/3} \log(N)^{2/3}))$ classical gates [17], i.e. resources that are exponential in N . This improvement, sometimes referred as “exponential quantum speed-up” (illustrated in [Fig. 1.7]) is therefore significant in the sense of Church-Turing thesis. However, it is not known if the best classical factoring algorithm known to date is the best possible classical algorithm. A detailed discussion of Shor’s factoring algorithm can

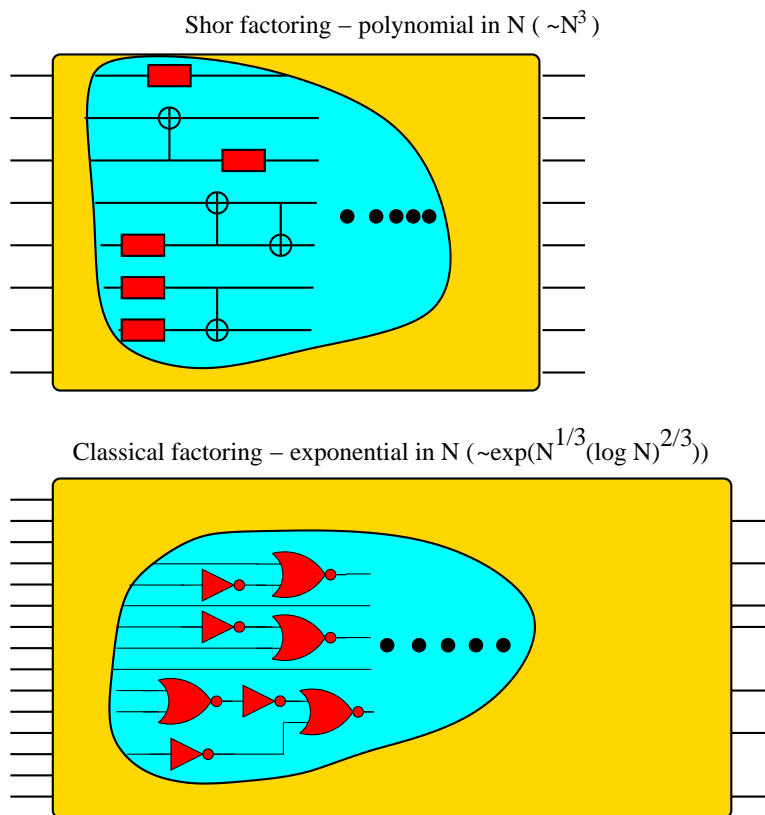


Figure 1.7. Comparison between complexities in classical and quantum circuit model. In this figure both classical and quantum circuit consist of a certain number of gates from appropriate universal sets. If the two circuits were designed to factor an N digit integer, classical using the best known classical algorithm and quantum using Shor's algorithm for factoring that can only be implemented in a quantum computer, the number of gates in classical circuit would grow like an exponential in N , while the number of quantum gates in the quantum circuit would be a polynomial.

be found in the review article of Ekert and Jozsa [18]. It is widely believed that factoring cannot be done significantly better on a classical computer, so it is equally widely believed that the quantum computer is a fundamental improvement of computing machinery.

It is still an open question just how powerful quantum computers really are, but they are extremely interesting from the point of view of computer science and in fact in any discussion about the ultimate limits of the power of algorithmic solutions to problems.

1.3 Physical Realizations

Computer science deals with idealized models of computation out of a need for rigorous and general definitions of the computing resources needed to solve a given problem. However, these models are useful only as long as they apply to computers that are, at least in principle, realizable in the real world. Therefore, the question about the computing power available in nature lies in the domain of natural sciences. Only the properties of real systems that perform computations determine if a given model of computation is an appropriate description of some real computing device.

For quantum computing the question of physical realization is very important for at least two reasons. The first reason is that quantum computing is possibly the most powerful computing model that does not violate the laws of nature as we know them. If quantum computers can not be realized there should be a good reason for that, hopefully involving novel insights into these laws. The second reason is that trying to build a quantum computer forces us to achieve complete control over a quantum system, offering many possibilities for learning about quantum mechanics in regimes where no experiments were done before.

For a quantum computer, the most important real world constraint is decoherence. Decoherence is a process in which a quantum system becomes entangled with its environment and thus makes a transition from a pure quantum state described by amplitudes into a statistical mixture of states described by probabilities alone (or, more precisely, a density matrix). Statistical mixtures cannot be used for quantum computation. Unfortunately, having qubits which interact with the environment is necessary, if we are going to be able to control them. This means that some amount of decoherence caused errors will always be present in any quantum computer. At first sight, then, it seems that a quantum computer can operate only for a finite and rather short period of time in which the transition from quantum state to statistical mixture takes place.

It is a remarkable fact, and one of the true triumphs of the theory of quantum information, that a quantum computer actually can function and maintain its advantage in performance over classical computers even in the presence of errors that are unavoidable due to decoherence. This result, due to Shor [19], Calderbank and Shor [20, 21], Steane [22] and Preskill [23] is known as quantum error correction and fault-tolerant quantum computation.

The main result of quantum error correction is the famous threshold result. This result states that if the error in a quantum operation has a probability p smaller than some constant error correction threshold p_{th} , it is possible to devise a procedure that will eliminate errors in the final results at the cost of a polylogarithmic increase in circuit complexity [24]. The exact value of the error correction threshold depends on the model of error and the estimates vary in a wide range $10^{-4} < p_{th} < 10^{-8}$. However, the very fact that the threshold exists proves that a quantum computer can, at least in principle function in the presence of errors without losing its power. A truly remarkable result.

Fighting decoherence and errors is not the only challenge facing the builders of quantum computers. The set of requirements that a device must meet in order to be a practical quantum computer are summarized in DiVincenzo's desiderata list for quantum computation [25]. The desiderata are:

1. **Qubits:** A quantum computer must be a scalable device with well characterized qubits. This property is important because quantum computers may be better than classical ones only for large sizes of input that requires a lot of qubits to encode and work with. Qubits are well characterized if there is only a small probability for the state of any qubit to leak outside of the space of linear combinations of logic basis states $|0\rangle$ and $|1\rangle$.
2. **Initialization:** Initialization of the computer in a specific state, like $|00\dots 0\rangle$ must be possible.
3. **Coherence:** Decoherence times must be much longer than the time needed to perform an elementary operation on the qubits. The probability of error in gate operation, which is bounded from below by a function of the ratio between time needed to perform a gate and the decoherence time, must be below the error correction threshold p_{th} .
4. **Universal Gates:** We must be able to apply every transformation from some universal set of gates. This requirement is very hard to meet, because the available set of gates is determined by the available interactions in a system. A wise choice of the universal set will contain gates implemented by control of the interactions between qubits that are already available in the system.

5. **Measurement:** We must be able to perform a measurement of the state of each qubit in the computational basis. The measurement requirement is necessary for the readout and application of the error correction procedures.

Many systems have been investigated as potential quantum computers. Some of the most notable ones are nuclear magnetic resonance in both liquid and solid state, ion and atom traps, cavity quantum electrodynamics systems, nonlinear optics, linear optics with measurement, quantum dots, Josephson junctions and nonabelian anyons. Topics discussed in this thesis are most relevant for the proposal for a quantum computer based on single electron quantum dots, due to Loss and DiVincenzo [26].

A common feature of all potential quantum computers is that they consist of systems with well established quantum behavior and a small subset of energy levels that can be isolated from the rest of the system and manipulated as a logical basis for a qubit. Most of the proposals come from areas of research with rich experimental practice and a great deal of experience with manipulation of the system.

Nuclear magnetic resonance (NMR) proposals use nuclear spins as qubits. They use a standard NMR setup using radio frequency pulses to address nuclear spins in magnetic fields. Preparation of the initial state, manipulation and measurement of the nuclear spins in this setup is an art form that is perfected through the experience of many researchers working in the field. Radio pulse sequences that perform various quantum operations are well known and, at the present stage of development, can be routinely developed. Nuclear spins have very long coherence times, due to their weak interaction with the environment, leaving the possibility for gate operations with very small errors. In nuclear magnetic resonance based proposals the complete computer fits on a single molecule and nuclei with different surroundings represent addressable qubits. The most powerful experimental demonstrations of quantum computing to date is factoring of the number 15 on 7 qubit NMR based quantum computer by Vandersypen *et al.* [27]. Currently, NMR quantum computers cannot be scaled up to useful numbers of qubits. Main problems with scaling are synthesizing large and complex molecules and strong damping of the NMR signal with molecule size.

Proposals based on traps use arrays of isolated atoms or ions [28]. Each trapped particle carries a qubit with logical states encoded in suitably chosen energy levels. Another alternative is the use of optical lattices. Manipulation of the qubits is done by shining

electromagnetic radiation of wisely chosen frequency and polarization, and interacting the qubit states with collective degrees of freedom and cavity photons. These systems have long coherence times, but somewhat involved control. Recent progress in designing ion traps on chips suggests that ion traps quantum computers may be scalable to useful scales [29].

Optics proposals use single photons to carry qubits encoded usually as states of the polarization or in spatial degrees of freedom. Single qubit operations on photons can be done using standard linear optics, and single photon detection allows for efficient measurements. The hard part of optical schemes are two-qubit operations that require nonlinear optical elements. An alternative to the circuit model, the one-way quantum computer of Raussendorf, Browne and Briegel [12] is considered as a way to remove the need for more than a single qubit operations. Optical qubits were the first ones with practical applications, in quantum cryptography [7, 8].

The most important solid state physics based proposals for quantum computation include Josephson junctions, phosphorus donors in silicon and our heroes, quantum dots, as carriers of qubits. In Josephson junction based approach, qubits are encoded into either flux or current through a junction or the charge of a superconducting island [30]. One interesting property of this proposal is that it uses quantum properties of a large collection of electrons. The phosphorus in silicon approach of Kane [31] uses qubits encoded into spin of phosphorus nuclei precisely implanted into a slab of silicon. Electrodes above the phosphorus donors influence the electron cloud of phosphorus atom and indirectly the nuclear spins. This proposal combines long coherence time of nuclear degrees of freedom with the indirect control through orbital degrees of freedom of electrons that are much easier to access. The main problem with this approach is the complexity of control and difficult fabrication of the device.

1.3.1 The Quantum Dot Quantum Computer

The quantum dot based proposal for realizing a quantum computer [26] is the most relevant one for the research presented in this thesis. In the original proposal of Loss and DiVincenzo, the qubits are spins of electrons bound to electrically gated coupled single electron quantum dots in GaAs, see [Fig. 1.8].

The control over these spins is then achieved through separate mechanisms for addressing single electron spins and interacting pairs of electron spins on neighboring dots. Single spins

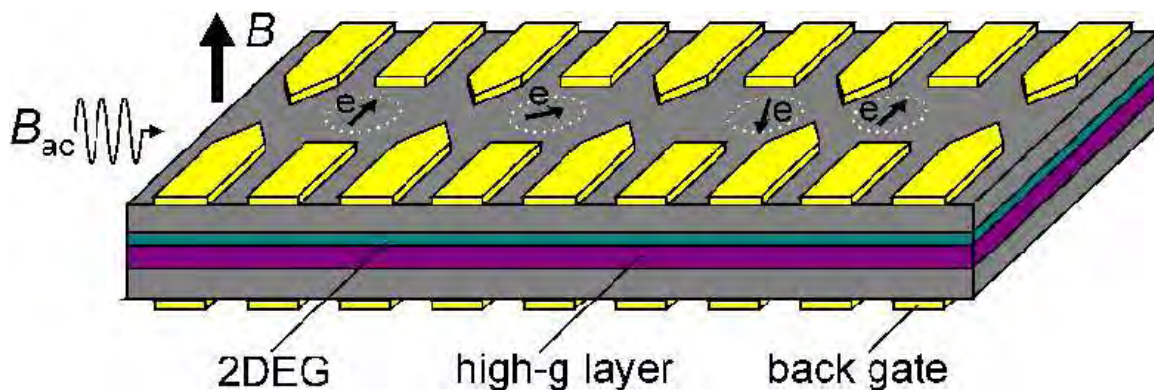


Figure 1.8. Quantum dot quantum computer, due to Loss and DiVincenzo. The qubits of this proposed computer are electron spins on coupled single electron quantum dots. Quantum dots are fabricated by electrostatic gating of a two dimensional electron gas in GaAs. In the original proposal, illustrated in this figure, the spins are manipulated via voltages on electrodes that define quantum dots and a combination of electron spin resonance techniques and manipulation of the Zeeman terms at the position of individual dots. In this figure two spin qubits on the left are decoupled, while spin qubits on the right interact through exchange coupling.

are accessed through local modulation of the Zeeman coupling via an external magnetic field, and electron spin resonance (ESR) techniques. Pairs of spins are interacted through the exchange coupling controlled by the potential on the electrode that separates the two quantum dot hosts.

Surprisingly, the mechanism for the control of pairs of electron spins is much simpler than the mechanism for accessing and controlling individual spins. Applying a two-qubit gate involves only sending a voltage pulse to one of the electrodes in the structure, while application of single-qubit gate involves modulation of the Zeeman coupling term $H^Z = \mu_0 g \mathbf{B} \cdot \mathbf{S}$ and applying an ESR pulse that will resonantly affect only one of the spins. The Zeeman coupling can be altered by either locally manipulating the magnetic field in the device or, again locally, changing the g -factor. Both the alteration of Zeeman coupling and application of an ESR pulse are considered to be much more involved operations than sending a voltage pulse which controls the interaction of a pair of spins.

This discrepancy in the difficulties connected with the control mechanisms for single-qubit and two-qubit gates has prompted a lot of effort to enable quantum computation in

these structures using only the voltage control. This approach is known as *exchange-only* quantum computation. An important result in exchange-only quantum computation was the demonstration of DiVincenzo *et al.* in [32] and Bacon *et al.* [33] that controllable isotropic exchange coupling of the form

$$H(t) = J(t)\mathbf{S}_1 \cdot \mathbf{S}_2, \quad (1.3)$$

where $J(t)$ is the coupling constant that depends on the externally controlled voltage and $\mathbf{S}_{1,2}$ are the spin operators of interacting electrons, is sufficient for the production of a universal set of quantum gates over qubits encoded into states of three spins.

The isotropic exchange gates (1.5) produced by the spherically symmetric exchange Hamiltonian preserve the total spin of affected spins. In order to construct a universal set of gates, the logical basis states $|0\rangle$ and $|1\rangle$ of a qubit must have the same total spin quantum numbers. The smallest number of spins that allows for such encoding is three. A construction of the universal set of gates over logical qubits of three spins with $S^{tot} = \frac{1}{2}$ and either $S_z^{tot} = \frac{1}{2}$ or $S_z^{tot} = -\frac{1}{2}$ is known, but it is rather complex, see [Fig.1.9], taken from [32].

This construction of a universal set of gates using isotropic exchange fails when the effective interaction of the spins deviates significantly from the isotropic form (1.3). In the context of quantum computing, a significant deviation is any deviation which produces an error that cannot be handled using quantum error correction codes.

Even with the optimistic assumption of the error correction threshold of $p_{th} = 10^{-4}$, naive estimate for the size of anisotropic corrections to the isotropic effective spin interaction (1.3) that are due to spin-orbit coupling are large enough to make voltage controlled quantum computing as proposed in [32] impossible. The first estimate of the size of spin-orbit coupling induced anisotropy and the corresponding pessimistic outlook on the possibility of exchange-only quantum computation was given by Kavokin [34].

One of the major results presented in this thesis resolves the problem of spin-orbit coupling induced errors in exchange-only quantum computing based on isotropic exchange interaction (1.3). We show that the anisotropy in a voltage controlled quantum gates can be smaller than the size of the interaction terms would suggest. With properly chosen time dependence of the control voltage, the effect of anisotropy in a quantum gate can be turned from a first order effect in spin-orbit coupling strength into a second order effect in spin-orbit

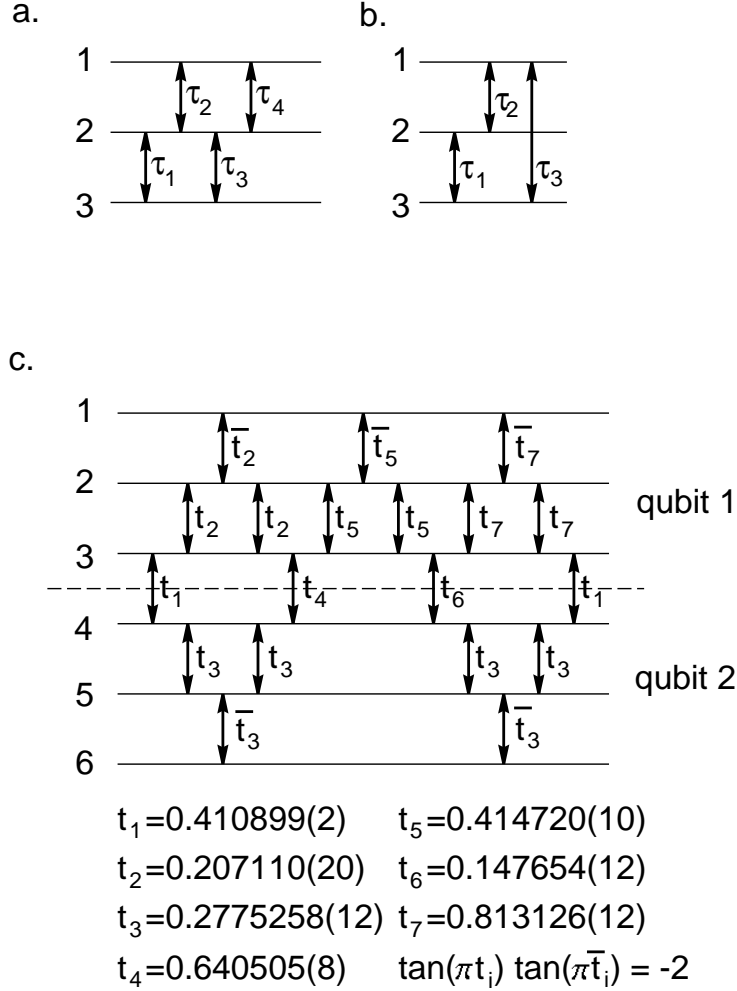


Figure 1.9. Circuits for implementing single-qubit and two-qubit rotations using isotropic exchange. a) Single-qubit rotations by nearest-neighbor interactions. Four exchanges (double-headed arrows) with variable time parameters τ_i are always enough to perform any such rotation b) Non-nearest neighbor interactions. Only three interactions are needed c) Circuit of 19 interactions that produce a CNOT between two coded qubits (up to one-qubit gates before and after). The durations of each interaction are given in units such that for $t = 1/2$ the rotation $U_{ij} = \exp(iJt\vec{S}_i \cdot \vec{S}_j/\hbar)$ is a SWAP, interchanging the quantum states of the two spins i,j . The \bar{t}_i parameters are not independent, they are related to the t_i s as indicated. (Figure due to DiVincenzo, Bacon, Kempe, Burkard and Whaley.)

coupling strength. More details about the procedure are given both later in the introduction and in the separate chapters of the thesis.

1.4 Spin-Orbit Coupling

The most important source of anisotropy in the effective spin interaction in coupled quantum dots is spin-orbit coupling. The details of the spin-orbit coupling interaction in the semiconductor hosting the quantum dots are important because they will determine the properties of the anisotropic interaction between the spins. We briefly review the physics of spin-orbit coupling in this context here. A more detailed discussion is given in chapter 3.

For electrons moving in the presence of an electric field in vacuum, spin-orbit coupling can be seen as a simple relativistic effect. A Lorentz transformation from the laboratory frame into the rest frame of the electron transforms the electromagnetic field, producing a magnetic component with the size of the order v/c , where v is the electron velocity and c is the speed of light. The spin magnetic moment of the electron will then couples to this magnetic field. Since the magnetic field in the rest frame is a function of electron velocity, the spin and orbital degrees of freedom are coupled through this effect.

In semiconductors, the source of spin-orbit coupling is, of course, the same relativistic effect described above; namely, an electron moving in the presence of the electric field of the background ions of the solid again feels an effective magnetic field which couples to its spin. However, the treatment of this effect is more complicated than that of a uniform electric field. To calculate the effect of spin-orbit coupling in this context it can be treated as a perturbation of the electronic band structure states labeled by the crystal momentum k . The resulting term that couples orbital and spin degrees of freedom then has the form

$$H^{SO} = \mathbf{h}(\mathbf{k}) \cdot \mathbf{S}, \quad (1.4)$$

where $\mathbf{h}(\mathbf{k})$ is an odd vector function of crystal momentum. This last fact follows from time-reversal symmetry — under time reversal both \mathbf{k} and \mathbf{S} changes sign, but H^{SO} cannot (spin-orbit coupling is time-reversal symmetric), thus we must have $\mathbf{h}(\mathbf{k}) = -\mathbf{h}(-\mathbf{k})$.

If the system is symmetric under inversion, the spin-orbit coupling will be absent. Under inversion the crystal momentum changes sign, $\mathbf{k} \rightarrow -\mathbf{k}$ and spin remains invariant $\mathbf{S} \rightarrow \mathbf{S}$. This implies that the time-reversal symmetric spin-orbit coupling Hamiltonian (1.4) is odd

under inversion and thus vanishes in systems that are inversion symmetric. Thus, we see that every source of spin-orbit coupling can be traced to inversion asymmetries of the system.

In the devices that are considered here, inversion asymmetry comes from two main sources. The first source is bulk inversion asymmetry of the crystal structure that hosts the dots. This source of spin orbit coupling was studied by Dresselhaus [35] and the contribution of crystal structure asymmetry to spin-orbit coupling Hamiltonian is usually referred to as the Dresselhaus term. Another spin-orbit coupling inducing inversion asymmetry comes from the structure fabrication. Quantum dots are fabricated near the boundary of two different semiconductors, and inversion would switch the materials, changing the system. Contribution of this structure inversion asymmetry to the spin-orbit coupling is called the Rashba term [36]. The strain at the contact of two semiconductors. induces spin-orbit coupling terms of Rashba form. These strain induced terms can be much stronger than the original Rashba terms, as shown in experiments of Kato *et al.* [37], and therefore important for spin manipulation.

Earliest inquiries into spin-orbit coupling in semiconductors concerned its effects on the band structure [35] and spin decoherence [38]. Also, an important proposal for a semiconductor device that uses both spins and charge, the Datta and Das spintronic transistor [39], uses spin-orbit coupling to influence spin degrees of freedom through electric fields. For the purpose of research presented here, details of the spin-orbit coupling interaction in a semiconductor hosting the quantum dots are important because its form will eventually determine properties of anisotropic interaction between the spins.

1.5 Symmetry and Control

The construction of a universal set of quantum gates in a quantum computing device can be formulated as a control problem. Imagine we are given a set of Hamiltonians that depend on the values of some set of external parameters. These external parameters are time dependent and under our control. As we change the values of these parameters in time, we apply a time-dependent Hamiltonian to the system that hosts the qubits and induce a unitary evolution, i.e. a quantum gate. The problem of complete control over our system

is solved when we find a set of time-dependent external parameters that will produce all of the gates from some universal set.

Whenever the interactions in the system have some degree of symmetry (for example, rotational symmetry in the case of the isotropic exchange interaction), there is an interesting trade off between the complexity of required control over the interactions and the set of gates that can be produced. Consider a given time-dependent Hamiltonian that has some fixed symmetry at every moment in time. The unitary evolution produced by this Hamiltonian will then have the symmetry as the underlying Hamiltonian. Also, the combination of two such symmetric evolution operators will also be symmetric. Therefore, the quantum gates that can be produced with time dependent pulses of control parameters will all have the symmetry of the underlying Hamiltonian and preserve its good quantum numbers. By definition, a combination of gates which form a universal set can implement arbitrary unitary transformation on qubits, including transformations that change good quantum numbers of Hamiltonian. Thus we see that symmetric gates can not be universal if qubits correspond to single spins.

In order to eventually produce a universal set of gates using symmetric elementary gates, logical qubit states have to be encoded into the states of more than one physical qubit (as in the discussion of exchange-only quantum computation given above). Here, we call a gate elementary if it is produced by a single voltage pulse. Then, a set of elementary gates with common symmetry operating on physical qubits can correspond to another set of gates on encoded logical qubits without common symmetry [33]. Another search through combinations of these gates can lead to a universal set. However, the search for a universal set of gates over encoded qubits can be hard. Therefore, the task of finding a universal set of gates becomes harder when the underlying interaction is symmetric, giving a negative side of the trade off.

On the positive side of the trade off, symmetry simplifies the control at the level of the design of pulses that produce an elementary gate. Since the Hamiltonian is symmetric throughout the application of the elementary gate, its good quantum numbers will remain unaltered by the applied gates. The form of resulting gate will be then constrained in order to preserve the good quantum numbers, and getting to the right gate in this restricted set will be much simpler.

The example of the spherically symmetric isotropic exchange interaction (1.3) can clarify this point about symmetry trade off. Let us assume that we apply a pulse of time dependent voltage which produces a time dependent coupling constant J : $H(t) = J(t)\mathbf{S}_1 \cdot \mathbf{S}_2$. Invariance under arbitrary rotation in spin space is preserved throughout any such pulse, and the resulting elementary gate must therefore also be spherically symmetric. There is only one spherically symmetric operator, apart from the irrelevant constant, that can be constructed from two spins. So, based on the symmetry of the problem alone, we can conclude that the resulting gate U has a very simple form

$$U(\lambda) = \exp -i\lambda\mathbf{S}_1 \cdot \mathbf{S}_2, \quad (1.5)$$

where the only dependence on the external parameters and the way they change in time comes through a single integrated coupling constant

$$\lambda = \int_{-\infty}^{\infty} J(t)dt. \quad (1.6)$$

The fact that there is only a single control parameter, λ , tells us that the control over this highly symmetric Hamiltonian is comparatively simple. The resulting elementary gate is fixed by a single parameter, as opposed to the 15 parameters of a general gate produced by an interaction with no symmetry. Also, there is only one simple property of the pulse — namely its integrated intensity — that matters at all in the elementary gate construction and needs to be controlled, as opposed to 15 functions of the time dependent Hamiltonian determining the gate when there is no symmetry. Parameters in asymmetric case are rather complex functions of time dependent interaction and hard to control. Control simplicity in symmetric case is the positive side of the trade-off.

1.5.1 Reduction of the Effects of Spin-Orbit Coupling in Exchange Gates

We have seen that symmetry is a useful guiding principle in solving problems that concern the control of spins in coupled quantum dots. Achieving this control is a crucial task for fulfilling the requirement of the existence of a universal set of gates from the desiderata list for the quantum computer proposal that uses spins of electrons on coupled single electron quantum dots as qubits.

Early experiments on spin manipulation in quantum dots suggested that control of a single spin is much harder task than control of the interaction between a pair of spins. For this reason, a lot of work has been aimed at minimizing the requirements that need to be imposed on single spin operations necessary for a quantum computer to function. While the set of all two-qubit gates is universal and also a randomly chosen two-qubit gate is almost certainly universal, the real problem lies in controlling such gates. In the light of the symmetry trade off described in the previous section, obtaining a desired quantum gate from an asymmetric interaction is hard.

In the original proposal [26] for a quantum computer based on electron spins on single electron quantum dots the effective interaction between spins was assumed to be isotropic (1.3). In fact, isotropic exchange is quite a good approximation to the real effective interaction for most purposes. However, due to the stringent requirements of quantum correction and fault-tolerant quantum computation, quantum gates have to be executed very precisely. The sources of anisotropic interaction between spins considered in the original proposal were direct dipolar coupling of spins and the spin-orbit coupling due to the electric field of the confining potential in the plane of the dots. The anisotropy from both of these sources was found to have negligible effect on the isotropy of the resulting effective interaction of the spins.

After taking Dresselhaus and Rashba contributions to spin-orbit coupling into account, the size of the anisotropic terms in the effective spin interaction was estimated by Kavokin [34] to be between 0.1 and 0.01 of the size of the dominant isotropic exchange interaction. If the gate anisotropy was comparable to the interaction anisotropy, the errors in the isotropic exchange gates due to spin-orbit coupling would make the error correction threshold of $p_{th} \sim 10^4 - 10^8$ unattainable.

The results presented in chapter 2 of this thesis will show that the error rate in isotropic exchange gate is not bounded from below by the size of anisotropic terms in the interaction relative to isotropic terms. To reduce the anisotropy in the gate, we use the freedom to shape the time dependence of the interaction that produces the gate. Since the isotropic part of the gate is determined by the integrated isotropic interaction strength (1.6) only, there is actually quite a lot of freedom left in the choice of time dependence for the Hamiltonian that implements the gate. When the underlying interaction is slightly anisotropic, this additional

freedom in the choice of time dependence can be used to reduce the error in the resulting gate. The required manipulation of the time dependence is remarkably simple. We only need to keep the time dependence of control parameters symmetric in time to prevent the strongest effects of anisotropy in the interaction from appearing in the resulting gate.

In general it is hard to fine tune the time dependence of an interaction to produce a desired unitary evolution. However, because for the specific case discussed in chapter 2 the requirement for the interaction can be stated in terms of symmetry alone, it translates into a very simple constraint on the pulses, that can again be stated in terms of symmetry alone.

With all of these requirements satisfied, the applied gates will be isotropic up to second order in spin-orbit coupling. For the range of anisotropic interaction strengths estimated by Kavokin, the difference in going from the first to the second order can be crucial for implementation of fault-tolerant quantum computation.

1.5.2 Using Spin-Orbit Coupling Effects for Spin Control

Any anisotropy in the effective interaction between spins on coupled quantum dots is an obstacle for isotropic exchange based quantum computing. However, if it is possible to control the form and size of the anisotropic terms in the gate, they can turn into a resource for spin manipulation.

Since single spin manipulation in coupled quantum dots is hard, various authors have proposed schemes for reducing the demands for single spin control in a spin-based quantum computer. Apart from using isotropic exchange for universal quantum computation over qubits encoded into states of three spins, there are various other sets of resources that are also sufficient.

For example, Kempe and Whaley [40] showed that one universal interaction is the XY Hamiltonian

$$H^{xy}(t) = J(t) (S_1^x S_2^x + S_1^y S_2^y), \quad (1.7)$$

where the spin components in plane, chosen to be xy , are coupled with equal strength, while the coupling of the third, out of plane z component is absent. This interaction would enable computation without the need for control over individual spins. Some other possible resources are gates generated by rotated exchange supplemented by the ability to control

local magnetic fields of constant direction, as shown by Benjamin [41], Levy [42] and Wu and Lidar [43]. Most of these proposals use a two spin interaction of reduced symmetry to do some of the work traditionally done by single spin operations.

In general breaking the symmetry makes the problem of finding a scheme for quantum computing easier. In deciding on the value of any particular scheme for reducing requirements placed on single spin manipulation, the crucial criterion is the availability of the considered interactions. Chapter 3 presents a study of the microscopic properties of a system of coupled single electron quantum dots for the purpose of finding a reasonable model for the effective interaction between the spins, including the effects of spin-orbit coupling. A very useful result of this analysis is that axially symmetric anisotropic exchange is available in carefully fabricated quantum dots.

Another original result presented in this thesis and relevant for the proposal for a quantum dot quantum computer is the idea that voltage control over anisotropy can be a useful resource in this system. This new resource may even be sufficient for universal computation when the details of the fabrication of the device and the control over pulse shape are arranged to achieve control over effects of anisotropic exchange in quantum gates, rather than eliminating them.

A scheme for implementing a universal set of quantum gates using axially symmetric anisotropy and pulse shaping is presented in chapter 4. There, control over an anisotropic, but axially symmetric, exchange interaction is considered as a source of control.

The control is achieved through voltage pulses only, which is a tremendous technical simplification. With both axial symmetry of the interaction, enforced by the device fabrication, and time symmetry of pulses that experimenters can enforce at will, the gates between a pair of spins are constrained to a simple form, determined by three parameters only.

While the form is constrained by symmetry, the parameters of a gate will depend on the detailed form of the time symmetric pulse used to implement it. The combination of interaction symmetry and control through time symmetric pulses in principle allows for complete control over encoded two-spin qubits. The amount of control is limited, but our estimates suggest that it is still a significant resource for spin control.

1.6 Summary of Results

The unifying theme of the work presented in this thesis is the use of symmetry as a guiding principle in solving the control problem for a pair of electron spins in coupled single electron quantum dots in the presence of anisotropic terms due to spin-orbit coupling.

The anisotropy caused by spin-orbit coupling is first treated as a problem for those quantum computation schemes which assume that spins interact through purely isotropic exchange, and later as a resource for spin control and application of a universal set of quantum gates.

It is shown that a novel symmetry that depends on the time dependence of the voltage used to switch on and off the exchange interaction can drastically reduce the anisotropy of the resulting quantum gates. Specifically, time-symmetric pulsing, combined with pulse shaping and a choice of local reference frames in the spin spaces of the qubits, reduces the effects of anisotropy in quantum gates from first order in spin-orbit coupling to second order.

A microscopic study of a realistic model of coupled quantum dots shows that dot fabrication can constrain the interaction of the spins to have an axially symmetric form (i.e., a form which is rotationally invariant about a particular axis in spin-space). Combining this axial symmetry of the interaction with time symmetry of the voltage pulses that implement quantum gates allows for a relatively simple solution to the complex problem of spin control. In particular, these gates can be combined to construct a universal set of gates over qubits encoded into pairs of spins. The range of available anisotropies in these gates is identified as a figure of merit for this control mechanism. Estimates of this figure of merit for realistic systems suggest that anisotropy in the spin interaction due to spin-orbit coupling can be a useful resource for spin manipulation.

CHAPTER 2

SPIN-ORBIT COUPLING AS A PROBLEM: REDUCING THE GATE ANISOTROPY

In Chapter 1 we have seen that the isotropic exchange interaction between two spin-1/2 qubits, $H = JS_1 \cdot S_2$, is a useful resource for quantum computation. In particular, this interaction can be used to construct a universal set of quantum gates for properly encoded qubits. Unfortunately, the interaction between electron spins in realistic systems is never exactly of this isotropic form. Even worse, for quantum dots realized in a GaAs two-dimensional electron gas, a good candidate for a solid-state quantum computer, spin-orbit coupling induces relatively large anisotropy in the exchange interaction. In this chapter we address this quantum computing “design problem” and show that by tailoring the time dependence of the control voltage pulses used to switch on and off the exchange interaction between neighboring spins we can make the resulting two qubit quantum gates significantly more isotropic than the underlying interaction.

2.1 Reduction of Control Complexity

The control of a large system of qubits to the extent that allows for the application of an arbitrary unitary evolution is an extremely complex problem. If the system consists of N qubits, the dimension of its state space is 2^N . The dimension of the space of all unitary operators with determinant 1 acting on this state space, i.e. the space of distinct quantum gates that can be applied to it, is $2^{2N} - 1$. The first item in the quantum computing desiderata list, mentioned in chapter 1, specifies that the system of qubits should be scalable. This means that adding new qubits to a computer should not significantly slow down its operation. This suggests that the control problem is very hard, because the dimension of

the gate space grows exponentially with the number of qubits while control has to remain possible for any number of qubits.

The complexity of this general control problem is more apparent when the gates are considered in terms of interactions that should be controlled in order to implement them. A matrix that represents a given gate in the computational basis of N qubits is an element of the group $SU(2^N)$, and is therefore an exponential of the corresponding $su(2^N)$ Lie algebra element. At the more intuitive level we may imagine the algebra element exponentiation as a gate implementation that consists of switching on the appropriate interaction H^{int} , keeping it on for some predetermined period of time and then switching it off to implement the gate

$$U = \exp -i\lambda H^{int}, \tag{2.1}$$

where $-i\lambda H^{int}$ is a convenient representation of the Lie algebra element that allows us to talk about the overall strength of interaction λ . (Here, and throughout this thesis, we will set Planck's constant \hbar equal to one.) Being able to apply arbitrary gates to the qubits thus corresponds to being able to switch on and off arbitrary interactions between qubits. This set of interactions includes all one-body terms interacting a qubit with external fields, all two-body interactions of arbitrary pair of qubits, all three-body interactions that naturally appear only as models of more fundamental two body interactions in systems of many particles, and all n -body interactions that can be imagined, which cannot be realized nor controlled. Obviously, a drastic simplification of control is necessary in order to move this complete control program anywhere further.

Fortunately there is a drastic simplification of the complete control problem, due to the notion of a universal set of gates. An analogous problem is also present in a classical digital computers. A computation consisting of taking an N bit input and transforming it into an M bit output of similar size is application of one out of $(2^M)^{(2^N)}$ possible transformations. The task would be impossible if each transformation corresponded to separate tuning of interactions in a computer. From the Turing machine model we can learn that one extremely complex tuning of interactions can be broken down into a possibly long succession of very simple operations. Similarly a quantum computation can proceed with repeated application of gates from a much smaller universal set. Such small sets of universal quantum gates do exist, as reviewed in chapter 1. More importantly, some universal sets consist solely of

gates that only act on one or two qubits at a time [44]. In the representation of gates by interactions (2.1), this means that it is sufficient to control one and two body interactions that commonly appear in nature. Repeated application of gates from a universal set can produce an arbitrary gate on a system of qubits of arbitrary size. Thus it is possible to trade a very complex construction of a gate that acts on a large collection of qubits for the repeated application of much simpler gates from a universal set.

2.2 Isotropic Exchange

In choosing a universal set of quantum gates for a particular design of a quantum computer, it is important to choose gates produced by interactions that are natural for the particular physical system being considered. In this thesis we are considering qubits that are encoded in electron spins. Spin $1/2$ is a good candidate for a qubit because it perfectly satisfies the desiderata requirement of having a well defined logical space. This requirement calls for having a small probability for a system to be in a state that does not correspond to any qubit state. For spin $1/2$ this probability is exactly zero, because the entire state space is two-dimensional. Another nice property of these qubits is that spin degrees of freedom are well isolated from all the other degrees of freedom. The criterion for having qubits with known properties hosted in systems that are studied in detail suggests electron spins in semiconductors are good candidate qubits. Furthermore, the rich experience gathered in studies of semiconductors in electronics eases the problems of fabrication and control of devices. It is then natural to ask which interactions of electron spins in semiconductors can efficiently produce quantum gates.

Recent experiments have shown that spins in semiconductors can have surprisingly long coherence times. For example, the experimental observation of long spin coherence times for electrons in GaAs in the experiments of Kikkawa and Awschalom [45] spurred interest in the possibility of using electron spin as a carrier of quantum information. Long coherence time is an indication of isolation of the spin degrees of freedom from both electron orbital degrees of freedom and degrees of freedom of the crystalline lattice.

It is interesting to note that the idealized assumption of perfect isolation of the spin degrees of freedom would determine the form of effective interaction between the spins.

Good isolation of spin from orbital degrees of freedom suggests that the Hamiltonian for an electron is, to a good approximation, of the form

$$H^e = H^{orb} \otimes \mathbf{1}^{spin}, \quad (2.2)$$

and therefore acts nontrivially only on the orbital degrees of freedom of the electrons. Such an interaction is invariant under arbitrary rotations in spin space. This suggests that the spin degree of freedom does not play any role in electron dynamics, and that the effective spin Hamiltonian for electrons is just the identity. However, this is not the case. Since electrons are fermions, the allowed wave functions of a pair of electrons must be antisymmetric with respect to exchange. Arbitrary transformation of spins can turn an antisymmetric spin state into symmetric, and the effective Hamiltonian can not be invariant under such a transformation.

As an example we may consider a state of a pair of electrons

$$|\psi\rangle = \frac{1}{2} (|ab\rangle^{orb} + |ba\rangle^{orb}) \otimes (|\uparrow\downarrow\rangle^{spin} - |\downarrow\uparrow\rangle^{spin}), \quad (2.3)$$

where a and b denote arbitrary orthogonal electron orbital states and \uparrow and \downarrow are spin states with projections $1/2$ and $-1/2$ on arbitrarily chosen quantization axis. If the Hamiltonian was symmetric under arbitrary spin transformation, the state

$$|\psi\rangle = \frac{1}{2} (|ab\rangle^{orb} + |ba\rangle^{orb}) \otimes (|\uparrow\uparrow\rangle^{spin} - |\downarrow\downarrow\rangle^{spin}), \quad (2.4)$$

obtained from (2.3) by rotation of the first spin would be an equally valid state of the pair of electrons. However, (2.4) is symmetric under the exchange of two electrons and can not be a state of a pair of fermions.

This means that even though the Hamiltonian acts trivially on spin states in (2.2), the effective spin Hamiltonian is not the identity, unless we explicitly take care of the electron statistics. Due to symmetry it must only be a constant in the subspace of all the symmetric spin states and possibly a different constant in the subspace of antisymmetric spin states. This fact alone fixes the form of effective spin Hamiltonian. Another way to find the form of effective spin Hamiltonian of a pair of electron spins interacting through (2.2) is through rotational symmetry in spin space. The real rotations that rotate both spins are symmetries of the system, so that the Hamiltonian has to be invariant under such rotation. There is

only one invariant quantity, up to an irrelevant constant, that can be constructed from two spins, the scalar product. This leads to the conclusion that the effective interaction of spins in the case when the electron Hamiltonian acts trivially in the spin space is

$$H^{int} = J\mathbf{S}_1 \cdot \mathbf{S}_2, \quad (2.5)$$

where J is a coupling constant determined by the details of orbital interaction and orbital states of electrons with spins $\mathbf{S}_{1,2}$.

Isotropic exchange interaction appears under rather general assumptions that concern only the electron Hamiltonian, and do not assume anything about the structure in which the electrons reside. Generically, the largest terms in a Hamiltonian of a pair of electrons are kinetic energy, interaction with external electromagnetic fields and Coulomb repulsion. All of these terms are spin independent and to a good approximation the electron Hamiltonian is of the form (2.2). The isotropic effective spin interaction arising from these terms is then the strongest interaction in a pair of electron spins.

This conclusion about the specific form of effective spin-spin interaction arising from the general properties of the underlying Hamiltonian is important from the point of view of spin control. There is a guarantee that the effective interaction will have a simple and symmetric form, even when the system itself is not symmetric. This fact was noted in the spin-based quantum computing proposals early on [26]. The most important aspect of this derivation is the fact that simple constraints on the Hamiltonian make the control of interaction between spins remarkably easy. No matter how the device is fabricated, no matter what the symmetry of the electron orbital wave functions and no matter which control mechanisms act on the orbital degrees of freedom, the effective spin interaction will have the simple form (2.5), as long as the spin degrees of freedom are neither directly affected by the interaction nor coupled to the orbital degrees of freedom. At every moment during the gate operation the effective interaction between spins will be

$$H^{int}(t) = J(t)\mathbf{S}_1 \cdot \mathbf{S}_2, \quad (2.6)$$

and only the coupling strength $J(t)$ will change. Since the set of available interaction is so constrained, all the complexity of control will be described with a single function of time, $J(t)$.

2.2.1 Simple Control

Simplicity of control brought by the triviality of spin part of the electron Hamiltonian does not end with the highly symmetric form (2.6) of the effective interaction. This symmetric interaction also implies simplicity of the quantum gates that can be produced.

Let us imagine that we are applying a gate using an arbitrary mechanism that produces a time-dependent orbital Hamiltonian while the spin interaction is both trivial and does not couple orbital and spin degrees of freedom. The only constraint we put on the gate is that its application takes finite time. The initial Hamiltonian at time $t \rightarrow -\infty$ and final Hamiltonian at $t \rightarrow \infty$ then must describe electrons in some orbital states with decoupled spins.

Spherical symmetry of the spin part of the electron Hamiltonian guarantees that the effective spin interaction is isotropic, with the strength of the effective isotropic coupling going to zero as time goes to plus or minus infinity. Quite generally the two spin gate produced by a time-dependent effective Hamiltonian $H^{int}(t)$ is given by the time ordered exponential

$$U = T \exp -i \int_{-\infty}^{\infty} H^{int}(t) dt, \quad (2.7)$$

where the symbol T represents the usual time ordering. The meaning of time ordering is that whenever Hamiltonians taken at different times appear in expansion of the exponential of (2.7), they should be commuted past each other so that the Hamiltonians with labels corresponding to earlier times act before Hamiltonians taken at latter times. For any product $H(t_1)H(t_2) \dots H(t_n)$ that appears in the exponential, it must be true that $t_1 \geq t_2 \geq \dots \geq t_n$.

In the case of an isotropic effective coupling, spin Hamiltonians taken at different times commute, because they are proportional to the same operator, $\mathbf{S}_1 \cdot \mathbf{S}_2$. The time ordering is then trivial and the resulting gate is of the extremely simple form

$$U(\lambda) = \exp -i\lambda \mathbf{S}_1 \cdot \mathbf{S}_2, \quad (2.8)$$

where the only parameter that determines the gate, λ , is the integrated interaction strength

$$\lambda = \int_{-\infty}^{\infty} J(t) dt. \quad (2.9)$$

This simplification in going from the most general unitary operator acting on two spins, to the extremely simple gate (2.8), determined by a single parameter is guaranteed whenever the

spin Hamiltonian is trivial and spin and orbital degrees of freedom do not interact. Because of this symmetry, all the potential complexity of arbitrary control mechanism is bundled in a single parameter λ , which is simple function of time dependent effective Hamiltonian.

This chain of symmetry induced simplifications leads from the reasonable assumption about the form of the electron Hamiltonian, through the specific form of the effective interaction of a pair of spins to the highly symmetric and simple form of any gate that can be applied using such an interaction, no matter how complex the control mechanism itself is. Such a simplification that is obtained without any need for special care about the device fabrication or the procedure for applying the gate suggests that the isotropic exchange gates (2.8) should be among the easiest gates to apply. It will be interesting to compare this bold prediction with the assessment of the actual possibility of control achievable in experiments on electron spins in quantum dots.

2.2.2 Universal Gate Set Using Isotropic Exchange

The gate produced by a time-dependent electron Hamiltonian with trivial spin part is very symmetric. It is invariant under rotations in spin space. In light of the symmetry trade off from the introductory chapter, a symmetry that allows for easy control of a single gate will make the problem of realizing a universal gate set construction harder if only the isotropic exchange gates are used.

If single qubit gates are also available, isotropic exchange can be used for a simple universal gate set construction. Isotropic exchange gates can add the necessary two-body interaction between spins to single qubit rotations to construct a universal set of gates. The standard choice of a universal set of quantum gates consists of all single qubit rotations and the CNOT gate. When qubits are spins of spin 1/2 electrons, we can choose the logical qubits as $|0\rangle = |\uparrow\rangle$ and $|1\rangle = |\downarrow\rangle$, and single spin rotations correspond to single qubit operations. The construction of a CNOT gate can be done using isotropic exchange gate \sqrt{SWAP} and single spin rotations, as shown by Loss and DiVincenzo [26];

$$CNOT = (\mathbf{1} \otimes H) \sqrt{SWAP} (\sigma_z \otimes \mathbf{1}) \sqrt{SWAP} (\mathbf{1} \otimes H), \quad (2.10)$$

where the square root of swap gate is

$$\sqrt{SWAP} = \exp -i \frac{\pi}{2} \mathbf{S}_1 \cdot \mathbf{S}_2, \quad (2.11)$$

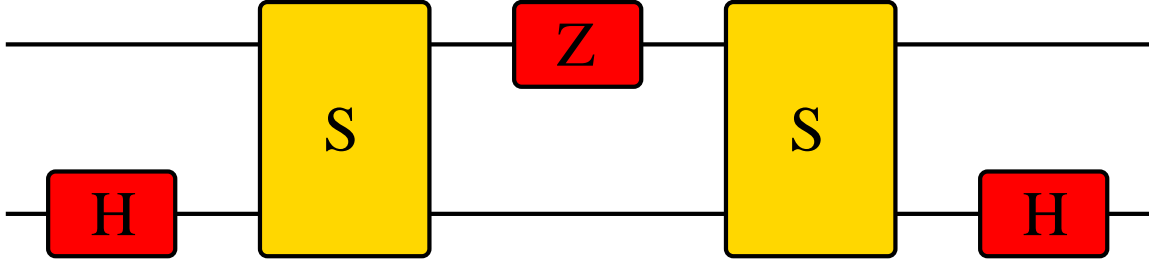


Figure 2.1. Controlled not (CNOT) gate construction using isotropic exchange gate $S \equiv U(\frac{\pi}{2}) = \sqrt{SWAP}$ and single qubit gates $Z = \sigma_z$ and Haddamard gate H . This construction demonstrates that isotropic exchange gates and single qubit rotations are sufficient for universal quantum computation over spin qubits.

and the Hadamard gate in the computational basis is

$$H = \frac{1}{\sqrt{2}} \begin{bmatrix} 1 & 1 \\ 1 & -1 \end{bmatrix}. \quad (2.12)$$

This construction is also shown in [Fig.2.1]. Therefore, control over isotropic exchange and single spin rotations is sufficient for universal quantum computation.

The perceived relative ease of applying the isotropic exchange gates on pairs of qubits stimulated a lot of research into the possibility of delegating some of the work performed by the single spin gates in the standard universal set of CNOT and single spin rotations to two spin gates.

The problem with isotropic exchange gates as a resource for universal quantum computation lies in the fact that they are too symmetric for this task if the qubits are taken to be the individual spins. Since the operator $\mathbf{S}_1 \cdot \mathbf{S}_2$ that appears in the isotropic exchange gates commutes with all of the spin rotations, spin quantum numbers remain invariant under the action of isotropic exchange gates. A universal set of gates must allow for application of an arbitrary unitary operation on a system of qubits and thus can not have any symmetry. Therefore, isotropic exchange gates can not be universal on spin qubits.

If universal quantum computation is to be performed using only isotropic exchange gates, logical qubit states must all have the same total spin and spin projection on arbitrary axis, because isotropic exchange gates cannot change these quantum numbers. The smallest system of spin-1/2 particles with a two dimensional subspace of states that all have the same

total spin and its projection on a fixed axis consists of three particles. In this case there are two subspaces with the required properties, states with $S = 1/2$, $S_z = 1/2$ and states with $S = 1/2$, $S_z = -1/2$. Universal quantum computation using isotropic exchange gates is indeed possible in both of these spaces. The explicit universal gate set constructions can be found in [32], and is based on the knowledge gathered in more general study of universal sets of quantum gates over encoded qubits [33]. One- and two-qubit gate constructions over encoded qubits are reproduced in [Fig.1.9].

2.3 Anisotropy

Hopefully we have convinced the reader that isotropic exchange is a powerful resource for quantum computation. It has the potential to be easy to control and at the same time sufficient for universal quantum computation over encoded qubits.

Unfortunately, the assumptions behind the simple argument for isotropic exchange as an effective spin interaction almost never hold exactly. In reality there will exist a nontrivial spin Hamiltonian and a nontrivial coupling of spin and orbital degrees of freedom. For example, a pair of spins will always interact through dipolar coupling of magnetic moments

$$H^{dip} \propto \frac{\mathbf{S}_1 \cdot \mathbf{S}_2 - 3(\mathbf{S}_1 \cdot \hat{\mathbf{r}})(\mathbf{S}_2 \cdot \hat{\mathbf{r}})}{r^3}, \quad (2.13)$$

where the vector \mathbf{r} connects the two spins. Another important source of anisotropy is spin-orbit coupling. Electrons in any solid state device will always move in the presence of the electric field produced by the background ions and the other electrons in the system. A Lorentz transformation from the frame of reference in which the lattice is stationary into the electron rest frame will transform this electric field into an electromagnetic field with a magnetic component of the order v/c , and the electron magnetic moment $g\mu_B\mathbf{S}$ will couple to that magnetic field. This coupling of the orbital quantity v to the electron spin will create a part of the Hamiltonian that couples orbital and spin degrees of freedom, leading to anisotropy. The source of this electric field can either be the external field used to localize electron spin qubit or very strong internal field in the crystal.

Terms that cause anisotropy are generically weaker than the kinetic energy, direct coupling to electric field and Coulomb repulsion terms responsible for isotropic exchange. However, the tolerance of a quantum computer to errors is low. It can function in the

presence of errors, but only if the probability of error in the gate operation is smaller than the error correction threshold p_{th} that is estimated to be $10^{-4} < p_{th} < 10^{-8}$ [24]. Demands for precision in the gate operation are very high and it is not obvious that various anisotropies are not going to push the deviation of a realistic gate from the intended isotropic exchange gate far enough to cross the threshold.

The anisotropy of the spin interaction in real semiconductor structures was first recognized as a potential problem for quantum computation by Kavokin [34]. His estimate for the strength of the anisotropic interaction relative to the dominant isotropic exchange was $\beta^K \sim 0.1 - 0.01$. If we imagine that a quantum gate is applied by switching on and off a slightly anisotropic exchange interaction instead of one which is purely isotropic, the size of Kavokin's β^K will then be the size of the amplitude for transitions into a state that generates an error in the gate. Therefore, the probability of error coming from this anisotropy will be of the order $(\beta^K)^2 \sim 10^{-2} - 10^{-4}$ and most probably larger than the error correction threshold.

Since isotropic exchange gates are controlled via simple voltage pulses and are still powerful enough for universal quantum computation these errors due to anisotropy are very unwelcome. This chapter describes in detail a procedure that allows for isotropic exchange based spin manipulation *even in the presence of anisotropic corrections predicted by Kavokin*. The procedure reduces the influence of anisotropy in the spin interaction on the applied gate, turning the part of the gate produced by the anisotropic interaction from a first order effect in the size of anisotropy into a second order effect. This reduction may push the error rate below the error correction threshold.

2.4 Time Dependence, Interaction and the Gate

In a quantum computer based on spin 1/2 qubits, the goal of spin manipulation through any two body interaction is to reliably produce a unitary transformation on a pair of spins. We are always interested in the gates that the interaction of spins produces, and (almost) never in the interaction itself.

The concept of a quantum gate is very similar to the S matrix of scattering theory. Let us consider a quantum gate acting on a pair of spins through a two-body interaction $H^{int}(t)$. At the initial $t \rightarrow -\infty$ and final $t \rightarrow \infty$ time the spins are decoupled, and their

states are $|\psi^{in}\rangle$ and $|\psi^{out}\rangle$, respectively. By definition, the gate is an evolution operator that connects these two states. If the system does not decohere or leak into a noncomputational state, the evolution operator U is unitary, and $|\psi^{out}\rangle = U|\psi^{in}\rangle$. The gate is then completely specified by the mapping from initial to final state. Obviously there are many time dependent interactions that produce the same gate.

Calculation of the gate produced by a given time dependent interaction involves solving the time-dependent Schrödinger equation for the evolution operator

$$i\frac{dU(t)}{dt} = H^{int}(t)U(t), \quad (2.14)$$

where $U(t)$ is the evolution operator evolving a state from time $-\infty$ to time t . The initial condition for $U(t)$ is that the initial state is indeed the state of the system at the beginning of evolution,

$$\lim_{t \rightarrow -\infty} U(t) = 1. \quad (2.15)$$

Equation (2.14) can not be solved analytically for the most general interaction H^{int} . The solution of this equation determines the gate produced by a given time-dependent interaction. As stated above, this correspondence between gates and time dependent interactions is not one to one. There are many time dependent interactions that produce the same gate.

2.4.1 Control through Pulse Shaping

From (2.14) we can also see that the quantum gate produced by a given time-dependent interaction is not determined solely by the form of the spin interaction. The specific form of the time dependence also plays a role. For example, the simple (and commonly used) model of a quantum gate applied by switching a constant interaction sharply on and off is a gross oversimplification in cases when the Hamiltonians describing the spin interaction taken at different times do not commute with each other.

In a quantum computer, the time dependence of the interaction will be under external control. For electron spins on coupled quantum dots, the interaction is a function of the potential on the electrode that separates two neighboring dots. This voltage and its time dependence are controllable.

This controllability can in principle be used to apply the quantum gate using a time dependent Hamiltonian, where the gate is determined by solving the Schrödinger equation

(2.14). The time dependence of the voltage can be therefore be considered as a handle for spin control. The voltage dependent Hamiltonian that causes a pair of spins to go through evolution that starts with a pair of noninteracting spins, continues with the change of state governed by some time dependent interaction and ends again in the decoupled spins in final state will be called a pulse. The corresponding voltage pulse is a time dependent potential on the electrode that is used to implement the gate.

The most important results presented in this thesis are insights into symmetry based control using time dependence. Time dependence is usually a rather weak control mechanism. Here we find that it is not weak because there are a few different gates that can be applied by carefully choosing the time dependence of the pulse. In fact, for an interaction without any symmetry, pulse shaping of the Hamiltonian can in principle produce an arbitrary gate acting on a pair of spins. The problem with this mechanism is in the complexity of required control.

2.4.2 Voltage Control Program

In the scenario where all the gates are to be applied by pulses of a two spin interaction, the difficulties are in finding the appropriate pulse forms and the generic complexity of such pulses. To find the required pulse shape, it is first necessary to solve the Schrödinger equation (2.14) with correct model for the interaction H^{int} . Even with the overly optimistic assumption that it is possible to find the correct model for an interaction in realistic system and a reasonable assumption that the resulting equation can be numerically solved to the required precision, the problem of control would not really be solved.

This solution would give the gate as a function of the time dependent Hamiltonian, which is an inverse problem of what we need for control. If the hard problem of inverting these solutions to find a time dependence of the correct model Hamiltonian needed to implement the gate can be solved, we would be able to know which time dependent Hamiltonian should be applied.

Only with yet another bold assumption, that a voltage pulse producing the required time dependent interaction can be found, would we be able to formally solve the control problem.

Apart from being extremely hard to obtain, this formal solution to the control problem is utterly useless. The list of unrealistic assumptions needed for formally solving the control

problem is quite impressive and includes the ability to model the realistic effective interaction between two spins in a semiconductor, the ability to solve the time dependent Schrödinger equation with this kind of Hamiltonian, the ability to invert the solution in order to find a time dependent realistic interaction that produces a given gate, and finally the ability to find the voltage pulse causing such a time dependent interaction. The list of problems with using time dependence as a control mechanism does not end there. Formal solution to the control problem, even if it is possible to find, is a voltage pulse as a function of two-spin quantum gate. The form of voltage pulse will generically be too complex for the contemporary or future electronics to produce. One of the requirements for a quantum computer from the desiderata list requires that the gates should be fast enough to prevent decoherence from putting the error rate of the gate beyond the error correction threshold. Therefore, voltage pulses would have to be both precision crafted and very fast. A drastic simplification in this scenario of achieving the spin control is necessary if the time dependence is to be useful in the control of spins.

The voltage control of a two spin system is a complex problem. However, the voltage pulses are technically the simplest mechanisms for control and it would be encouraging if the voltage control over available interactions proves to be sufficient for the control required for the universal quantum computation. Applicability of the voltage control is determined by the available interactions. It was already shown that highly symmetric isotropic exchange can in principle be easily controlled, and because of its simple form, the fine tuning of pulse shapes is not needed in this case.

In this chapter the freedom of crafting the pulse shape beyond what is needed for the control over isotropic part of interaction is used to reduce the effects of the remaining anisotropic terms on the performed gate. In the final analysis, the applicability of this approach is determined by the form of effective spin interaction in the actual device. In the case of spin-orbit coupling caused anisotropy, the symmetry of the underlying interaction, manifested in the form of the effective coupling of the spins, allows for the simple design of pulse shapes that reduce the gate anisotropy. However the problem of control using general anisotropic coupling is still practically unsolvable. For general anisotropy, problems connected with the stringent requirements on control of pulse shape make voltage control impractical.

2.5 Simplifications from Symmetry

A drastic simplification of the control required to reduce the effects of anisotropy in a quantum gate implemented by the pulse of an almost isotropic interaction comes from symmetry. An isotropic interaction is itself highly symmetric, and the dominant anisotropic terms in the effective spin interaction will also have definite symmetries. Regularity in the interaction between spins leads to simple predictions about the form of the resulting gate. In the case of small anisotropy caused by spin-orbit coupling these predictions are sufficient to prepare a recipe for the pulse control that reduces the errors in isotropic exchange-based gates below the error correction threshold.

The analysis of this chapter is most useful for reducing the errors in isotropic exchange gates caused by spin-orbit coupling. An appropriately modified procedure can in principle reduce anisotropy in gates caused by anisotropies of different origin. The quantum computer design that inspired this procedure is the coupled single electron quantum dots proposal of Loss and DiVincenzo [26].

In this proposal the only significant source of anisotropy is spin-orbit coupling. Symmetry properties of spin-orbit coupling allow for a needed drastic simplification of the control problem that is sufficient for the removal of first-order anisotropy in a quantum gate.

The source of spin-orbit coupling for a free particle is, as we have described above, a relativistic effect. Electron that moves in the purely electric field experiences an electromagnetic field with nonzero magnetic component in its rest frame. The magnetic field strength is of the order v/c , where v is the electron velocity, and c is the speed of light. This magnetic field couples to electrons magnetic moment which is proportional to spin. This coupling includes both the orbital degrees of freedom through the velocity v and the spin degrees of freedom through the electron spin. In a crystal, the form of this coupling is

$$H^{SO} = \mathbf{h}(\mathbf{k}) \cdot \mathbf{S}, \quad (2.16)$$

where $\mathbf{h}(\mathbf{k})$ is an odd function of electron crystal momentum \mathbf{k} , and \mathbf{S} is electron spin (see chapter 1).

In a semiconductor system with a localized pair of electrons, the dominant effective interaction between spins will be isotropic exchange. If spin-orbit coupling is treated as

a small correction to this dominant interaction, it is useful to write down the effective interaction between spin at any time t as

$$H^{int}(t) = J(t) (\mathbf{S}_1 \cdot \mathbf{S}_2 + A^{int}(t)), \quad (2.17)$$

where $J(t)$ is the instantaneous strength of the isotropic part and $A^{int}(t)$ is the strength of anisotropic part of the interaction, scaled by the size of the dominant isotropic part.

The symmetry of spin-orbit coupling under parity can help us find the structure of the anisotropic term A^{int} of (2.17). With complete generality, we can write down A^{int} as

$$A^{int}(t) = \boldsymbol{\beta}^{int}(t) \cdot (\mathbf{S}_1 \times \mathbf{S}_2) + \mathbf{S}_1 \cdot \boldsymbol{\Gamma}^{int}(t) \cdot \mathbf{S}_2, \quad (2.18)$$

where $\boldsymbol{\beta}^{int}(t)$ is a vector and $\boldsymbol{\Gamma}^{int}(t)$ is a symmetric rank two tensor. This particular parametrization of the anisotropic part of the interaction in (2.17) is useful because it separates terms that are of different order in spin-orbit coupling. The term $\boldsymbol{\beta}^{int}$ acting between localized spins and caused by spin-orbit coupling was considered for the first time from the point of view of symmetry by Dzyaloshinskii [46] and microscopically by Moriya [47]. They found that the antisymmetric anisotropy term $\boldsymbol{\beta}^{int}$ is first order in the strength of spin-orbit coupling, while the symmetric anisotropy term $\boldsymbol{\Gamma}^{int}$ is second order in spin-orbit coupling.

This observation of Dzyaloshinskii and Moriya is a simple consequence of the fact that spin-orbit coupling is odd under parity. This can be seen by noting that under inversion, the crystal momentum of a given electron changes sign $\mathbf{k} \rightarrow -\mathbf{k}$, while its spin, which is an axial vector, does not $\mathbf{S} \rightarrow \mathbf{S}$. Thus, since the spin-orbit field $\mathbf{h}(\mathbf{k})$ is an odd function of \mathbf{k} , the spin-orbit Hamiltonian $H_{SO} = \mathbf{h}(\mathbf{k}) \cdot \mathbf{S}$ also changes sign $H_{SO} \rightarrow -H_{SO}$ under inversion. Therefore, the $\boldsymbol{\beta}^{int}(t)$ term of (2.18) that couples to a spin operator ($\mathbf{S}_1 \times \mathbf{S}_2$) that is odd under exchange of two spins must itself be odd inversion and at most first order in spin-orbit coupling strength. And by similar reasoning the $\boldsymbol{\Gamma}^{int}(t)$ term of (2.18) that couples to a spin operator that is even under exchange of the two spins must be of even order in spin-orbit coupling. Since the interaction is isotropic when spin orbit-coupling is absent ($\boldsymbol{\Gamma}^{int}(t) = 0$ in that case), $\boldsymbol{\Gamma}^{int}(t)$ is at most second order in spin-orbit coupling strength.

2.6 Removal of First Order Anisotropy

The separation of anisotropy into terms of different order in spin-orbit coupling strength is helpful in the search for voltage controlled gates with reduced anisotropy. When the task is specified to eliminating the first order anisotropy, the hierarchy of terms allows for calculating the gate applied by pulse (2.17) using perturbation theory with spin orbit coupling strength playing the role of a small parameter.

2.6.1 Calculation of the Gate

We have found that in our analysis it is useful to define something we refer to as the “gate Hamiltonian.” To define the gate Hamiltonian imagine that a given quantum gate implemented by a particular pulse (i.e. time-dependent interaction) was in fact implemented by switching on and off a constant Hamiltonian — this constant Hamiltonian is then what we refer to as the gate Hamiltonian. Put another way, the gate Hamiltonian is nothing more than the Hermitian operator which is exponentiated to produce a given quantum gate. As we shall see, the usefulness of the gate Hamiltonian is that it makes the symmetries of the corresponding quantum gate transparent.

A priori there is no reason to expect the gate Hamiltonian to have any special form — it can be the most general two-spin Hamiltonian possible. A useful parametrization of the gate Hamiltonian, which is analogous to the parametrization of interaction discussed above, is then

$$\begin{aligned}
 U &= \exp -i\lambda H \equiv \exp -i\lambda (\mathbf{S}_1 \cdot \mathbf{S}_2 + A) \equiv & (2.19) \\
 &\equiv \exp -i\lambda \left(\mathbf{S}_1 \cdot \mathbf{S}_2 + \boldsymbol{\beta} \cdot (\mathbf{S}_1 \times \mathbf{S}_2) + \mathbf{S}_1 \cdot \boldsymbol{\Gamma} \cdot \mathbf{S}_2 + \frac{\boldsymbol{\alpha}}{2} \cdot (\mathbf{S}_1 - \mathbf{S}_2) + \frac{\boldsymbol{\mu}}{2} \cdot (\mathbf{S}_1 + \mathbf{S}_2) \right),
 \end{aligned}$$

where the gate parameter λ measures the overall strength of the pulse, and the remaining parameters are vectors $\boldsymbol{\alpha}$, $\boldsymbol{\beta}$ and $\boldsymbol{\mu}$ and a rank two symmetric tensor $\boldsymbol{\Gamma}$. The interaction H appearing in the gate parametrization (2.19) is the gate Hamiltonian and time independent operator A is the anisotropic part of the gate Hamiltonian.

The gate parameters ($\boldsymbol{\alpha}$, $\boldsymbol{\beta}$, $\boldsymbol{\mu}$, $\boldsymbol{\Gamma}$) will depend on the the details of the pulse shape (2.17). Note that the parameter λ is arbitrary, because only the product λH enters the definition of the gate Hamiltonian. The freedom of choosing the value of λ can be used to define it as

Table 2.1. Behavior of gate parameters under parity (P) and time reversal (T). Quantities that are even(odd) under parity are of even(odd) order in spin interaction anisotropy. Gate parameters odd under time reversal vanish from the gates implemented by time-symmetric pulses.

symmetry	λ	$\boldsymbol{\alpha}$	$\boldsymbol{\beta}$	$\boldsymbol{\Gamma}$	$\boldsymbol{\mu}$
P	+	-	-	+	+
T	+	-	+	+	-

$$\lambda = \int_{-\infty}^{\infty} J(t) dt. \quad (2.20)$$

With this convention, λ is the control parameter of the isotropic gate that would be implemented in the limit of zero spin-orbit coupling strength. This definition allows us to see that the gate Hamiltonian H defined in (2.19) as an isotropic gate Hamiltonian we would like to implement plus a correction A due to the anisotropy of interaction.

2.6.1.1 Parity and Time Reversal

Before starting the calculation of gate, we can do a quick symmetry analysis, analogous to the symmetry analysis of Dzyaloshinskii, and estimate the sizes of the terms which will appear in the gate Hamiltonian. This analysis is summarized in table (2.6.1.1). Recall that spin-orbit coupling, which produces all the anisotropic terms in the gate, is odd under parity $\mathbf{S}_1 \leftrightarrow \mathbf{S}_2$. The gate parameters also behave simply under parity; the vectors $\boldsymbol{\alpha}$ and $\boldsymbol{\beta}$ change sign, while the vector $\boldsymbol{\mu}$ and symmetric rank two tensor $\boldsymbol{\Gamma}$ remain invariant. That implies that parameters $\boldsymbol{\alpha}$ and $\boldsymbol{\beta}$ are first order in spin orbit coupling, while $\boldsymbol{\mu}$ and $\boldsymbol{\Gamma}$ are second order. Another important symmetry of spin-orbit coupling is time reversal ($\mathbf{S}_i \rightarrow -\mathbf{S}_i$), where $i = 1, 2$. Under time reversal, parameters $\boldsymbol{\beta}$ and $\boldsymbol{\Gamma}$ are invariant, while $\boldsymbol{\alpha}$ and $\boldsymbol{\mu}$ change sign. The terms $\boldsymbol{\alpha}$ and $\boldsymbol{\mu}$, odd under time reversal and corresponding to staggered and uniform magnetic field, will vanish unless time reversal symmetry is broken.

The symmetry properties summarized in Table (2.6.1.1) immediately give us a method to eliminate one of the strong (i.e. first-order in spin-orbit coupling) anisotropic terms from the gate. Since the interaction (2.17, 2.18) is invariant under time reversal, the only way to create the $\boldsymbol{\alpha}$ term, which is odd under time reversal and first order in spin-orbit coupling, is to break time reversal symmetry. And the only possible source of time reversal symmetry

breaking is in the actual time dependence of the pulse used to implement the gate, as we prove in the next section.

2.6.1.2 Time Reversal Symmetric Interactions and Time Symmetric Pulses

In this section, we prove the following important result: A time symmetric pulse will preserve the time reversal symmetry of the resulting gate.

It is important to make the distinction between invariance under time reversal of the interaction Hamiltonian and the time symmetry of the pulse. Invariance under time reversal of the interaction is here taken in the standard sense. Let us consider some Hamiltonian and the evolution governed by it, starting at time t_0 from the state $|\psi(t_0)\rangle$. We let the evolution proceed under the influence of this Hamiltonian to time t . At time t , we change the current state of the system $|\psi(t)\rangle$ into time reversed version $T|\psi(t)\rangle$ and let the system keep evolving under the influence of the Hamiltonian from t to $t + (t - t_0)$. If the state of the system at $t + (t - t_0)$ is the same as the initial state at t_0 for an arbitrary initial state and values of t and t_0 , we say that the Hamiltonian is invariant under time reversal. Time symmetry of the pulse, on the other hand, means simply that the time dependent Hamiltonian $H(t)$ is an even function of time, $H(t_0 + t) = H(t_0 - t)$ for every time t , where t_0 is the center of the pulse. Time symmetric pulses are easy to produce because the time symmetry of the classical control parameters, which can be, in principle, directly controlled in an experiment, guarantees that the corresponding Hamiltonian pulse will also be time symmetric.

We can now precisely state the proposition to be proved: A time symmetric pulse of a time reversal symmetric Hamiltonian produces a time reversal symmetric gate. Here is a formal proof of this statement.

Let $H_P(t)$ be a time symmetric pulse i.e. $H_P(t) = H_P(-t)$ for every time t , and let it be invariant under time reversal at any point in time. Evolution generated by this time dependent Hamiltonian, $U = \exp -i\lambda H$ has a time reversal symmetric gate Hamiltonian H .

The time reversal operation for any quantum system can be represented by an antiunitary operator Θ [48]. An orthonormal basis $\{|M_i\rangle\}$ for the Hilbert space of this system is time symmetric if

$$\Theta|M_i\rangle = |M_i\rangle \tag{2.21}$$

for all i .

For any Hamiltonian H acting on a state $|M_i\rangle$ in this basis we can write

$$H|M_i\rangle = \sum_j \langle M_j|H|M_i\rangle|M_j\rangle. \quad (2.22)$$

Under time reversal H is transformed into $\Theta H\Theta^{-1}$. Using the invariance of the $\{|M_i\rangle\}$ basis and the antiunitarity of Θ we can then also write

$$\Theta H\Theta^{-1}|M_i\rangle = \Theta H|M_i\rangle = \Theta \sum_j \langle M_j|H|M_i\rangle|M_j\rangle = \sum_j \langle M_j|H|M_i\rangle^*|M_j\rangle. \quad (2.23)$$

Comparing (2.22) and (2.23) leads to the conclusion that if H is time reversal symmetric, i.e. $H = \Theta H\Theta^{-1}$, then the Hamiltonian matrix is purely real in the $\{|M_i\rangle\}$ basis.

Since H is real in the $\{|M_i\rangle\}$ basis if and only if H is time reversal symmetric it follows that the unitary operator $U = \exp -i\lambda H$ is symmetric, i.e. $U = U^T$, if and only if H is invariant under time reversal.

Now consider a time dependent pulse $H_P(t)$. We assume that $H_P(t)$ is invariant under time reversal at all times, i.e. $H_P(t) = \Theta H_P(t)\Theta^{-1}$ for all t . The corresponding unitary evolution operator U which evolves the system from time t_I to t_F can be written

$$U = \lim_{N \rightarrow \infty} U(t_N)U(t_{N-1}) \cdots U(t_2)U(t_1) \quad (2.24)$$

where

$$U(t_i) = e^{-i\Delta t H_P(t_i)}, \quad (2.25)$$

with $\Delta t = (t_F - t_I)/N$ and $t_1 \equiv t_I$ and $t_N \equiv t_F$.

Since $H_P(t_i)$ is time reversal symmetric the above arguments imply $U^T(t_i) = U(t_i)$ when $U(t_i)$ is expressed in the time-symmetric basis $\{|M_i\rangle\}$. Thus, in this basis, we have

$$U^T = \lim_{N \rightarrow \infty} (U(t_N)U(t_{N-1}) \cdots U(t_2)U(t_1))^T \quad (2.26)$$

$$= \lim_{N \rightarrow \infty} U^T(t_1)U^T(t_2) \cdots U^T(t_{N-1})U^T(t_N) \quad (2.27)$$

$$= \lim_{N \rightarrow \infty} U(t_1)U(t_2) \cdots U(t_{N-1})U(t_N). \quad (2.28)$$

For a time-symmetric pulse $H_P(t_i) = H_P(t_{N+1-i})$ and so $U(t_i) = U(t_{N+1-i})$. This allows us to reverse the order of the operators in (2.28) which then implies

$$U^T = U. \quad (2.29)$$

Thus if we write U in terms of an effective Hamiltonian,

$$U = \exp -i\lambda H, \quad (2.30)$$

the matrix elements of H must be real in the time-symmetric basis. H must therefore be time reversal symmetric, i.e. $H = \Theta H \Theta^{-1}$.

2.6.2 Perturbative Evaluation of the Gate

After proving this crucial result regarding time reversal symmetry for general quantum gates, we now return to the task of perturbatively solving (2.14) for the gate (2.19) produced by the pulse (2.17). We take as the small parameter of the perturbation theory the strength of spin-orbit coupling.

The formal exact solution of (2.14) is the time ordered exponential (2.7). Here the unperturbed Hamiltonian (i.e. the Hamiltonian in the absence of spin-orbit coupling) is isotropic exchange $H_0(t) = J(t)\mathbf{S}_1 \cdot \mathbf{S}_2$, and the unperturbed evolution is trivial to find, because the unperturbed Hamiltonians taken at different times commute $[H_0(t_1), H_0(t_2)] = 0$ for every pair of times t_1, t_2 . This means we can safely ignore the time-ordering operator, and the unperturbed evolution operator is

$$U_0(t) = T \exp -i \int_{-\infty}^t J(t') \mathbf{S}_1 \cdot \mathbf{S}_2 dt' = \exp -ix(t) \mathbf{S}_1 \cdot \mathbf{S}_2, \quad (2.31)$$

where

$$x(t) = \int_{-\infty}^t J(t') dt', \quad (2.32)$$

is the integrated pulse strength from the beginning of the pulse up to time t . Pulsing the unperturbed interaction produces an unperturbed gate (i.e. an isotropic exchange gate) $\lim_{t \rightarrow \infty} U(t) = U_0(\lambda) = \exp -i\lambda \mathbf{S}_1 \cdot \mathbf{S}_2$ where λ is the usual strength of entire pulse (2.9). Anisotropy will appear as a correction to this form of this gate.

Since the unperturbed problem is solved and we are interested in presenting the perturbative solution in the form (2.19) that clearly separates the unperturbed and perturbative parts of the gate, it is useful to keep track of the orders of perturbation theory in the interaction

picture, with the picture operator defined by the unperturbed evolution operator (2.31). In this picture the state of the system at time t , $|\psi_I(t)\rangle$, is

$$|\psi_I(t)\rangle = U_0^\dagger(t)|\psi(t)\rangle, \quad (2.33)$$

where $|\psi(t)\rangle$ is the state in the standard Schrödinger picture, and $U_0^\dagger(t)$ is given by (2.31). The state in this interaction picture then evolves only under the influence of anisotropic part of the Hamiltonian,

$$i\frac{d}{dt}|\psi_I(t)\rangle = J(t)A_I(t)|\psi_I(t)\rangle, \quad (2.34)$$

where the anisotropic part of the Hamiltonian must, of course, also be taken in the same interaction picture, with

$$A_I(t) = U_0^\dagger(t)A(t)U_0(t). \quad (2.35)$$

The form of the Schrödinger equation in the interaction picture is the same as in the Schrödinger picture, with the operator $J(t)A_I(t)$ playing the role of a time dependent Hamiltonian. By analogy, the formal solution for the evolution operator in interaction picture is again the time ordered exponential

$$U_I(t) = T \exp -i \int_{-\infty}^t J(t')A_I(t')dt', \quad (2.36)$$

where the initial condition $\lim_{t \rightarrow -\infty} U_I(t) = 1$ is assumed. This evolution operator maps a state at the initial time $t \rightarrow -\infty$ into a state at time t when both states are in the interaction picture. Note that the picture operator at the initial time is the identity, $U_0(t \rightarrow -\infty) = 1$. The initial state in the interaction picture is then the same as in the standard Schrödinger picture. On the other hand, the final states at $t \rightarrow \infty$ do differ because $\lim_{t \rightarrow \infty} U_0(t) = \exp -i\lambda \mathbf{S}_1 \cdot \mathbf{S}_2$.

To calculate the gate parameters (2.19) corresponding to this gate, we need to compare our perturbative result for the gate with the gate that would be produced by a pulse of the gate Hamiltonian H of (2.19) with the same isotropic interaction strength. Of course the comparison is meaningful only when both operators are taken in the same picture.

The gate produced by the gate Hamiltonian in the Schrödinger picture is, by definition U of (2.19). From the transformation rule between states in the Schrödinger and interaction pictures, we can easily conclude that the interaction picture of this evolution operator is

$$U_I = \lim_{t \rightarrow \infty} U_0^\dagger(t)U(t) = \exp(i\lambda \mathbf{S}_1 \cdot \mathbf{S}_2) U. \quad (2.37)$$

The goal of this calculation is then to find the gate produced by a pulse (2.17). The result should be correct up to second order in the strength of spin-orbit coupling, which translates in to second order in $\beta^{int}(t)$ and first order in $\Gamma^{int}(t)$. Since the perturbation $A^{int}(t)$ contains both of these terms, we would need to work out the second order perturbation. For this precision it is sufficient to keep the first two terms in the Dyson series expansion of (2.36). This gives

$$U_I = 1 - i \int_{-\infty}^{\infty} J(t)A_I^{int}(t)dt + \frac{(-i)^2}{2} \int_{-\infty}^{\infty} dt_1 \int_{-\infty}^{t_1} dt_2 J(t_1)J(t_2)A_I^{int}(t_1)A_I^{int}(t_2) + o(SO^2), \quad (2.38)$$

where $o(SO^2)$ are terms of higher than second order in spin orbit coupling strength.

Using the two expressions for the gate in the interaction picture, (2.37) and (2.38), we arrive at a set of 16 equations for the matrix elements, 15 of which are independent. The condition that reduces the number of equations is the fact that both the traceless time dependent Hamiltonian $H^{int}(t)$ and traceless gate Hamiltonian H produce gates with determinant 1, represented by an $SU(4)$ matrix. These equations can then be solved for the parameters of the gate Hamiltonian.

The result of this rather lengthy computation are the following perturbative expressions for the gate parameters:

$$\alpha = \frac{1}{2 \sin(\lambda/2)} \int_{-\infty}^{\infty} \beta^{int}(t) \sin\left(x(t) - \frac{\lambda}{2}\right) J(t)dt, \quad (2.39)$$

$$\beta = \frac{1}{2 \sin(\lambda/2)} \int_{-\infty}^{\infty} \beta^{int}(t) \cos\left(x(t) - \frac{\lambda}{2}\right) J(t)dt, \quad (2.40)$$

$$\mu = \frac{1}{4\lambda} \int_{-\infty}^{\infty} J(t_1)dt_1 \int_{-\infty}^{t_1} J(t_2)dt_2 \mathbf{m}(t_1, t_2), \quad (2.41)$$

where

$$\mathbf{m}(t_1, t_2) = (\beta^{int}(t_1) \times \beta^{int}(t_2)) \cos(x(t_1) - x(t_2)) + 2(\alpha \times \beta) \sin(x(t_1) - x(t_2)), \quad (2.42)$$

and

$$\Gamma_{ab} = \frac{1}{\lambda} \int_{-\infty}^{\infty} \Gamma_{ab}^{int}(t) J(t) dt + \frac{1}{4\lambda} \int_{-\infty}^{\infty} J(t_1) dt_1 \int_{-\infty}^{t_1} J(t_2) dt_2 I_{ab}(t_1, t_2) \sin(x(t_1) - x(t_2)), \quad (2.43)$$

where

$$\begin{aligned} I_{ab}(t_1, t_2) &= 2 (\boldsymbol{\beta}^{int}(t_1) \cdot \boldsymbol{\beta}^{int}(t_2) - \beta^2 - \alpha^2) \delta_{ab} - \\ &- (\beta_a^{int}(t_1) \beta_b^{int}(t_2) + \beta_a^{int}(t_2) \beta_b^{int}(t_1) - 2\beta_a \beta_b - 2\alpha_a \alpha_b). \end{aligned} \quad (2.44)$$

These results are valid when $|\lambda\alpha| \ll 1$ and $|\lambda\beta| \ll 1$ and correct up to second order in spin orbit coupling strength. They obviously diverge in the limit $\lambda \rightarrow 2n\pi$ for integer n . The reason for this divergence is in the fact that the unperturbed gate U_0 approaches the identity, and the corrections cannot be small. In the $\lambda \rightarrow 0$ limit, α and β do diverge, but the products $\lambda\alpha$ and $\lambda\beta$ have finite values and the result represents a valid gate. Since only the gate has direct meaning, the gate parametrized by a value of λ close to an even multiple of π can always be mapped to another gate with the value of λ close to zero. The result of this remapping will generically be far from the real gate applied by the considered pulse and in that sense perturbative results do break down for these values of λ .

It is gratifying to note that these perturbative results are consistent with our rigorous result that time symmetric pulses produce gates described by a time reversal symmetric gate Hamiltonian. To see this note that the expressions (2.39) for $\boldsymbol{\alpha}$ and (2.41) for $\boldsymbol{\mu}$ corresponding to staggered and homogeneous magnetic field do indeed vanish when the pulse $H^{int}(t)$ is time symmetric. The vanishing of the $\boldsymbol{\alpha}$ term in (2.39) is obvious for symmetric pulses. We can introduce the quantity x of (2.32) as a new integration variable and use $J(t)dt = dx(t)$. The sine function is odd about the center of the pulse, i.e. changes sign on mapping $\frac{\lambda}{2} \pm x \rightarrow \frac{\lambda}{2} \mp x$, and the prefactor is even under the same transformation. Integration over x goes from 0 to λ , an interval symmetric about $\frac{\lambda}{2}$, so that the value of $\boldsymbol{\alpha}$ is zero. For $\boldsymbol{\mu}$, we can do a similar trick, and show that the cross product term vanishes after separating the first integration into intervals from 0 to $\frac{\lambda}{2}$ and from $\frac{\lambda}{2}$ to λ and switching variables in the two integrals. The term with $\boldsymbol{\alpha}$ vanishes, because $\boldsymbol{\alpha}$ is zero for time symmetric pulses.

The symmetry predictions for the size of the anisotropic terms also hold. The gate parameters $\boldsymbol{\alpha}$ and $\boldsymbol{\beta}$ are first order in the time dependent $\boldsymbol{\beta}^{int}(t)$, i.e. first order in spin orbit coupling, while $\boldsymbol{\Gamma}$ and $\boldsymbol{\mu}$ are second order.

2.6.3 Local Symmetry

We have seen that time symmetric pulsing of anisotropic exchange gates removes one of the undesirable first order anisotropic terms (i.e. the $\boldsymbol{\alpha}$). Unfortunately, such a symmetrically pulsed gate will still be anisotropic, but the remaining anisotropy will only have the terms that correspond to interactions which are invariant under time reversal. The remaining first order $\boldsymbol{\beta}$ term in (2.19) can not be removed by simple pulse shaping. However, the perturbative expression for $\boldsymbol{\beta}$ (2.40) suggests that this term can be controlled by the choice of the pulse shape that fixes the form of $\boldsymbol{\beta}^{int}(t)$.

While we cannot use the control gained from pulse shaping to make $\boldsymbol{\beta}$ vanish, we *can* use it to *effectively* eliminate this term. To see how, note that the gate Hamiltonian of a symmetrically pulsed gate is

$$H = \mathbf{S}_1 \cdot \mathbf{S}_2 + \boldsymbol{\beta} \cdot (\mathbf{S}_1 \times \mathbf{S}_2) + \mathbf{S}_1 \cdot \boldsymbol{\Gamma} \cdot \mathbf{S}_2, \quad (2.45)$$

where, again, the problematic term is $\boldsymbol{\beta}$, because it is of the first order in spin-orbit coupling strength.

The isotropic exchange gate (1.5) we are trying to implement is very useful because of its symmetry properties. Any rotation in spin space leaves it invariant. However, the rotations that leave the gate invariant are global. Both spins that the gate affects must be rotated about the same axis and through the same angle in order to keep the gate isotropic. However if the spin rotations are not equal the isotropic form will not be preserved.

Under rotations, the spin operators behave like vectors, and simple geometry can tell us what happens with a scalar product when spins are rotated by a different angle. From elementary geometry, the change of a vector \mathbf{S} under a small rotation is

$$\mathbf{S} \rightarrow \mathbf{S}' = \mathbf{S} + \boldsymbol{\phi} \times \mathbf{S}, \quad (2.46)$$

where $\hat{\boldsymbol{\phi}}$ is the rotation axis and the rotation angle is ϕ . Under such a local rotation, the isotropic exchange gate Hamiltonian will transform into

$$\mathbf{S}_1 \cdot \mathbf{S}'_2 = \mathbf{S}_1 \cdot \mathbf{S}_2 + \sin \phi \hat{\boldsymbol{\phi}} \cdot (\mathbf{S}_1 \times \mathbf{S}_2) + (\cos \phi - 1) \left(\mathbf{S}_1 \cdot \mathbf{S}_2 - \left(\hat{\boldsymbol{\phi}} \cdot \mathbf{S}_1 \right) \left(\hat{\boldsymbol{\phi}} \cdot \mathbf{S}_2 \right) \right). \quad (2.47)$$

In the special case, when the symmetric tensor $\boldsymbol{\Gamma}$ in gate (2.45) satisfies

$$\Gamma_{ab} = \frac{\sqrt{1 - \beta^2} - 1}{\beta^2} (\beta^2 \delta_{ab} - \beta_a \beta_b), \quad (2.48)$$

all the anisotropy can be absorbed into a relative rotation of spins. This kind of gate is called a rotated exchange gate, and its gate Hamiltonian is a rotated exchange interaction.

Comparing these changes of vector and scalar product with the gate Hamiltonian for a symmetric pulse we see that, up to the first order in spin-orbit coupling, a symmetrically pulsed gate can always be interpreted as an isotropic exchange gate between a spin \mathbf{S}_1 and slightly rotated spin \mathbf{S}_2

$$\mathbf{S}_1 \cdot \mathbf{S}_2 + \boldsymbol{\beta} \cdot (\mathbf{S}_1 \times \mathbf{S}_2) = \mathbf{S}_1 \cdot R(\boldsymbol{\beta})\mathbf{S}_2 + O(SO^2), \quad (2.49)$$

where the currently unimportant terms of second and higher orders are lumped together into $O(SO^2)$.

Within this interpretation, the first order anisotropy in a symmetrically pulsed gate is just a measure of the relative rotation of the two spins involved in an isotropic exchange gate. Therefore all the first order anisotropy in a symmetrically pulsed quantum gate can be absorbed into a choice of the spin quantization axis on one of the spins, regardless of the form of the symmetric anisotropy because it is always second order.

We apply this idea to a general gate produced by a time symmetric pulse. With standard spin quantization axes, the gate is

$$U = \exp -i\lambda (\mathbf{S}_1 \cdot \mathbf{S}_2 + \boldsymbol{\beta} \cdot (\mathbf{S}_1 \times \mathbf{S}_2) + \mathbf{S}_1 \cdot \boldsymbol{\Gamma} \cdot \mathbf{S}_2), \quad (2.50)$$

i.e. it is generated by the gate Hamiltonian (2.45). The convention for the overall pulse strength λ is that it is the strength of the isotropic gate that would be applied if spin-orbit coupling was turned off. When represented in terms of spins \mathbf{S}_1 and $\mathbf{S}'_2 = R(\phi)\mathbf{S}_2$ which is slightly rotated \mathbf{S}_2 this same gate is

$$U = \exp -i\lambda (\mathbf{S}_1 \cdot \mathbf{S}'_2 + \mathbf{S}_1 \cdot \boldsymbol{\Gamma}' \cdot \mathbf{S}'_2), \quad (2.51)$$

when the axis and angle of rotation $R(\phi)$ are determined by the requirement that the first order anisotropic term $\boldsymbol{\beta}$ gets absorbed in the relative rotation of the two spins. Note that the relative rotation of the spins has also caused a change in the symmetric tensor part of

the gate, from Γ to Γ' , because of second order terms in (2.47). The new symmetric second order anisotropy is

$$\Gamma'_{ab} = \Gamma_{ab} + \frac{1}{2} (\beta^2 \delta_{ab} - \beta_a \beta_b) + O(\beta^4). \quad (2.52)$$

The absorption requirement determines the local rotation completely. The rotation that exactly removes the β term from (2.50) is about the $\hat{\beta}$ axis and the angle of rotation is $\arcsin \beta$.

The exact form of this rotation is not important at this point, because we only aim at removing the first order anisotropic effects. With this in mind, we expand the required rotation up to first order in orbit coupling and find that it is about an axis $\hat{\beta}$ and through an angle β . The corresponding rotation matrix is

$$R_{ab} = \delta_{ab} + \sum_c \epsilon_{abc} \beta_c - \frac{1}{2} (\beta^2 - \beta_a \beta_b) + O(\beta^3), \quad (2.53)$$

with the remaining terms $O(\beta^3)$ being of third order in spin orbit coupling.

A choice of spin reference frames that are local for spins in a computer (i.e., a choice of gauge) can remove the first order anisotropy from any gate applied by a given time symmetric pulse. If all quantum are done in this gauge, the first order correction will not affect the computation, again in first order in spin-orbit coupling. Even better, the choice of gauge is not an actual operation applied to the spins. It is merely a choice in the way in which define “up” and “down” spins on the two quantum dots. There is no additional spin control requirement involved with a change of gauge.

There are only two times in a quantum computation when the actual spin reference frame matters. At the beginning of a computation, the spins have to be prepared in initial states that are defined in a fixed gauge. Also the spin projection measurements at the end of the computation are done along axes defined in the same fixed gauge. Because the initial and final steps of a quantum computation have to be done in the same gauge, it is necessary that the entire computation proceeds in a fixed gauge. The anisotropy reducing gauge is illustrated in [Fig. 2.2].

The requirement that the entire computation take place in a fixed gauge, however, presents a problem. The anisotropy canceling rotation (2.53) that determines the gauge is a function of the pulse used to implement the gate. On the other hand the spin quantization

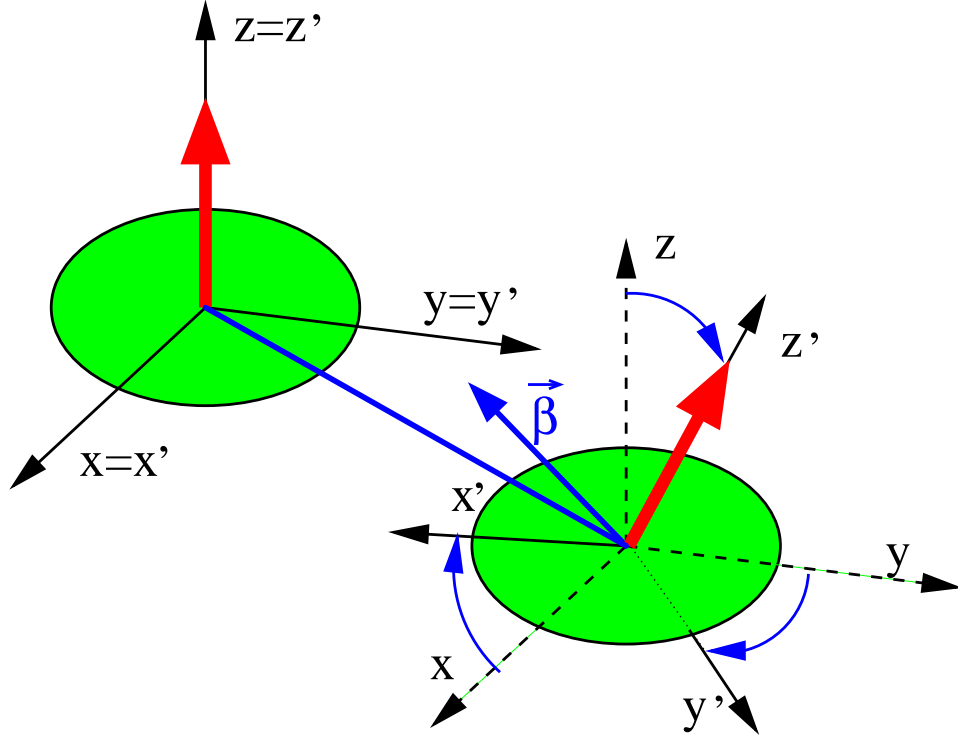


Figure 2.2. Illustration of local reference frames. If every two-qubit exchange gate that acts on a pair of spins produces the same first order anisotropy β , the anisotropy in rotated reference frame will be second order in interaction anisotropy β^{int} . Rotation connecting the two local reference frames is about the axis $\hat{\beta}$, and rotation angle is β up to second order in interaction anisotropy. It maps the reference frame (x, y, z) , represented with dashed axes into (x', y', z') , represented with solid axes. Actual reference frames matter only in initialization and readout of the spin qubit. To reduce anisotropy, the spins should be prepared and measured along local z' axes. Red arrows represent spins immediately after initialization.

axis of a fixed spin is determined by the gauge and must not change during the computation. Therefore the gauge fixing is possible only if every gate applied to a pair of spins requires the same canceling rotation for that particular pair. Since the canceling rotation (2.53) is a function of the gate parameter β , every symmetric pulse applied to a given pair of spins must produce the same first order anisotropy, regardless of the isotropic exchange gate that was implemented.

In the search for a set pulses that produces all possible isotropic exchange gates (1.5) while keeping the first order anisotropy fixed, the perturbative result (2.40) can be quite useful. To illustrate this point, let us find a set of pulses that produce gates with a fixed value of β for all the values of the isotropic part strength λ in a simple but illustrative model.

We consider a family of pulses of the form (2.17) with time dependent isotropic interaction strength

$$J(t; \lambda) = \frac{J_0(\lambda)}{\cosh^2 \frac{2t}{\tau(\lambda)}}, \quad (2.54)$$

and first order anisotropy proportional to isotropic interaction strength

$$\beta^{int}(t) = \beta_1 J(t; \lambda). \quad (2.55)$$

The time dependence is set by the pulse strength $J_0(\lambda)$ and the decay time $\tau(\lambda)$. For all of these pulses, the integrated strength of the isotropic part of interaction is $\int_{-\infty}^{\infty} J(t; \lambda) dt = J_0(\lambda)\tau(\lambda)$. With this simple model of pulse time dependence and the anisotropy strength, equation (2.40) for the value of gate parameter β can be integrated analytically. The resulting first order anisotropy parameter is

$$\beta = \beta_1 \frac{4J_0(\lambda)}{\lambda^2} \left(2 - \cot \frac{\lambda}{2} \right), \quad (2.56)$$

and it is easy to find a set of pulses that keep (2.56) constant, while the integrated isotropic gate strength varies. Solving for the parameters $J_0(\lambda)$ and $\tau(\lambda)$ of such a set of pulses of the form (2.54) we find

$$J_0(\lambda) = J_0(\pi) \frac{2\lambda^2}{\pi^2} \frac{1}{2 - \lambda \cot \frac{\lambda}{2}}, \quad (2.57)$$

and

$$\tau(\lambda) = \tau(\pi) \frac{\pi}{2\lambda} \left(2 - \lambda \cot \frac{\lambda}{2} \right). \quad (2.58)$$

With these parameters the gate anisotropy is independent of λ , but the integrated pulse strength of the isotropic part $J_0(\lambda)\tau(\lambda) = \lambda$ is different for different pulses. Note also that the pulses are time symmetric. The shape of these pulses is shown on [Fig.2.3].

In realistic systems the goal of keeping the first order anisotropy fixed for all gates would be achieved through calibration in experiments, rather than calculation. The reason for this is the obvious difficulties connected with finding the actual form of the first order anisotropy of interaction that we have conveniently modeled using (2.55).

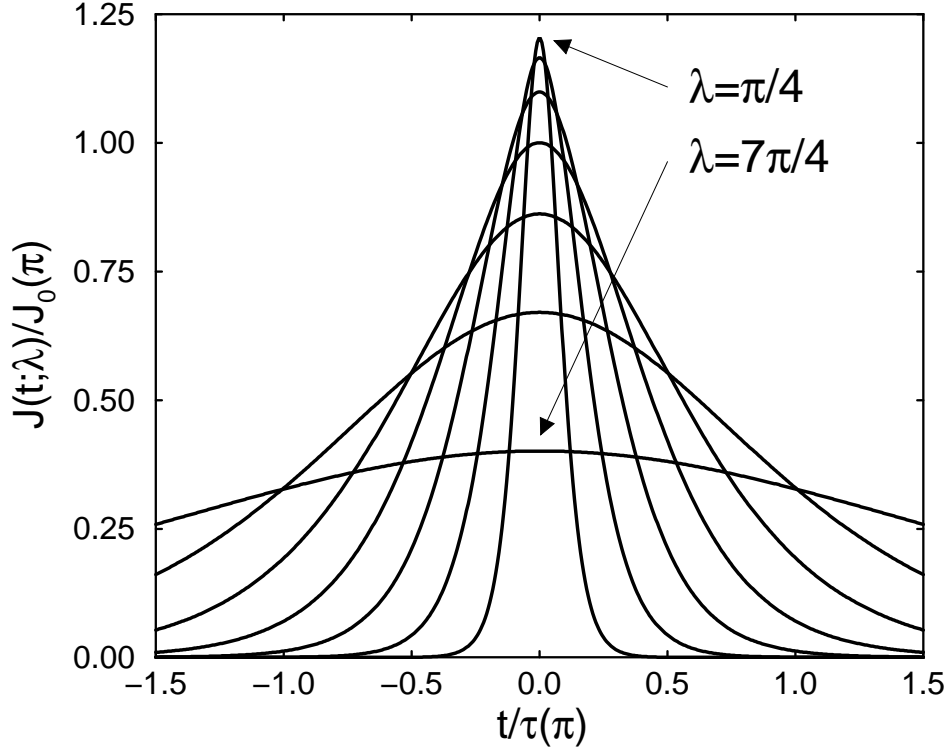


Figure 2.3. A family of pulses that implement different isotropic exchange gates that all have the same first order anisotropy. Time dependence of isotropic exchange coupling strength $J(\lambda; t)$ is plotted as a function of time measured in units of characteristic time scale τ . The sharpest pulse gives the integrated isotropic exchange $\lambda = \pi/4$. Other pulses give $\lambda = 2\pi/4 \dots 7\pi/4$ in steps of $\pi/4$. For the identity $\lambda = 2\pi$ pulse, the width would have to diverge in order to keep anisotropy constant.

If an analogous set of pulses could be found in a realistic device, the entire quantum computation could proceed without any first order anisotropic corrections, provided that initialization and readout were done in the correct gauge.

The anisotropy reducing gauge does not exist for all the topologies of spins connected by two spin gates. In fact, whenever the net of spins connected by two spin gates contains closed loops, such a gauge does not exist. The problem is that each link in such a net defines a reference frame of spin on one of its ends. Starting from one of the spins in the network

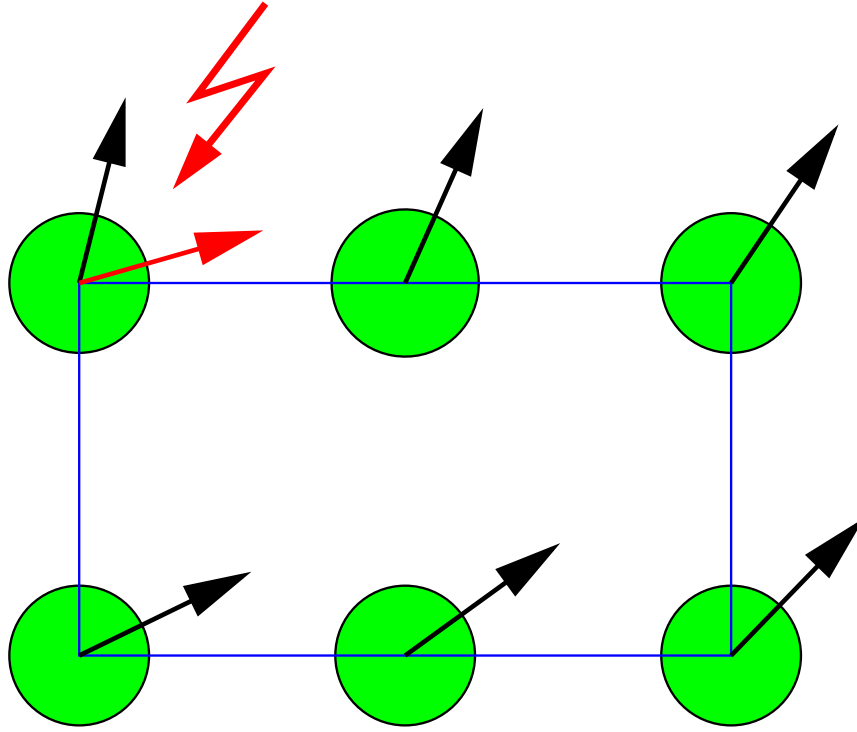


Figure 2.4. Inconsistency of the definition of local reference frames in the presence of loops. Quantization axes in the anisotropy reducing gauge are determined by the spin position. On each step between spins connected by a two spin gate, quantization axis is rotated by a fixed amount. Going around a loop will give two contradictory prescriptions for a spin quantization axis. In this figure, the quantization axis for the spin in upper left corner is set at the beginning and set again after transversing a loop.

and going around a loop will define a reference frame for every spin on the path. The last step in the loop will require defining the reference frame at the position of the spin at which we started transversing this loop. However, this frame was defined before, at the start of the loop. The new definition set in the last step of the loop will generally be inconsistent with the old one. The required anisotropy reducing gauge therefore does not exist, see [Fig. 2.4]. This method of anisotropy reduction works only for networks of spins connected by two spin gates with the topology of a tree i.e. without any loops. Two examples of tree topology are given in [Fig.2.5].

The idea of an anisotropy reducing gauge in spin based quantum computer was formalized by Wu and Lidar in [49], where they have introduced the formalism of dressed qubits and

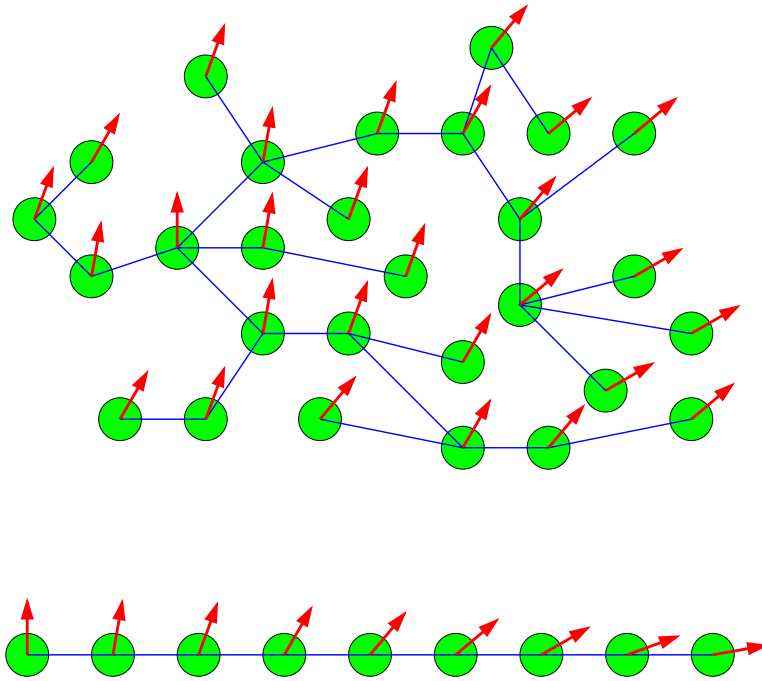


Figure 2.5. Two examples of spin nets with tree topology. If two spin gate is going to act between a pair of spins during quantum computation, they are connected by a blue link. If every exchange gate produces the same anisotropy, local reference frames at the ends of a link will be related by a constant rotation. At initialization all the spins in a network point in the direction of local quantization axis z . Initial configuration is represented by red arrows. Because there are no loops of spins connected by exchange gates, it is possible to consistently define local reference frames in a net with tree topology.

applied it to gates produced by switching on and off the rotated exchange interaction (2.47). In this case, they have found that the gauge choice completely removes the anisotropy from the gate. (A point we also made in [50]).

The main advantage of the procedure for the reduction of anisotropy advocated here is that the new requirements on control are surprisingly simple. All that is required is that the voltage pulses be time symmetric and both initialization and readout performed in local reference frames, with independent axes at the position of every spin. It is especially important that the requirements on pulse shapes are not tremendously more complex than in the case of isotropic interaction. The intuition that the time dependence of voltage pulses needed to perform any useful task is prohibitively complex was probably the reason why

their time dependence was never considered to be such a useful method for spin control prior to this work.

2.7 Summary of the Results

The method described here can be applied to improve any anisotropic exchange gate. It would be particularly useful if the anisotropy of the spin interaction in a system is already small, but still above the error correction threshold. For small anisotropies this method roughly squares the error rate.

Apart from learning how to use pulse shaping and gauge fixing to improve quantum gates, we can also learn about spin control through time dependent pulses. The most important lesson to be learned is that the extremely complex requirements of generic control through a time dependent interaction is drastically simplified if we are only trying to constrain the symmetry of the resulting gate. While it is not true that the interaction Hamiltonian equals the gate Hamiltonian, symmetry constraints can stay satisfied when some care is taken about the symmetry of the pulse. It is reasonable to expect that similar techniques are able to efficiently control the spins in situations when the symmetry of resulting gate is crucial.

There are two main implementations of the universal gate sets that use isotropic exchange. One is exchange only quantum computation that was already shown to benefit from symmetry based control. Another approach is to use isotropic exchange and the single spin rotations for CNOT construction and then proceed with the standard universal set consisting of CNOT and all the single spin rotations.

Standard implementations of the universal gate sets are dependent on isotropic exchange gates. Results about symmetrically pulsed gates as a simple way to obtain symmetric gates, with gate Hamiltonian (2.45), encouraged several authors to study them, rather than isotropic exchange as a natural, easily implemented, two spin gates in a system of coupled quantum dots.

An important result of Burkard and Loss [51] showed that the standard construction of the CNOT gate based on isotropic exchange also works exactly with any symmetric gate generated by (2.45). In the gate parametrization (2.19) it means that whenever $\alpha = 0$ and $\mu = 0$, the CNOT construction is going to be exact. This result shows the value of symmetrically pulsed gates beyond the immediate application in reducing the gate

anisotropy. Similarly, when aided by the controllable Zeeman splitting $H^Z = g\mu (\mathbf{B} \cdot \mathbf{S})$ the symmetric gates were shown to be universal for quantum computation over encoded qubits by Wu and Lidar [43].

CHAPTER 3

MICROSCOPIC DERIVATION OF SPIN INTERACTION

I wish to God these calculations had been executed by steam.

Charles Babbage

The power of the isotropic exchange interaction, $H^{int}(t) = J(t)\mathbf{S}_1 \cdot \mathbf{S}_2$ as a control tool in a spin-based quantum computer was the main motivation for the work presented in the previous chapter. There, we developed a method for effectively eliminating anisotropic corrections, by using time-symmetric pulses and tailoring of the pulse shapes. However, isotropic exchange is not the only useful tool for the construction of a universal set of quantum gates. Other, less symmetric forms of the interaction can be equally useful. Burkard and Loss [51], for example, have shown that the standard construction of a controlled not (CNOT) gate, using the isotropic \sqrt{SWAP} gates (see [Fig. 2.10]) also works *exactly* when the isotropic \sqrt{SWAP} gates are replaced by any gate of the form

$$U^{\pi/2}(\beta, \gamma) = \exp -i\frac{\pi}{2} (\mathbf{S}_1 \cdot \mathbf{S}_2 + \beta (S_{1x}S_{2y} - S_{1y}S_{2x}) + \gamma (S_{1x}S_{2x} + S_{1y}S_{2y})), \quad (3.1)$$

with *arbitrary* values of parameters β and γ . In this chapter, we show that time symmetric pulsing of a Hamiltonian that includes the effects of spin-orbit coupling will produce a quantum gate of this useful form. Unlike the method presented in the previous section, however, detailed tailoring of the pulse shapes is *not* necessary.

Our demonstration will proceed within a model of the quantum dot quantum computer. This microscopic approach will allow us to study the properties of the anisotropic corrections to the isotropic exchange gates in a real device. Such a study will prove valuable in the design of gates that *use* anisotropy as a resource for control of spins. Such gates will be presented

and discussed in chapter 4 of this thesis. To appreciate the reasons for using the microscopic approach, we now discuss the usefulness of the results of the previous chapter, obtained for the purpose of reducing the gate anisotropy, in design of a spin-based quantum computer.

The perturbative results (2.39)-(2.41) that predict the quantum gate produced by a given time-dependent Hamiltonian can not immediately tell us which gates can be produced in a realistic device. In order to use these results, we would have to know the interaction between spins as a function of time. For practical use, therefore, it is necessary to supplement these perturbative results with some model of the interaction between the spins. Prior work in modeling the spin interaction in these devices was mainly concerned with the isotropic exchange coupling [52]. The original results we present here are about the anisotropy of the effective spin interaction caused by spin orbit coupling.

Constructing a solvable microscopic model of the exchange interaction in a double quantum dot system that would be accurate enough to allow us to use the perturbative expressions derived in the last chapter to predict the quantum operation is impossible. The connection between a given time dependent interaction and the gate produced by it is only a useful estimate of what we expect in future experiments on spin control in quantum dots. For any quantum computing application, the interaction parameters would have to be calibrated in experiment, rather than calculated theoretically. All the results of the calculations presented below should therefore be seen as proofs of principle rather than accurate design specifications.

One of the main result of this chapter, that axial symmetry of symmetrically pulsed (in time) gates is, however, to a large extent independent of the details of interaction. The details of the device construction that are modeled with simplicity, rather than accuracy, in mind are not going to change the symmetry of the interaction. They will, however give us an insight into the effects of spin-orbit coupling in spin-based quantum computing and motivate a study of these effects as a source of control in the quantum dot quantum computer discussed in Chapter 4.

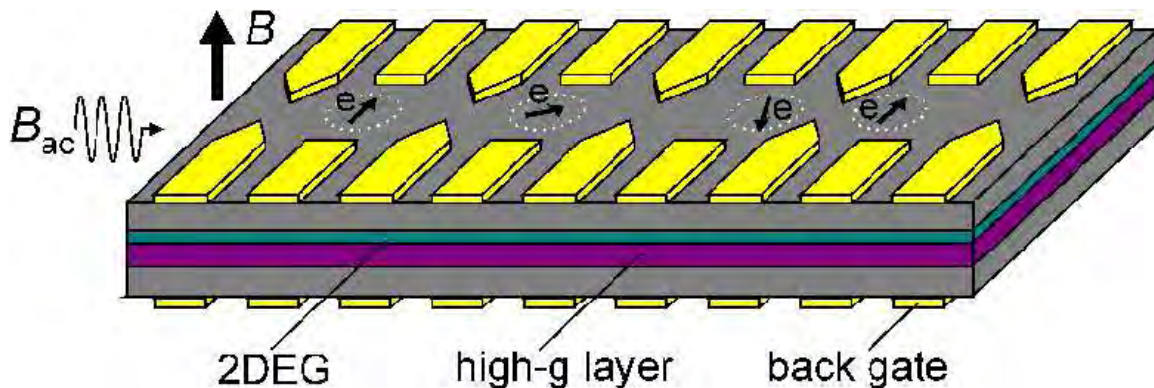


Figure 3.1. Quantum dot quantum computer, due to Loss and DiVincenzo. The qubits of this proposed computer are electron spins on coupled single electron quantum dots. Quantum dots are fabricated by electrostatic gating of a two dimensional electron gas in GaAs. In the original proposal, illustrated in this figure, the spins are manipulated via voltages on electrodes that define quantum dots and a combination of electron spin resonance techniques and manipulation of the Zeeman terms at the position of individual dots. In this figure two spin qubits on the left are decoupled, while spin qubits on the right interact through exchange coupling.

3.1 The Model of Quantum Dots Quantum Computer

The calculations presented here are all based on the Loss-DiVincenzo proposal [26] for a quantum dot quantum computer. This proposal was reviewed in Chapter 1, and for ease of reference, a sketch of the proposed device is given again in [Fig. 3.1].

Recall that the quantum dot quantum computer consists of an array of single electron quantum dots, fabricated by electrical gating of a two dimensional electron gas (2DEG) in GaAs. Each dot contains a single electron, and the spin of that electron represents a qubit. The proposed control mechanism for single qubit operations is electron spin resonance (ESR). Addressing of the spin qubits is done through local manipulation of the Zeeman Hamiltonian $H^Z = g\mu_0(\mathbf{S}_1 \cdot \mathbf{B})$ at the position of individual dots. Preparation of the computer into an initial state is achieved by cooling in a uniform magnetic field. The proposed readout mechanism is to transform spin information into charge information by spin selective tunneling to a polarized dot or lead [53].

For describing the two-qubit quantum gates in this device, and in particular the effects of spin-orbit coupling on these gates, the most important aspects of the actual device design in this proposal are the confinement mechanisms and the voltage control of the interaction between spins. We will now discuss these properties in greater detail and introduce the model we are going to use to calculate the behavior of an actual device.

3.1.1 Confinement to Two Dimensions

Hosts of electron spin qubits in the proposed quantum computing device considered here are quantum dots. A quantum dot is a system of electrons confined in all three dimensions to the extent that it exhibits a discrete spectrum.

For quantum computing applications it is necessary that confinement can change during gate operation. Tunable confinement is possible in electrically gated quantum dots. This kind of confinement is achieved in two steps. The first step consists of confining electrons to a two dimensional electron gas (2DEG). This is typically done by fabricating a semiconductor heterostructure consisting of layers of semiconductors with different energy gaps (e.g. GaAs and $\text{Al}_x\text{Ga}_{1-x}\text{As}$). Band bending at the boundary between the two semiconductors creates a potential well for electrons in the growth direction. The motion of electrons along the growth direction is then quantized into so-called subbands. If the temperature of the sample is much less than the subband level splitting then a truly two-dimensional gas of electrons forms [54]. To put it more colorfully, we have created an electron "flatland."

In the calculation of the effective Hamiltonian for electrons on coupled single electron quantum dots and in the presence of spin orbit coupling, this step in confinement is important. In the introduction to this thesis, it was mentioned that spin orbit coupling exists in systems that lack inversion symmetry. One of the sources of this inversion asymmetry is the potential that restricts the motion of electrons in one direction and produces a 2DEG. We will model the growth direction potential by a triangular well,

$$V_t(z) = \begin{cases} -eEz, & z \geq 0 \\ \infty, & z < 0 \end{cases} \quad (3.2)$$

where $e = -|e|$ is the electron charge, and E is the effective electric field that is taken to point along the z axis [Fig. 3.2]. This description looks crude, but it is in fact quite adequate for the purpose of deriving the effective spin Hamiltonian. It captures the essential

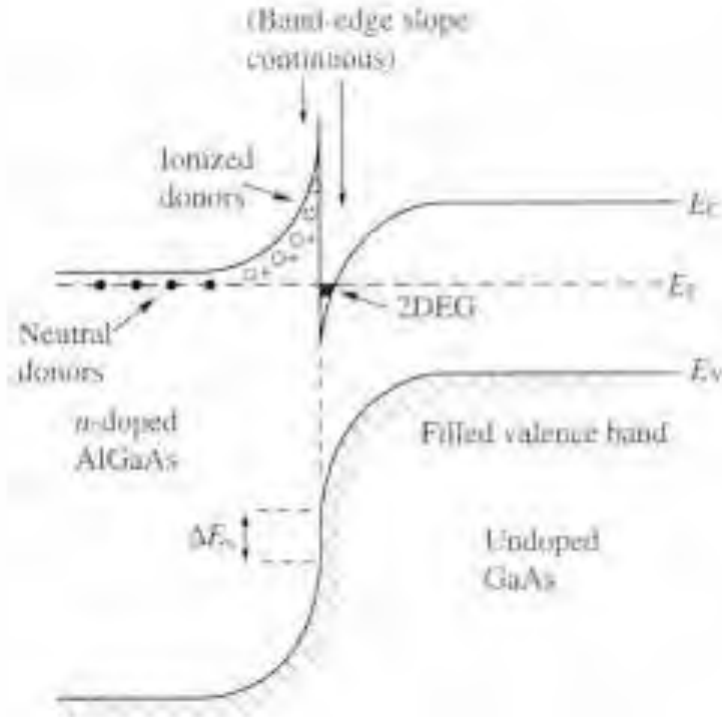


Figure 3.2. Two dimensional electron gas, formed in the potential well at the interface of two semiconductors. The well appears due to electrostatic attraction of the ionized donors. Electrons in this well have their motion in the direction normal to the interface confined to the ground state and they are effectively two-dimensional.

symmetry properties of the asymmetric confining potential because it breaks the inversion symmetry in the z direction, while being symmetric with respect to transformations in xy plane. The linear form of the potential is a reasonable approximation for a well with cusp near its bottom. In the limit of a very steep well, we can expect that both the form of the potential will be close to triangular well and that the low lying states will be similar to the eigenstates of such a well. For concreteness, we will assume that the growth direction of the semiconductor heterostructure is along the $[001]$ crystallographic direction of the GaAs layer hosting the quantum dots.

The electronic state in the growth direction is then the ground state of triangular potential. In position representation this state is an Airy function. The entire state is

given by

$$\langle z|\psi^{tot}\rangle = C\kappa Ai(\kappa z - \xi_1)|\psi\rangle, \quad (3.3)$$

where $|\psi^{tot}\rangle$ is the state of an electron, and $|\psi\rangle$ is the factor in the state that describes orbital degrees of freedom in the plane of the 2DEG and the spin degree of freedom. The width of the wave function in z direction is determined by the parameter $\kappa = (2m^*E|e|)^{1/3}$ of (3.3), where m^* is the effective electron mass. The constant $\xi_1 \approx -2.34$ is the first zero of Airy function and the normalization constant is $C \approx 1.43$.

The structural inversion asymmetry in the growth direction due to this triangular well will give rise to the Rashba [36] type of spin orbit coupling. The form of this term is the same as the spin-orbit coupling of a free electron coupled to an electric field pointing in the growth direction. In our model, we have assumed that the growth direction is along the [001] crystalline axis of GaAs, which we also denoted as the z direction, and the Rashba term is then

$$H_R^{SO} = 2\alpha_R E e (k_{[010]}S_{[100]} - k_{[100]}S_{[010]}), \quad (3.4)$$

where $k_{[abc]}$ is the projection of crystalline momentum to the $[abc]$ crystalline axis, and $S_{[abc]}$ is the analogous projection of electron spin. The parameter α_R is a property of the material hosting the 2DEG. It is then convenient to define the strength of Rashba term as

$$f_R \equiv 2\alpha_R E e. \quad (3.5)$$

Confinement in the plane will also affect the Dresselhaus contribution to spin-orbit coupling due to the bulk inversion asymmetry of the zinc-blende crystal structure of GaAs (see Chapter 1) [35]. In the system of crystallographic axes, the form of the Dresselhaus term in bulk is

$$H^D = \gamma_C (k_{[100]} (k_{[010]}^2 - k_{[001]}^2) S_{[100]} + cycl. + H.C.), \quad (3.6)$$

where *cycl.* denotes cyclic permutation of axes [100], [010] and [001], *H.C.* is the Hermitian conjugate, and γ_C is again a property of GaAs hosting the dots.

When electrons are confined to a 2DEG in the (001) plane, the electric field determines the width of the electron wave function in the [001] (z) direction. We can always replace the

square of the crystal momentum component k_z by its expectation value in the state described by the Airy function and given in (3.3),

$$\langle k_{[001]}^2 \rangle = 0.78\kappa^2 = 1.24 (m^* E |e|)^{2/3}. \quad (3.7)$$

This expectation value is set by the strength of the electric field. We can also set odd powers of the component of the crystal momentum in the growth direction to zero, $k_z = \langle k_z \rangle = 0$.

In a typical quantum dot, the confinement through heterostructure fabrication is much tighter than the confinement in the plane of the 2DEG. The tight confinement leads to large expectation values of the square of the momentum, i.e.

$$\langle k_{[001]}^2 \rangle \gg \langle k_{[100]}^2 \rangle, \langle k_{[010]}^2 \rangle, \quad (3.8)$$

and the Dresselhaus contribution to spin-orbit coupling takes an approximate linear form

$$H_1^D = 2\gamma_C \langle k_{[001]}^2 \rangle (-k_{[100]} S_{[100]} + k_{[010]} S_{[010]}). \quad (3.9)$$

In the rest of this chapter, we will neglect the remaining bulk inversion asymmetry contributions to spin orbit coupling that are cubic in in-plane momentum components and call H_1^D the linear Dresselhaus term.

For convenience, we define the strength of the linear Dresselhaus term f_D as

$$f_D = 2\gamma_C \langle k_{[001]}^2 \rangle. \quad (3.10)$$

From the dependence of the linear Dresselhaus (3.9) and Rashba (3.4) terms in the spin-orbit coupling Hamiltonian on the growth direction electric field, we can immediately see that the size of this electric field controls the relative size of the two terms. The size of the Rashba term is linear in the confining field E , while the Dresselhaus term scales as $E^{2/3}$.

A very important fact about the control of spin-orbit coupling via in-plane confinement and heterostructure growth is that the change of the order of layers relative to the [001] direction corresponds to a switch in the sign of electric field. This change of sign will change the sign of Rashba term in spin-orbit coupling, but will not change the Dresselhaus term. Therefore, the heterostructure orientation can make the contributions of the Dresselhaus and Rashba terms add up constructively or destructively.

3.1.2 Confinement in Plane, from Two to Zero Dimensions

The earliest quantum dots were produced by chemically etching a semiconductor heterostructure containing a 2DEG into pillars [55]. The geometry of such dots is set by the confinement and fixed in fabrication. For quantum computation, it is essential to allow for the change of quantum dot properties after they are produced. A tunable confinement potential in the plane of 2DEG is achieved by fabricating metallic electrodes on top of the 2DEG [56]. (Whenever possible, throughout this thesis the metallic gates controlling this confinement will always be referred to as electrodes, to avoid confusion with quantum gates.)

Electrodes that define quantum dots are connected to an external voltage source and their potentials can be changed at will. The electrode potential modifies the electrostatic confinement in the plane of the 2DEG (the xy plane). By supplying an external voltage to an electrode, we form a potential well in the xy plane, with a minimum under the electrode. This minimum provides confinement in two dimensions and binds electrons from the 2DEG to form a quantum dot. Electrons in a quantum dot are then have the discrete energy levels of both the triangular well in z direction and the electrostatic potential of an electrode in xy plane. The dot properties will depend on electrode potentials and can be manipulated after fabrication.

As in the problem of confinement into s 2DEG, the exact form of the electrostatic binding potential is hard to predict. For example, numerical calculations of the potential well produced by square metallic electrode, based on the Poisson-Schrödinger equation and self consistently including up to ten electrons by Kumar, Laux and Stern [57] demonstrated that the potential is to a good approximation circularly symmetric and has a radius significantly smaller than the dimensions of the electrode. In their calculation the side of square electrode was $300nm$ and the diameter of the produced circular dot was approximately $100nm$. Since the confining potential is hard to predict the best strategy when calculating the device properties is to use a simple potential which models it.

Some guidance in the choice of the model binding potential is based on both experimental and theoretical studies of the discrete spectra in quantum dots. Spectroscopy in the far infrared region showed that the excitation spectrum of a quantum dot is independent of the number of electrons and the interaction between them. Work of Brey, Johnson and Halperin

[58], Maksym and Chakraborty [59], and Bakshi, Broido and Kempa [60] on generalizations of the Kohn theorem [61] have shown that these properties, as well as the observed structure of the spectrum are to be expected in wells with parabolic confinement. Parabolic well shape is also a natural approximation to any smooth potential around its minimum. These two observations suggest that the parabolic well is a reasonable approximation for the potential in the plane of electrically confined quantum dot.

The problem of a two dimensional electron in a parabolic potential well with a magnetic field orthogonal to the electron plane was solved long before the development of quantum dots by Fock [62] and Darwin [63]. Their results come from the fact that the Hamiltonian for this system can be written in the form

$$\begin{aligned} H^{FD} &= \frac{1}{2m^*} \left(\mathbf{p} - \frac{e}{c} \mathbf{A} \right)^2 + \frac{1}{2} m^* \omega_0^2 r^2 \\ &= \frac{\mathbf{p}^2}{2m^*} + \frac{1}{2} m^* (\omega_0^2 + \omega_L^2) r^2 - \omega_L l_z, \end{aligned} \quad (3.11)$$

where \mathbf{r} is electron position, \mathbf{p} its momentum, ω_0 is the frequency of an electron in a well, $\mathbf{A} = B/2[y, -x, 0]$ is the vector potential of a uniform magnetic field of strength B pointing in growth direction of the 2DEG z , $\omega_L = |e|B/(2m^*c)$ is the Larmor frequency of the electron in this field, and l_z is the orbital angular momentum of two dimensional electron. From the similarity of the form of the Fock-Darwin Hamiltonian (3.11) with that of a two-dimensional simple harmonic oscillator, it is clear that the eigenstates in this system are eigenstates of a two dimensional simple harmonic oscillator of frequency $\Omega = \sqrt{\omega_0^2 + \omega_L^2}$ and mass m^* that are at the same time eigenstates of the angular momentum projection on the z axis. The spectrum consists of equidistant two dimensional simple harmonic oscillator energies, shifted by the Larmor term $-\omega_L l_z$.

Within the approximations of a triangular well in the growth direction and a harmonic well in the plane, the ground state of an electron in a single electron quantum dot is an Airy function in the z direction (3.3) and a magnetically squeezed simple harmonic oscillators state in the plane of the 2DEG. These states will be used in further microscopic evaluation of the spin behavior.

3.1.3 Control Mechanisms

The control mechanisms for single spin and two spin operations in the quantum computer proposal considered here are clearly different. Single spin operations are done using electron paramagnetic resonance (ESR) techniques or local magnetic fields. In order to address separated spins through ESR, the transition frequencies for electron spins on individual dots are modified by local manipulation of the Zeeman coupling, either through direct local control of magnetic fields or g-factor manipulation [64]. Similar manipulations are also necessary for direct addressing of spins by magnetic fields. Manipulation of either quantity on the length scales of $\sim 10nm$ and the time scale of picoseconds is necessary for single spin control, but also very demanding. It is widely believed that single spin operation are very hard to achieve in this configuration. (For a review of spin manipulation in this structure see [65].)

There has been a great deal of interest in reducing the requirements for single qubit operations in this quantum computer proposal. One direction of work aims at methods that will allow for some computing tasks that in the standard implementation require single spin operations to be applied by two spin interactions only [40], [32]. These methods require either encoding of logical qubits into more than one spin or control over novel two spin interactions. Another set of methods aims at quantum computation with less than complete control over the magnetic field. For example, universal quantum computation is possible with controllable local magnetic fields of fixed direction [43] or with global fields and encoding [66, 42]. However, it is generally believed that minimizing the required single spin manipulations in any quantum computing scheme is preferable in practice.

Two spin operations are much easier to perform in this device. A pair of quantum dots is separated by a barrier set by a potential on the electrode sitting above it. Changing the potential on this electrode, which is comparatively easy to do in electrically gated dots, will make the potential barrier between the dots higher or lower. The low barrier will make the two electrons interact, while the high one will decouple them. Application of a two spin operation then consist of starting with the low voltage on the control electrode, producing a high barrier corresponding to uncoupled dots, continues with application of high voltage that lowers the barrier and couples the electrons on the dots, and than separating the dots by lowering the voltage and raising the barrier again [Fig. 3.3].

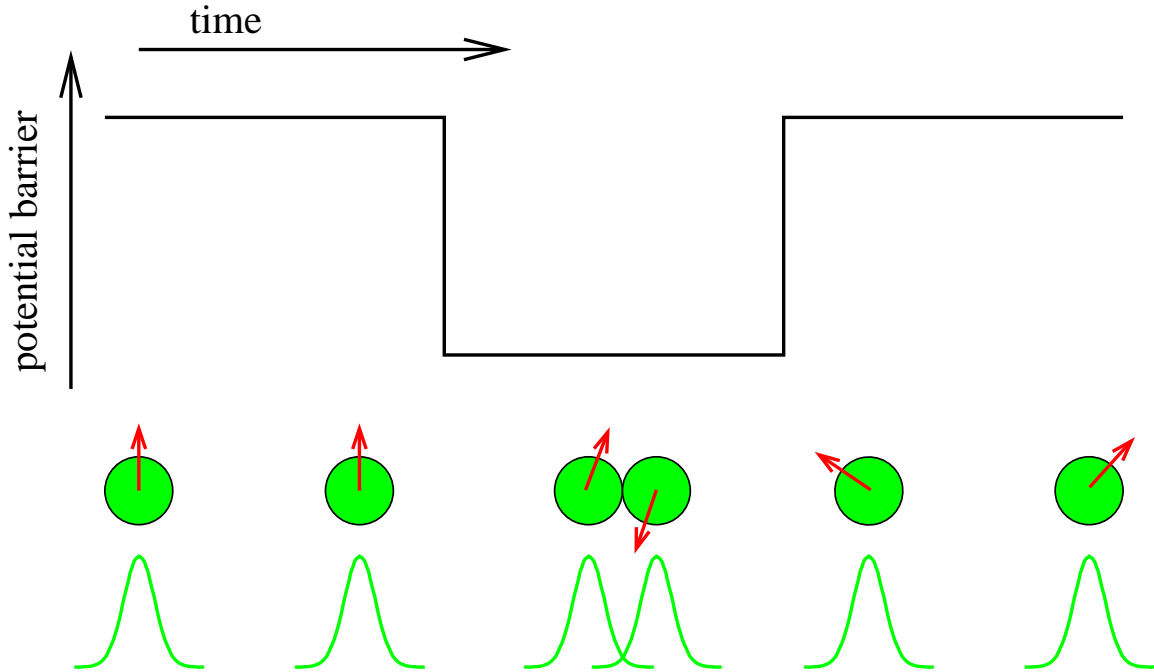


Figure 3.3. Voltage control of the spin gate. At the beginning of the gate application, the barrier between the dots is high and the spins are not interacting. Lowering the the barrier by changing the potential of the control electrode make the electron orbitals overlap and turns on the effective spin interaction. At the end, the barrier is turned again high, the spins do not interact and they are in a different state.

The effective spin interaction in the absence of spin orbit coupling will be isotropic exchange (1.3), and the only input from microscopic properties of the device will be the strength of this exchange. This coupling strength was calculated by Burkard, Loss and DiVincenzo [52] and their result is reproduced in [Fig. 3.4]. In this chapter we are deriving an effective spin Hamiltonian for nonzero spin orbit coupling and discuss the dependence of this interaction on the external classical control parameters.

To model a quantum gate acting on a pair of spins, we consider a system of two electrostatically confined quantum dots with one electron in each dot. For concreteness, we assume the dots are formed in a two-dimensional electron gas realized in a GaAs heterostructure.

The system is modeled by the Hamiltonian

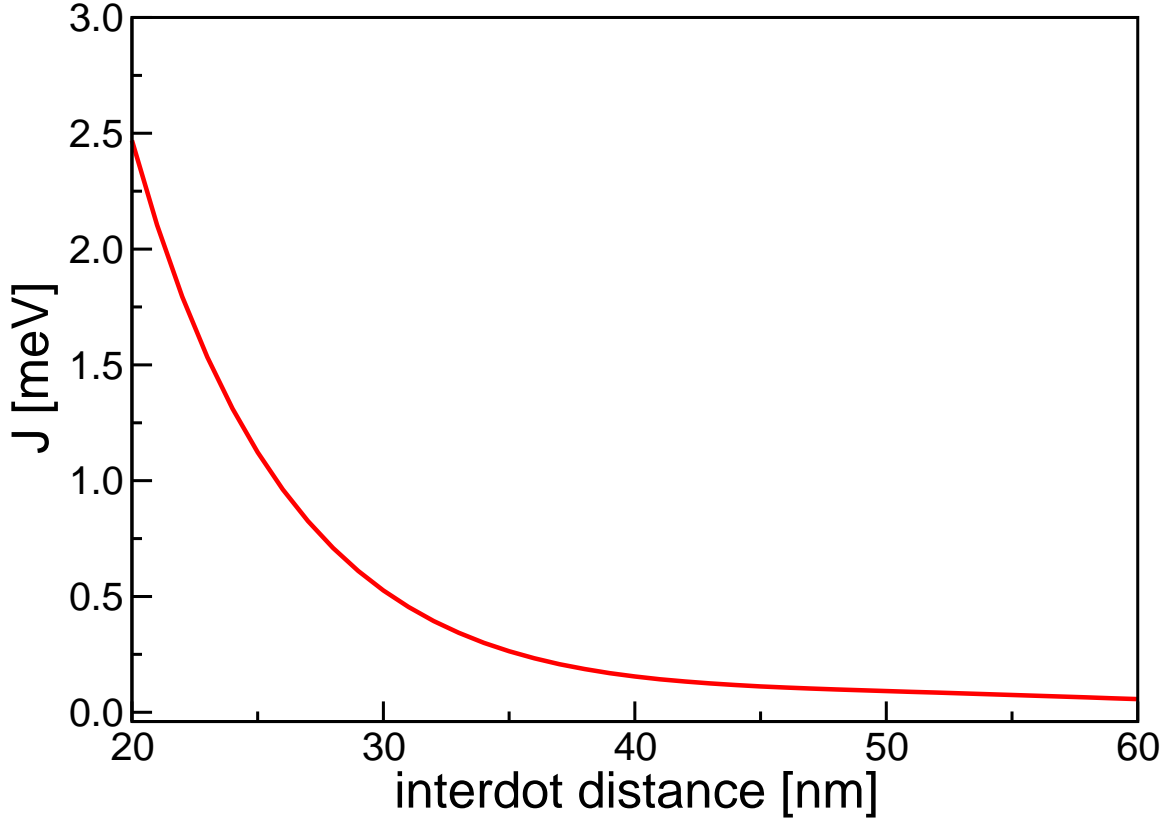


Figure 3.4. Isotropic exchange coupling strength as a function of distance between two single electron quantum dots, adapted from Burkard, Loss and DiVincenzo. The radius of the dots is 20 nm, and they are fabricated in GaAs. Effects of the spin-orbit coupling are not included.

$$H = T + C + H^{SO}. \quad (3.12)$$

Here T is the Hamiltonian that describes kinetic energy of two dimensional electrons and their binding to the modeled electrostatic gate potential in C is the Coulomb repulsion term. This part of Hamiltonian (3.12) was studied in [52]. It is given by $T = \sum_i h_i$ with

$$h_i = \frac{1}{2m^*} \left(\mathbf{p}_i - \frac{e}{c} \mathbf{A}(\mathbf{r}_i) \right)^2 + V(\mathbf{r}_i), \quad (3.13)$$

and $C = e^2/\epsilon|\mathbf{r}_1 - \mathbf{r}_2|$ is the Coulomb repulsion between electrons. We take the 2DEG the dots are formed in to lie in the xy plane, and for concreteness take $m^* = 0.067m_e$ and $\epsilon = 13.1$, corresponding to GaAs. For completeness we include a vector potential $\mathbf{A} = (-y, x, 0)B/2$ which couples the orbital motion of the electrons to a uniform magnetic field $\mathbf{B} = B\hat{z}$.

Note that the Zeeman coupling of spins to this magnetic field is explicitly excluded. While for typical values of the magnetic field the Zeeman coupling is small [52], it can become comparable to the spin-orbit coupling effects considered here for some values of dot parameters. If this is the case, the general conclusions based on time reversal symmetry we derive below will no longer be valid. As opposed to Zeeman coupling, the orbital effects of a magnetic field, included in the single particle Hamiltonian (3.13) through minimal substitution and the vector potential \mathbf{A} will *not* alter these time reversal symmetry based conclusions.

As in [52] lateral confinement of the dots is modeled by a double-well potential,

$$V(x, y) = \frac{m^* \omega_0^2}{2} \left(\frac{1}{4a^2} (x^2 - a^2)^2 + y^2 \right). \quad (3.14)$$

This potential describes a pair of quantum dots at the points $(x, y) = (\pm a, 0)$ [Fig. 3.5].

When the dots are well separated, i.e. the interdot distance scale a is much bigger than the characteristic length scale of the harmonic oscillator of mass m^* and frequency ω_0 , this potential describes two decoupled harmonic wells. Application of a quantum gate can be described by the potential of the form (3.14) with time dependent interdot distance a that goes to infinity at the beginning and the end of the pulse, for times $t \rightarrow \pm\infty$.

3.2 Hund-Mulliken Approximation

To better understand the choice of approximation used in the description of a system of coupled single electron quantum dots, we will first briefly review an elementary, but revealing, estimate of the effective spin interaction. Let us imagine a pair of electrons in localized orbitals $|A\rangle$ and $|B\rangle$ that are ground states of some confining potential. Let us also imagine that the centers of these orbitals can be moved around so that in the limit of very large distance between the centers the two orbitals become orthogonal $\langle A|B\rangle = 0$, and at smaller distance they begin to overlap.

The properly antisymmetrized states of the pair will be

$$|Singlet\rangle = \frac{1}{\sqrt{2(1 + |\langle A|B\rangle|^2)}} (|AB\rangle + |BA\rangle) \otimes |S\rangle \quad (3.15)$$

$$|Triplets\rangle = \frac{1}{\sqrt{2(1 - |\langle A|B\rangle|^2)}} (|AB\rangle - |BA\rangle) \otimes |T \pm 0\rangle, \quad (3.16)$$

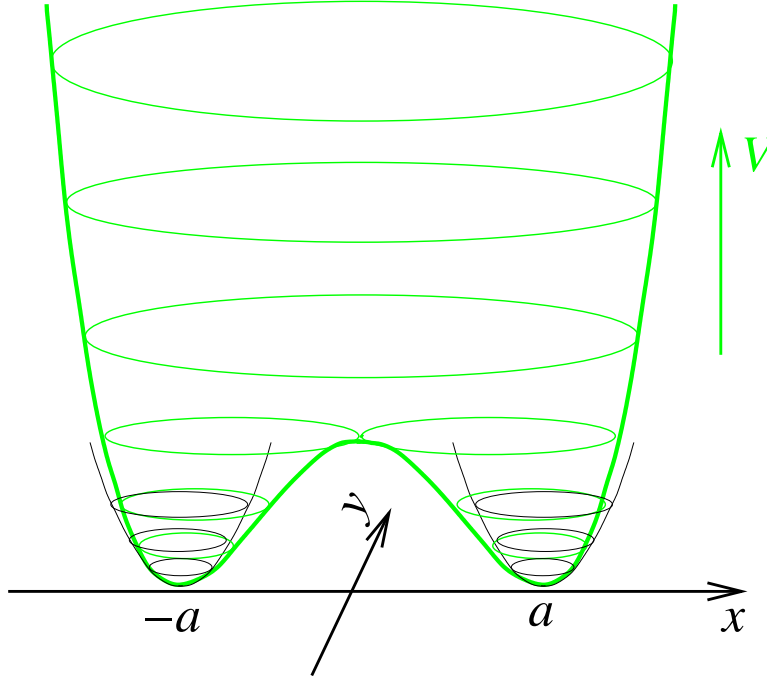


Figure 3.5. The model electrostatic potential that defines the quantum dots in a plane of 2DEG. Dots form around the minima of this potential at the points $(x, y) = (\pm a, 0)$. Near this minima, the binding potential is parabolic in both x and y direction and eigenfrequency of corresponding to the potential near the minimum is ω_0 .

where $|S\rangle$ and $(|T \pm 0\rangle)$ label a spin singlet and three spin triplet states. If the electrons interact through some two-body interaction W , the energies of these two states will differ by

$$E_T - E_S = J = \langle Triplets \pm 0 | W | Triplets \pm 0 \rangle - \langle Singlet | W | Singlet \rangle. \quad (3.17)$$

This energy difference between triplets and singlets can be reinterpreted in terms of spins as an isotropic exchange interaction $J\mathbf{S}_1 \cdot \mathbf{S}_2$. The crucial assumption behind this interpretation is that the spins state uniquely specifies the total state of the system. Only in that case we can label the states by spins.

A similar situation occurs in our system of quantum dots when the barrier is high. The orbital states are ground states in the dots and the total state is completely describes by spins.

When the barrier is lowered, the low lying two-electron states will have a significant amplitude for both electrons to be on the same dot or for electrons to be in excited states of the dots. These states are not completely described by spins. For example a pair of electrons in a spin singlet state can be in an orbital state with one electron on each dot, but they can also be in a state in which both electrons are on the same dot. For that reason, the Hamiltonian that describes both of those states and the transitions between them cannot be written as a function of just the two spins. Therefore an exact effective spin Hamiltonian does not exist in this case. An approximate spin Hamiltonian exists only when the probability for having the electrons in orbitally excited states is small.

In order to describe the situation when a spin Hamiltonian does not exist, we need to include the orbital excitations into our calculation. The energy scales that define important excitations are excitation energies in a single dot E_e and Coulomb energy cost of double occupancy E_C . These energy scales measure the gaps from the orbital state of two electrons in ground states on their dots to excited orbital states with an electron excited into a higher energy state (E_e) or with both electrons on the same dot (E_C).

A good spin qubit will spend most of the time during gate operation in the orbital ground state of its dot and must be in the ground state of its dot at the end of the operation. That will be the case if both energies E_e and E_C are large and the tunneling amplitude between the two dots is small. This property of a good spin qubit suggests that a useful approximation in deriving the properties of such a qubit would be to take into account only orbital ground states of the dots and low lying excitations.

Our choice of approximation is to take into account only one orbital —the ground state — per dot, but allow for the two-electron states in which both electrons occupy the ground state of the same dot. This is the famous Hund-Mulliken approximation of molecular physics. In our system, it is justified when the Coulomb repulsion energy scale E_C is significantly smaller than the energy scale of the single dot orbital excitations E_e . This limit of Coulomb repulsion dominating over orbital excitations corresponds to small quantum dots. The orbital excitation energy is proportional to the inverse square of the dot size, while the Coulomb repulsion energy is proportional to the inverse of the dot size. For small dots the energy cost of orbital excitations will be greater than the energy cost of double occupancy.

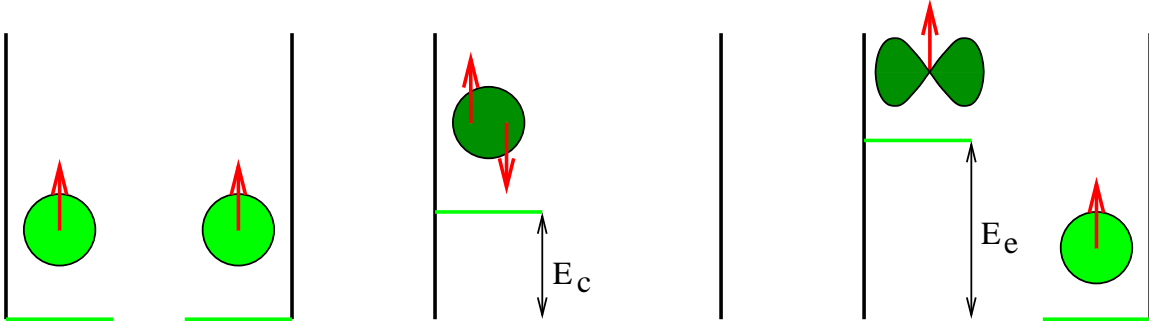


Figure 3.6. Orbital excitations. Two-body states with both single-body ground states occupied by an electron correspond to qubits. Hund-Mulliken approximation also takes into account the orbital excitations with doubly occupied one-body states that do not represent a spin qubit. These states are separated from the ground state by an energy gap E_c . Other orbital excitations, not included in Hund-Mulliken approximation, with electrons in excited one-body orbitals are separated from the ground state by an energy gap $E_e \approx \omega_0$.

Apart from describing a qubit, the Hund-Mulliken approximation also describes one of its important “failure modes.” The inclusion of doubly occupied states in the approximation scheme enables us to consider errors in gate operation due to transitions of electrons into orbital states that do not correspond to any state of a qubit. If electrons end up in such a state, qubits are lost from the computer.[Fig. 3.6].

In the limit of decoupled dots, and ignoring spin-orbit coupling, the single electron ground states will be the ground states of the Fock-Darwin Hamiltonian (3.11), centered at $(x, y) = (\pm a, 0)$,

$$\phi_{\pm a}(x, y) = \sqrt{\frac{m^* \Omega}{\pi}} \exp\left(-\frac{m^* \Omega}{2} \left((x \mp a)^2 + y^2\right) \pm iay/2l_B^2\right). \quad (3.18)$$

Here $\Omega = \sqrt{\omega_0^2 + \omega_L^2}$ is the frequency of the magnetically squeezed oscillator where $\omega_L = |e|B/(2m^*c)$ is the Larmor frequency and l_B is the magnetic length given by $2l_B^2 = 1/(m^* \omega_L)$. In zero magnetic field, the size of these wave functions is set by the effective Bohr radius $a_B = (m\omega_0)^{-1/2}$.

The Fock-Darwin states can be orthogonalized to obtain the Wannier states

$$|\Phi_1\rangle = \frac{1}{\sqrt{1-2Sg-g^2}}(|\phi_a\rangle - |g|\phi_{-a}\rangle), \quad (3.19)$$

$$|\Phi_2\rangle = \frac{1}{\sqrt{1-2Sg|-g^2}}(|\phi_{-a}\rangle - g|\phi_a\rangle), \quad (3.20)$$

where $S = \langle\phi_{-a}|\phi_a\rangle$ and $g = (1 - \sqrt{1 - S^2})/S$. We can then introduce second quantized operators $c_{1\alpha}^\dagger$ ($c_{1\alpha}$) and $c_{2\alpha}^\dagger$ ($c_{2\alpha}$) which create (annihilate) electrons in the states $|\Phi_1\rangle$ and $|\Phi_2\rangle$ with spin $\alpha = \uparrow, \downarrow$. These states are taken to be the single particle levels of the two electron system. Obviously, for large separation of the dots they turn into Fock-Darwin states on dots 1 and 2.

To proceed with the calculation, we represent two electron states as built by populating the low lying Wannier states (3.19). This approximation takes into account only one orbital per dot, the ground state of corresponding Fock-Darwin potential. The approximation takes into account the states in which electrons stay in lowest lying levels on their dots, but also includes the doubly occupied states in which both electrons lie in the same orbital. This amounts to restricting the full Hilbert space of the problem to the six-dimensional Hilbert space spanned by the states

$$|S_1\rangle = \frac{1}{\sqrt{2}}(c_{1\uparrow}^\dagger c_{2\downarrow}^\dagger - c_{1\downarrow}^\dagger c_{2\uparrow}^\dagger)|0\rangle, \quad (3.21)$$

$$|S_2\rangle = \frac{1}{\sqrt{2}}(c_{1\uparrow}^\dagger c_{1\downarrow}^\dagger + c_{2\downarrow}^\dagger c_{2\uparrow}^\dagger)|0\rangle, \quad (3.22)$$

$$|S_3\rangle = \frac{1}{\sqrt{2}}(c_{1\uparrow}^\dagger c_{1\downarrow}^\dagger - c_{2\downarrow}^\dagger c_{2\uparrow}^\dagger)|0\rangle, \quad (3.23)$$

$$|T_-\rangle = c_{1\downarrow}^\dagger c_{2\downarrow}^\dagger|0\rangle, \quad (3.24)$$

$$|T_0\rangle = \frac{1}{\sqrt{2}}(c_{1\uparrow}^\dagger c_{2\downarrow}^\dagger + c_{1\downarrow}^\dagger c_{2\uparrow}^\dagger)|0\rangle, \quad (3.25)$$

$$|T_+\rangle = c_{1\uparrow}^\dagger c_{2\uparrow}^\dagger|0\rangle, \quad (3.26)$$

where the S states are spin singlets, and the T states are triplets. States $|S_1\rangle$, $|T_-\rangle$, $|T_0\rangle$ and $|T_+\rangle$ are all singly occupied, i.e. each electron is in separate Wannier orbital, while singlets $|S_2\rangle$ and $|S_3\rangle$ are doubly occupied, i.e. both electrons are in the same orbital.

We proceed by calculating the matrix representation of the Hund-Mulliken Hamiltonian in this basis. The problem of determining the effective spin interaction for this Hamiltonian, but without spin orbit coupling, was solved before [52]. We will use these results, and present in detail the calculation of the spin orbit coupling contribution to interaction.

In the case of zero spin orbit coupling, the Hund-Mulliken Hamiltonian is described by the Hubbard model [67] with the direct exchange term added,

$$H^{Hubbard} = \sum_{\alpha=\uparrow,\downarrow} -t_H \left(c_{1\alpha}^\dagger c_{2\alpha} + H.c. \right) + V (\mathbf{S}_1 \cdot \mathbf{S}_2 + 3/4) + U_H (n_{1\uparrow} n_{1\downarrow} + n_{2\uparrow} n_{2\downarrow}). \quad (3.27)$$

Here

$$\mathbf{S}_\mu = \frac{1}{2} \sum_{\alpha,\beta=\uparrow,\downarrow} c_{\mu\alpha}^\dagger \boldsymbol{\sigma}_{\alpha\beta} c_{\mu\beta} \quad (3.28)$$

is the spin operator on site $\mu = 1, 2$,

$$V = \langle S_1 | C | S_1 \rangle - \langle T | C | T \rangle \quad (3.29)$$

is the ferromagnetic direct exchange,

$$U_H = \langle S_2 | C | S_2 \rangle - \langle S_1 | C | S_1 \rangle \quad (3.30)$$

is the Coulomb energy cost of doubly occupying a dot, and

$$t_H = -\frac{1}{2} \langle S_1 | T + C | S_3 \rangle \quad (3.31)$$

is the interdot tunneling amplitude. Expressions for these quantities as functions of the properties of the pair of quantum dots hosting the electrons can be found in [52].

This model describes a pair of electrons on two sites, 1 and 2. They can hop between the sites with transition amplitude t_H . Double occupancy of any site increases the system energy by on-site Coulomb repulsion U_H . Electrons also interact through direct exchange coupling V that splits singly occupied singlets and triplets.

3.2.1 Spin Orbit Coupling Hamiltonian

Spin-orbit coupling enters the Hamiltonian through the term

$$H^{SO} = \sum_{i=1,2} \mathbf{h}(\mathbf{k}_i) \cdot \mathbf{S}_i, \quad (3.32)$$

where $\mathbf{k} = \mathbf{p} - \frac{e}{c} \mathbf{A}$ is the canonical momentum of an electron in a magnetic field. Time-reversal symmetry requires that $\mathbf{h}(\mathbf{k})$ is an odd function of \mathbf{k} , $\mathbf{h}(\mathbf{k}) = -\mathbf{h}(-\mathbf{k})$. Thus \mathbf{h} is nonzero only in the absence of inversion symmetry.

For definiteness, we have taken the 2DEG in which the dots are formed to lie in the plane perpendicular to the [001] crystalline axis of GaAs, which then points along the z -axis. However, we allow the x -axis, which is parallel to the displacement vector of the two dots, to have any orientation with the respect to the [100] and [010] structural axes. To describe the dependence of the spin-orbit field \mathbf{h} on the crystal momentum \mathbf{k} , it is convenient to introduce unit vectors $\hat{\mathbf{e}}_{[110]}$ and $\hat{\mathbf{e}}_{[\bar{1}10]}$ which point in the [110] and $[\bar{1}10]$ structural directions, respectively, and define $k_{[110]} = \mathbf{k} \cdot \hat{\mathbf{e}}_{[110]}$ and $k_{[\bar{1}10]} = \mathbf{k} \cdot \hat{\mathbf{e}}_{[\bar{1}10]}$. We then have, following Kavokin [34],

$$\mathbf{h}(\mathbf{k}) \simeq (f_D - f_R)k_{[110]}\hat{\mathbf{e}}_{[\bar{1}10]} + (f_D + f_R)k_{[\bar{1}10]}\hat{\mathbf{e}}_{[110]}. \quad (3.33)$$

Here f_D is the strength of Dresselhaus contribution [35, 46] due to the bulk inversion asymmetry of the zinc-blende crystal structure of GaAs [Fig. 3.7], and f_R is the strength of Rashba contribution [36] due to the inversion asymmetry of the quantum well used to form the 2DEG. These quantities depend on details of the 2DEG confining potential and so will vary from system to system.

It was pointed out in [68] that H_{SO} has a special symmetry when $f_D = \pm f_R$. This can be seen directly from (3.33). When $f_D = f_R$ ($f_D = -f_R$) the direction of \mathbf{h} is independent of \mathbf{k} and is fixed to be parallel to $\hat{\mathbf{e}}_{[110]}$ ($\hat{\mathbf{e}}_{[\bar{1}10]}$). The full Hamiltonian (3.12) is then invariant under rotations in spin space about this axis. We will see below that this special case has a number of attractive features.

Since \mathbf{h} in (3.32) is a sum of direct products of single particle operators that are linear in components of \mathbf{k} with spin projections, the matrix elements of H^{SO} can be written as

$$\langle orb_1, spin_1 | H^{so} | orb_2, spin_2 \rangle = \sum_{\alpha=1,2} \sum_{j,l=x,y} h_{j,l} \langle orb_1 | k_{j,\alpha} | orb_2 \rangle \langle spin_1 | \mathbf{e}_l \cdot \mathbf{S}_\alpha | spin_2 \rangle, \quad (3.34)$$

where \mathbf{e}_l is a unit vector in the direction of the crystal axis. The index α counts electrons. The model we are considering is recovered from (3.34) when $-h_{x,x} = h_{y,y} = f_D$ (Dresselhaus terms), $h_{x,y} = -h_{y,x} = f_R$ (Rashba terms), with all the other components of \mathbf{h} being zero. This form of bulk inversion asymmetry induced spin-orbit coupling corresponds to dots in a thin two dimensional electron gas.

The spin orbit coupling Hamiltonian in second quantized notation is

$$H^{SO} = \sum_{\alpha,\beta=\uparrow,\downarrow} (-i\mathbf{P} \cdot c_{1\alpha}^\dagger \boldsymbol{\sigma}_{\alpha\beta} c_{2\beta} + H.c.). \quad (3.35)$$

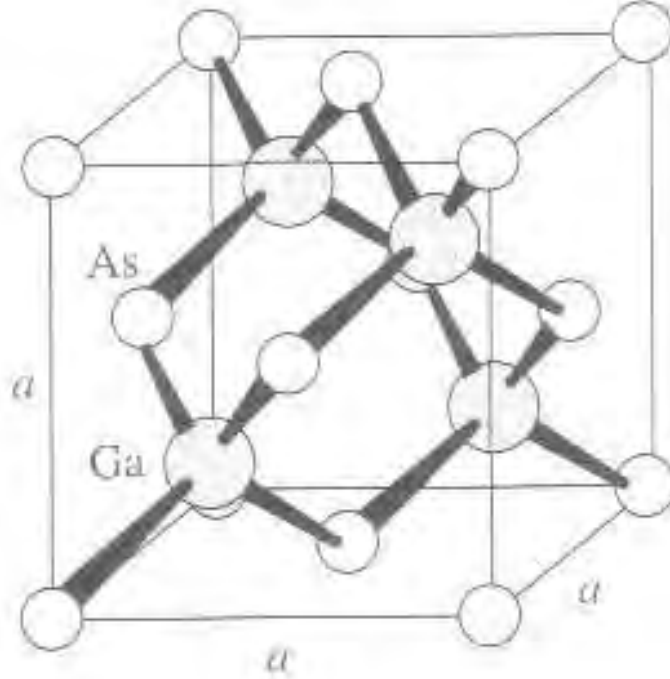


Figure 3.7. Zinc-blende crystalline structure of GaAs. The lattice consists of two face centered cubic lattices, one made of Ga and another of As ions, displaced along the diagonal of a cube by a quarter of its length. This crystal structure is not symmetric under inversion and its inversion asymmetry gives rise to Dresselhaus terms in spin-orbit coupling.

It describes a tunneling from one dot to the next with a spin flip around the axis $\hat{\mathbf{P}}$. The amplitude for this process is given by P . Details of the calculation of P are given in the Appendix.

Adding the spin-orbit coupling Hamiltonian (3.35) to the extended Hubbard model, we have shown that the Hamiltonian of the electrons on coupled quantum dots is of the form

$$\begin{aligned}
 H^{HM} = \sum_{\alpha, \beta = \uparrow, \downarrow} & - \left(c_{1\alpha}^\dagger (t_H \delta_{\alpha\beta} + i\mathbf{P} \cdot \boldsymbol{\sigma}_{\alpha\beta}) c_{2\beta} + H.c. \right) \\
 & + V (\mathbf{S}_1 \cdot \mathbf{S}_2 + 3/4) + U_H (n_{1\uparrow} n_{1\downarrow} + n_{2\uparrow} n_{2\downarrow}).
 \end{aligned} \tag{3.36}$$

Effects of spin-orbit coupling in this system are described by a single parameter $P = |\mathbf{P}|$. An intuitive picture of this modification of the extended Hubbard model by spin-orbit

coupling can be seen if we rewrite the hopping part of the Hund-Mulliken Hamiltonian (3.36) as

$$\sum_{\alpha,\beta=\uparrow,\downarrow} - \left(c_{1\alpha}^\dagger (t_H \delta_{\alpha\beta} + i\mathbf{P} \cdot \boldsymbol{\sigma}_{\alpha\beta}) c_{2\beta} + H.c. \right) = \sum_{\alpha,\beta=\uparrow,\downarrow} -t \left(c_{1\alpha}^\dagger R(\psi, \mathbf{e}_{\mathbf{P}})_{\alpha\beta} c_{2\beta} + H.c. \right), \quad (3.37)$$

where $t = \sqrt{t_H^2 + P^2}$ is the hopping amplitude, and $R(\psi, \mathbf{e}_{\mathbf{P}})$ is a spin rotation by the angle $\psi = 2 \arctan \frac{P}{t_H}$ about the axis parallel to \mathbf{P} , given by

$$R(\psi, \mathbf{e}_{\mathbf{P}})_{\alpha\beta} = \cos \frac{\psi}{2} \delta_{\alpha\beta} - i \sin \frac{\psi}{2} \hat{\mathbf{P}} \cdot \boldsymbol{\sigma}_{\alpha\beta}. \quad (3.38)$$

With (3.37) and (3.38) we can interpret the influence of spin orbit coupling on spin interaction as a precession of spin when it tunnels from one quantum dot to the next. Spin-orbit coupling induces tunneling with a spin flip about the axis \mathbf{P} and standard Hubbard model parameter t_H gives an amplitude for tunneling without a flip. The sum of these two processes corresponds to tunneling with a new amplitude t into a state with rotated spin. This modification of interaction is illustrated in [Fig. 3.8]. Given the physics of spin-orbit coupling, it is not surprising to see that it enters as a small spin precession which occurs whenever an electron tunnels between the dots.

The only remaining task in calculating the spin orbit Hamiltonian in Hund-Mulliken approximation is finding the value of the parameter \mathbf{P} . It is given by the matrix element

$$i\mathbf{P} = \langle \Phi_1 | \mathbf{h}(\mathbf{k}) | \Phi_2 \rangle = \langle \Phi_1 | (p_x - \frac{e}{c} A_x) | \Phi_2 \rangle \boldsymbol{\eta}, \quad (3.39)$$

where

$$\boldsymbol{\eta} = (f_D - f_R) \cos \theta \hat{\mathbf{e}}_{[\bar{1}10]} + (f_D + f_R) \sin \theta \hat{\mathbf{e}}_{[110]}. \quad (3.40)$$

Here θ is the angle the x -axis makes with the $[110]$ structural direction. This term introduces a small spin precession about an axis parallel to \mathbf{P} through an angle $\psi = 2 \arctan(P/t_H)$ when an electron tunnels between dots.

It is convenient to express the spin-orbit matrix element as $\mathbf{P} = s \mathbf{l}_{SO}$ where

$$s = \frac{\sqrt{(f_D - f_R)^2 \cos^2 \theta + (f_D + f_R)^2 \sin^2 \theta}}{a_B \omega_0} \quad (3.41)$$

is a dimensionless measure of the strength of spin-orbit coupling. As stated above, f_D and f_R depend on details of the potential confining the electron to the 2DEG. Thus θ , f_D and f_R

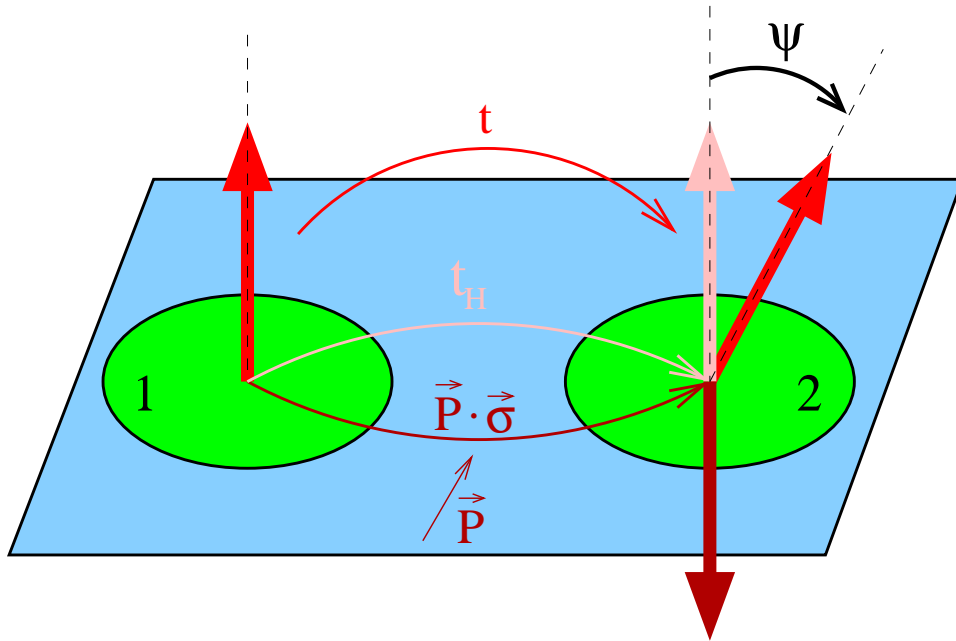


Figure 3.8. Precession on hopping. Spin-orbit coupling induces tunneling of an electron from one dot to the next. During the tunneling, the spin of electron is flipped about the \mathbf{P} axis. This process is represented by a dark red arrow. Hubbard model tunneling induces the same orbital transition, but keeps the spin orientation unchanged and it is represented by a pink arrow. Combined effect of these two processes is tunneling with a spin precession about the flip axis by an angle that depends on the ration of amplitudes for the two tunneling processes, represented by the red arrow.

are all parameters that in principle can be engineered to control the value of s . For example, if $\theta = 0$ then $s = |f_D - f_R|/(a_B\omega_0)$. Thus, for this orientation of the dots, if it is possible to design a system in which $f_D = f_R$, s can be made to vanish. Even if such perfect cancellation cannot be achieved, minimizing the difference $f_D - f_R$ will reduce s .

The parameter s lumps together all of the dependence of the spin orbit coupling contribution to the spin interaction on the material properties and dot parameters fixed during fabrication. In the remaining part of this section it will be treated as a free parameter. For typical parameters in GaAs quantum dots, its value is $s < 0.1$, based on the estimates of [34]. The remaining factor in \mathbf{P} is

$$\mathbf{l}_{SO} = \frac{\hbar\omega_0}{2} \frac{1-g^2}{1-2Sg+g^2} \frac{d}{b} e^{-d^2b(2-1/b^2)} \hat{\boldsymbol{\eta}}, \quad (3.42)$$

where $d = a/a_B$ is a dimensionless measure of the distance between dots, $b = \Omega/\omega_0$, and $\hat{\boldsymbol{\eta}} = \boldsymbol{\eta}/\eta$.

The Hund-Mulliken Hamiltonian (3.36) is a description of a pair of single electron quantum dots. Our goal is the extraction of the effective spin interaction. As discussed earlier, orbital excitations in the form of doubly occupied states indicate that strictly speaking the effective spin interaction does not exist, because the orbital degrees of freedom play some role in the system dynamics. An effective spin interaction is an approximation to the true system behavior when the orbital excitations do not play a significant role. This is the case when on-site Coulomb repulsion is much bigger than the amplitudes of both direct tunneling and tunneling mediated by spin orbit coupling, $U_H \gg t_H, |\mathbf{P}|$. This description gives the derivation of effective spin Hamiltonian and also determines the range of its applicability.

3.3 Axial Symmetry of the Effective Spin Interaction

When the Hund-Mulliken Hamiltonian (3.36) describes a pair of spins in singly occupied one-electron orbitals, the spins of these two electrons are spin qubits. Neglecting the doubly occupied states, the interactions in this system can be described by an effective spin Hamiltonian. That will be the case when the energy cost of double occupancy U_H is much larger than the hopping amplitude t_H and the spin orbit coupling parameter P . We begin by noting that the system has an axial symmetry around the direction of the spin orbit coupling induced vector \mathbf{P} . This implies that the spin interaction will have the same axial symmetry and will then be of the form

$$H^m(J, \beta^{int}, \gamma^{int}) = J (\mathbf{S}_1 \cdot \mathbf{S}_2 + \beta^{int} (S_{1x}S_{2y} - S_{1y}S_{2x}) + \gamma^{int} (S_{1x}S_{2x} + S_{1y}S_{2y})). \quad (3.43)$$

This is the most general axially symmetric form of a two spin interaction. The parameter J is the strength of isotropic coupling. Because of axial symmetry, the direction of the vector coupling β^{int} and the form of the symmetric tensor coupling $\boldsymbol{\Gamma}^{int}$ are fixed and we only need one scalar parameter to completely specify each of them, β^{int} measures the strength of vector

and γ^{int} of the tensor coupling. We now take the z axis in spin space to be the symmetry axis, i.e. an axis parallel to the precession vector \mathbf{P} .

We determine the values of the parameters J , β^{int} and γ^{int} by solving (either exactly or perturbatively) both the model spin Hamiltonian (3.43) and the microscopic Hund-Mulliken Hamiltonian (3.36) and matching the eigenvalues and eigenvectors. Our earlier symmetry analysis tells us that the isotropic exchange J term exists even in the absence of spin orbit coupling, the antisymmetric anisotropy β^{int} is first order, and the symmetric anisotropy γ^{int} is second order in spin-orbit coupling. The matching of solutions proceeds by doing a perturbatively expansion in powers of \mathbf{P} of the eigenvalues and eigenvectors of the microscopic Hund-Mulliken Hamiltonian. We then fit the parameters of the model spin Hamiltonian (3.43) to get the same spectrum up to second order in \mathbf{P} and the same eigenstates up to first order. The result is

$$J = J_0 + 4P^2 \frac{\cos^2 \frac{\theta}{2}}{J_0 - 2V + U_H} + o(SO^2) \quad (3.44)$$

$$\beta^{int} = 4P \frac{\sin \frac{\theta}{2}}{J} + o(SO^3) \quad (3.45)$$

$$\gamma^{int} = 8P^2 \frac{V}{J(V(V - U_H) - 4t_H^2)} - \frac{\beta^2}{2} + o(SO^2), \quad (3.46)$$

where J_0 is the strength of anisotropic exchange without spin orbit coupling, V is the strength of direct ferromagnetic exchange interaction, and the angle θ is given by

$$\sin \theta = \frac{4t_H}{\sqrt{U_H^2 + (4t_H)^2}}, \quad (3.47)$$

which measures the relative sizes of the hopping amplitude and the on-site Coulomb repulsion.

The dependence of the parameters of the spin interaction on the interdot distance is shown in [Fig. 3.9].

The equations (3.43) and (3.44)-(3.46) define an effective low energy spin Hamiltonian for electrons on coupled quantum dots that perturbatively includes the effects of spin orbit coupling. We have shown that for the configuration of the dots that we investigate the only new parameters to be calculated from the microscopic Hamiltonian is P .

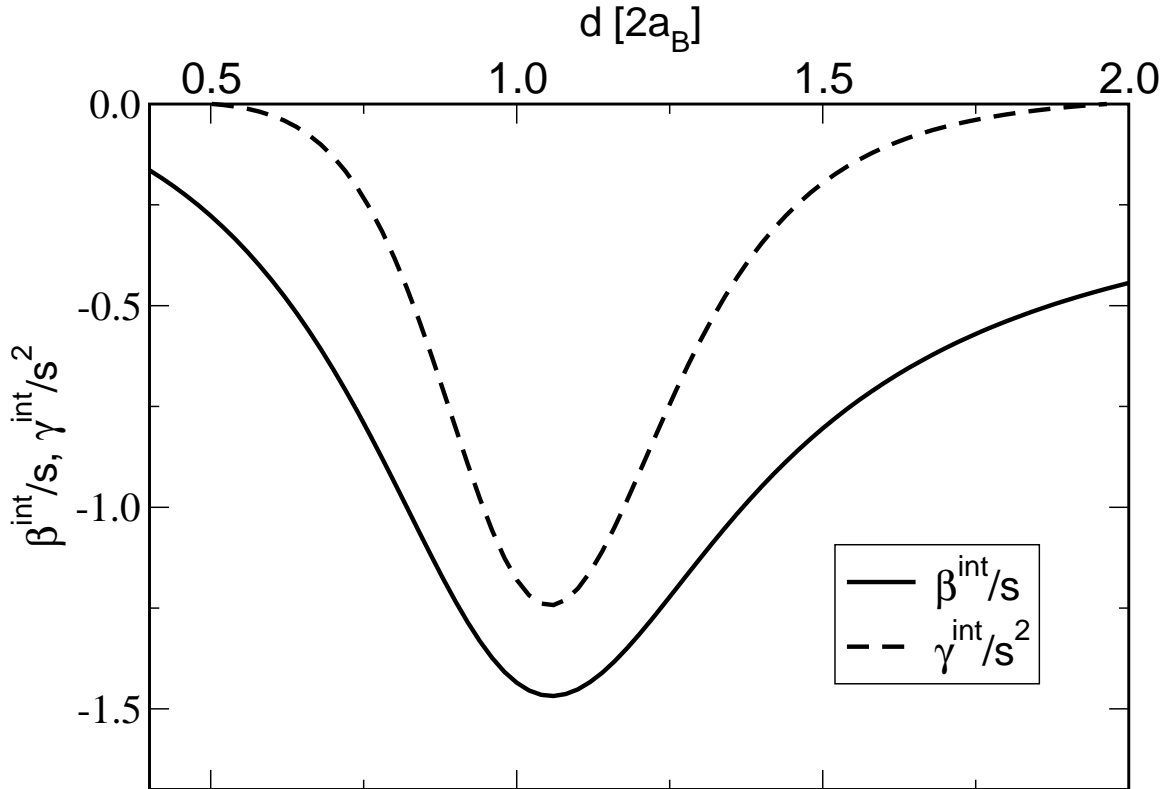


Figure 3.9. Strengths of anisotropic terms in effective spin Hamiltonian as a function of the interdot distance. Plotted quantities are β^{int}/s and γ^{int}/s^2 , where s is the dimensionless measure of spin orbit coupling strength (3.41). Data points are calculated from results (3.45) and (3.46). The system is a pair of GaAs quantum dots of the Bohr radius $a_B \approx 20nm$, corresponding to the simple level spacing of $\omega_0 = 3meV$, and for this calculation it was assumed that $s = 0.01$.

3.4 Pulses of Hund-Mulliken Hamiltonian

We now consider pulsing the Hund-Mulliken Hamiltonian H^{HM} by varying the distance between the dots, the barrier height, or some combination of the two, in such a way that the two electron spins interact for a finite period of time, but are well separated at the beginning and end of the pulse. We assume the initial state of the system is in the four-dimensional Hilbert space describing two qubits, i.e. the space spanned by the singly occupied states $|S_1\rangle, |T_0\rangle, |T_-\rangle$ and $|T_+\rangle$. As the pulse is carried out, the eigenstates of H^{HM} at any given instant in time can be grouped into four low-energy states separated by a gap of order U_H

from two high-energy states. If the pulse is sufficiently adiabatic on a time scale set by $\sim \hbar/U_H$, the amplitude for nonadiabatic transitions which would leave the system in the excited state $|S_2\rangle$ at the end of the pulse can be made negligibly small [69]. If this condition holds, the final state of the system can also be assumed to be in the four-dimensional Hilbert space of two qubits. We will see that this condition is easily achieved below.

One way to theoretically study the effect of such a pulse would be to first reduce H^{HM} to an effective anisotropic spin Hamiltonian acting on the four-dimensional low-energy Hilbert space, as we have done in the previous section, and then consider pulsing this effective model using the perturbative results of Chapter 2. The problem with this approach is that any such effective spin Hamiltonian will only be valid if the pulse is adiabatic, not only on the time scale \hbar/U_H , but also on the much longer time scale set by the inverse of the small energy splittings within the low-energy space due to the spin-orbit induced anisotropic terms. However, it is precisely the nonadiabatic transitions induced by these terms which give rise to the quantum gate corrections we would like to compute.

Although we may not be able to define an instantaneous effective spin Hamiltonian during the pulse, we can define one which describes the net effect of a full pulse. This definition, which is essentially the same as the "gate Hamiltonian" defined in Chapter 2, amounts to parameterizing the quantum gate produced by the pulse as

$$U = \exp -i\lambda H, \tag{3.48}$$

where U acts on the four-dimensional Hilbert space of the initial and final spin states. H is then an effective spin Hamiltonian, i.e. it can be expressed entirely in terms of the spin operators \mathbf{S}_1 and \mathbf{S}_2 .

We have seen from symmetry arguments that time symmetric pulsing of an axially symmetric Hamiltonian, such as H^{HM} when f_D and f_R are constant, which is itself time-reversal symmetric at all times, will automatically produce an axially and time reversal symmetric gate of the form (2.50), provided the pulse is adiabatic so that the initial and final states of the system are in the four-dimensional Hilbert space of two qubits. It is natural to then ask what the effect of the inevitable deviations from time symmetric pulsing will be on the resulting gate. To investigate this we have performed some simple numerical simulations of coupled quantum dots.

In our calculations, we imagine pulsing the dots by varying the dimensionless distance d between them according to

$$d(t) = d_0 + \left(\frac{t}{\tau + rt} \right)^2. \quad (3.49)$$

Here d_0 is the distance at the point of closest approach, τ is a measure of the pulse duration, and r is a dimensionless measure of the time asymmetry of the pulse. This form describes the generic behavior of any pulse for times near the pulse maximum ($t = 0$). Note that for large $|t|$, and for $r \neq 0$, the distance $d(t)$ will saturate, and has a singularity for some negative t . We have taken r to be small enough so that the dots decouple long before this leads to any difficulty.

For our calculations, we work in zero magnetic field and take $\hbar\omega_0 = 3$ meV and $d_0 = 1$, corresponding to $a \simeq 20$ nm at closest approach. The resulting time dependences of the parameters in H_{HM} are shown in [Fig. 3.10]. Note that the spin-orbit matrix element plotted in this figure is l_{SO} , while the spin-orbit matrix element appearing in H_{HM} is $\mathbf{P} = sl_{SO}\hat{z}$ where s is the dimensionless measure of spin-orbit coupling.

For a given pulse $H_{HM}(t)$ we integrate the time-dependent Schrödinger equation to obtain the evolution operator U for the full pulse. If the pulse is adiabatic then the matrix elements of U which couple the singly occupied states $|S_1\rangle$ and $|T_0\rangle$ to the doubly occupied state $|S_2\rangle$ can be made negligibly small [69]. The quantum gate is then obtained by simply truncating U to the 4×4 matrix acting on the two-qubit Hilbert space. By taking the log of this matrix we obtain $\lambda H = i \log U$ and thus the parameters $\lambda, \alpha, \beta, \gamma$. Note that when calculating $\log U$, there are branch cuts associated with each eigenvalue of U , and as a consequence λH is not uniquely determined. We resolve this ambiguity by requiring that as the pulse height is reduced to zero and U goes continuously to the identity that $\lambda H \rightarrow 0$ without crossing any branch cuts.

We fix the pulse width τ by requiring that if we turn off spin-orbit coupling ($s = 0$) we obtain a $\lambda = \pi/2$ pulse, i.e. a square-root of swap. For the parameters used here we find this corresponds to taking $\tau = 23.9/\omega_0 \simeq 5$ ps. We have checked that these pulses are well into the adiabatic regime. The magnitudes of the matrix elements coupling singly occupied states to the doubly occupied state $|S_2\rangle$ are on the order of $|\langle S_1|U|S_2\rangle| \sim 10^{-6}$ and $|\langle T_0|U|S_2\rangle| \sim s10^{-6}$.

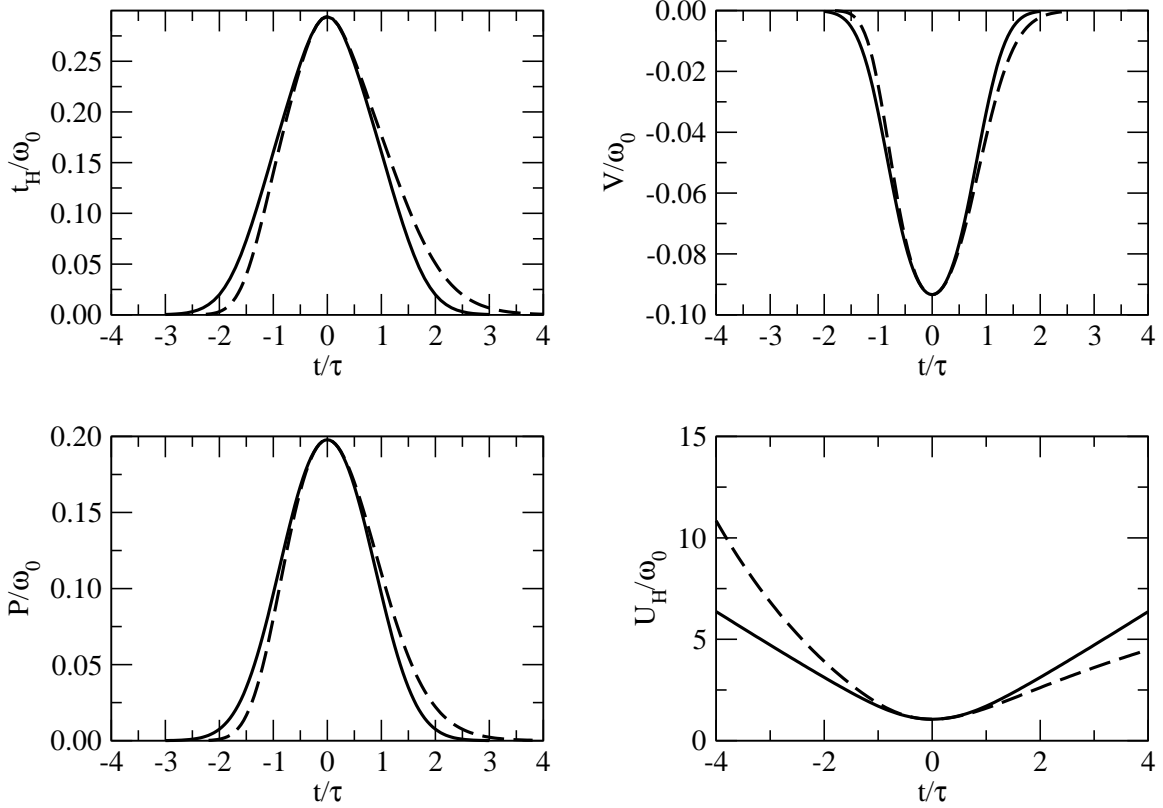


Figure 3.10. Time dependence of the terms in Hund-Mulliken Hamiltonian. Graphs are for spin independent hopping t_H , direct exchange V , spin orbit coupling induced hopping with spin flip P and energy cost of double occupancy U_H . The energy scale on all the graphs is the splitting of harmonic oscillator levels in isolated dots ω_0 . The time scale is characteristic time scale of the pulse τ . Pulses in the figure are tailored to produce a square root of swap (\sqrt{SWAP}) gate in the limit of zero spin orbit coupling. The solid line is a time symmetric pulse with asymmetry parameter $r = 0$. The dashed line is the most asymmetric pulse we have considered, corresponding to asymmetry parameter $r = 0.1$.

3.4.1 Slightly asymmetric pulses

Once τ is fixed, there are two parameters characterizing each pulse, s and r , and four parameters characterizing the resulting gate, λ , α , β , and γ . The transformation properties of these parameters under parity (P) and time reversal (T) are summarized in Table I. These properties follow from the fact that under time reversal $\mathbf{S}_\mu \rightarrow -\mathbf{S}_\mu$ and $r \rightarrow -r$, while $\mathbf{P} = s l_{SO} \hat{\mathbf{z}}$ is invariant and under parity $\mathbf{S}_A \leftrightarrow \mathbf{S}_B$ and $\mathbf{P} \rightarrow -\mathbf{P}$, while r is invariant. Note

Table 3.1. Symmetry properties of the pulse parameters r and s , and gate parameters λ , α , β and γ under parity P and time reversal T .

	r	s	λ	α	β	γ
P	+	-	+	-	-	+
T	-	+	+	-	+	+

that, as defined in (3.41), the parameter s is positive. Here we allow s to change sign when the direction of the vector \mathbf{P} is reversed, thus under parity $s \rightarrow -s$.

These symmetry properties imply that if s and r are small, the parameters of the effective Hamiltonian will be given approximately by

$$\alpha \simeq C_\alpha r s, \tag{3.50}$$

$$\beta \simeq C_\beta s, \tag{3.51}$$

$$\gamma \simeq C_\gamma s^2, \tag{3.52}$$

$$\lambda \simeq \lambda_0 + C_\lambda s^2, \tag{3.53}$$

where the coefficients should be of order 1. For the pulses we consider here $\lambda_0 = \pi/2$.

The results of our calculations are shown in [Fig. 3.11]. Each point corresponds to a separate numerical run. The plots for λ , β and γ show their dependence on s when $r = 0$. The dependence of the parameter α on pulse asymmetry is shown by plotting α/s vs. r . For the s values we have studied, up to $|s| = 0.1$, the numerical results for α/s are essentially independent of s for a given r . These results are clearly consistent with the above symmetry analysis.

3.5 Robust CNOT

There are two main implementations of the universal gate sets that use isotropic exchange. One is exchange only quantum computation that was already shown to benefit from symmetry based control. Another approach is to use isotropic exchange and the single spin rotations for CNOT construction and then proceed with the standard universal set consisting of CNOT and all the single spin rotations.

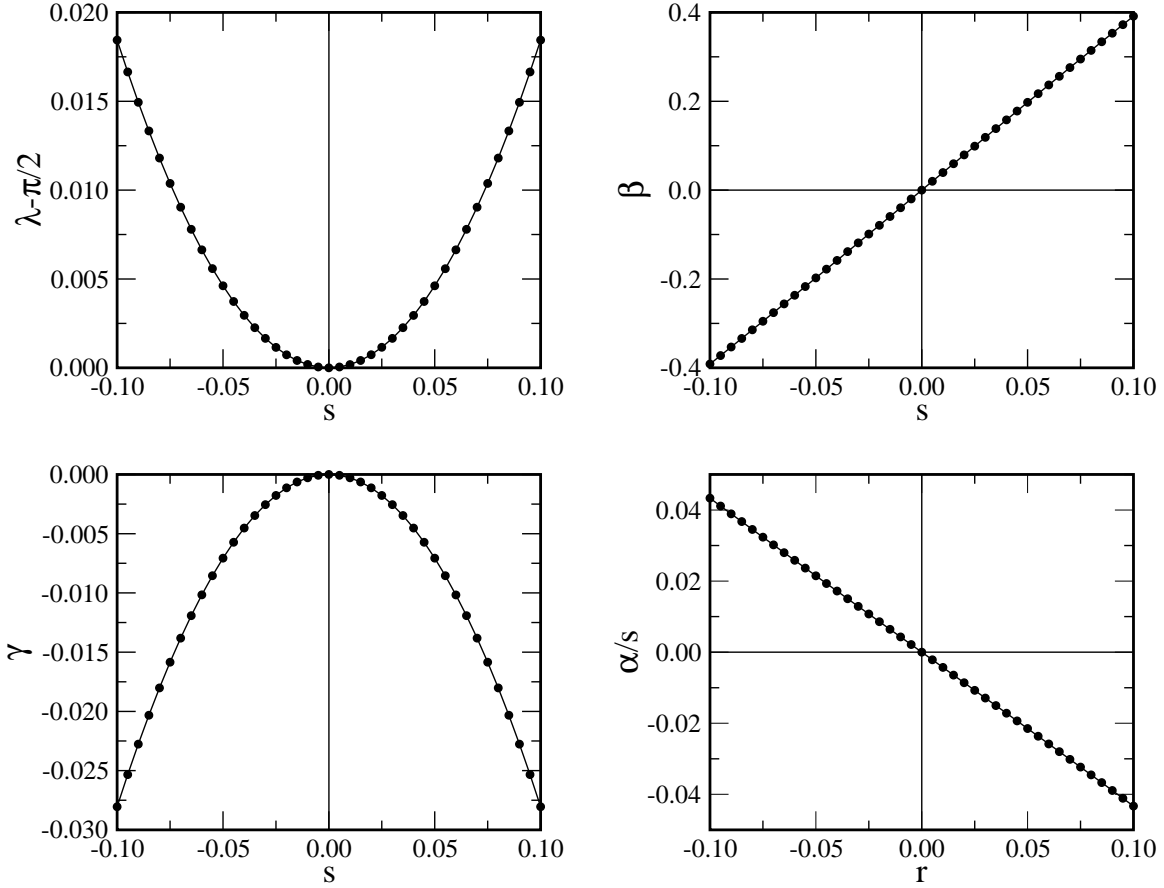


Figure 3.11. Parameters appearing in the gate Hamiltonian derived from pulses. The parameters for isotropic pulse strength λ , antisymmetric anisotropy β and symmetric anisotropy γ are shown as functions of dimensionless spin orbit coupling strength s for the case of time symmetric pulses ($r = 0$). For α the quantity α/s is plotted vs. pulse anisotropy r . We have verified that the ratio α/s is essentially independent of s for all values we have considered ($|s| \leq 0.1$).

Standard implementations of the universal gate sets are dependent on isotropic exchange gates. Results about time symmetric pulses as a simple way to obtain time reversal symmetric gates, presented in Chapter 1 of this thesis, encouraged a couple of authors to study these gates, rather than isotropic exchange, as a natural easily implemented two spin manipulation in a system of coupled quantum dots.

An important result of Burkard and Loss [51] showed that the standard construction of the CNOT gate based on isotropic exchange also works exactly with any symmetric gate of

the form (3.1). If we try to implement the CNOT gate using standard construction with \sqrt{SWAP} isotropic exchange gate, errors due to anisotropy of spin interaction may spoil the result. Instead of a CNOT construction considered in Chapter 2 and illustrated in [Fig. 2.1], in the presence of anisotropy a more general gate

$$U\left(\frac{\pi}{2}; \alpha, \beta, \gamma\right) = \exp\left(-iH^m\left(\frac{\pi}{2}; \alpha, \beta, \gamma\right)\right), \quad (3.54)$$

with axially symmetric Hamiltonian H^m defined in (3.43) is applied whenever the original construction calls for isotropic \sqrt{SWAP} gate.

Our microscopic consideration shows that the decoupled triplets with $S_z = \pm 1$ are not affected by the spin-orbit coupling. Action of anisotropic gates on these states is the same as the action of corresponding isotropic gate. We will now see how anisotropic gates act in the remaining two dimensional space.

In the pseudospin space defined with singlet state of two spins representing pseudospin up and triplet state with zero projection representing pseudospin down, the axially symmetric gate is a pseudospin rotation

$$U(\lambda; \alpha, \beta, \gamma) \rightarrow \exp\left(-\frac{i}{2}\mathbf{b} \cdot \boldsymbol{\sigma}\right), \quad (3.55)$$

parametrized by the vector $\mathbf{b} = \lambda(\alpha, \beta, 1 + \gamma)$ in the convention where the vector parametrizing a rotation points along the rotation axis and has an intensity equal to the rotation angle. Anisotropy effects on the essential two-qubit part of the CNOT circuit are shown in figure [Fig. 3.12]. When there is no anisotropy $\alpha = \beta = \gamma = 0$ and the vector \mathbf{b} points along the pseudospin z axis. The role of anisotropy is to pull the pseudospin rotation axis away from z direction.

Single qubit $Z \otimes \mathbf{1}$ operation sandwiched between the two-qubit gates is a rotation about the pseudospin x axis by the angle π . It is represented by pseudospin Pauli matrix with a phase factor, iX .

If there was no anisotropy, the sequence of gates in a circuit of [Fig. 3.12] would act as a simple phase factor of i on the pseudospin space. In this space, it is a sequence of $\pi/2$ rotation about z axis, π rotation about x with an extra factor i and finally another $\pi/2$ rotation about z . Since the x rotation by π flips all the vectors in yz plane, the second z rotation will cancel the initial one, and the phase factor will be the only change of states in the pseudospin space.

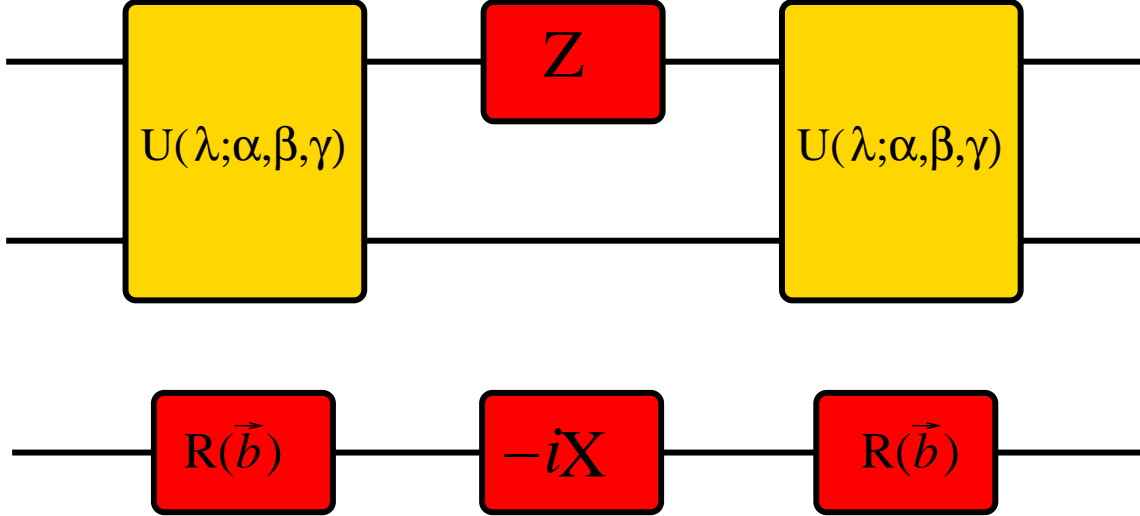


Figure 3.12. Effect of axially symmetric anisotropy on a CNOT construction.

When there is anisotropy, the pseudospin rotations that describes two-qubit gates will not be about z axis, but about an axis parallel to $\mathbf{b} = \lambda(\alpha, \beta, 1 + \gamma)$. However, the previous argument showing that the combination of gates from [Fig. 3.12] gives only a phase factor holds whenever the rotations caused by two-qubit gates are about a fixed axis in yz plane, and not necessarily about the z axis.

Therefore, this CNOT construction is exact when the vector \mathbf{b} has a vanishing component in pseudospin x direction. At the level of a two qubit gates (3.54) it means that the gate construction is exact whenever $\alpha = 0$. This condition is satisfied for time symmetric pulses.

Microscopic considerations of this chapter are therefore immediately useful in application of a CNOT gate. The condition for validity of the construction is immediately satisfied when the voltage pulses that produce the gate are symmetric in time and the interaction is axially symmetric. Even when the interaction is not isotropic, time symmetric pulses will produce a gate that is axially symmetric up to first order in spin-orbit coupling.

Apart from immediate usefulness in CNOT construction, the results about the gate symmetry based on microscopic model can help in the quantum gate design. Intensities of various interaction terms calculated here are dependent on the details of device fabrication,

but the overall symmetry of the gates is not. Since the symmetry of the gates is a robust property, application of symmetric gates is less sensitive to the details of device design.

CHAPTER 4

SPIN-ORBIT COUPLING AS A RESOURCE: USING THE GATE ANISOTROPY

Brothers and sisters, the time has come for each and every one of you to decide whether you are going to be the problem or you are going to be the solution...

Brother J.C. Crawford

In the previous chapters, we have shown that the effect of spin orbit coupling induced anisotropy on quantum gates performed in a spin-based quantum computers can be reduced using pulse shaping and device fabrication techniques. These studies taught us that the anisotropy in a quantum gate can be controlled. Now we show that control over anisotropy can be *used* to apply quantum gates, becoming a computational resource, rather than an obstacle in the design of quantum gates.

The techniques of pulse shaping and fabrication that reduce the effects of anisotropy lead to quantum gates with specific symmetries. The requirement of time symmetric pulsing imposes time reversal symmetry on the resulting gate. Microscopic calculation shows that the gate symmetry is further increased in dots fabricated along specific crystalline axes, when the resulting gate also shows axial symmetry.

In this chapter we construct a universal set of quantum gates over qubits encoded into pairs of spins out of “elementary” quantum gates with both axial and time reversal symmetry. We define an elementary gate as a gate produced in a single voltage pulse. Later in the chapter, we examine the control of the symmetric interaction and estimate the amount of control over anisotropy in a realistic device. It will turn out that the constraints on the available amount of control will come from details of the spin interaction in the system and more importantly from the physical processes that produce errors in gate operation for

voltage pulses that either take a long time on the time scale set by the decoherence, or a short time on the time scale set by the nonadiabatic orbital transitions.

4.1 Universal Gate Set Construction

In this section we give a construction of a universal set of quantum gates over qubits encoded into pairs of electron spins that uses only elementary gates with both axial and time reversal symmetry. Elementary operations in this construction act on a pair of electron spins on coupled single electron quantum dots aligned along a specific axis of a crystal with zinc-blende structure. Control is achieved using *only* voltage pulses on electrodes that define the dots. Such voltage-only control is a great advantage in implementation of spin-based quantum computing, because voltages are the simplest control parameters in quantum dot quantum computer.

Microscopic analysis of spin-orbit coupling effects, presented in chapter 3, shows that axial symmetry of the spin interaction is present in quantum dots aligned along the [110] axis and lying in (001) plane of GaAs for any value of the control voltages. Axial symmetry of the interaction throughout the pulse implementing an elementary gate implies that the resulting gate will also be axially symmetric. The most general form of axially symmetric gate, acting between neighboring spins \mathbf{S}_1 and \mathbf{S}_2 is

$$U(\lambda, \alpha, \beta, \gamma) = \exp -i\lambda \left(\mathbf{S}_1 \cdot \mathbf{S}_2 + \beta (S_{x1}S_{y2} - S_{y1}S_{x2}) + \right. \quad (4.1) \\ \left. + \gamma (S_{x1}S_{x2} + S_{y1}S_{y2}) + \frac{\alpha}{2} (S_{1z} - S_{2z}) - \frac{1}{4} \right),$$

where we have chosen the symmetry axis to point along the z direction in spin space. Note that the “ $\boldsymbol{\mu}$ ” term that would correspond to a homogeneous magnetic field pointing in symmetry direction is allowed by axial symmetry, but it is missing from the general axially symmetric gate (4.1). This term is absent, because it can not be generated by a pulse of axially symmetric interaction, as can be inferred from perturbative expressions for gate parameters, (2.41) and (2.42). A constant term $-1/4$ is added for later convenience.

In terms of the gate Hamiltonian, the Hermitian operator that would reproduce this gate if exponentiated, (4.1) is

$$U(\lambda, \alpha, \beta, \gamma) = \exp -i\lambda H^{gate}(\lambda, \alpha, \beta, \gamma), \quad (4.2)$$

with the gate Hamiltonian H^{gate} of the form

$$H^{gate}(\lambda, \alpha, \beta, \gamma) = \mathbf{S}_1 \cdot \mathbf{S}_2 + \beta (S_{x1}S_{y2} - S_{y1}S_{x2}) + \gamma (S_{x1}S_{x2} + S_{y1}S_{y2}) + \frac{\alpha}{2} (S_{1z} - S_{2z}) - \frac{1}{4}. \quad (4.3)$$

The symmetry of the gates with respect to rotations about the z axis implies that the total spin projection on this z axis will be conserved in any applied gate. A universal set of gates, on the contrary, contains gates that can produce arbitrary operation on qubits through repeated application. It is now clear that the repeated application of elementary gates with axial symmetry (4.1) can not lead to all the gates from any universal set acting on single spins as qubits. As in [32], the symmetry of our elementary operation forces us to use qubits encoded into states that all have the symmetry of underlying interaction.

In our case of axial symmetry all the qubit states must have the same projection of the total spin on z axis. The smallest number of electron spins that allows for such encoding is two. To describe this encoding, we associate a pseudospin space with every nearest-neighbor pair of spins i and $i + 1$. This space is spanned by the states

$$|S\rangle_{i,i+1} = \frac{1}{\sqrt{2}}(|\uparrow_i\downarrow_{i+1}\rangle - |\downarrow_i\uparrow_{i+1}\rangle), \quad (4.4)$$

$$|T_0\rangle_{i,i+1} = \frac{1}{\sqrt{2}}(|\uparrow_i\downarrow_{i+1}\rangle + |\downarrow_i\uparrow_{i+1}\rangle), \quad (4.5)$$

where the associated pseudospin states are

$$|S\rangle_{i,i+1} \equiv |\uparrow'\uparrow'\rangle \quad (4.6)$$

$$|T_0\rangle_{i,i+1} \equiv |\uparrow'\downarrow'\rangle. \quad (4.7)$$

Within this pseudospin space axially symmetric gates correspond to spin rotations. Triplet states with nonzero total spin projection on the symmetry axis are decoupled, as we demonstrated in appendix. The phase convention in (4.1) is chosen so that the spin states without assigned pseudospin remain invariant under the action of elementary gates. The space of these decoupled states is orthogonal to pseudospin space and spanned by $|T_+\rangle_{i,i+1} = |\uparrow_i\uparrow_{i+1}\rangle$ and $|T_-\rangle_{i,i+1} = |\downarrow_i\downarrow_{i+1}\rangle$.

Given these definitions and a phase convention, the action of elementary gates in pseudospin space is

$$U_{i,i+1}(\lambda, \phi) = \exp\left(i\frac{\lambda}{2}\right) \exp\left(-\frac{i}{2}\phi \cdot \boldsymbol{\sigma}^{(i,i+1)}\right), \quad (4.8)$$

where $\phi = \lambda(\alpha, \beta, 1 + \gamma)$ and the components of $\sigma = (\sigma_x, \sigma_y, \sigma_z)$ are Pauli matrices, with the superscript $(i, i + 1)$ indicating that they act in the pseudospin space associated to spins i and $i + 1$. These gates are pseudospin rotations by an angle

$$\phi = \lambda\sqrt{1 + \alpha^2 + \beta^2 + 2\gamma + \gamma^2} = \lambda + O(SO^2), \quad (4.9)$$

with the dominant part determined by isotropic component of the interaction and a correction that is of the second order in axial anisotropy caused by spin-orbit coupling, indicated by $O(SO^2)$ term. The pseudospin rotation axis is parallel to ϕ .

Outside the pseudospin space, states remain invariant under the action of any axially symmetric gate (4.1)

$$U_{i,i+1}(\lambda, \phi)|T_{\pm}\rangle_{i,i+1} = |T_{\pm}\rangle_{i,i+1}. \quad (4.10)$$

Note that while this invariance is a consequence of phase convention, it is relevant. In order to keep the states invariant in (4.10) we had to keep the overall phase factor $\exp(i\lambda/2)$ in (4.8) that is irrelevant if we only care about pseudospin states. In the construction of a universal set of gates we are going to need this phase. Since computational and noncomputational states of a pair of spins get different phases in gate application, these phases will be of importance when the gate acts between spins that do not belong to the same qubit.

Axial symmetry will be set in the fabrication of quantum dots. All control over gate parameters will come from pulse shaping. The isotropic part of the spin interaction will approximately determine the angle of pseudospin rotation, λ , and the anisotropic corrections that depend on the details of the pulse will determine the pseudospin rotation axis through spin-orbit coupling induced terms α , β and γ .

The pulse shape control was investigated in chapter 2 and chapter 3 and we do know some properties of the gate produced by a pulse of axially symmetric interaction. Following the general discussion of chapter 2, we know that if the pulses are symmetric in time, the resulting gate will be invariant under time reversal. Thus, the α term is odd under time reversal, it vanishes for time symmetric pulses. In what follows, we assume that the pulses are time symmetric and $\alpha = 0$. Allowing for nonzero α would not simplify universal gate set construction.

Pulse shaping beyond keeping the pulses symmetric in time will give us some control over the integrated isotropic exchange λ , antisymmetric anisotropy β and symmetric anisotropy

γ in (4.8). We will be able to vary λ at will, β will be first order in spin-orbit coupling and γ second order. Different pulse shapes will control the values of β and γ , but the amount of control will be limited. Also, β will be larger than γ and will vary in a wider range.

When time symmetric voltage pulses are used to implement the gate, the gate applied in a single pulse will consist of pseudospin rotations about an axis in yz plane. Isotropic exchange is the dominant interaction of spins so β and γ will be small and β will be larger and easier to control than γ . The range of available rotation axes will be continuous and it will span a wedge in yz plane in the vicinity of pseudospin z axis. Width of the wedge of available axes will change slightly with the rotation angle ϕ , but to a good approximation we may assume that it is constant. The opening angle θ_m of wedge of available axes is a measure of our ability to control spins. This wedge may or may not contain the z axis that corresponds to isotropic exchange. The wedge of available pseudospin rotation axes is sketched in [Fig.4.1].

We now show how the available pseudospin rotations can be combined to perform all the single qubit rotations and the CNOT gate, thus providing a universal set of quantum gates [44]. The setup of our quantum computer is a linear array of quantum dots. The dots are aligned along [110] crystalline axis of a zinc blende semiconductor to enforce axial symmetry of spin-orbit interaction. Within this array, each qubits is encoded into a pair of spins on dots i and $i + 1$ for odd i . We choose logical basis states

$$|0_L\rangle_{i,i+1} = |S\rangle_{i,i+1} \quad (4.11)$$

$$|1_L\rangle_{i,i+1} = |T_0\rangle_{i,i+1}. \quad (4.12)$$

These states also correspond to a basis in the pseudospin space of same pair of spins

$$|0_L\rangle_{i,i+1} = |\uparrow'\uparrow'\rangle_{i,i+1} \quad (4.13)$$

$$|1_L\rangle_{i,i+1} = |\uparrow'\downarrow'\rangle_{i,i+1}. \quad (4.14)$$

This identification of the logical qubit basis and the pseudospin basis lets us identify single qubit gates with pseudospin rotations. It is now obvious that in order to apply all single qubit operations we must be able to perform all pseudospin rotations. We can now rely on ordinary geometric intuition in construction of the single qubit gates from a universal set.

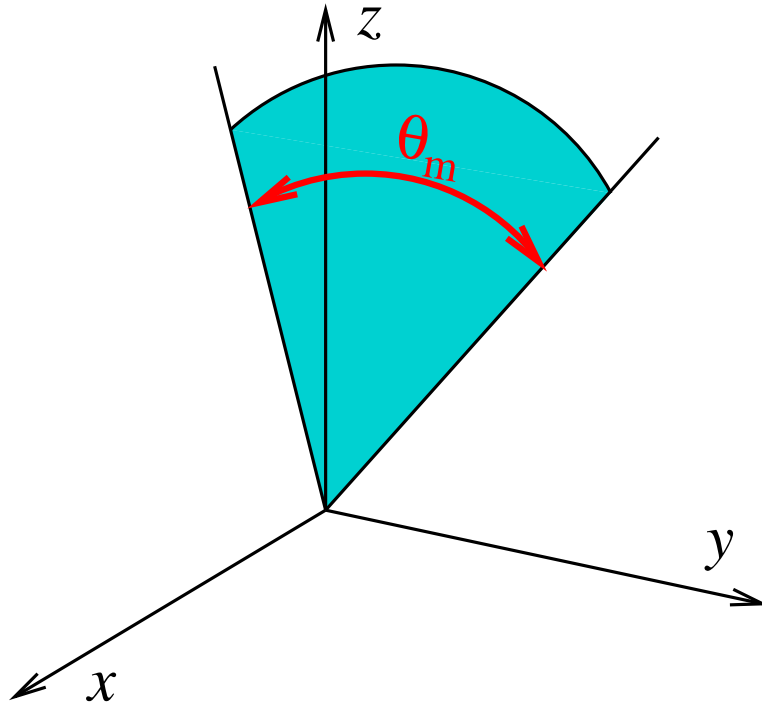


Figure 4.1. Rotation axes in the pseudospin space of two neighboring spins. The wedge lying in the plane perpendicular to x and sweeping out the angle θ_m contains rotation axes which can be achieved using time symmetric pulses in a system fabricated so that the spin interaction has axial symmetry about z axis.

If the pseudospin rotation acts on a pair of spins that do not encode a qubit there is no simple geometric interpretation of the gate action. Such pseudospin rotation are important in the application of gates on pairs of encoded qubit. For designing two qubit gates we will have to rely on formalism, rather than intuition.

4.1.1 Single Qubit Gates

Any rotation can be represented as a composition of elementary rotations about any pair of noncolinear axes. It is then obviously true that the set of available pseudospin gates is sufficient to perform an arbitrary single qubit gate. A more interesting question is how many elementary rotations are necessary for constructing an arbitrary rotation. To answer this

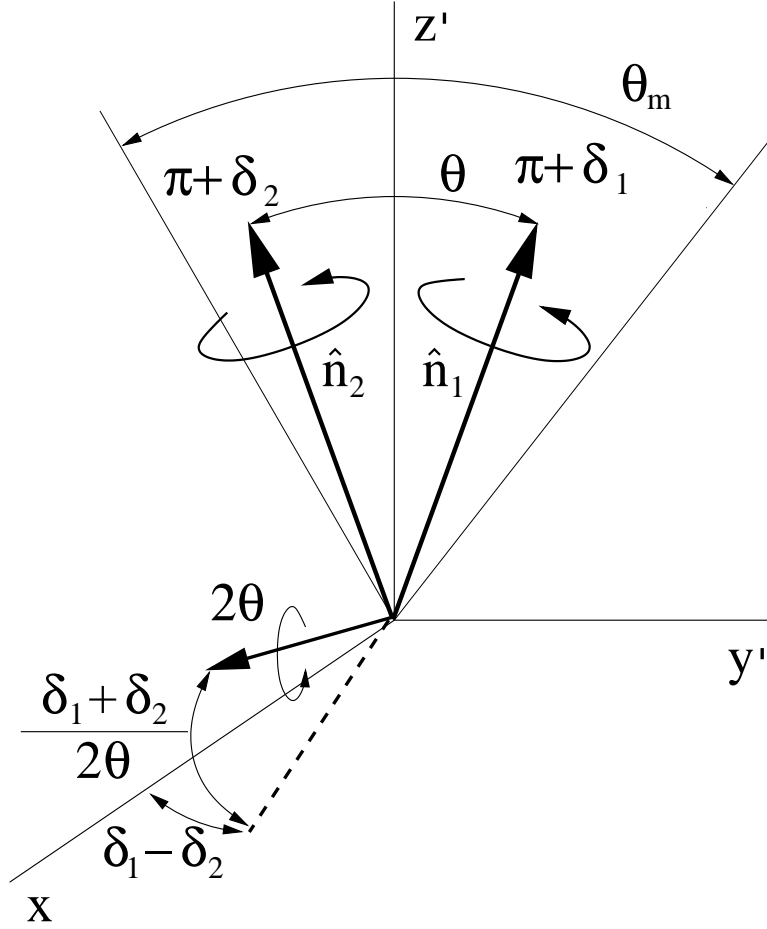


Figure 4.2. Pseudospin rotation about the x axis. Successive π rotations about $\hat{\mathbf{n}}_1$ and $\hat{\mathbf{n}}_2$, with $\hat{\mathbf{n}}_1 \cdot \hat{\mathbf{n}}_2 = \cos \theta$, result in a 2θ rotation about the x axis. The effect of errors in the rotation angles, δ_1 and δ_2 , on the net rotation axis is also shown. Here $\hat{z}' \parallel (\hat{\mathbf{n}}_1 + \hat{\mathbf{n}}_2)$ and $\hat{y}' = \hat{z}' \times \hat{x}$.

question we first explicitly present a way to do single qubit rotations, and then argue that it is optimal.

It is clear that the rotations about axes inside the wedge can be implemented with just one pulse. Rotations which will require the longest sequence of elementary gates are going to be about axes far from the wedge. Specifically, we will consider a pseudospin rotation about an axis normal to the wedge, x . This operation can be performed by a sequence of π rotations about available axes lying in the wedge. Two such axes, \mathbf{n}_1 and \mathbf{n}_2 , making an

angle $\theta \leq \theta_m$ are shown in [Fig. 4.2]. A π rotation about \mathbf{n}_1 followed by a π rotation about \mathbf{n}_2 then results in a 2θ rotation about the x axis. The sense of this rotation can be reversed by reversing the order of the π rotations. Since a continuous range of axes within the wedge are available, a rotation about the x axis through an arbitrary angle Θ can be carried out by an even number, $2[\Theta/(2\theta_m)] + 2$, of π rotations, where $[x]$ denotes the greatest integer function of x . So, the hard rotations about x axis take a number of elementary rotations that scales as θ_m^{-1} and in the worst case this number N_x is

$$N_x = 2[\pi/(2\theta_m)] + 2. \quad (4.15)$$

Once we know how to perform an arbitrary x rotation, we can do an arbitrary rotation about an arbitrary axis by completing the standard Euler construction with one of the axes in the wedge. Therefore the number of pulses needed to perform an arbitrary single qubit gate on our encoded qubits is $N_x + 2$. This number goes to infinity as the wedge width shrinks to zero.

The scaling of N_x with the wedge width as $(\theta_m)^{-1}$ is optimal. A simple way to see that we cannot do a single qubit gate construction that scales better than θ_m^{-1} , is to consider the images of the wedge after repeated rotations. If we want to be able to apply arbitrary rotation, we must be able to rotate the wedge axis to any position in yz plane. Optimal way of moving the wedge axes is sequence of π rotations about the axes on the edge of wedge. With each new rotation, the axis of the wedge moves at most by an angle $\theta_m/2$ from its previous position. Covering the entire yz plane, therefore takes on the order of θ_m^{-1} elementary rotations, and there is no way to produce all the rotations in a number of steps that scales any better than θ_m^{-1} .

As θ_m is reduced, this construction also becomes increasingly sensitive to errors. To see this, let us consider the case when the π rotations about $\mathbf{n}_{1(2)}$ are slightly wrong, and the angles are $\pi + \delta_{1(2)}$, where $\delta_{1(2)}$ are errors. If we take the z' axis to be parallel to $\mathbf{n}_1 + \mathbf{n}_2$ and the y' axis parallel to $\hat{z}' \times \hat{x}$ then the composition of these two rotations will yield an overall $2\theta + O(\delta^2/\theta)$ rotation about an axis deviating from the \hat{x} axis by an angle $\delta_1 - \delta_2$ in the y' direction and $(\delta_1 + \delta_2)/2\theta$ in z' direction (see [Fig. 4.2]). Thus, the larger θ_m is, the more robust this construction is against errors.

We have shown that arbitrary rotations of a single encoded qubit can be performed using axially and time reversal symmetric gates. The number of elementary gates in this construction and the dominant error in the resulting gate both scale like an inverse of the range of available rotation axes.

4.1.2 Two Qubit Gates

Encoding of qubits in pairs of spins was chosen so that all the elementary gates applied to a pair of spins forming a qubit correspond to single qubit operations. Therefore, these gates will never enact two qubit gates when applied in this way. However, if the elementary pseudospin rotation acts in the pseudospin space of spins that belong to two different but neighboring qubits, the elementary gate changes the state of both qubits. Therefore, we may use such operations to interact qubits.

Now consider the two logical qubits shown in [Fig.4.3]. A two-qubit gate between the 12 qubit and the 34 qubit can be carried out by a sequence of pulses acting on spins 2 and 3. Because the pseudospin space of spins 2 and 3 does not correspond to a logical qubit, rotations in this space will, in general, mix in noncomputational states resulting in leakage errors. To avoid such errors, the net unitary transformation must be diagonal in the $\{\uparrow_1\downarrow_2\uparrow_3\downarrow_4, \uparrow_1\downarrow_2\downarrow_3\uparrow_4, \downarrow_1\uparrow_2\uparrow_3\downarrow_4, \downarrow_1\uparrow_2\downarrow_3\uparrow_4\}$ basis of the four spins. The most general unitary operator of the form (4.8) for which this is the case consists of a rotation about the x -axis in pseudospin space. It follows that the net gate must be of the form

$$U_{23}(\Lambda, \Phi) = \prod_k U_{23}(\lambda_k; \phi_k) = \exp\left(i\frac{\Lambda}{2}\right) \exp\left(-i\frac{\Phi}{2}\sigma_x^{(2,3)}\right), \quad (4.16)$$

where $\Lambda = \sum_k \lambda_k$ is the net phase and Φ is the rotation angle about the x -axis produced by the sequence of rotations $\{\phi_k\}$. Note that both Λ and Φ are defined modulo 4π .

The gate (4.16) can be expressed in terms of operators acting on the logical qubits as follows,

$$U_{23}(\Lambda, \Phi) = \exp\left(i\frac{\Lambda}{4}\right) \exp\left(i\frac{\Lambda}{4}\sigma_x^{(1,2)}\sigma_x^{(3,4)}\right) \exp\left(i\frac{\Phi}{4}\sigma_x^{(1,2)}\right) \exp\left(i\frac{\Phi}{4}\sigma_x^{(3,4)}\right). \quad (4.17)$$

This gate can be combined with single qubit gates we already know how to implement to give a CNOT and complete the universal gate set construction.

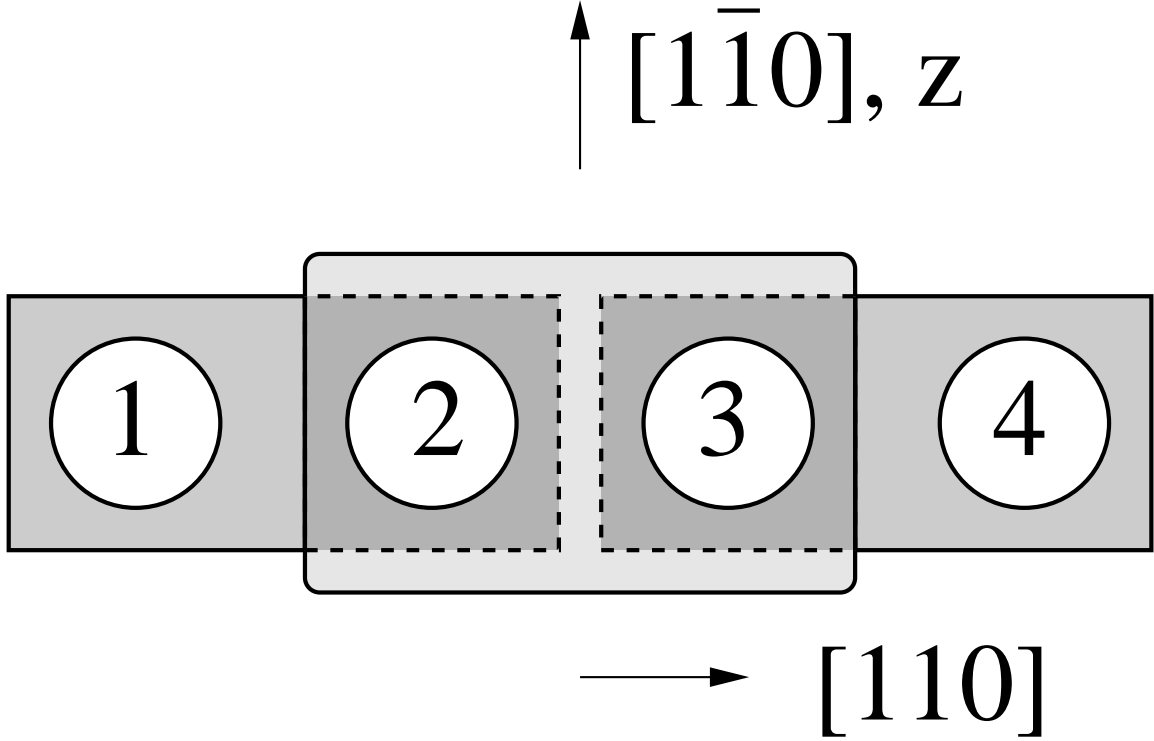


Figure 4.3. Sketch of two logical qubits, one composed of spins on dots 1 and 2, and another composed of spins on dots 3 and 4. Gates between spins that belong to the same qubit will enact single qubit gates. The two qubits can interact via same kind of gates, performed between spins 2 and 3 that belong to different qubits.

In the search for the gates of the form (4.17) that can make a CNOT, we use a two qubit gate canonical form [70]. The canonical form $E(\theta_x, \theta_y, \theta_z)$ of a two qubit gate is

$$E(\theta_x, \theta_y, \theta_z) = \exp -i (\theta_x \sigma_x \otimes \sigma_x + \theta_y \sigma_y \otimes \sigma_y + \theta_z \sigma_z \otimes \sigma_z), \quad (4.18)$$

where the parameters θ_x , θ_y and θ_z satisfy condition

$$\frac{\pi}{4} \geq \theta_x \geq \theta_y \geq |\theta_z|, \quad (4.19)$$

and σ operators are the Pauli matrices. Any two qubit gate can be decomposed into a gate of canonical form and at most four single qubit gates. For any $U \in SU(4)$, there are $U_{1L} \dots U_{2R}$ so that

$$U = U_{1L} \otimes U_{2L} E(\theta_x, \theta_y, \theta_z) U_{1R} \otimes U_{2R}, \quad (4.20)$$

and the decomposition is unique in a sense that single qubit rotations can not change the canonical form of a gate.

By expressing the (4.17) in its canonical form [70], it can be shown to be equivalent to a CNOT gate, up to single qubit rotations, if and only if

$$\Lambda = \sum_k \lambda_k = (2n + 1)\pi. \quad (4.21)$$

Detailed discussion of the condition (4.21) is given in the Appendix.

Below we outline two procedures for simultaneously satisfying (4.16) and (4.21).

For the first procedure, we use the fact that the phase shift λ in any elementary gate is approximately equal to the rotation angle. Therefore, we try to construct a rotation about the x axis from rotations with angles that approximately sum up to an odd multiple of π .

Let $R_x(\pi)$ be a π rotation about the x axis. Using the single qubit rotation scheme described above, this rotation can be performed through a sequence of $2n = 2[\pi/(2\theta_m)] + 2$ rotations about available axes. If $A(\phi)$ is then a ϕ rotation about a particular available axis lying in the yz plane, the sequence of rotations $A(\phi)R_x(\pi)A(\phi)$ will have the form (4.16) with $\Phi = (2n + 1)\pi$ regardless of the value of ϕ . According to (4.9) the contribution of $R_x(\pi)$ to the total phase Λ will then be $2n\pi + \mu$ where $\mu \sim O(s^2/\theta_m) \sim O(s)$. To satisfy (4.21) we therefore require $\phi = \pi/2 + O(s)$, where the $O(s)$ adjustment must be chosen so that $\lambda = \pi/2 - \mu/2$ for $A(\phi)$ and thus $\Lambda = (2n + 1)\pi$. This procedure is similar to those proposed in the two spin encoding schemes of [41, 42, 43]. The main difference is that in these constructions the R_x rotation is generated by an inhomogeneous Zeeman field, whereas in ours it is generated entirely by a sequence of exchange gates corresponding to π rotations in the wedge of available axes. As for single qubit rotations, as θ_m goes to zero, the number of required pulses scales as $1/\theta_m$ and the construction becomes increasingly sensitive to errors.

The second procedure uses the fact that the phase shift in elementary gate and the rotation angle do differ. We do a series of 2π rotation that are equivalent to x rotations as far as leakage is concerned, because they are pure phases. While doing this, we wait for the difference between the sum of angles and the sum of phases to grow to π .

This second procedure requires more pulses in the limit of small θ_m , but is simpler and less susceptible to error. The idea is to perform a sequence of 2π pseudospin rotations about any available axis or axes and use the spin-orbit induced mismatch between ϕ and λ to

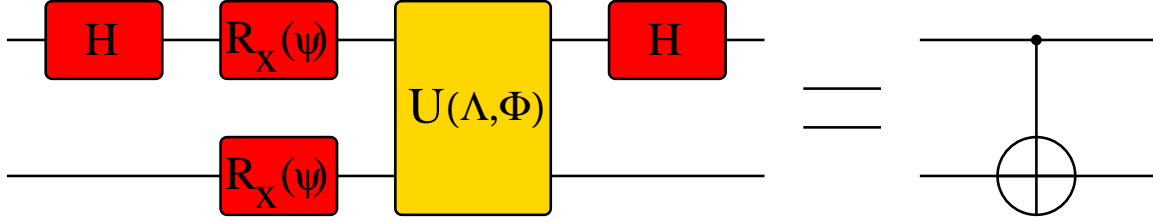


Figure 4.4. A quantum circuit implementing the CNOT gate. Each line represents a qubit encoded in the state of two spins. Circuit consists of a two-qubit part $U(\Lambda, \Phi)$ and four one-qubit gates. Angle of single qubit rotations is $\psi = (\Phi + \Lambda)/2$ and the Haddamard gate H is $1/\sqrt{2}(\sigma_x + \sigma_z)$.

accrue the extra π phase required to satisfy (4.21). The resulting gate will then have the form (4.42) with $\Phi = 2n\pi$ where n is the number of 2π rotations. For the i th rotation the corresponding phase factor will be $\lambda_i = 2\pi + \nu_i$, where $\nu_i \sim O(s^2)$. For a sequence to satisfy the constraint (4.21) the sum of all phases, and hence $\sum_i \nu_i$, must be an *odd* multiple of π . Given control of spin-orbit coupling, there will be a continuous range of achievable ν values for each 2π rotation, with $\nu_1 < \nu < \nu_2$ where $\nu_1, \nu_2 \sim O(s^2)$. If this range includes 0 then (4.21) can always be satisfied with $\lceil \pi/\nu_{max} \rceil + 1$ rotations, where $\nu_{max} = \max(|\nu_1|, |\nu_2|)$. If this range does not include 0 it will still always be possible to satisfy (4.21) with, at most, $\lceil \nu_{max}/(\nu_2 - \nu_1) \rceil + 2 + \lceil \pi/\nu_{max} \rceil$ rotations.

Regardless of which procedure is used, single qubit gates acting on logical qubits 12 and 34 are required to complete the CNOT construction. One procedure for doing this is shown in [Fig.4.4].

This gate construction establishes that axially and time reversal symmetric gates are universal for quantum computing over qubits encoded in pairs of electron spins. Universality is not such an exciting feature by itself. In fact, almost any two qubit gate is universal [71]. The present construction is exciting because it uses gates that are constrained by the symmetries of both interaction and time dependence. Such symmetry constrained gates are usually easier to apply than generic unconstrained gate, and the scheme that uses them may have advantages implementation. Another important result of the gate construction is identification of the width of a wedge of available axes θ_m as a figure of merit for a device

that should host a quantum computer. Both the efficiency and the precision of a universal set of quantum gates depend on θ_m and we will investigate its size in the real devices.

4.2 Control Range

As shown in the previous section, a universal set of quantum gates over qubits encoded in states of a pair of spins can be constructed from elementary quantum gates that are both axially and time-reversal symmetric. Application of these elementary gates does not require excessive tuning of fabrication and in principle does not require very involved control through voltage pulses. Requirements for their application are fabrication of an array of quantum dots along [110] crystalline axis of a semiconductor with zinc-blende structure and symmetry in time dependence of the control voltage pulses.

Explicit construction of a universal set of quantum gates depends crucially on the ability to independently control both the axis and angle of a pseudospin rotation, i.e. both the length and direction of the vector parameter ϕ in pseudospin rotation (4.8). Manipulation of the pseudospin rotation angle is relatively simple, because the main contribution to this angle comes from the integrated strength of the isotropic exchange interaction. To achieve a desired pseudospin rotation angle we only need to fix the integrated strength of the pulse. We are then still left with a lot of freedom for further tailoring of the pulse shape.

The requirement for control over the axis of the pseudospin rotation is harder to meet. If the interaction between spins was isotropic, the parameters α , β and γ of an elementary gate (4.1) would all be zero and the pseudospin rotation (4.8) along ϕ would always be about the z axis. In order to controllably move the pseudospin rotation axis away from the z axis we have to control the anisotropic terms in the elementary gate.

The number of pulses needed to produce a generic gate from a universal set depends on the available range on pseudospin rotation axes. In our construction, the width of this range was called θ_m and the number of pulses per implementation of a gate from the universal set scales as θ_m^{-1} . Also, the dominant contribution to the error in such a gate scales as θ_m^{-1} . The applicability of our universal gate set construction depends on the range θ_m in real quantum dot devices being large enough to allow for meaningful control.

This section presents an estimate of the available range of anisotropies in a system of quantum dots in zinc-blende structures. Detailed discussion of this range is limited to the

case of GaAs quantum dots. The reason for this is that the most sophisticated experiments are done in this material [72], and fabrication techniques are better developed than in the case of other zinc-blende semiconductors.

Control over anisotropy in a quantum gate depends on the fabrication of the device and on the way it is operated. The only significant source of anisotropy for our scheme is spin-orbit coupling. In chapter 3 the effects of spin-orbit coupling were divided into (i) device specific interaction strength, described by a parameter s and defined in (3.41), and (ii) the part that changes during the application of an elementary quantum gate because it depends on the current state of control parameters, \mathbf{I}_{SO} defined in (3.42).

In the present discussion of the available range of anisotropies we make the division into fabrication level and pulse level control. We find this division useful because the types of control coming from these two sources are different. Our scheme for application of a universal set of quantum gates calls for successive application of quantum gates with different anisotropies. Control through fabrication is fixed once and cannot be changed between gate applications. We use this type of control to impose axial symmetry and find the device parameters that gives a useful range of anisotropic interaction when control parameters i.e. electrode voltages vary while the gate is implemented.

A figure of merit for our proposal, θ_m , is determined by the range of anisotropies of quantum gates implemented by sending voltage pulses of various shapes to electrodes. Below, we estimate this figure of merit in a device that uses both ways to influence the resulting gate.

4.2.1 Control at Fabrication Level

First choices that will influence anisotropy in quantum gates are made at the fabrication level. Properties of the device set at fabrication do not change during the gate operation. Therefore, fabrication is the preferable stage for setting the symmetry properties of the interaction. In the implementation of quantum computing using isotropic exchange, the goal of fabrication is to reduce the anisotropy of interaction and choosing the material with weak spin-orbit coupling, like in silicon design of [73], would solve the problem of anisotropy. In our scheme, the goal is not to reduce the anisotropy, but to make it symmetric and controllable.

The most important control task that needs to be solved at the fabrication stage is making the interaction of spins axially symmetric. The range of available axially symmetric anisotropies in the interaction should also be as large as possible. The range of anisotropies available in the gates will ultimately be determined by the control through pulse shaping. Later in this chapter, we will show that having a wide range of anisotropies in the interaction before considering the time dependence implies a larger set of available quantum gates.

The most common materials considered for spin-based quantum computing in quantum dots are III-V semiconductors. Among these materials GaAs holds the greatest promise because it is easiest to fabricate the necessary structures from it. Important III-V semiconductors that are commonly used for quantum dots fabrication have zinc-blende crystalline structure [74]. As discussed in chapter 3, the zinc-blende structure is not symmetric under inversion and this bulk inversion asymmetry causes Dresselhaus type spin-orbit coupling. Structure inversion asymmetry in the layered heterostructure of semiconductors will produce Rashba type spin-orbit coupling. Both of these couplings can be influenced in the stage of fabrication of two dimensional electron gas (2DEG) by choosing the width and orientation of potential well in which 2DEG is formed.

Recall that two important contributions to the spin-orbit-coupling of electrons in (001) crystallographic plane are Dresselhaus

$$H^D = \gamma_C (k_{[100]}(k_{[010]}^2 - k_{[001]}^2)S_{[100]} + cycl. + H.C.), \quad (4.22)$$

and Rashba term

$$H^R = 2\alpha_R E e (k_{[010]}S_{[100]} - k_{[100]}S_{[010]}). \quad (4.23)$$

In (4.22), γ_C is the property of the particular III-V semiconductor in which the dots are fabricated. The equation is given in the system of crystallographic axes, $k_{[abc]}$ is a projection of canonical momentum to the crystallographic axis $[abc]$, and similarly $S_{[abc]}$ is a projection of spin. The symbol *cycl.* to denotes cyclic permutations and *H.C.* is Hermitian conjugation. We will not consider the effects of external magnetic field now, but hermitian conjugate adds a factor of two to the result. In (4.23), α_R is again the property of material, e is electron charge and E is the strength of electric field in $[001]$ direction binding the electrons into 2DEG. A detailed description of the spin-orbit coupling effects in two dimensional systems

can be found in Winkler's monograph [75]. Since the spin-orbit coupling Hamiltonian was already discussed in chapter 3, we will here only review its dependence on device properties.

There are two main ways of influencing spin-orbit coupling in a 2DEG, before fabrication of the quantum dots using electrodes to bind 2DEG electrons into the quantum dots. The first way is control through the choice of the material that alters constants γ_C and α_R . These constants will determine the relative size of Dresselhaus (4.22) and Rashba (4.23) contribution to the total spin-orbit coupling Hamiltonian. Since the two terms have different functional dependencies on momentum components, altering their size will alter the form of resulting coupling. Other material properties that influence spin-orbit coupling are the effective mass of the electron and the dielectric constant. For our purpose of getting large spin-orbit coupling the advantageous material should have large γ_C and α_R . However, the main concern in fabrication is the technology of producing the 2DEG and fabrication of electrodes to produce quantum dots. These technological concerns single out quantum dots in GaAs as the best candidate for quantum computing device.

The second important parameter set at the stage of 2DEG fabrication that will influence spin-orbit coupling is the width of the potential well in growth direction.

The earlier discussion of the influence of the growth direction electric field in the regime of a strong field that induces strong confinement in growth direction,

$$\langle k_{[001]}^2 \rangle \gg \langle k_{[100]}^2 \rangle, \langle k_{[010]}^2 \rangle, \quad (4.24)$$

presented in chapter 3, gives the following expression for the spin-orbit coupling Hamiltonian

$$H_1^{SO} = (k_{[100]}(-f_D, -f_R) + k_{[010]}(f_R, f_D)) \cdot (S_{[100]}, S_{[010]}). \quad (4.25)$$

The strengths of Dresselhaus and Rashba terms are

$$f_D = 2\gamma_C \langle k_{[001]}^2 \rangle = 2.48\gamma_C \kappa (m^* E |e|)^{2/3}, \quad (4.26)$$

and

$$f_R = 2\alpha_R E e, \quad (4.27)$$

where E is the growth direction electric field. Other parameters in spin-orbit coupling strengths are material properties γ_C and α_R electron charge e and its effective mass m^* .

The expression (4.25) has some interesting properties. There is a special symmetry in the case

$$f_D = \pm f_R. \quad (4.28)$$

In both of these cases (4.25) describes coupling of the orbital crystalline momentum to fixed projection of the spin. In the first case, $f_D = f_R$, we have

$$H_1^{SO}(f_D; f_R = f_D) = f_D(k_{[100]} + k_{[010]})(-1, 1) \cdot \mathbf{S}, \quad (4.29)$$

and coupling of orbital degrees of freedom to the spin projection in $[\bar{1}10]$ direction, for any values of the matrix elements of in plane momentum components. Similarly, for $f_D = -f_R$

$$H_1^{SO}(f_D; f_R = -f_D) = f_D(-k_{[100]} + k_{[010]})(1, 1) \cdot \mathbf{S}, \quad (4.30)$$

again coupling only the $[110]$ spin component in any orbital state to the orbital degrees of freedom.

Achieving (4.28) in regime (4.24) would be very useful, because it imposes an approximate rotational symmetry of the spin-orbit coupling Hamiltonian about a fixed axis, regardless of symmetry of actual orbital electron states in the system. Effects of this symmetry on spin coherence in transport were studied by Schliemann, Egues and Loss [68].

Parameters f_D and f_R have different dependence on growth direction electric field, $f_D \propto E^{2/3}$, $f_R \propto E$. Note that the sign of f_R changes when the sign of the electric field along the crystal axis $[001]$ is changed, while the sign of f_D does not. For that reason the condition for axial symmetry (4.28) can be satisfied at some fields in any III-V material. Whether such fields can be produced in real heterostructure is a separate and complex question.

After production of the 2DEG, the next step in designing a device is fabrication of quantum dots by putting metallic electrodes on top of the heterostructure hosting the 2DEG. There, we can choose a direction of dot alignment.

In the Hund-Mulliken approximation that takes into account only rotationally invariant orbital ground states of each dot, the only component of momentum with nonzero matrix elements connecting ground state orbitals on dots will be along the direction connecting the dots. This property will impose a constant ratio of matrix elements of $k_{[100]}$ and $k_{[010]}$, because they are projection of the momentum operator in the direction connecting the dots,

which is fixed during fabrication. This allows for a new way of controlling the spin-orbit coupling Hamiltonian and keeping it axially symmetric.

As described earlier, adjusting the values of f_D and f_R by engineering the 2DEG could produce coupling to a single component of the spin, under the assumption of a narrow well (4.24). Equation (4.25) tells us that the roles of f_D and f_R on one hand and $k_{[100]}$ and $k_{[010]}$ on the other hand are similar when the ratio of appropriate \mathbf{k} matrix elements is kept constant. This property becomes manifest if we rewrite (4.25) using parameters f_D, c defined by $f_R = cf_D$, intensity of the momentum in the direction connecting the dots k , and the angle θ between $[100]$ axis and that direction:

$$H_1^{SO}(k, f_D, c, \theta) = kf_D(-\cos\theta - c\sin\theta, c\cos\theta + \sin\theta) \cdot \mathbf{S}. \quad (4.31)$$

The direction of spin-orbit coupling field \mathbf{h} is

$$\hat{\mathbf{h}} = (1 + c^2)^{-1/2}(-\cos\theta - c\sin\theta, c\cos\theta + \sin\theta), \quad (4.32)$$

and in the case $\theta = (2n + 1)\pi/4$ giving, $\cos\theta = \pm\sin\theta$ it is independent of c and points either in $[110]$ or $[\bar{1}10]$ direction. This is in principle another way of achieving coupling of only one component of spin to the orbital degrees of freedom, resulting in the axially symmetric spin-orbit coupling Hamiltonian for any values of f_D and f_R .

By manipulating the width of the 2DEG we were able to impose axial symmetry in the approximation of a very thin well, where (4.24) holds. If we carefully choose the direction along which the dots are fabricated, axial symmetry of the spin interaction will be imposed by the symmetry of the problem. Then, the condition of a thin well (4.24) is not necessary for axial symmetry of the dots. Adding the cubic Dresselhaus terms, the ones that contain third powers of crystal momentum components in (001) plane of the 2DEG, is not going to spoil the axial symmetry. Therefore, in an array of quantum dots fabricated in (001) plane and aligned along either $[110]$ or $[\bar{1}10]$ crystallographic direction, the spin interaction will be axially symmetric.

In the intuitive picture of anisotropy as spin precession on hopping [50], illustrated on [Fig. 3.8], uniaxiality means that the axis of relative spin rotation points in the same direction for any interdot distance. The dependence of the precession angle on interdot distance in GaAs quantum dots fabricated along $[110]$ crystalline direction and in (001) plane is plotted

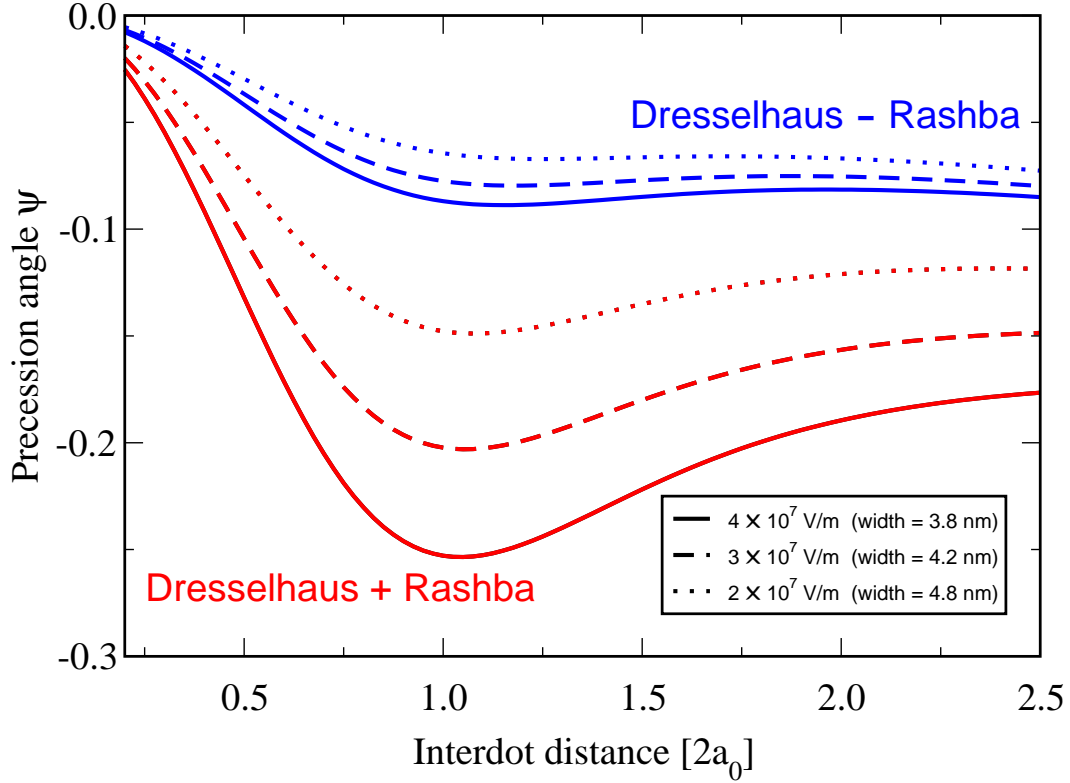


Figure 4.5. Angle of precession on hopping as a function of the device parameters. Spin-orbit coupling causes precession of the electron spin when it hops from one dot to the next. Precession angle is plotted against interdot distance for various electric fields in growth direction. Dots are fabricated in GaAs and their Bohr radius is $a_0 \approx 20\text{nm}$, corresponding to level spacing of 3meV . Red curves correspond to the direction of the electric field in which contributions of Dresselhaus and Rashba coupling to the precession add up, and on blue curves they interfere destructively. Pronounced dip shows that the anisotropy of interaction changes with the interdot distance.

in [Fig. 4.5]. The precession angle shows a pronounced dip when the orbital states on dots start to overlap significantly. This implies that there will be a range of available anisotropies of the interaction.

The precession angle is a function of the ratio of amplitudes for two types of electron hopping. One amplitude is for hopping between the dots with a spin flip, caused by the spin-orbit coupling. The other is an amplitude for hopping without a change in spin state, standard Hubbard model t_H . Combination of the two types of hopping gives a hopping with

precession about the vector spin-orbit coupling parameter in Hund-Mulliken Hamiltonian. The precession angle is

$$\psi = 2 \arctan \frac{P}{t_H}, \quad (4.33)$$

where P is a matrix elements of the spin-orbit coupling Hamiltonian, discussed in the chapter 3 and in the Appendix B.

Interaction parameter β^{int} is closely related to spin precession angle. If the Hund-Mulliken Hamiltonian did not include the direct exchange V term, the interaction would be rotated exchange. The Hund-Mulliken Hamiltonian without direct exchange is,

$$H_0^{HM} = \sum_{\alpha, \beta = \uparrow, \downarrow} -t \left(c_{1\alpha}^\dagger R(\psi, \mathbf{e}_P)_{\alpha\beta} c_{2\beta} + H.c. \right) + U_H (n_{1\uparrow} n_{1\downarrow} + n_{2\uparrow} n_{2\downarrow}), \quad (4.34)$$

where $t = \sqrt{t_H^2 + P^2}$ is the hopping amplitude, $R(\psi, \mathbf{e}_P)$ is a spin rotation by the angle $\psi = 2 \arctan \frac{P}{t_H}$ about the \mathbf{P} axis and U_H is energy cost of double occupancy. Redefining the local reference frame of the second spin, in a way similar to anisotropy reducing gauge of chapter 2, and remembering that the standard Hubbard model predicts isotropic exchange spin interaction [67], we find

$$H_0^{int} = J_H \mathbf{S}_1 \cdot R(\psi) \mathbf{S}_2, \quad (4.35)$$

where

$$J_H = \frac{4t^2}{U_H}, \quad (4.36)$$

and t is the total amplitude that includes hopping induced by spin-orbit coupling. For small precession angles the equation (4.35) gives the interaction anisotropy $\beta_0^{int} = \sin \psi \approx \psi$.

Direct exchange will, in the lowest order, change the strength of isotropic exchange from the Hubbard value J_H (4.36) to $J = J_H + V$. With the new strength of isotropic exchange, the anisotropic interaction strength will change to

$$\beta^{int} = \sin \psi \frac{J_H}{J_H + V}. \quad (4.37)$$

Since the direct exchange is ferromagnetic, $V = -|V|$, this correction increases the anisotropy. Direct exchange changes fast when orbitals begin to overlap, in the region that coincide with the dip in precession angle versus distance plot. Therefore, direct exchange can make the dip in anisotropic interaction of spins versus interdot distance significantly larger

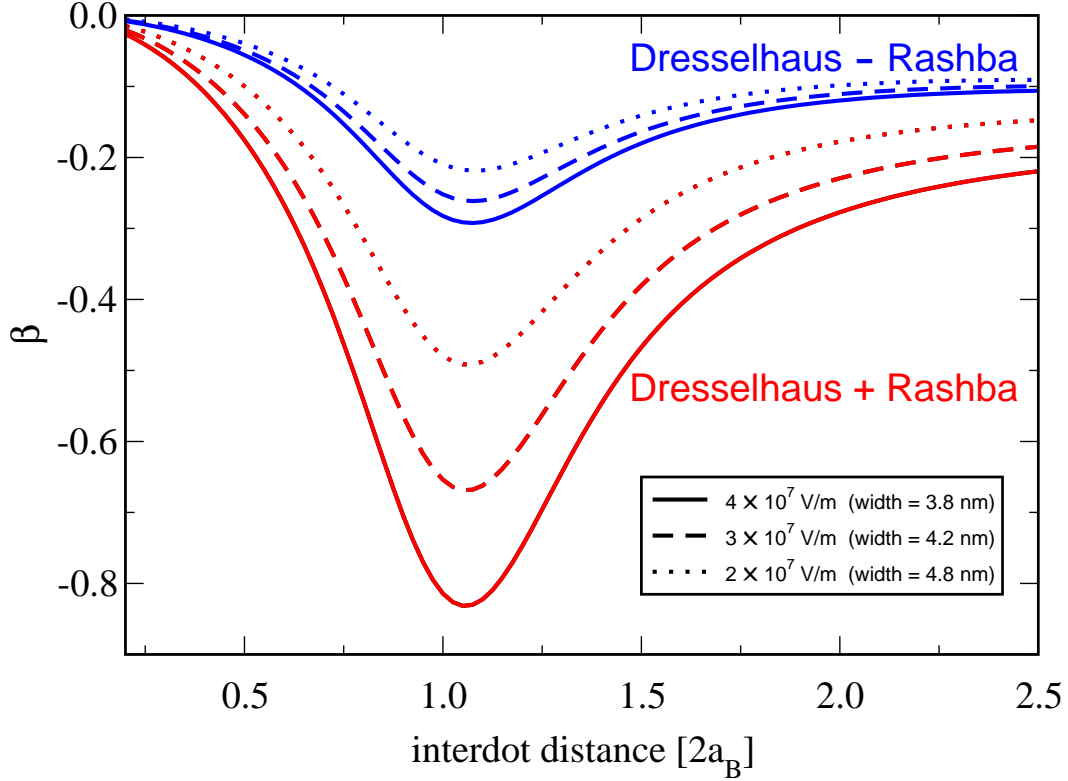


Figure 4.6. Strength of the dominant term in spin interaction β^{int} , plotted against interdot distance for various electric fields in growth direction. Dots are fabricated in GaAs and their Bohr radius is $a_0 \approx 20nm$, corresponding to level spacing of $3meV$. Red curves correspond to the direction of the electric field in which contributions of Dresselhaus and Rashba coupling to the precession add up, and on blue curves they interfere destructively. Pronounced dip shows that the anisotropy of interaction changes with the interdot distance.

than the dip in precession angle. Explicit calculation of anisotropic interaction strength confirms this intuition as shown in [Fig. 4.6].

At the fabrication level we set two important properties that will persist throughout the gate application. First, we can ensure axial symmetry of the interaction by alignment of the dots along crystallographic direction [110]. An alternative way of setting the axial symmetry through fabrication is matching of the magnitudes of Dresselhaus and Rashba coupling, $|f_D| = |f_R|$ in a very thin 2DEG. Second important characteristic of the device set at the fabrication stage is the effective spin interaction. Although the effective spin interaction in the strict sense does not always exist, setting its approximate form so that it varies widely

with the interdot distance would allow for the more efficient manipulation of spins using voltage pulses.

4.2.2 Control through Time Dependence

The effective interaction between spins does not specify the gate that will be applied by the pulse of such interaction. As discussed earlier, a quantum gate is the evolution operator connecting states in distant past with states in far future. This evolution is governed by the time dependent interaction. When the interaction operators taken at different times commute, the corresponding quantum gate is just the exponential of the interaction Hamiltonian times the integrated interaction strength. In our case, however, interactions at different times do not commute, and the gate can be more complex than the interaction. Manipulations of time dependence were used in chapter 1 to reduce the gate anisotropy and make it smaller than the anisotropy of interaction. Now, our goal is to find out how much the anisotropy in the gate can be controlled by pulse shaping.

For spin control, the most important gate parameter is β , because it is the largest and most controllable, once the overall isotropic exchange strength is fixed. It is of the first order in spin-orbit coupling and when the time dependence of underlying interaction is even β is the only gate parameter that is first order in anisotropy. The perturbative result for β in (2.40) for an axially symmetric spin interaction is

$$\beta = \frac{1}{2 \sin(\lambda_J/2)} \int_{-\infty}^{\infty} \beta^{int}(t) \cos\left(x(t) - \frac{\lambda_J}{2}\right) J(t) dt, \quad (4.38)$$

where

$$x(t) = \int_{-\infty}^t J(t') dt', \quad (4.39)$$

and $\lambda_J = \lim_{t \rightarrow \infty} x(t)$ is the strength of isotropic part of the interaction, integrated over the entire pulse. Up to second order in spin-orbit coupling λ_J is equal to the gate parameter λ of (4.1).

The perturbative result (4.38) shows that, to first order in spin-orbit coupling, the gate parameter β is an average of the time dependent interaction parameter $\beta^{int}(t)$. The weight function for this average is a product of the strength of the isotropic exchange and the cosine of the integrated isotropic exchange strength, starting from the beginning of the pulse. The

cosine factor is phase shifted so that its maximum falls in the middle of the pulse. The isotropic exchange factor in the weight function makes the anisotropy of the interaction between spins at small distance more important. The cosine term imposes the proper symmetry in time. This result also implies that the available range of gate anisotropies is similar to the available range of interaction anisotropies. For gates applied through a change in the interdot distance, starting from infinitely separated dots, suddenly bringing them close together, keeping them at that distance until enough pulse strength λ_J is accumulated and again suddenly pulling them back apart, this range corresponds to all of the values of β^{int} plotted in [Fig. 4.6]. Such gates can not be applied in realistic systems. Sudden changes of the potential would excite arbitrary orbital levels, and the description in terms of spin degrees of freedom becomes meaningless.

In realistic systems that are to be used for quantum computation, anisotropy of the interaction is not necessarily a good estimate for anisotropy in the gate, as we demonstrated in chapter 2. The fundamental problem with identifying the interaction anisotropy β^{int} with the gate anisotropy β applied by some pulse lies in the fact that the effective spin interaction, for which β^{int} is one of the parameters is a meaningful concept only when the orbital states of spin carrying electrons are well defined orbital qubit states.

In reality the orbital state of a pair of electrons involved in the gate has some overlap with orbitally excited states that cannot be described with a spin Hamiltonian. The Hund-Mulliken approximation can model such excitations, but the effective spin Hamiltonian cannot. Amplitude for orbital excitations is suppressed by the energy gap between qubit and orbitally excited states. This gap was studied in a system of quantum dots by Hu and Das Sarma [76]. Orbital excitations can make the concept of effective spin interaction inapplicable, but still allow for the quantum gate operation if the transitions in a final state are suppressed due to adiabaticity [69]. Destruction of a qubit due to orbital excitations happens only if the amplitude for orbital excitations is high at the end of the pulse.

Since orbital excitations can not be modeled by an effective spin interaction, we have chosen to study the effects of time dependence on the gate operation using a time dependent Hund-Mulliken Hamiltonian. This way we can account for the orbital excitations and study the gate errors caused by them.

Our model of a time dependent interaction of electrons in a quantum gate is a Hund-Mulliken Hamiltonian derived from the potential (3.14) with variable interdot distance a . The model system are $20nm$ quantum dots in GaAs and we assumed that the fabrication sets axial symmetry and produces the 2DEG corresponding to an electric field giving the widest range of anisotropies in interaction in [Fig. 4.6].

Distance between the dots is described by parameter a of (3.14). It is time dependent and

$$a(t) = a_0 \left(1 + \left(\frac{t}{\tau} \right)^2 \right), \quad (4.40)$$

where a_0 is the value of parameter at the distance of closest approach. Pulse duration is set by τ . At any time t the distance between dot centers is $2a(t)$. Variable distance produces a time dependent Hund-Mulliken Hamiltonian $H^{HM}(t)$. At the beginning and end of a pulse, as $t \rightarrow \pm\infty$, the dots are decoupled.

We are interested in independent control over integrated pulse strength λ and gate anisotropy β . In order to set λ to a fixed value, we have to impose a relation between the distance of closest approach a_0 and the pulse duration τ . Integrated pulse strength λ is to a good approximation equal to the integrated time dependent isotropic exchange coupling strength $J(a(t))$. We have studied a set of pulses with integrated isotropic exchange strength fixed to π

$$\int_{-\infty}^{\infty} J(a(t)) dt = \pi. \quad (4.41)$$

Since $J(a)$ is roughly an exponential of a square of the interdot distance [52], condition (4.41) will make the pulse duration grow very fast with the distance of closest approach a_0 . This dependence is illustrated in [Fig. 4.7]. Very long pulses will present a problem, because of decoherence. As the pulse times get comparable to the decoherence times, the error in a gate will grow beyond the power of error correcting codes to repair it. Decoherence puts a fundamental limit on the pulse duration on the side of long pulses.

By solving the Schrödinger equation for a time dependent Hund-Mulliken Hamiltonian with the interdot distance set by (4.40) we can study both the gates produced by these pulses and the errors caused by orbital excitations in a form of double occupancy at the end of a pulse.

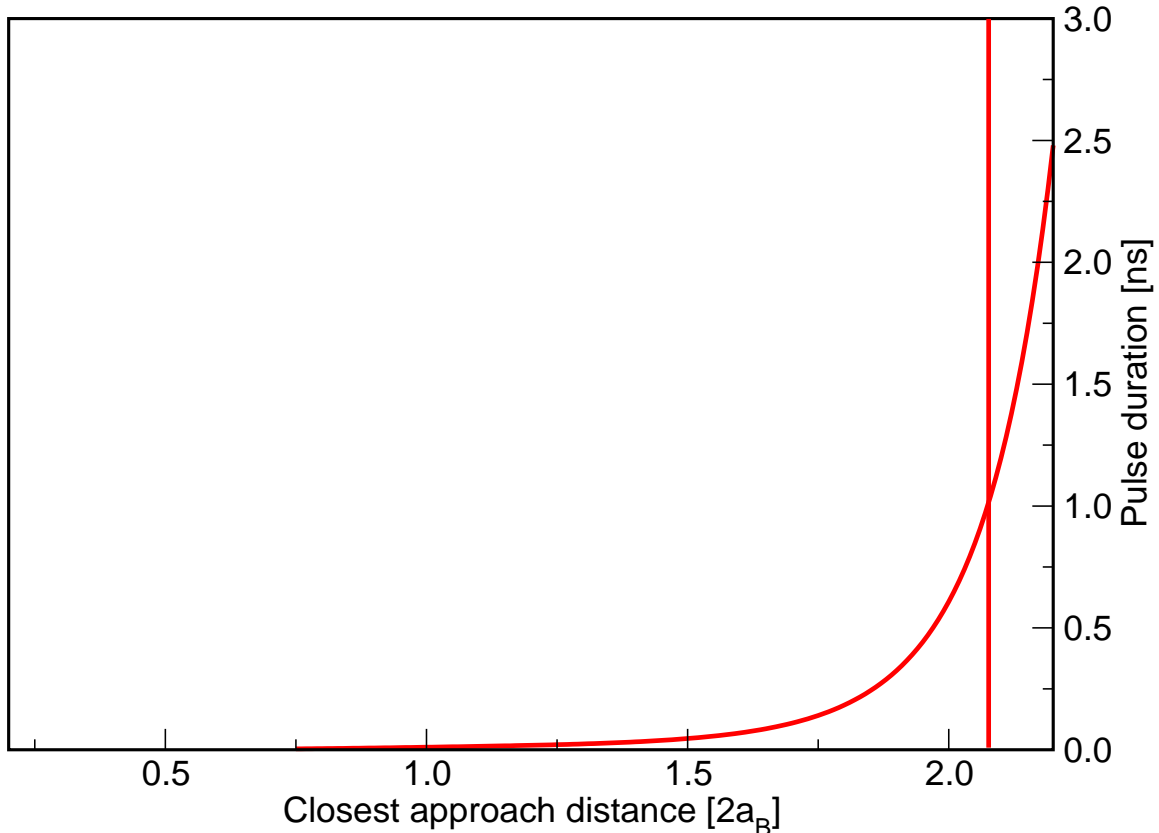


Figure 4.7. Decoherence for slow pulses. Model pulses (4.40) that produce the gates with fixed integrated isotropic exchange strength, $\lambda_J = \pi$ have their duration, measured by τ fixed by the distance of closest approach. In this figure, the pulse duration is plotted against the distance of closest approach. As pulse times get longer, the errors caused by decoherence will prevent the gate from being correctly executed. The red vertical line is the bound on the distance of closest approach, set by the error rate due to decoherence. To set this bound, we used decoherence time $\tau \sim 10\mu s$ and $p_{th} \sim 10^{-4}$.

For short pulses another process will limit our ability to tailor them. As the distance of closest approach gets smaller, the pulses will get faster. For fast pulses, the probability of nonadiabatic transitions into orbitally excited states grows.

Numerical solution of the Schrödinger equation with a time dependent Hamiltonian $H^{HM}(a(t))$ is a unitary operator in the variational space of the Hund-Mulliken approximation. Probabilities for having orbital excitations at the end of a pulse are given by squared moduli of the amplitudes for a system to be in one of doubly occupied states. We have solved

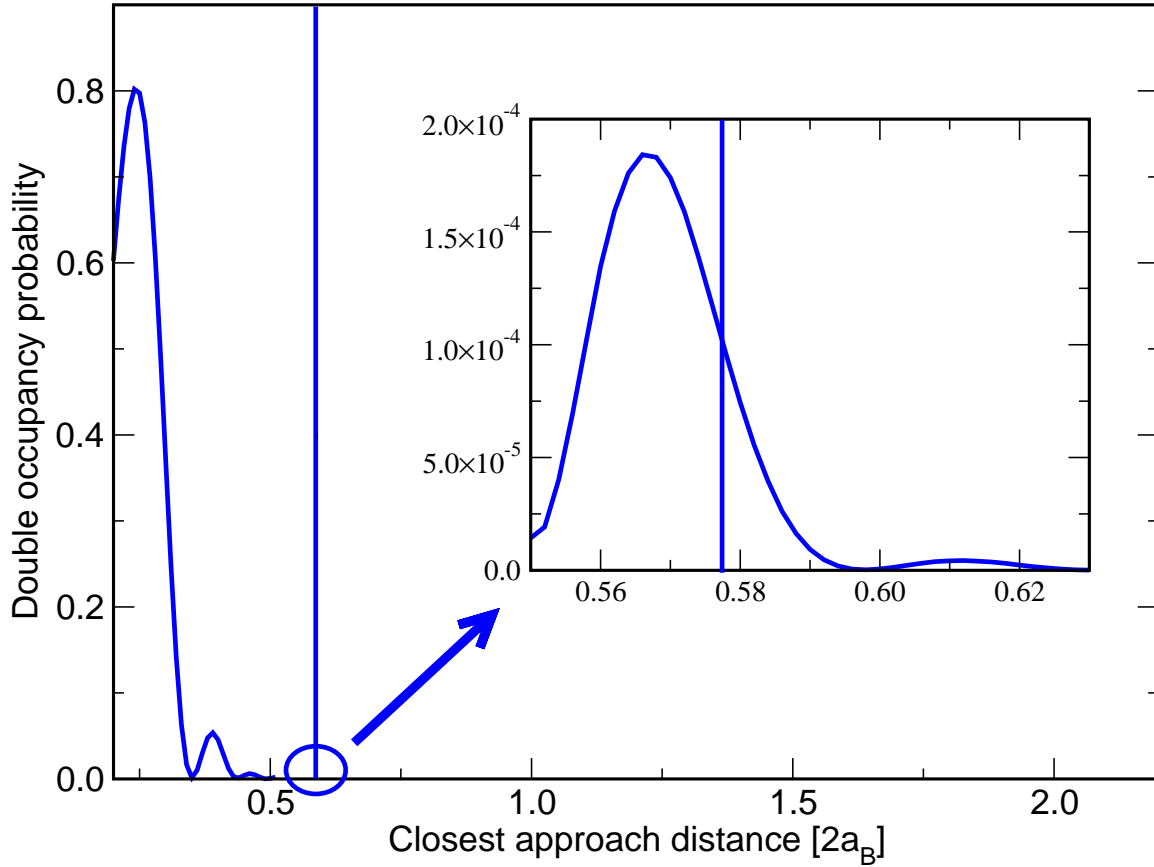


Figure 4.8. Double occupancy for fast pulses. Double occupancy at the end of a π pulse described in the caption of the previous figure. As the pulses get faster, the probability of double occupancy caused error grows. If we want this probability to be smaller than the error correction threshold, the pulses must be slower than the bound set by the vertical blue line. Inset shows the details of error around the intersection with the error correction bound.

the Schrödinger equation for a range of pulses that satisfy (4.41). The results for a double occupancy probability as a function of the distance of closest approach are given in [Fig. 4.8]. We see that the probability of errors due to double occupancy at the end of the pulse grows very fast when the $\lambda_T = \pi$ pulses get faster as the distance of closest approach gets smaller. Beyond some distance of closest approach, double occupancy errors will overcome quantum error correction, and the gate will again become inoperable.

Between the limits of very long pulses that make the gate inoperable due to decoherence, and very short pulses that make the gate inoperable due to double occupancy in the final

state, lies the region of pulses that can drive the quantum gate. These pulses produce various anisotropies β for the fixed integrated isotropic exchange strengths λ . They are a handle for control over axially symmetric anisotropic gates. The range of anisotropies available in the gates produced by these pulses spans the control wedge [Fig. 4.1] of width θ_m and determines how much control over the anisotropic gates is available. If the intuition about the gate anisotropy as an average of the interaction anisotropy is correct, the first estimate of this control range is a variation of the anisotropic interaction strength β^{int} between the distances of closest approach corresponding to the fastest and the slowest pulse allowed by the limited tolerance for errors.

There is a procedure for calculating a gate produced by a pulse of the Hund-Mulliken Hamiltonian, even when the effective spin Hamiltonian does not exist throughout the pulse application. This procedure was already used in chapter 3. We begin by solving the Schrödinger equation with a time dependent Hund-Mulliken Hamiltonian for the unitary evolution operator in the entire variational space. If the probability of double occupancy at the end of the pulse is small, we can neglect it and obtain the parameters for the gate by taking

$$i \log U^{gate} = \lambda H^{gate}, \quad (4.42)$$

where U^{gate} is a slightly nonunitary operator in a qubit space obtained by truncating the orbitally excited states from the unitary evolution in the space of Hund-Mulliken approximation. The gate parameter β is fitted from the gate Hamiltonian.

Results of such calculation are presented in [Fig. 4.9], together with the bounds on pulses that can be implemented. For comparison the dependence of interaction anisotropy β^{int} obtained from effective spin interaction is plotted on the same graph. Intuition about the gate anisotropy as an average of interaction anisotropy with a weight function pulling strongly toward the short distance is valid in this case. Range of gate anisotropies predicted in our calculation with optimistic prediction for error correction threshold of $p_t h = 10^{-4}$ and decoherence time $T = 10 \mu s$ is very large. We find $\Delta\beta \approx 0.5$. This result is not very sensitive to the exact values of decoherence time and error correction threshold, because both curves that limit the available closest approach distances for the pulses are very steep.

With this estimate of the available range of axially symmetric anisotropies, spin control using control over anisotropy would be an attractive procedure for spin manipulation, either

in a quantum computer or for any other purpose. However, numbers that came out of this calculation, like $\Delta\beta = 0.5$ should not be trusted as an accurate estimate for the control range in a realistic device. But it does suggest that axially symmetric spin-orbit coupling caused anisotropy may be a useful resource for spin manipulation.

4.3 Summary

This chapter shows that anisotropy caused by spin-orbit coupling can be a resource for universal quantum computation. Applicability of anisotropy for the purpose of universal quantum computing depends on the numerical values of different device parameter that are hard to calculate. Applicability for spin manipulation is, however, clear. More importantly it is clearly demonstrated that tailoring of the time dependence in voltage pulses implementing the gate can control the effects of anisotropy. Requirements on pulse shape go beyond the fixing of the integrated isotropic exchange strength, but, due to symmetry, do not go far beyond that. It is enough to keep them symmetric in time and slightly change their shape to influence the anisotropy of the resulting gate.

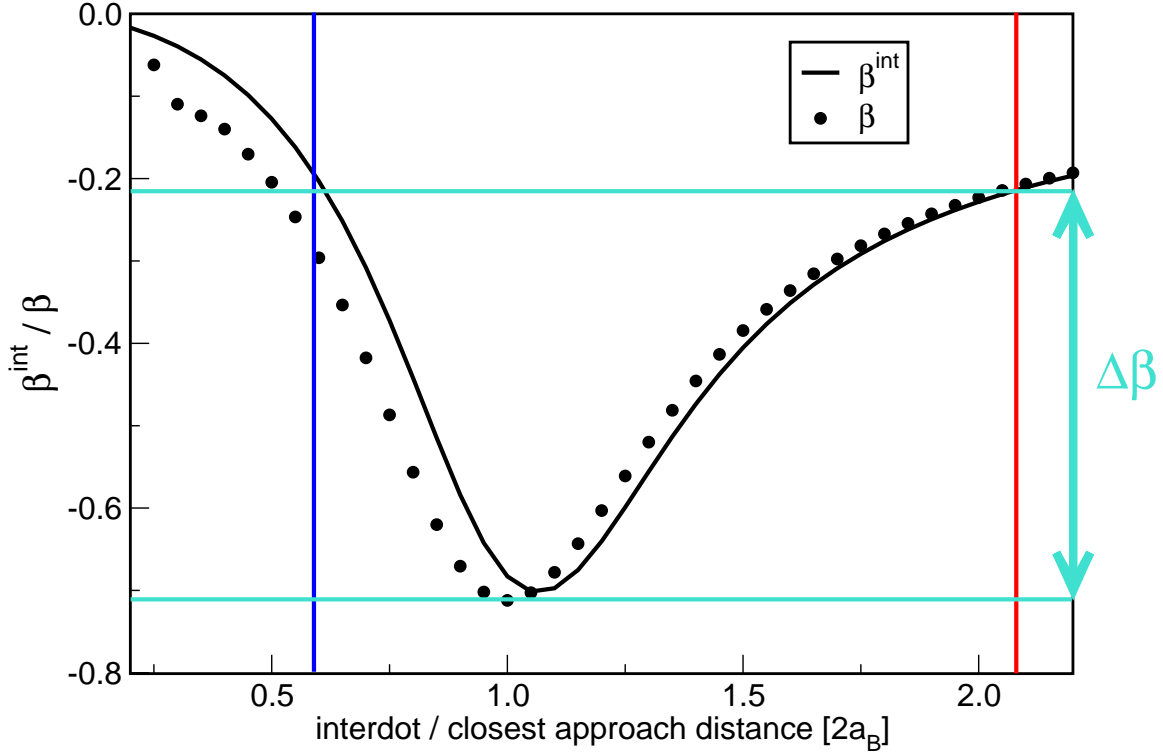


Figure 4.9. Control of Anisotropy Using the Pulse Shape. Black dots represent the size of anisotropic term in the gate, β is plotted against the distance of closest approach in a pulse implementing an isotropic gate $U(\pi, 0, 0, 0)$ in the limit of zero spin-orbit coupling. The data points come from the numerical solutions to a time dependent Schrodinger equation. As discussed in the text, the pulses with smaller distance of closest approach are faster and the pulses with large distance of closest approach are slower. Limit on pulse duration that come from the decoherence in the case of slow pulses is represented by a red line. For the fast pulses, the limiting factor are errors caused by double occupancy in the final state and the limit is represented by the blue line. The available range of gate parameters is denoted by $\Delta\beta$. For the reference, the dependence of interaction anisotropy β^{int} as a function of the interdot distance is plotted as a solid black line.

APPENDIX A

AXIALLY SYMMETRIC GATE FOR CNOT CONSTRUCTION

Discussion of two qubit gates is more convenient if we choose a basis consisting of $|\uparrow\downarrow\rangle = 1/\sqrt{2}(|0\rangle + |1\rangle)$ and $|\downarrow\uparrow\rangle = 1/\sqrt{2}(|0\rangle - |1\rangle)$ in computational space for qubits. If the qubits are in computational states, states of electron spins on the four dots that encode two qubits are spanned by the vectors

$$|\uparrow\downarrow\uparrow\downarrow\rangle = 1/\sqrt{2}(|0\rangle + |1\rangle) \otimes 1/\sqrt{2}(|0\rangle + |1\rangle), \quad (\text{A.1})$$

$$|\uparrow\downarrow\downarrow\uparrow\rangle = 1/\sqrt{2}(|0\rangle + |1\rangle) \otimes 1/\sqrt{2}(|0\rangle - |1\rangle), \quad (\text{A.2})$$

$$|\downarrow\uparrow\uparrow\downarrow\rangle = 1/\sqrt{2}(|0\rangle - |1\rangle) \otimes 1/\sqrt{2}(|0\rangle + |1\rangle), \quad (\text{A.3})$$

$$|\downarrow\uparrow\downarrow\uparrow\rangle = 1/\sqrt{2}(|0\rangle - |1\rangle) \otimes 1/\sqrt{2}(|0\rangle - |1\rangle). \quad (\text{A.4})$$

Note that the two middle (we will call them interacting) spins upon which the elementary gate is going to act do not lie in the computational space for a single qubit. Therefore, we will need to care about states with both $S_z = 0$ and $S_z = \pm 1$. State of the interacting spins uniquely determines the state of all four spins, provided that the state is computational.

An elementary gate acting on interacting spins may lead to the leakage of the state of four spins outside of the computational space for two qubits. Specifically, if we change any of the interacting spins configurations that appear in the basis (A.1) at least one of the qubits will leak outside of the computational space. To stay within computational space, unitary transformation on qubits, induced by applying an elementary gate to interacting spins, must be diagonal in the basis (A.1). We call these transformations diagonal.

Axially symmetric gates will always be diagonal in the subspace spanned by states with $S_z = \pm 1$, and eigenvalues corresponding to the two states will be equal.

Therefore, the most general operator from $SU(4)$ that is both diagonal and can be implemented using axially symmetric gate is of the form

$$U = e^{-i\frac{\phi_1+\phi_2}{4}} \begin{bmatrix} e^{i\phi_1} & 0 & 0 & 0 \\ 0 & 1 & 0 & 0 \\ 0 & 0 & 1 & 0 \\ 0 & 0 & 0 & e^{i\phi_2} \end{bmatrix}, \quad (\text{A.5})$$

in the basis (A.1). It is parametrized by two real phases ϕ_1 and ϕ_2 .

Since application of two qubit gates using elementary gates acting on interacting spins may lead to the leakage outside of computational space, we would like to minimize their number in constructing a universal set of gates. Writing the gate in form (A.5) enables us to find a set of operations on interacting spins that allow for the construction of $CNOT$ gate with a single application of unitary operation on interacting spins.

First we note that we can go from the computational basis of two qubits to the basis (A.1) using single qubit Hadamard gates. Therefore, the set of operations that can be implemented using (A.5) and single qubit gates is equal to the set of operations that can be implemented using an operator V , defined as an operator with the same matrix form but in computational basis, and single qubit gates.

Next we consider the condition the phases ϕ_1 and ϕ_2 have to fulfill in order to create maximally entangling gate. Since the $CNOT$ gate is maximally entangling gate, only some other maximally entangling gate may produce it in single application, with the help of single qubit gates.

Following Kraus and Cirac [70], [77], the entanglement capability can be extracted from the eigenvalues of $V^T V$, when transpose is taken in the magic basis. In the magic basis operator V takes the form of V_m

$$V_m = e^{-i/4(\phi_1+\phi_2)} \begin{bmatrix} \frac{1}{2}(e^{i\phi_1} + e^{i\phi_2}) & \frac{-i}{2}(e^{i\phi_1} - e^{i\phi_2}) & 0 & 0 \\ \frac{i}{2}(e^{i\phi_1} - e^{i\phi_2}) & \frac{1}{2}(e^{i\phi_1} + e^{i\phi_2}) & 0 & 0 \\ 0 & 0 & 1 & 0 \\ 0 & 0 & 0 & 1 \end{bmatrix}. \quad (\text{A.6})$$

Matrix $V_m^T V_m$ is diagonal and magic basis vectors are its eigenvectors.

$$V_m^T V_m = \begin{bmatrix} e^{\frac{i}{2}(\phi_1+\phi_2)} & 0 & 0 & 0 \\ 0 & e^{\frac{i}{2}(\phi_1+\phi_2)} & 0 & 0 \\ 0 & 0 & e^{-\frac{i}{2}(\phi_1+\phi_2)} & 0 \\ 0 & 0 & 0 & e^{-\frac{i}{2}(\phi_1+\phi_2)} \end{bmatrix}. \quad (\text{A.7})$$

Double eigenvalues are $v_j = e^{-2i\lambda_j}$ and we read of λ s of Kraus and Cirak recipe:

$$\lambda_1 = \lambda_3 = -\frac{1}{4}(\phi_1 + \phi_2) \quad (\text{A.8})$$

$$\lambda_2 = \lambda_4 = \frac{1}{4}(\phi_1 + \phi_2). \quad (\text{A.9})$$

This set of λ s translates into $(\alpha_x, \alpha_y, \alpha_z) = (\frac{1}{4}(\phi_1 + \phi_2), 0, 0)$, using the convention of [77]. Criterion for the gate to be maximally entangling is either $\alpha_x + \alpha_y \geq \pi/4$ and $\alpha_y + \alpha_z \leq \pi/4$ or $\max_{k,l} |\sin(\lambda_k - \lambda_l)| = 1$. When we take into account the fact that entanglement capacity is periodic with the period $\pi/2$ and symmetric around $\pi/4$ in α_x , α_y and α_z , and also that phases of the eigenvalues are periodic with the period 2π and subject to constraint that their sum is equal to zero, we find that *CNOT* can be performed with a single application of a two-qubit gate iff

$$\phi_1 + \phi_2 = (2n + 1)\pi, \quad (\text{A.10})$$

where n is an arbitrary integer.

APPENDIX B

MATRIX ELEMENTS OF HUND-MULLIKEN HAMILTONIAN

We work in the basis

$$|2S\rangle = \frac{1}{\sqrt{2}} (|\Phi_{+a}\Phi_{+a}\rangle + |\Phi_{-a}\Phi_{-a}\rangle) \quad (\text{B.1})$$

$$|2A\rangle = \frac{1}{\sqrt{2}} (|\Phi_{+a}\Phi_{+a}\rangle - |\Phi_{-a}\Phi_{-a}\rangle) \quad (\text{B.2})$$

$$|1S\rangle = \frac{1}{\sqrt{2}} (|\Phi_{+a}\Phi_{-a}\rangle + |\Phi_{-a}\Phi_{+a}\rangle) \quad (\text{B.3})$$

$$|1A\rangle = \frac{1}{\sqrt{2}} (|\Phi_{+a}\Phi_{-a}\rangle - |\Phi_{-a}\Phi_{+a}\rangle) \quad (\text{B.4})$$

where $\Phi_{\pm a}$ are orthogonalized Wannier states on the two dots.

The spin-orbit coupling term in the Hamiltonian is

$$H_{SO} = \mathbf{h}(\mathbf{k}_1) \cdot \mathbf{S}_1 + \mathbf{h}(\mathbf{k}_2) \cdot \mathbf{S}_2 \quad (\text{B.5})$$

where

$$\mathbf{h}(\mathbf{k}) = (-f_D k_x + f_R k_y, f_D k_y - f_R k_x, 0). \quad (\text{B.6})$$

Here f_D is the Dresselhaus term and f_R is the Rashba term. In a magnetic field \mathbf{k} is replaced by the canonical momentum $\boldsymbol{\kappa} = \mathbf{k} - (e/c)\mathbf{A}$.

In what follows we will assume the displacement of the dots is in the x direction. It is trivial to rotate (B.6) if this is not the case, so nothing that follows hinges on this assumption.

Explicit calculation gives

$$\langle \Phi_{\pm a} | \boldsymbol{\kappa} | \Phi_{\pm a} \rangle = 0 \quad (\text{B.7})$$

$$\langle \Phi_{-a} | \kappa_y | \Phi_{+a} \rangle = 0 \quad (\text{B.8})$$

with the only nonvanishing matrix element being

$$\langle \Phi_{-a} | \kappa_x | \Phi_{+a} \rangle = -iam\Omega n^2 (1 - g^2) \left(1 - \frac{1}{(2l_B^2 m \Omega)^2} \right) \exp \left(-a^2 m \Omega \left(1 + \frac{1}{(2l_B^2 m \Omega)^2} \right) \right) \quad (\text{B.9})$$

where a is half the dot spacing, l_B is the magnetic length, and $\Omega = \omega_0 \sqrt{1 + (\omega_L/\omega_0)^2}$ and ω_L is the Larmor frequency, and n is the normalization constant of two-electron states.

Given these matrix elements, the Hund-Mulliken Hamiltonian matrix is

$$H = \begin{bmatrix} V & 0 & -i2P \\ 0 & 0 & -2t_H \\ i2P & -2t_H & U_H \end{bmatrix} \quad (\text{B.10})$$

where the matrix is 3×3 because the state $|2A\rangle$ decouples and so we work only in the $|1A\rangle$, $|1S\rangle$, $|2S\rangle$ basis. It is understood that the two other triplet states $|1A, S=1, S_z = \pm 1\rangle$ have decoupled from the problem and both have energy V . Note that we take the z axis in spin space to be parallel to the vector $(-f_D, -f_R, 0)$

Here V , U_H and t_H are the matrix elements calculated in [52]. There is only one new matrix element due to spin-orbit coupling,

$$2iP = \langle 2S | H^{SO} | 1A \rangle \quad (\text{B.11})$$

and

$$P = \frac{\rho}{2} am\Omega n^2 (1 - g^2) \left(1 - \frac{1}{(2l_B^2 m \Omega)^2} \right) \exp \left(-a^2 m \Omega \left(1 + \frac{1}{(2l_B^2 m \Omega)^2} \right) \right) \quad (\text{B.12})$$

where $\rho = \sqrt{m\omega_0}(f_D^2 + f_R^2)$ is a measure of the strength of spin-orbit coupling.

In summary, we have shown that the Hamiltonian of the electrons on coupled quantum dots is of the form (B.10). Effects of the spin-orbit coupling in this system are described by a single parameter P when we choose the appropriate axis of quantization for the total spin.

REFERENCES

- [1] David Hilbert. Mathematische Probleme. *Nachrichten von der Konigl. Gesellschaft der Wiss. zu Gottingen*, pages 253–297, 1900.
- [2] A.M. Turing. On computable numbers, with an application to the entscheidungsproblem. *Proceedings of the London Mathematical Society*, 42:230–265, 1936.
- [3] Alonzo Church. A note on the entscheidungsproblem. *Journal of Symbolic Logic*, 1:40, 1930.
- [4] Alonzo Church. An unsolvable problem of elementary number theory. *American J of Math.*, 58:345, 1936.
- [5] Claude E. Shannon. A mathematical theory of communication. *Bell System Technical Journal*, 27:379, 1948.
- [6] Claude E. Shannon. A mathematical theory of communication. *Bell System Technical Journal*, 27:623, 1948.
- [7] C. H. Bennett and G. Brassard. Quantum cryptography: Public key distribution and coin tossing. In *Proceedings of IEEE international Conference on Computers, Systems and Signal Processing, Bangalore, India*, page 175, New York, 1984. IEEE Press.
- [8] I. Marcikic, H. de Riedmatten, W. Tittel, H. Zbinden, M. Legre, and N. Gisin. Distribution of time-bin entangled qubits over 50 km of optical fiber. *Physical Review Letters*, 93:180502, 2004.
- [9] J. S. Bell. On the Einstein-Podolsky-Rosen paradox. *Physics*, 1:195, 1964.
- [10] J. S. Bell. Speakable and unspeakable in quantum mechanics. *Physics*, 1:195, 1964. (Cambridge University Press, Cambridge, 1987).
- [11] E. Farhy and S. Gutmann. An analog analogue of a digital quantum computation. *Physical Review A*, 57:2403, 1998.
- [12] Robert Raussendorf, Daniel E. Browne, and Hans J. Briegel. Measurement-based quantum computation on cluster states. *Physical Review A*, 68:022312, 2003.
- [13] D. P. DiVincenzo. Two-bit gates are universal for quantum computation. *Physical Review A*, 51(2):1015, 1995.
- [14] E. Fredkin and T. Toffoli. Conservative logic. *International Journal of Theoretical Physics*, 21(3/4):219, 1982.

- [15] L. K. Grover. Quantum mechanics helps in searching for a needle in a haystack. *Physical Review Letters*, 79(2):325, 1997.
- [16] P.W. Shor. Algorithms for quantum computation: discrete logarithms and factoring. In *35. Annual Symposium on Foundations of Computer Science*. IEEE Press, Los Alamitos, CA, 1994.
- [17] A. K. Lenstra, H. W. Lenstra, M. S. Manassee, and J. M. Pollard. The number field sieve. In *Proc. 22nd. Ann. ACM Symp. on Theory of Computing*, 1990.
- [18] Artur Ekert and Richard Jozsa. Quantum computation and shor’s factoring algorithm. *Rev. Mod. Phys.*, 68:733, 1996.
- [19] Peter W. Shor. Scheme for reducing decoherence in quantum computer memory. *Phys. Rev. A*, 52:R2493, 1995.
- [20] A. R. Calderbank and P. W. Shor. Good quantum error-correcting codes exist. *Phys. Rev. A*, 54:1098–1105, 1996.
- [21] A. R. Calderbank, E. M. Rains, P. W. Shor, and N. J. A. Sloane. Quantum error correction and orthogonal geometry. *Physical Review Letters*, 78:405, 1997.
- [22] A. M. Steane. Error correcting codes in quantum theory. *Physical Review Letters*, 77:793, 1996.
- [23] J. Preskill. Reliable quantum computers. *Proc. R. Soc. Lond. A*, 454:385, 1998.
- [24] D. Aharonov and M. Ben-Or. Fault-tolerant quantum computation with constant error rate. In *Proc. 29th. Ann. ACM Symp. on Theory of Computing*, 1997. Longer version quant-ph/9906129.
- [25] D. P. DiVincenzo. Quantum computation. *Science*, 270:255–261, 1995.
- [26] D. Loss and D. P. DiVincenzo. Quantum computation with quantum dots. *Physical Review A*, 57:120–126, 1998.
- [27] L. M. K. Vandersypen, M. Steffen, G. Breyta, C. S. Yannoni, M. Sherwood, and I. L. Chuang. Experimental realization of Shor’s quantum factoring algorithm using nuclear magnetic resonance. *Nature*, 414:883, 2001.
- [28] A. M. Steane. The ion-trap quantum information processor. *Applied Physics B*, 64:623, 1997.
- [29] D. Kielpinsky, C. Monroe, and D. J. Wineland. Architecture for a large-scale ion-trap quantum computer. *Nature*, 417:709, 2002.
- [30] A. Shnirman, G. Schön, and Z. Hermon. Quantum manipulations of small Josephson junctions. *Phys. Rev. Lett.*, 79:2371–2374, 1997.
- [31] B. Kane. A silicon-based nuclear spin quantum computer. *Nature*, 393:133, 1998.

- [32] D. P. DiVincenzo, D. Bacon, J. Kempe, G. Burkard, and K. B. Whaley. Universal quantum computation with the exchange interaction. *Nature*, 408:339, 2000.
- [33] D. Bacon, J. Kempe, D. DiVincenzo, D. A. Lidar, and K. B. Whaley. Encoded universality in physical implementations of a quantum computer. In *Proceedings of the International Conference on Experimental Implementation of Quantum Computation (IQC'01)*, Australia, 2001. Rinton Press.
- [34] K. V. Kavokin. Anisotropic exchange interaction of localized conduction-band electrons in semiconductors. *Physical Review B*, 64:075305, 2001.
- [35] G. Dresselhaus. Spin-orbit coupling effects in zinc-blende structures. *Physical Review*, 100:580, 1955.
- [36] E. I. Rashba. *Fizika Tverdogo Tela (Leningrad)*, 2:1109, 1960.
- [37] Y. Kato, R. C. Myers, A. C. Gossard, and D. D. Awschalom. Coherent spin manipulation without magnetic fields in strained semiconductors. *Nature*, 427:50, 2004.
- [38] R. J. Elliot. *Physical Review*, 96:266, 1954.
- [39] S. Datta and B. Das. *Applied Physics Letters*, 56:665, 1990.
- [40] J. Kempe and K. B. Whaley. Exact gate-sequences for universal quantum computation using the XY-interaction alone. *Phys. Rev. A*, 65 (5):52330, 2002.
- [41] Simon C. Benjamin. Simple pulses for universal quantum computation with a Heisenberg ABAB chain. *Phys. Rev. A*, 64:054303, 2001.
- [42] Jeremy Levy. Universal quantum computation with spin-1/2 pairs and Heisenberg exchange. *Phys. Rev. Lett.*, 89:147902, 2002.
- [43] L.-A. Wu and D. A. Lidar. Power of anisotropic exchange interactions: Universality and efficient codes for quantum computing. *Phys. Rev. A*, 65:042318, 2002.
- [44] M. A. Nielsen and I. L. Chuang. *Quantum Computation and Quantum Information*. Cambridge University Press, Cambridge, UK, 2000.
- [45] J. M. Kikkawa and D. D. Awschalom. Resonant spin amplification in n-type GaAs. *Phys. Rev. Lett.*, 80:4313, 1998.
- [46] I. Dzyaloshinskii. *Journal of Physics and Chemistry of Solids*, 4:241, 1958.
- [47] Toru Moriya. Anisotropic superexchange interaction and weak ferromagnetism. *Phys. Rev.*, 120:91, 1960.
- [48] Kurt Gottfried. *Quantum Mechanics*, volume 1. W. A. Benjamin, Reading, Mass., 1966.
- [49] L.-A. Wu and D. A. Lidar. Dressed qubits. *Phys. Rev. Lett.*, 91:097904, 2003.

- [50] N. E. Bonesteel, T. M. Rice, and F. C. Zhang. Spin-orbit coupling and spirals in doped La_2CuO_4 . *Phys. Rev. Lett.*, 68:2684, 1992.
- [51] Guido Burkard and Daniel Loss. Cancellation of spin-orbit effects in quantum gates based on the exchange coupling in quantum dots. *Phys. Rev. Lett.*, 88:047903, 2002.
- [52] Guido Burkard, Daniel Loss, and David P. DiVincenzo. Coupled quantum dots as quantum gates. *Phys. Rev. B*, 59:2070, 1999.
- [53] Patrik Recher, Eugene V. Sukhorukov, and Daniel Loss. Quantum dot as spin filter and spin memory. *Phys. Rev. Lett.*, 85:1962, 2000.
- [54] L. L. Chang, L. Esaki, and R. Tsu. Resonant tunneling in semiconductor double barriers. *Applied Physics Letters*, 24:593, 1974.
- [55] M. A. Reed, R. T. Bate, K. Bradshaw, W. M. Duncan, W. R. Frensley, J. W. Lee, and H. D. Shih. Spatial quantization in gaas-algaas multiple quantum dots. *J. Vacuum Sci. Technol. B*, 4:358, 1986.
- [56] M. A. Reed. Quantum dots. *Scientific American*, 268:118, 1993.
- [57] Arvind Kumar, Steven E. Laux, and Frank Stern. Electron states in a gaas quantum dot in a magnetic field. *Phys. Rev. B*, 42:5166, 1990.
- [58] L. Brey, N. F. Johnson, and B. I. Halperin. Optical and magneto-optical absorption in parabolic quantum wells. *Phys. Rev. B*, 40:10647, 1989.
- [59] P. A. Maksym and Tapash Chakraborty. Quantum dots in a magnetic field: Role of electron-electron interactions. *Phys. Rev. Lett.*, 65:108, 1990.
- [60] P. Bakshi, D. A. Broido, and K. Kempa. Electromagnetic response of quantum dots. *Phys. Rev. B*, 42:7416, 1990.
- [61] Walter Kohn. Cyclotron resonance and de Haas-van Alphen oscillations of an interacting electron gas. *Phys. Rev.*, 123:1242, 1961.
- [62] V. Fock. Bemerkung zur Quantelung des harmonischen Oszillators in Magnetfeld. *Z. Phys.*, 47:446, 1928.
- [63] C.G. Darwin. The diamagnetism of the free electron. *Proc. Cambridge Phil. Soc.*, 27:86, 1930.
- [64] Y. Kato, R. C. Myers, D. C. Driscoll, A. C. Gossard, J. Levy, and D. D. Awschalom. Gigahertz electron spin manipulation using voltage-controlled g-tensor modulation. *Science*, 299:1201, 2003.
- [65] D. D. Awschalom, D. Loss, and N. Samarth. *Semiconductor Spintronics and Quantum Computation*. NanoScience and Technology. Springer, Berlin, 2002.
- [66] L.-A. Wu, D.A. Lidar, and M. Friesen. One-spin quantum logic gates from exchange interactions and a global magnetic field. *Phys. Rev. Lett.*, 93:030501, 2004.

- [67] J. Hubbard. Electron correlations in narrow energy bands. *Proc. Roy. Soc. London A*, 276:238, 1963.
- [68] John Schliemann, J. Carlos Egues, and Daniel Loss. Nonballistic spin-field-effect transistor. *Phys. Rev. Lett.*, 90:146801, 2003.
- [69] John Schliemann, Daniel Loss, and A. H. MacDonald. Double-occupancy errors, adiabaticity, and entanglement of spin qubits in quantum dots. *Phys. Rev. B*, 63:085311, 2001.
- [70] B. Kraus and J. I. Cirac. *Physical Review A*, 63:062309, 2002.
- [71] Seth Lloyd. Almost any quantum logic gate is universal. *Phys. Rev. Lett.*, 75:346, 1995.
- [72] Hans-Andreas Engel, L. P. Kouwenhoven, Daniel Loss, and C. M. Marcus. *Experimental Aspects of Quantum Computing: Controlling Spin Qubits in Quantum Dots*, volume 3. Springer Science+Business Media B.V., Formerly Kluwer Academic Publishers B.V., 2004.
- [73] Mark Friesen, Paul Rugheimer, Donald E. Savage, Max G. Lagally, Daniel W. van der Weide, Robert Joynt, and Mark A. Eriksson. Practical design and simulation of silicon-based quantum-dot qubits. *Phys. Rev. B*, 67:121301(R), 2003.
- [74] Lucjan Jacak, Pawel Hawrylak, and Arkadiusz Wojs. *Quantum Dots*. Springer, Berlin, 1998.
- [75] R. Winkler. *Spin-orbit Coupling Effects in Two-Dimensional Electron and Hole Systems*. Springer, Berlin, 2003.
- [76] Xuedong Hu and S. Das Sarma. Hilbert-space structure of a solid-state quantum computer: Two-electron states of a double-quantum-dot artificial molecule. *Phys. Rev. A*, 61:062301, 2000.
- [77] K. Hammerer, G. Vidal, and J. I. Cirac. *Physical Review A*, 66:062321, 2002.

BIOGRAPHICAL SKETCH

Dimitrije Stepanenko

Department of Physics and
National High Magnetic Field Laboratory
Florida State University
Tallahassee, FL 32310

Email: didef@magnet.fsu.edu
Phone: (850) 644 6825
Fax: (850) 644 5038

EDUCATION

- | | |
|-------------------|--|
| Ph. D. in Physics | Florida State University, 2005.
Thesis: Symmetry and Control in Spin-Based Quantum Computing
Advisor: Nicholas Bonesteel |
| B. S. | University of Belgrade, 1998.
Thesis: Duality in Field Theories
Advisor: Branislav Sazdović |

EMPLOYMENT

- | | |
|--------------------|--|
| 06/1993 to 08/1998 | Lecturer, Petnica Science Center. Lectured and supervised student research projects in the program of education through research for high school students. |
| 09/1998 to 09/2000 | Presidential graduate fellow and teaching assistant, Boston University. Recitation in Quantum Mechanics, Electromagnetism and Introductory Physics lab and recitation. |
| 08/2000 to present | Research assistant, National High Magnetic Field Laboratory and Department of Physics, Florida State University. |

HONORS AND SCHOLARSHIPS

- Dirac-Hellman award for research in theoretical physics, awarded for the study of spin-orbit coupling in solid state based quantum computer, Florida State University, 2003.

- Presidential University Graduate Fellowship, Boston University, 1998-2000.
- National Scholarship of the Department of Science and Technology, Serbia and Montenegro, 1993-1998.

PUBLICATIONS

- D. Stepanenko, N. E. Bonesteel: *Universal Quantum Computation through Control of Spin-Orbit Coupling*, Physical Review Letters, **93**, 140501 (2004).
- D. Stepanenko, N. E. Bonesteel, D. P. DiVincenzo, G. Burkard and Daniel Loss: *Spin-Orbit Coupling and Time-Reversal Symmetry in Quantum Gates*, Physical Review B **68**, 115306 (2003).
- N. E. Bonesteel, D. Stepanenko and D. P. DiVincenzo: *Anisotropic Spin Exchange in Pulsed Quantum Gates*, Physical Review Letters, **87**, 207901 (2001).
- D. Stepanenko and N. E. Bonesteel, Control of Anisotropic Exchange Interaction in Coupled Quantum Dots (in preparation).

CONFERENCE PRESENTATIONS

- *Anisotropic Spin Exchange in Pulsed Quantum Gates*, March Meeting of the American Physical Society, Indianapolis 2002.
- *Spin-Orbit Coupling and Time-Reversal Symmetry in Quantum Gates*, poster presentation, Gordon Research Conference on Quantum Information Science, Ventura, 2002.
- *Spin-Orbit Coupling and Time-Symmetric Pulsing of Quantum Gates*, March Meeting of the American Physical Society, Austin, 2003.
- *Universal Quantum Computation with Axially Symmetric Anisotropic Exchange*, poster presentation, Gordon Research Conference on Quantum Information Science, Ventura, 2004.

- *Universal Quantum Computation through Control of Spin-Orbit Coupling*, poster presentation, Frontiers in Nanoscale Science and Technology workshop, Boston, 2004.

VISITS

- IBM T. J. Watson Research Center, October 2004.
- Condensed Matter and Surface Science Program, Ohio University, November 2002.